LATE PLEISTOCENE ENVIRONMENTS ACROSS NORTH-CENTRAL INDIA AND IMPLICATIONS FOR HOMININ ADAPTATIONS WITH SPECIAL REFERENCE TO THE LOWER SON VALLEY, SONBHADRA, UTTAR PRADESH

Shashi Bhushan

A thesis submitted for the partial fulfillment of

the degree of Doctor of Philosophy

Department of Humanities and Social Sciences

Indian Institute of Science Education and Research Mohali

Knowledge city, Sector 81, SAS Nagar, Manauli PO, Mohali 140306, Punjab, India.

July 2023

To everyone,
who dared to step out and explore!

Declaration

The work presented in this thesis has been carried out by me under the guidance of Dr. Parth R. Chauhan at the Indian Institute of Science Education and Research Mohali. This work has not been submitted in part or in full for a degree, a diploma, or a fellowship to any other universityor institute. Whenever contributions of others are involved, every effort is made to indicate this clearly, with due acknowledgement of collaborative research and discussions. This thesis is a bonafide record of original work done by me and all sources listed within have been detailed in the bibliography.

Shashi Bhushan

In my capacity as the supervisor of the candidate's thesis work, I certify that the above statementsby the candidate are true to the best of my knowledge.

Dr. Parth R. Chauhan

Acknowledgements

First and foremost, I would like to express my deep appreciation for Dr. Parth R. Chauhan, my supervisor and mentor, who has been a constant source of academic support and guidance throughout this study. His valuable advice and encouragement were instrumental in helping me complete this thesis. I also want to extend my heartfelt gratitude to Dr. V. Rajesh and Dr. Anu Sabhlok, who provided academic support in their roles as department heads. Their unwavering support has been critical to my success in this research.

I am immensely grateful to Dr. Anoop Ambili for his input and guidance in understanding the complex geological concepts, methods, and interpretation of palaeoenvironmental reconstructions. I want to express my gratitude towards Prof. Rajeev Patnaik (Panjab University) for helping me understand different geological and taphonomic concepts and fossil identification. I also appreciate Prof. Rajeev Patnaik and Dr. Anoop Ambili's valuable feedback and support as committee members for my doctoral research. Their encouragement and guidance have been truly invaluable.

I would also like to thank the University Grants Commission for awarding the Junior and Senior Research Fellowship, which enabled me to pursue this research. I am also thankful to the Indian Institute of Science Education and Research Mohali and the STARS grant (Project ID, 651) from the Ministry of Education (MOE) (awarded to Dr. Parth R. Chauhan) for providing the necessary fieldwork and logistical support.

I want to acknowledge the Uttar Pradesh State Archaeology Department, Lucknow and the Archaeological Survey of India, Delhi, for granting Dr. Parth R. Chauhan the necessary permit for explorations and lithic collection in the study area. Their support and permission have been critical in completing this research.

Further, I want to express my deep appreciation to Dr. Krishna Mohan Dubey and Dr. Swtantra Kumar for their friendship and unwavering support during fieldwork in Sonbhadra, Uttar Pradesh. Their compassion and camaraderie made the challenging fieldwork a genuinely memorable experience.

I am deeply grateful to Prof. Ajay Pratap of the Department of History and Prof. Prabhakar Upadhyay of the Department of Ancient Indian History, Culture, and Archaeology at Banaras Hindu University (BHU) in Varanasi for generously offering their time and invaluable support during my visits to BHU.

I am grateful to Mr. Gopesh Jha, Mr. Kaleeswarvan, Ms. Swati Verma, Ms. Shweta Pandey, Mr. Manish Chobey and Mr. Rajesh Poojari for their invaluable assistance during the fieldwork. Their interest, dedication and hard work during field explorations have made this research possible. Furthermore, I extend my heartfelt thanks to Dr. Vivek Singh, Mr. Ravindra Devra, Ms. Bharti Jangra, Ms. Swati Verma, Mr. Yezad Pardiwalla, Mr. Anil Devra, Ms. AnubhavPreet Kaur, Ms. Diptimayee Behra, Mr. Nishant, Mr. Atharva Deshpande, Ms. Aarya Joshi, Mr. Mihir Tanksale and Mr. Dhruva Sambrani for their exceptional involvement to this study. Their tireless efforts, from fieldwork to laboratory analysis, have played a crucial role in the success of this research. I would also like to express my gratitude towards the other alums and present members of PalaeoArch Lab: Dr. Nupur Tiwari, Dr. Akash Srinivas, Dr. Jayashree Mazumder and for their support throughout the research process.

I cannot express enough how grateful I am to Dr. Ravish Lal, Dr. Toshabanta Padhan, Mr. Shubham Pal, and Mr. Shantanu Katiyar for their exceptional efforts in collecting fossils and calcrete samples from various sites in Narsinghpur, Sehore and Narmadapuram Districts, Madhya Pradesh. The fieldwork and logistical support of sample collection was made

possible through the University Grants Commission-Israel Science Foundation research grant (Application no. 2712/16) awarded to Dr. Parth R. Chauhan.

I sincerely thank Dr. Prabhin Sukumaran from CHARUSAT, Gujarat, and Dr. Neeraj Awasthi from Veer Bahadur Singh Paranuchal University, Jaunpur, for providing valuable geological insights during the fieldwork. Their expertise and guidance were invaluable in helping me understand the geological complexities of the study area.

Furthermore, I extend my gratitude to Dr. Vimal Singh, Mr. Arkaprabha Sarkar from University of Delhi and Dr. Naveen Chauhan, Ms. Monika Devi from Physical Research Laboratory, Ahmedabad, for their help and guidance in OSL sample collection and dating of the study area, which was a crucial part of my research. I am also thankful to Dr. Shailesh Agrawal and Mr. Sandeep from BSIP, Prof. Debajyoti Paul and Mr. Abhishek for their guidance in understanding the method and concepts and conducting stable isotope analysis.

I express my sincere gratitude to Prof. Ajithprasad from Maharaja Sayajirao University (MSU), Baroda and Dr. August Costa from Rice University, USA for granting access to the fossils from Gopnath, which were stored in MSU repository. Their cooperation and support were crucial in facilitating my research work, and I am deeply grateful for their assistance. I would also like to thank the Department of Ancient History and Archaeology at MSU, particularly Mr. Anil Devra and Dr. Ritvik Balvally, for facilitating my visit to MSU.

Additionally, I extend my appreciation to Prof. Vijay Sathe from Deccan College for assisting me in accessing fossils from the Narmada Valley stored at Deccan College repository. I also want to thank the Department of Ancient Indian History Culture and Archaeology, Deccan College for allowing me to access their library and present my work. I

thank Mr. Chandan from Deccan College for his assistance in arranging my visit to Deccan College.

I sincerely appreciate Prof. Bruce Bradley from the University of Exeter, UK, who introduced me to knapping. Additionally, I would like to thank Dr. Andrew Kandel from the University of Tubingen, Germany, for his invaluable input on lithic collection and general discussion of lithic typo technology, which enriched this research.

I am also profoundly thankful to "The Role of Culture in Early Expansions of Humans" (ROCEEH) project for facilitating my visit to the University of Tubingen and allowing me to participate in the project. Their support and encouragement have been instrumental in my academic and professional growth. Furthermore, I extend my gratitude to the University of Tubingen for allowing me to participate in the excavation at the cave site of Hohle Fels, a crucial aspect of my research career.

I want to express my sincere gratitude to the reviewers for taking the time to review and provide feedback on the thesis. Their valuable insights, suggestions, thorough evaluation and constructive comments have contributed significantly to the improvement and refinement of the work.

I want to thank Mr. Arun, Mr. Pappu Mishra, Mr. Ritesh, Mr. Ramesh, and Mr. Rahul for their valuable assistance in providing vehicles during my research work. Their support and cooperation were crucial in facilitating transportation during the project, and I am deeply thankful for their contributions. Their assistance allowed me to conduct my research with ease, and I appreciate their willingness to help me with the project.

I also extend my gratitude to Mr. Anand Agarwal Ji for providing suitable field accommodation. I thank the villagers of Kargara, especially Mr. Sudin ji, for allowing and helping in the geological excavation in the field.

I express my profound appreciation to the Department of Humanities and Social Sciences and IISERM, for their generous financial support and infrastructure assistance in facilitating my research work. It is a great honour for me to acknowledge the Directors, Deans, and other esteemed officials of IISERM for their invaluable support throughout my academic pursuit.

Lastly, I want to thank my parents and brothers from the bottom of my heart for always believing in me and supporting me. I am thankful for their support and advice, which have helped me get where I am today. I extend my special thanks to my younger brother, cousins, nephew, and nieces, who have provided me with invaluable support and entertainment throughout the process.

Shashi Bhushan

07-07-2023

Abstract

Climate change is increasingly recognised as a significant component in the biological evolution and cultural development of our species. It is widely assumed that it has an impact on behavioural plasticity, as well as the development of more efficient technologies and associated subsistence strategies. However, detailed research on such possibilities has not yet been explored in South Asia, despite the fact that our knowledge of palaeoenvironmental records from the Late Pleistocene have improved in this region and South Asia plays an important role in human migrations outside of Africa. Late Pleistocene habitation in South Asia currently spans a diverse range of ecologies, from desert to tropical rainforest and from large low-lying river basins to high-altitude settings. North-central and western India probably acted as vital biogeographic dispersal corridors and cultural and biological crossroads for diverse hominin populations, including modern humans, for a large part of the Quaternary. The current study aims to better understand the hominin-environmental interface by investigating various types of paleoanthropological sites in western India (Gopnath, Gujarat), central India (Different localities in Narsinghpur, and Nehlai in Madhya Pradesh) and north-central India (Doma in Uttar Pradesh). It also explicitly focuses on understanding the Palaeolithic/microlithic assemblages and related palaeoenvironmental dynamics of the Lower Son Valley (LSV) in the Sonbhadra District of Uttar Pradesh in north-central India. This research incorporates three different aspects: 1) A. To carry out surveys to locate new Palaeolithic and microlithic sites in the LSV, Sonbhadra, Uttar Pradesh, B. To collect sediment samples from a geological trench to characterise the Quaternary stratigraphy and palaeoenvironments of the study area. 2) Compile published sources for the Late Pleistocene palaeoenvironmental reconstruction of South Asia; 3) To visit the previously reported Late Pleistocene Palaeolithic and fossil sites or museum/university collections to collect enamel samples of fossil teeth and carbonates for the reconstruction of Late Pleistocene

paleoenvironments. To achieve the objectives, five seasons of geological, palaeontological and archaeological field surveys have been conducted from 2017-2021. During these surveys, 61 new Palaeolithic and microlithic sites have been identified along with three vertebrate fossil sites in the LSV, Sonbhadra, Uttar Pradesh. Furthermore, a ~11-meter-deep geological excavation was also conducted to reconstruct the regional Late Pleistocene palaeoenvironmental framework and date the associated sediments through collaboration. Along with that, fossil enamel samples or carbonate samples were collected from select sites mentioned above for palaeoenvironmental reconstructions. It is the first such project that attempts to understand the Late Pleistocene environments and hominin adaptations in the Indian subcontinent via multidisciplinary techniques and through a multi-site study. The study incorporates the lithic analysis of Palaeolithic and microlithic artefacts, the stable isotope analysis on fossil tooth enamel, calcrete collected from western and central India, grain size analysis, X-ray fluorescence (XRF) geochemistry and OSL dating on sediments from LSV. For lithic analysis, Palaeolithic and microlithic artefacts were collected from seven sites in LSV belonging to periods ranging from Late Acheulean to microlithic age, probably spanning from ~140 kyr to 48 kyr based on currently-known evidence. The Late Acheulean to Upper Palaeolithic sites were generally located on the south side of the Son River, while microlithic sites were found all around the study area. The dominant raw material porcellanite is quite versatile and unique in nature which allowed Late Acheulean to microlithic populations to exploit it for artefact production. Preference for other raw materials was observed for successive technologies, especially those found away from the raw material sources. Compiled published resources: Late Pleistocene environmental studies conducted to date in South Asia and associated implications are broadly derived from different proxies, i.e., sediment, carbonate, ostrich eggshell, pollen, speleothem, and multiproxy approaches, including some archaeological sites. The compiled records tentatively show that the period

from 125-80 kyr was predominantly characterised by humid environments and was followed by varied results/changes in climatic conditions at 79-70 kyr and arid environments at 69-60 ka. Between 59 and 30 kyr, South Asia's environmental conditions were again generally humid. The period from 29-20 kyr again represents varied results, which were later followed by arid conditions from 19-11 kyr, following the Last Glacial Maximum or LGM.

Table of Content

List of Figures

List of Tables

List of Plates

1 Introduction

1.1 Human Evolution: A broad perspective

The oldest hominins known are *Sahelanthropus tchadensis* (6-7 myr) from Chad (Brunet et al., 2002) and *Orrorin tugenensis* (5-6 myr) from Kenya (Senut et al., 2001). *Australopithecus* appeared roughly four million years ago, with the first specimens discovered in South Africa in 1924 (Dart, 1925). *Australopithecus* was a highly successful genus that endured for about three million years, based on the abundance of fossils found in eastern and southern Africa. Famous *Australopithecus* species include *A. afarensis* (3.6–2.9 myr) and *A. africanus* (3.2–2.0 myr) from East Africa. The *Australopithecus* foot may have had a human-like arch, according to fossilised Laetoli footprints and metatarsals (Ward et al., 2011). The oldest *Homo* fossil mandible was discovered from Ledi-Geraru research area, Afar Regional State, Ethiopia, and dated to 2.8 myr. The oldest member of the genus *Homo*, *H. habilis* (2.3–1.4 myr), is associated with butchered animal bones and simple stone tools in East Africa (Blumenschine et al., 2003). Its more formidable and ubiquitous descendant, *H. erectus*, was distributed throughout Africa and Eurasia and survived from 1.9 myr to 100 kyr and possibly later (Anton, 2003). Its spatiotemporal persistence implies that *H. erectus* was ecologically adaptable and had the cognitive capacity to flourish in drastically different environments. *H. erectus* has smaller molars than *Australopithecus*, reflecting its softer, more nutritious diet. Around 700 kyr or maybe earlier, *H. erectus* in Africa gave rise to *H. heidelbergensis*, a species remarkably similar to us in body proportions, dental adaptations, and cognitive ability (Rightmire, 2009). The lineage of *H. sapiens* presumably originated in Africa at least 500 kyr (Stringer, 2016), and eventually, *H. sapiens* evolved around 315 kyr (Hublin et al., 2017; Scerri et al., 2018).

1.2 Modern Human origins

The origin and dispersal of *H. sapiens* has drawn both popular and academic interest (O'Shea and Delson, 2018). The discovery of a fossilised forehead of the cranium at Zuttiyeh in Israel, dated between 500 and 200 kyr, indicates that it is either an early Neanderthal or from a population ancestral to both Neanderthals and *H. sapiens* (Freidline et al., 2012). Additionally, Sima de Los Huesos site (Atapuerca, Spain) dates possibly early *H. Neanderthalensis/sapiens* to 430 kyr (Arsuaga et al., 2014). It is nearly universally accepted that *H. sapiens* evolved in Africa, with the first representative of our species dating to approximately 315 kyr at site Jebel Irhoud, Morocco (Hublin et al., 2017) and roughly 260 kyr at site Florisbad, South Africa (Grun et al., 1996). Also, see Scerri et al. (2018) for multiple origins of *H. sapiens* within Africa. Fossilised hominin crania from Herto, Middle Awash, Ethiopia, dating to 160-154 kyr, possibly bridge the gap between archaic African hominin species and modern humans (Clark et al., 2003; White et al., 2003). Fossil remains of modern humans from the Kibish Formation of the lower basin of the Omo River, southern Ethiopia, were dated to 195 kyr (Aubert et al., 2012; Butzer, 1969).

Apidima Cave in Greece contains the oldest *H. sapiens* fossil outside of Africa, dating back to 210 ka (Harvati et al., 2019). This discovery shows that two hominin species (humans and human relatives, i.e., Neanderthals) inhabited southeastern Europe for roughly 200 kyr (Delson, 2019). A jaw of an early modern human from Misiliya Cave in Israel has been dated between 194 - 177 kyr (Hershkovitz et al., 2018). Skhul and Qafzeh include another 130–90 kyr old human fossil (Groucutt et al., 2019). These early Eurasian human fossils represent what may be termed a failed dispersal from Africa (Delson, 2019). A phalanx of *H.* Denisov was discovered from Denisova Cave and dated between 48 to 30 kyr (Krause et al., 2010). *H.* Denisova fossils have also been found from the Tibetan Plateau, dating to 160 ka (Chen et

al., 2019). The qualitative and quantitative studies of the parietal bones, mandible, and lower second molar of Nesher Ramla *Homo* fossils from Israel, dated to 140 – 120 kyr, revealed that this *Homo* group possessed a unique combination of Neanderthal and archaic characteristics. It is postulated that these fossils represent the late survivors of a Middle Pleistocene paleodeme that was most likely involved in the evolution of the Middle Pleistocene *Homo* in Europe and East Asia (Hershkovitz et al., 2021).

Multiple locations in China have revealed fossils believed to represent early *H. sapiens* (Michel et al., 2016), with the most recent discovery of *Homo longi* dated to 146 ka (Ni et al., 2021). Other discoveries include teeth from Fuyan Cave, which were estimated to be older than 80 kyr based on the dating of an underlying speleothem a few metres from the fossils (Liu et al., 2015) and teeth from Luna Cave, which were discovered in strata dated between 129.9 ka and 70.2 ka (Bae et al., 2015). Teeth and a jawbone from China's Zhiren Cave have been attributed to *H. sapiens*, but additional species attributions are plausible (Liu et al., 2010). *H. sapiens* bones recovered in Tam Pa Ling, Laos, date between 86 and 46 kyr (Demeter et al., 2017; Freidline et al., 2023). *H. sapiens* teeth from the Lida Ajer Cave in Sumatra were found in a breccia dating to 68 ka, with fauna dating to 75 ka (Westaway et al., 2017). The metatarsals recovered from Callao Cave (Northern Luzon, Philippines) have been assigned to a new *Homo* species, *H. luzonensis* dating to 67 ka (Détroit et al., 2019; Mijares et al., 2010). A complete skeleton of *H. sapiens* was recovered from Lake Mungo in Australia, which dates to 62 ka (Throne et al., 1999).

H. floresiensis fossils, cranial and some post-cranial remains from Liang Bua Cave of Indonesia date between 38 ka to 18 ka (Brown et al., 2004; Morwood et al., 2004). Another fossil similar to *H. floresiensis* was found in Mata Menge of So'a Basin of central Flores, dating to 700 ka (Van den Bergh et al., 2016). It is currently a matter of debate whether *H.*

floresiensis and *H. luzonensis* evolved from early Asian *Homo erectus* or from an older genus like *Homo habilis* (see Argure et al., 2017; Roberts et al., 2023).

A handful of fossils of *H. sapiens* have been found in South Asia dating between 38 ka to mid-Holocene at Fa Hien Cave in Sri Lanka (Deraniyagala, 1992; Kennedy, 1999, 2000; Kennedy and Deraniyagala, 1989; Kennedy et al., 1987; Perera, 2010; Wijeyapala, 1997). *H. sapiens* fossils found from Sarai Nahar Rai, Uttar Pradesh, date to 10 ka (Dutta 1984).

Other notable hominin fossils found in India are *Homo* sp. indet. (Athreya, 2007), from Hathnora (Sonakia, 1984; Sonakia and Biswas, 1998) with a maximum age of 236 ka (Patnaik et al., 2009) and another hominin from Netankheri is to ~ 80 – 70 ka (Sankhyan, 2012).

1.2.1 Dispersals of *Homo sapiens* out of Africa and the distribution of other Late Pleistocene species across Eurasia

There is considerable interest in determining the timing and location of successful and unsuccessful dispersals of hominins (including modern humans) from Africa. *H. erectus* is believed to have been the first hominin species to leave Africa approximately two million years ago and colonise Asia (Dennell and Roebroeks, 2005). A second wave of migration occurred between 800 and 600 kyr when the ancestor species that gave rise to Neanderthals entered Europe. *H. sapiens* were likely the third group to depart Africa during the Late Pleistocene (Delson, 2019). During the Late Pleistocene, two models of dispersal are prevalent: 1) The traditional "out of Africa" model, which proposes a dispersal of modern *H. sapiens* across Eurasia as a single wave around 60 – 50 kyr (Marine Isotope Stage (MIS) 3) and the subsequent replacement of all indigenous populations (Stringer and Andrews, 1988); and 2) multiple dispersals beginning at the start of the Late Pleistocene (MIS 5) (Bae et al.,

2017; Boivin et al., 2013; Dennell and Petraglia, 2012; Groucutt et al., 2015; Petraglia et al., 2010).

The first model is supported by early genetic research and, to various extents, archaeology, geochronology and palaeoanthropology (Krings et al., 1997; Klein, 2008; Macaulay et al., 2005, Mellers, 2006; Oppenheimer, 2003; Oppenheimer, 2009). The 60 ka dispersal is still predominantly supported by genetic studies of present-day human population variance across the globe. Given the genetic clock's unpredictability (because of different mutation rates and other uncertainties), it is plausible that this event occurred before or after the 60 ka marker (Oppenheimer, 2009; Scally and Durbin, 2012). Recent whole-genome investigations (Malaspinas et al., 2016; Mallick et al., 2016; Mondal et al., 2016) imply that "all present non-Africans diverged from a single ancestral population" [(Tucci and Akey, 2016), p. 179] during the Late Pleistocene (Sikora, 2017). Archaeologists have also established the border between 60 and 50 ka based on the behavioural and technological shift from the Middle to Upper Palaeolithic (Kaifu et al., 2015; Klein, 2008; Mellers, 2006).

Given the increasing number of palaeontological and archaeological reports of *H. sapiens* from sites across Eurasia that supposedly predate 60 ka, it appears that earlier dispersals out of Africa reached the Levant, Greece, Qafzeh, Skhul and perhaps also South, East, and Southeast Asia (Bae et al., 2014; Demeter et al., 2012; Harvati et al., 2019; Petraglia et al., 2007; Liu et al., 2010, 2015; Michel et al., 2016; Mijares et al., 2010; Norton and Jin, 2009; Shen et al., 2002; Westaway et al., 2017). At least some remnants of these earlier dispersals are likely to exist in the modern record. 2% of the DNA of current Papua New Guineans derives from the lineage that precedes the hypothesised 60 ka expansion of modern humans out of Africa, according to a recent genomic study (Pagani et al., 2016).

1.2.2 Interbreeding

Neanderthals and Denisovans are extinct human species (of the genus *Homo*) closely related to modern humans (Hublin, 2009; Krause et al., 2010). Recent genetic studies have revealed a higher Neanderthal admixture in East Asians than in Europeans (Vernot and Akey, 2015), indicating that at least two independent gene flow events must have occurred in early modern humans and that the early ancestors of East Asians experienced more admixture than those of Europeans after the divergence of these two groups (Kim and Lohmueller, 2015; Vernot and Akey, 2015). Before the ancestors of current non-Africans moved across Eurasia, the first interbreeding with Neanderthals occurred in the Middle East. The progenitors of present Europeans and Asians were then separated from this migrant group (Kim and Lohmueller, 2015), along with the beginning of interbreeding between the ancestors of East Asians with Neanderthals again. It is estimated that the first humans with proto-Neanderthal characteristics existed in Eurasia between 350 – 600 kyr, while the first population with classic Neanderthal characteristics appeared between 200 – 250 kyr. This discovery suggests that Neanderthals and Denisovans were more closely connected than either was to contemporary humans (Harmon, 2012). Studies have established the influence of Denisovan heritage in the islands of Oceania, particularly Papua, New Guinea, and some parts of mainland Asia, such as Tibet, despite the disputed extent of Denisovan territory (Reich et al., 2011).

Prehistoric ancestors of all living *H. sapiens* have interbred with Neanderthals, Denisovans, or other hominins. We know that these hominin groupings persisted longer and interbred more in some world regions than others. Besides Denisovans and Neanderthals, archaic hominin species were replaced by *H. sapiens* that moved out of Africa. Still, substantial interbreeding with Denisovans and Neanderthals in Eurasia left a significant impression on

contemporary human DNA (Prüfer et al., 2014). Contemporary South Asian populations preserve substantial evidence for Denisovan introgression, as compared to South West Asians (Sankararaman et al., 2016), suggesting that Denisovan populations inhabited South Asia during the expansion of modern humans into Asia.

1.3 The Late Pleistocene Period

The Late Pleistocene (Upper Pleistocene or the Tarantian) is a stage of the Pleistocene Epoch (Rafferty, 2011). The beginning of the stage is defined by the base of the Eemian interglacial phase before the final glacial episode of the Pleistocene ~126,000 years ago. The end of the stage is put nearly 11,700 years ago (Cohen and Gilbbard, 2011). The Late Pleistocene is further divided into four MIS stages: 1) MIS 2 (14-29 ka), 2) MIS 3 (29-57 ka), 3) MIS 4 (57 – 71 ka), 4) MIS 5 (71-126 ka).

Changes in climate across the last glacial cycle in the Northern Hemisphere and the melting of high-latitude ice sheets at the end of MIS 6 around 130 ka marked the end of the last glacial period. A brief interglacial followed deglaciation during MIS 5e (128 - 120 ka) that ended approximately 117 to 115 ka when glacial inception during MIS substage 5d started building enormous ice sheets over Europe and North America, and the sea level was low, and ice volume was high (Kukla, 2000). MIS 5d culminated at 111 ka, followed by the brief interstadial MIS 5c that lasted until 106 ka, a progressive climatic degradation throughout MIS 4 (71-57 ka) led to complete glacial conditions (Imbrie et al., 1984). Throughout the last glacial cycle, there was a gradual but variable decline in global relative sea levels, beginning with a peak a few metres above the present level around MIS 5e (Lambeck et al., 2002) and reaching between 118 and 135 m below the present levels during the Last Glacial Maximus (LGM; Clark and Mix, 2000; Shannon et al., 2009).

Timmermann and Friedrich (2016) conducted a climate-induced human dispersal experiment, which accounts for a numerical representation of gradual human adaptation to climatic conditions over the past 125 ka. According to their simulations, approximately at 115–106 kyr, the first low-density migrant wave of *H. sapiens* diffused through vegetated regions and reached the coast of northeast Africa along the Bab-el-Mandeb. Two rapid dispersals occurred between 107–95 and 90–75 kyr, coinciding with wet phases that made the Arabian Peninsula and Sinai favourable pathways for migration. Southern Europe is projected to have had extremely low densities from 95 to 72 kyr. The following arid conditions during the period 71–60 ka (MIS4) prevented the interaction between the inhabitants in north-eastern Africa and the rapidly expanding population in southern Asia. It contradicts prior claims (Oppenheimer, 2012) that the southern Arabian Peninsula was an active migration corridor during this time. During the succeeding precession minimum (increased boreal summer insolation) between 60 and 47 kyr, the simulation model predicts that the increase in rainfall increased net primary output in northern Africa, the Levant and the Arabian Peninsula. A second significant migration wave exited northern Africa approximately around 60 kyr, correlating with the youngest estimates of the L3-haplogroup-based age range for the time to the most recent common ancestor (Oppenheimer, 2012; Soares et al., 2012) and the subsequent development of mitochondrial DNA (mt DNA) haplogroups M, N, and R. This wave eventually merges with the Eurasian population, increasing population density throughout Europe and southern Asia. Approximately 60 thousand years ago, *H. sapiens* crossed the Indonesian archipelago, altered by sea-level changes, arriving in Papua New Guinea and Australia.

For the subsequent 60–30 kyr (MIS 3), the model predicts a continuous Africa/Eurasia flow of *H. sapiens* across the Levant and a second wave (45–30 kyr) across the Bab el-Mandeb

and the Arabian Peninsula. The Laschamps Excursion at 42 kyr caused a global environmental crisis, resulting in the extinction of the Neanderthals and many large mammals during the Late Quaternary, which occurred during geomagnetic field strength minima (Channell et al., 2019; Cooper et al., 2021). *H. sapiens* completed the simulated grand trip from Africa to the Americas by crossing the Bering Land Bridge into North America between 14 and 10 thousand years ago. As a result of rising sea levels, the Bering Land Bridge was submerged near the end of the glacial period, terminating the geographical connection between Asia and North America. In congruence with a plethora of studies (Field et al., 2007 Groucutt et al., 2005; Liu et al., 2015; Nicholson et al., 2022; Petraglia et al., 2010), Timmermann and Friedrich's (2016) research also shows the early exit climate/human dispersal simulation reproduces an early MIS 5 exodus of *H. sapiens* out of Africa and a rapid dispersal along the southern rim of Asia into southern China and eventually into Australia during MIS 3 and MIS 4.

Thus, the effect of climatic change on the timing of early human migrations has been a topic of extensive research and discussion. All hypotheses share the fundamental premise that climate influences resource abundance, which, in turn, determines a region's carrying capacity - the maximum population that can be supported; this then guides the distribution of humans. Other different factors can also affect resource richness and, ultimately, dispersal/migration, including significant volcanic eruptions (Ambrose, 1998), glacial "Heinrich events" associated with ice-sheet collapse (Carto et al., 2009), orbital monsoonal rainfall changes (every 21,000 years, Earth's orbit undergoes slight changes in its rotational axis, which affects seasonal solar radiation and thus monsoonal climate) (Castaneda et al., 2009; Eriksson et al., 2012; Osborne et al., 2008) and sea-level changes (Armitage et al., 2011).

The Late Pleistocene is a time of relatively quick technological replacements, variations in behaviour, rapid movements of *H. sapiens (Table 1)* and several significant environmental events. There are different technological and hominin species overlaps in the Late Pleistocene (e.g., Bruggemann et al., 2004; Clark and Brown, 2001; Lee, 2013; Li et al., 2018; Li et al., 2019; Michel et al., 2013) and variable climatic conditions. The Acheulean culture could possibly last until 120 -29 kyr globally (Key et al., 2021). The origins of the Middle Stone Age/Middle Palaeolithic can be traced to 500 kyr (Porat et al., 2010) and lasted up to 20-10 kyr (Lombard et al., 2012; Scerri et al., 2021). While the origins of symbolic behaviours might be difficult to trace (Nowell, 2010), one of the earliest appearances is evident at 105 kyr for the intentional collection of non-utilitarian objects (calcite crystals) and ostrich eggshells in the southern Kalahari Basin (Wilkins et al., 2021). The collection of quartz crystals intentionally transported to the site of Singi Talav with no clear utilitarian purpose (d'Errico et al., 1989) marks the oldest dated non-utilitarian objects in the South Asian record (Blinkhorn et al., 2021). The origin of microlithic technology at Pinnacle Point at the African sites of (71 ka) (Brown et al., 2012; Wilkins et al., 2017) and Howiesons Poort (65-60 kyr) (Guerin et al., 2013; Roberts et al., 2016; Tribolo et al., 2009) is associated with and without the impact of climate change, respectively.

Table 1. List of species present during the Late Pleistocene.

Sr. No.	**Name of the Species**
1	*Homo erectus*
2	*Homo neanderthalensis*
3	*Homo floresiensis*
4	*Homo luzonensis*
5	*Homo* Denisova
6	*Homo longi*
7	Naser Ramla *Homo*
8	*Homo sapiens*

Understanding the effect of the environment on hominin adaptation and the effect of anthropogenic activities on environments (Foley and Lahr, 2015) has led to many long-standing debates. The former has been the most intriguing for Palaeolithic archaeologists (Rodriguez et al., 2010; Zhao et al., 2021; Zingher et al., 2013, to name a few), and most of the studies show that technological innovation/adaptation occurs due to environmental change (McHall et al., 2007; Fronco et al., 2016; Wilkins et al., 2017; Zhao et al., 2021; Zingher et al., 2013), while some imply no effect of environment on technological change (Roberts et al., 2016; Rodriguez et al., 2010).

1.3.1 Late Pleistocene Extinctions - Overkill Hypothesis

Paul Martin, a palaeontologist, proposed in 1967 that humans were the primary cause of Late Pleistocene megafaunal extinctions. Megafauna represents animals whose mature body weight exceeds 44 kg (Martin, 1984). He proposed that a) large mammals were decimated during the Late Pleistocene, b) small mammals (except on islands) were relatively untouched, c) large mammals survived best in Africa, d) the extinctions were often quite abrupt, e) regional extinctions were diachronous, f) the extinctions occurred without replacement by new taxa, g) the extinctions followed in man's footsteps and h) archaeology of extinction is obscure.

Martin hypothesised that big-game Palaeolithic hunters preferred large mammals. Species in continents never colonised by humans have little to no fear of humans, making them easier to kill. Martin envisioned waves of human hunters fanning into newly colonised North and South America and Australia and killing large mammals in a "blitzkrieg," triggering megafauna extinction. Conversely, megafaunal losses in Eurasia and Africa were less severe due to lengthy coexistence with humans. He hypothesised that human advent on "colonised continents" led to the extinction of megafauna.

Mosimann and Martin (1975) and Martin (1984, 2005) hypothesised that the slaughter occurred so quickly that it left little trace in the fossil record, mainly in response to the perception that there were too few 'kill sites' (i.e., sites with projectile weapons and megafaunal remains) in North America. Computer modelling by Alroy (2001) and others support the notion that human hunting could have resulted in extinctions, mainly if the model permits the hunters to switch to other more common prey yet maintain opportunistic hunting of rarer slow-breeding species.

Some scholars argue that anthropogenic extinctions began when the first modern humans left Africa between 200 and 100 kyr, which is supported by recent megafaunal extinctions in Australia, New Zealand, and Madagascar (Kolbert, 2014). The most compelling evidence for this theory is that 80% of North American large mammal species vanished within 1000 years of humans arriving in the western hemisphere (Martin, 1984).

1.3.2 Late Pleistocene fauna and its extinction in the Indian Subcontinent

All Quaternary vertebrate fossil evidence can be arbitrarily divided into three broad chronological groups: a) the Early Pleistocene evidence, which is primarily found in the Siwalik Hills of Pakistan, India, and Nepal; b) fossil assemblages found in several river valleys, which are generally assigned to the Late Pleistocene; and c) the Holocene fossils, sub-fossils, and unfossilised bones (Chauhan, 2023). The areas yielding Late Pleistocene - Holocene fossils include river valleys: Ganga, Son, Narmada, Godavari, Mahanadi, Manjra, Krishna, Ghod and other areas such as Kurnool Cave complex, northeastern India, West Bengal, Rajasthan, Gujarat, Tamil Nadu and Sri Lanka (See Badam, 1988; Badam, 2002; Chauhan 2008). Most of the recovered species belong to the orders Artiodactyla, Perissodactyla, and Proboscidea. Most sites were devoid of carnivorans, primates, small mammals, birds, and other vertebrates (Jukar et al., 2021). Chauhan (2023) highlights the

lack of identification and absolute dates for fauna within Middle Pleistocene contexts in the subcontinent, except for the Middle Pleistocene fauna from the Kurnool Caves, which shows their continuity to Late Pleistocene and modern times (Roberts et al., 2014).

During the end Pleistocene and earliest Holocene, the Indian subcontinent underwent an extinction that was highly size (large) biased but of low significance. Climatically, the period is distinguished by the last glacial maximum (LGM), Heinrich Event I (H1), and Younger Dryas (YD) (Jukar et al., 2021). The monsoon intensity decreased throughout these seasons, particularly in H1, resulting in widespread droughts (Dutt et al., 2015; Stager et al., 2011; Tierney et al., 2015). During the late Quaternary, the Indian Peninsula witnessed the extinction of four large animal species and one avian species. Although the four species comprise 4% of the mammalian fauna, they account for 20% of the megafauna of the Indian subcontinent (Jukar et al., 2021). The extinction magnitude is most like that observed in regions of Africa, consistent with the findings of regional research (Roberts et al., 2014) and giving direct evidence to support the co-evolution concept for megafaunal persistence outside Africa (Faurby and Svenning, 2015; Sandom et al., 2014). While the substantial size bias is evidence of human impact (Smith et al., 2018), the low magnitude shows that most faunas were resistant to prehistoric *H. sapiens*. However, preliminary chronology indicates that faunal extinctions did not begin until at least 20,000 years after the arrival of modern *H. sapiens* to India (Bae et al., 2017). In addition, *H. sapiens* in the Indian subcontinent may have favoured smaller forest-dwelling prey (such as monkeys and rodents) over larger species, as observed in Sri Lankan Palaeolithic populations (Roberts et al., 2015; Wedage et al., 2019).

1.4 Indian Subcontinent

The Indian subcontinent[1] is a land with abundant geomorphic diversity and magnificent scenery, and it correlates with South Asia's political region (Bangladesh, Bhutan, India, Nepal, Pakistan, and Sri Lanka). The Subcontinent comprises practically every geomorphic feature on Earth, from glacier-carved valleys and ice summits to extensive mangrove swamps, coral island chains, and a burned rocky sand desert. Additionally, the Indian subcontinent contains some of the oldest rocks on the Earth's surface, ranging in age from the Archean to the Quaternary can be found (Kale, 2014). The Indian dubcontinent consists of five significant provinces (1) the Himalayas, (2) the Indo-Gangetic Plains, (3) the Irrawaddy Plains, (4) the mountains, uplands and plateaus of Peninsular India, and (5) the Coastal Plains. Each of these divisions is a contrasting structurally, lithologically and physiographically separate geomorphic region with a distinct evolutionary history. Interestingly, about 11 % of the geographic area of India comprises high mountains above 2100 metres (m) mean sea level, 18 % area is small mountains and hills of elevation 900–2100 m, and 28 % is made up of plateaus in the altitudinal range of 300–900 m, and 43 % area encompasses the plains (Valdiya, 2016)

The Himalayan Mountain belt divides India from the rest of Eurasia by bordering the Indian subcontinent in the northwest, north, and northeast like a massive wall. The mountainous province consists of several curved mountain ranges, including the Kirthar and Sulaiman in the west, the central Himalaya in the centre, and the Patkai–Naga–Arakan Yoma in the east.

---

[1] Valdiya, K.S., 2016. Physiographic layout of Indian subcontinent. In *The Making of India* (pp. 1-19). Springer, Cham.
Kale, V.S., 2014. Geomorphic history and landscapes of India. In *Landscapes and landforms of India* (pp. 25-37). Springer, Dordrecht.

The Himalayas consists of four contrasting physiographic and lithostructural terranes, mainly between the Ravi in the west and the Arun in the east: Siwalik, the Himachal (Lesser Himalaya), the Himadri (Greater Himalaya) and the Tethys Himalaya. In the Holocene, the Brahmaputra, Ganga, and Sindhu River systems created the world's most extensive alluvial plains in front of the Himalaya Mountain range. The plains span 3,200 kilometres from the southern boundary of the Ganga–Brahmaputra delta in the east to the terminal of the Sindhu delta and the Rann of Kachchh in the west. Between the Patkai–Naga–Chin–Arakan, Yoma Ranges in the west and the Kachin–Shan–Tenasserim Ranges in the east are lowlands produced by the Irrawaddy, its tributary Chindwin and the Sittang rivers that run north to south. The Irrawaddy Basin consists of various plains, including the Putao and Hukawang plains, with Indaw Lake in the upper reaches of the Irrawaddy and Chindwin, respectively.

Peninsular India is about 1600 kilometres long in the north-south direction and 1400 kilometres wide in the east-west direction. The southernmost point of the triangle, Kanyakumari, is its apex. It consists of three major physiographic units: mountain ranges along its borders on three sides, uplands and plateaus inside the bounds of the bordering ranges and coastal plains along the eastern and western coastlines. Peninsular India is divided into two sections by the Satpura Range. The northern section contains the Malwa, Bundelkhand and Vindhyan plateaus in Maharashtra, Karnataka, and Andhra Pradesh, and the southern section contains the Deccan, Mysore and Telangana plateaus. While the southern portion gently slopes eastward, the northern portion's rivers flow northward. The 500–600 m high Malwa Plateau consists of flat-topped hills and undulating plains of Late Cretaceous lavas and is drained by the Banas and Chambal rivers, which flow northeast. It encompasses the 250–300 m undulating terrain of the eastern Rajasthan Aravalli Range. Bundelkhand Upland, 300–600 m above mean sea level and composed of Late Archaean gneisses and

granites, is located to the northeast. Before joining the Yamuna River, the Chambal, Betwa, and Dhasan rivers carve their valleys through the undulating terrain of Bundelkhand, creating deep gorges and stunning ravine land known as the Chambal Badlands. The Vindhyan Plateau in Madhya Pradesh is surrounded by Kaimur in the north and the Bhander in the south. Both have frontal escarpments and a general elevation of 300–650 m. The 610-meter-high Kaimur cliff overlooks the Yamuna and Ganges alluvial plain in southeast Uttar Pradesh.

The Chambal, Sind, Betwa, and Ken rivers drain northward from the Proterozoic sedimentary strata that compose the Vindhyan Plateau. South of the Satpura Range and east of the Sahyadri, the Deccan Plateau stretches across almost all of Maharashtra and portions of Telangana and Karnataka. The landscape comprises flat terraces of Late Cretaceous lavas, some of which contain a lateritic mantle. The Deccan has an average elevation of 600 m, and it is drained by the Godavari and Krishna rivers, which flow east-southeast. The rivers have carved out narrow valleys in highland Maharashtra around the foot of the Sahyadri Range, but their middle reaches are vast with gentle valley slopes. The Mysore Plateau is composed of Archaean gneisses, granites, and high-grade metamorphic rocks, and it encompasses all of Karnataka and portions of Tamil Nadu and Telangana. It consists of two distinct regions: Malnad, a dissected hilly tract adjacent to the Sahyadri, and Maidan, a rolling flat region in the east. Several NNW hills traverse the plateau–SSE- to N–S-trending linear hills and chains of isolated hillocks, such as Bababudan with its 1913-m-tall Mullayanagiri Hill, Ramanagaram with its 1255-m-tall Madhugiri peak, the Bangalore range with its 1467-m-tall Nandidurga Hill, the Chitradurga Range, the Kolar Range and so the Bangalore range with gneissic hills stretches south with a gradual increase in altitude, giving place to the charnockitic Biligirirangan–Mahadeswaramalai Ranges in eastern Tamil Nadu. The highest

point of the Biligirirangan is a 1,750-meter peak, whereas the highest points of the Mahadeswaramalai are 1,487- and 1,316-meter peaks. The 500–600 m planation surface of the Andhra Pradesh Telangana Plateau flanks the 900 m Bangalore surface to the northeast.

The narrow coastal plains along the seaboards of Peninsular India are over 6,000 kilometres long, extending from the deltas of the Sindhu and Saraswati (Ghaggar–Nara) rivers in the west, through the southern tip of the peninsula, to the delta of the Ganga–the Brahmaputra and then along the Arakan Coast to the deltas of the Irrawaddy and Salween rivers in the east. Vast coastal plains surround the island of Sri Lanka.

1.4.1 Monsoon

According to India's Meteorological Department Climate Profile, the average southwest monsoon (June to September) rainfall is 877.2 mm, accounting for around 74.2 % of the annual rainfall (1,182.8 mm). The monsoon is a stable atmospheric system that has never failed and has fluctuated by roughly 20–30% around a mean southwest monsoon value of ~ 877 mm. There is significant regional and temporal variability in monsoon rainfall, which leads to droughts and floods. Thus, 20–30% less rainfall signals dryness in a location and more widespread rainfall may indicate floods.

On the other hand, the long-term average of rainfall remains practically constant. The rainfall varies geographically, with the lowest average annual rainfall of ~ 130 mm in Jaisalmer and the maximum average annual rainfall of 11,410 mm in Mawsynrum (near Cherrapunji) in Meghalaya. The oceans, notably the Bay of Bengal, provide a large portion of the moisture. Thermal stratification is essential for monsoon formation, with the essential sea surface temperature being ~28°C. The Arabian Sea contains colder waters and is extensively mixed with wind fields. As a result, except for the western parts, it does not contribute significantly

to precipitation across the subcontinent. The Sun-Earth geometry, the state of the North Atlantic Ocean, the level of snow cover in Eurasia, vegetation change, El Nino Southern Oscillation (ENSO), and other factors affect seasonal monsoon strength; determining their precise impact and long-term stability is challenging. Statistical studies show that the monsoon system is 50% predictable at best; factors like rainfall commencement, duration and intensity cannot be forecast with the accuracy necessary for the planning of water resources and agriculture (Kelkar, 2009; Singhvi and Kale, 2009; Singhvi et al., 2010). The impacts of past monsoon cycles have been studied only to Holocene archaeological data (Lasker and Bohra, 2021; Sarkar et al., 2016) and not for prehistoric records barring a few exceptions (Blinkhorn et al., 2021; Paddayya and Petraglia, 1993).

1.4.2 Toba, LGM and other events

Global geological events such as Toba supereruption and LGM, among others, are also expected to have affected the ecology of the Indian subcontinent. There is an ongoing debate about the Younger Toba Tephra (YTT) and its potential impact of the eruption on global climate and ecology. The YTT is known to occur at multiple locations across India, and some African locations, representing its largest terrestrial extent. Tephra deposits found at Indian Acheulean sites, such as Morgaon and Bori, have been thought to belong to the Older Toba Tephra (Gaillard et al., 2010; Mishra et al., 2005), but recent studies indicate younger ages (Biswas et al., 2013).

Various hypotheses have been proposed by different researchers regarding the ecological and biological impacts of the YTT events. Ambrose (1998) suggested that the eruption likely had significant repercussions on global climate and ecology 74 kyr, which may have impacted the

adaptations of hominin groups and resulted in possible population bottlenecks. However, Petraglia and colleagues (2007; Blinkhorn et al., 2012; Clarkson et al., 2012; Haslam and Petraglia, 2010; Haslam et al., 2010a; 2012a) challenged this theory, proposing that Middle Palaeolithic artefacts found below and above the YTT in southern India statistically compare with those made by modern humans in southern Africa, suggesting that modern humans must have reached South Asia before ~74 kyr and that the supereruption had minimal impact overall.

Despite these theories, the exact impacts of the supereruption on regional environments, hominin groups, and their behavioural adaptations and lithic technologies across India are still uncertain (see Williams, 2012b). More research is necessary to determine how much the YTT influenced the development of hominin adaptations in the region.

During the Last Glacial Maximum or LGM, cold and dry conditions prevailed over the Indian subcontinent, and the southwest monsoon was weak (Bolton et al., 2013; Caley et al., 2011; Clemens and Prell, 2003; Singhvi and Kale, 2010). The geomorphological archives of environmental conditions immediately following the LGM are diverse, including a combination of sand dune accretion and fluvial reactivation, which resulted in the formation of numerous playas in blocked drainages across the Thar (e.g., Achyuthan et al., 2007; Deotare et al., 2004).

The LGM also had an impact on vegetation and animal populations in India. Studies have shown that the colder and drier climate during the LGM caused a shift in vegetation patterns and the extinction of some animal species (Clarkson et al., 2009; Jukar et al., 2020).

Lonar Lake, also known as Lonar crater, is a lagoon lake formed by a meteorite collision impact approximately 52,000 ± 6,000 years ago (Sengupta et al., 1997) or 576,000 ± 47,000

years ago (Jourdan et al., 2011). The exact age and its formation are a matter of debate. One theory suggests that the lake was formed by a meteorite impact, while others propose that it was formed by volcanic activity or tectonic activity, with the former being the more popular theory.

Despite its unique geological formation, Lonar Lake has not been studied in detail from a paleoanthropological perspective. It is possible that the lake may contain significant evidence of prehistoric human activity, as the region of Maharashtra is known to have been inhabited by prehistoric hominin populations.

1.5 Late Pleistocene dynamics of the Indian Subcontinent

With the spread of *H. sapiens* from Africa and their interbreeding with archaic species (Clarkson et al., 2012; Green et al., 2010; Rasmussen et al., 2011; Reich et al., 2010), human demography and behaviour in Asia changed substantially during the Late Pleistocene (Athreya, 2015; Deraniyagala, 1992; Liu et al., 2015). Because of its physical location with major east-west human migration routes across Asia, the Indian subcontinent is a vital region to explore to understand human dispersals (Blinkhorn and Petraglia, 2017; Boivin et al., 2013; Petraglia et al., 2010; Reyes-Centeno et al., 2014). However, understanding the Late Pleistocene of the Indian subcontinent is both necessary and challenging. Researchers must deal with various factors to conclude, such as 1) which species were dominant on the Indian subcontinent during the Late Pleistocene: a) modern humans or b) archaic hominins or both? 2) What kind of technologies did they employ to make their adaptations in different landscapes and environments? 3) What impact did environmental factors have on the expansion of hominin populations? 4) How did the Toba super-eruption affect the hominin populations? 5) How did incoming populations gradually replace archaic populations? 6) How many dispersals of *H. sapiens* were there into the Indian subcontinent?

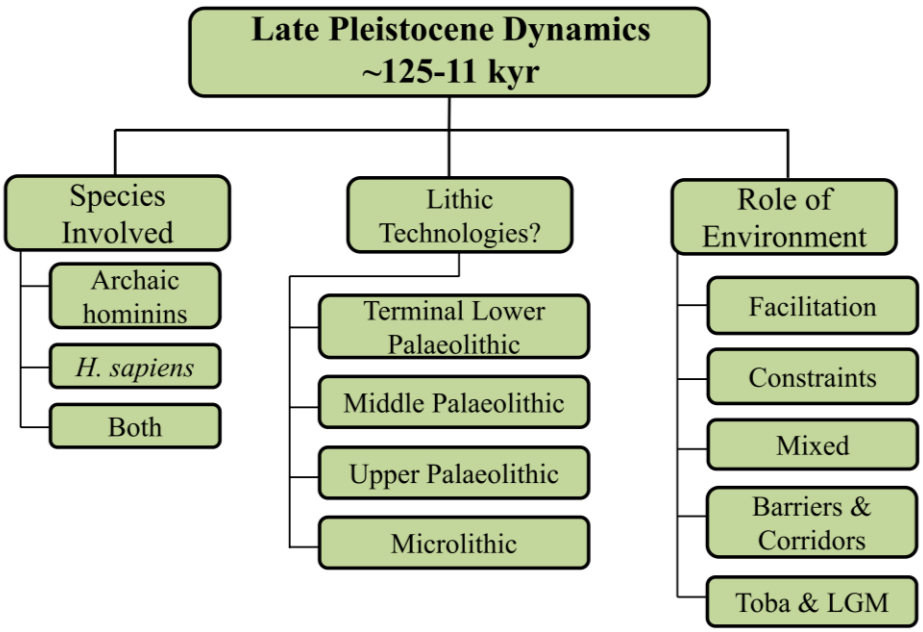

Figure 1. Late Pleistocene dynamics of the Indian subcontinent.

Considering the dearth of hominin remains in the Indian subcontinent, Palaeolithic tools have served as the primary source of interpretation for the species that may have produced them. Present scenarios show that the Indian subcontinent could have been inhabited by archaic hominins (Haslam et al., 2011) and *H. sapiens* (Deraniyagala, 1992; Mellars et al., 2013; Mishra et al., 2013; Perera et al., 2011; Petraglia, 2007) populations during the Late Pleistocene. It is also evident that South Asian hominin/human populations were utilising 1) Lower Palaeolithic (Blinkhorn et al., 2021; Haslam et al., 2011), 2) Middle Palaeolithic (Blinkhorn, 2013; Blinkhorn et al., 2019; Perera et al., 2011; Petraglia, 2007), 3) Upper Palaeolithic (Dennell et al., 1992; Funaki et al.,2022) and 4) microlithic technologies (Basak and Srivastava 2017; Clarkson et al., 2020; Mellars et al., 2013; Mishra et al., 2013) during the Late Pleistocene period. It is challenging to infer the plausible manufacturers of these technologies because of the lack of definite dates and chronological overlaps (*Figure 1, 2*).

As mentioned above, understanding the effect of the environment on hominin adaptation and the effect of anthropogenic activities on the environment is a long-standing debate. In the Indian subcontinent, only a few attempts have been made to understand the palaeoenvironments and hominin adaptations, and the data shows fragmented evidence. The predation of ostriches and the exploitation of OES by Late Pleistocene populations (for engravings, bead making and as water containers) specify a significant geographic overlap of humans and ostriches in Sahel-like and savannah habitats (Cooper et al., 2009). The presence of ostrich in the Late Pleistocene before 60 kyr in India favours the rapid coastal dispersal of modern humans with advanced technological and social adaptations (Blinkhorn et al., 2013, Mellars et al., 2013). Ostriches appear to be restricted to Sahel-like vegetation, while modern humans have the capability to adapt to different environments. If the Sahel-like environment was a factor in the dispersal of ostriches and human populations, then it can be considered that both taxa could have dispersed during MIS 5, based on the available palaeoenvironmental reconstructions (Blinkhorn et al., 2013). While Chauhan et al. (2015) suggest that the expansion of ostriches and modern humans in South Asia is associated with palaeoenvironmental changes, the correlation between particular lithic technologies and OES specimens remains currently weak in the subcontinent. The comparison of the Middle-Late Pleistocene (100 kyr) fossil record from the Billasurgam Cave complex, Indian subcontinent, with contemporary faunal ranges indicates some geographical redistribution of mammalian taxa within India; this suggests that most taxa adapted to ecological change in suitable habitats (Roberts et al., 2014).

Furthermore, it is suggested that deteriorating environmental conditions at 38 ka in Jwalapuram led modern humans to develop microlithic technology (Petraglia et al., 2009). Middle Palaeolithic technologies were widespread in the Thar Desert during MIS 5 when

wetter conditions supplied riverine corridors, greater vegetation diversity and landscape stability (Blinkhorn et al., 2013). The absence of evidence for occupation during MIS 4 is likely linked to prohibitive levels of aridity, yet Middle Palaeolithic occupations resume at the onset of MIS 3 (Baskaran et al., 1986; Blinkhorn, 2013). Middle Palaeolithic technology did not dramatically alter in the face of the 74-kyr old super eruption and any subsequent climatic effects at the onset of MIS 4 (Petraglia et al., 2012), nor did Late Palaeolithic microlithic technology vary substantially across the LGM (Clarkson et al., 2009). Much research has been done on the Toba super-eruption (e.g., Ambrose, 1998; Blinkhorn et al., 2012; Clarkson et al., 2012; Clarkson et al., 2020; Petraglia, 2007; Williams et al., 2009), but its understanding is still contentious. Ambrose (1998) suggested a consequence of the behaviour of hominin groups and possible population bottlenecks due to volcanic winters caused by the Toba super-eruption. Williams et al. (2009) suggested a change of vegetation from C_3 to C_4 type due to Toba. However, some researchers (Blinkhorn et al., 2012; Clarkson et al., 2012; Clarkson et al., 2020; Haslam and Petraglia, 2010; Haslam et al., 2010a, 2012a; Petraglia et al., 2007) suggested the minimal impact of Toba, based on the presence of Middle Palaeolithic stone tools from below and above the YTT, meant to highlight the lack of technological change across the extreme event.

The Lower Palaeolithic in the Late Pleistocene is denoted by the terminal or Late Acheulean artefacts from Middle Son Valley, Madhya Pradesh, dated 140-120 kyr and 85 kyr at Singi Talav in Rajasthan (Blinkhorn et al., 2021; Haslam et al., 2011). It is suggested that these tools were made by the last surviving archaic hominin species (Haslam et al., 2011). The younger Middle Palaeolithic of the Indian subcontinent is thought to represent the earliest arrival of *H. sapiens* in the Indian subcontinent during MIS 5 (Blinkhorn et al., 2015; Haslam et al., 2012a; Petraglia, 2007), although fossil evidence for this is currently lacking.

The Middle Palaeolithic is also present in Sri Lanka around 80 kyr (Deraniyagala, 1992; Perera, 2010).

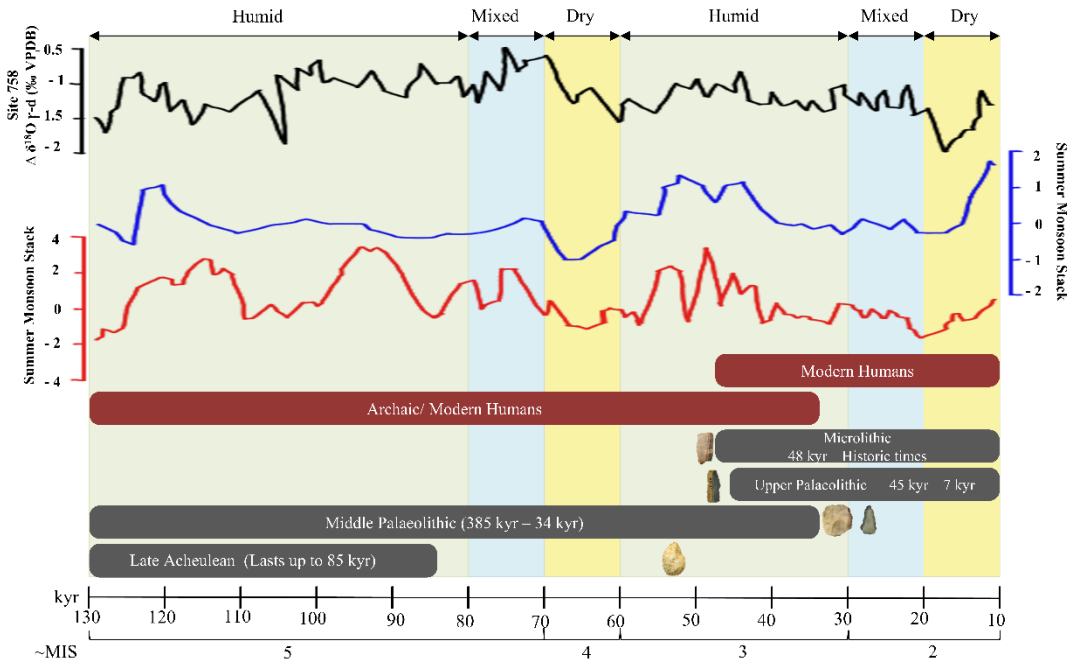

Figure 2. Late Pleistocene technological and human evolution dynamics in the Indian subcontinent, along with three archives of monsoonal intensity, including oxygen isotope records from the Bay of Bengal (Bolton et al., 2013), and two alternative Summer Monsoon Stacks from the Arabian Sea (middle Clemens and Prell, 2003; and bottom Caley et al., 2011).

Furthermore, the Late Pleistocene hominin adaptations in South Asia are driven by two opposing concepts about the initial arrival of prehistoric modern humans in the region. One idea connects the Middle Palaeolithic technologies in India to the arrival of modern humans from Africa during MIS 5 (130-70 kyr), with populations surviving the Toba super-eruption at 74 ka (Groucutt et al., 2015; Petraglia, 2007; Petraglia et al., 2010). Due to deteriorating environmental conditions, these modern humans are assumed to have later innovated microlithic technology (Clarkson et al., 2009, 2018; Petraglia et al., 2009). Discoveries of

older microliths challenge the alleged impact of later environmental deterioration on technological innovation, which is younger (elaborated upon later). The second idea links the Indian Middle Palaeolithic with pre-existing archaic species, emphasising the initial appearance of modern humans with microlithic assemblages and other cultural and behavioural traits only after MIS 4 or 3 (71-57 ka) (Mellars et al., 2013; Mishra et al., 2013)

The discovery of Middle Palaeolithic assemblages at Sandhav in Gujarat at 114 ka (Blinkhorn et al., 2019), Katoati in Rajasthan at 95 ka (Blinkhorn et al., 2013), and Jwalapuram in Andhra Pradesh at 77 ka (Korisettar, 2014) may provide evidence to support the first theory (Petraglia et al., 2007). In contrast, new data from Attirampakkam, Tamil Nadu (Akhilesh et al., 2018) and Andhra Pradesh (Anil et al., 2022) demonstrate a limited Lower to Middle Palaeolithic changeover at about 385 ka and 247 ka showing that the latter was developed locally rather than being brought into India by incoming dispersals. A new question arises: What are the evolutionary and technological links between older and younger Middle Palaeolithic evidence? Do they represent the continuity of archaic populations or represent multiple species (including *Homo sapiens*) using the same technology?

The South Asian Upper Palaeolithic remains ambiguous due to a lack of chronological dates and multidisciplinary excavations despite the presence of stratified, multicultural sequence sites such as 16R (Blinkhorn, 2013; Singhvi et al., 2010), Bhimbetka (Misra, 1982; Wakanker, 1973), Dhaba (Haslam et al., 2012b), Patne (Sali, 1989), including stratigraphically exclusive Upper Palaeolithic assemblages. These assemblages provide insights into the long-term hominin occupation and ecological stability in the region. Some stratigraphic breaks are observed at these sites; it is thus hard to distinguish between the absence of hominin occupation and post-depositional disturbance/destruction of cultural layers (Chauhan, 2009). In short, interpretations of the transition from terminal Middle

Palaeolithic to Upper Palaeolithic and Upper Palaeolithic to microlithic phases in India remain contentious. Moreover, the disconformities in the number of species producing Middle Palaeolithic in the Old World, compounded by Middle Palaeolithic, Upper Palaeolithic and microlithic evidence denoting high technological diversity and overlap across India during Late Pleistocene, makes it challenging to identify associated hominin species (Akhilesh et al., 2018; Chauhan et al., 2015; Clarkson et al., 2012).

1.5.1 Late Pleistocene lithic technologies in the Indian Subcontinent

The Indian subcontinent has a rich history of technological advancements, with evidence of nearly every known technology discovered thus far. These include Acheulean (Lower Palaeolithic) (1.5 Ma – 85 kyr), Prepared Core (Middle Palaeolithic) (385 – 38 kyr), Laminar (Upper Palaeolithic and microlithic) (48 kyr – historical times), arguably Oldowan (2.6, 2.0 myr) as well, except Lomekwien (Akhilesh et al., 2018; Blinkhorn et al., 2021; Clarkson et al., 2020; Dennell et al., 1992; Sao et al., 2016; Harmand et al., 2015; Hurcombe 2017; Mishra et al., 2013; Pappu et al., 2011; Rendell et al., 1987).

1.5.1.1 Late Acheulean (Lower Palaeolithic)

Late Acheulean assemblages are characterised by a low proportion of bifaces, a high ratio of cleavers to handaxes, an exceptionally high ratio of flake tools such as scrapers, and the extensive use of the soft-hammer and Levallois and discoid core techniques (Misra, 1987). The bifaces are generally smaller, thinner, and more morphologically refined, with increased retouching and controlled thinning and flaking (Pappu, 2002). Most South Asian Late Acheulean evidence is in central and peninsular India, including parts of Rajasthan, Gujarat, Maharashtra, Madhya Pradesh, Bihar, Karnataka, Andhra Pradesh, and Tamil Nadu (Chauhan, 2009; Pappu, 2001). The recent advancement and use of scientific methods on Palaeolithic sites in India have helped us assign dates to Palaeolithic assemblages/cultures.

The Indian subcontinent has produced the allegedly youngest Acheulean (Late Acheulean) in the world, dated to 140-120 kyr at Bamburi and Patpara, north-central India (Haslam et al., 2011) and at Singi Talav (85 kyr), western India (Blinkhorn et al., 2021). Additionally, the earliest date of Acheulean at 1.5 Ma from Attirampakkam (Pappu et al., 2011) indicates a long-lasting Acheulean culture in India. At 385 ka (Akhilesh et al., 2018), the site with the oldest known Acheulean evidence (Attirampakkam) also has the oldest known early Middle Palaeolithic evidence in South Asia outside Africa. This suggests that the shift from the Lower Palaeolithic to the Middle Palaeolithic in South Asia was long, irregular in geography and chronology, and behaviourally complicated. Defining the Late Acheulean remains complicated whether the presence of bifaces is a cultural maker for determining a Palaeolithic assemblage as (Late) Acheulean (Haslam et al., 2011; Shipton et al., 2013) or is it also an integral part of the Indian Middle Palaeolithic (Akhilesh et al., 2018 and references therein). In the Middle Son Valley, Late Acheulean assemblages are also associated with Levallois and blade elements, while Bifaces at Patpara (n=26) form only 1% of the total assemblage (n= 2284) (Shipton et al., 2013) and at Bamburi (n= 2), comprising only 4% of the complete assemblage (n= 47). This may indicate that many (if not all) of the Middle Son Valley bifaces are part of the regional Middle Palaeolithic record, as initially noted by Blumenschine et al. (1983). Bifaces from Layer 3 (85 kyr and defined as Late Acheulean) at Singi Talav are represented by only handaxes (n = 3), without any cleavers, and these handaxes form only 0.75% of the total assemblage (n = 401) of Layer 3 (Blinkhorn et al., 2021; Gaillard and Rajaguru, 2017; Gaillard et al., 1985). Overall, it is more significant to analyse the transition from Lower to Middle Palaeolithic by looking at a wide range of variables rather than just one, such as the presence or lack of bifaces (as suggested by Dennell, 2021).

1.5.1.2 Middle Palaeolithic

The Middle Palaeolithic assemblages appear to have been first collected in 1893 from the Son Valley of Uttar Pradesh (Kennedy, 2000). Nevertheless, the credit for identifying the Middle Palaeolithic in India goes to Sankalia (1956), who discovered a flake industry comprising scrapers, points and borers made on siliceous materials such as chert chalcedony, agate, and jasper at Nevasa. The Middle Palaeolithic assemblages are developed from the Lower Palaeolithic assemblages (Akhilesh et al., 2018; Anil et al., 2022; Kennedy, 2000). Essential tools of the assemblage are flakes and scrapers, usually made using the Levallois technique. In comparison with the South Asian Acheulean, it is distinguished by four features: (a) a decrease in the size of the artefacts, (b) a noticeable shift from large Acheulean bifaces to smaller, specialised tools, (c) an increase in the prepared core technique and (d) a preference for fine-grained raw material crypto-crystalline silica, such as chert, jasper and chalcedony (Kennedy, 2000). The Middle Palaeolithic assemblages are found all over the Subcontinent, including the Himalayas, sub-Himalayas, western, central, eastern, southern and coastal regions (Pal, 2002).

The Middle Palaeolithic of the Indian subcontinent was thought to represent the earliest arrival of *H. sapiens* during MIS 5 (Blinkhorn et al., 2015, 2019; Haslam et al., 2011; Petraglia et al., 2007). However, a recent study by Akhilesh et al. (2018) suggests an indigenous development of the Indian Middle Palaeolithic at Attirampakkam, which dates to 385 ka, and re-evaluates the African models. While recent work at Hanumanthunipadu in Andhra Pradesh has established a date of 247 kyr for the local MP there (Anil et al., 2022), and the Middle Palaeolithic site of Sandhav in Gujarat dates to 114 kyr (Blinkhorn et al., 2019). In contrast, there is some dispute regarding the carriers of these technologies, whether they were modern or archaic humans. However, the archive demonstrates the prevalence of cultural variability alongside the development of many technologies. The Middle Palaeolithic

is also reported from Sri Lanka at around 80 kyr (Deraniyagala, 1992; Perera, 2010). The Middle Palaeolithic industries were widespread across the Subcontinent until the appearance of Late Palaeolithic technologies, such as microlithic tool-kits associated with bone tools and personal ornamentation from at least 36 kyr (Clarkson et al., 2009) and possibly 48-45 kyr (Basak and Srivastava, 2017; Clarkson et al., 2020; Mishra et al., 2013).

The debate continues over the relationship between the Middle Palaeolithic and microlithic industries, with which *H. sapiens* inhabited South Asia. Proponents of a quick, single southern path of human dispersal from Africa around 60 kyr point to the similarities between contemporary industries in Africa and South Asia (Mellars, 2006; Mishra et al., 2013). In contrast, indigenous transitions from the Middle Palaeolithic to microlithic, encouraged by contextual demographic and environmental shifts, have been utilised to infer a more gradual, early human dispersals into South Asia from Africa, as well as local technological development (Lewis et al., 2014; Petraglia et al., 2009). According to a preliminary assessment (Pers. Comm. with Mr. Yezad Pardiwalla) (Chauhan, 2020) of published data, at least 750 Middle Palaeolithic/Middle Stone Age sites are reported in India. While previous scholars recognised Middle Palaeolithic sites based on the absence of bifaces, the prevalence of flake-based assemblages, and the presence of Levallois elements, many Middle Palaeolithic assemblages may lack an unambiguous signature of this phase.

1.5.1.3 Upper Palaeolithic

The presence of the Upper Palaeolithic in South Asia was recognised in the 19th century with the discovery of osseous bone tools in Kurnool Caves (Foote, 1885; Newbold, 1844) and blade-and-burin tools (Brown, 1889). Nevertheless, the position of the Upper Palaeolithic in South Asia remained uncertain until the 1970s, when discoveries of stratified sites, bone tools, art and radiocarbon dating enabled its recognition (Raju and Venkatasubbaiah, 2002).

While the Upper Palaeolithic remains enigmatic and ranges from 45 kyr (Site 55 in Pakistan) up to ~7 kyr (Baghor) (Dennell et al., 1992; Misra, 1989, Funaki et al., 2022), some scholars use *Late Palaeolithic* to include chronologically overlapping technologies, specifically Upper Palaeolithic blade elements and microlithic technologies (James and Petraglia, 2005). However, the recent dates for the microlithic assemblage at Mehtakheri, Batadombalena and Dhaba display the distinct presence of this technology as early as 48 kyr, contradicting the '*Late Palaeolithic'*. While the Upper Palaeolithic chronology remains problematic and overlaps with Middle Palaeolithic and microlithic, the Subcontinent preserves well-marked examples of Upper Palaeolithic, i.e., multiple blade and burin dominated sites and site complexes across India, some clear examples being Gunjana Valley, Reningunta, Cuddapah region, Kurnool Caves, Site 55, Bhimbetka, Birbhum region and Mayurbhanj region among many others. Although these sites lack absolute dates, the blade and burin components are known to occur in three contexts at the pan-Indian level: overlapping with terminal Middle Palaeolithic elements, occurring exclusively and overlapping with early microlithic elements. According to preliminary data from published sources (Pers. Comm. with Ms. Martina Narzary), India has at least 530 reported Upper Palaeolithic/Late Stone Age sites (Chauhan, 2020). This technological stage is distinguished by the increased production of more specialised laminar implements such as blades and burins. Flakes, awls, borers, scrapers, cores, choppers, and bone tools were also used at this time. Even though multiple sites have been documented, there are few absolute dates for most of the Upper Palaeolithic assemblages in India. The single known date for a blade-dominated assemblage in the Subcontinent is 45 kyr for Site 55 in Pakistan (Dennell et al., 1992), which corresponds to late Middle Palaeolithic assemblages in northern India (Tewari et al., 2002) and microlithic assemblages in central India and Sri Lanka (Clarkson et al., 2020; Langley et al., 2020; Mishra et al., 2013).

Aside from chronology and ecological adaptations, the nature of transitions in South Asia between the Middle Palaeolithic, Upper Palaeolithic and early microlithic is a critical topic still inadequately understood. The dearth of associations between Upper Palaeolithic assemblages and symbolic behaviour (James and Petraglia, 2005) is the likely cause for insufficient investigation and preservation during the period. Given the spatial mosaic of ecological variation over the Indian subcontinent, classic Upper Palaeolithic technologies are likely to exist as distinct techno-chronological entities only in a few areas. Their absence in other geographical zones could be explained by a lack of suitable raw materials, such as siliceous rocks (e.g., chert, fine-grained quartzite), as well as other factors, such as a lack of geographic movement in some zones because of various climatic, ecological, and adaptive constraints. More surveys and research are needed to describe, characterise and date the Upper Palaeolithic in South Asia.

1.5.1.4 Microlithic

Microliths are an essential component of the Mesolithic period, but the antiquity of microlithic technology is much older. The first microliths were discovered by Carlleyle in 1867 from the Vindhyan rock shelters, Mirzapur district (now Mirzapur and Sonbhadra) of Uttar Pradesh (Misra 2002). The microliths dated to ~50 kyr are reported from various localities in South Asia; Dhaba (48 kyr), Mehtakheri (48-45 kyr), Jwalapuram 9 rock shelter (34 kyr), Kitulgala, Batadombalena, Fa Hien Cave (30 – 48 kyr) and Mahadebbera and Kana in West Bengal (25 and 42 kyr) (Basak and Srivastava, 2017; Clarkson et al., 2009; Clarkson et al., 2020; Mishra et al., 2013; Roberts and Petraglia, 2015; Roberts et al., 2015; Wedage et al., 2019). The presence of microliths is continuously debated over its timing and appearance in the Indian subcontinent; this has led to two opposing views for their genesis 1) indigenously developed due to climate deterioration, or 2) microlithic technology was introduced by modern humans dispersed from Africa. The indigenous development of

microliths was suggested by Petraglia et al. (2009) due to climatic deterioration from the Jwalapuram 9 site dated 38 ka. The second theory suggests the introduction of microlithic technology by modern humans from Africa around 60-50 kyr (Mellars et al., 2013, Mishra *et al.,* 2013). Moreover, the arrival of modern humans in South Asia remains contested. Two dominant schools of thought are prevalent 1) the initial arrival of modern humans in the Subcontinent with Middle Palaeolithic technology possiblely during MIS 5 (Blinkhorn et al., 2015a, 2019; Haslam et al., 2011; Petraglia et al., 2007); 2) arrival with microlithic technology during MIS 4-3 (Mellars, 2006; Mishra et al., 2013). Mellars proposed the introduction of microliths (2006a, 2006b, Mellars *et al.,* 2013) based on similarities between the microlithic assemblages of South Africa's Howieson Poort and Indian microliths and the presence of beads and engraved artefacts in both regions. Lewis (2015) and Lewis et al. (2014) undertook a detailed comparative study of the Howieson's Poort and South Asian microlithic assemblages from India and Sri Lanka. A considerable variation was found within all three; additionally, the Howieson's Poort and South Asian assemblages indicated different technological systems and did not have much in common. "Not only have geometric shapes such as segments shown to be in the minority at all of the sites analysed here, but the proportions of microlithic morphologies vary considerably between sites" (Lewis et al., 2014, pp 17).

Microlithic technologies first appeared in the archaeological record in South Asia around 48 kyr and were used by hunter-gatherer populations for much of the Holocene (3 kyr), when they are known as Mesolithic industries (Clarkson et al., 2020; Mishra et al., 2013) until early Historical Times (IAR 1976-1977: 29-30). Microlithic sites have been discovered almost everywhere in the subcontinent, from near Peshawar in the northwest to the tip of the peninsula in the south, including Sri Lanka, and from Saurashtra in the west to West Bengal

in the east (Misra and Kanungo, 2019). The long temporal span of microliths in South Asia is accompanied by the development of symbolic representations such as rock art, burials, and ornamentations (Misra, 2002). Evidence for symbolic social behaviours has been found as early as 48 kyr at Fa-Hien Lena Cave in Sri Lanka (Langley et al., 2020), where perforated shell beads were discovered. A fragment of ostrich eggshell carved with an intricate "bounded crisscross" design dating to 30 kya has been discovered in Patne, India (Sali, 1989).

1.6 Introduction to the Research

Climate change is increasingly recognised as a significant component in the biological evolution and cultural development of our species. It is widely assumed that it has an impact on behavioural plasticity, as well as the development of more efficient technology and subsistence strategies. However, detailed research on such possibilities has not yet been done in South Asia, although paleoenvironmental records from the Late Pleistocene have improved in this region, and South Asia plays a vital role in human migrations outside of Africa. Late Pleistocene habitations in South Asia currently span a diverse range of ecologies, from desert to tropical rainforest (Deraniyagala, 1992; Perera et al., 2011; Roberts et al., 2017; Wedage et al., 2019) and from large low-lying river basins to high altitude regions (Corvinus et al., 2007; Petraglia et al., 2012). The Indian subcontinent has been studied extensively from archaeological perspectives. However, few attempts have been made to study the impact of the environment on human dispersal, landscape adaptation, and technological development/innovation. The current study aims to better understand the hominin-environmental interface by investigating previously collected faunal samples from various sites in western (Gopnath, Gujarat) and central (Davakachar, Talyaghat, and Nehlai, Madhya Pradesh) India. It also focuses on understanding the Palaeolithic and palaeoenvironmental dynamics of the Lower Son Valley (LSV), Sonbhadra district of Uttar Pradesh in north-

central India. North-central and western India probably acted as a vital dispersal corridor and cultural and biological crossroads for diverse hominin populations, including modern humans, for a large part of the Quaternary (Chauhan et al., 2017; Field et al., 2006). The nearby Middle Son Valley has produced one of the youngest Late Acheulean sites in the region (Haslam et al., 2011). The study area has also reported the first-ever discovery of Middle Palaeolithic (Kennedy, 2000) and microliths (Misra, 2002) in the Subcontinent. It makes the area highly suitable for understanding the Late Acheulean to microlithic period transitions and the possible impact of climate change (if any) on those transitions. This study incorporates stable isotope analysis on fossil teeth collected from western and central India, grain size analysis and X-ray fluorescence (XRF) geochemistry on sediments collected from the LSV. It is the first-ever project to attempt to understand the Late Pleistocene environments and hominin adaptations across northern India through multidisciplinary techniques.

2 Late Pleistocene environments of South Asia: A review of multidisciplinary research and palaeoanthropological implications[2]

2.1 Introduction

Palaeoclimatic studies play a significant role in improving our understanding of past climate variability on lengthy timescales. Different types of records, such as lacustrine (e.g. Anoop et al., 2013; Rosenmeier et al., 2002), marine (e.g. Gupta et al., 2003; Ponton et al., 2012), speleothems (e.g. Burns et al., 2002; Kotlia et al., 2015), tree rings (e.g. Borgaonkar et al., 2011; Yadav et al., 2011) and ice cores (e.g. Jouzel et al., 2007; Lorius et al., 1985; Petit et al., 1999) have been used to document climate variability during the Late Quaternary period in many parts of the world. At a broader level, palaeoenvironmental data from Europe, Africa and the Levant have been variably applied to explain milestones in relation to hominin evolution, dispersals, adaptations, and cultural transitions (e.g., Collard et al., 2016; deMenocal and Stringer, 2016; Potts, 2013). In this thesis, an attempt has been made to obtain a broader picture of Late Pleistocene environmental variability across South Asia. An integrated review of different climatic proxies, i.e., pollen, carbonate, sediment, varve, and speleothem, is presented geographically and historically, a few of which include archaeological evidence while the majority do not. Almost all the compiled data is presented here collectively for the first time, while some of the data has already been reviewed earlier by some researchers (e.g. Deo et al., 2004). The studies reviewed in this thesis are primarily restricted to well-dated ones published in recent decades as the historically-older studies warrant further scientific attention using modern methods to confirm or challenge the original results. The compiled palaeoenvironmental data has been presented geographically by

[2] This is an updated version of published article by Mehra and Chauhan, 2021.

broadly dividing the Subcontinent into the following broad zones: Himalayan (H) includes Himachal Pradesh, Ladakh, Jammu and Kashmir, Kashmir, Pakistan and Nepal; northwestern (NW) includes Rajasthan, Gujarat and Arabian Sea; Ganga plains (GP) includes Uttar Pradesh, central (C) includes Madhya Pradesh and Chhattisgarh; northeastern (NE) includes Manipur, Meghalaya, West Bengal, Bay of Bengal, Arunachal Pradesh and Bangladesh; and southern (S) includes Andhra Pradesh, Kerala, Tamil Nadu, Maharashtra, East coast of India, Arabian sea core and Sri Lanka. This is followed by a discussion of the implications of the data for understanding human adaptations and natural events, including the extinction of specific species at the end of the Pleistocene. The ecological mosaic of South Asia may suggest that different populations across the subcontinent responded differently to environmental/climatic change (Boivin et al., 2013). Likewise, the entry-exit opportunities and the timing of arrival of modern humans into different zones (Langgut et al., 2018) need not match a specific condition, distance, group size, dispersal speed, intermediate climate, barrier, environment and so forth.

South Asia, or the Indian subcontinent, is a landmass with a mosaic of diverse ecozones such as the Thar Desert, the Himalayas, the Ganga plains, the Eastern and Western Ghats, various plateaus (including Chotanagpur and Deccan), tropical and rainforest environments such as parts of southern and northeastern India, temperate environments and patches of grasslands, an 18-myr-old bi-annual monsoon (Retallack et al., 2018) and home to the wettest place on Earth (Murata et al., 2017). The region also has a unique vertebrate faunal history (Roberts et al., 2014), preserves the largest terrestrial source of Youngest Toba Tephra (Williams, 2012b) and geographically links various palaeoanthropological records by being located in the centre of the Old World.

A minimum number of 120 studies have been addressed here, with broadly seven proxies (sediments, carbonates, ostrich eggshell (OES), pollen, fossil teeth/wood/seed, and multi-proxy) in the region *(*see *Figure 3-6; Table 2-7*). The sediment proxy approach has been reported at the maximum level, followed by multi-proxy, pollen, carbonates and fossil teeth/wood/seed. Only two ostrich eggshells and three speleothem datasets were found for understanding the palaeoclimates. The studies with palaeoclimatic inferences drawn only on sediment types/correlation without any absolute dates or those focussing primarily on the Holocene period were excluded in this review.

A comprehensive comparison of available records from South Asia reveals that there is a lack of concordance between the studies and as a result, it is not possible to ascertain a regional context of the environmental factors. Over and above, several drawbacks and limitations of individual proxy records, a lack of uniformity in representing the data and a variable resolution of analysis further contribute to the uncertainty of comparison comparative approach. For example, the data presented in the studied articles are interpreting the signatures of environmental settings during a particular phase in terms of at least 39 different terminologies (*Figure 6*). That warrants a regional scale understanding of the Quaternary environments and a focused long-term planning to address major issues. Considering these aspects and the requirement of focused research to be incorporated by Quaternary scientists to obtain a common regional understanding, this is an attempt to comprehend the studies through only two different aspects, viz., based on a chronological perspective and geographical level. We assume this work should provide the first-hand ready reference for researchers working on aspects of Late Pleistocene climates and associated human adaptations. We constrain ourselves from making any major critical evaluations of the

reported results due to the major geographic, chronological and methodological gaps, and rather, focus more on quantifying the factual figures and discussing their implications.

2.2 Late Pleistocene signatures from a chronological perspective

2.2.1 MIS 5 (~126-70 kyr)

The onset of the Late Pleistocene is characterised by high intensified monsoonal rainfall due to which climatic conditions were broadly humid. Within this period, 23 studies have been reported, out of which 12 are from the NW region (Achyuthan et al., 2007; Blinkhorn et al., 2017; Blinkhorn et al., 2019; Blinkhorn et al., 2021; Caley et al., 2011; Jain et al., 2005; Juyal et al., 2000; Juyal et al., 2006; Kathayat et al., 2016; Prabhu et al., 2004; select references in Sinha et al., 2020; Thokchom et al., 2017) and two from the NE region (Alam et al., 1997; Bolton et al., 2013) represent humid or high precipitation environments throughout MIS 5. Four studies demonstrate humid environments as specific periods i.e., Juyal et al. (2006) for 90-80 kyr, Agrawal et al. (2012) for 110-100 kyr, Blinkhorn et al. (2017) for 100 -80 kyr from NW region and Alam (1997) for 125-110 kyr from the NE region. Raghvan (1987) (also see Deo et al., 2004) reported a semi-arid to arid environment for the Thar Desert throughout the Late Pleistocene, Dhir et al. (2004) also demonstrates arid climates during the Late Pleistocene within Jodhpur, Birla, and Nagaur regions of the Thar Desert. Likewise, Pal et al. (2005) denote semi-arid environments from the Middle Son Valley (C region), while William et al. (2009) reported cold climatic conditions in Middle Son Valley, Kalpi in the GP region (110-100 kyr), and arid climatic from 100-90 kyr. Farooqui et al. (2014) and Reddy et al. (2013) report arid conditions at 90 ka, Kajale (1979) and Umarjikar (1984) report semi-arid conditions from 110-80 kyr. Allu et al., 2015 (in Sinha et al., 2020) denote high precipitations at 82-80 kyr in S region (see Deo et al., 2004 for the most recent review of such studies).

2.2.2 MIS 4 (~70-57 kyr)

MIS 4 in the Indian subcontinent is represented by 15 studies, all of which reported dominantly arid climatic conditions except select references in Sinha et al., 2020, which show high fluvial aggradation during that period. Overall, arid conditions are demonstrated by (Andrews et al., 1998; Caley et al., 2011; Kathayat et al., 2016; Juyal et al., 2006; Pandarinath et al., 1999; Prabhu et al., 2004) from the NW region, Bolton et al. (2013) from the NE region and Singh (2005) and Srivastava et al. (2003) from the GP region. Studies in the southern (S) region yielded both semi-humid (Reddy et al., 2013) and semi-arid (Kajale, 1979 and Umarjikar, 1984, see Deo et al., 2004) conditions throughout the Late Pleistocene.

2.2.3 MIS 3 (~57-29 kyr)

A total of 43 studies dated to MIS 3 have been reported from all six regions across India. At this stage, a shift in climatic conditions was observed, and environments tended to be more humid than arid. This period showed similar environments throughout the Subcontinent and is identified with intensified monsoon/ rainfall and humid climate. However, intensified monsoon/ rainfall and humid climate are not recorded at all studied sites dated to this time period. Out of the 43 studies reported, 33 of them represent humid conditions (Andrews et al., 1998; Blinkhorn et al., 2017; Caley et al., 2011; Jain et al., 2005; Juyal et al., 2000; Juyal et al., 2006; Kar et al., 2001; Kathayat et al., 2016; Pandarinath et al., 1999; Prabhu et al., 2004; Srivastava et al., 2001; Tewari et al., 2002) from the NW region, (Bhandari et al., 2009; Kotlia et al., 1997; Nag and Phartial, 2015; Owen et al., 1997; Phartriyal et al., 2005 (sub-tropical to warm)) from the H region; (Pal et al., 2005; Quamar, 2015) from C region, (Agarwal et al., 2012; Chauhan et al., 2015; Pal et al., 2005; Singh et al., 2005; Srivastava et al., 2003; Tewari et al., 2002) from GP region; (Bolton et al., 2013; Bhattacharya et al., 2014; Dutt at al. 2015) from the NE region, (Babeesh et al., 2017; Maya et al., 2017; Powar et al.,

1993; Rajagopalan et al., 1997; select references in Sinha et al., 2020; Tiju et al., 2021) from the S region. While nine studies (Pandarinath et al.,1999; Srivastava et al., 2001) from the NW region (Singh, 2005; Srivastava et al., 2003; Trivedi et al., 2012), from the GP region (Verma and Rao, 2011) and S region represent arid environments until 32 kyr and after that, largely semi-arid; (Bhattacharya, 1989; Kotila et al., 1997; Phartiyal et al., 2005; Ranthora et al., 2007) from the H region and Sadakata et al. (1995) from the S region shows arid conditions. Although many more studies are required, there is currently no clear evidence for widespread climatic deterioration at the subcontinental level after ~40 kyr (contra Petraglia et al., 2009). Mishra et al. (2013) suggest an expansion of modern humans from India to adjoining regions during interglacial climates of MIS 3.

2.2.4 MIS 2 (~29-14 kyr)

Between 30 – 11 kyr, the environment across the Indian subcontinent was broadly characterised by more arid conditions and is represented by the maximum number of scientific inferences (n = 85).

2.2.5 Period 29 – 20 kyr

This sub-period has at least 38 studies but has a weak resolution in terms of chronological continuity. It suggests a broad shift from humid to arid conditions and probably marks the end of the Last Glacial Maximum (LGM); 15 of these studies infer humid conditions until 25 kyr, and 17 studies represent arid conditions after 25 kyr. The NW region shows mostly arid conditions except Andrews et al. (1998) who show a humid climate until 25 kyr. The work of Kale et al. (2003) demonstrates a catastrophic flood in the central Narmada valley at 25 ka, while Patnaik et al. (2009) shows arid conditions at 24 ka, also in the C region and Sanwal et al. (2019) also shows arid conditions at 22-18 kyr.

2.2.6 Period 19-11 kyr

The general trend from the period 19-11 kyr is observed to be largely arid and this period provides the maximum number of studies (n = 53). Here, 20 studies (Achyuthan et al., 2007; Agrawal et al., 2012; Andrews et al., 1998; Basavaiah et al., 2004; Bhattacharya, 1989; Bolton et al., 2013; Deotare, 2004; Ghosh et al., 2014 in Kar and Quamar, 2020; Kajale and Rajaguru, 1989; Pandarinath et al., 1999; Prabhu et al., 2004; Rajendran 1979; Sharma et al., 2006; Srivastava et al., 2001; Srivastava et al., 2003; select references in Sinha et al., 2020; Thokchom, 1987; Trivedi et al., 2012; Vaidyanadhan and Ghosh, 1993) represent absolute dry climatic conditions. The span of arid conditions is also noticed in patches from the following studies: (Bera et al., 1996; Bhattacharyya et al., 2011; Bohra et al., 2017; Rajagopalan et al., 1997; Rajaguru et al., 2011; Sadakata et al., 1995; Sharma, 2001; Sharma et al., 2004; Singh, 2005; Quamar and Chauhan, 2012; Quamar and Bera, 2017; Van Campo, 1986; Wünnemann et al., 2010).

Only six studies (Jain et al., 2005; Khonde et al., 2017; Lasker et al., 2010 (NW region), Nag and Phartiyal, 2015; Sanwal et al., 2019; Khan et al., 2022 from (H region)) show absolute humid climates, while patches of humid climate can be observed from different parts of South Asia reported by (e.g., Bera et al., 1996; Bohra et al., 2017; Dixit and Bera, 2013; Ranhotra et al., 2018 and Sadakata et al., 1995). Broadly, the subcontinent exhibits a cool and dry climate until 15 kyr and at the onset of Holocene, when more intensified precipitation and humid climate is recorded.

2.3 Late Pleistocene environments at a regional geographic level

The Himalayan region includes Jammu and Kashmir, Uttrakhand, Himachal Pradesh, Nepal and parts of Pakistan. The Upper Alaknanda basin shows the large extension of glaciers due

to high precipitation during 80-65 kyr (Singhvi and Kale, 2010). The Kathmandu valley (present-day Nepal) witnessed a change from subtropical to warm climate between at 53-49 kyr (Bhandari et al., 2009), and from 50-25 kyr, a comparatively cold climate was reported (Phartiyal et al., 2005). Between 40-20 kyr, a humid climate was reported with high precipitation (Babeesh et al., 2017 (41 ka); Bookhagen et al. 2005; Dar et al., 2015; Datta et al., 2012 in Sinha et al., 2020; Gupta et al., 1982; Ghosh and Bhattacharya, 2003; Kotlia et al., 1997; Ranthora et al., 2007) and a contemporaneous study (Bhattacharya, 1989) reported a cold and dry climate at the period of 30-28 kyr. After 28 kyr, the Himalayan belt shows significant variation in climate, warm and humid climate was reported between 24-18 kyr, followed by a cold and dry climate (Bhattacharya, 1989), contemporaneous studies in Bharatpur, Upper Lahaul valley sequentially shows an arid phase (24-22 kyr), followed by an increase in monsoonal precipitation (22-20 kyr), followed by a decrease in precipitation with arid conditions (20-18 kyr) and humid climate at 18-11 kyr (select references in Sinha et al., 2020) before ending with warm and humid climate between 18-15 kyr (Bohra et al., 2017).

The Northwest region (Thar Desert) includes mostly Rajasthan and Gujarat and presents longest continuous Late Pleistocene records retrieved from the Indian subcontinent are from this region, covering the period from 126 kyr to 11 kyr. A minimum of 28 studies have been done with absolute dates and associated palaeoenvironmental interpretations. The period from 130 kyr to 70 kyr broadly indicates high precipitation with warm and humid climates in the general desert area (Blinkhorn et al., 2017, 2019, 2021; Caley et al., 2011; Dhir et al., 2004; Jain et al., 2005; Juyal et al., 2000, 2006; Kathayat et al., 2016; Prabhu et al., 2004; Thokchom et al., 2017) while the river valleys in Gujarat were reported to have high fluvial deposition (Raj et al., 2016) and intense monsoon. From the 70-60 kyr context, only a few studies were reported with overlaps, which indicate a broad shift towards an arid climate

(Andrews et al., 1998; Caley et al., 2011; Juyal et al., 2006; Kathayat et al., 2016; Pandarinath et al., 1999; Prabhu et al., 2004; select references in Sinha et al., 2020). This is followed again by a period of high and intensified monsoon and humid climate, which lasts until ~30 kyr (Andrews et al., 1998; Blinkhorn et al., 2017; Caley et al., 2011; Jain et al., 2005; Juyal et al., 2000; 2006; Kar et al., 2001; Kathayat et al., 2016; Mishra and Rajaguru 2001; Pandarinath et al., 1999; Srivastava et al., 2001; Raj et al., 2016). From 30 to ~15/12 kyr, a climate shift is broadly indicated from humid to arid environment (Andrews et al., 1998; Dhir et al., 2004; Juyal et al., 2003; Mishra and Rajaguru 2001; Srivastava et al., 2001) and after 15/12 kyr, re-establishment of the monsoon was reported with a humid climate (Jain et al., 2005; Juyal et al., 2003; Lasker et al., 2010; Parbhu et al., 2004; Srivastava et al., 2001).

The Ganga plains region includes floodplains of the river Ganga which are mostly present in the state of Uttar Pradesh. In this northern region, periods of intensified monsoon were reported at 100 ka, 40 ka, 25 ka (Agrawal et al., 2012) and arid to humid climate shift is reported between 100-75 kyr by Jha et al., 2020. Humid climate at Kalpi between ~50-40 kyr (Singh, 2005; Srivastava et al., 2003; Tewari et al., 2002), Belan and Yamuna at 60-45 kyr (Pal et al., 2005) has been reported. A contemporaneous study shows cool and dry climate at Jalesar Tal between 42-13 kyr (Trivedi et al., 2012) and from 15-13 kyr, dry climates with low rainfall was reported with an exception Kumar et al. (2022) showing humid conditions; after 13 kyr, the climate became more humid with high rainfall (Chauhan et al., 2015; Sharma et al., 2006).

The Central region broadly includes Madhya Pradesh, Chhattisgarh and Odisha. In comparison with other regions, a limited number of palaeoenvironmental studies have been done in the C region. Pal et al. (2005) studied the palaeoclimate of the Quaternary formations

of the Middle Son Valley and which were bracketed to the Late Pleistocene. Palaeoclimatic interpretations of this valley include a semi-arid climate with irregular rainfall prior to 100 kyr, and a relatively dry climate at ~100 kyr. Williams et al., 2009 suggest cold climatic conditions at Middle Son Valley after 73 kyr. Quamar (2015) further assessed the Late Quaternary here as a period of humid climate. At 32 ka, and ~12 kyr to 7 ka cool and dry climates were reported from the Hoshangabad (Madhya Pradesh) area and the Baikunthpur forest range (Chhattisgarh) (Quamar and Bera, 2017; Quamar and Chauhan, 2012; Verma and Rao 2011). For the period from 30.5 ka to 24.5 ka, Verma and Rao (2011) reported warm and semi-arid conditions at Shakarghat and Chahin Nala in the central Narmada valley and Kale (2003) reported a catastrophic flood in the same region at ~25 kyr and arid conditions were demonstrated at Hathnora at ~ 24 kyr (Patnaik et al., 2009), ~16-15 kyr in the same region (Jukar et al., 2019) and at 17 ka in Pratappur (Odisha) (Patnaik et al., 2019).

A minimum of 13 studies have been reported from the northeast region of the Subcontinent including Bangladesh. The earliest Late Pleistocene palaeoclimate record is currently known from Darjeeling, West Bengal, where the following conditions were revealed: low monsoon and high temperature between 46.4-31 ka, high precipitation and cooler temperature between 31-22.3 ka and low temperature and low precipitation after 22.3 ka onwards (Ghosh et al., 2015). The Ziro Valley, Arunachal Pradesh, showed an increase in the SW monsoon from 43-34 kyr, and after that, a relative decline in rainfall; the area experienced a peak warm and humid phase around 36-34 kyr (Bhattacharyya et al., 2014). Dutt et al. (2015) shows a strong wet phase at 33.5-32.5 ka and a weak and dry phase at 26 – 23.5 ka and very weak phase from 17-15 ka. The work of Alam et al. (1997) shows a humid climate at Chandril village (northwest Bangladesh) during the Late Pleistocene. The semi-arid conditions within an overall sub-humid phase are reported from Terafeni Valley, West Bengal at 18 ka (Basak et

al., 1998) and a very less amount of precipitation is observed in the Bay of Bengal and Andaman Sea during 18.2-14.6 ka (Rashid et al., 2011). Ghosh et al. (2014) in Kar and Quamar (2020) show humid conditions at 20 kyr and dry conditions after 20 kyr onwards. The Manipur valley shows dry conditions during the terminal Late Pleistocene (Thokchom, 1987). The persistent fluvial activity from ~15-12 kyr and from ~12-10 kyr cool and dry climate with weakened monsoonal precipitation is also reported from Kamrup (Assam) by Dixit and Bera (2013). Also, see Bolton et al. (2013) in (*Table 5*) for palaeoclimatic inferences based on a marine core from the Bay of Bengal.

The Southern region includes Maharashtra, Kerala, Karnataka, Tamil Nadu, Andhra Pradesh, Goa and Sri Lanka. Based on the present climate, the parts of southern region and Sri Lanka are wet regions getting high precipitation throughout the year (John, 2018; Wedage et al., 2019). Reddy et al. (2013) report a semi-humid climate at Kanigiri in Andhra Pradesh during Late Pleistocene with arid phases at 90 ka, 48-45 kyr, 33-30 kyr, 21 kyr, and at 11 kyr. Farooqui et al. (2010) reported a warmer climate with intensified monsoon from 80-40 kyr from Vazhapally and Chaganachery (Kerala). The work of Allu et al. (2015) denotes a dry climate at MIS 5c and Farooqui et al. (2014) show intense precipitation at MIS 5a. During MIS 3 (57/46 kyr), evidence for a strong monsoon was reported from Kerala (Maya et al., 2017), and the Pravara River basin, Maharashtra (Sadakata et al., 1995). A study by (Tiju et al., 2021) shows marine transgression at 42-40 kyr on a Kerala coast. A shift from warm to a wetter climate was linked with the tectonic upliftment of the Konkan coastal belt (Powar et al., 1993). Climate aridity and a decrease in rainfall were reported from 40-25 kyr from the Pravara River basin, Maharashtra (Sadakata et al., 1995, also see Jagtap and Deo, 2016 for an absolute chronology of the Maharashtra region), low surface productivity denoting less precipitation is observed from the Arabian sea during 42-20 kyr (Singhvi and Kale, 2010) and

warm and semi-arid conditions from Coimbatore were reported at 30-21 kyr (Achyuthan et al., 2012). The contemporaneous studies, however, in the Nilgiris in Tamil Nadu indicated high monsoonal precipitation at 40-28 kyr (Rajagopalan et al., 1997) and at the Kerala coast at >40 and 28 kyr (Tiju et al., 2021). During 25-14 kyr, a decrease in rainfall/weakening of monsoon and arid conditions were reported (Kajale and Rajguru, 1989; Rajagopalan et al., 1997, Sadakata et al., 1995, Tiju et al., 2021; Vaidyanadhan and Ghosh, 1993; Van Campo 1986;) as well as a cold and dry climate (Bera et al., 1996 and Kumar et al., 2017) and a dry humid climate (Premathilake and Risberg, 2003). From 15 kyr to the Holocene, a humid climate was reported from an Arabian Sea core and Berijam Lake in Tamil Nadu (Bera et al., 1996; Kumar et al., 2017; Van Campo, 1986). Based on geomorphic studies at different river basins (Luni, Mahi, Sabarmati, Narmada, Tapti, Godavari, and Bhima) (Mishra and Rajaguru, 2001) shows a humid climate at 50- 30 kyr and a rapid transformation from glacial to post-glacial environment at 14 kyr.

2.4 Late Pleistocene hominins and environmental adaptations in South Asia

Contexts near the Middle-to-Late Pleistocene transition (~150-100 kyr) in South Asia have yielded both Lower Palaeolithic evidence at 140-120 kyr (Haslam et al., 2011) and Middle Palaeolithic evidence spanning from 385-74 kyr (Akhilesh et al., 2018) in north-central and southern India, respectively. With the exception of 16R in Rajasthan, which preserves a multi-cultural sequence from the last ~200 kyr (see Singhvi et al., 2010), there are currently no well-dated palaeoanthropological sites spanning the entire Late Pleistocene in the Subcontinent *(Table 2-8)*. After the Large Flake Acheulean disappears at ~100 kyr, the South Asian record is first dominated by Middle Palaeolithic assemblages with diminutive bifaces, followed by exclusively flake-based Middle Palaeolithic assemblages from about ~80 kyr until 38 kyr (Korisettar, 2014). However, these technological overlaps are chronologically

variable across the subcontinent, and very few absolute dates are available to provide a clear picture of the transitions. While the Lower Palaeolithic is generally associated with archaic hominins (Haslam et al., 2011), our current understanding of Late Pleistocene hominin adaptations in South Asia is dominated by two opposing theories regarding the initial arrival of prehistoric modern human into the region. One theory relates Middle Palaeolithic in India with the arrival of modern humans from Africa during MIS 5 (130-70 kyr), with populations surviving the Toba super-eruption at ~74 kyr (Groucutt et al., 2015; Petraglia et al., 2007; Petraglia et al., 2010). These modern populations are thought to have later developed microlithic technology due to deteriorated climatic conditions (Clarkson et al., 2009; 2018; Petraglia et al., 2009). The second theory associates the Indian Middle Palaeolithic with pre-existing archaic species and highlights the first arrival of modern humans with microlithic assemblages and other cultural and behavioural features only after MIS 4 or 3 (71-57 kyr) (Mellars et al., 2013; Mishra et al., 2013). The former theory may be supported by Middle Palaeolithic assemblages found at Sandhav in Gujarat at 114 ka (Blinkhorn et al., 2019), Katoti in Rajasthan at ~95 kyr (Blinkhorn et al., 2013) and Jwalapuram in Andhra Pradesh at 77 Ka (Petraglia et al., 2007). However, new data from Attirampakkam suggests a localised Lower-Middle Palaeolithic transition at ~385 ka (Akhilesh et al., 2018), suggesting the indigenous development of the latter instead of its introduction into India via incoming dispersals. As that evidence includes a highly diverse tool-kit including large bifaces, diminutive bifaces, Levallois elements, points and laminar technology (i.e. blades and blade cores), we need to be more cautious about automatically linking all Middle Palaeolithic technologies in South Asia with *Homo sapiens*. It is also possible that the entire South Asian Middle Palaeolithic was innovated, utilised, and dispersed by different hominin species over time, including archaic and *H. sapiens*, all conjectures that future fossil discoveries can better confirm. For instance, the multiple Late Pleistocene absolute dates obtained for the

depositional context at the fossil hominin site of Hathnora (Patnaik et al., 2009) suggest the possibility of late survival of archaic species in India and, thus, complex interactions with the first incoming moderns (whenever that may have been). It is also possible that archaic populations were declining in the subcontinent due to various factors prior to their integration with moderns. Due to the lack of fossils and adequate palaeoenvironmental evidence, it is unclear whether there were multiple dispersals of moderns in India, and what specific environmental factors stimulated and facilitated their arrival(s), as well as their subsequent spread within the subcontinent.

One key topic of contention has been the impact of the Toba volcanic eruption (Sumatra) on existing hominin populations ~74 kya (Williams, 2012a; 2012b). Today, the Younger Toba Tephra (YTT) is known to occur at multiple locations across India, representing its largest terrestrial source including some African locations. Tephra deposits at Indian Acheulean sites, such as Morgaon and Bori, thought by some to belong to the Older Toba Tephra (Gaillard et al., 2010; Mishra et al., 2005), indicate younger ages (Biswas et al., 2013) and thus may actually be reworked YTT. Regarding the debate of the ecological and biological impacts of the YTT, several hypotheses have been proposed by different researchers. Ambrose (1998) was one of the first to hypothesize that the eruption probably had significant repercussions on global climate and ecology 74 kyr, and as a consequence, on the behaviour of hominin groups and possible population bottlenecks. Petraglia and colleagues (2007; Blinkhorn et al., 2012; Clarkson et al., 2012; Haslam and Petraglia, 2010; Haslam et al., 2010a; 2012a) challenged that, based on new evidence from southern India where they reported Middle Palaeolithic stone tools from below and above the YTT. They then proposed that the Jwalapuram artefacts statistically compare with those made by modern humans in southern Africa, and thus modern humans must have reached South Asia >74 kyr and that the

supereruption had minimal impact overall. Multiple issues later arose in relation to the dating results, contexts of the artefacts and interpretations (Balter, 2010; Petraglia et al., 2012; Williams, 2012a, 2012b; also see Chauhan et al., 2015). Additionally, some researchers (Mellars et al., 2013) have also challenged the presence of modern humans at Jwalapuram, stating that the first such dispersal involved microlithic technology. Indeed, it is possible that such assemblages reflect independent but parallel technological progression rather than a dispersal event from elsewhere. In the absence of fossil evidence and the contemporaneous timing of the Lower to Middle Palaeolithic transition across the Old World between 500 and 300 kyr, including India (Akhilesh et al., 2018), archaic hominin species can still be considered as a candidate responsible for (some if not all of) the younger Middle Palaeolithic assemblages also. While the Jwalapuram work yielded a problematic wide age range (77 kyr and 38 kyr) for the pre-and-post-Toba lithic evidence, a similar investigation at the site of Dhaba in north-central India has chronologically narrowed that gap to 79 kyr and 65 kyr encouraging another interpretation of no technological change (Clarkson et al., 2020). Nonetheless, the large time gap of 10,000 years after the Toba event makes it challenging to draw major conclusions regarding true occupational continuity. It is also not clear if fluvial or other processes facilitated occupational/technological continuity by minimizing the ecological impact of the Toba tephra in the immediate region. Thus, it remains ambiguous exactly how the supereruption may have impacted regional environments, hominin groups, and their behavioural adaptations and lithic technologies across India (see Williams, 2012a). From a broader theoretical perspective, Jones (2010; 2012) has suggested that the YTT probably had variable impacts across the entire subcontinent, and a single widespread, homogeneous effect should not be expected. Singh and Srivastava's (2022) research suggests that the YTT eruption had a limited impact on Southeast Asia's climate and ecology, with minimal effects on hominins, vegetation, ecosystems, and animal species. During most of the

Late Quaternary to Holocene period, warm and arid to semi-arid climatic conditions alternated, which were favourable for living populations, including flora. It is asserted that human populations did not disappear outright from the Indian subcontinent; nonetheless, they may have suffered marginally. The first record of rhizospheres, preserved in the pre-tephra Quaternary succession of the entire Purna alluvial basin in Central India, indicates the existence of vegetation long before the YTT eruption and the continuation of the same after the above-said eruption, suggesting that the eruption had minimal impact on the vegetation. In addition, it is inferred that the mixed C_3- C_4 vegetation existed long before and during the YTT eruption, although various changes in the same have been observed during the past 75 kyr. Still, these variations had no direct relationship with the effects of the YTT eruption. In addition, it is concluded that there is no direct relationship between the human bottleneck and their movement, deforestation, animal mortality and the YTT-induced climate hostility.

Further understanding of the presence of Toba ash as a stratigraphic marker remains ambiguous. Geethanjli et al. (2020) date Toba ash deposits in Sagileru and Gundlakamma Valley, Andhra Pradesh, between 65 kyr – 0.35 kyr, suggesting the presence of Toba ash is not a reliable chronological marker in South Asia. Furthermore, research is required at the site-specific level (Toba ash associated with Palaeolithic artefacts) in pan-India before any conclusive statements can be made about the actual short-term and long-term impacts of Toba.

Despite the earliest microliths occurring at 48 kyr in Sri Lanka (Wedage et al., 2019) and at 48-45 kyr in central India (Mishra et al., 2013; Clarkson et al., 2020), the Middle Palaeolithic persists until 38 kyr in southern India (Clarkson et al., 2009; Petraglia et al., 2012) and perhaps other zones also. The Middle Palaeolithic is also present in Sri Lanka c. 80 kyr and appears to be the earliest evidence of human occupation of the island (Deraniyagala 1992;

Perera 2010). The Middle Palaeolithic assemblages occur extensively across the subcontinent until the appearance of 'Late Palaeolithic' technologies (James and Petraglia, 2005), including microlithic toolkits, associated with bone tools and personal ornamentation from at least 36 kyr (Clarkson et al., 2009) and perhaps 45 kyr onwards (Mishra et al., 2013; Basak et al., 2014). Proponents of a rapid, single southern route of human dispersal from Africa ~60 kyr argue for the dispersal of microlithic industries from Africa and across South Asia (Mellars, 2006; Mishra et al., 2013). By contrast, suggestions of indigenous transitions from the Middle to Late Palaeolithic, stimulated by contextual demographic and environmental changes, have been used to suggest more gradual, early human dispersals into South Asia from Africa and local technological development (Clarkson et al., 2018; Lewis et al., 2014; Petraglia et al., 2009).

A review of archaeological and palaeoenvironmental data from three different ecological regions of South Asia i.e., Thar desert, Jurreru River Valley and Sri Lanka's wet zone broadly demonstrate the effect of climate change leading to the development of the new technologies and cultural behaviours rather than developing independently without any external factors (Roberts et al., 2017). While the Thar Desert, shows humid climates during MIS 5, favouring the hominin occupations, and climatic aridity led to the discontinuity of occupations at Katoati during MIS4 (Blinkhorn et al., 2017). At the site of Jwalapuram, the transition from Middle Palaeolithic to the Late Palaeolithic industries is thought to happen due to climatic deterioration. The wetlands of Sri Lanka were exploited by human foragers, utilising bone tools and Late Palaeolithic microlithic around ~36 kyr (Roberts et al., 2017).

However, the alleged innovation of microliths due to population expansion and climate deterioration after 40 kyr (Petraglia et al., 2009) is now challenged by the discovery of older microliths at 48 kyr in Sri Lanka (Wedage et al., 2019) and 48-45 kyr in central India

(Clarkson et al., 2020; Mishra et al., 2013). While it remains unclear whether South Asian microliths were indigenous innovations or introduced through dispersals, the link between climate change and microlithic innovation is currently tenuous, and more multidisciplinary evidence is required to test it. Not only is the current palaeoenvironmental evidence inadequate to identify clear climatic deterioration at a pan-Indian level, but the South Asian Upper Palaeolithic itself remains an ambiguous entity (Chauhan, 2019; James and Petraglia, 2005; Haslam et al., 2010a). For example, ample evidence of laminar technology has been reported from various parts of the subcontinent. However, the associated assemblages appear to spatially and chronologically overlap with the preceding Middle Palaeolithic technologies and the following microlithic technologies, in addition to occurring exclusively at numerous sites (Chauhan, 2009). Despite this abundance of evidence, almost no absolute dates exist for the South Asian Upper Palaeolithic, except Site 55 in Pakistan, where Dennell et al. (1992) have reported blade-dominated assemblages dated to 45 kyr. The Upper Palaeolithic horizon in the 16R dune cultural sequence in Rajasthan was recently re-dated to 80-40 kyr by Singhvi et al. (2010), and thus this archaeological sequence was re-classified by Blinkhorn (2013) as Middle Palaeolithic. The site shows intermittent occupation dated to MIS 5 and MIS3 with humid climates.

2.5 Discussion and conclusions

Based on the broad review above, the number of studies is currently of low resolution to reveal any discrete geographic and chronological patterns for Late Pleistocene environments, with the possible exception of some northern zones and those dated to <50 kyr, especially closer to the terminal Pleistocene. This chronological disparity appears to be due to research bias, preservation bias, variable abundance of geological exposures, logistical access to stratigraphic sampling and methodological limitations in geochronology. Another major issue

why a critical comparison of different regions and time periods is not yet possible is because the environmental results of these studies are highly variable and subjective. For example, the results of many of these studies include humid, semi-humid, less arid, arid, semi-arid, semi-humid to semi-arid and wet-semi-arid. From all of these known studies, even fewer have focused on palaeoenvironmental reconstructions at prehistoric sites, infact only a handful of such examples are known. Most Late Pleistocene environmental reconstructions have been done in the Himalayan zone, the Thar Desert, and the Ganga plains. The remaining studies are more randomly scattered throughout central, western, northeastern and southern India, as well as in Sri Lanka and deep-sea cores in the Arabian Sea. Major geographic gaps need to be critically filled through future work across India, in addition to Pakistan, Nepal, Bhutan, Bangladesh and Sri Lanka. In India, vast areas of central India, northeastern India and peninsular India require focused attention through problem-oriented multidisciplinary projects. For example, future palaeoenvironmental datasets may help answer key questions regarding the following issues (among others): i) technological dispersals, innovations and transitions; ii) the absence of specific technologies and technological dispersals across some geographic zones (e.g., northeast India see Jamir et al., nd); iii) pan-Indian impact of the Toba super-eruption; and iv) factors of hominin and other faunal extinctions like *Palaeoloxodon namadicus*, *Stegodon namadicus*, *Hexoprotodon sp.*, *Equus namadicus* and *Struthio camelus* (see Jukar et al., 2020). At a broad and tentative level, the Late Pleistocene climatic framework for the region represents a linear trend with a relatively humid climate throughout the period, with some exceptions at 69-60 kyr and 19-11 kyr, representing arid climates. One primary explanation for such a trend from 125 to 80 kyr might be the lack of adequate research: only 15 studies have been reported, of which nine are from the NW region. The period from 79-70 kyr shows almost equal inferences for humid and dry climates with a total number of 15 studies. In the period from 69-60 kyr, more studies show a dry climate and for the period from 59-30 kyr, out of a total of 84 inferences, 60 represent humid climate. Again

from 29-20 kyr, almost an equal number of inferences are drawn for both humid and arid climates and demonstrate the dynamic climatic history of the region during the Late Pleistocene. The terminal Late Pleistocene (19-11 kyr) shows 35 dry environmental examples out of 49 inferences, while the remaining are humid, semi-humid or semi-dry. For the time being, almost all studies representing MIS 5 show humid climatic conditions, probably due to regional research bias. MIS 3 is the only phase that is represented by studies across all six regions. Based on current evidence, there is no marked climatic deterioration at the subcontinental level at ~40 kyr. In fact, the current data also does not show any chronological congruency at the subcontinent level, highlighting the sub-regional ecological and climatic diversity across South Asia. Therefore, to better understand the Late Pleistocene environments of South Asia and linked palaeoanthropological events, significant work needs to be done at the regional level and preferably approached from 'bio-eco-geographic' perspective. We also need to develop a high resolution palaeoclimate database for South Asia and associated palaeoanthropological records. Further, there is major scope for multi-proxy approaches which will provide more definitive scientific evidence to strengthen palaeoclimatic inferences at key sites. To understand human-environment interactions during the Quaternary, emphasis needs to be given for developing regional/site specific palaeoenvironmental records from prehistoric archaeological sites and also contemporaneous non-archaeological contexts in surrounding regions (including well-preserved geological contexts without any diagnostic evidence preserved, such as lithic assemblages or Toba tephra). This compiled section has aimed to provide an empirical update of Late Pleistocene environments in South Asia, and associated implications for different specialists in Quaternary studies, palaeoanthropology, prehistoric archaeology and vertebrate palaeontology. The compilation also shows which geographic zones require urgent scientific attention across South Asia, especially in light of widespread anthropogenic activities that are rapidly destroying key Quaternary geological features and related sites of scientific relevance.

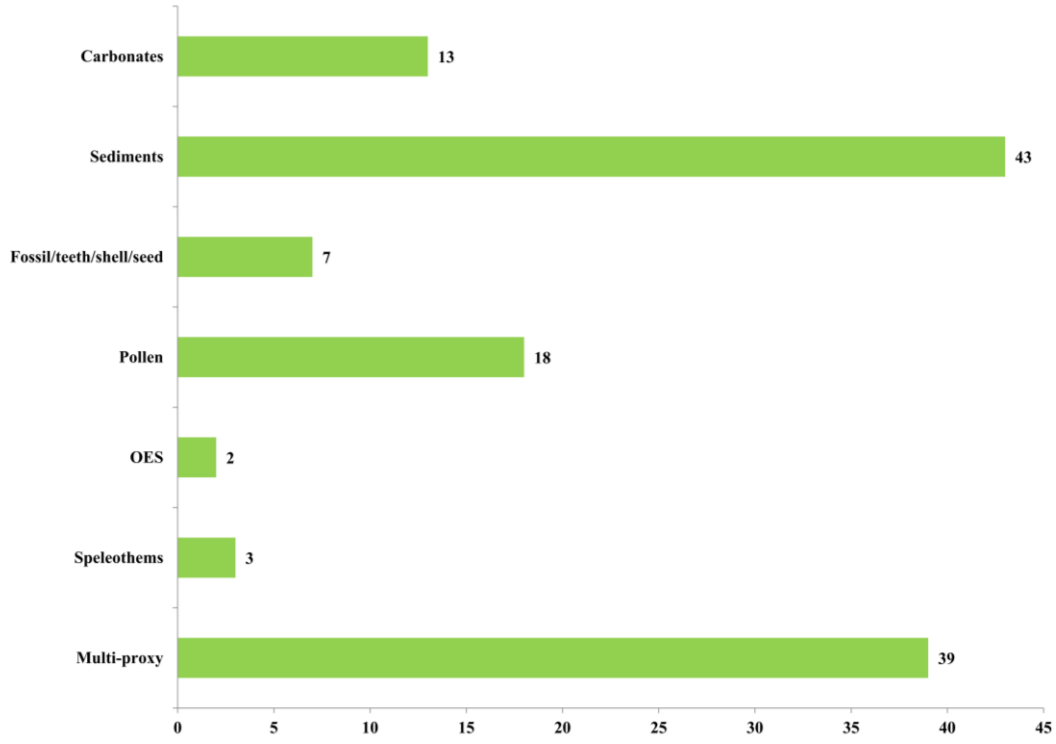

Figure 3. Number of palaeoclimatic reconstruction studies proxy-wise.

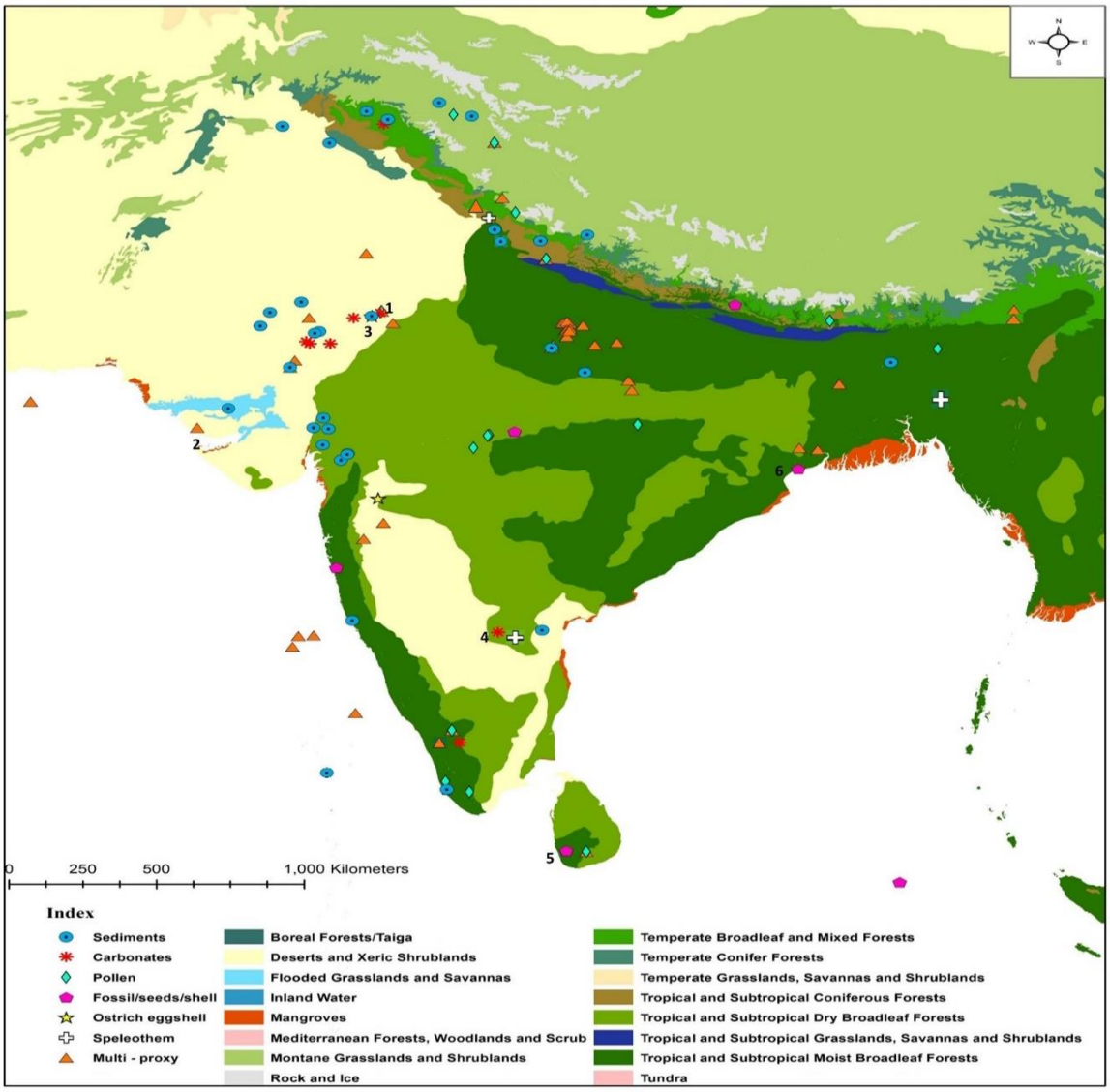

Figure 4. Map of South Asia showing the Late Pleistocene palaeoclimatic studies with different proxies (source: ArcGIS).

Table 2. Region-wise palaeoclimatic inferences in South Asia (Northwest Region = NW Region)

Sr. No.	Site	Material/Proxies	Method/Age	Inferred Palaeoclimate	Reference
NW1	16R Dune (RJ)	Carbonate nodules/ Stable isotope	TL/ C-14 126 kyr – 70 kyr 26 kyr – 13 kyr	126 kyr – 70 kyr (High values of δ13C values which represent high % C_4 plants) 26 kyr – 13 kyr (Lower δ13C value consistent with a higher proportion of C_3 vegetation. The % of summer rains is determining factor, C_4 plants coincide with a period of greater summer rains (High monsoon)	Achyuthan et al., 2007
NW 2	Shergarh (RJ) Shergarh Tri-junction	Carbonate nodules/stable isotope	OSL, Infrared 70 kyr - 25 kyr 50 kyr – 14 kyr	70 kyr - 60 kyr (Arid) 60 kyr – 25 kyr (Strengthened monsoon) 25 kyr – 10 kyr (Arid) (C_3 and C_4 vegetation) 50 kyr -30 kyr - Humid climate 25 kyr -14 kyr – Major phase of Late Pleistocene aridity 14 kyr – Rapid transition from glacial to post-glacial climate	Andrews et al., 1998 Mishra and Rajaguru, 2001
NW 3	Thar Desert (Jhodpur, Birla and Naguar group) (RJ)	Carbonate nodules/stable isotope	ESR 150 kyr – 60 kyr 27 kyr – 14 kyr	Mid Pleistocene – More arid conditions Late Pleistocene – Progressively drier conditions	Dhir et al., 2004
NW 4	Bikampur (Bikaner) Nacha (Jaisalmer) Awai (Jaisalmer) (RJ)	Sediments-Chronology and sand profiles	TL) 39.6 kyr - 5.5 kyr	Enhancement in sand mobilisation at 14 kyr, but at 13 kyr, sand mobilisation is weakened, representing a transition from arid to semi-arid climate	Chawla, 1992
NW 5	Karna, Sindhari, Khudala (Luni Basin) (RJ)	Sediments/Palaeosol/calcrete Stable isotope	OSL 200 ka, 80 kyr - 1 kyr	80 kyr – 1 kyr (OIS 5 – OIS 1) shows distinct depositional environments suggesting strong climatic control, following record correlates with arid, humid cycles during the last glacial-interglacial cycle. Humid phase (OIS 1 and OIS 5) Reddening and Warm-humid climate (70 kyr -30 kyr), Intensified monsoon around 14 kyr.	Jain et al., 2005
NW 6	Southern Thar Desert (Dharoi, akhaj, Dabka, Tajpura) (GJ)	Sediment, Dune building	Blue-green light stimulated luminescence 26 kyr - 0.6 kyr	Before 26 kyr humid phase, around 26 kyr shifts from humid to arid phase. 11 kyr – 8 kyr more humid phase due to intensified SW monsoon.	Juyal et al., 2003
NW 7	Chamu, and Chirai (RJ)	Sediment-profiles	C14 > 40 kyr ,7 kyr	Alternation of wet and dry phases dated to 7 kyr, 15 kyr and >40 kyr.	Agrawal, 1980

NW 8	Bap – Malar (RJ)	Sediments,Pollen and carbonates – stable isotope	AMS 18,430 Yrs, 8, 320 Yrs	>15 kyr – Shallow ephemeral lake 11 kyr to 10 kyr – Shallow and seasonal lake at times dry.	Deotare, 2004
NW 9	Sambhar playa (RJ)	Organic fraction of core sediments/carbonate – stable isotope /evaporate mineralogy/geochemical ratio	AMS Upto 30 kyr	>30 kyr – Semi-humid to Semi-arid climate 30 kyr – 24 kyr – Lake shows low to moderate salinity, Semi- humid to Semi-arid climate 24 kyr to 20 kyr – Low lake level with large fluctuations, variable salinity 20 kyr to 16 kyr – Shallow lake with moderate salinity; gradual strengthening of the monsoon 16 kyr to 7.5 kyr – Fluctuating lake with variable salinity; moderate precipitation semi-humid phase	Sinha et al., 2006
NW 10	(Kalibangan) Ghaggar Plains (RJ)	Sediments- Sr isotope, Carbonates – stable isotope	OSL ~75 kyr	Intense summer monsoon (Wet conditions)	Singh et al., 2016
NW 11	Nal Sarovar (RJ)	Crystallinity of Illite	75 kyr	A continuous spell of aridity between 7 and 73 kyr, a single wet phase around 50 kyr was identified.	Pandarinath et al., 1999
NW 12	Khudala(RJ)	Sediments/stratigraphic correlation	TL, IGSL, IRSL >100 kyr	Aeolian Phase at >100 kyr, followed by Channel Activation phase at ca. 90 kyr, another Aeolian phase at 86 kyr, a more humid phase from 50 to 30 kyr and a climatically unstable phase between 13 kyr and 8 kyr	Kar et al., 2001
NW 13	Didwana(RJ)	Pollen	20 kyr	20 kyr – 13 kyr hypersaline conditions, indicating weekend monsoon and higher winter precipitation	Singh et al., 1990
NW 14	Didwana, Nevasa(RJ)	Colluvio-alluvial calcretised sediment; (Correlation)	~125 kyr to 10 kyr	Arid (22 – 18 kyr BP) to dry-semi-arid with short wet-semi-arid phases (125 – 100 kyr, 60-30 kyr)	Rajaguru et al., 2011
NW	Luni-Mahi-Sabarmati basins Narmada - Tapti – Godavari- Bhima basins		50 kyr -14 kyr 30 kyr -14 kyr	50 kyr -30 kyr - Humid climate 14 kyr – Rapid transition from glacial to post-glacial climate 30 kyr -20 kyr - Humid climate 14 kyr – Rapid transition from glacial to post-glacial climate	Mishra and Rajaguru, 2001

NW 15	Sabarmati Basin (GJ)	Sediments stratigraphy	TL 54 kyr -30 kyr, 12 kyr	(54 kyr – 30 kyr) less aridity and stronger SW monsoon activity 30 kyr -12 kyr arid 12 kyr - reestablishment of SW monsoon	Srivastava et al., 2001
NW 16	Jhanjhari (Vatrak River basin) (GJ)	Sediments/ litho-stratigraphic, textural analysis, mineral magnetic analysis	OSL 55 kyr – 26 kyr	100 kyr to 55 kyr – Fluvial deposition 55 kyr to 41 kyr – Aggradation by ephemeral fluvial processes under semi-arid conditions 41 kyr to 26 kyr – Fluvio-aeolian 26 kyr onward – Aeolian	Raj et al., 2016
NW 17	Dhordo, Berada (Great rann of kutch basin) (GJ)	Clay Mineralogy	C-14 17.7 – 7 kyr	Intensified monsoon (17.7 – 16.3 kyr), Monsoon became stronger before ~8.4 kyr	Khonde et al., 2016
NW 18	Sabarmati River Valley (GJ)	Sediments	OSL ~ 90 kyr, ~63 kyr	Enhanced monsoonal condition during MIS -5	Thokchom et al., 2017
NW 19	Kanjetha Cliff (GJ)	Sediment	C-14/ ~15 kyr	~15 kyr to 10 kyr – Humid climate 12.5 kyr – Enhanced Monsoon Phase	Lasker et al., 2010
NW 20	Eastern Arabian Sea (sk 128a – 30, and 31) (ArbS)	Sediments, Pollen	Oxygen isotopic chronology, C-14 dating Up to 200 kyr	MIS (2,4,6) glacial periods – Low precipitation, cold and dry climate MIS (1,3,5) interglacial periods – High precipitation, warm and wet conditions	Prabhu et al., 2004
NW 21	Mohhammadpura, Jaspur, Dabka etc. Mahi Basin (GJ)	Feldspar	IRSL 82 kyr – 10 kyr	Two phases of fluvial aggradations – first during Oxygen isotope sub-stage 5 and second from 50 kyr to 30 kyr – both represent a humid environment	Juyal et al., 2000
NW 22	Thar Desert (RJ)	Sand dunes, salt lakes, palaeosols, calcrete	C-14 and Th-Ur methods	Increased aridity during early quaternary, while it fluctuated from semi-arid to arid and vice versa during the Mid to Late Pleistocene	Raghvan, 1987
NW 23	Orsang River Valley (Bahadarpur, Aritha) (GJ)	Sediment chronology	90 kyr	90 – 70 kyr – Enhanced Monsoon 70 – 60 kyr – Weak Monsoon 60 – 30 kyr – Enhanced Monsoon	Juyal et al., 2006

NW 24	Bittoo Cave (HP) MD042861 (ArbS)	Speleothem Arabian sea marine core	Monsoon	MIS 5 – Intense Monsoon Precipitation MIS 4 – Decline in Precipitation MIS 3 – reestablishment of intense monsoon at the beginning of MIS 3 and a decline is observed at the end ~21 kyr – Minimum monsoon intensity observed	Kathayat et al., 2016 Caley et al., 2011
NW 25	Katoati (RJ)	Sediments/ OES Stable Isotope	OSL/ 95 kyr	MIS 5 -96- 60 kyr – humid environments MIS 4 – arid climate MIS 3 – humid climate	Blinkhorn et al., 2013,2015, 2017
NW 26	Sandhav (GJ)	Sediments/carbonates - Stable isotope	IRSL/ 114 kyr	C_4 vegetation with enhanced monsoon	Blinkhorn et al., 2019
NW 27	Ghaggar Hakra	Sediments	OSL/86 kyr – 4 kyr	Aggradation – 86 – 59 kyr	Select references in Sinha et al., 2020
NW 28	Arabian Sea core	Sediments	42 kyr -20 kyr	Lower surface productivity (a proxy for monsoon)	Singhvi and Kale, 2010
NW30	Sighvi Talav	Calcrete /Pollen	177-65 kyr	C_4 vegetation with humid climates	Blinkhorn et al., 2021

RJ – Rajasthan, GJ – Gujarat, ArbS – Arabian Sea

Table 3. Region-wise palaeoclimatic inferences in South Asia (Central Region = C Region)

Sr. No	**Site**	**Material/Proxies**	**Method/Age**	**Inferred Palaeoclimate**	**Reference**
C1	Son Valley (MP)	Grain polymineralic samples Shell Feldspar Sample correlation	IRSL, C 14 ~100 kyr (11870+- 120 yrs) (50 +- 6 kyr – 19 +-2 kyr)	Sihawal formation (>100 kyr) – Semi-arid characterized by erratic rainfall Clay layer of Sihawal formation (~100 kyr) – Formed in a relatively dry climate by low energy streams Patpara formation (58 kyr to 45 kyr) – Moist conditions followed by a return to drier conditions Baghor formation (39 kyr to 20 kyr) – formed due to an intermediate flow regime within a low sinuosity bed load channel Khetaunhi formation (10 kyr to 8 kyr) – Formed under less humid and more variable rainfall conditions.	Pal et al., 2005

C2	Middle Son Valley (Khunteli, Hirapur, Rehi)	Calcrete/Pollen	73 kyr	C_3 to C_4 vegetational change with a cold environment	Williams et al., 2009
C3	Lakadandh Swamp, Baikunthpur Forest Range of Koriya (CH)	Pollen	C-14/~ 12,785 – 9035 cal. Yrs. B.P.	Cool and dry climate (probably reduced precipitation)	Quamar and Bera, 2017
C4	Nitaya Village Hoshagabad (MP)	Pollen	C-14/12,700 – 7,150 cal. Yrs B.P	Cool and dry climate (probably reduced precipitation)	Quamar and Chauhan, 2012
C5	Southwestern Madhya Pradesh (Hoshangabad, Sehore, Harda and Betul) (MP)	Non-Pollen palynomorphs (Pollen)	Late Quaternary	Humid climate	Quamar, 2015
C6	Central Narmada Valley (MP)	Pollen	C-14/ ~ 32 kyr	32000 yr B.P. – cool and dry climate 30,500 to 24,500 yr B.P. – warmer and semi-arid climate 23,700 to 19,700 yr B.P. – extreme arid and cool climate	Verma and Rao, 2011
C7	Bhedaghat (MP)	Sedimentary Aggradation	C-14/ 25,160 kyr	Narmada catastrophic flood	Kale et al., 2003
C8	Hathnora (MP)	Pollen	C-14/24 kyr	Cool and dry conditions (24 kyr)	Patnaik et al., 2009
C9	Pratappur (OD)	Fossil teeth	C-14/ 17875 cal BP	Arid environments	Patnaik et al., 2019
C10	Baneta, Narmada Valley (MP)	Fossil teeth	AMS/ 16467 – 15660 cal BP	Arid environments	Jukar et al., 2019

MP – Madhya Pradesh, CH – Chhattisgarh, OD – Odisha

Table 4. Region-wise palaeoclimatic inferences in South Asia (Himalayan Region = H Region)

Sr. No.	Site	Material/Proxies	Method/Age	Inferred Palaeoclimate	Reference
H1	Goting, Garhwal (UK)	Calcite	C-14 42 kyr – 18 kyr	Increased rainfall due to enhanced southwest monsoon (40.2, 38.2, 36.2, 34.2, 32.7 and 29.4 kyr) where sharp, negative shifts in δ18O and δ13C of carbonates were observed. During (41.5, 37 and 35 kyr) short positive shifts in δ18O were observed, indicating a weakening of the southwest monsoon,	Ghosh et al., 2003
H2	Kashmir valley (Sankerpoora and khan sahib) (J&K)	Pedogenic carbonates	Late Pleistocene	Cold arid to semi-arid climate	Dar et al., 2015
H3	Lower Karewas (K)	Sediments Comparison	TL 110 kyr +-10 kyr	80 – 50 kyr – Humid conditions	Bronger et al., 1987
H4	Dun Valley (UK)	Sediments Aggradation	OSL 40 kyr – 10 kyr	26 kyr, 20 kyr – Intensified summer monsoon	Pandey et al., 2014
H5	Bhimtal-Naukuchiata Lake (UK)	Charcoal-rich muddy soil/ magneto Stratigraphy/carbon isotope	TL 25 kyr, 21 kyr	>40 kyr – Arid phase 25.6 kyr /21.5 kyr – Arid phase, between 40 kyr – 25 kyr, it was reported to be a humid phase	Kotlia et al., 1997
H6	Wadda Lake (esater Kumaun Himalaya)	Sediments, Pollens	C-14 35 -10 kyr	34,200 – 32,200 years B.P – humid climate 32,200 – 30,700 years B.P – dry climate 30,700 – 29,000 years B.P – warm and humid climate 29,000 – 21,700 years B.P – cool and arid climate 21,700 – 18,200 years B.P – humid climate	Kotlia et al., 2000
H7	Potwar (Pak)	Loess	TL /130 kyr – 18 kyr	Loess deposition	Rendell, 1988
H8	Peshawar (Pak)	Loess	TL /66 kyr – 30 kyr	Loess deposition	Rendell, 1988
H9	Garbayangbasin	Sediments,	OSL/20 kyr -10	20 kyr to 13 kyr – Glacial conditions, A short-lived relatively warm lacustrine	Juyal et al., 2004

	(UK)	magnetic susceptibility	kyr	environment around 13 kyr and cooler conditions at <13 kyr.	
H10	Indus River valley, between Nimo and Batalik (Ldkh)	Sediment	C-14/Up to 35 kyr	~35,000 – 26,000 BP (Lamayuru palaeolake) –Cold and Humid phase followed by the LGM 17,000 – 13,000 BP (Rizong palaeolake) – Deglaciation, rising temperatures and monsoonal activity 14,000 – 5000 BP (Khalsie Saspol palaeolake) – high temperatures and monsoon	Nag and Phartiyal, 2015
H11	Garbyang and Goting (UK)	Sediment, mineral magnetic, magnetic susceptibility	29 kyr to 10 kyr	Major cooling events at 18 kyr and 11 kyr.	Basavaiah et al., 2004
H12	Dokriani Valley, (Garhwal) (UK)	Glacio-lacustrine sediment,/ Palynology done	C-14/12,400 to 5,400 yr BP	12,406 and 10,633 cal yr BP – cool-dry	Bhattacharyya et al., 2011
H13	Ladakh (J&K)	Sediment	C-14/50 kyr - 25 kyr	Cold Climate, Limited Chemical weathering and rapid erosion (Lakes are formed by Damming of the Indus river and its tributaries	Phartiyal et al., 2005
H14	Naukuchiya Tal (UK)	Pollen	16 kyr	High Precipitation	Gupta, 1982
H15	Tso Kar (Ldkh)	Lacustrine Pollen, magnetic susceptibility, sedimentology	(ca.15.2 to 14 kyr BP) (12.9 and 12.5 kyr BP) (ca. 12.2–11.8 kyr BP)	Dry and cold conditions Improved moisture conditions Weak monsoon	Wünnemann et al., 2010
H16	Lamayuru (Trans-Himalaya)	Pollen, Palynology	C-14/35 kyr	>40 kyr – Semi-arid climate 35 kyr – Comparatively less arid 22 kyr – became more arid	Ranthora et al., 2007
H17	Tso kar (Ldkh)	Pollen	30 kyr – 9 kyr	>30,000 – prevalence of dry alpine steppe under the cold and dry climate regime 30,000 – 28,000 – a drastic change from cold and dry to warm and humid environments (Gupta et al., 1992) 28,000 – 24,000 – cold and dry climate 24,000 – 18,000 – warm and humid climate 18,000 – 12,000 – cold and dry climate	Bhattacharya 1989

H18	Khadmandu Valley (NPL)	Fossil Seeds	AMS /53,170 ± 820 yrs. BP and 49,300 ± 2100/1700 yrs. BP.	Subtropical to warm climate	Bhandari et al., 2009
H19	Rukti valley, Kinnaur (HP)	Palynological and magnetic susceptibility	~16.6 kyr –3.5 kyr	The climate was warm and moist during ~16.6 kyr and changed to cool ~at 13.3 kyr, followed by increasing Indian summer monsoon since ~11.5 kyr.	Ranhotra et al., 2018
H20	Bharatpur, Upper LahaulValley (Ldkh)	Varvite sediments/ magnetic susceptibility	C-14/~24.3 and 7.2 kyr BP	~ ca. 24.3 and 22.6 kyr BP – arid phase. ~ ca. 22.6–20.5 kyr BP – a slight increase in monsoonal precipitation ~ca. 20.5 to 18 kyr BP – decrease in precipitation ~ca.18 to 15.7 – warm and humid climatic ~ ca. 15.7 to 11.5 – cold event may correspond to the Younger Dryas (YD) which in turn is followed by a phase of maximum moisture of the Holocene Climate Optimum (HCO) (ca. ~11.5–7.2 kyr BP)	Bookhagen et al., 2005
H21	Satluj Valley (Northern Himalayas)	Lacustrine deposits, sediments	29 kyr	29 – 24 kyr – Intense precipitation	Bookhagen et al., 2005
H22	Lahul (Western Himalayas)	Drumlins	OSL/ 43 400 ± 10 300 and 36900 ± 8400 yr	Indicates that glaciers probably started to retreat between	Owen et al., 1997
H23	Frontal Himalaya, Yamuna Valley	Sediments	OSL/37 kyr to >2 kyr	Aggradation – 37-24 kyr and 15-12 kyr Incision – 24 kyr and 11 kyr	Dutta et al., 2012 in Sinha et al., 2020
H24	Alaknanda Valley	Sediments	OSL/49 kyr to 8 kyr	Aggradation – 49-25 kyr and 18-11 kyr Incision - <11 kyr	Select references in Sinha et al., 2020
H25	Upper Alaknanda Vbasin		MIS 4 (80-65 kyr)	Larger extension of the glacier than MIS 2 due to high precipitation	Singhvi and Kale, 2010
H26	Manasbal, Kashmir Valley	Loess like Palaeosol	OSL/ 41 kyr	MIS 3 – 41 kyr – wet climate	Babeesh et al., 2017
H27	Northwest Himalaya, Including Tso-Kar lake	Pollen/vegetation	77-10 kyr	77-10 kyr - Mostly Cold and arid with warm-moist fluctuations at 30-28 kyr, 21-18 kyr, 16 kyr and 10 kyr	Bhattacharyya, 1983 in Kar and Kumar, 2020

H28	Makaibagh, Kashmir Valley	Loess sediments	OSL/ ~65- 14 kyr	65.8 – 44 kyr – Moderate climatic conditions 44 – 43 kyr – Extreme dry/arid conditions 43 – 34.7 kyr - warm and moist climates 34.7 – 14.7 kyr – dry/arid climates	Shah et al., 2020
H29	Parvati valley, Kullu, HP	Pollen/Sediment/stable carbon isotope	OSL/ 15.1 kyr – 9.2 kyr	15.2 – 12.7 kyr – Cool and Moderate humid climate 12.7 – 9.2 Warm and humid climate	Khan et al., 2022
H30	Dwarahat Township, Kumaun, Central Himalaya	Stable Carbon Isotope on sediment profile	C-14 / 25,330 – 19797 Cal years BP	25 kyr – Warm and moist conditions 22-18 kyr – Arid conditions 15 kyr – Enhanced monsoon, moist and warm conditions	Sanwal et al., 2019

Uk – Uttarakhand, HP – Himachal Pradesh, Ldkh – Ladakh, NPL – Nepal, J&K – Jammu and Kashmir, K – Kashmir, Pak – Pakistan

Table 5. Region-wise palaeoclimatic inferences in South Asia (Northeast Region = NE Region)

Sr. No.	**Site**	**Material/Proxies**	**Method/Age**	**Inferred Palaeoclimate**	**Reference**
NE1	Ziro valley (AP)	Sediments/pollen	C-14/43 kyr - <20 kyr	An increase in SW monsoon from (43,000 cal. yr BP – 34,000 cal. yr BP) and after that decline is reported. The area experienced a peak warm and humid phase around 36,181 cal. yr BP – 34,145 cal. yr BP During (LGM) a decline in monsoon is evident when the forest turns into a savannah type.	Bhattacharyya et al., 2014
NE 2	Chandril Village (BAN)	Sediment and pedogenic carbonate correlation	Middle and Upper Pleistocene	Upper Pleistocene – Humid Climate	Alam et al., 1997
NE 3	Tarafeni Valley (WB)	Sediment, Pollen, fauna	18 kyr	Semi-aridity in the overall sub-humid phase	Basak et al., 1998
NE 4	Kamrup (Assam)	Pollen	C-14/~15 kyr to 10 kyr	14,895 to 12,450 cal BP – persistent fluvial activity 12,450 to 10,810 cal BP – Cool and dry climate with weakened monsoonal precipitation	Dixit and Bera, 2013

NE 5	Kolaghat (WB)	Pollen, Sediment	C-14/32 kyr , 7 kyr	8 Phases- fluvial – estuarine- estuarine with strong tidal effects, shallow marine- fluvial – fluvial with arid sub-phases- estuarine with moderate tidal effects- fluvial. Mangrove swamps	Hait et al., 1996
NE 6	Site 758 (BOB)	Marine core, Stable isotope 67characterise species	Late Pleistocene	MIS 5 – Intense Monsoon Precipitation MIS 4 – Decline in Precipitation MIS 3 – re-establishment of intense monsoon at the beginning of MIS 3, and a decline is observed at the end ~21 kyr – Minimum monsoon intensity observed	Bolton et al., 2013
NE 7	Ganol and Rongraam Valleys (MG)	Colluvial-alluvial deposits	~18 kyr	Excessive soil stripping caused by drier climatic conditions during LGM (~18 kyr)	Sharma, 2001
NE 8	Manipur valley (MN)	Fluvial and colluvial fans, morphological and lithological characters of sediments	Late Pleistocene	Arid climate during the terminal Pleistocene	Thokchom, 1987
NE 9	Bay of Bengal and the Andaman Sea	Sediment core	18.2 kyr and 14.8 kyr interval	Less precipitation	Rashid et al., 2011
NE 10	Darjeeling (WB)	Pollen	~50 kyr	46.4 – 31 kyr – Low monsoon and high temperature 31 kyr – 22.3 kyr – Higher precipitation and cooler temperature After 22.3 kyr – low temperature and low precipitation	Ghosh et al., 2015
NE 11	Ziro Lake basin	Pollen/ phytolith	C-14/ 19.5 kyr to Present	19.5 kyr – Humid Climate 19.5 -10 kyr – Cooler and drier	Ghosh et al., 2014 in Kar and Qumar, 2020

NE 12	Subankhata Swamp (Assam)	Pollen	C-14/ 27 kyr to present	~27 – 22 kyr – cool and dry climate 22 – 18 kyr – less cool and arid than the previous phase 18 – 14 kyr – warm and humid climate	Basumatary et al., 2014
NE13	Mawmluh Cave (Meghalaya)	Speleothem	U/Th	33,500–32,500 years B.P. – strong wet phase 26,000 to 23,500 years B.P. - a weak/dry phase from 17,000 to 15,000 years B.P. - a very weak phase 15000 – early Holocene onward – abrupt increase in monsoon	Dutt et al., 2015

MN – Manipur, MG – Meghalaya, BOB – Bay of Bengal, WB – West Bengal, BAN – Bangladesh, AP – Arunachal Pradesh

Table 6. Region-wise palaeoclimatic inferences in South Asia (Southern Region = S Region)

Sr. No.	Site	Material/Proxies	Method/Age	Inferred Palaeoclimate	Reference
S1	MD 76131, MD 77194 (ArbS)	Calcrete, pollen	Oxygen isotope /22 kyr	22 kyr to 18 kyr – Very arid period 11 kyr – humid period	Van Campo, 1986
S2	Coimbatore (TN)	Calcrete	C-14/21 kyr – 30 kyr	Warm and semi-arid conditions	Achyuthan et al., 2012
S3	Horton Plains (SL)	Pollen	AMS 24 kyr – 0.15 kyr	Relatively dry, humid conditions due to the monsoon regime, the onset of monsoon caused a semi-humid climate resulting in an expansion of the Upper Montane rain forest.	Premathilake et al., 2003
S4	Horton plains (SL)	Pollen, Spores, macrofossils	C-14	16,200 to 15900 yrs – rains 13,700 to 13,000 yrs – humid phase 13000 to 11,900 yrs – semi-arid	Premathilake et al., 2012
S5	Near Kanigiri town, Prakasham (ANP)	Sand Dunes (Sediments)	OSL /90 kyr to 1.7 kyr	Semi-humid landscape with short-lived arid phases (90 kyr, 45–48 kyr, 30–33 kyr, 21 kyr, 11 kyr,)	Reddy et al., 2013
S6	Nilgiri (TN)	Pollen	25 kyr, 15 kyr	Moist Climate	Gupta, 1982
S7	Vazhapally, Chaganachery (KL)	Pollen	80 kyr - >40 kyr	Anoxic fluvio-marine/estuarine depositional environments during warmer climates with the intensified Asian monsoon	Farooqui et al., 2010
S8	Sandynallah, Nilgiris (TN)	Pollen	C-14/Late Quaternary	Montane grasslands persisted in the area since ca. 30,000 yr B.P.	Vasanthy 1988

S9	Berijam lake (TN)	Pollen	C-14, /20 kyr	20 kyr -17 kyr – Dry spell (Cold and dry climate), 17 kyr – 14.5 kyr – Wet phase (Humid Climate), 14.5 kyr – 7 kyr – Wet Phase (Humid Climate)	Bera et al., 1996 (Kumar et al., 2017)
S10	Pravara River Basin (MH)	Shells and Gravels	C-14/Middle Pleistocene to Late Holocene	Arid Climate phases (40 – 25 kyr, 19 – 16 kyr, 13 – 10 kyr) OIS 3 – Strong Monsoon LGM (16 – 21 kyr) – Weak Monsoon with an arid climate Terminal Pleistocene (10 – 13 kyr) – Weak Monsoon with an arid climate	Sadakata et al., 1995
S11	Konkan coastal Belt (MH and Goa)	Elevated Lignite beds	50 kyr (tectonic Upliftment)	Warm to wetter climate due to upliftment	Powar et al., 1993
S12	Kanyakumari and Madapam (ECOI)	Aragonite of Pelycypods/shell	C-14, TL, ESR /38 kyr – 1 kyr	Flora from north of Madras – Indicate tropical climate Gypsum pseudomorphs in the inner shelf sediments off Masulipatnam bay of Krishna delta front indicate aridity during Late Pleistocene Certain mammals from quaternary sediments in Southeastern coastal Tamil Nadu suggest a warmer climate during the Pleistocene.	Vaidyanadhan and Ghosh, 1993
S13	Nirgudsar (Ghod Valley) (MH)	Fossil wood, Sediments	C-14/38 kyr -10 kyr	20 kyr – 10 kyr (Decrease in rainfall)	Kale and Rajaguru, 1989
S14	Nilgiri Hills (Peat) (TN)	Organic Matter/peat stable isotope	C-14/~40 kyr	40 kyr to 28 kyr (Monsoonal Precipitation) 28 kyr to ~16 kyr (Arid conditions)	Rajagopalan et al., 1997
S15	Kerala (KL)	Shell, Wood, Pollen, Sediments Stable isotope	C-14/46,570 ± 3,480 yrs BP and 20,600 ± 1,030 yrs BP	Heavy rainfall and wet climate during Late Pleistocene	Maya et al., 2017
S16	Krishna and its tributaries (MH)	Alluvial fills, calcretes, ferricretes	Late Pleistocene	No drastic climatic changes; semi-arid climate throughout the Late Pleistocene	Umarjikar, 1984
S17	Konkan coast (MH)	Littoral deposits	C-14/Late Quaternary	Sea level changes during Late Quaternary	Guzder, 1980
S18	Chaul and Sopra (MH)	Coastal sediments-beach rock	Late Quaternary	Sea level changes during Late Quaternary	Ghate, 1985
S19	Ghod valley (MH)	Alluvial fills-silt, gravel and Palaeontological records	Late Pleistocene	Semi-arid climate	Kajale, 1979

S20	Kerala (KL)	Littoral deposits	End Pleistocene	Aridity during the low sea level phase of the end Pleistocene	Rajendran, 1979
S21	Kangvai well (MH)	Fossil Flora (Coexistence approach)	Late Pleistocene (44 kyr)	Humid climate	Kumaran et al., 2013; Srivastava et al., 2015
S22	Fa Hien cave (SL)	Enamel Stable isotope	OSL/ 36 kyr	Wet climates	Roberts et al., 2017
S23	Jwalapuram (ANP)	Carbonate Stable isotope	77 kyr	a mixed C_3/ C_4 environment (Variable rainfall)	Haslam et al., 2010a
S24	Patne (MH)	OES Stable isotope	25 kyr	Arid	Baptista, 2012
S25	Belum Cave (ANP)	Speleothem	U-Th/ (108-99 kyr)	Abrupt reduction in monsoon rains during MIS 5c led to increased droughts	Allu et al., 2015 in Band and Yadava, 2020
S26	SK-129/CR-05 (Arb S)	Sediments	Oxygen isotope record of planktic foraminifera/MIS 6 –MIS 1	MIS 5a – Intense precipitation	Farooqui et al., 2014
S27	Kerala Coast	Sediment Core	C-14/42 kyr	Marine transgression at 42 - 40 kyr BP High Rainfall at > 40 kyr and 28 kyr Arid climate during LGM	Tiju et al., 2021

ANP – Andhra Pradesh, KL – Kerala, MH – Maharashtra, SL – Sri Lanka, ECOI – East coast of India, TN – Tamil Nadu, Arb S – Arabian Sea Core.

Table 7. Region-wise palaeoclimatic inferences in South Asia (Ganga Plains = GP Region)

Sr. No.	Site	Material/Proxies	Method/Age	Inferred Palaeoclimate	Reference
GP1	Ganga Plains a) Kalpi, b) IITK, c) Firozpur, d)Bhognipur (UP)	Carbonate nodules, Soil organic matter Stable isotope	OSL /100 kyr – 25 kyr	Three periods of intensified monsoon at 100 kyr, 40 kyr and 25 kyr. A decrease of 20% in rainfall during LGM.	Agrawal et al., 2012
GP 2	Kalpi Yamuna valley (UP)	Sediments	IRSL /45 kyr -40 kyr	Humid Climate	Tewari et al., 2002
GP 3	Kannauj (Ganga Valley) (UP)	Sediment Cores	OSL /MIS 5,4,3,2	Episodes of aggradations were recorded during MIS 5,4, the mid part of MIS 3, late MIS 3 (23 kyr -30 kyr) and Late MIS 2 to MIS 1 (11 kyr -16 kyr)	Roy et al., 2012
GP 4	Belan Valley(UP) Yamuna (UP)	Grain polymineralic samples, Shell	IRSL, C 14/ (90 +- 20 kyr – 16+-3 kyr) (15,540+- 540 yrs) (26,270+- 660 yrs)-(18,055+-150 yrs)	Unit I (>100 kyr) – Semi-arid 71 characterised by erratic rainfall Unit II (~100 kyr) – Formed in a relatively dry climate by low energy streams Cemented gravel II (58 kyr to 45 kyr) – Moist conditions followed by a return to drier conditions Upper gravel III & IV (39 kyr to 20 kyr) – formed due to an intermediate flow regime within a low sinuosity bed load channel	Pal et al., 2005
GP 5	Jalesar Tal, Unnao (UP)	Pollen, sediment	C-14/42,490 – 13,560 cal. Yrs B. P	Cool and dry climate	Trivedi et al., 2012
GP 6	Saini lake (UP)	Sediments, pollen	AMS C-14, Pollen, Geochemical /15 kyr	15 – 13 kyr – Dry Climate 13 – 5 kyr – Humid Climate	Sharma et al., 2006 (Kumar et al., 2017)
GP 7	Karela lake (UP)	Sediments, pollen	14 kyr	14- 12.5 kyr – Dry Climate 12.5 – 8.7 kyr – Humid Climate	Chauhan et al., 2015 (Kumar et al., 2017)
GP 8	Ganga Plains (UP)	Sediments	IRSL /76 kyr -22 kyr	The deposits of the Marginal Plain Upland Surface (MP) show evidence of a humid climate in 50 kyr to 40 kyr	Srivastava et al., 2003

GP 9	Ganga Plains (UP)	Mineralogical, Chemical, faunal, palynological, and teeth enamel	80 kyr – 1300 yrs	80 – 50 kyr BP, the climate in southern Ganga Plain was dry with a few humid cycles 50 – 25 kyr BP = High rainfall with short dry spells 25 – 13 kyr BP = Low rainfall 13 – 5 kyr BP = High rainfall	Singh, 2005
GP 10	Kalpi (UP)	Sediments	IRSL /76 kyr – 32 kyr	Moist grasslands (50 kyr – 40 kyr)	Singh, 2005
GP 11	Meerut and Yamuna Puram (western Ganga Plains)	Sediments; clay mineralogy	ISRL / 50- 30 kyr	50- 30 kyr - humid climate	Singh et al., 2003
GP 12	Sanai tal Lake (UP)	Shells and sediments	15 kyr – 11.5 kyr	Low rainfall (15 kyr – 13 kyr) (Lake formation) Aquatic plant taxa increase, sedges decline, and grasses dominate (13 – 11.5 kyr), probably high rainfall?	Sharma et al., 2004
GP 13	Belan Valley	Palaeosol, Calcium Carbonate, n-alkane	100 kyr to Present	100 – 75 kyr – Climates shift from arid to humid phase with mixed C_3- C_4 vegetation 75 – 25 kyr – Fluctuation in rainfall and transition from C_3- C_4 vegetation 25 – 18 kyr – Arid conditions 18 – Present – Strengthen monsoon	Jha et al., 2020
GP 14	Ganga plain, Rajaura, Lakhimpur Kheri, UP	δ13C values, χlf, pollen, phytoliths and non-Pollen Palynomorphs	AMS C-14, OSL/ 15.2 – 7 kyr	15.2 – 14.5 kyr – enhanced hydroclimatic conditions with good precipitation and overall humid climatic condition	Kumar et al., 2022

UP – Uttar Pradesh

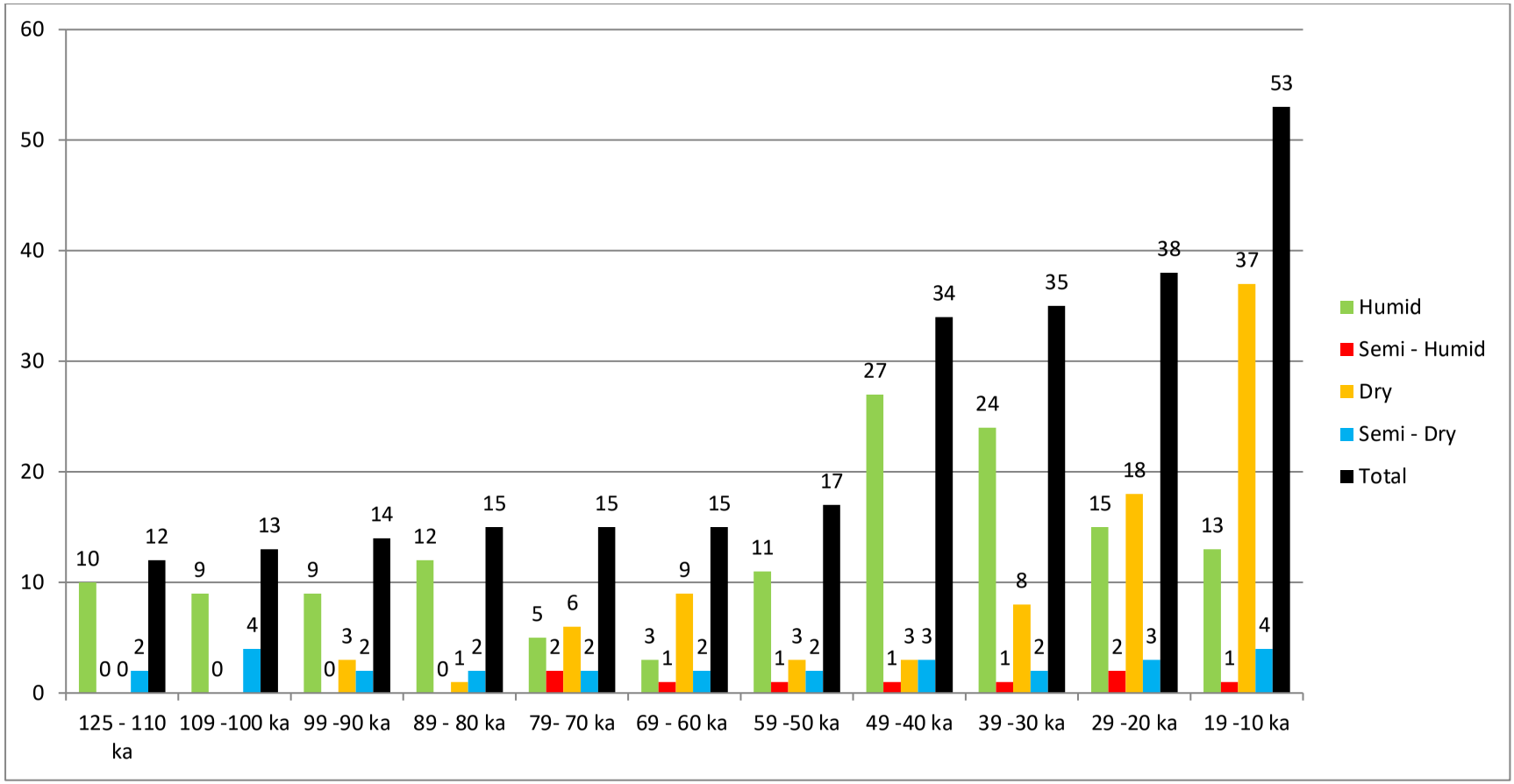

Figure 5. Graph representation of the number of studies with climatic inferences carried out per ten thousand years in Late Pleistocene South Asia

Table 8. Prehistoric archaeological sites with palaeoenvironment reconstructions (see Figure 4 for locations).

Sr. No.	Site	Age	Technology	Palaeoclimate	References
1	16 R	126- 70 kyr	Late Acheulean? Middle Palaeolithic	C_4 vegetation	Achyuthan et al., 2007
2	Sandhav	114 kyr	Middle Palaeolithic	C_4 vegetation with enhanced monsoon	Blinkhorn et al., 2019
3	Katoti	96-60 kyr	Middle Palaeolithic	Humid environments	Blinkhorn et al., 2017
4	Jwalapuram	80-38 kyr	Middle Palaeolithic	Mixed C_3/C_4 environment, Variable rainfall	Haslam et al., 2010a
5	Fa Hien cave	36 kyr	microlithic	Wet Climate	Roberts et al., 2017
6	Pratappur	17875 Cal BP	microlithic	C_4 arid environments	Patnaik et al., 2019
7	Singi Talav	177 – 65 kyr	Late Acheulean – Middle Palaeolithic	C_4 vegetation with warm and humid climates	Blinkhorn et al., 2021

| | | Time / Reference regionwise | Northwest region | | |

	Time / Reference regionwise	Himalayan region											
		Ranhotra et al. 2017	Bohra et al. 2017	Bookhagen et al. 2005	Owen et al. 1997	Dutta 2012 in Sinha et al. 2020	select ref. in Sinha et al. 2020	Singhvi and kale 2010	Babeesh et al. 2017	Bhattacharyya in 1983, Kar and Kumar 2020	Sanwal et al.2019	Khan et al. 2022	Shah et al. 2020
MIS1	10	8	1				29			1		35	
	11		21			29	18			21		35	
	12		21			18	18			21		35	
	13	21	21			18	18			21		37	
MIS2	14		21			18	18			21		37	2
	15		21				18			21	8	37	2
	16	1	1				18			1			2
	17		1				18			21			2
	18		1				18			1	2		2
	19		19							1	2		2
	20		19							1	2		2
	21		19							1	2		2
	22		8							21	2		2
	23		2							21			2
	24		2	8		29				21			2
	25			8		18	18			21	35		2
	26			8		18	18			21			2
	27			8		18	18			21			2
	28			8		18	18			1			2
	29			8		18	18			1			2
MIS3	30					18	18			1			2
	31					18	18			21			2
	32					18	18			21			2
	33					18	18			21			2
	34					18	18			21			2
	35					18	18			21			1
	36				28	18	18			21			1
	37				28	18	18			21			1
	38				28		18			21			1
	39				28		18			21			1
	40				28		18			21			1
	41				28		18		9	21			1
	42				28		18			21			1
	43				28		18			21			2
	44				28		18			21			2
	45				28		18			21			30
	46						18			21			30
	47						18			21			30
	48						18			21			30
	49						18			21			30
	50									21			30
	51									21			30
	52									21			30
	53									21			30
	54									21			30
	55									21			30
	56									21			30
	57									21			30
	58									21			30
	59									21			30
MIS4	60									21			30
	61									21			30
	62									21			30
	63									21			30
	64									21			30
	65								8	21			30
	66								8	21			30
	67								8	21			
	68								8	21			
	69								8	21			
MIS5	70								8	21			
	71								8				
	72								8				
	73								8				
	74								8				
	75								8				
	76								8				
	77								8				
	78								8				
	79								8				
	80								8				
	81												
	82												
	83												
	84												
	85												
	86												
	87												
	88												
	89												
	90												
	91												
	92												
	93												
	94												
	95												
	96												
	97												
	98												
	99												
	100												
	101												
	102												
	103												
	104												
	105												
	106												
	107												
	108												
	109												
	110												
	111												
	112												
	113												
	114												
	115												
	116												
	117												
	118												
	119												
	120												
	121												
	122												
	123												
	124												
	125												
	126												

Time	Northeast region									
	Bhattacharyya et al. 2014	Basak et al. 1998	Dixit and Bera, 2012	Bolton et al. 2013	Sharma, 2001(Deo et al. 2004)	Rashid et al. 2011	Ghosh et al. 2015	Ghosh et al. 2014 in Kar and Kumar 2020	Basumatary et al. 2014	Dutt et al. 2015
10			21				21	21		8
11			21				21	21		8
12			21				21	21		8
13			16				21	21		8
14			16			21	21	21	1	8
15							21	21	1	8
16							21	21	1	34
17							21	21	1	34
18		4			2	21	21	21	26	
19							21	21	26	
20	19						21	1	26	
21				2			21		26	
22				1			8		21	
23				1			8		21	34
24				1			8		21	34
25				1			8		21	34
26				1			8		21	34
27				1			8		21	
28				1			8			
29				1			8			
30				1			8			
31				1			21			
32				1			21			9
33				1			21			9
34	1			1			21			9
35	1			1			21			
36	8			1			21			
37	8			1			21			
38	8			1			21			
39	8			1			21			
40	8			1			21			
41	8			1			21			
42	8			1			21			
43	8			1			21			
44				1			21			
45				1			21			
46				1			21			
47				1						
48				1						
49				1						
50				1						
51				1						
52				1						
53				1						
54				1						
55				1						
56				1						
57				1						
58				1						
59				1						
60				2						
61				2						
62				2						
63				2						
64				2						
65				2						
66				2						
67				2						
68				2						
69				2						
70				1						
71				1						
72				1						
73				1						
74				1						
75				1						
76				1						
77				1						
78				1						
79				1						
80				1						
81				1						
82				1						
83				1						
84				1						
85				1						
86				1						
87				1						
88				1						
89				1						
90				1						
91				1						
92				1						
93				1						
94				1						
95				1						
96				1						
97				1						
98				1						
99				1						
100				1						
101				1						
102				1						
103				1						
104				1						
105				1						
106				1						
107				1						
108				1						
109				1						
110				1						
111				1						
112				1						
113				1						
114				1						
115				1						
116				1						
117				1						
118				1						
119				1						
120				1						
121				1						
122				1						
123				1						
124				1						
125				1						
126				1						

Time	Southern region																		
	Van Campo 1986	Achyuthan et al. 2012	Premathilake et al. 2012	Reddy et al. 2013	Gupta, 1982	Farooqui et al. 2010	Bera et al. 1996 (Kumar et al. 2017)	Sadakata et al. 1995	Powar et al. 1993	Kajale and Rajaguru, 1989	Rajagopalan et al. 1997	Maya et al. 2017	Kumaran et al. 2013; Srivastava et al. 2015	Roberts et al. 2017	Haslam et al. 2010	Baptista et. al, 2012	Allu et al in Band and Yadava et al. 2020	Tiju et al. 2021	Farooqui et al. 2014
10				3			9	2		19									
11	1		4	2			9	2		19									
12			4	3			9	2		19									
13			4	3			9	2		19									
14			1	3			9	2		19									
15				3	1		9	2		19									
16			8	3			9	2		19	2								
17				3			21	2		19	2								
18	2			3			21	2		19	2								
19	2			3			21	2		19	2							2	
20	2			3			21	2		19	2	8						2	
21	2	4		2							2							2	
22	2	4		3							2							2	
23		4		3							2							2	
24		4		3							2								
25		4		3	1			2			2					2			
26		4		3				2			2								
27		4		3				2			2								
28		4		3				2			8								
29		4		3				2			8								
30		4		2				2			8								
31				2				2			8								
32				2				2			8								
33				2				2			8								
34				3				2			8								
35				3				2			8								
36				3				2			8			9					
37				3				2			8								
38				3				2			8								
39				3				2			8								
40				3		8		2			8								
41				3		8		8											
42				3		8		8										36	
43				3		8		8											
44				3		8		8					1						
45				2		8		8											
46				2		8		8				8							
47				2		8		8											
48				2		8		8											
49				3		8		8											
50				3		8		8	9										
51				3		8		8											
52				3		8		8											
53				3		8		8											
54				3		8		8											
55				3		8		8											
56				3		8		8											
57				3		8		8											
58				3		8		8											
59				3		8		8											
60				3		8		8											
61				3		8													
62				3		8													
63				3		8													
64				3		8													
65				3		8													
66				3		8													
67				3		8													
68				3		8													
69				3		8													
70				3		8													
71				3		8													
72				3		8													
73				3		8													
74				3		8													
75				3		8													
76				3		8													
77				3		8									31				
78				3		8													
79				3		8													
80				3		8													8
81				3															8
82				3															8
83				3															8
84				3															8
85				3															8
86				3															8
87				3															8
88				3															8
89				3															8
90				2															8
91																			
92																			
93																			
94																			
95																			
96																			
97																			
98																			
99																	19		
100																	19		
101																	19		
102																	19		
103																	19		
104																	19		
105																	19		
106																	19		
107																	19		
108																	19		
109																	19		
110																			
111																			
112																			
113																			
114																			
115																			
116																			
117																			
118																			
119																			
120																			
121																			
122																			
123																			
124																			
125																			
126																			

Time	Ganga plain region											
	Agrawal et al. 2012	Tiwari et al. 2002	Trivedi et al. 2012	Sharma et al. 2006 (Kumar et al. 2017)	Chauhan et al. 2015 (Kumar et al. 2017)	Srivastava et al. 2003	Singh 2005	Singh 2005	Singh et al. 2013	Sharma et al. 2004a	Kuamr et al. 2022	Jha et al. 2020
10				1	1		8			8		8
11				1	1		8			8		8
12				1	2		8			8		8
13			21	2	2		19			19		8
14			21	2	2		19			19	8	8
15			21	2			19			19	8	8
16			21				19					8
17			21				19					8
18			21				19					2
19			21				19					2
20	19		21				19					2
21			21				19					2
22			21				19					2
23			21				19					2
24			21				19					2
25	8		21				8					2
26			21				8					33
27			21				8					33
28			21				8					33
29			21				8					33
30			21				8		1			33
31			21				8		1			33
32			21				8		1			33
33			21				8		1			33
34			21				8		1			33
35			21				8		1			33
36			21				8		1			33
37			21				8		1			33
38			21				8		1			33
39			21				8		1			33
40	8	1	21			1	8	32	1			33
41		1	21			1	8	32	1			33
42		1	21			1	8	32	1			33
43		1				1	8	32	1			33
44		1				1	8	32	1			33
45		1				1	8	32	1			33
46						1	8	32	1			33
47						1	8	32	1			33
48						1	8	32	1			33
49						1	8	32	1			33
50						1	2	32	1			33
51							2					33
52							2					33
53							2					33
54							2					33
55							2					33
56							2					33
57							2					33
58							2					33
59							2					33
60							2					33
61							2					33
62							2					33
63							2					33
64							2					33
65							2					33
66							2					33
67							2					33
68							2					33
69							2					33
70							2					33
71							2					33
72							2					33
73							2					33
74							2					33
75							2					1
76							2					1
77							2					1
78							2					1
79							2					1
80							2					1
81												1
82												1
83												1
84												1
85												1
86												1
87												1
88												1
89												1
90												1
91												1
92												1
93												1
94												1
95												1
96												1
97												1
98												1
99												1
100	8											1
101												
102												
103												
104												
105												
106												
107												
108												
109												
110												
111												
112												
113												
114												
115												
116												
117												
118												
119												
120												
121												
122												
123												
124												
125												
126												

Figure 6. Compilation of Late Pleistocene palaeoclimate reconstructions carried out in the Subcontinent. CODES: 1-humid; 2-arid; 3-semi-humid; 4- semi-arid; 5- less arid; 6- semi humid to semi-arid;7- low lake level with large fluctuation and variable salinity; 8- monsoon strengthening /strong monsoon; 9- wet; 10- aeolian phase; 11-channel activation phase;12-unstable climate;13- hyper-saline; 14- wet-semi-arid; 15- rapid transition from glacial to post glacial climate; 16- fluvial deposition; 17- fluvio-aeolian; 18- aggradation; 19- weak monsoon; 20- low surface activity (a proxy for monsoon); 21- cool and dry climate; 22-flood; 23- deglaciation; 24- cooling event; 25-cold climate; 26- less arid; 27- subtropical to warm; 28- glacier retreat; 29- incision; 30- moderate climatic conditions; 31- C_3/ C_4 plants; 32- moist grasslands; 33- fluctuation in rainfall; 34- weak and dry phase; 35- warm and moist/humid; 36- Marine transgression; 37- cool and moderate humid climate; C_3 - high C_3 plants; C_4 - high C_4 plants.

3 Study Area and Background

3.1 Sonbhadra

Lying between 23.52 and 25.32°N latitude and 82.72 and 83.33°E longitude, Sonbhadra District is the second largest district in Uttar Pradesh; it extends from north to south with a maximum length of 79.36 km and 74.56 km in the east-west direction covering an area of approximately 6788 km^2. Sonbhadra District is bounded by the districts of Rohatas (Bihar) and Palamu (Jharkhand) in the east, while the Sarguja District of Chhattisgarh and the Sidhi District of Madhya Pradesh form the southern and western boundaries, respectively. Administratively, the district is divided into eight blocks, i.e., Robertsganj, Ghorawal, Chatara, Nagawa, Chopan, Meyorpur, Dudhi and Babhani.

Sonbhadra District has the highest percentage of forest cover in Uttar Pradesh. The district has 35.29% forest cover, with 138.32 km^2 of very dense forests, 940.62 km^2 of moderately dense forests, and 1357.81 km^2 of open forests. The district also has scrub forests covering 30.18 km^2 (ISFR, 2021).

The part of the district north of the Son River lies in the dry deciduous forest ecoregion of the Lower Gangetic plains. The portion south of the Son lies in the Chhota Nagpur dry deciduous forests ecoregion. The Kaimur Wildlife Sanctuary is located primarily within the district, generally reaching east and west along the spine of the Kaimur Range and extending to the Son River at its eastern end.

The temporal pattern of land use shows forest (48.01%), barren cultivable wasteland (2.02%), present fallow land (6.28%), other fallow lands (2.91%), barren and non-cultivable land (1.92%), land put to non-agricultural use (8.44%), pasture land (0.03%), bush, forest and gardens (6.67%) and Net sown area (23.73%).

The year is divided into winter (November to February), summer (April to mid-June) and rainy (late June to October) seasons due to the tropical monsoon climate. The average monthly minimum temperature ranges from 13.4 ° C to 30.7 ° C, while the average monthly maximum temperature ranges from 23.4 ° C to 40.2 ° C. Due to the southwest monsoon, approximately 87% of the total annual precipitation (mm) falls during the wet season, which lasts approximately three months. Average precipitation ranges from 850 to 1300 millimetres, and approximately 85% of annual precipitation occurs during the rainy season of the southwest monsoon (Sunita and Meenal, 2013).

3.2 Flora and Fauna

The region north of the Son River is part of the humid deciduous forest ecoregion of the Lower Gangetic plains. The ecoregion of the Chhotanagpur Plataeu is a dry deciduous forest that forms the area south of the Son River. The northern section of the district is part of the Vindhyan Range Plataeu and is flooded by tributaries of the Ganga River, such as the Belan and Karmanasha rivers. The Son River, which flows from west to east through the district, is located south of the steep escarpment of the Kaimur Range. The southern half of the district is hilly, with fertile stream valleys intermingled. The entire area is covered with scrub vegetation and thick forests in some places. A consistent horizontal stratification of rocks characterises almost the entire plateau. The top of the plateau is unfavourable for the growth of broad-leaved plants and is characterised by homogeneous scrubby dry vegetation. Broad-leaved plants are commonly found on the slopes of the plateau. The forest is mainly dry deciduous, but there are few evergreen trees in the ravines. The forest type in the Sonbhadra District is dry tropical deciduous, according to a new classification of forest types in India by Champion and Seth (1968). Due to the variable plains, slopes, hills, and climate of the district, the entire region offers a remarkable range of flora and vegetation, represented by dry

deciduous vegetation, natural scrub, jungle, grass patches and dense forests. The entire district is densely forested, with trees at the top, shrubs in the intermediate, herbs, climbers, and twiners at the ground level; identified 705 angiosperm species in 459 genera and 110 families, including 78 cultivated species that had been established in the region for various purposes. That has a land area of 500.73 km^2 in the semi-arid zone of northern India (Rodgers et al., 2000) with a geographical extent of 82°20' 15" E to 24°52' 00" N and 83°08' 23" E to 24°27' 51" N.

The Kaimur Wildlife Sanctuary in the district is separated into four administrative ranges: Halia, Ghorawal, Robertsganj, and Gurma. Geologically, most of the sanctuary's topography is mountainous and undulating. The soil of this area is red clay, which is hard and ferruginous in composition. The dry bamboo brakes make up the bamboo forest, and the scrub forest is surrounded by open dry scrubby vegetation. On the other hand, the dry deciduous forest comprises mixed dry deciduous woody species. (Biodiversity Impact Assessment Report, 2019, OCBTL, Bareilly, Uttar Pradesh).

3.3 General Geology

Geologically, the district comprises diverse rock formations, including Chhotanagpur Granite Gneiss Complex (CGGC), Vindhyan Supergroup and Gondwana Supergroup, and younger alluvium ranging in age from Archaean to sub recent. The oldest exposed rock (CGGC) in Sonbhadra District belongs to the Archaean age, occupying the southernmost part of the Dudhi Tahsil, covering an area of 1694 km^2. Since they are the bases for successive younger rocks, they are also known as the basement rocks of the basement complex (granite, amphibolite, magnetite, gneisses, and mica-schist). The Vindhyan Supergroup comprises the Mahakoshal Group (slate, phyllites, dolerite dykes, sandstone), the Semri Group (limestone, sandstone, porcellanite, shale) and the Kaimur Group (sandstone, shale, minor carbonates);

the Gondwana Supergroup (sandstones and shales) and Quaternary alluvium of the Son River and associated tributaries consist of gravels, sand, silt and clay. The Vindhyan Supergroup comprises stratified, metamorphosed groups (Semri and Kaimur) of rocks mainly represented by sandstones, shales, and limestones-porcellanitic rocks (*Table 9*). Lower Vindhyan rocks consist mainly of limestone, shales, sandstone and porcellanitic beds. In the study area, these outcrops are located in the Son Valley, which occupies approximately 653 km^2 of area. The Gondwana Supergroup overlies the Vindhyan rocks and is divided into two subgroups: 1) the Lower Gondwana and 2) the Upper Gondwana. The Sonbhadra District is occupied by Lower Gondwana, which consists of carbonaceous shales and coal seams. In general, the Lower Gondwana in Sonbhadra is spread over about ~259 km^2 and is of very little importance in the development of topography, and more than 90% of this outcrop forms the bottom of the G.B. Pant Sagar Reservoir (Census of India, Sonbhadra, 2011; Maharana and Tripathi, 2018).

The Vindhyan Supergroup comprises the Semri and Kaimur Groups; archaeologically, both groups are essential and well-exposed *(Figure 7-9)* in the region. 1) Semri Groups consist of different rocks from which porcellanite is used as the primary raw material for making Palaeolithic artefacts, and 2) in the Kaimur Groups, the Kaimur sandstone is used for the depiction of prehistoric and younger art in the region.

Table 9. Stratigraphic succession of Sonbhadra (after Census of India, Sonbhadra 2011; Maharana and Tripathi 2018).

Group	**Sub-groups & Formation**	**Lithology**	**Period**
Quaternary	Alluvium	Sand, Silt and Clays	Recent
Gondwana Supergroup		Shale and Coal	Permo-Carboniferous
----------Unconformity----------			
Vindhyan Supergroup	Kaimur	Sandstone, shale, minor carbonates	Neoproterozoic
	Semri	Limestone, Sandstone, Porcellanite, Shale	Meso - Proterozoic
----------Unconformity----------			
	Mahakoshal Group	Slate, Phyllites, Dolerite dykes, Sandstone	Palaeo- Proterozoic
----------Tectonic Contact----------			
Chhotanagpur Granite Gneiss Complex (CGGC)		Granite, Amphitotite, Magnatite, Gneisses, mica-schist	Archean

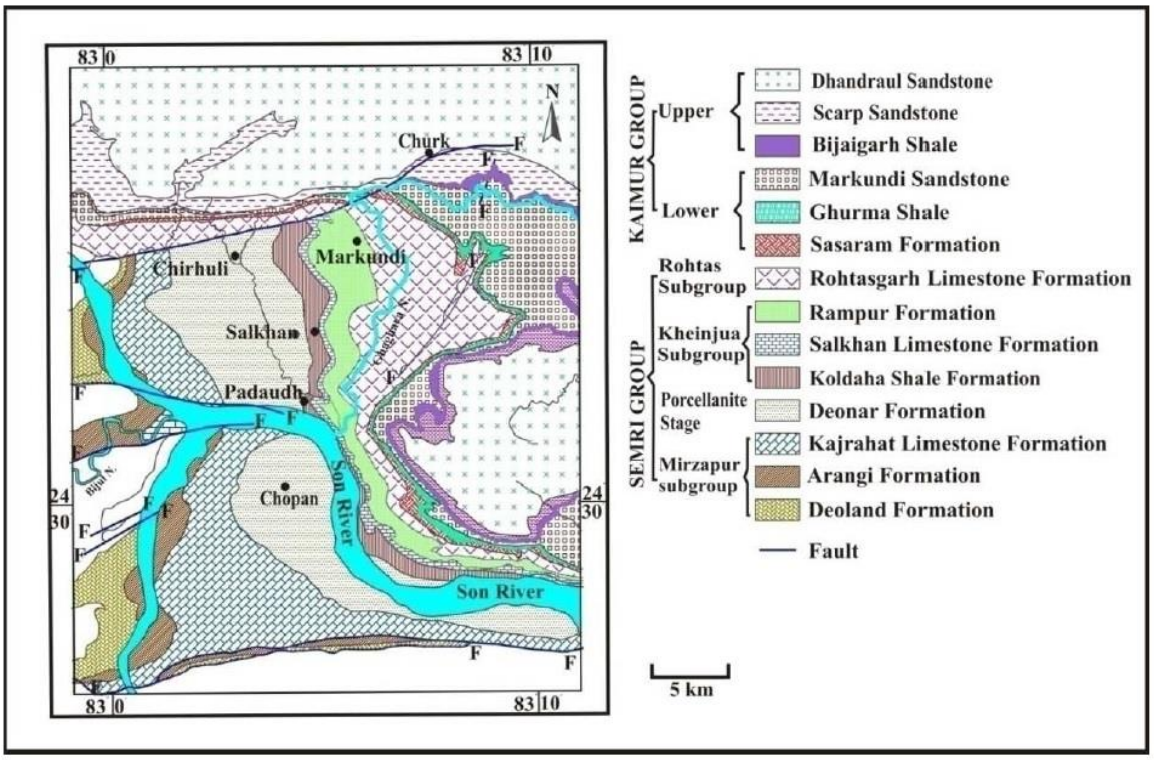

Figure 7. Detailed geological map of Vindhyan Supergroup in and around Sonbhadra and Mirzapur districts, U.P., India (modified after Auden, 1933).

Semri Group – It overlies Mahakoshal in the Son Valley by distinctive mappable units such as Patherwa, Arangi, Kajrahat, Chopan Porcellanite, Kheinjua shale, Fawn limestone, Glauconitic sandstone, and Rohtas limestone. The Chopan porcellanite unit is the primary source of Palaeolithic raw material.

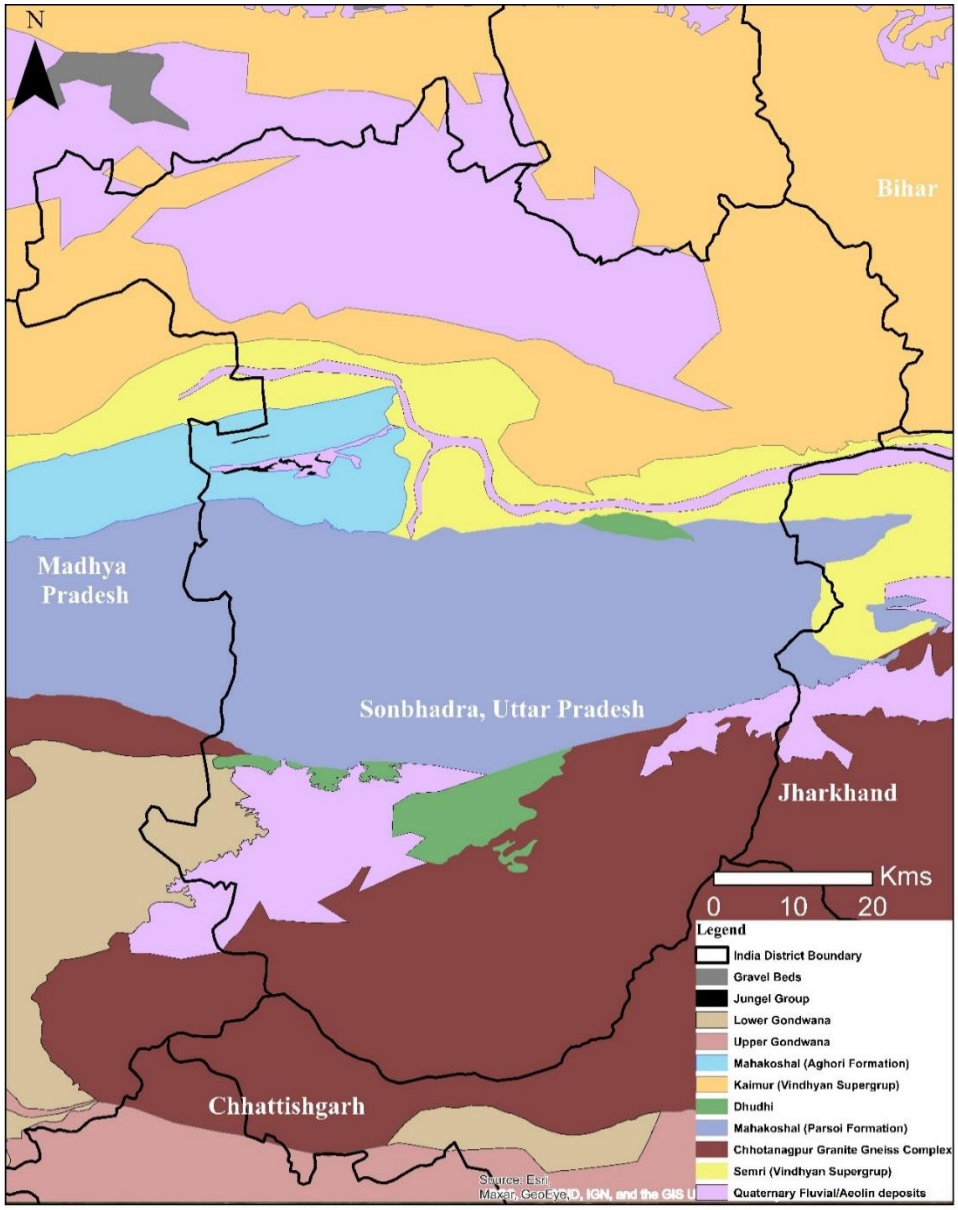

Figure 8. Detailed geological map of Vindhyan Supergroup, Group and Formations in and around Sonbhadra, Uttar Pradesh.

3.4 Raw Material

Porcellanite rocks (an impure form of chert) constitute an essential formation of the Lower Vindhyan (Semri Group) stretching over a distance of 380 km in the Son Valley region, extending from Palamu District of Jharkhand towards the east and Sidhi District of Madhya Pradesh in the west (Mehrotra and Banerjee 1983; Srivastava et al., 2003). It is associated with tuffaceous shale, sandstone, pyroclastic breccia, banded cherty rock and porcellanite.

The Porcellanite Formation is attested to be of explosive origin by many earlier workers (Auden, 1933; Chakrabarti et al., 2007; Ghosh, 1971; Law, 1954; Mishra et al., 2017; Srivastava, 1977; Singh and Srivastava, 1982). This formation is referred to as Chopan Porcellanite (in the eastern part) and Deonar Porcellanite (in the western part) of the Vindhyan Supergroup exposed in the Son Valley (Bhattacharyya, 1996).

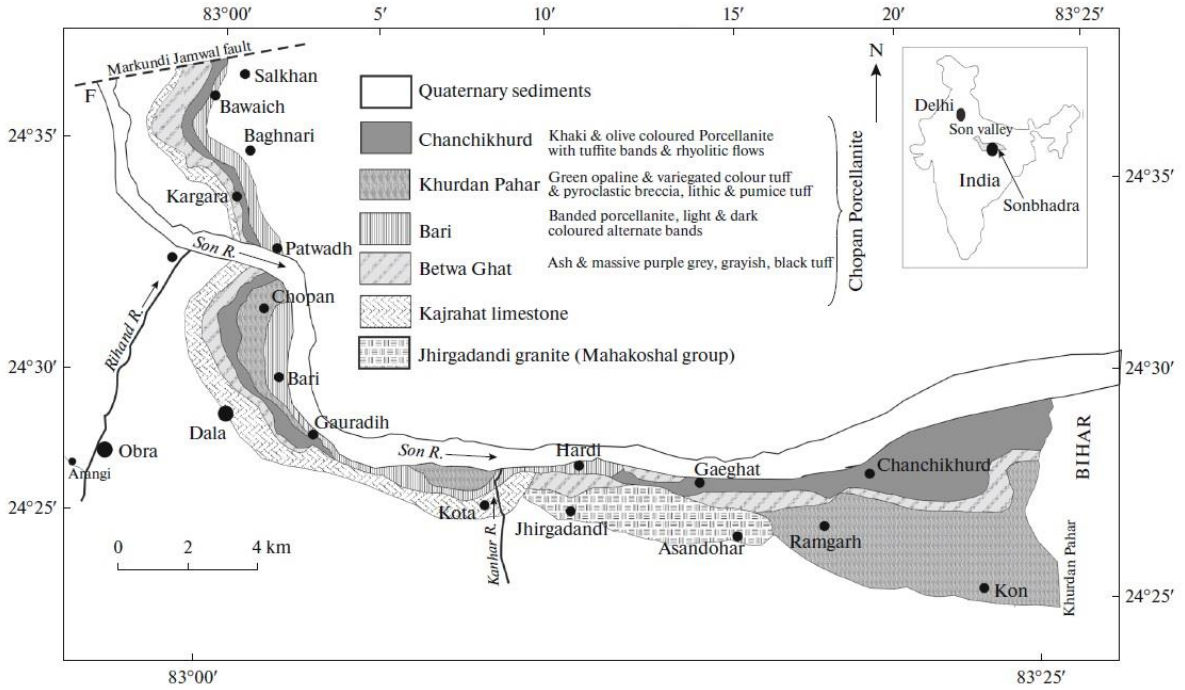

Figure 9. Geological map of Chopan Porcellanite along Son River (modified after Srivastava et al., 2003

The Chopan Porcellanite Formation (CPF) comprises pyroclastics of mainly tuffaceous sediments that occur in both massive and banded varieties. The black and white bands in the banded porcellanite are parallel to the general strike of the Vindhyan Supergroup. The banded variety of porcellanite constitutes 80% of the total porcellanite exposure in Son valley. Massive tuffaceous sediments occur in variegated colours ranging from opaline green, grey, buff, olive green, bluish grey and black. In the area around Kone, massive black and buff varieties of tuffaceous porcellanite are exposed (*Figure 10-11*) (Srivastava et al., 2003).

Figure 10. a) Different shapes and sizes of porcellanite clasts available in the study area, b) porcellanite clast representing the original colour in the centre (dark olive/black) and outer cortex in yellow (Site: Doma).

Figure 11. Exposure of Semri Group (porcellanite) near Sugwa Ghati.

The compact massive black porcellanite is thickly bedded, and quartz phenocrysts and calcite-filled vesicles can be observed with the naked eye. The buff-coloured porcellanite is thinly bedded. The thin section study indicates that the black and buff-coloured massive porcellanite are welded to ignimbrites displaying various textures such as spherulitic and porphyritic (Mishra et al., 2017).

3.5 The Son River and its drainage

The Son River is a significant tributary of the Ganga River and covers a course of 784 km. Its basin stretches from 22°37′58.6″ N to 25°43′48.12″ N latitude and 80°5′35.68″ E to 84°58′31.47″ E longitude. The basin area is ~68 km^2 and includes parts of Madhya Pradesh, Uttar Pradesh, Bihar and Jharkhand. The Son River originates from the Amarkantak hills of

the Maikal range at an elevation of ~600 m in Madhya Pradesh, and it flows north-northwest through Madhya Pradesh and turns east after encountering the southwest-northeast running Kaimur range of Vindhyan Supergroup and covers Sonbhadra District of Uttar Pradesh and merges with the Ganga River in Patna, Bihar (Rai et al., 2017; Maharana and Tripathi, 2018). The Son has been known to change its course, as is noticeable from numerous old beds near its east bank. The valley itself owes its formation partly to tectonics and partly to the action of the river. In these areas, tributaries of Son discharge their waters and sediments, forming accordant junctions from the right hand and a complex one from the left *(Figure 12,13).* In general, the valley is flat, with high walls of the highlands that overlook it from the north and south, differing significantly in the nature of their local elevations (Rai et al., 2017).

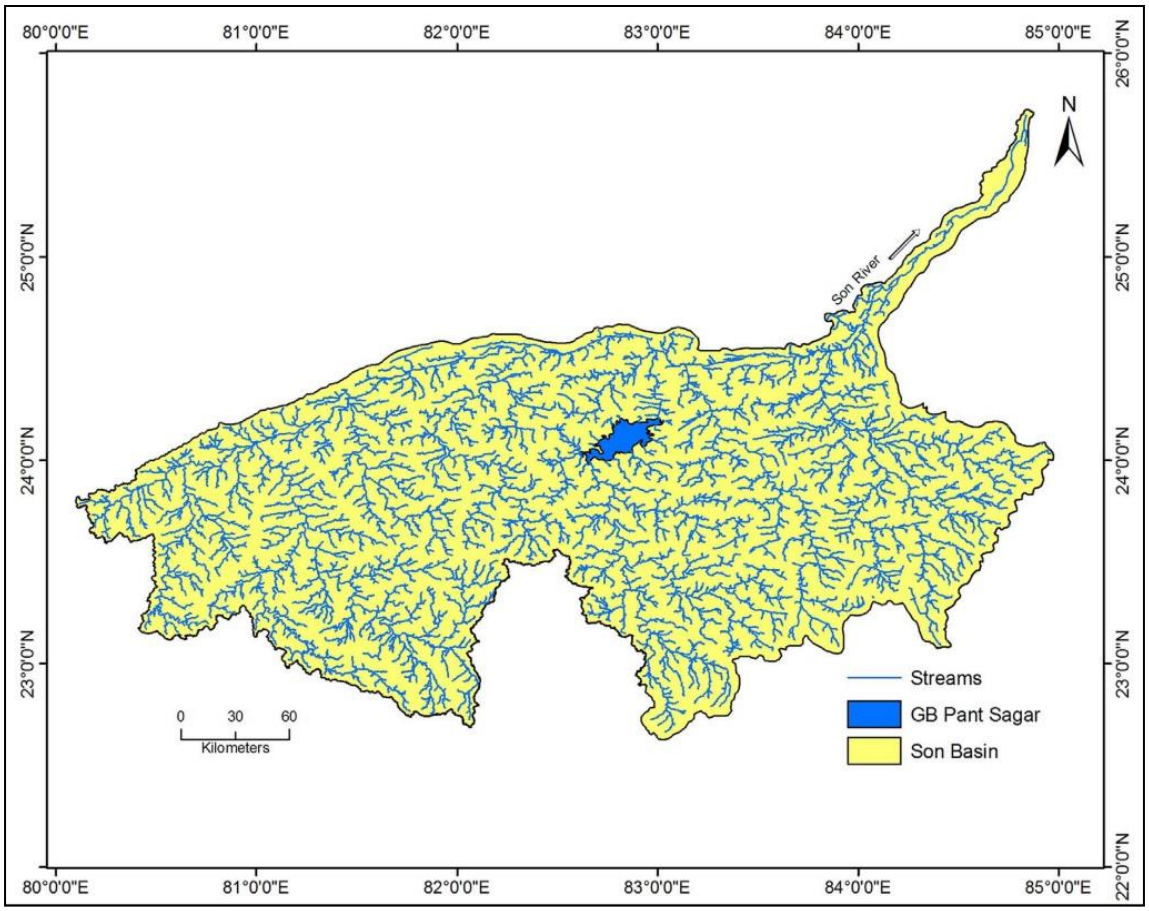

Figure 12. Drainage network within Son Basin (after Rai et al., 2017).

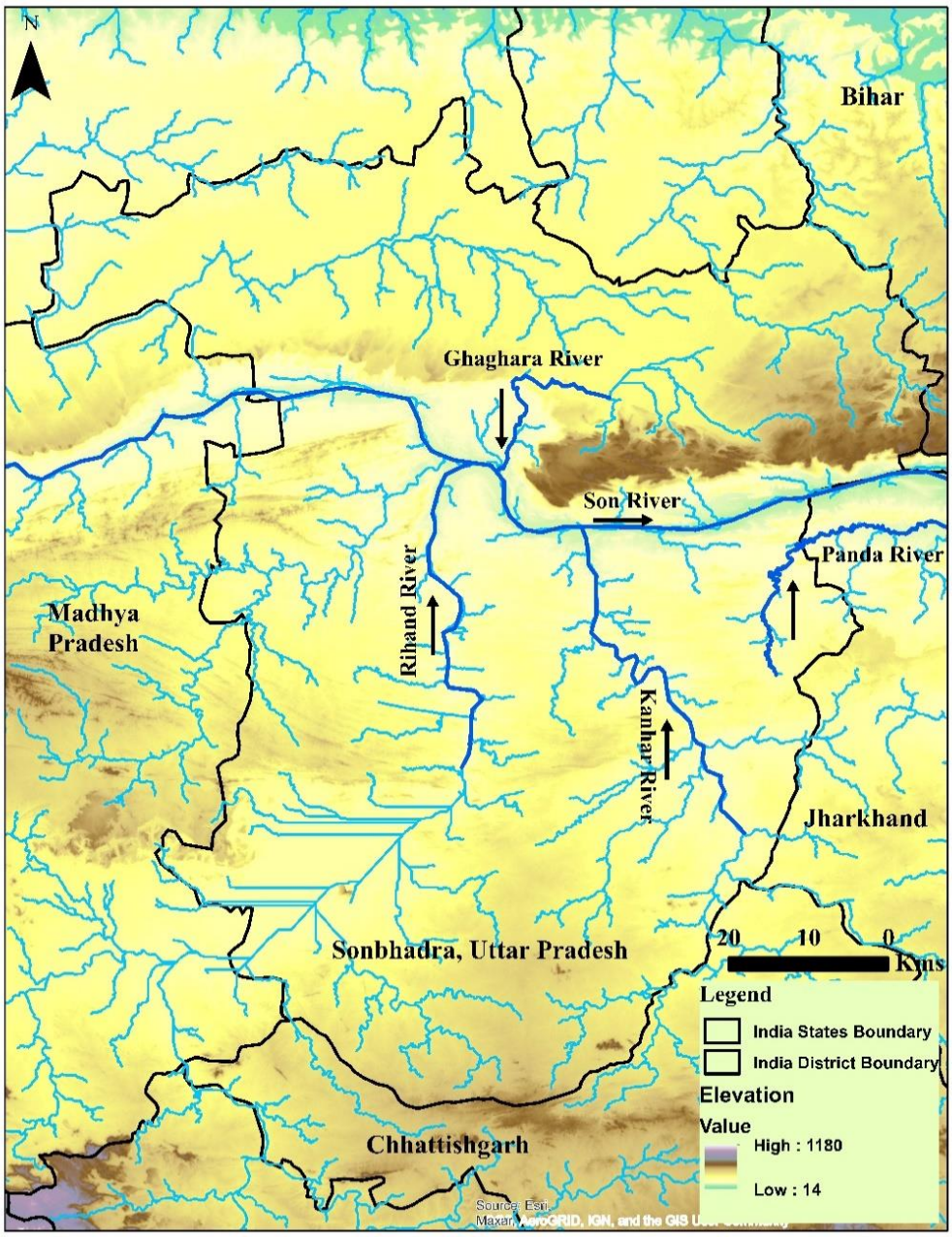

Figure 13. Drainage pattern and elevation in Sonbhadra, Uttar Pradesh.

3.5.1 Drainage System

3.5.1.1 Karamnasa River

It begins near Sarodag, on the northern side of the Shahabad continuation of the eastern Kaimur and flows approximately 26 km west to Rohtasgarh in Bihar. It flows from north to

south through rocky and forested terrain in the Sonbhadra, Chanduli and Varanasi Districts of Uttar Pradesh. It is a border between Uttar Pradesh and Bihar for a considerable distance and consists of the Nagwa Block and the eastern part of the Chatara Block of Sonbhadra District (Tewari, 2013).

3.5.1.2 Ghaghar River

The Ghaghar River is a tributary of the Son River; it starts in Pargana, Vijaygarh and joins Son near Markundi Valley after flowing through Nagwa Block. The Dhandraul dam was built on Ghaghar in 1917 to help with irrigation.

3.5.1.3 Rihand River

The Rihand River is also a tributary of the Son River that flows through Chhattisgarh, Uttar Pradesh and Madhya Pradesh in India. The Rihand River Basin has three sub-basins: Moran, Mahan, and Ghunghutta. The Rihand River originates in the Matiranga hills, southwest of the Mainpat plateau, approximately 1100 m above mean sea level. The river flows roughly north for 160 km through the central Surguja District. It flows north into Sonbhadra District, Uttar Pradesh, via Singrauli District of Madhya Pradesh, known as Rhed, before joining the Son (Kumar et al., 2018; Verma and Patel, 2021).

3.5.1.4 The Kanhar River

The Kanhar River is an important Son tributary; it flows through Chhattisgarh, Jharkhand and Uttar Pradesh, covering an area of 5,654 km^2. The Kanhar originates at Gidhadhodha on the Khudia plateau in the Jashpur District of Chhattisgarh. It initially flows north, forming the boundary with Garhwa District in the Palamu division of Jharkhand. After that, it flows about 100 km through the Surguja District of Chhattisgarh. Subsequently, it runs parallel to the Son River in Garhwa District, turns northwest, and flows through the Sonbhadra district in the Mirzapur division of Uttar Pradesh. The Kanhar River confluences with the Son River

northeast of the Kota village. The elevation of the basin ranges from a low height of 180 m, where the Kanhar meets the Son River, to 1,223 m (Gaurlpat) at Kavradara in Sarguja District of Chhattisgarh. The tributaries of the Kanhar River are Pangan, Thema, Lauwa, Malia, Pandu, Goitha, Banki, Hathi nala[3], Suria, Chana, Sendur, Kursa, Galphulla, Semarkhar Rigar, Cherna nala (Rao 1975; Rai 2017; Maharana and Tripathi, 2018).

3.5.1.5 The Panda River

Panda River, one of the tributaries of the Son River, is in the Chopan block of Sonbhadra District and has a drainage area of 216 km^2. Panda originates near Kuarava village in Sonbhadra district and flows northward, eventually meeting Son in Garhwa district, Jharkhand (Raju et al., 2011).

3.6 Son Valley and its Archaeological background

From an archaeological perspective, the Son Valley can be divided into three parts; 1) Upper Son Valley, 2) Middle Son Valley (Sidhi district) and 3) Lower Son Valley (Sonbhadra district, Uttar Pradesh). Prehistoric explorations in the region started in the early 1960s in the Upper Son Valley, including the districts of Jabalpur, Shahdol, Sidhi, and Bilaspur (Bilaspur is now in Chhattisgarh). A total of 65 Stone Age sites belonging to the Early, Middle, and Later Stone Age have been located in Upper Son Valley, including the famous sites of Nakjhur Khurd, Sihawal, Bahgor Ramnagar (all in Sidhi District in the 1960s) (Ahmad, 1984). Later, in the 1980s, Son Valley in Sidhi district was termed Middle Son Valley.

In the early 1980s, extensive palaeoanthropological, archaeological, and geological research was carried out in the Middle Son Valley (mainly in the Sidhi District of Madhya Pradesh),

[3] Nala = small seasonal stream

leading to the discovery of more than 6000 animal fossils, at least 47 Lower Palaeolithic, 86 Middle Palaeolithic, and 120 Upper Palaeolithic sites and ash deposits from the 74,000-year-old Toba supereruption *(Figure 14*) (Haslam, 2011; Haslam and Petraglia, 2010; Haslam et al., 2012a; Clarkson et al., 2020; Sharma and Clark, 1982; Sharma and Clark, 1983; Williams and Clarke, 1984; Williams and Royce, 1982; Williams et al., 2009).

The late Quaternary sedimentary sequence of the Middle Son Valley has been extensively analysed, and five wide-spread alluvial formations were mapped and defined (Williams and Clarke, 1995; Williams and Royce, 1983; Williams et al., 2006). The chronology of the oldest to youngest formations is the Sihawal Formation, Khunteli Formation, Patpara Formation, Baghor Formation and Khetaunhi Formation. The most important and well-studied evidence of the Formations is summarised below for comparative purposes.

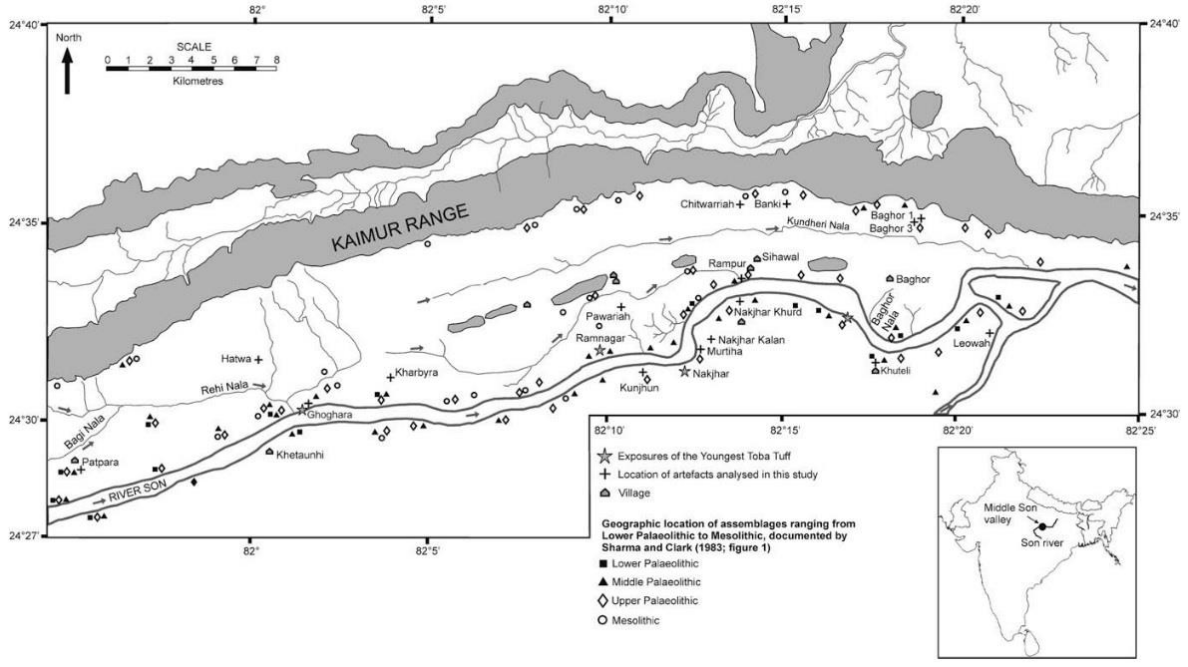

Figure 14. Location of Palaeolithic to Mesolithic sites and Toba tephra exposures in Middle Son Valley (after Jones and Pal, 2009).

3.6.1 Sihawal Formation

The initial excavation at Sihawal resulted in a 1.5 m deep sequence *(Figure 15*) divided into three primary members, underlined by shale bedrock (Kenoyer and Pal, 1983). The lower member is a gravel deposit comprising rolled to angular clasts of quartzite, sandstone, chert, and shale, within a clay matrix, with a higher ratio of calcium carbonate and iron/manganese components that attain greater convergence at the base of the stratum. The upper part is a culturally sterile, mottled-brown clay loam up to 0.5 m thick, with a high concentration of carbonate nodules at its base. The lower gravel unit yielded 119 artefacts with handaxe and cleaver forms, a discoidal core, and a range of flake tools reported from the site (Haslam et al., 2011; Shipton et al., 2013).

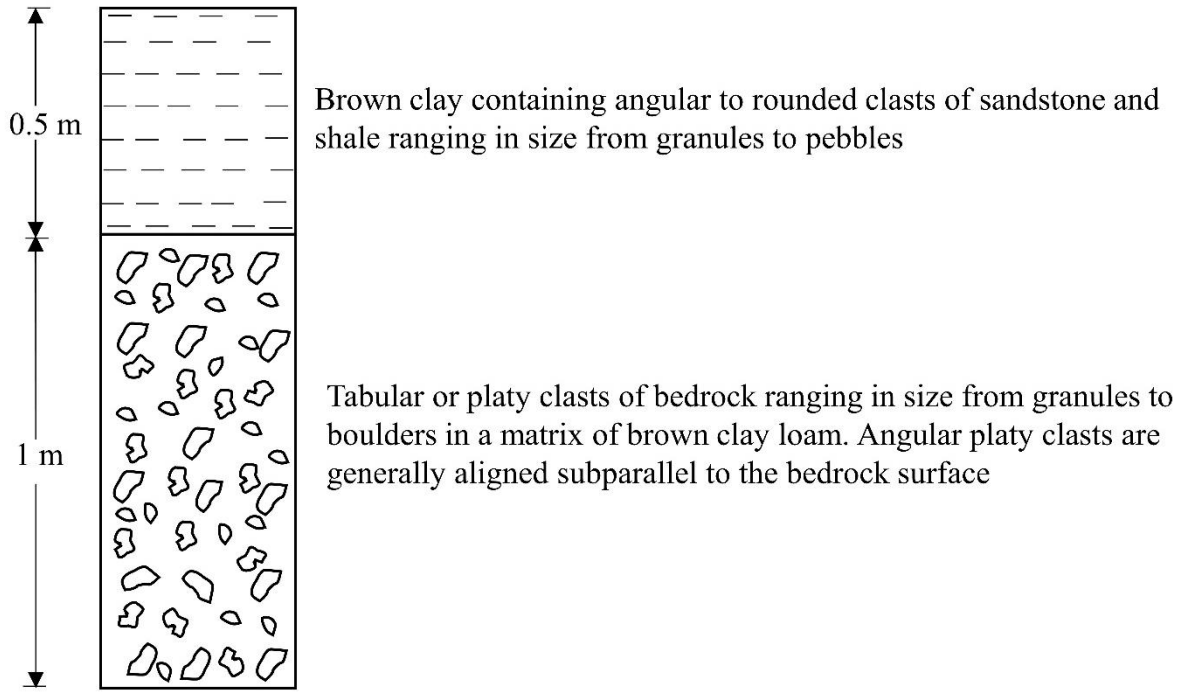

Figure 15. Type-section of Sihawal Formation - Sihawal village (William and Royce, 1983).

3.6.2 Khunteli Formation

A new formation was identified on the right bank of the Son, near the village of Khunteli. This formation dates before the Patpara Formation and precedes the Sihawal Formation. This formation has a maximum exposed thickness of 10 m. A basal unit of unconsolidated pale yellow-brown medium sand is up to 6 m thick, a discontinuous bed of pure volcanic ash up to 1.5 m thick, at least 4 m of a cross-bedded and planar-bedded medium, coarse sand and fine gravel, and an upper unit of carbonate-cemented gravels make up the formation *(Figure 16*) (Williams et al., 2006). A lateral version of this formation is a 30 m thick portion on the left bank of the Son River near its confluence with the Rehi River, which comprises a locally obscured base unit of medium brown sand up to 8m thick, capped by a laterally discontinuous unit of pure volcanic ash up to 4m thick (Williams and Royce, 1983). The ash acts as a channel filler, although it is eroded and partially replaced by multiple lenses of alluvial gravel.

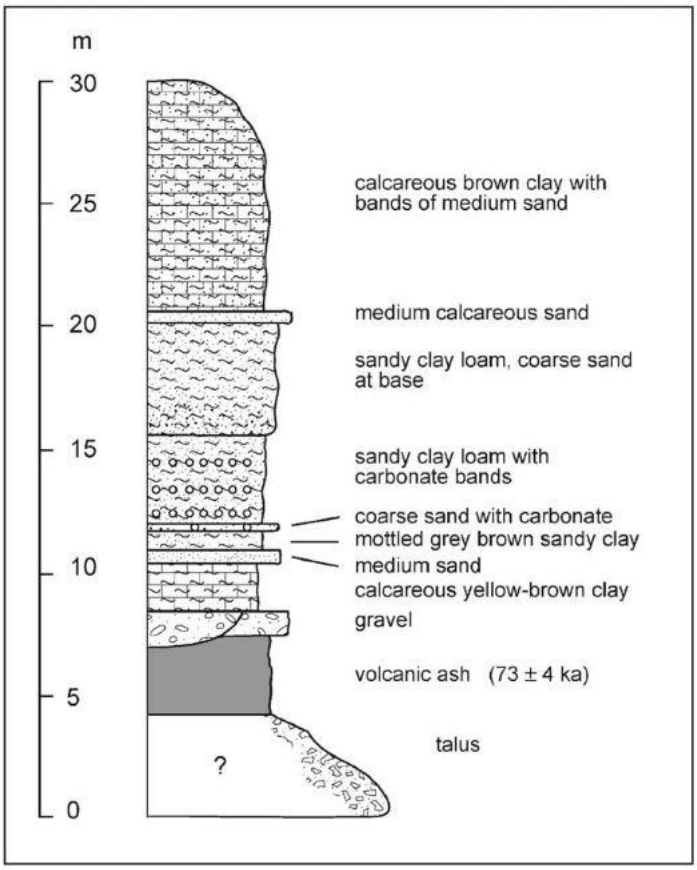

Figure 16. Type-section of Khunteli Formation (Williams et al., 2006).

3.6.3 Patpara Formation

The Patpara Formation is at least 10 m thick and overlies the Khunteli Formation. It has a distinctive reddish colour and contains rounded to sub-angular quartz, sandstone, and mudstone clasts like the underlying bedrock; agate, chalcedony, and other microcrystalline silicic rocks are also found in abundance. The Deccan Trap basalts in Son's headwaters gave rise to these far-flung clasts. The size of the sediments/clasts varies from coarse sand to cobbles, with 1–2 cm pebbles being the most prevalent, all set in a clay-rich matrix. The bedding comes in various shapes and sizes, from large to flat or undulating laminations (*Figure 17*). Iron is partially cemented in the formation, giving the sediments their distinctive reddish colour. Unless terminated by the overlying Baghor Formation, the formation is

overlain by up to 1 m of hard, dark reddish-brown, mottled silty clay (Williams et al., 2006). Most of the artefacts belonging to the Lower and Middle Palaeolithic are recovered from the lowest, dark red, clayey-sand layer, dating to 137–140 kyr (Haslam et al., 2011). The Palaeolithic site of Patpara has produced 2284 artefacts showing both Lower and Middle Palaeolithic components; most of these were made of quartzite and chert (Sharma and Clark, 1983; Haslam et al., 2011).

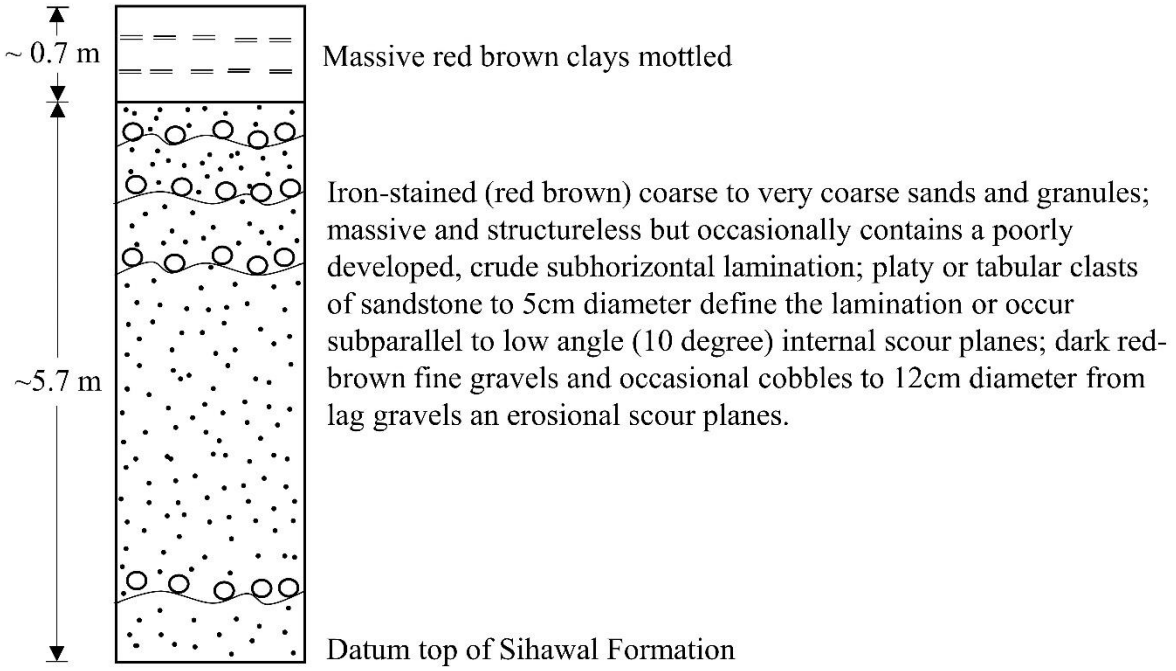

Figure 17. Type-section of Patpara Formation - Patpara excavation site (William and Royce, 1983).

3.6.4 Baghor Formation

An erosional unconformity separates the Baghor Formation (20 m thick) from the underlying Patpara Formation. The lower coarse and fine upper members comprise two distinct members, each around 10 m thick. Individual sets of unconsolidated cross-bedded medium to coarse sands comprise the coarse component, particularly sets 5–85 cm thick and generally

limited by planar horizontal surfaces (*Figure 18*). Sandstone, mudstone, quartzite, chalcedony, agate and chert lenses, ranging in size from granules to pebbles, commonly appear as pebble trains on scour surfaces between cross-bedded layers. Throughout the coarse component, discontinuous sheets of enormous carbonate cemented sands contain well-preserved fossils such as buffalo, hippo, crocodile, antelope, elephant and tortoise, as well as rolled and abraded Middle Palaeolithic artefacts. With an elevation of at least 30 m above low water level, the fine member forms the highest aggradation surface in the Son Valley and rests conformably on the coarse member with no trace of an erosional break. It is made up of interbedded silt, clay, and fine sand. Each bed is 1 to 4 m thick and can be tracked 2 to 3 km laterally. Soil-forming processes have altered primary depositional structures, and irregular carbonate nodules, tubules and plates occur in well-defined layers. The concretions become more concentrated, moving up the fine member, indicating extended periods of little flood-plain sedimentation and longer periods of soil formation. Fresh Upper Palaeolithic artefacts have been discovered *in-situ* inside the fine member's silt and clay and on the surface.

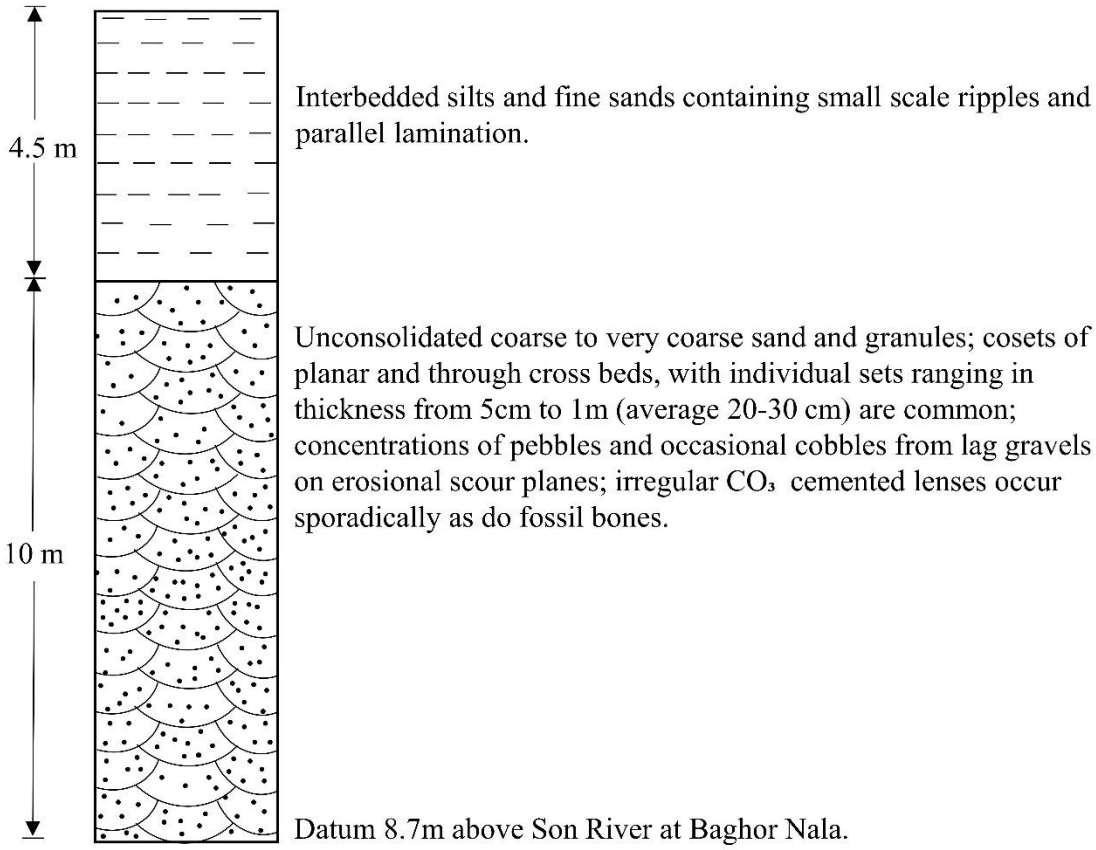

Figure 18. Type-section of Baghor Formation - Baghor Nala (William and Royce, 1983).

3.6.5 Khetaunhi Formation

The Khetaunhi Formation is 10 m thick and consists of interbedded silts, clays, and fine sands that form a well-defined alluvial terrace (*Figure 19*). Laterally homogeneous parallel lamination can be seen in the silts and clays, while ripples and ripple cross-laminations can be seen in the fine sands. The current Son may overtop the terrace during a flood, allowing sedimentation to continue. The strata dip 10–15^0 towards the current river along the right bank opposite the Sihawal Formation and exhibit exceptionally well-preserved sedimentary features, indicating a relatively rapid deposition of the beds in recent times.

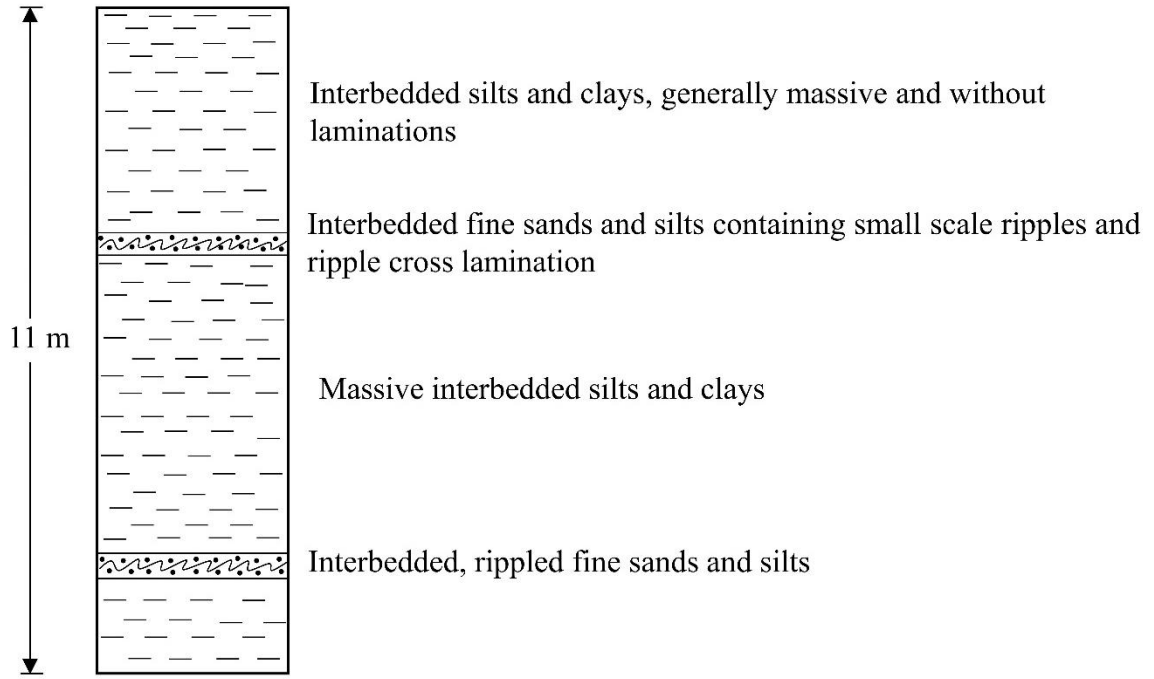

Figure 19. Type-section of Khetaunhi Formation, opposite Son River and Rehi River confluence (William and Royce, 1983).

As discussed above, comprehensive research has been carried out in the Middle Son Valley, but only a few archaeological explorations have been carried out in the Upper (Ahmad 1984) and Lower Son Valley in the 1970s-80s (IAR 1977; Tewari et al., 1995). Researchers laid the foundation of archaeological investigations in the geographical area of the LSV in the late nineteenth century by discovering some painted rock shelters depicting scenes of prehistoric people hunting, dancing and other activities (Cockburn 1883, 1899). During his investigations in what are now Mirzapur and Sonbhadra districts in the 1950s, G.R. Sharma unearthed various Palaeolithic, microlithic, and rock art sites (*Indian Archaeological Review,* 1957). Lower Palaeolithic sites have yielded cores, handaxes, cleavers and scrapers made on quartzite and chert. Cores, flakes, and various types of scrapers, points, and blades made on

quartzite, chert and quartz have been found at Middle Palaeolithic sites. *(*IAR 1956, 1962, 1977, 1980, 1982*;* Tewari et al., 1995). The Upper Palaeolithic and microlithic artefacts were made on various raw materials such as chert, quartz, and jasper (*Table 10*). Six hundred faunal fossil remains eroding from cemented gravel/sand strata have also been recorded from Patvadh, Rendia, Mahalpur and other sites, including faunal genera such as *Bos, Elephas, and Gharialis* (*IAR,* 1980).

Although some post-Acheulean sites have been discovered in the LSV (*IAR*, 1980, 1983), no systematic multidisciplinary investigations have been conducted. This is remarkable because it is an extension of the nearby Middle Son Valley, where intriguing palaeoanthropological evidence has been identified and examined using a variety of multidisciplinary approaches (Sharma and Clark, 1983; Jones and Pal, 2005; 2009).

Table 10. Pre-reported sites in the LSV.

Sr. No.	Site Name	Site Type	Reference
1	Devagarh	Microlithic	Narain and Pant, 1962-63, p. 132
2	Bhagahi	Microlithic	IAR- 1977-78, p. 56-57; Misra, 1977, p. 45
3	Chaura	Middle Palaeolithic and Microlithic	IAR- 1980-81, p. 73; Pant, 1982: 32
4	Nevari	Upper Palaeolithic	IAR- 1977-78, p. 56
5	Rijula	Upper Palaeolithic and Microlithic	IAR- 1977-78, p. 56; IAR- 1956-57, p. 48
6	Semia	Upper Palaeolithic	IAR- 1977-78, p. 56-57
7	Mandaha	Microlithic	Narain and Pant, 1962-63, p. 132
8	Ghoria	Upper Palaeolithic	IAR- 1977-78, p. 56
9	Chitwar	Upper Palaeolithic	IAR- 1977-78, p. 56-57
10	Alaur	Upper Palaeolithic	IAR- 1977-78, p. 56
11	Bijara	Middle Palaeolithic and Microlithic	IAR- 1980-81, p. 73
12	Mitapur	Middle Palaeolithic	IAR- 1977-78, p. 56
13	Gothani	Lower Palaeolithic	IAR- 1977-78, p. 56; Misra, 1977, p. 45
14	Mahalpur	Middle and Upper Palaeolithic	IAR- 1977-78, p. 56
15	Bardiya	Microlithic	IAR- 1977-78, p. 56-57; Misra, 1977, p. 45
16	Kandakot	Microlithic	IAR- 1956-57, p. 13-14
17	Bashauli	Microlithic	IAR- 1956-57, p. 13-14
18	Kurhul	Upper Palaeolithic	IAR- 1977-78, p. 56
19	Rendia	Middle and Upper Palaeolithic	IAR- 1977-78, p. 56
20	Sinduria	Middle Palaeolithic and Microlithic	IAR- 1977-78, p. 56-57; Misra, 1977, p. 45
21	Obra	Microlithic	Narain and Pant, 1962-63, p. 130
22	Chopan	Middle Palaeolithic and Microlithic	IAR- 1962-63, p. 33,37; IAR-1977-78, p. 56-57; IAR-1980-81, p. 73; IAR- 1982-83, p. 145; Misra, 1977, p. 33; Narain and Pant, 1962-63, p. 130, Pant, 1983, p. 91.
23	Patvadha	Tool Series I	IAR- 1977-78, p. 56; IAR- 1956-57, p. 48
24	Salai Banava	Microlithic	IAR- 1977-78, p. 56; IAR- 1956-57, p. 48
25	Kotta	Upper Palaeolithic	IAR- 1977-78, p. 56
26	Raja Nala ka Tilla	Stone artefacts, scrapers	Tiwari and Srivastava, 1994
27	Kone	Upper Palaeolithic	IAR- 1977-78, p. 56

*Microlithic sites associated with rock shelters and sites with coordinates are not mentioned above. For that, see (Tiwari et al., 1995).

*The table provides info and terminology as originally reported, and most reports show inconsistent format.

Considering the above information, the Sonbhadra District of Uttar Pradesh was selected for the research. The selected study area includes the downstream extension of the Son River but has not produced much Lower Palaeolithic evidence; therefore, by thoroughly studying the area, one can try to fill the technochronological gaps. The primary objective of the current

research was to perform 1) a systematic exploration to understand the palaeoanthropological potential of the region, 2) to locate new prehistoric sites and associated transitional assemblages (Lower Palaeolithic to microlithic) with dateable context as found in the Middle Son valley to the west, and 3) to locate new vertebrate and invertebrate fossil locations. These preliminary objectives were partially obtained in the first year (2017) of fieldwork by discovering 48 new prehistoric sites, tentatively ranging from the Middle Palaeolithic to the microlithic periods and two vertebrate fossil sites, thus confirming that the area is suitable for further research.

3.7 Research Objectives

Based upon the study area's importance (discussed above), and archaeological and geographical gaps in the region, the following objectives were aimed to be achieved.

1) a} To carry out surveys to locate new Palaeolithic and microlithic sites in the Lower Son Valley (LSV), Sonbhadra District, Uttar Pradesh, b} To collect sediment samples from a geological excavation to characterise the stratigraphy and palaeoenvironment of the study area.

- Landscape-level comparison between Late Acheulean to microlithic sites from the LSV (raw material variability and selection, regional adaptations, site formation differences, lithic typo-technology)
- Optical Luminescence (OSL) dating of a part of the LSV to understand the chronology and link the paleoenvironmental data with lithic occurrences

2) Compile published sources for the Late Pleistocene palaeoenvironmental reconstruction of South Asia.

3) To visit the previously reported Late Pleistocene Palaeolithic and fossil sites or museum/university collections to collect enamel samples of fossil teeth and carbonates to reconstruct Late Pleistocene paleoenvironments.

3.8 Methodology

Numerous methods have been applied to fulfil the objectives mentioned above, i.e., surveys, collection of artefacts, lithic analysis, stable isotope analysis and OSL dating.

3.8.1 Survey and site mapping

The study region is limited to the Sonbhadra District of Uttar Pradesh, with a total area of 6788 km^2, with only 1897 km^2 along the north and south of the Son River considered for surveying and named LSV for this study. Preliminary surveys were conducted in the first week of June 2017 to locate previously known sites for mapping and to understand the geomorphological setting of the region. Based on previously documented sites, different survey strategies were organised to explore the selected area. Exploration undertaken by the author aimed to locate stratified sites in the region with a dateable context and understand their distribution during different periods in the study area. A two-layer survey strategy was applied to cover the whole area 1) Systematic surveys (Renfrew and Bahn 2012, 2016) were conducted in June 2017, May – June 2018, April – May 2019, December 2019, February – March 2020 and February – March 2021; arbitrary grids (~3X3 kms^2) (*Figure 20*) were plotted in Google Earth, and then particular squares were targeted for surveying based on analysing specific topographic, geographic and geological features. 2) Unsystematic and systematic survey methods were applied in those squares. In the unsystematic survey, in one selected square, walking across each part of the area was involved to locate a site. In the systematic survey, transect surveys were conducted within the square. Features such as small

streams, river channels, small hills and their sections, exposures and raw material outcrops were also targeted for surveying.

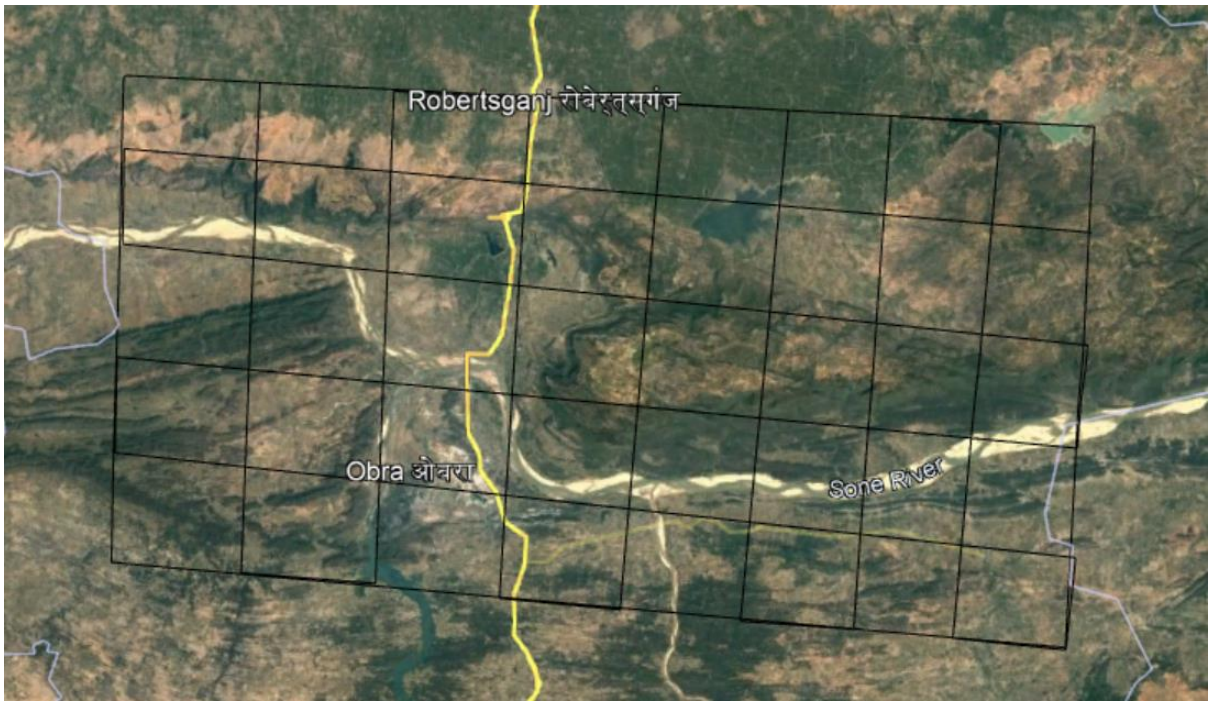

Figure 20. Arbitrary grids with (~3X3 kms^2) squares plotted in Google Earth.

Extensive photographic documentation was done during the fieldwork, and sites were plotted using a GARMIN eTrex 10.

"A site is concentration of humanly modified materials, associated materials and landscape features, regardless of the concentrating agency (Foley 1981). An archaeological site can be defined as a place where artefacts, features, structures, and organic and environmental remains can be found together. However, finding all these landmarks at a Palaeolithic site is very difficult; it can be simplified as a place where significant traces of human activities are found (Renfrew and Bahn 2016). Off-site or non-site is the area with low density of artefacts, which should be located and recorded in order to understand landscape archaeology (Foley 1981; Issac 1972; Renfrew and Bahn 2012). During the surveys conducted in the LSV, a site

was defined as an area with an artefact density of ten or more artefacts, while areas with less than ten artefacts were classified as off/non-sites due to their low density as compared to other sites in the valley. There is no underlying assumption dictating the specific 500-meter radius for defining a locality. Instead, this determination is based on several factors, including typology, artefact types, and sedimentation patterns observed at each site. Typically, these are made with consideration for the topographic characteristics of the area such as hills, or riverbank or nearby villages.

The plotted sites were further transferred to Google Earth, later classified into different periods, and utilised through Global mapper, QGIS, and ArcGIS for mapping. The surveyed areas without sites are highlighted with a red cross (*Figure 21*).

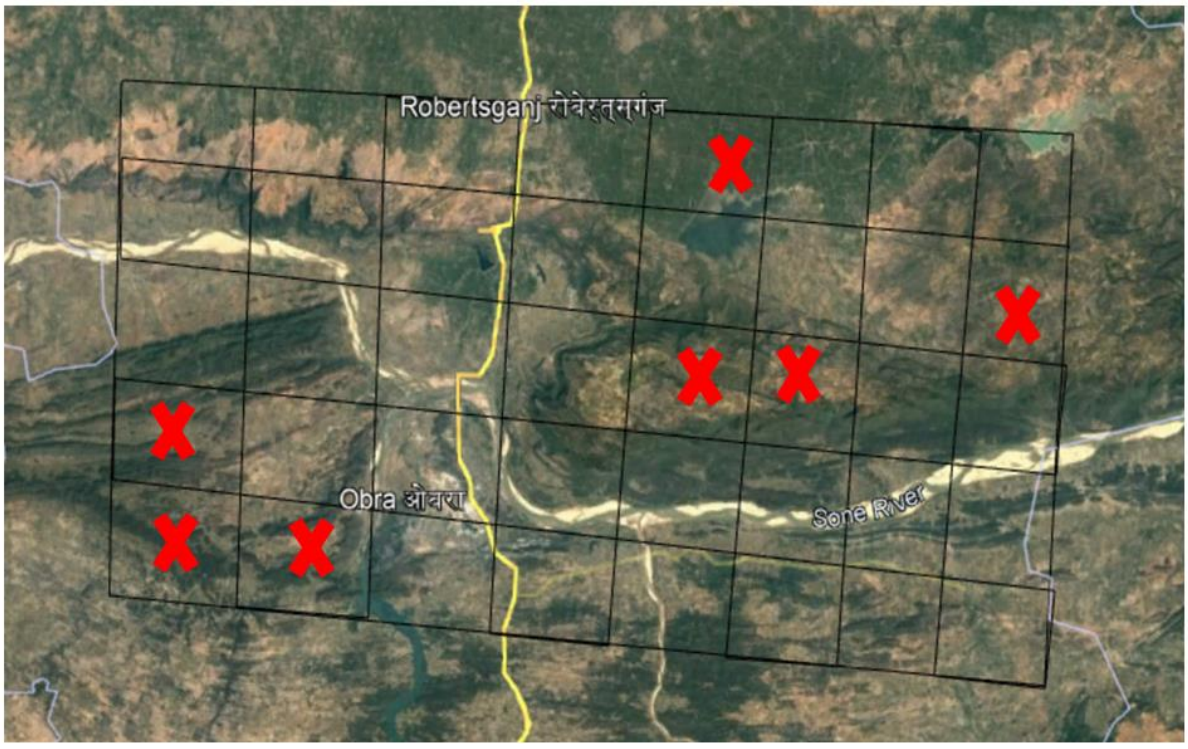

Figure 21. Red crosses represent the surveyed area without any site.

3.8.2 Results

Six seasons of surveys (mentioned above) have led to the discovery of (*n* = 61) prehistoric sites (*Figure 22*) belonging to Late Acheulean to microlithic periods and vertebrae fossil localities. Rock-art sites were also located during the survey but were not considered for the study.

On a typological basis, these sites (*Table 11*) were categorised as Late Acheulean (*n* = 1), Middle Palaeolithic (*n* = 8); Middle/Upper Palaeolithic (*n* = 13); Upper Palaeolithic (*n* = 7); Upper Palaeolithic/ Microlithic (*n* = 15); microlithic (*n* = 12); Middle Palaeolithic/Upper Palaeolithic/microlithic (*n* = 3). The sites were defined as: (1) Late Acheulean - manufacture of large flake blanks for bifaces production (Sharon 2007); (2) Middle Palaeolithic – prepared core and flake based technology (Akhilesh *et al.*, 2018; Akhilesh *et al.*, 2018; Misra and Rajaguru 1978; Pappu 2001; Sankalia 1964; White *et al.*, 2011); (3) Upper Palaeolithic - blades: flakes that are twice as long as they are wide, with a parallel margin and parallel dorsal flake scars (Mackay, 2008) and (4) microlithic - artefacts <3 cm long (Shea, 2016).

As mentioned, most of the sites are described on a typological basis; the true nature of the site can only be determined after technological and statistical analysis.

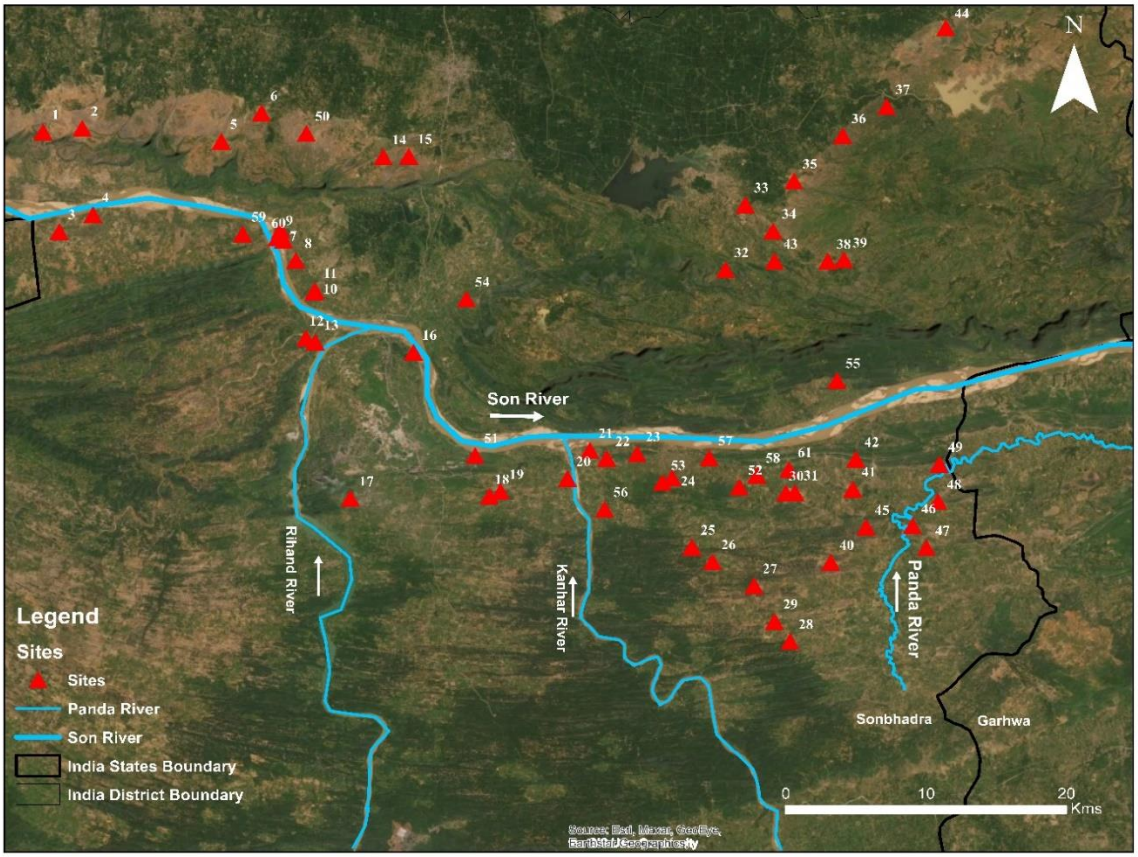

Figure 22. Map showing newly discovered Palaeolithic and microlithic sites in the LSV (site number correlates with Table 11. New discovered Palaeolithic and microlithic sites in the LSV.

Table 11. New discovered Palaeolithic and microlithic sites in the LSV.

Sr. No.	Sites	Location	Raw Material	Probable period*
1	Parva Chinguri	Foothill	Porcellanite, Chert, Chalcedony, Quartz, Agate	Microlithic
2	Domakhari	Hill slope	Chert, Chalcedony, Quartz, Agate	Microlithic
3	Newari	Streambank	Porcellanite, Chert, Chalcedony, Quartz	Microlithic
4	Shemiya	Top of hillock/River bank	Porcellanite, Chalcedony, Agate	Upper Palaeolithic
5	Tilha	Foothill	Porcellanite, Chalcedony	Middle Palaeolithic
6	Mahulia	Top of hillock	Porcellanite, Chert, Chalcedony, Quartz, Agate	Microlithic
7	Kargara Loc. 1	River bank	Porcellanite, Chert, Chalcedony, Quartz	Middle Palaeolithic/ Upper Palaeolithic/Microlithic
8	Kargara Loc.2	Riverbank/foothill	Porcellanite, Chalcedony, Quartz	Middle Palaeolithic/ Upper Palaeolithic/Microlithic
9	MitapurLoc 1	Foothill	Chert, Chalcedony, Quartz	Upper Palaeolithic
10	MitapurLoc 2	River bank	Chert, Chalcedony, Quartz	Upper Palaeolithic
11	Mahalpur	Foothill	Porcellanite, Chert, Chalcedony, Quartz	Upper Palaeolithic/ Microlithic
12	Bardiya	Top of hillock	Porcellanite, Chalcedony, Quartz, Agate	Microlithic
13	Kandakot	Top of hillock	Porcellanite, Quartz	Upper Palaeolithic/ Microlithic
14	Bhandar Khurd	Top of hillock	Porcellanite, Chalcedony, Quartz, Agate	Microlithic
15	Chopan	Riverbank	Chalcedony, Quartz	Upper Palaeolithic/ Microlithic
16	R. Salai Banwa	Foothill	Chalcedony, Quartz	Microlithic
17	Salai Banwa Loc 1	Foothill	Porcellanite, Chert, Chalcedony, Agate, Quartz	Upper Palaeolithic/ Microlithic
18	Salai Banwa Loc 2	Foothill	Porcellanite, Chert, Chalcedony, Agate, Quartz	Upper Palaeolithic/ Microlithic
19	Kota	Foothill/Streambank	Porcellanite, Chalcedony, Quartz	Upper Palaeolithic
20	Devarta	Foothill	Porcellanite, Chalcedony, Quartz	Middle Palaeolithic/ Upper Palaeolithic
21	Piperhawa	Foothill	Porcellanite, Chalcedony, Quartz	Middle Palaeolithic/ Upper Palaeolithic
22	Hardi Tola	Foothill	Porcellanite, Chalcedony, Quartz	Upper Palaeolithic/ Microlithic
23	Chilbilia	Hill slope	Porcellanite, Chalcedony, Quartz	Middle Palaeolithic/ Upper Palaeolithic
24	Bhalu Kudhur	Forest/foothill	Porcellanite, Chert, Chalcedony, Quartz, Agate	Upper Palaeolithic/ Microlithic
25	Ismaila Nagar	Forest/foothill	Porcellanite, Chert, Chalcedony, Quartz	Upper Palaeolithic/ Microlithic
26	Mid Kone Range	Forest/foothill	Porcellanite, Chert, Chalcedony, Quartz	Upper Palaeolithic/ Microlithic
27	Dharanwa Loc 1	Foothill	Porcellanite, Chert, Chalcedony, Quartz	Upper Palaeolithic/ Microlithic
28	Dharanwa Loc 2	Foothill	Porcellanite, Chert, Chalcedony,	Upper Palaeolithic/

			Quartz	Microlithic
29	Khorcha Kholi	Foothill	Porcellanite, Chalcedony, Quartz	Middle Palaeolithic/ Upper Palaeolithic
30	Nodiha	Foothill	Porcellanite, Chert, Chalcedony, Quartz, Agate	Upper Palaeolithic/ Microlithic
31	Mardaha	Top of hillock	Chert, Chalcedony, Quartz	Upper Palaeolithic
32	Patana	Streambank	Porcellanite, Chalcedony	Middle Palaeolithic/ Upper Palaeolithic
33	Darama	Streambank	Porcellanite, Chalcedony	Middle Palaeolithic/ Upper Palaeolithic
34	Siltham	Top of hillock	Porcellanite, Chalcedony, Quartz	Upper Palaeolithic/ Microlithic
35	Kirhulia	Top of hillock	Porcellanite, Chert, Chalcedony, Quartz	Microlithic
36	Silhat	Top of hillock	Porcellanite, Chert, Chalcedony, Quartz	Microlithic
37	Deenari	Top of hillock	Porcellanite	Middle Palaeolithic
38	Baijnath	Top of hillock	Porcellanite	Middle Palaeolithic
39	Roravra	Foothill	Porcellanite, Chalcedony, Quartz	Middle Palaeolithic
40	Khempur	Foothill	Porcellanite, Chalcedony	Middle Palaeolithic
41	SugwaGhati	Foothill/Streambank	Porcellanite, Chalcedony	Middle Palaeolithic/ Upper Palaeolithic
42	Karaundiya	Hill slope	Porcellanite, Chert, Chalcedony, Quartz, Agate	Upper Palaeolithic/ Microlithic
43	Rahiya	Foothill	Porcellanite, Chalcedony, Quartz	Middle Palaeolithic/ Upper Palaeolithic
44	Navai Tola	Foothill	Porcellanite, Chalcedony, Quartz	Middle Palaeolithic
45	Bagia	Foothill	Porcellanite, Chalcedony	Middle Palaeolithic
46	Mitihiniya	Foothill	Porcellanite	Middle Palaeolithic
47	Saemar Khand	Foothill	Porcellanite, Chalcedony	Upper Palaeolithic
48	Doma	Foothill+ Riverbank	Porcellanite	Late Acheulean to Upper Palaeolithic
49	Kone	Foothill	Porcellanite, Chert, Chalcedony	Microlithic
50	Basuhari	Foothill	Porcellanite, Chert, Chalcedony, Quartz	Microlithic
51	Dala Picnic point	Foothill	Chert, Chalcedony, Quartz, Agate	Upper/Microlithic
52	Negai	Foothill	Porcellanite, Chert, Chalcedony	Middle/Upper Palaeolithic
53	Padarach	Foothill	Porcellanite	Middle/Upper Palaeolithic
54	Belach	Foothill	Porcellanite, Chert, Chalcedony, Quartz	Microlithic
55	Parari	Foothill	Porcellanite, Chalcedony	Upper Palaeolithic
56	Dubey Kudwa	Foothill	Porcellanite, Chert, Chalcedony	Middle/Upper Palaeolithic
57	Harra (DBT)	Colluvium + foothill	Porcellanite	Middle/Upper Palaeolithic
58	Maheshwer temple(3 localities)	Colluvium + foothill	Porcellanite, Chert, Chalcedony	Middle/Upper Palaeolithic/Microlithic
59	Barganwa	Surface+ Riverbank	Porcellanite, Chert, Chalcedony	Middle/Upper Palaeolithic

3.8.2.1 Late Acheulean

Only one site (Doma) has been categorised as Late Acheulean in the study area. Doma (*Figure 23*) comprises a range of artefacts such as bifaces (average length ~ 12 cm), large flakes (>10 cm), prepared cores, prepared flakes, points, flakes, and blades (>3 cm) made on locally available porcellanite (black/olive green). The maximum density of artefacts was reported within an area of 200 m^2 along the slopes. Around 2 km of territory was investigated to determine the full extent of the site. The location was the first to be discovered with bifacial technology in the research area. The evidence at the site is part of a multicultural sequence that may extend up to the Upper Palaeolithic, and adequate verification will require long-term multidisciplinary research.

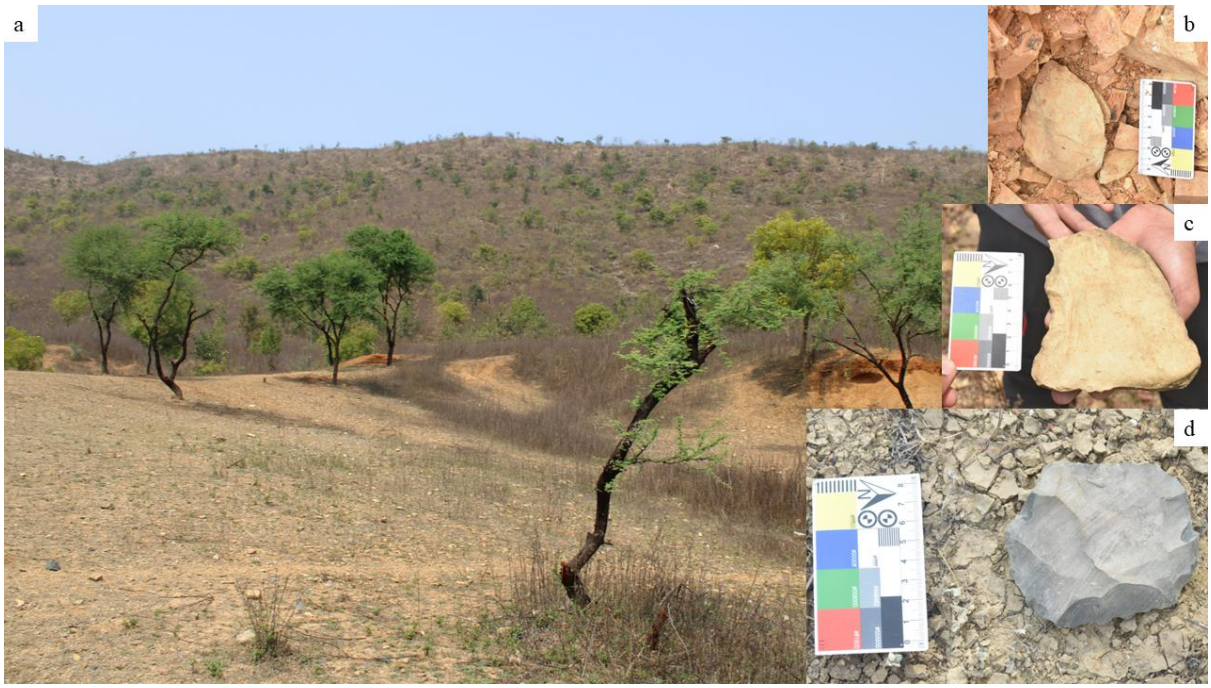

Figure 23. a) Landscape view of Doma, b) In-situ biface in colluvium, c) large flake, d) prepared core.

3.8.2.2 Middle Palaeolithic

The Middle Palaeolithic sites appear to be clustered around raw material sources. The Middle Palaeolithic in the study region is best represented by the sites of Khempur and Bagia, located near the foothills, within the vicinity of 4 – 5 km from the raw material sources. The sites comprise prepared cores, Levallois flakes, prepared flakes, scrapers, and retouched flakes. At Khempur, artefacts can be located in a 50-100 meter radius around a hillock, while Bagia has an extension of around 200 L × 100 W meters. Hominins have used porcellanite, readily available in the area, from raw material outcrops and colluvial deposits for artefact production. Artefacts were discovered on the surface and eroding out of fine-grain sediments (sand and silt) of a reddish-brown colour at the Khempur site. Bagia (*Figure 24*) is situated in a ploughed field, with artefacts eroding from yellow-grey sediments and resting on worn bedrock nearby. All artefacts discovered at the site have a yellowish-cream patina.

Figure 24. a) Landscape view of Bagia, b) flake with calcrete, c) various flakes, d) prepared core.

3.8.2.3 Middle/Upper Palaeolithic

The Middle/Upper Palaeolithic sites could be considered transitional evidence and represent the mixing of different technologies because they contain artefacts from both the Middle and Upper Palaeolithic periods. More research is needed to rule out geomorphological mixing or multiple (hominin) groups using the same region over time. The Maheshwer temple site (*Figure 25*), a fine example of this type of mixed assemblage, is located in the foothill (200 L × 100 W meter extension). Various artefacts, prepared cores, prepared flakes, scrapers, retouched flakes, and blades have all been found at the site. Hominins used locally available porcellanite and other raw materials like chalcedony and quartz for artefact production. Artefacts were discovered on bedrock and eroding out of fine-grain sediments (sand and silt) of a reddish-brown colour at the location.

Figure 25. a) Landscape view of Maheshwer temple, b) discoid core, c) distally snapped blade, d) various flakes.

3.8.2.4 Upper Palaeolithic

The Upper Palaeolithic sites in the valley consist of blades, blade cores, fluted cores, and scrapers without any or minimum presence of Levallois elements. Most sites feature a minimum of 10 blades with an average length of 4-5 cm; these specimens are significantly larger than microlithic blades. These Upper Palaeolithic sites can be found on the hillslopes, foothills and hilltops of the Vindhyan range. Porcellanite, chert and chalcedony were the preferred raw materials, which were most likely transported at least some distance at a few sites because the raw material outcrops were unavailable in proximity. Other raw materials, such as agate and quartz, were also used. The site of Samaer Khand (*Figure 26*) is located at the foothill, and artefacts can be located within a 50–100 meter radius of the hill. Artefacts like blade core, blade, and scrapers can be found at the site.

Figure 26. a) Landscape view of Samaer Khand, b) artefact scatter, c) blade core d) blade and flake.

3.8.2.5 Upper Palaeolithic/microlithic Sites

Artefacts from the Upper Palaeolithic (blades, blade cores, fluted cores, scrapers) and microlithic (microblades and microblade cores) periods can be found at these sites. Like the Upper Palaeolithic sites, these sites are found on the hill slopes, foothills, and hilltops of the Vindhyan ranges. The primary raw materials used at these sites are chalcedony, chert, and quartz; porcellanite was used sometimes. The site of SalaiBanwa (*Figure 27*) is an excellent example of this type of site, with artefacts like flakes, blades, microblades, and fluted cores. The artefacts can be located with an extension of 100 L × 100 W meters.

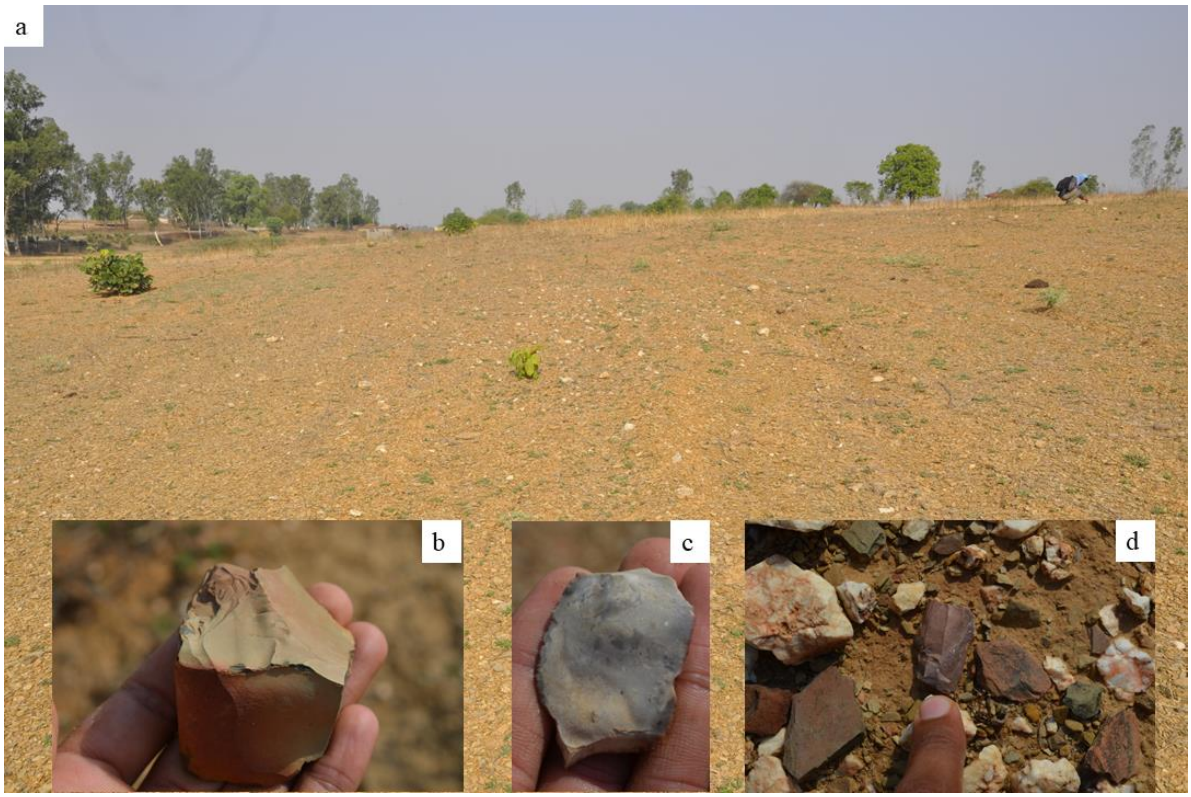

Figure 27. a) Landscape view of SalaiBanwa, b) core, c) flake, d) artefacts scatter highlighting microblade core.

3.8.2.6 Microlithic

Microlithic sites can be found all across the study area and were produced on quartz, chert, chalcedony, and agate. Microblades, fluted cores, and points make up the majority of microlithic assemblages in the area. During this technological phase, chert was the most common raw material used in the area. Domakhari (*Figure 28*) is located on a hillside leading to a rock shelter, and the rich scattering of more than 300 microliths, including microblades, fluted cores, and points, covers an area of approximately 100 m^2. Because the site is on a hillside, artefacts were discovered on the surface without any sedimentation.

Figure 28. a) Landscape view of Domakhari, b) hammerstone with pit marks, c) various points, d) artefacts scatter, e) various microlithic artefacts.

3.8.3 Contexts of the sites

The sites were generally open-air and found near water sources, foothills, hill slopes, and hilltops. Although several scattered sites were adjacent to rock shelters, this study did not include a survey of rock shelters. The artefacts have been discovered on the surface and *in-situ,* eroding from underlying fine-grain sediments. In the future, a few sections of the river or stream that preserve *in-situ* artefacts will be considered for test trenches for retrieving samples for dating. During the fieldwork, the following general trends were observed: sites north of the Son River on the tableland were mostly Upper Palaeolithic or microlithic, with very little sedimentation, whereas on the south side, most of the sites were Middle Palaeolithic, sedimentation appears to be relatively higher, with artefacts *in-situ* and eroding out of sediments. The discovered sites were primarily in the foothills and were associated with fine-grained sediments or exposed bedrock outcrops. The assemblages on bedrock were more abraded than those in fine-grained sediments. Sand and silt make up the fine-grained sediments, ranging in colour from reddish-brown to reddish-orange to yellowish-brown. The deposits contain calcrete primarily on the surface at some spots. Although most of the sites are on the surface or have been eroded from sediments, two main stratigraphic findings have been made: 1) artefacts eroding just a few millimetres above bedrock from sediments or weathered bedrock; 2) artefacts eroding from fine sediments or fine sediments with calcrete where bedrock is not visible (*Figure 29*). The site of Chopan appears in a primary context and is promising for more in-depth multidisciplinary research, including absolute dating. Aside from these contexts, the artefacts can also be found in regolith and colluvial deposits.

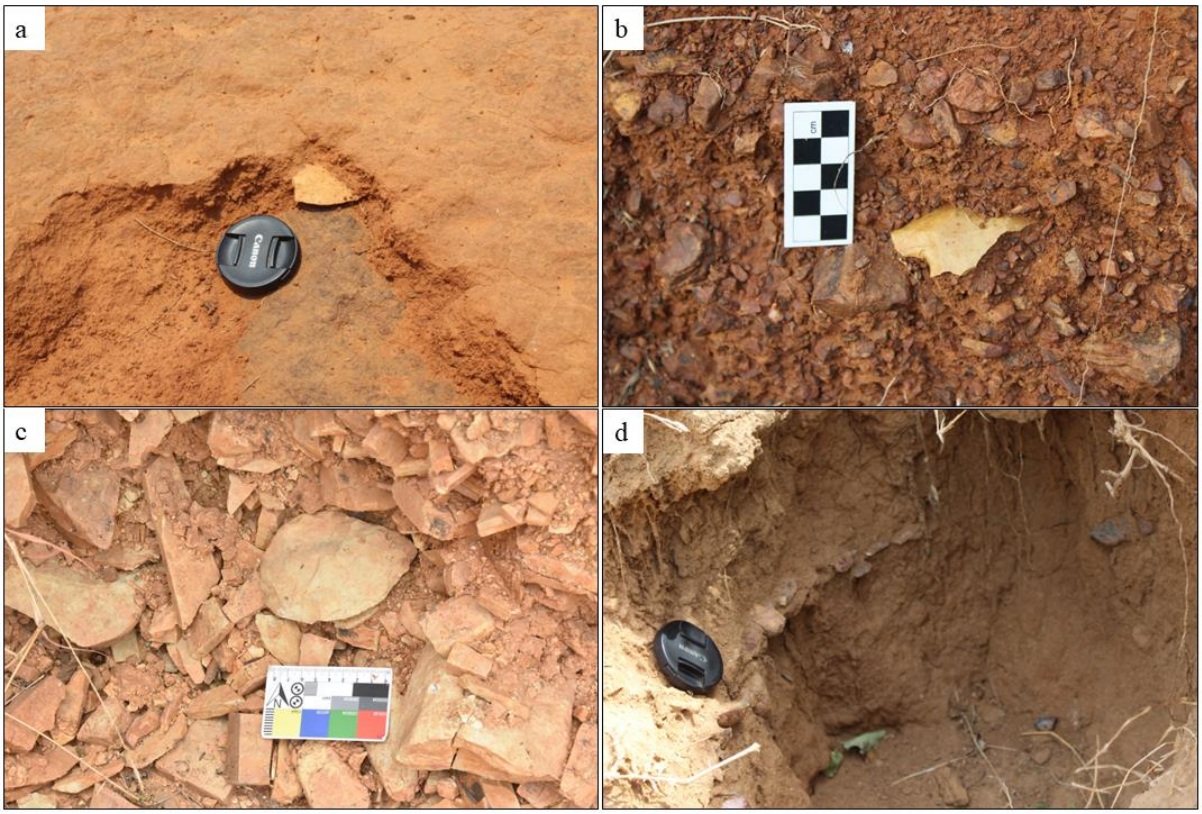

Figure 29. a) Artefacts eroding just a few millimetres above bedrock from sediments/weathered bedrock at Baijnath, b) artefacts embedded in the regolith at Khempur, c) refined handaxe in colluvial deposit at Doma, d) artefact layer in fine sediments at Chopan.

3.8.4 Lithic Collection

A systematic and random/comprehensive collection (Renfrew and Bahn 2016, Peregrine 2018) of lithic artefacts from sites - Khempur, Doma, Kone, Kargara, Bagia, Parva Chinguri and Newari from the LSV, Sonbhadra, Uttar Pradesh was done (*Table 12*) in February-March 2020 after Dr. Parth Chauhan acquired the permit from the Archaeological Survey of India (ASI). The random/comprehensive collection was made from sites with a low concentration of artefacts and was collected wherever available from the site. Grid collection was made from sites with a high concentration of artefacts with a less disturbed context. For systematic collection, different sizes of grids were placed, and artefacts were collected square by square; each square and artefacts were labelled accordingly. Grid collection was made only from two sites 1) Doma and 2) Kone. At Doma, a 30 × 20 meter grid was placed with 24 squares of 5 × 5 meter, the squares were labelled D_1 to D_{24}, and a serial number was provided to the artefacts in each square. At Kone, an 8 × 6 meter grid was placed with a total of 12 squares ($K_1 – K_{12}$) of 2 × 2 meters, and serial numbers were provided for the artefacts from K_1 to K_{12} squares. All artefacts collected from the sites were first brought to the base in the field; some of the artefacts were washed and labelled at the base. After that, all artefacts were packed in trunks and transported to the Palaeoanthropology and Archaeology (Palaeo – Arch) Lab at IISER Mohali via SUVs and Indian Railways.

Artefacts were cleaned with water and a soft brush in the field and lab. Each artefact was given a three-letter code related to the site name/code and a numerical number for identification. A plastic 150 mm vernier calliper, an Aero Space 200 mm vernier calliper, and a 180-degree national goniometer were used for various measurements. Some selected artefacts were photographed using a Canon 1500D digital camera with 18-55 mm and 55-200 mm lenses, while smaller artefacts were captured using a magnifying glass lens in front of the

mouth of the 18-55 mm lens and an Amazon Basics 60-inch lightweight tripod support. All artefacts were photographed in the lab using artificial light, and all pictures were edited in Photoshop. The artefacts were individually packaged in zip-lock bags with their unique identifying numbers. The zip-lock bags were then classified and stored in stainless steel trunks.

Table 12. The number of sites, their area, number of artefacts collected, collection method and respective period.

Sr. No.	Site	Size (m)	Artefacts	Collection Method	Period
1	Doma	300 L x 100 W	820	Grid	Late Acheulean to Upper Palaeolithic
2	Khempur	50-100 meter radius around the hill	153	Comprehensive/Random	Middle Palaeolithic
3	Kone	200 L × 70 W	510	Grid	Microlithic
4	Kargara	100 L × 50 W	225	Comprehensive/Random	Middle/Upper Palaeolithic /Microlithic
5	Bagia	200 L × 100 W	164	Comprehensive/Random	Middle Palaeolithic
6	Parva Chinguri	100 L × 50 W	443	Comprehensive/Random	Microlithic
7	Newari	30 L × 50 W	567	Comprehensive/Random	Microlithic

3.8.5 Lithic analysis

After collecting lithic artefacts from the study area, they were washed and analysed in the Palaeo-Arch Lab at IISER Mohali using various quantitative and qualitative methods. Quantitative variables include measurements of artefacts and other attributes, i.e., length, width, thickness, weight, edge angle, flake scars shape and the percentage of original cortex retained (*Table 13-16*). Qualitative variables include raw material type, tool type, general morphology, edge damage, retouching levels, and the amount of weathering *(Table 13-16)*. This resulted in a comprehensive typo-technological assessment of the assemblages. The

primary lithic analysis will be restricted only to the evidence collected from the LSV (U.P.). The study area has yielded different sites, tentatively attributed to Late Acheulean, Middle and Upper Palaeolithic and microlithic, that appear to be broadly contemporary with most of the other selected sites for study outside the LSV. Broadly, the LSV lithics comprise flakes, cores, bifaces, blades, microblades, scrapers, points, and notches, which are defined below:

Flake: Any piece of stone detached from a nucleus, be it a core/ another flake/ from a tool during its manufacturing by percussion or pressure, that possesses one of the combinations of the following: ring crack, platform, eraillure, positive bulb of percussion or clearly discernible dorsal and ventral surfaces (Andrefsky and Andrefsky, 1998, Inizan et al., 1999).

Core: A nucleus/mass of rock/ block of raw material that shows the sign of detached piece removal/flakes to produce tool blanks. These are different from core tools as core tools are made by reducing the core by removal of flakes until it has a desired shape or edge and used for chopping, cutting or some activity other than as a source of detached pieces (i.e., flakes) (Andrefsky and Andrefsky, 1998, Inizan et al., 1999, Banning, 2022)

Bifaces: In the bifaces category, only handaxes are found in the LSV. 'In general, a handaxe is a flake or core blank that has been reduced on both faces from two parallel but opposing axes through percussion' (Kelly, 1988, p. 718).

'A tool with two surfaces that meet to form a single edge that circumscribes the tool. Both faces usually contain flake scars that travel at least halfway across the face.' (Andrefsky and Andrefsky, 1998, xxi).

Blade: The flakes that are twice as long as they are wide, with parallel or almost parallel lateral margins and parallel dorsal flake scars (Mackay, 2008, p. 88).

Microlith: Backed/truncated flake/flake fragments less than 3 cm long and less than 1 cm wide (Shea, 2016); for this study, we consider blades which are <3 cm long with 1.5 cm or less width, whether backed or not. Similarly, blade cores which are <3 cm are categorised as microblade cores.

Notch: Notching refers to the production of a single, relatively deep concavity on the flake margin. It can be produced in two ways: by a single blow or by several small, continuous retouch scars that shape the concavity (Bordes, 1961; Debenath and Dibble, 1994).

Point: A flake or blade, Levallois or not, having convergent lateral edges or is modified/retouched and is usually triangular or subtriangular in shape with a pointed end (Bordes, 1961; Debenath and Dibble, 1994)

Scraper: An artefact made on flake or blade can be Levallois or not, with a continuous retouch that is flat or abrupt, scaled or not on one or more margins, in order to produce a more or less straight, convex or concave cutting edge with no deliberate notching or denticulation (Bordes, 1961; Debenath and Dibble, 1994)

Measurements for the flakes, blades, and microblades were done along the technological axis, while the morphological axis was considered for cores and handaxes. The lithic attributes for analysis were adapted from various authors (Andrefsky and Andrefsky, 1998; Blinkhorn, 2012; Bordes, 1961; Boëda, 1993; Debenath and Dibble, 1994; Högberg, 2016; Inizan et al., 1999; Sharon, 2007; Thompson et al., 2014; Villa et al., 2018; Wojtczak, 2014).

The following attributes have been recorded on the artefacts (if an attribute is absent then denoted as NA: not applicable/available).

Table 13. Flake Attributes

Flakes		
Attributes		**Features**
1	**Site Name/code/year**	LSV…
2	**Length**	Maximum in mm
3	**Width**	Maximum in mm
4	**Thickness**	Maximum in mm
5	**Weight**	Weight in grams (g)
6	**Type of Flake**	Regular, side, oblique, end, indeterminate
7	**Shape of flake**	Square, triangular, rectangular, elongated, amorphous
8	**Eraillure**	Present, absent
9	**Bulb of percussion**	Flat, prominent, broken
10	**Platform width**	Width of platform orientated by flaking axis (mm)
11	**Platform thickness**	Perpendicular to platform width at point of percussion (mm)
12	**Platform preparation**	Plain, facetted, dihedral convex, dihedral flat, punctiform, cortical, indeterminate, abraded
13	**Platform appearance**	Crushed, small, big, oval, squared, rectangle
14	**Exterior Platform angle**	Angle between platform and dorsal surface
15	**Interior Platform Angle**	Angle between platform and ventral surface
16	**No. of Dorsal flake scars**	Total number of flake scars present on dorsal surface
17	**No. of ventral flake scars**	Total number of flake scars present on dorsal surface
18	**Dorsal flake scar pattern**	Unidirectional, bidirectional, centripetal, crossed, irregular, indeterminate, absent
19	**Ventral flake scar pattern**	Unidirectional, bidirectional, centripetal, crossed, irregular, indeterminate, absent
20	**Flake termination**	Step, feather, hinge
21	**Retouch**	Present, absent
22	**Retouch position**	Direct, inverse, alternating, alternate, bifacial, crossed
23	**Retouch delineation**	Rectilinear, convex, concave, denticulate, notch, shouldered, nose, tanged, irregular
24	**Retouch angle**	Low (10 or less), semi-abrupt (11-45), abrupt (46-90)
25	**Retouch localisation**	Right lateral, left lateral, mesial, proximal, distal
26	**Retouch morphology**	Scaled, stepped, parallel, sub-parallel
27	**Retouch distribution**	Continuous, discontinuous, partial
28	**Retouch extent**	Short, long, invasive, covering
29	**Tool Type**	Point, scraper, notch
30	**Raw material**	Chert, porcellanite, quartz, quartzite, limestone, agate, chalcedony
31	**Blank type**	Angular clast, rounded clast (cobble), rounded clast (pebble), sub-angular clast, indeterminate
32	**Artefact condition**	(1-5) (1 – fresh, 5 – completely rolled)
33	**Position of cortex**	A, B, C, D (4 quadrant)
34	**Amount of cortex**	In %
35	**Completeness**	Complete, incomplete, broken
36	**Patination**	Patinated, double patinated
37	**Surface**	Abraded, plain
38	**Modern edge damage**	Present, absent
39	**Utilization marks**	Present, absent
40	**Affected by natural weathering/exfoliation**	Present, absent
41	**Remarks**	

Table 14. Blade Attributes

Blades		
Attributes		**Features**
1	**Site Name/code/year**	LSV…
2	**Length**	Maximum in mm
3	**Width**	Maximum in mm
4	**Thickness**	Maximum in mm
5	**Weight**	Weight in grams (g)
6	**Shape**	Rectangle, point
7	**Fragmentation**	Distal, Mesio-distal, Mesial, Mesio-proximal, Proximal, Complete, Indeterminate
8	**Blade Curvature/Profile**	1 -Straight, 2- Curved along distal part, 3- curved along medial part, 4- Curved along proximal part, 5- Curved, 6- Twisted, 7 - Indeterminate
9	**Cross- section**	1- Flat, 2- Triangular, 3- Trapezoid, 4- U-shaped, 5- Rectangular, 6- Polyhydric, 7-Indeterminate
10	**Platform width**	Width of platform orientated by flaking axis (mm)
11	**Platform thickness**	Perpendicular to platform width at point of percussion (mm)
12	**Platform preparation**	Plain, facetted, dihedral convex, dihedral flat, punctiform, cortical, indeterminate, abraded, absent (not applicable)
13	**Platform appearance**	Crushed, small, big, oval, squared, rectangle
14	**Dorsal cortex**	Presence of cortex on dorsal surface
15	**Dorsal ridges**	Number of Dorsal ridges extending over more than three-quarters of the length of the blade
16	**Dorsal flake scars**	Number of Dorsal flake scars extending over more than three-quarters of the length of the blade
17	**Opposite negative scars**	Number of dorsal flake scars run in the opposite direction to which the blade has been detached from the core.
18	**Axial percussion**	Parallel to length axis, from left, from right
19	**Termination**	Overshot, hinge, feathered, intermediate, step
20	**Shoulders**	1 – No shoulder, 2 – Shoulder slightly pronounced on one side (left or right), 3 – Pronounced shoulder on both sides, 4 – Concave shoulder on one or both sides
21	**Transition line between platform and ventral side**	1- Smooth, 2- Marked, 3- Rhombic, 4- wing, 5- Double impact, 6 Double line
22	**Eraillure**	Present, absent
23	**Exterior platform angle**	Angle between platform and dorsal surface
24	**Interior platform angle**	Angle between platform and ventral surface
25	**Lip**	Present, absent
26	**Bulb of percussion**	Flat; prominent, broken
27	**Exterior core surface**	1-Blunt Platform; 2- Abraded platform; 3- Small preparation flakes on dorsal side by platform edge; 4- One single preparation flake running down the dorsal side; 5- One single preparation flake running down to the left on the dorsal side; 6- One single preparation flake running down to the right on the dorsal side; 7- Several preparation flakes running down the dorsal side; 8- Several preparation flakes of same size running down of dorsal surface; 9- Blade lacks preparation
28	**Raw material**	Chert, porcellanite, quartz, quartzite, limestone, agate, chalcedony
29	**Blank type**	Angular clast, rounded clast (cobble), rounded clast (pebble), sub-angular clast, indeterminate
30	**Artefact condition**	(1-5) (1 – fresh, 5 – completely rolled)
31	**Position of cortex**	A, B, C, D (4 quadrant)
32	**Amount of cortex**	In %
33	**Completeness**	Complete, incomplete, broken

34	**Patination**	Patinated, double patinated
35	**Surface**	Abraded, plain
36	**Modern edge damage**	Present, absent
37	**Utilisation marks**	Present, absent
38	**Affected by natural weathering/exfoliation**	Present, absent
39	**Remarks**	

Table 15. Core Attributes

Cores		
Attributes		**Features**
1	**Site Name/code/year**	LSV…
2	**Length**	Maximum in mm
3	**Width**	Maximum in mm
4	**Thickness**	Maximum in mm
5	**Weight**	Weight in grams (g)
6	**No. of flake scars on face 1**	Total number of flake scars present
7	**No. of flake scars on face 2**	Total number of flake scars present
8	**No. of flake scars on face 3**	Total number of flake scars present
9	**No. of flake scars on face 4**	Total number of flake scars present
10	**Technique of percussion**	Direct, indirect, pressure
11	**Method of flaking**	Regular, discoid, prepared, kombewa, centripetal, laminar
12	**Flake scar direction**	Unidirectional parallel, unidirectional convergent, radial/centripetal, bidirectional-opposed, bidirectional, irregular, bidirectional convergent
13	**Flaking pattern**	Unidirectional, Centripetal unidirectional, Bidirectional, Orthogonal, Bipolar, Multidirectional, Centripetal, Discoid, Core-on-flake
14	**Type of core**	Centripetal, prepared, Levallois, blade, discoid, multi-platform, amorphous, exhausted, core-on-flake, bidirectional, single platform (unifacial), single platform (bifacial), double platform (unifacial)
15	**Raw material**	Chert, porcellanite, quartz, quartzite, limestone, agate, chalcedony
16	**Blank type**	Angular clast, rounded clast (cobble), rounded clast (pebble), sub-angular clast, indeterminate
17	**Artefact condition**	(1-5) (1 – Fresh, 5 – completely rolled)
18	**Position of cortex**	A, B, C, D (4 quadrants)
19	**Amount of cortex**	In %
20	**Completeness**	Complete, incomplete, broken
21	**Patination**	Patinated, double patinated
22	**Surface**	Abraded, plain
23	**Modern edge damage**	Present, absent
24	**Utilization marks**	Present, absent
25	**Affected by natural weathering/exfoliation**	Present, absent
26	**Remarks**	

Table 16. Biface Attributes

Bifaces		
Attributes		**Features**
1	**Site Name/code/year**	LSV…
2	**Length**	Maximum in mm
3	**Width**	Maximum in mm
4	**Thickness**	Maximum in mm
5	**Weight**	Weight in grams (g)
6	**L1**	Distance from the base to the point of maximum width
7	**Width at the tip (B1)**	Width at 1/5th Length
8	**Width at the base (B2)**	Width at 4/5th Length
9	**Width at Mid-point (B3)**	Width at 1/2nd Length
10	**Thickness at Tip (T1)**	Thickness at 1/5th Length
11	**Thickness at Base (T2)**	Thickness at 4/5th Length
12	**Thickness at Mid-point (T3)**	Thickness at 1/2nd Length
13	**Tip angle**	Measured in degree
14	**No. of flake scars on dorsal**	Total number of flake scars present
15	**Flake scar length**	Maximum in mm
16	**Flake scar width**	Maximum in mm perpendicular to length
17	**No. of flake scars on ventral**	Total number of flake scars present
18	**Flake scar length**	Maximum in mm
19	**Flake scar width**	Maximum in mm perpendicular to length
20	**Working edge length**	Maximum in mm
21	**Working edge shape**	Straight, convex, concave, sinous, jagged, irregular
22	**Type of Flake**	Regular, end, side, oblique, indeterminate
23	**Bulb of percussion**	Flat; prominent, broken
24	**Platform width**	Maximum in mm
25	**Platform thickness**	Maximum in mm perpendicular to width
26	**Biface shape**	Ovate, pick, triangle
27	**Butt shape**	Square, round, point
28	**Raw material**	Chert, porcellanite, quartz, quartzite, limestone, agate, chalcedony
29	**Blank type**	Angular clast, rounded clast (cobble), rounded clast (pebble), sub-angular clast, indeterminate
30	**Artefact condition**	(1-5) (1 – Fresh, 5 – completely rolled)
31	**Position of cortex**	A, B, C, D (4 quadrants)
32	**Amount of cortex**	In %
33	**Completeness**	Complete, incomplete, broken
34	**Patination**	Patinated, double patinated
35	**Surface**	Abraded, plain
36	**Modern edge damage**	Present, absent
37	**Utilisation marks**	Present, absent
38	**Affected by natural weathering/exfoliation**	Present, absent
39	**Remarks**	

3.8.6 Stable Isotope Analysis

The atomic number of an element is the number of protons present in its atom. The atomic mass of an element is the number of protons and neutrons present in its atom. Isotopes are atoms of an element with the same atomic number but different atomic mass; they have different numbers of neutrons.

There are two kinds of isotopes: radioactive (unstable) isotopes and stable isotopes. Radioactive isotopes are isotopes that have an unstable ratio of neutrons and protons. Stable isotopes have a stable proton-neutron pair that do not decay and hence produce no radiation. The number of neutrons present in the nucleus determines the stability of the atom. The stable isotopes of interest generally include H, C, N, O, S, B, and Li. Isotopic fractionation is the relative partition of lighter and heavier isotopes in a natural system between two coexisting phases. The slightly variable binding energy of each isotope causes isotope fractionation. The heavier isotopes react at a slower rate and have stronger bonds. The reaction rate and bonding energy difference are proportional to the isotope mass difference. Isotopic fractionation is more evident in lighter elements than in heavier elements. The most abundant elements on Earth are highly prone to isotopic fractionation: H, C, N, O, and S.

In this research, we are only focussing on carbon and oxygen isotopes. Stable isotope analysis can be performed on different materials, but this research will focus on vertebrate fossil teeth. The author collected the sample for stable isotope analysis and analysed by Dr. Shailesh Agrawal, Birbal Sahni Institute of Palaeosciences (BSIP), Lucknow.

3.8.7 Carbon Isotopes

Carbon have three isotopes, which are used in palaeoclimate reconstruction and determining age. Carbon-12 (^{12}C) is the most prevalent carbon isotope, with six protons and neutrons. Carbon-13 (^{13}C), which has seven neutrons, is the next heaviest isotope of carbon. Both

carbon isotopes are stable since they do not decay further; the ratio of these two isotopes is used to reconstruct the past ecology. Carbon-14 (^{14}C), the rarest of the three isotopes, has eight neutrons in its nucleus and is radioactive, unlike the other two. Almost 99% of all carbon on Earth is ^{12}C, with ^{13}C accounting for the remaining 1% and ^{14}C accounting for less than 0.0001%.

3.8.8 Oxygen Isotopes

There are three stable isotopes of oxygen: ^{16}O, ^{17}O, and ^{18}O. Based on natural abundance, ^{16}O is the most abundant on Earth (99.76%), whereas the other two, ^{17}O and ^{18}O, account for 0.04% and 0.20% of the total oxygen existing on the planet, respectively. ^{16}O has eight neutrons and 8 protons, ^{17}O has nine neutrons, and ^{18}O has ten neutrons and eight protons. ^{16}O and ^{18}O are classified as light and heavy isotopes based on their mass, and the ratio of these isotopes is commonly used to reconstruct the palaeoclimate.

3.8.9 Carbonates

Carbonates are widely used as proxy records of palaeoclimatic change. Oxygen ($\delta^{18}O$) and carbon ($\delta^{13}C$) isotopic signatures are indicative of temperature, aridity or vegetation at the time of calcrete formation. The standard procedure for processing carbonate samples is adopted from previously established studies (McLaren et al. 2012; Agrawal et al. 2013; Adamson et al. 2015) - 1) Rinse carbonates nodules in distilled water and treats in ultra-sonic bath for some 3 min. to remove adhering sediments. 2) Fine grained carbonate nodules are preferred for analysis, nodules are crushed to powder; 3) For $\delta^{13}C$ and $\delta^{18}O$ values, ~100–300 μg of powdered carbonate samples is required, further putting the powder into screw capped glass vials; divided into two parts. 4) One part is used for making a thin section for microscopic study and the remaining part was used for isotopic analysis of carbonates and organic matter. 5) The vials are flushed with pure Helium (He) gas followed by injected

~100% phosphoric acid manually into each vial at 72°C temperature bath. The evolved CO_2 will be purified by Nafion tube and Porapack column in Gas Bench and allowed into Continuous Flow Isotope Ratio Mass Spectrometer (CFIRMS) for analysis. Each measurement comprised of three pulses of reference followed by six pulses of sample CO 2 gas. The tank reference gas was calibrated by using IAEA 603. All samples including standards were measured with respect to the calibrated tank gas. The isotopic data are reported against VPDB with a precision of ±0.1‰ (1σ) for both $\delta^{18}O$ and $\delta^{13}C$ values.

3.8.10 Fossil teeth enamel

Generally, stable isotope analysis on fossilised material can provide information about drinking water using $\delta^{18}O$ values, and carbon ($\delta^{13}C$ values) reveals dietary preference (Besado et al., 2010). Several studies have been conducted internationally that undertake stable isotope analysis on fossil/modern vertebrate tooth/teeth; 1) tooth enamel of 9 middle Miocene mammalian herbivores from Fort Ternan, Kenya, were analysed for δ^{18} O and $\delta^{13}C$ values. Where the $\delta^{18}O$ value of tooth enamel was compared with pedogenic and diagenetic carbonate, this study confirms the use of stable isotope analysis of tooth enamel as a palaeoenvironmental indicator. The $\delta^{18}O$ values show differences in water sources between animals (Cerling et al., 1997). 2) In Lower Awash Valley, Ethiopia analysis of $\delta^{18}O$ and $\delta^{13}C$ isotopic comparison on 80 herbivore tooth enamel samples was performed; $\delta^{13}C$ signified a wide range of foraging strategies and ($\delta^{18}O$) isotopic enrichment between evaporation sensitive and insensitive taxa, indicates high rainfall season (Bedaso et al., 2010). 3) In the Narok and Nakuru districts of southwest Kenya (Balasse and Ambrose, 2005), 40 modern tooth samples of goats and sheep were analysed for distinguishing sheep and goats using dental morphology and stable carbon isotopes in C_4 grassland environments, and different $\delta^{13}C$ values were assigned for sheep and goats showing their different dietary preferences.

For the thesis, fossil teeth samples were collected from 1) Nehlai, Sihore, Madhya Pradesh; 2) various localities from Narsinghpur, Madya Pradesh; 3) Gopnath, Bhavnagar, Gujarat; 4) Doma (the LSV), Sonbhadra, Uttar Pradesh. The sample cleaning and collection methods were followed from Millers et al. (2018).

1) The outer surface of the tooth was cleaned (~0.1 mm) with gentle abrasion using a handheld drill with a clean diamond-tipped drill bit. 2) Drilling was conducted at the Palaeo-Arch Lab IISER Mohali, Maharaja Sayajirao University of Baroda and Deccan College, Pune, in a well-ventilated room wearing a mask and goggles. 3) Approximately 4-8 mg of sample powder was collected, transferred to a 1.5 ml microcentrifuge tube, and labelled with the sample designation. 4) Used drill bits were cleaned with 0.5 M HCl and then acetone before drilling each new tooth. 5) The workspace was thoroughly cleaned and wiped with a dustpan, brush, and methanol (*Figure 30*).

The mechanism for the stable isotope[4] analysis comes from standard established procedures (e.g., Balasse et al., 2002, Bedaso et al., 2010; Cerling et al., 1997). The pure enamel sample (10-20 μg) is prepared from the individual tooth by removing all dentine. Cleaned enamel powder was treated in 3% hydrogen peroxide (H_2O_2) to extract organic matter, followed by rinsing in 1M acetic acid-calcium acetate buffer to remove secondary carbonates. A ~2-3 μg of samples and three carbonate standards (NBS 18, IAEA603 and Carrara marble) were kept in individual screw-capped glass vials. After flushing with He gas, 100% orthophosphoric acid (H_3PO_4) was injected into each vial which was kept at a 72ºC temperature bath for two hours. The evolved CO_2 was purified by a Nafion tube and Pora pack column in Gas Bench

[4] All the samples were measured at the stable isotope facility at Birbal Sahni Institute of Palaeosciences by Dr. Shailesh Agrawal and at stable isotope facility at IIT Kanpur by Prof. Debajyoti Paul.

and allowed into Continuous Flow Isotope Ratio Mass Spectrometer (CFIRMS, MAT 253) for isotopic analysis. Each measurement comprised three pulses of reference followed by six pulses of sample CO_2 gas. The tank reference gas was calibrated by using IAEA 603. All samples, including standards, were measured with respect to the calibrated tank gas. The isotopic data are reported against VPDB with a precision of ±0.1‰ (1σ) for $\delta^{18}O$ and $\delta^{13}C$ values.

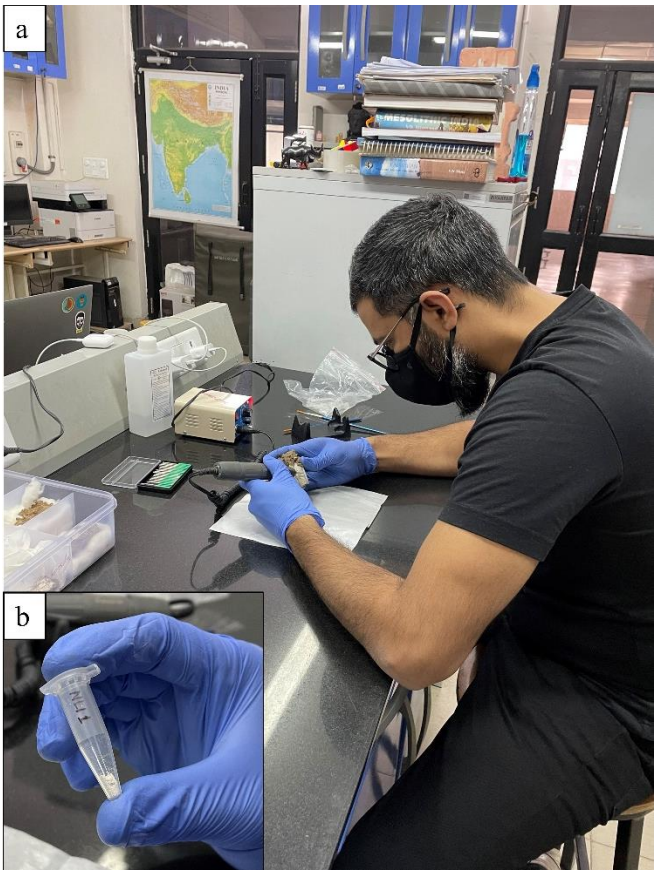

Figure 30. a) Extracting enamel powder from fossil tooth using a handheld drill for stable isotope analysis, b) collection of drilled enamel powder in a 1.5ml tube with the label.

3.8.11 OSL (Optical Stimulated Luminescence) dating [5]

The OSL dating method utilises the dosimetric properties of mineral grains found in sediments and man-made materials (Aitken, 1998; Huntley et al., 1985). In the LSV, OSL dating was applied to sediment samples collected from a geological trench located in Kargara. The step trench was approximately 11 meters in depth, and the samples were collected using an aluminium tube measuring approximately 30 cm in length and 8-10 cm in diameter. Before sample collection, the trench steps were scraped, and a meter scale was used to measure the depth of the samples. The tube was inserted horizontally *(Figure 31)* into the centre of the section with the help of a steel hammer. Sample collection was conducted after sunset, with no natural light allowed to enter the sampling area during or before sample collection. After the tube was fully inserted into the sediment, it was extracted carefully by removing the surrounding sediment, and the mouth of the tube was closed with a cap and labelled accordingly. A total of nine samples were collected from the trench. Subsequently, these samples were analysed for OSL dating in designated laboratories.

[5]Prof. Vimal Singh first analysed these samples at the Department of Geology, University of Delhi. Unfortunately, very few quartz grains were recovered, which was insufficient for dating purposes. Subsequently, these samples were transferred to the Physical Research Laboratory in Ahmedabad for another dating attempt using alternate luminescence methods. Dr. Naveen Chauhan subsequently evaluated these samples for IRSL (Infrared stimulated luminescence) feldspar dating. The OSL dating methods and results were provided by Dr. Naveen Kumar.

Figure 31. OSL sample collection from step-trench at Kargara.

Samples were analysed and handled under the subdued red light. The samples were processed using routine procedure; treated with 1N HCl acid for 24 hours and Hydrogen Peroxide (H_2O_2) for 12 hours to remove carbonates and organic materials, respectively (Wintle, 1997). Grains having 90-150 µm in diameter were separated through dry sieving. Quartz and feldspar grains were separated using a Frantz® magnetic separator. The feldspar grains were subsequently etched with 10% hydrofluoric (HF) acid for 40 minutes to remove the alpha-irradiated skin (Duval et al., 2018). The etched feldspar grains were treated with concentrated HCl (37%) for 30 minutes to dissolve the residual fluorides. Infrared stimulation was generated using IR-LEDs (850 nm with FWHM 33 nm) in a Risø TL/OSL DA-20 reader.

The post-IR IR single aliquot regeneration (pIRIR-SAR) protocol was used for the estimation of palaeo-dose (*Table 17*) (Buylaert et al., 2011). A preheat of 320º C for 60s was used, and pIRIR was measured at 290º C for 100s (Buylaert et al., 2011; Thomsen et al., 2011). The preheat temperature was taken from a preheat plateau test conducted on the natural sample (*Figure 32*). An arithmetic mean of the equivalent dose (D_e) of three aliquots for each preheat was used to estimate the final D_e. The doses for 280º C, 300º C, 320º C, and 340º C fell

within 5% of the estimated paleo-dose (*Figure 32*). The typical shine down curve of pIRIR is shown in (*Figure 33*). The initial 2s luminescence signal was used as the signal, and a final 20s signal was used as the background.

Table 17. Parameters used in pIRIR-SAR protocol.

Steps	*A*
1	*Dose*
2	*Preheat @320 ℃ for 60 s*
3	*IRSL @50 ℃ for 100 s*
4	*IRSL @290 ℃ for 100 s*
5	*Test dose*
6	*Preheat @320 ℃ for 60 s*
7	*IRSL @50 ℃ for 100 s*
8	*IRSL @290 ℃ for 100 s*
9	*IRSL @ 325 ℃ for 200 s*
10	*Return to step 2 (Repeat up to 5 cycles)*

The dose estimation central age model (CAM) was used as the dose scatter was much less (*Figure 33*). For all samples, the acceptance criteria were recuperation ratio < 5%; recycling ratio < 10% of unity.

A dose recovery test was conducted to test the applicability of the used pIRIR-SAR protocol. Five aliquots of the OSL-8 sample were first bleached in the 300W Ultra vitalux solar lamp and filtered through a borax glass for up to 5 hours. Aliquots were then irradiated with a known beta dose of 220 Gy, and the dose recovered was 216 ± 8 Gy, giving a dose recovery ratio of 0.98 ± 0.04.

Five aliquots of the OSL-8 sample were bleached under a solar lamp for 5 hours to check the residual level of the dose that remained after bleaching. The residual dose estimated was 18.7 ± 0.8 Gy. This residual dose was subtracted from the estimated D_es to obtain the true paleo-dose.

The fading rates (*g*-values) were estimated using the procedure outlined by Auclair et al., 2003. It involves bleaching the sample, given the known laboratory dose equal to palaeo-doses estimated for respective samples, preheating it and measuring luminescence intensity at different time delays. The time delays ranged from prompt measurements to up to 2 days. Fading rate (% per decade) was estimated from the slope of the graph plotted between delayed intensities and logarithmic delayed time, as shown in (*Figure 34*) (Huntley and Lamothe, 2001). Fading rates ranged from 0.9 to 2.3 % per decade. The doses were corrected for fading using (Huntley and Lamothe, 2001).

The concentration of Uranium, Thorium and potassium nuclides were measured using a high purity Germanium (HPGe) detector. All samples were first dried, powdered, and homogenized before the measurements. Further, these concentrations were used to estimate the total dose rate assuming an infinite matrix assumption and all nuclides are in secular equilibrium (Beck and de Planque, 1985).

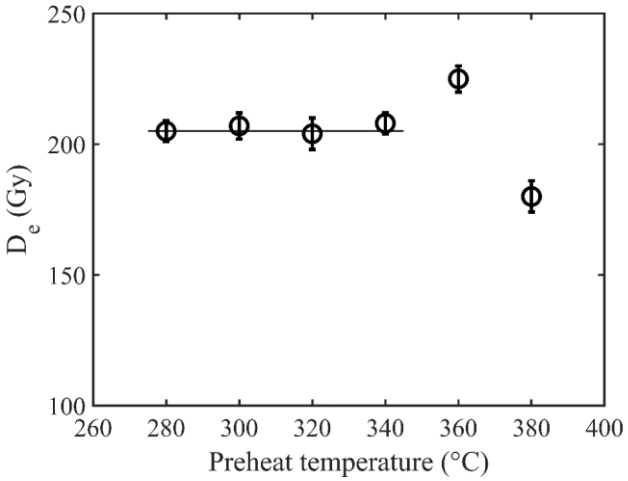

Figure 32. Equivalent dose (De) variation with preheat temperature. Preheat plateau is observed between 280 to 340°C preheat temperature.

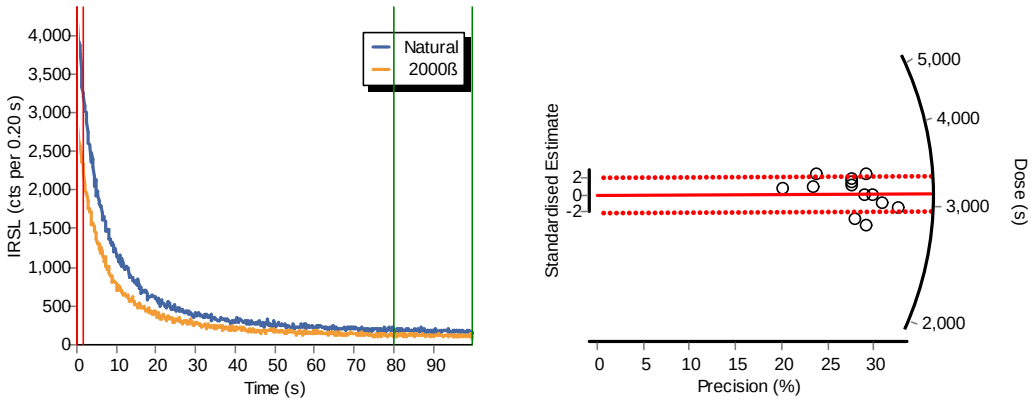

Figure 33. Results of pIRIR analyses of OSL-8 sample. A) Typical feldspar shine down curve; b) Radial plot representing the estimated paleo-doses.

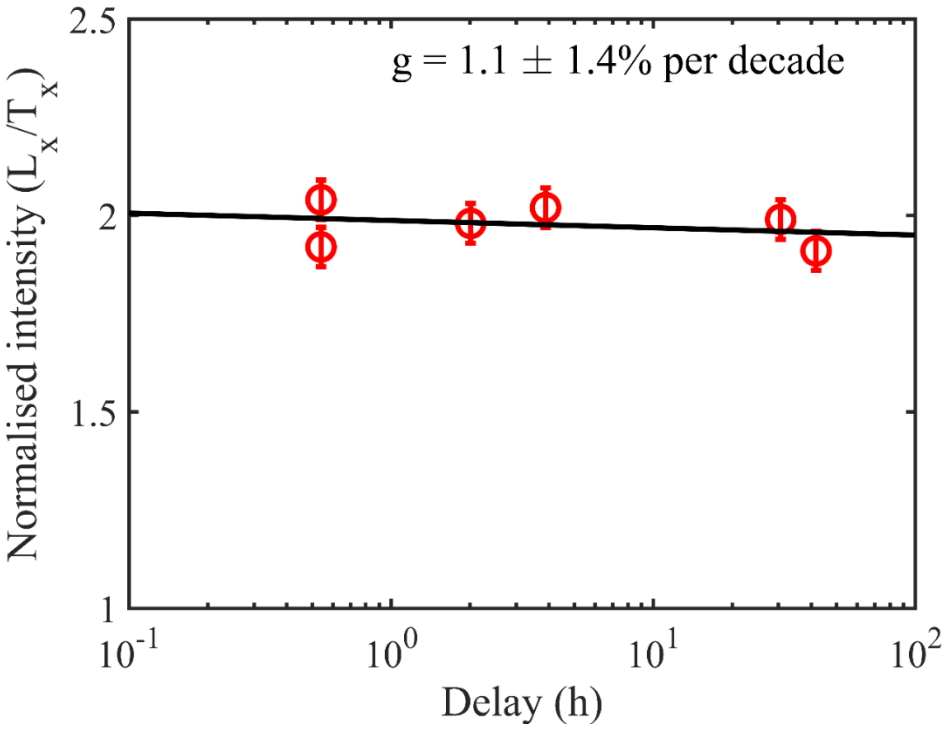

Figure 34. The normalised intensity with delay time for the OSL-8 sample.

3.8.12 Grain Size Analysis

Grain size analysis is a common analytical technique employed in the earth sciences and routinely performed in the laboratory. It is also utilised frequently by disciplines such as archaeology and geoarchaeology. It is a sedimentological analysis performed to determine the size of the various particles that make up a specific unconsolidated sedimentary deposit, sedimentary rock, archaeological site, or soil unit. This procedure's primary objective is to determine the type of environment and energy associated with the transport mechanism at the deposition time; this is accomplished by inference from the sizes and distributions of the sediment particles analysed.

The grain size analyses were performed following the methodology outlined in Ajay et al. (2021) and Bulbul et al. (2021). The sediment samples (n=216) for grain-size analysis (~2-5 g) were pre-treated with H_2O_2 (30%) to remove the organic matter incorporated in the sediments. Furthermore, the samples were treated with 1N HCl to eliminate detrital/authigenic carbonates (*Figure 35 a*). After removing carbonates and organic matter, the samples were centrifuged (using double distilled water) and decanted thrice to remove the excess acidic fraction (*Figure 35 b*). The grain-size analysis was carried out using a laser particle size analyser (Malvern Mastersizer 3000) coupled to a Hydro EV (Extended Volume) wet dispersion unit with a standard operating procedure of 20s measurement time, obscuration of 5–20% and dispersion speed of 2500 rpm (*Figure 35 c*). Three measurement cycles were recorded for each sample, and their mean value was considered. The grain-size distribution was intended for 100 grain-size classes (particle size ranging from 0.02 to 2000 μm), and the analytical error was less than 1%. The De Brouckere mean diameter (D [4, 3]) was obtained, and the results are reported in a volume percentage of sand, silt and clay according to a textural class of grain size (Folk and Ward, 1957).

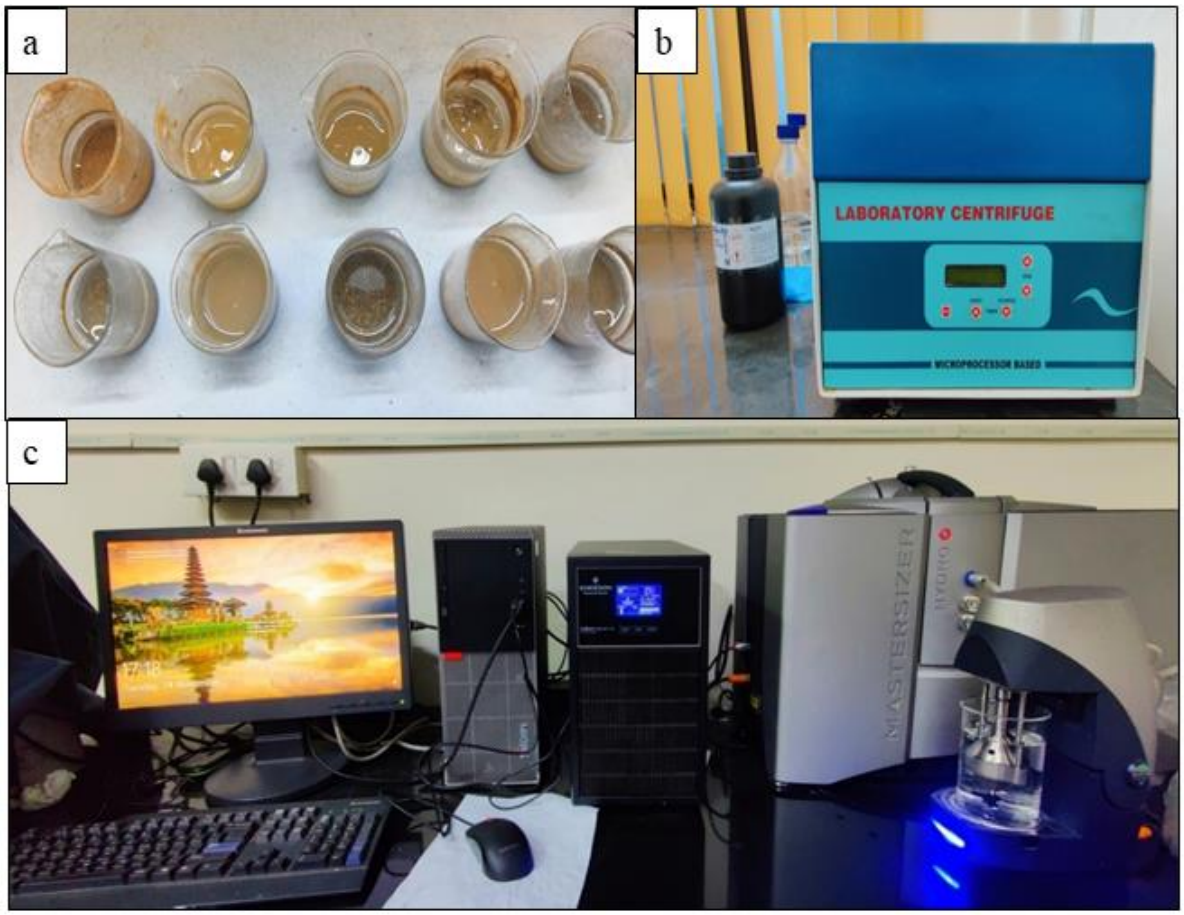

Figure 35. (a) Treatment of samples with H_2O_2 and HCl, (b) centrifuging samples using laboratory centrifuge, (c) Grain size analysis was performed using MASTERSIZER 3000E.

3.8.13 XRF Analysis

The X-Ray Fluorescence (XRF)[6] method was used to know about the chemical composition of the samples. Here, WDXRF (wavelength dispersive system) spectrometer was used because it has a wide elemental range than EDXRF (energy dispersive system). The precision and reproducibility of XRF are very high. In the sample preparation, 5 grams were taken

[6] The XRF analysis was conducted on a payment basis by Dr. Manoj Kumar Jaiswal and Mr. Biswajit Giri from IISER Kolkata, who also provided the materials and methods for the study.

from each sample and finely ground using a mortar and pestle at Palaeo - Arch Lab IISER Mohali. Then the prepared samples were sent to IISER Kolkata for analysis.

The XRF analysis was performed following the methodology described elsewhere (Dipti et al., 2022). The collected sediment samples were powdered to the size of approximately ~200 mesh for major and minor elemental concentrations. The powdered samples were then dried at 50 °C for 12h. For pallet preparation, powdered samples (ca. 5g) were mixed with sodium tetraborat and placed in an aluminium cup pressed under a hydraulic pressure of 20t for 1 min. The major element concentration was determined using X-ray fluorescence technique.

3.9 Selected sites for comparative analysis

Numerous archaeological surveys and descriptions of collected lithic assemblages have been reported from other regions across India. However, very few of these studies have also incorporated discrete comparisons with chronologically similar sites using multi-disciplinary scientific methods. Therefore, this project also aims to generate new comparative data to supplement and complement the LSV (U.P.) paleoanthropological evidence. Specific paleoanthropological sites have been selected for their respective scientific significance due to their broad chronological overlap with the LSV. They include exclusive vertebrate fossil sites, exclusive lithic sites and sites with these materials preserved together in various combinations and contexts. All selected five sites are described briefly below, along with their scientific justifications concerning the overall research questions addressed in this thesis. They are located in Gujarat, and Madhya Pradesh and different proxies (calcrete or fossil enamel) were targeted, respectively, depending on the material preserved at each site. Some of these sites have been known for decades, and various researchers have made collections of fossil and artefact specimens. Therefore, some sites were studied through step-trenching for primary sample collection of fossils and calcrete. In contrast, other sites such as

Gopnath (also visited by the author to understand the context) and Amonda were studied through previously made collections housed at Deccan College in Pune and the M.S. University of Baroda, Vadodara, respectively.

3.9.1 Gopnath

Gopnath is a small fishing village in Bhavnagar District (coastal Gujarat), nearly 5.5 km south of the present mouth of the Shetrunji River. It marks the southeastern point of the Saurashtra peninsula and the boundary between the Gulf of Cambay and the Arabian Sea. Vertebrate fossils at Gopnath were noted for the first time by Khadkikar and Basavaiah (2004). Recent work at the site by Costa (2011, 2017) yielded a new reduncine (*Sivacobus sankaliai*) that is unique in the Middle to Late Pleistocene record of Eurasia (Vrba et al., 2015). The Gopnath fossils complement Acheulean artefacts recovered from a nearby area at Madhuban *(Figure 36, 37)*; the locality around the site consists of carbonate blocks from which fossils were collected (Costa, 2017).

The fossil samples were collected by Dr. Augusta Costa during 2011-15 and were stored in the Department of Archaeology and Ancient History, Faculty of Arts, The Maharaja Sayajirao University, Baroda, India. I visited the site to get an idea about the stratigraphy and landscape and extracted samples of enamel from Dr. Costa's collection (GPN 1(Canid), GPN 14,79,96 (Bovid)) for stable isotope studies. This site is selected as a comparison with all other inland sites that preserve different fauna. The site is stratigraphically assigned to 57-26 kyr (Costa, 2017) and is consistent with our compiled data showing humid climatic conditions during MIS 3. Another date for Gopnath shows that it belongs to Late Middle Pleistocene (156 kyr) (Sharma et al., 2012).

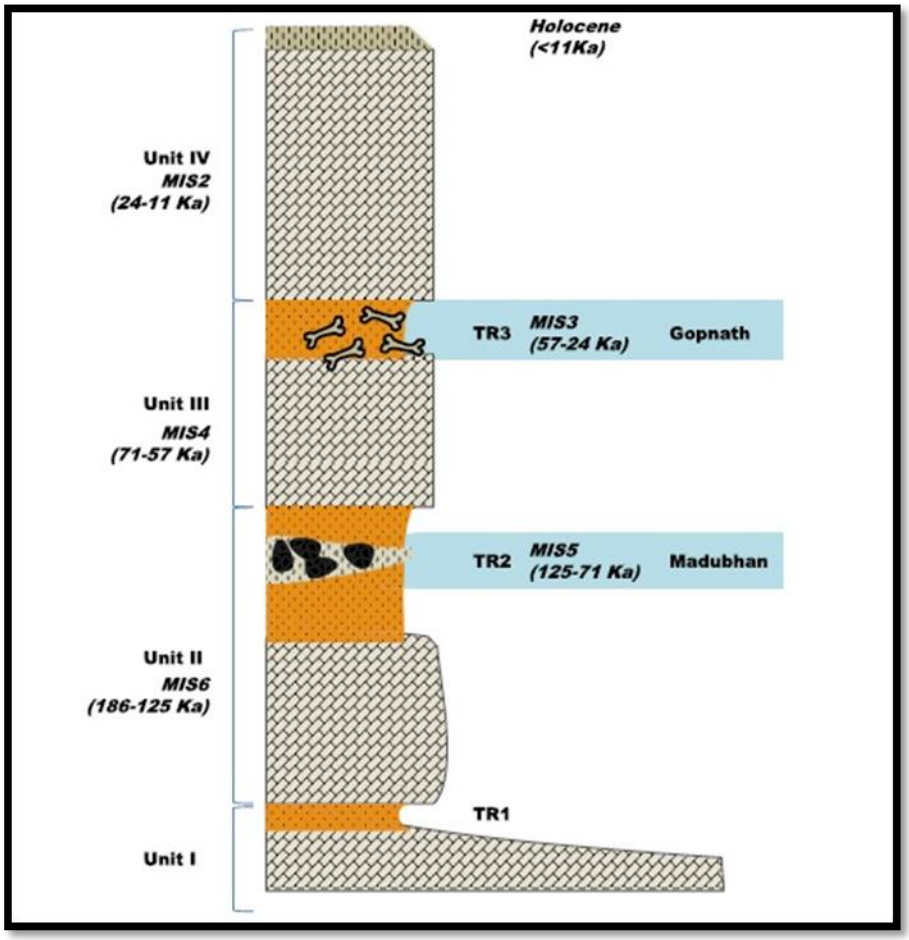

Figure 36. A composite succession of coastal carbonate aeolianites and terra rossa deposits in southeastern Bhavnagar (Gopnath Formation). Relative chronology is based on alternating environmental conditions and the assumption that the Indian Summer Monsoon tracks global glacial-interglacial phases (Costa et al., 2015).

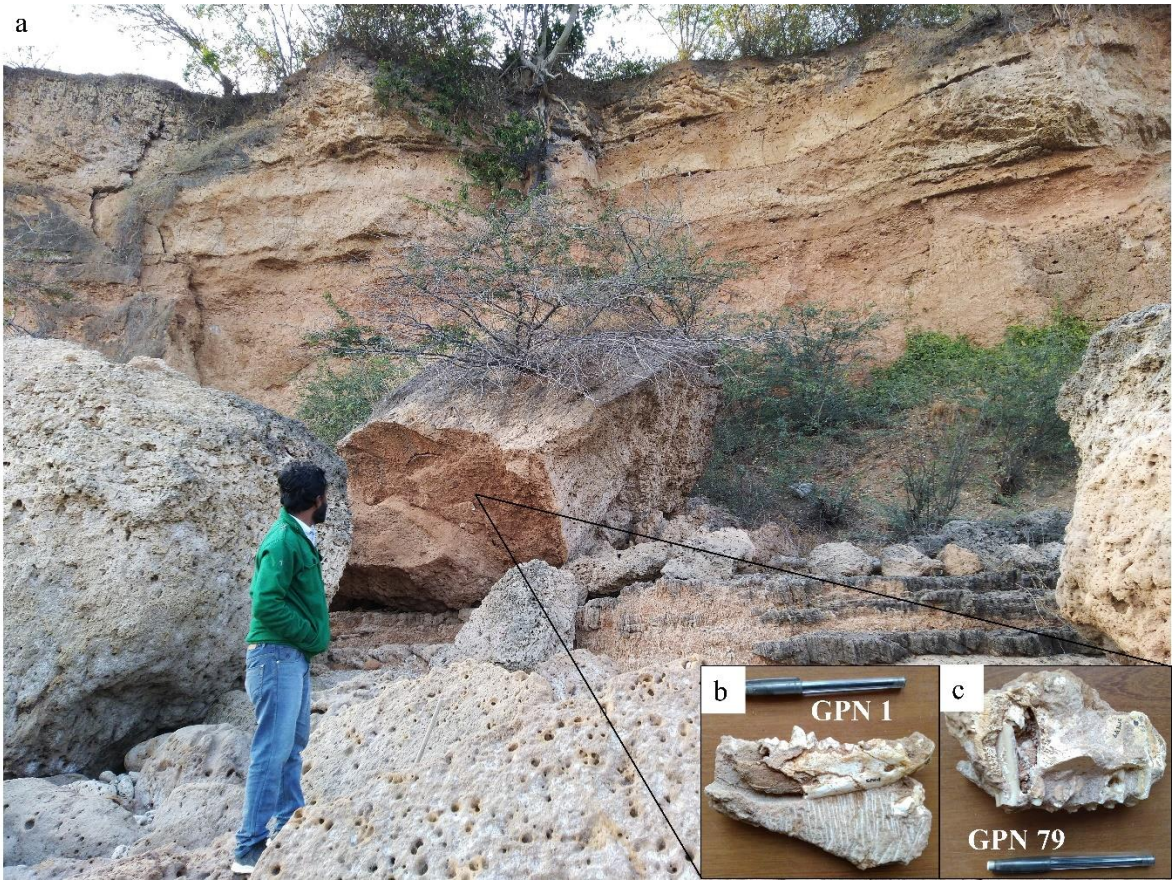

Figure 37. a) Gopnath site from where fossils were recovered by Dr. Costa b) GPN 1 fossil lower mandible of canid c) GPN 79 fossil teeth of Bovid.

3.9.2 Narsinghpur Region (Devakachar)

The site is located in the central Narmada Valley in Narsinghpur District (Madhya Pradesh); this site has yielded different vertebrate and invertebrate fossils, including a large number of cranio-dental and skeletal elements of elephant, crocodile, antelope, micromammal fossil and also molluscan shells and Middle and Upper Palaeolithic artefacts (Badam, 1979; Patnaik, 1995). An interesting worked bone, possibly a prehistoric chisel, was found in association with fossil rodents in the top gravel bed (Sharma and Misra, 2003). K. P. Oakley carried out a chemical study on the fossil bone from the site, and it was found that the nitrogen values of

the site are similar to the Upper Pleistocene of Africa and Europe. A radiocarbon date was assigned to the site around 31,750 years (+_1650) (Agrawal and Kusumgar, 1974).

Recently, new dating techniques have been developed further, and this site was excavated in 2018-19 (by my colleagues Bharti Jangra, Dr. Ravish Lal and Dr. Toshabanta Padhan) for characterising the stratigraphy *(Figure 38-39)*. A rolled artefact from the trench between 17-18m from the gravel layer was located. Sediment samples for OSL dating and calcrete samples for stable isotope analysis were collected from the trench. Besides the trench at Devakachar, many fossils in the nearby area were collected by my colleagues. Comparison with other research in the region shows that the Hirdepur Formation (tentatively dated <74 kyr), predominantly visible in the Narsinghpur region, can also be assigned to the deposits in the trench (Kotlia and Joshi, 2010; Tiwari and Bhai, 1997). Another date for the Middle and Upper Palaeolithic assemblages in the region was estimated to be ~ 30 ka (Agrawal and Kusumgar, 1974); therefore, most of the fossils collected from the region belong to Late Pleistocene, probably dated between 74-30 kyr[7] (more in-depth work is required for a confirmed date).

[7] This date is based on stratigraphic, and correlation as the youngest Middle Palaeolithic in South Asia is 38 ka, and in the Narsinghpur region, the youngest date of the site with fossils goes back to 31 ka and the Hirdepur Formation exposed in the region has the maximum age of 74 kyr.

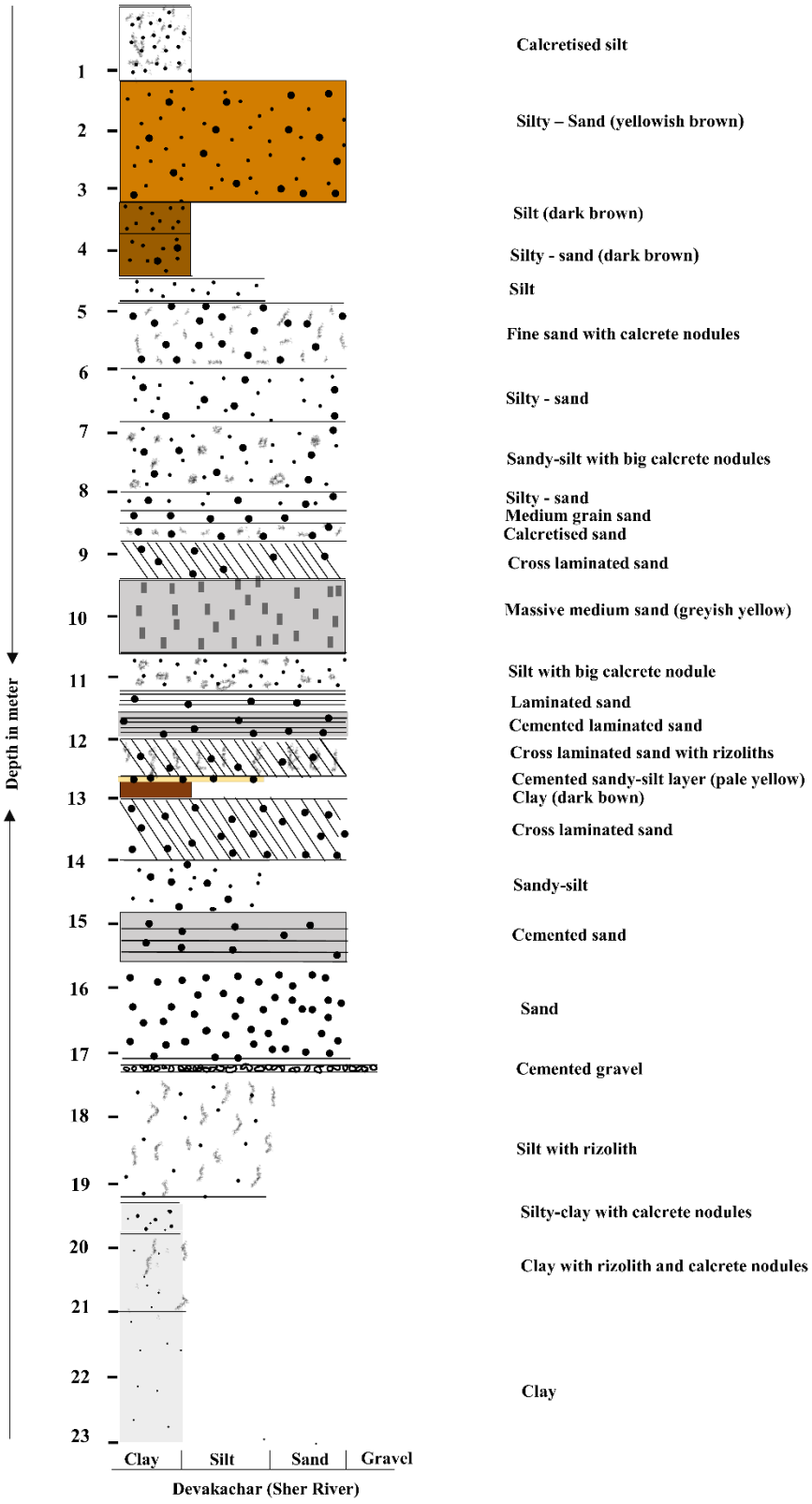

Figure 38. Stratigraphy of Devakachar.

Figure 39. a) Step trench at Devakachar, b) rolled artefact found at 17-18m from the gravel layer.

3.9.3 Narsinghpur Region (Talyaghat)

As Devakachar, the Talyaghat site is also located in the central Narmada Valley in Narsinghpur District (Madhya Pradesh) and has yielded numerous vertebrate fossils and artefacts. Although Bos sp., Equus sp., antelope, crocodile and turtle fossils were found at the site, it was especially rich in hippo fossils. Both known varieties of fossil hippos, namely, *Hexaprotodon namadicus* and *H. palaeindicus*, are found. The artefacts and fossils were collected between 2.0-2.5m depth (Loose pebbly sand with gravels of quartz, andesite, and agate). The artefacts were prepared on chalcedonic silica and comprised end flakes, side flakes, thick blades, scrapers, and cores. The assemblage represents Middle Palaeolithic culture, and artefacts were moderately rolled (IAR 1985-86, p. 53).

A systematic step-trench was conducted in 2019 by my colleagues (Bharti Jangra, Dr. Ravish Lal and Dr. Toshabanta Padhan); a total of 23-meter was excavated with eight units observed as follows 1) Sandy silt, 2) Planner bedded fine sand, 3) Sandy clay, 4) Sand, 5) Coarse grain sand layer, 6) Clay layer, 7) Sand layer with fossils and bivalves, 8) Sandstone bedrock in the river bed (*Figure 40*). Various samples, OSL samples, calcrete, sedimentary and fossil specimens were collected from the trench.

Similar to Devakachar, based on geology, palaeontology and archaeology, the site can be bracketed under Late Pleistocene (Kotlia and Joshi, 2011; IAR 1985-86, p. 53; Tewari and Bhai, 1997)

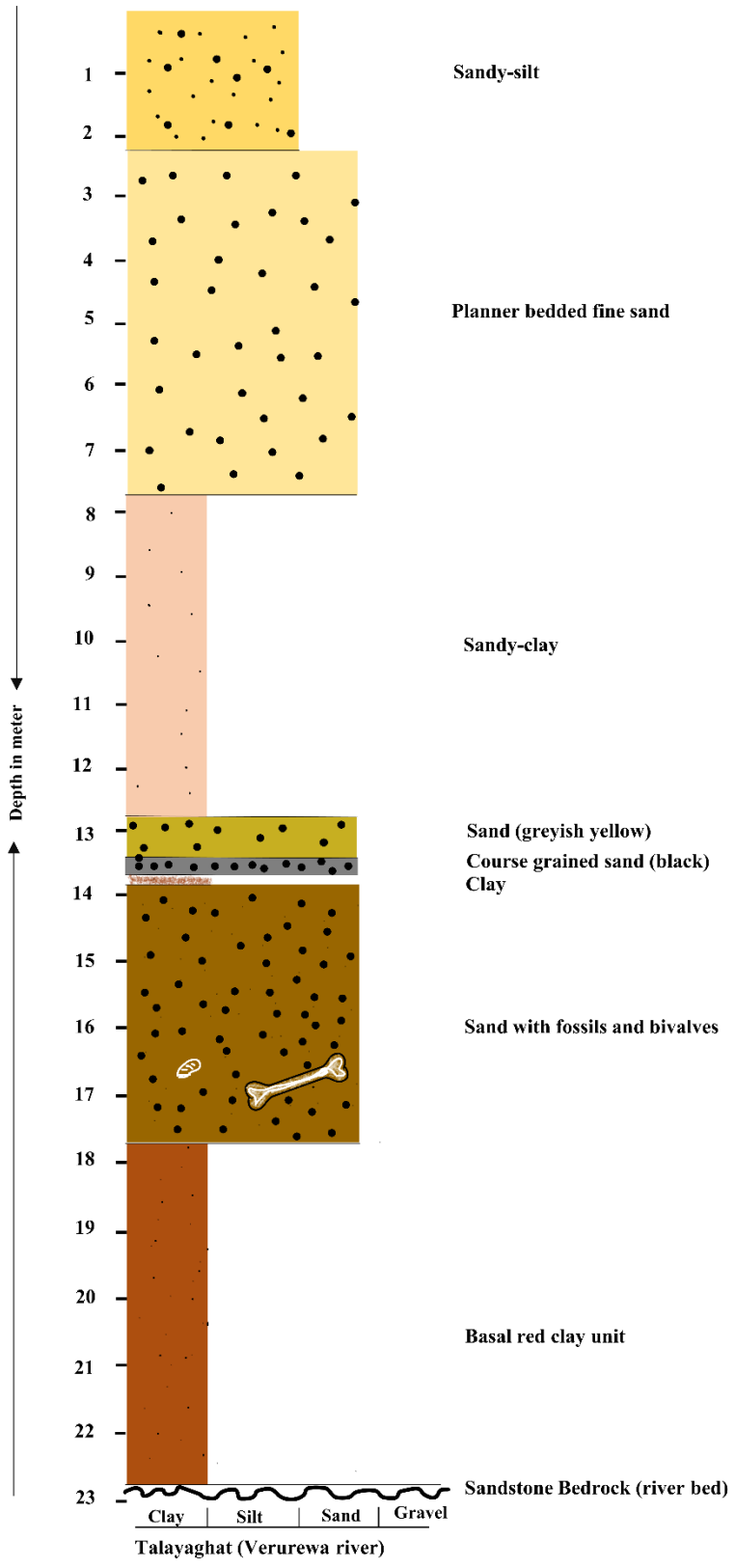

Figure 40. Stratigraphy of Talayaghat showing eight different units and fossil bone and bivalve location.

3.9.4 Nehlai, Sehore, Madhya Pradesh

Nehali ghat is around 68 km west of Hoshangabad (now Narmadapuram) in Sehore District, Madhya Pradesh and has yielded fresh choppers, primary flakes, and some vertebrate fossils. The geological trench (1x1m trench) and a step-trench were carried out at the site in May 2017. Flakes and vertebrate fossils were recovered during the excavation from both trenches at different stratigraphic levels; 394 artefacts were collected from the surface context from the site by placing grids of various sizes. While excavating the step trench (*Figure 41*), Dr. Vivek Singh and the author recovered flakes associated with fossil fragments, burnt soil and charcoal samples were also found in association. The silty sediments at Nehlai belong to the Baneta Formation, which can be broadly dated between ~ 84 to 8 kyr (Kale et al., 2020; Patnaik et al., 2009; Tiwari and Bhai, 1997; Pers. Comm. with Dr. Vivek Singh)).

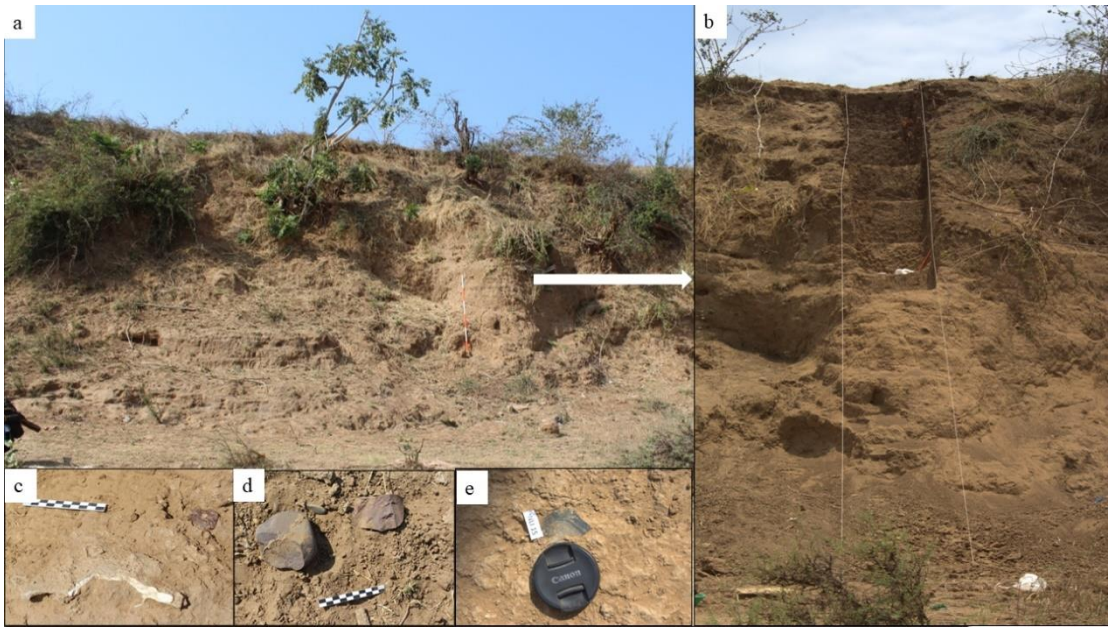

Figure 41. a) General view of Nehlai, b) step-trench at Nehlai, c) in-situ artefact and fossil from the trench, d) artefacts scattered at the site, e) in-situ artefact at the site.

3.9.5 Pilikarar, Sehore, Madhya Pradesh

This site is located 10 km west of Hoshangabad (now Narmadapuram), the formation of the site is considered to be the oldest Quaternary formation in the central Narmada Basin (Tiwari and Bhai 1997). However, a contradicting interpretation by Patnaik *et al.*, (2009) suggests that the oldest Quaternary deposits, may be the Dhansi Formation. This site is known for yielding early Acheulean artefacts such as handaxes and cleavers from the Pilikarar Formation (Patnaik *et al.*, 2009; Chauhan and Patnaik 2017) and microliths have been seen to erode out of the younger deposits, presumably of the Baneta Formation which can be broadly dated between ~ 84 to 8 kyr (Kale et al., 2020; Patnaik et al., 2009; Tiwari and Bhai, 1997; Pers. Comm. with Dr. Vivek Singh)) (*Figure 42,43*).

Two geological trenches were placed by my colleague Dr. Vivek Singh along with me and interns (Shantanu Katiyar and Shubham Pal), sediments from both trenches were collected for OSL dating. The first trench was 1 x 0.50 m in dimension with a depth of 03.5 m and located at the type-section of Pilikarar Formation on the Kaliadoh stream. It took three and a half steps (single step = 50 cm) to reach the regolith, which is defined as being a part of the Pilikarar Formation by Tiwari and Bhai (1997). The second trench was 2 x 2 m in dimension and was located at the main artefact locality in the foothills. This trench was three meters deep, and 12 luminescence samples were taken due to the clayey nature of the sediments. The Acheulean horizon was not reached in the trench because the early monsoon disrupted the investigation. According to Tiwari and Bhai Acheulean artefacts are located in the Pilikarar formation and on top of that lies the Baneta formation, as the Acheulean horizon was not reached in trench 2, hence it is assumed here that this might belong to Baneta formation which dates back to Late Pleistocene and calcrete samples were collected from here for palaeoenvironment reconstruction.

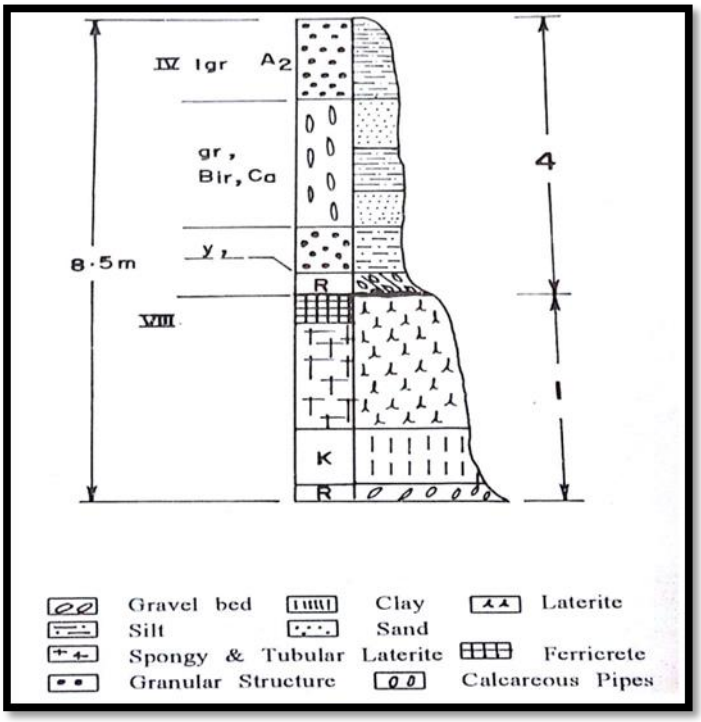

Figure 42. Stratotype section of the Pilikarar Formation (1) and Baneta Formation (4). Left Column Weathering Profile, Right Colum Stratotype (Tiwari and Bhai, 1997).

Figure 43. Step-trench at Pilikarar (PC – Vivek Singh)

Table 18. Select sites for comparative study.

Sr.No.	Site	Tool type	Proxies	Importance to research
1	Gopnath, Gujarat	No artefacts	Fossil teeth enamel	This site is unique due to its geographical location at the Arabian Sea; it yielded fossilised partial cranium of an antelope species, *Sivacobus sankaliai* and other different fossils; this site provides an insight that it may have served as a corridor for different species to migrate in the subcontinent
2	Different localities in Narsinghpur, Madhya Pradesh	Middle Palaeolithic artefacts	Fossil teeth enamel and Calcrete	1) Vertebrate fossils, Micro mammal fossils 2) Mammalian fossils were found in the same strata as Middle Palaeolithic artefacts
3	Nehlai, Madhya Pradesh	Choppers and flake tools	Fossil teeth enamel	Fossil teeth and carbonates associated with flakes
4	Pilikarar, Madya Pradesh	Mircoliths	Calcrete	Calcrete collected from Baneta formation

4 Lithic Analysis

This chapter describes the lithic analysis of 1196 artefacts from seven sites (see Appendix *Table A 1 to Table A 20*) (total number of artefacts collected = 2882). Only complete artefacts were subjected to lithic and statistical analysis. The presence of a large number of artefacts in a semi-primary context or a relative lack of disturbance compared to other sites led to the selection of these seven sites. The lithic collection methods include grid and comprehensive collection. The random/comprehensive collection was made from sites with a low concentration of artefacts, whereas the grid collection was made from sites with a high concentration of artefacts. These sites include Doma, Bagia, Khempur, Kone, Kargara, Parva Chinguri, and Newari.

4.1 Doma

Doma is located between Misari and Doma villages on the left bank of the Panda River and on the left side of the main Ramgarh-Kone road. Along the foothills, artefacts were discovered within a 300 L x 100 W m area. The site is unique in the region because it is the only known location with bifaces (represented here by handaxes), despite extensive surveys. Handaxes, prepared cores, Levallois cores, blade cores, prepared flakes, Levallois flakes, flakes and blades make up the assemblage. All artefacts were made on black or olive green porcellanite. The assemblages at and near the site include artefacts from various technological periods, such as Late Acheulean, Middle and Upper Palaeolithic. The site is ideal for determining the stratigraphy and ages of the local assemblages (Mehra, 2021).

In total, 820 artefacts were systematically collected (*Table 19*) from the site using a 15 x 15m grid and through random/comprehensive sampling.

Table 19.Assemblage composition and frequency at Doma.

Typology	N (820)	%	Complete specimens				
			N (418)	%	Mean (SD)		
					Length (mm)	Breadth (mm)	Thickness (mm)
Biface (handaxe)	5	0.6	3	0.7	116.3(16.4)	87.3(14.1)	30(4.24)
Core	61	7.4	60	14	83.9(24.5)	69.9(18.3)	33.8(10)
Prepared			14	3.3	92.4(31.1)	77.4(23.3)	32.7(8.9)
Levallois			2	0.5	88(2)	81(1)	33(9)
Discoid			3	0.7	66(10.7)	60(11.4)	37(4.3)
Blade			8	1.9	84.4(24)	59.3(17.9)	34.5(11.7)
Multi-Platform			2	0.5	55(10)	53.5(0.5)	23(2)
Centripetal			7	1.6	89.1(15)	70.3(14.4)	33.4(10)
Core-on-flake			4	0.9	87.3(36.2)	72.3(16.7)	25(6.1)
Amorphous			13	3	86.3(15.2)	74.8(13.1)	40.3(9.6)
Exhausted			7	1.6	69.9(16.8)	61(11.1)	30.1(6.5)
Flake	608	74.1	340	79.3	53.4(19.3)	43.4(17.1)	13.4(6.9)
Regular			35	8.2	44.2(13.6)	42.3(14.6)	12.1(5.3)
End			166	38.7	59.5(17.9)	38.2(11.9)	12.6(5.6)
Oblique			66	15.4	56.1(19.3)	42.6(16.3)	14.4(6.3)
Side			73	17	41.3(17.2)	57.4(21.4)	15.1(9.6)
Blade	60	7.3	14	3.3	77.4(15)	30.3(5.5)	9.8(3.1)
Blade flake	32	3.9	12	2.8	80.2(14.1)	35.9(7.2)	12.1(1.7)
Core fragment	37	4.5	0	-	-	-	-
Core/flake fragment	5	0.6	0	-	-	-	-
Angular fragment	10	1.2	0	-	-	-	-
Debitage	2	0.2	0	-	-	-	-
Total	820	~100	429	~100	-	-	-

4.1.1 Bifaces (handaxe) from Doma

A total of five bifaces have been recovered from the site; out of these five, only three were complete and considered for analysis. Bifaces make up only 0.7% of the entire assemblage. The average dimensions[8] for the bifaces were 116.3 × 87.3 ×30 mm. The bifaces were

[8] Mean or average dimensions of artefacts are represented as length × width × thickness.

collected from a find-spot where the colluvium rubble of Unit III (*Figure 23 b*) was exposed due to anthropogenic activities, mostly digging for agricultural purposes. All artefacts were patinated; three specimens (no. DMA 1(*Plate 1. b*), 2, 823) were found without abrasion, while two were rolled (no. DMA 3,6).

4.1.2 Cores from Doma

Sixty artefacts were classified as cores, making up 14% of the assemblage. These cores were mostly made on angular clasts; only a few were on rounded clasts. There were 14 prepared cores with average dimensions of 92.4 × 69.9 × 33.8 mm. These cores were the most common type, followed by amorphous cores, with 13 specimens showing average dimensions of 86.3 × 74.8 × 40.3 mm, with an irregular flaking pattern. After prepared and amorphous cores, blade cores were the most common, with eight specimens with average measurements of 84.4 × 59.3 × 34.5 mm. A total of seven centripetally flaked cores and seven exhausted cores were reported with average dimensions of 89.1 × 70.3 × 33.4 mm and 69.9 × 61 × 30.1 mm, respectively. There were only two Levallois cores (*Plate 1. c, e*) and two multi-platform cores documented with overall dimensions of 88 × 81 × 33 mm and 55 × 53.5 × 23 mm, respectively. A total of four core–on–flake and three discoid core specimens were documented with average dimensions of 87.3 × 72.3 × 25 mm and 66 × 60 × 34 mm, respectively.

Because the shape of the raw material is primarily angular, the cores were usually flatbacked. The presence of cortex and high patina was observed. In most cores, a single surface has been used for flaking, and the flake scars on the second surface are mainly used as a platform. The cores appear to have been reduced in every possible way, indicating a wide range of flaking patterns, e.g., unidirectional, bidirectional, centripetal and irregular flaking methods.

4.1.3 Flakes from Doma

This category outnumbers every other category in artefact counts, with 340 specimens and an overall frequency of 79.3%. In this category, regular flakes (n = 35) were dominated by a square shape with average dimensions of 44.2 × 42.3 × 12.1 mm. Compared to other flakes, end-struck flakes outnumber other flakes with a total count of 166 and have an average size of 59.5 × 38.2 × 12.6 mm and are rectangular. A total of 66 oblique-struck flakes show average measurements of 56.1 × 42.6 × 14.4 mm, these flakes were also rectangular, but their length and breadth ratio were less than end flakes. A total of 73 side-struck flakes show average dimensions of 41.3 × 57.4 × 15.1 mm and are rectangular. The latter two types of flakes appear to be similar in their average dimensions regardless of their morphologies, and some flakes appear to be used and retouched. The flake assemblage consists of numerous tools, including scrapers, points, and notches, and most flakes were found with the presence of cortex and patination.

4.1.4 Blades and Blade flakes from Doma

Blades (n = 60) are a unique feature of the site, with a frequency of 7.3%. Most blades were snapped (n = 46), but 14 specimens were complete with average dimensions of 77.4 × 30.3 × 9.8 mm. Some of the artefacts were patinated, and some had cortex. A total of 32 blade flakes specimens were observed, out of which only 12 were complete with average dimensions of 80.2 × 35.9 × 12.1 mm.

4.2 Bagia

This site is located five kilometres southeast of the main village centre of Kone and at the foothills on the right bank of the Panda River. The site has an approximate expansion over ~ 200 L x 100 W m. Most of the artefacts in the collection were flake tools, such as scrapers,

blades, prepared flakes, and prepared and blade cores. Comprehensive collection at Bagia reported 164 artefacts, of which 75 were complete specimens (*Table 20*). The artefacts were made on porcellanite rocks that can be found within a 4-5 km radius.

Table 20. Assemblage composition and frequency at Bagia.

Typology	**N (164)**	**%**	**Complete specimens**				
			N (76)	**%**	**Mean (SD)**		
					Length (mm)	**Breadth (mm)**	**Thickness (mm)**
Core	42	25.6	35	46.7	75.3(28.8)	57(16.2)	28.8(14.3)
Prepared			16	21.3	74.3(15.9)	60.9(13.5)	21.9(6.1)
Levallois			1	1.3	63	60	23
Discoid			1	1.3	85	75	39
Blade			6	8	52.2(20.9)	38.3(5.2)	22.8(4.5)
Multi-platform			5	6.7	95.2(31.9)	65.6(19.4)	52.2(14.7)
Double Platform			1	1.3	76	63	55
Single Platform Unifacial			1	1.3	53	43	28
Single Platform Bifacial			1	1.3	180	81	51
Core-on-flake			1	1.3	54	45	18
Exhausted			2	2.7	64(14)	47.5(3.5)	28.5(2.5)
Flake	70	42.7	40	53.3	67(24.8)	51.2(18.2)	15.8(5.8)
Regular			2	2.7	45.5(4.5)	44(3)	12(1)
End			25	3.3	75(23)	47.5(15.3)	17(5.8)
Oblique			4	5.3	70(21.4)	57.3(16)	14(1.9)
Side			9	12	48.2(20.7)	60.3(23.5)	14.3(6.7)
Blade	8	4.9	0	-	-	-	-
Flake fragment	36	21.9	0	-	-	-	-
Angular fragment	8	4.9	0	-	-	-	-
Total	164	100	75	100	-	-	-

4.2.1 Cores from Bagia

Thirty-five artefacts were classified as cores, making up 46.7% of the assemblage. These cores were mostly made on angular clasts; only a few were on rounded clasts. There were 16 prepared cores with average dimensions of 74.3 × 60.9 × 21.9 mm. These cores were the

most common type, followed by blade cores (*n* = 6) and multi-platform cores (*n* = 5), with average dimensions of 52.2 × 38.3 × 22.8 mm and 95.2 × 65.6 × 52.2 mm, respectively. Other types were also present and were primarily observed in singular quantity, Levallois (63 × 60 × 23 mm) (*Plate 2. b*), discoid (85 × 75 × 39 mm), double platform (76 × 63 × 55 mm), single platform unifacial (53 × 43 × 28 mm), single platform bifacial (180 × 81 × 51 mm), core-on-flake (54 × 45 × 18 mm), along with these two exhausted cores with average measurement of 64 × 47.5 × 28.5 mm, were reported.

4.2.2 Flakes from Bagia

This category contains 40 artefacts with an aggregate frequency of 53.3%. End-struck flakes (*n* = 25) in this category have a rectangular shape and average dimensions of 75 × 47.5 × 17 mm. These were followed by the side-struck flakes, with a total count of nine specimens and an average measurement of 48.2 × 60.3 × 14.3 mm; these flakes were also rectangular. Four oblique-struck flakes with average dimensions of 70 × 57.3 × 14 mm were rectangular, and two regular flakes with average dimensions of 45.5 × 44 × 12 mm of square shape were observed. The presence of cortex and patination was observed in most flakes.

4.3 Khempur

The site is near a small hill on the left side of the Ramgarh-Kone road, near Khempur primary school. Artefacts were found within a 100 m radius of the hill. The assemblage consists mainly of cores (*n* = 30) and flakes (*n* = 60), including flake tools (scrapers, Levallois flakes), blades and prepared and blade cores (*Plate 3*). The artefact collection was conducted comprehensively at the site, and 153 artefacts were collected (*Table 21*), of which 92 were complete. Artefacts were made mainly on porcellanite available within 2-3 km of the vicinity.

Table 21. Assemblage composition and frequency at Khempur.

Typology	**N (153)**	**%**	**Complete specimens**				
			N (92)	**%**	**Mean (SD)**		
					Length (mm)	**Breadth (mm)**	**Thickness (mm)**
Core	40	26.1	30	32.6	59.4(15.7)	49.2(14.2)	32.2(11.16)
Prepared			6	6.5	76.3(15.8)	63.2(11.2)	36.3(13.5)
Blade			3	3.26	61.3(13.1)	50.3(14.4)	20(2.4)
Multi-platform			14	15.2	53.1(10)	42.6(11.6)	33.4(9.1)
Single Platform Unifacial			2	2.2	72(3)	62(10)	42.5(0.5)
Single Platform Bifacial			1	1.1	49	45	29
Core-on-flake			2	2.2	37(2)	33(8)	16.5(1.5)
Exhausted			2	2.2	65(10)	57(2)	37.5(7.5)
Flake	97	63.4	60	65.2	50.2(12.1)	43.1(13.7)	12.7(4.6)
Regular			12	13	42.4(8.8)	40.8(10.2)	11.9(5.1)
End			29	31.5	54.2(12.4)	38.4(11.3)	11.3(3.4)
Oblique			10	10.9	50.6(8.9)	45(12.5)	14.7(4.2)
Side			9	9.8	47.1(12.6)	59.1(13.9)	15.9(5.5)
Blade	2	1.3	2	2.2	49(1)	19.5(2.5)	9.5(1.5)
Flake fragment	14	9.2	0	-	-	-	-
Total	153	100	92	100	-	-	-

4.3.1 Cores from Khempur

Thirty artefacts were classified as cores, making up 32.6% of the assemblage and mainly were made on angular clasts. There were 14 multi-platform cores with average dimensions of 53.1 × 42.6 × 33.4 mm. These were the most common core type, followed by prepared cores with six specimens with average dimensions of 76.3 × 63.2 × 36.3 mm. After prepared and multi-platform core, blade cores were most commonly present, with three specimens with average dimensions of 61.3 × 50.3 × 20 mm, other core types were primarily observed in singular quantity, single platform bifacial (49 × 45 × 29 mm), and double quantity; single platform unifacial (72 × 62 × 42.5 mm), exhausted core (65 × 57 × 37.5 mm), core-on-flake (37 × 33 × 16.5 mm).

4.3.2 Flakes from Khempur

This category consists of 60 artefacts with an overall frequency of 65.2%. In this category, end-struck flakes (*n* = 29) were dominated by a rectangular shape with average dimensions of 54.2 × 38.4 × 11.3 mm. It was followed by regular flakes with a total count of 12 artefacts and have average size of 42.4 × 40.8 × 11.9 mm and were predominantly square shaped. A total of 10 oblique-struck flakes show average measurements of 50.6 × 45 × 14.7 mm, and a total of nine side-struck flakes show average dimensions of 47.1 × 59.1 × 15.9 mm, both were predominantly rectangular shaped. Most of the flakes were observed to have the presence of cortex and patination.

4.3.3 Blades from Khempur

The whole assemblage consists of two blades; both were complete. The average blade measurements were 49 × 19.5 × 9.5 mm.

4.4 Parva Chinguri

Parva Chinguri site is located on the Kaimur Plateau on the left side of the Son River. The landscape of the site consists of many rock shelters and agricultural fields; only one has ochre rock paintings. The site consists of flake tools, blade cores, fluted cores, blades, backed blades, microblades, and a borer.

The artefact collection was made comprehensively from the site, and a minimum of 443 artefacts were collected (*Table 22*).

Table 22. Assemblage composition and frequency at Parva Chinguri.

Typology		**N (443)**	**%**	**Complete specimens**				
				N (96)	**%**	**Mean (SD)**		
						Length (mm)	**Breadth (mm)**	**Thickness (mm)**
Core		39	8.8	24	25	44.5(16.3)	29.3(14.5)	20.3(12.5)
	Prepared			1	1	30	24	20
	Blade			12	12.5	47.4(8.6)	27.5(7.9)	17(4.3)
	Single Platform Unifacial			3	3.13	73.3(1.2)	59(3.6)	45.7(13.3)
	Microblade			4	4.2	25(0.7)	15.3(2.2)	11.25(1.5)
	Exhausted			4	4.7	37.5(15.3)	28(13.4)	20.5(12)
Flake		64	14.5	45	46.9	30.6(10.5)	27.9(8)	8.2(3.2)
	Regular			2		25.5(7.5)	25.5(7.5)	9(3)
	End			25		35.2(10.9)	26.2(8.14)	8.5(3.7)
	Oblique			3		33(3.7)	24.3(5.2)	7.7(0.5)
	Side			15		23.3(5.4)	31.9(6.7)	7.7(2.5)
Blade		214	48.3	15	15.6	39.8(6.5)	15.2(5.7)	6.8(3.5)
Microblade		12	2.7	12	12.5	23(3.7)	9.7(2.3)	3.7(1.7)
Flake fragment		113	25.5	0	-	-	-	-
Angular fragment		1	0.2	0	-	-	-	-
Total		443	100	96	100	-	-	-

4.4.1 Cores from Parva Chinguri

Twenty-four artefacts were classified as cores, making up 25 % of the assemblage. There were (n = 12) blade cores with average dimensions of 47.4 × 27.5 × 17 mm. These cores were the most common type, followed by exhausted cores with an irregular flaking pattern and microblade cores. A total of four specimens of each category were observed with average measurements of 37.5 × 28 × 20.5 mm and 25 × 15.6 × 11.6 mm, respectively. After blade, exhausted and microblade cores, single platform unifacial cores (*Plate 4. a*) were most frequently present with three specimens and average dimensions of 73.3 × 59 × 45.7 mm. Only a single prepared core with average dimensions of 30 × 24 × 20 mm was observed.

4.4.2 Flakes from Parva Chinguri

This category outnumbers every other category in artefact counts, with 45 artefacts and an overall frequency of 46.9 %. In this category, regular flakes (n = 2) were square-shaped with average dimensions of 25.5 × 25.5 × 9 mm. In comparison, end-struck flakes outnumber other flakes with a total of 25 specimens and have an average size of 35.2 × 26.2 × 8.5 mm and were rectangular. A total of three oblique-struck flakes show average measurements of 33 × 24.3 × 7.7 mm, and a total of 15 side-struck flakes show average dimensions of 23.3 × 31.9 × 7.7 mm; both categories were dominated by a rectangular shape.

4.4.3 Blades from Parva Chinguri

Blades (n = 15) show a frequency of 15.6 % of the total assemblage. Most of the blades were snapped (n = 199), but 15 specimens were complete with average dimensions of 39.8 × 15.2 × 6.8 mm.

4.4.4 Microblades from Parva Chinguri

A total of 12 microblade specimens were observed, showing average dimensions of 23 × 9.7 × 3.7 mm.

4.5 Kargara

Kargara is situated on the left bank of the Son River, on a calcrete-rich hill composed of fine sediments. The site has an area of ~ 100 L × 50 W metres (Location 1) and ~ 200 L × 100 W m (Location 2). The collection contains various artefacts, including prepared flakes, fluted cores, blades, microblades, points, and cores. Various raw materials were utilised, including

chert, chalcedony, agate, and porcellanite. Artefact collection was made comprehensively from the site, and at least 225 artefacts were collected (*Table 23*) from Location 1.

Table 23. Assemblage composition and frequency at Kargara.

Typology	**N (225)**	**%**	**Complete specimens**				
			N (115)	**%**	**Mean (SD)**		
					Length (mm)	**Breadth (mm)**	**Thickness (mm)**
Core	46	20.4	31	26.9	50.2(22.3)	35(14.3)	26.6(14.9)
Prepared			2	1.7	50(5)	44.5(6.5)	35(16)
Discoid			1	0.9	63	47	32
Blade			8	7	42.3(10.2)	28.8(6)	21.5(6.1)
Multi-platform			4	3.5	60(9.7)	43.8(5.7)	33.5(9)
Double Platform			1	0.9	48	33	27
Single Platform Unifacial			3	2.6	98.3(30.3)	60.7(22.1)	57(19.6)
Core-on-flake			5	4.3	44.6(12.2)	27(4.7)	16.8(4.5)
Microblade			2	1.7	27(2)	18.5(0.5)	11.5(1.5)
Exhausted			5	4.3	39(12.9)	31.4(8.9)	22.2(5.3)
Flake	93	41.3	75	65.2	34(11.4)	32(11.6)	10.8(4.2)
Regular			2	1.7	37(10)	37(10)	12.5(2.5)
End			39	33.9	35.9(10.3)	26.7(8.2)	10(3.5)
Oblique			4	3.5	37(18.2)	35.8(19.5)	11(5.8)
Side			30	26.1	30.9(10.8)	38.1(10.8)	11.8(4.6)
Blade	24	10.7	4	4.5	41.3(7.6)	13.8(4.3)	4.5(0.5)
Microblade	3	1.3	3	2.6	27(1.6)	12(2.8)	3.3(0.5)
Flake fragment	57	25.3	0	-	-	-	-
Hammerstone	2	0.9	2	1.7	78(25)	62.5(11.5)	34(12)
Total	225	~100	115	~100	-	-	-

4.5.1 Cores from Kargara

Thirty-one artefacts were classified as cores, making up 26.9 % of the assemblage. There were eight blade cores (*Plate 5c*) with average dimensions of 42.3 × 28.8 × 21.5 mm. These cores were the most common type, followed by exhausted cores and core-on-flake, a total of five specimens each, with average dimensions of 39 × 31.4 × 22.2 mm and 44.6 × 27 × 16.8

mm, respectively. After exhausted cores and core-on-flake, multi-platform cores were the most common, with four specimens with average measurements of 60 × 43.8 × 33.5 mm. Microblade cores follow these multi-platform cores with two specimens with average dimensions of 27 × 18.5 × 11.5 mm. Other core types were discoid and double platform cores observed in a single quantity with average dimensions of 63 × 47 × 32 mm and 48 × 33 × 27 mm, respectively. Only three single platform unifacial cores *(Plate 5b*) were observed with overall dimensions of 98.3 × 60.7 × 57 mm.

4.5.2 Flakes from Kargara

This category outnumbers every other category in artefact counts, with 75 artefacts and an overall frequency of 65.2%. In this category, regular flakes (n = 2) were dominated by a square shape with average dimensions of 37 × 37 × 12.5 mm. In comparison, end-struck flakes outnumber other flakes with a total count of 39 and have average size of 35.9 × 26.7 × 10 mm and were predominantly rectangular. A total number of four oblique-struck flakes show average measurements of 37 × 35.8 × 11 mm and were dominated by a square shape. A total of 30 side-struck flakes offer average dimensions of 30.9 × 38.1 × 11.8 mm with a dominant rectangular shape.

4.5.3 Blades from Kargara

A total of 24 blades were observed at the site, and most of the blades were snapped (n = 20), but four specimens were complete with average dimensions of 41.3 × 13.8 × 4.5 mm.

4.5.4 Microblades from Kargara

A total of three microblade specimens were observed, showing an average dimension of 27 × 12 × 3.3 mm.

4.5.5 Hammerstones from Kargara

A total of two hammerstones were observed at the site, which was unique, as it is the only known occurrence of hammerstones in the valley. Hammerstones show average dimensions of 78 × 62.5 × 34 mm; on one hammerstone (*Plate 5a*), battering marks were observed all over its peripheral surface, indicating a possible use as an anvil, as it shows pit marks at its centre.

4.6 Newari

The location is adjacent to the Newari village on the right bank of the Son River. Various artefacts, such as fluted cores, blades, and microblades, were found all over the surface of a hill. The artefacts were produced from cryptocrystalline material such as chert, agate and chalcedony. The density of the artefact was relatively high compared to other sites in the valley; approximately 30-40 artefacts per metre square, with the site spread across an area of roughly 10×10 metres.

A minimum of 551 artefacts were collected (*Table 24*) from the site using a random/comprehensive sampling technique.

Table 24. Assemblage composition and frequency at Newari.

Typology		**N (567)**	**%**	**Complete specimens**				
				N (256)	**%**	**Mean (SD)**		
						Length (mm)	**Breadth (mm)**	**Thickness (mm)**
Core		101	17.8	101	39.4	35(12.3)	25.8(9.5)	18.9(7.7)
	Prepared			1	0.4	25	35	27
	Blade			38	14.8	40.7(7.5)	27.4(8)	20.1(7)
	Multi-platform			2	0.8	62.5(21.5)	48.5(16.5)	30(15)
	Single Platform Unifacial			3	1.2	56.3(23.5)	36.3(10.7)	31.7(14.1)
	Single Platform Bifacial			1	0.4	65	60	41
	Core-on-flake			6	2.3	28.2(3.3)	20.2(5)	9(2.2)
	Microblade			32	12.5	24.9(4.6)	20.5(4.4)	16.1(3.9)
	Amorphous			7	2.7	39(7.7)	29.7(7.9)	21.1(4.1)
	Exhausted			11	4.3	33.3(7.7)	25.6(7.9)	18.1(5.1)
Flake		166	29.3	139	54.3	29.5(8.7)	25.8(8.5)	9(3.5)
	Regular			3	1.2	26.3(7.6)	26.3(7.6)	6.3(1.7)
	End			79	30.8	30.4(8.2)	20.7(6.5)	8.4(3.7)
	Oblique			25	9.8	35.2(8.1)	27.7(6)	9.8(2.9)
	Side			32	12.5	23(6)	32.5(8.2)	10.1(3.3)
Blade		20	3.5	11	4.3	38.5(6.8)	15.5(4.2)	5.5(2.1)
Microblade		5	0.9	5	2	23.6(3.9)	10(2.8)	3.8(1.6)
Core fragment		51	9	0	-	-	-	-
Core/Flake fragment		9	1.6	0	-	-	-	-
Flake fragments		124	21.9	0	-	-	-	-
Angular fragment		3	0.5	0	-	-	-	-
Blade fragment		88	15.5	0	-	-	-	-
Total		567	100	256	100	-	-	-

4.6.1 Cores from Newari

A total of 101 artefacts were classified as cores, making up 39.4 % of the assemblage. There were 38 blade cores (*Plate 6*) with average dimensions of 40.7 × 27.4 × 20.1 mm. These cores were the most common type, followed by microblade cores with (n = 32) specimens and exhausted cores (n = 11) specimens, with average dimensions of 24.9 × 20.5 × 16.1 mm and 33.3 × 25.6 × 18.1 mm, respectively. After these, amorphous and core-on-flake were

most common, with a total of seven and six specimens with average dimensions of 39 × 29.7 × 21.1 mm and 28.2 × 20.2 × 9 mm, respectively. A total of three single platform unifacial and two multi-platform cores were observed with average dimensions of 56.3 × 36.3 × 31.7 mm and 62.5 × 48.5 × 30 mm, respectively. There were only single specimens of prepared and single platform bifacial cores with overall dimensions of 25 × 35 × 27 mm and 65 × 60 × 41 mm, respectively.

4.6.2 Flakes from Newari

This category outnumbers all other categories in artefact count, with 139 artefacts and an overall frequency of 54.3%. In this category, regular flakes (n = 3) were dominated by a square shape and have average dimensions of 26.3 × 26.3 × 6.3 mm. In comparison, end-struck flakes outnumber other flakes with a total count of 79 specimens and have an average size of 30.4 × 20.7 × 8.4 mm with a dominant rectangular shape. A total number of 25 oblique-struck flakes were dominated by rectangular shape and show average measurements of 35.2 × 27.7 × 9.8 mm, and a total of 32 side-struck flakes show average dimensions of 23 × 32.5 × 10.1 mm with a dominant rectangular shape.

4.6.3 Blades from Newari

A total of 20 blade specimens were observed, half of the blades were snapped (n = 9), and 11 specimens were complete with average dimensions of 38.5 × 15.5 × 5.5 mm.

4.6.4 Microblades from Newari

A total of five microblade (*Plate 6. i*) specimens were observed, showing an average dimension of 23.6 × 10 × 3.8 mm.

4.7 Kone

The site is near a foothill about one kilometre south of Kone centre. The site has an expansion of 200 L × 70 W m, and various artefacts, including scrapers, blades, Levallois flakes, prepared cores, blade cores, fluted cores and flakes, were observed at the site. These artefacts were primarily made on porcellanite and chert. The artefacts were collected from the site by methodically laying out a 8 × 6 m grid. At least 510 artefacts were collected from the site (*Table 25*).

Table 25. Assemblage composition and frequency at Kone.

Typology	**N (510)**	**%**	**Complete specimens**				
			N (133)	**%**	**Mean (SD)**		
					Length (mm)	**Breadth (mm)**	**Thickness (mm)**
Core	33	6.5	31	23.3	43.8(13.6)	32.5(9.6)	23.1(7.2)
Blade			19	14.3	43.2(8.8)	32(8.1)	22(5.1)
Multi-platform			2	1.5	49(5)	45.5(6.5)	34.5(0.5)
Single Platform Unifacial			4	3	58.8(22.3)	37.3(6.4)	29.3(9.8)
Single Platform Bifacial			1	0.75	51	49	20
Core-on-flake			1	0.75	44	19	14
Microblade			3	2.6	24.7(3.3)	20.7(3.3)	17.3(5.4)
Exhausted			1	0.75	37	32	25
Flake	159	31.2	95	71.4	36.6(13.5)	30.7(12.8)	10.2(3.9)
Regular			6	4.5	31.7(6.2)	34.2(16)	12(4.9)
End			53	39.8	39.8(14.4)	26.2(9.1)	9.9(4)
Oblique			8	6	41.3(11.9)	28.4(11.3)	10.1(3.3)
Side			28	21	30.3(10.1)	39.4(13.8)	10.2(3.5)
Blade	9	1.8	5	3.75	43.8(10.4)	15.8(2.3)	7.4(2.6)
Microblade	3	0.6	2	1.5	26(1)	13(1)	4.5(0.5)
Core fragment	22	4.3	0	-	-	-	-
Core/Flake fragments	35	6.9	0	-	-	-	-
Flake fragment	179	35.1	0	-	-	-	-
Blade fragment	33	6.5	0	-	-	-	-
Angular fragment	34	6.7	0	-	-	-	-
Split clast	3	0.6	0	-	-	-	-
Total	510	100	133	100	-	-	-

As the site is near Kone town, it has been heavily disturbed by anthropogenic and livestock trampling, resulting in few complete specimens (*n* = 133).

The assemblage comprises of cores (*n* = 31), flakes (*n* = 95), blades (*n* = 4), and microblades (*n* = 3). Because the site has been heavily disturbed, many artefacts were incomplete and were indicated mainly by flake fragments (179), blade fragments (33), flake/core fragments (35), core fragments (22) and angular pieces (34).

4.7.1 Cores from Kone

Thirty-one artefacts were classified as cores, making up 23.3 % of the assemblage. There were (*n* = 19) blade cores (*Plate 7. c*) with an average dimension of 43.2 × 32 × 22 mm. These cores were the most common type, followed by single platform unifacial cores (*n* = 4) (*Plate 7 h*) and microblade cores (*n* = 3), with average dimensions of 58.8 × 37.3 × 29.3 mm and 24.7 × 20.7 × 17.3 mm, respectively. A total of two multi-platform cores, one single platform bifacial, one core-on-flake and one exhausted core were reported with average dimensions of 49 × 45.5 × 34.5 mm, 51 × 49 × 20 mm, 44 × 19 × 14 mm and 37 × 35 × 25 mm, respectively.

4.7.2 Flakes from Kone

This category has 95 artefacts, making 71.4 % of the overall assemblage. The end-struck flakes (*n* = 53) in this category were dominated by a rectangular shape with average dimensions of 39.8 × 26.2 × 9.9 mm. It was followed by side-struck flakes with a total count of 28 specimens and average dimensions of 30.3. × 39.4 × 10.2 mm, also dominated by a rectangular shape. A total of eight oblique-struck flakes were dominated by rectangular shapes and had average measurements of 41.3 × 28.4 × 10.1 mm. Six regular flakes were predominated by square shape with average dimension of 31.7 × 34.2 × 12 mm.

4.7.3 Blades from Kone

This category represents 3.75% of the total assemblage, with only four complete specimens while others were broken. The overall dimensions of the blades (*Plate 7. f, g*) were 43.8 × 15.8 × 7.4 mm.

4.7.4 Microblades from Kone

A total of three microblades specimens were observed, showing average dimensions of 26 × 13 × 4.5 mm.

4.8 Artefact types and their frequencies

A total of 1196 complete artefacts were studied for lithic analysis (*Table 26*). Doma site shows maximum artefact counts (*n* = 429, 38.86%), followed by Newari (*n* = 256, 21.40%), Kone (*n* = 133, 11.12%), Kargara (*n* = 115, 9.61%), Parva Chinguri (*n* = 96, 8.02%), Khempur (*n* = 92, 7.69%) and Bagia (*n* = 75, 6.27%). These numbers represent only complete collected specimens, a sample from the total present at the site.

A total of 22 types of artefacts were observed, i.e., biface, prepared core, Levallois core, discoid core, centripetal core, blade core, microblade core, multi-platform core, double platform core, single platform unifacial core, single platform bifacial core, core-on-flake, amorphous core, exhausted core, regular flake, end flake, side flake, oblique flake, blade, blade flake, microblade and hammerstone from the study area.

Table 26. Artefact type and their frequency.

Artefact type/Sites	Doma	Kone	Kargara	Khempur	Bagia	Newari	Parva Chinguri	Total	Frequency (%)
Biface	3 (0.25)							3	0.25083612
Prepared Core	14 (1.17)		2 (0.17)	6 (0.5)	16 (1.33)	1 (0.8)	1 (0.8)	40	3.34448161
Levallois Core	2 (0.17)				1 (0.8)			3	0.25083612
Discoid Core	3 (0.25)		1 (0.8)		1 (0.8)			5	0.4180602
Centripetal Core	7 (0.58)							7	0.58528428
Blade Core	8 (0.67)	19(1.6)	8 (0.7)	3 (0.25)	6 (0.50)	38 (3.2)	12 (1)	94	7.85953177
Microblade core		3 (0.3)	2 (0.2)			32 (2.7)	4 (0.3)	41	3.42809365
Multi-platform Core	2 (0.17)	2 (0.17)	4 (0.33)	14 (1.17)	5 (0.42)	2 (0.17)		29	2.42474916
Double Platform Core			1 (0.8)		1 (0.8)			2	0.16722408
Single Platform Unifacial Core		4 (0.33)	3 (0.25)	2 (0.17)	1 (0.8)	3 (0.25)	3(0.25)	16	1.33779264
Single Platform Bifacial Core		1 (0.8)		1 (0.8)	1 (0.8)	1 (0.8)		4	0.33444816
Core-on-flake	4 (0.33)	1 (0.8)	5 (0.42)	2 (0.17)	1 (0.8)	6 (0.5)		19	1.58862876
Amorphous Core	13(1.1)					7 (0.58)		20	1.6722408
Exhausted Core	7 (0.58)	1 (0.8)	5 (0.42)	2 0.17)	2 (0.17)	11 (0.92)	4 (0.33)	32	2.67558528
Regular flake	35 (2.92)	6 (0.50)	2 (0.17)	12 (1)	2 (0.17)	3 (0.25)	2 (0.17)	62	5.18394649
End flake	166 (13.9)	53 (4.43)	39 (3.26)	29 (2.42)	25 (2.09)	79 (6.6)	25 (2.09)	416	34.7826087
Side flake	73 (6.10)	28 (2.34)	30 (2.50)	9 (0.75)	9 (0.75)	32 (2.68)	15 (1.25)	196	16.3879599
Oblique flake	66 (5.51)	8 (0.67)	4 (0.33)	10 (0.84)	4 (0.33)	25 (2.09)	3 (0.25)	120	10.0334448
Blade	14 (1.17)	5 (0.4)	4 (0.33)	2 (0.17)		11 (0.92)	15 (1.25)	51	4.26421405
Blade flake	12 (1)							12	1.00334448
Microblade		2 (0.17)	3 (0.25)			5 (0.42)	12 (1)	22	1.83946488
Hammerstone			2 (0.17)					2	0.16722408
Total	429	133	115	92	75	256	96	1196	100
Frequency (%)	35.86957	11.1204013	9.61538462	7.6923077	6.270903	21.4046823	8.02675585	100	

The Doma and Kargara sites include the highest variety of artefact types (n = 16), followed by Newari (n = 15), Bagia (n = 14), Kone (n = 13), Khempur (n = 12), Parva Chinguri (n = 11).

From the overall assemblage, the flake artefacts show the highest frequency, the end struck flakes count (n = 416) with an overall frequency of 34.78%, followed by the side struck flakes with a total of 196 artefacts owing 16.38% of the entire assemblage. Oblique-struck flakes come next in overall count (n = 120), making 10.03 % of the total assemblage. After the flake artefacts, the maximum frequency was shown by blade cores, with 94 artefacts with an overall frequency of 7.86%. After blade cores, regular flakes show the highest frequency, with artefacts (n = 62) contributing 5.18% of the total assemblage. It was followed by the blades, which comprise 4.26% of the total assemblage with artefacts (n = 51). After the blades, the microblade cores show the maximum frequency with artefacts (n = 41), representing up to 3.42% of the total artefacts. Prepared cores show maximum frequency after microblade cores, with 40 artefacts making 3.34% of the total assemblage. After the prepared cores, the exhausted cores show the maximum number of artefacts (n = 32), representing 2.67% of the entire assemblage. After exhausted cores, multi-platform cores show the maximum frequency with 29 artefacts owing to 2.42% of the total assemblage. The microblades show the maximum frequency after exhausted cores with (n = 22) artefacts with an overall frequency of 1.84%. After microblade, amorphous cores show a maximum frequency of 1.67% with 20 artefacts.

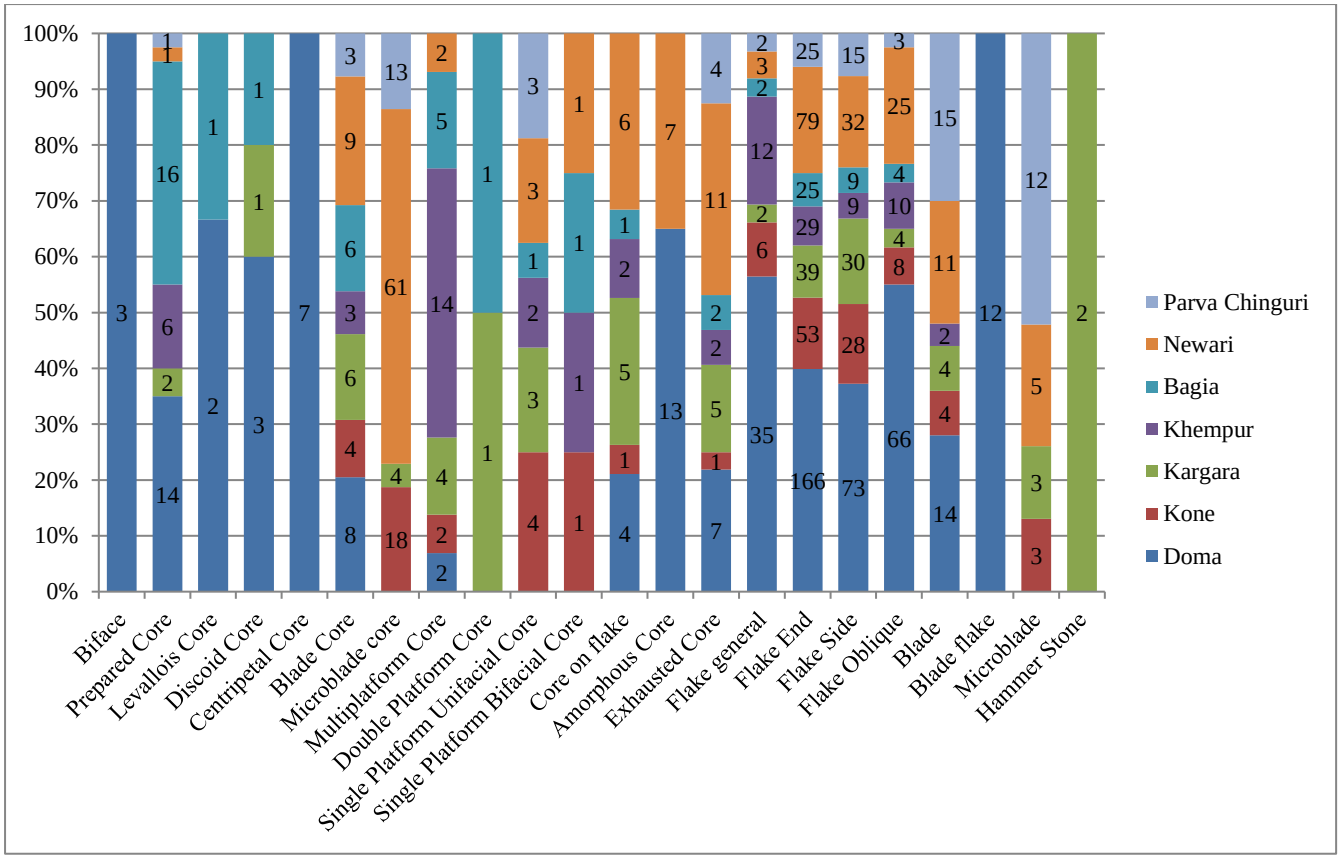

Figure 44. Artefact types site-wise.

Amorphous cores were followed by core-on-flake, single platform unifacial cores and blade flakes with a total count of 19, 16 and 12 and an overall frequency of 1.58%, 1.33%, and 1%, respectively. Blade flakes were followed by centripetal cores, discoid cores and single platform bifacial cores with a total count of 7, 5, and 4, making up 0.58%, 0.41% and 0.33% of the complete assemblage, respectively. Single platform bifacial cores were followed by Levallois cores, bifaces, double platform cores and hammerstones with 3, 3, 2, 2 artefacts making 0.25%, 0.25%, 0.16% and 0.16% of the entire assemblage, respectively.

4.9 Finished tool types

In the LSV, 137 finished tools across 15 different tool types were identified (*Figure 44*, *Table 27*). Most tool types were produced using flakes (n = 59), followed by blade tools with 51

artefacts. Microblade tools were the third most commonly found, with 21 artefacts identified. Bifaces and choppers were also present, with only 3 and 1 artefacts identified, respectively.

The flake tools consist of different categories, i.e., scraper (*n* = 14, 10.22%), side scraper (*n* = 15, 10.94%), end scraper (*n* = 6, 4.37%), convergent scraper (*n* = 1, 0.72%), transverse scraper (*n* = 1, 0.72%), point (*n* = 14, 10.21%), notch (*n* = 5, 3.64%), knife (*n* = 1, 0.7.2%) and perforator (*n* = 2, 1.45%). The core tools consist of a chopper observed at Bagia, forming 0.84% of the total finished tools assemblage.

Blade tools consist of points (*n* = 2, 1.45%), retouched/modified blades (*n* = 6, 4.37%) and unretouched/unmodified blades (*n* = 43, 31.38%). Microblade tools consist of retouched/modified microblades (*n* = 2, 4.37%) and unretouched/unmodified blades (*n* = 21, 15.32%). The bifacial tools consisted of only handaxes (*n* = 3, 2.52%) and were only observed at Doma. The core tool consists of a chopper (*n* = 1, 0.72%) observed at Bagia.

Doma (*n* = 41, 32.77%), followed by Parva Chinguri (*n* = 29, 21.16%) and Newari (*n* = 26, 18.97%) and represent the highest number of finished tools. Kargara has only 14 finished artefacts making up 10.21% of the total finished assemblage. Kone has only 12 finished artefacts making up 8.76% of the assemblage. Khempur represents (*n* = 11, 9.24%) finished artefacts of the complete assemblage. The lowest number of finished tools was observed at Bagia, with (*n* = 4) forming 2.92% of the total assemblage.

Table 27. Finished tool types.

Finished Tool Types		Doma	Bagia	Khempur	Kargara	Parva Chinguri	Kone	Newari	Total	Frequency
Flake Tools	Scraper	4	2	6	1			1	14	10.218978
	Side Scraper	8			1	1	3	2	15	10.948905
	End Scraper	2		1			2	1	6	4.379562
	Convergent Scraper	1							1	0.729927
	Transverse Scraper	1							1	0.729927
	Point	6	1	1	2	1		3	14	10.218978
	Notch	1		1	2			1	5	3.649635
	Knife	1							1	0.729927
	Perforator				1			1	2	1.459854
Core Tools	Chopper		1						1	0.729927
Blade Tools	Point	2							2	1.459854
	Retouched/Modified				1	2		3	6	4.379562
	Unretouched/Unmodified	12		2	3	13	5	8	43	31.386861
Microblade	Retouched/Modified				1			1	2	1.459854
	Unretouched/Unmodified				2	12	2	5	21	15.328467
Bifaces	Handaxe	3							3	2.189781
Total		41	4	11	14	29	12	26	137	100
Frequency		29.93	2.92	8.029197	10.21898	21.16788321	8.76	18.978	100	

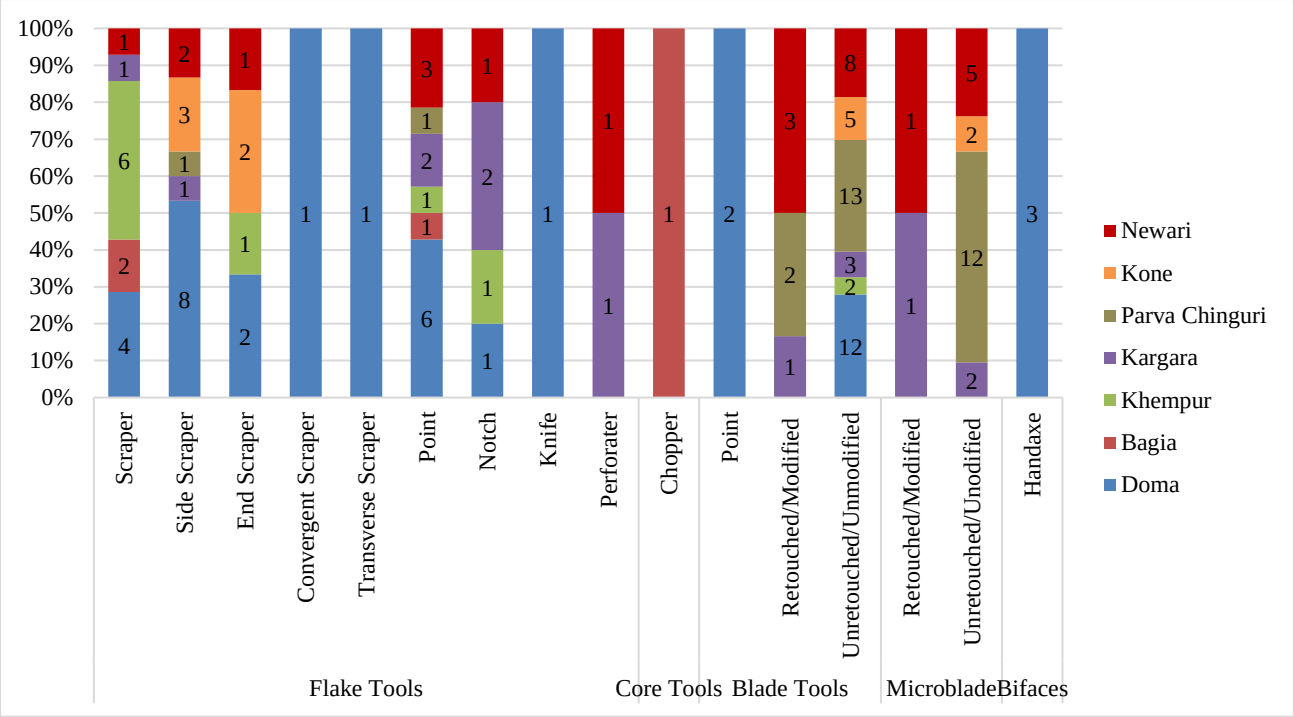

Figure 45. Finished tool types.

4.10 Distribution of raw materials

In the LSV, seven types of raw materials were identified as primary resources for tool production. These raw materials included porcellanite, chert, chalcedony, quartz, agate, quartzite, and limestone *(Figure 46, 47)*. Among these raw materials, porcellanite was the most commonly used, accounting for 69.39% (n = 830) of the complete artefacts out of a total of 1196 artefacts. After porcellanite, chert was most utilised, with (*n* = 273) artefacts that form 22.83% of the total assemblage. Quartz was the third most common raw material used at the sites, with (*n* = 48) artefacts accounting for 4.01% of the total assemblage. In addition, other raw materials such as chalcedony (*n* = 28), quartzite (*n* = 10), agate (*n* = 6), and limestone (*n* = 1) were used, accounting for 2.34%, 0.83%, 0.5%, and 0.08% of the total assemblage, respectively.

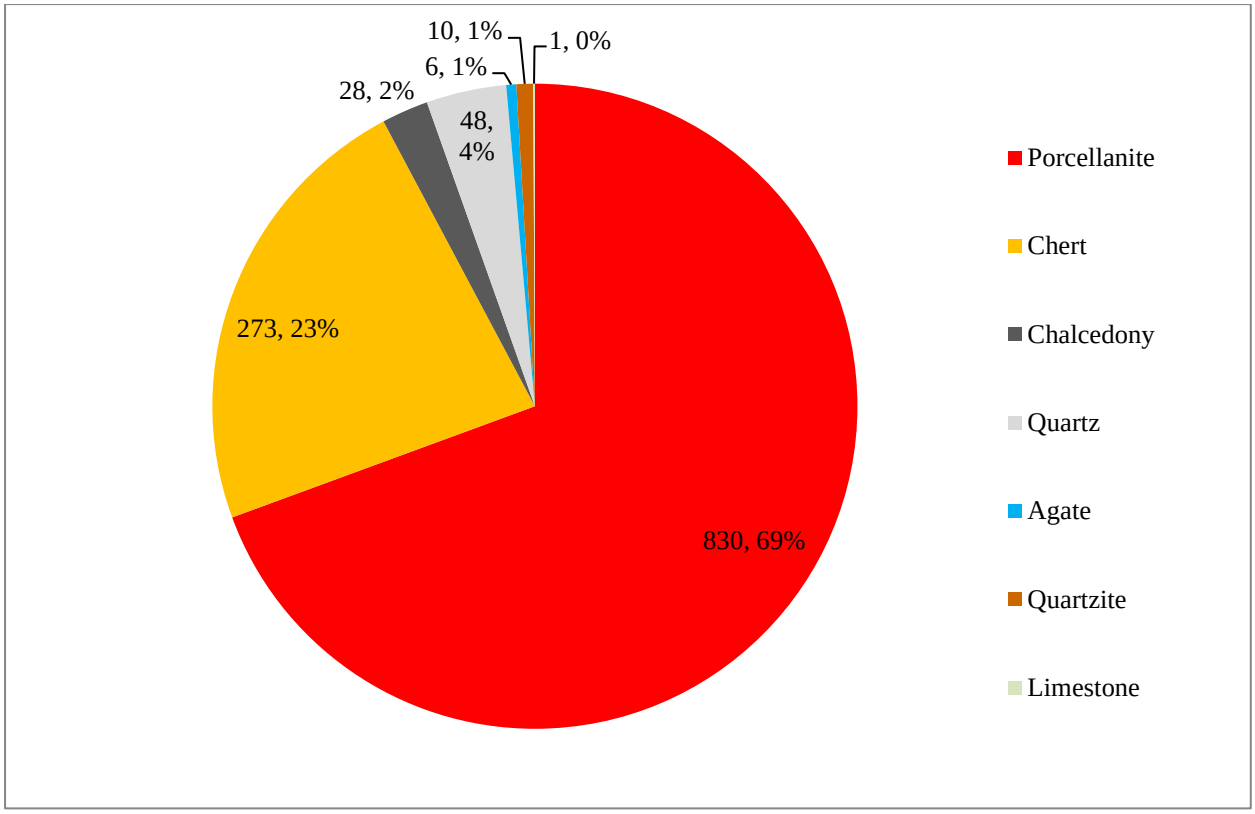

Figure 46. Raw material distribution in the LSV (n = 1196)

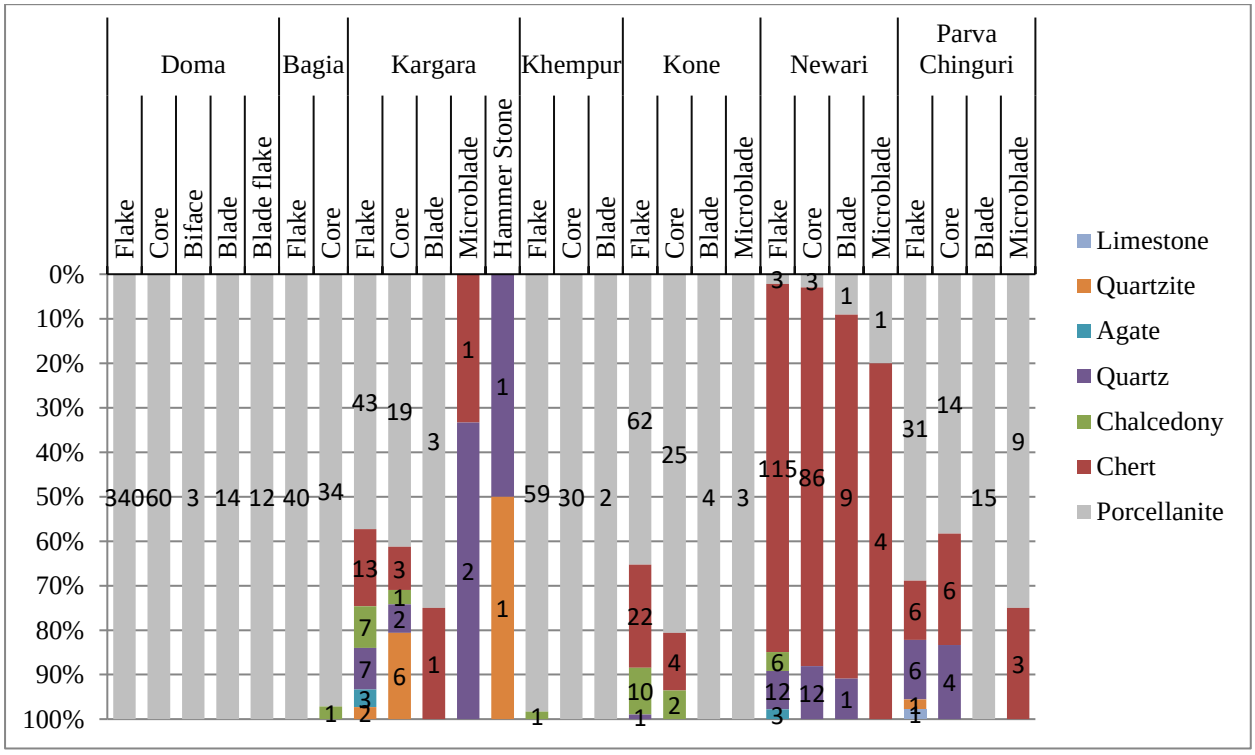

Figure 47. Site-wise raw material distribution (Bar columns) in the LSV.

4.10.1 Raw material distribution site-wise

This section presents the raw material usage patterns observed in seven sites of the LSV: Doma, Bagia, Kargara, Khempur, Kone, Newari, and Parva Chinguri.

At Doma, all 429 artefacts, including bifaces, cores, flakes, blades, and blade flakes, were made exclusively (100%) on porcellanite. Similarly, at Khempur, out of 92 complete artefacts, 91 (99%) were made on porcellanite, and only one was made on chalcedony. At Bagia, most artefacts (*n*=74) were made on porcellanite, and only one was made on chalcedony.

At Kargara, almost all raw materials were used except for limestone. Of the total assemblage (*n*=115), 56% (*n*=65) of artefacts were made on porcellanite, 16% (*n*=18) on chert, 10% (*n*=12) on quartz, 8% (*n*=9) on quartzite, 7% (*n*=8) on chalcedony, and 3% (*n*=3) on agate.

At Kone, out of 133 artefacts, 71% (*n*=94) artefacts were made on porcellanite, followed by chert with 19% (*n*=26) artefacts, chalcedony with 9% (*n*=12), and only one artefact was observed on quartz.

At Newari, out of 256 artefacts, the majority (84%, *n*=214) artefacts were made on chert, followed by 10% (*n*=25) artefacts made on quartz, 3% (*n*=8) on porcellanite, 2% (*n*=6) on chalcedony, and 1% (*n*=3) on agate.

Further, at Parva Chinguri, out of 96 artefacts, 72% (*n*=69) artefacts were made on porcellanite, followed by chert with 16% (*n*=15) and quartz with 10% (*n*=10) artefacts. Single specimens on quartzite and limestone were also observed at the site (*Figure 48, Table 28*).

Overall, these findings highlight the variable use of raw materials across different sites in the LSV, with porcellanite being the most commonly used material across all sites except for Newari.

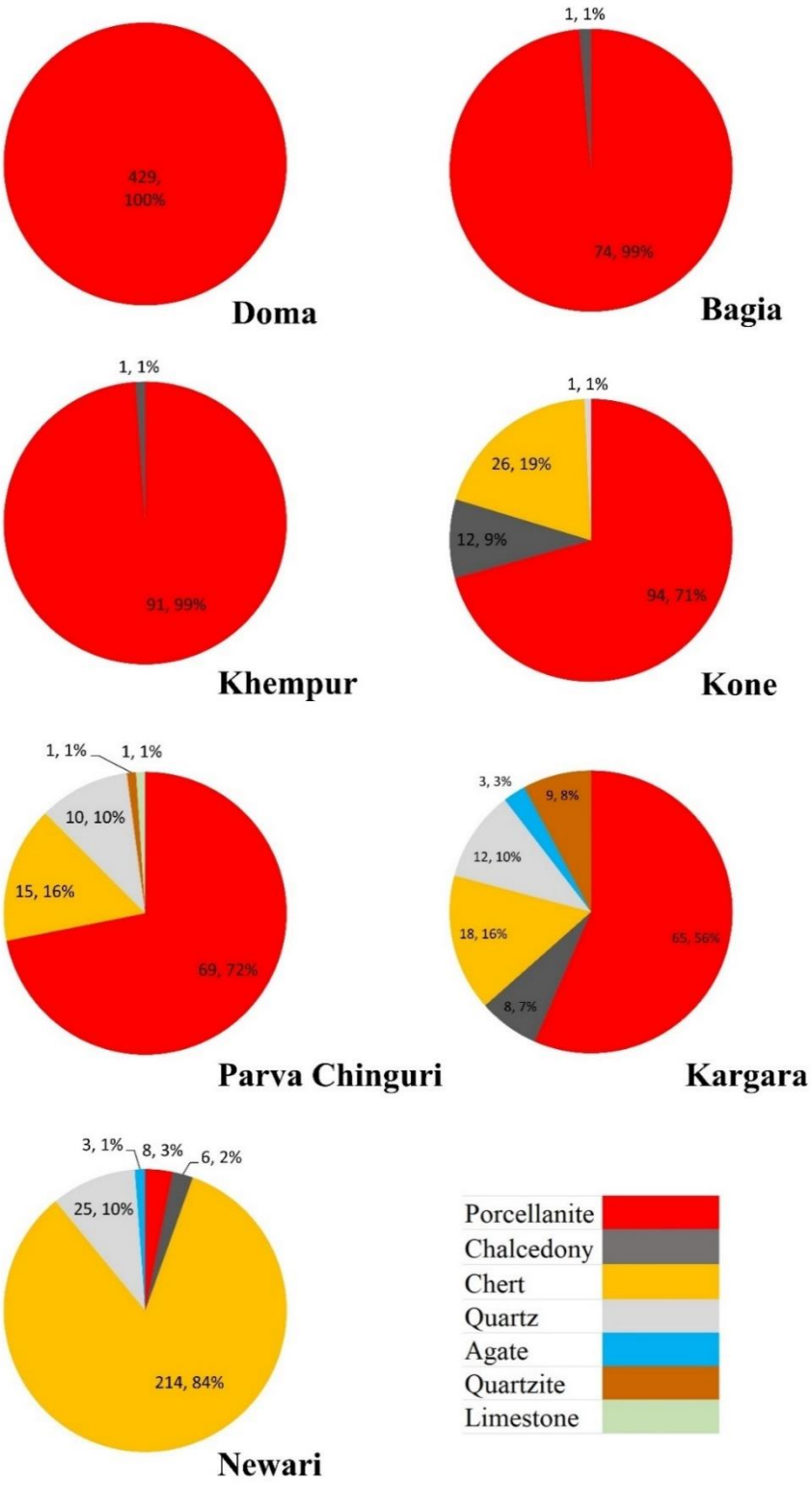

Figure 48. Site-wise raw material distribution (Pie Chart) in the LSV.

Site/Raw Material		Porcellanite (%)	Chert (%)	Chalcedony (%)	Quartz (%)	Agate (%)	Quartzite (%)	Limestone (%)
Doma	Flake	340(28.42)						
	Core	60(5.01)						
	Biface	3 (0.25)						
	Blade	14(1.17)						
	Blade flake	12(1)						
Bagia	Flake	40(3.34)						
	Core	34(2.84)		1(0.08)				
Kargara	Flake	43(3.59)	13(1.08)	7(0.58)	7(0.58)	3(0.25)	2(0.16)	
	Core	19(1.58)	3(0.25)	1(0.08)	2(0.16)		6(0.50)	
	Blade	3(0.25)	1(0.08)					
	Microblade		1(0.08)		2(0.16)			
	Hammerstone				1(0.08)		1(0.08)	
Khempur	Flake	59(4.93)		1(0.08)				
	Core	30(2.50)						
	Blade	2(0.16)						
Kone	Flake	62(5.18)	22(1.83)	10(0.83)	1(0.08)			
	Core	25(2.09)	4(0.33)	2(0.16)				
	Blade	5(0.41)						
	Microblade	2 (0.16)						
Newari	Flake	3 (0.25)	115(9.61)	6(0.50)	12(1)	3 (0.25)		
	Core	3 (0.25)	86(7.19)		12(1)			
	Blade	1(0.08)	9(0.75)		1(0.08)			
	Microblade	1(0.08)	4(0.33)					
Parva Chinguri	Flake	31(2.59)	6(0.50)		6(0.50)		1(0.08)	1(0.08)
	Core	14(1.17)	6(0.50)		4(0.33)			
	Blade	15(1.25)						
	Microblade	9(0.75)	3 (0.25)					
Total		830(69.39)	273(22.83)	28(2.34)	48(4.01)	6(0.50)	10(0.83)	1(0.08)
Frequency		69.3979933	22.83	2.34113712	4.0134	0.502	0.83612	0.083612
Total		1196						

Table 28. Raw material distribution in the LSV and their frequency.

4.10.2 Raw material distribution technology-wise

4.10.2.1 Late Acheulean/ Middle Palaeolithic

4.10.2.1.1 Doma

The possible presence of the Late Acheulean in the valley can be found at Doma. A total of five bifaces (two refined) were reported from the site and distinguishable in different strata from the Middle Palaeolithic and Upper Palaeolithic assemblages. Despite the presence of handaxes and large flakes (>10 cm), the site was dominated by Middle Palaeolithic cores (e.g., prepared, Levallois, discoid, centripetal), (n = 26) and flakes (n = 340). The site also preserves eight blade cores and 14 blades. All artefacts at the site were made exclusively on porcellanite (*Figure 49*).

4.10.2.1.2 Khempur

Middle Palaeolithic cores and flakes dominate the site. Different types of cores were found at the site, i.e., prepared, multi-platform, single platform unifacial, single platform bifacial, core-on-flake, exhausted and blade cores (n = 30); all cores were made on porcellanite. In total, 60 flakes were collected from the site, of which 59 were made on porcellanite; the remaining flake was on chalcedony. Only two blades made on porcellanite were recovered from the site.

4.10.2.1.3 Bagia

At Bagia, different types of cores were found (prepared, Levallois, discoid, multi-platform, double platform, single platform unifacial, single platform bifacial, core-on-flake, exhausted and blade). A total of 40 flakes were located at the site, and despite the availability of blade cores, no blades were found at the site. All the artefacts were made on porcellanite.

4.10.2.2 Multiple technologies

4.10.2.2.1 Kargara

The site shows the maximum variability in the use of raw materials (i.e., porcellanite, chert, quartz, agate, quartzite, and chalcedony), and it also demonstrates the presence of different technologies, i.e., prepared core (Middle Palaeolithic) and laminar (Upper Palaeolithic and microlithic). It represents various cores, including prepared, discoid, multi-platform, double platform, single platform unifacial, core-on-flake, exhausted, blade and microblade. Of the cores, including the prepared and discoid core (n = 3 specimens), two were made on porcellanite, and one was made on quartzite. A total of eight blade cores were found at the site; seven of these cores were made on porcellanite, and one was made on quartz. Additionally, the microlithic cores were made on porcellanite (n = 1) and chert (n = 1). The flakes were produced primarily on porcellanite (n = 43) followed by chert (n = 13), chalcedony (n = 7), quartz (n = 7), agate (n = 3) and quartzite (n = 3). The blades were made on porcellanite (n = 3) and chert (n = 1). The microblades were made on chert (n = 1) and quartz (n = 2). The use of quartzite as a raw material was unique to the site (*Figure 49*).

4.10.2.3 Microlithic

The presence of laminar elements dominates at microlithic sites. As the sites were primarily present on the surface, most microblades are broken/snapped; hence, significantly few complete microblades are observed at the sites (*Figure 50*).

4.10.2.3.1 Kone

The site also shows the dominant use of porcellanite. The cores at Kone demonstrate the use of porcellanite predominantly in the blade and microblade cores (n = 19, blade; n = 3,) along with the utilisation of chert (n = 2) and chalcedony (n = 1) only in microblade cores. The flakes were produced on different raw materials such as porcellanite (n = 62), chert (n = 22), chalcedony (n = 10) and quartz (n = 1). The blades (n = 5) and the microblades (n = 2) were

made only on porcellanite, although a few microblade cores were found on chert and chalcedony.

4.10.2.3.2 Parva Chinguri

The Parva Chinguri site represents laminar technology with blade (*n* = 12) and microblade (*n* = 4) cores. Porcellanite was predominantly used to produce blade (*n* = 6) and microblade elements (*n* = 4). The blade cores were also made on quartz (*n* = 1) and chert (*n* = 5). At Parva Chinguri, flakes were made from different raw materials, predominantly porcellanite (*n* = 31), followed by chert (*n* = 6), quartz (*n* = 6), quartzite (*n* = 1) and limestone (*n* = 1). The use of limestone is unique to the site. The blades (*n* = 12) at the site were made exclusively on porcellanite. The microblades were also predominantly produced on porcellanite (*n* = 4) and chert (*n* = 1).

4.10.2.3.3 Newari

Newari is the only known site in the valley to demonstrate the dominance of laminar technology, blade cores (*n* = 38) and microblade cores (n = 32). The dominant raw material used at the site was chert, and porcellanite was almost absent at the site, except few artefacts. A single prepared core and single platform bifacial core were observed at the site. A total of 35 blade cores were observed on chert, and three were made on quartz. Of the 32 microblade cores, 26 were made on chert, and six were made on quartz. The flakes were produced on a variety of raw materials, predominantly on chert (*n* = 115) followed by quartz (*n* = 12), chalcedony (*n* = 6), agate (*n* = 3) and porcellanite (*n* = 3). The blades were also produced on different raw materials, predominantly on chert (*n* = 9), followed by quartz (*n* = 1) and porcellanite (*n* = 1). The microblades were produced mainly on chert (*n* = 4) and followed by porcellanite (*n* = 1).

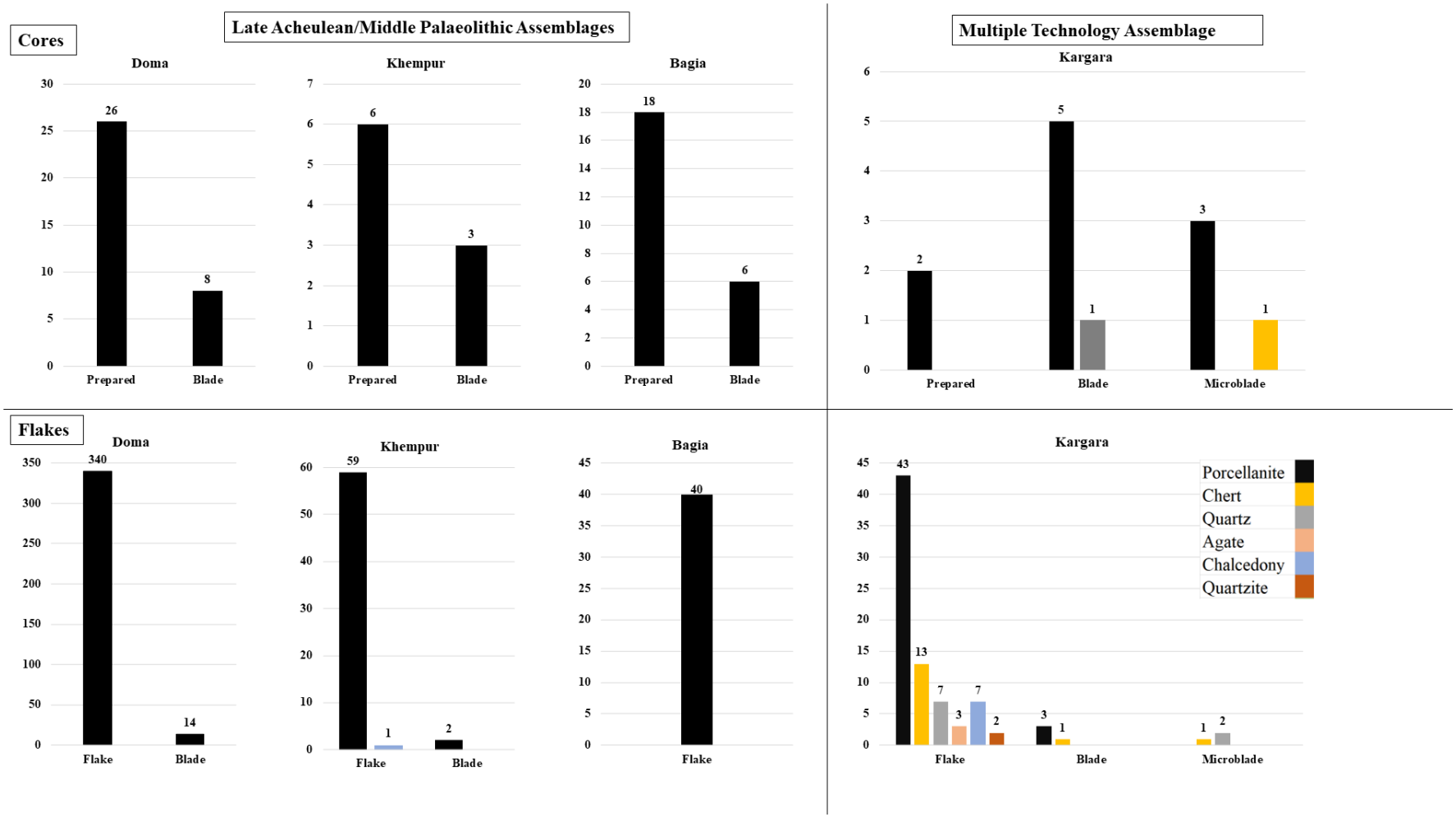

Figure 49. Late Acheulean/Middle Palaeolithic and multiple technology assemblage showing raw material distribution in accordance with technological change.

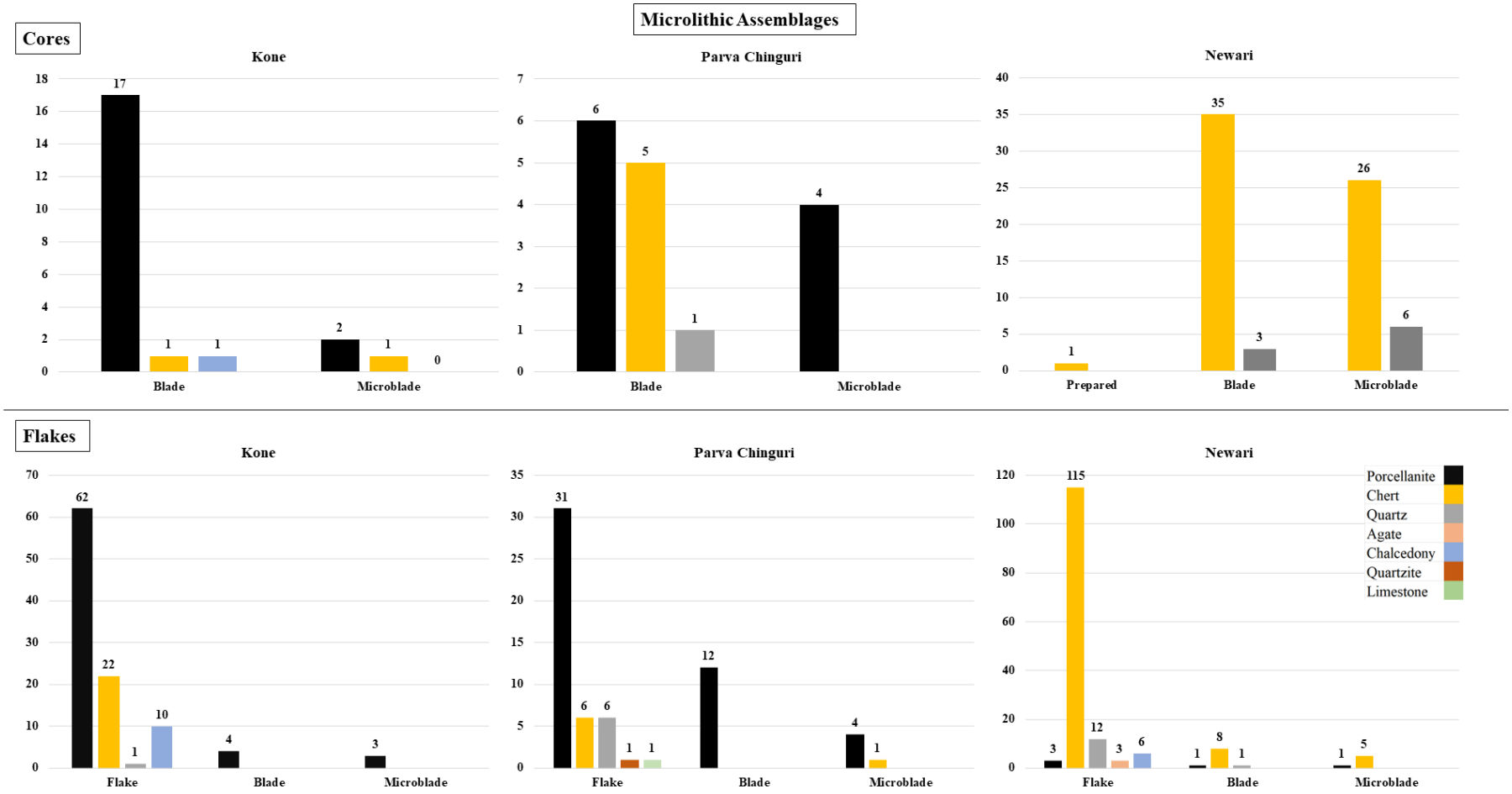

Figure 50. Microlithic assemblages showing raw material distribution.

4.11 Raw material procurement

When the procurement of raw materials at the outcrops is linked to studies of the lithic assemblages found in archaeological deposits, we connect the two ends of the lithic chaîne opératoire, from acquisition to discard (*Figure 51*). As mentioned above, porcellanite is the primary raw material utilised at almost all sites. The hills representing raw material sources are located on the right bank of the Son River from Harra village in the Sonbhadra District, Uttar Pradesh, to Kosdehra village in the Garhwa District of Jharkhand. The author here presumes that all the porcellanite used in the LSV was possibly obtained from the rock sources between the villages mentioned.

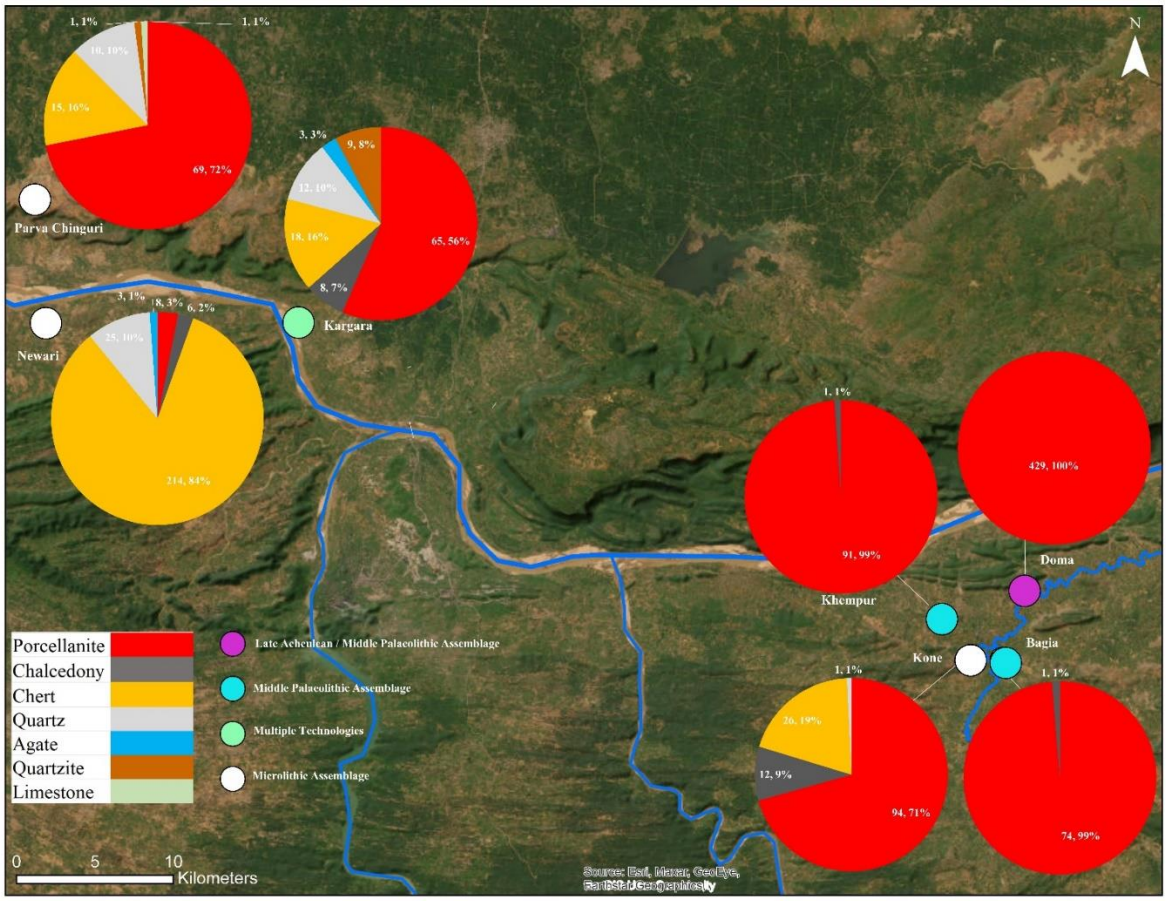

Figure 51. Location of the studied sites along with different technologies and raw material distribution.

4.11.1 Late Acheulean/Middle Palaeolithic sites

The Doma site is located in the foothills, and angular, subangular, and rounded colluvial clasts of porcellanite can be observed. The Doma site represents the presence of Late Acheulean technology, the predominant use of prepared core technology, and laminar technology. The Late Acheulean artefacts were located in colluvial deposits, while prepared and blade artefacts were found on the surface and in fine sediments. Overall, the site is in a semi-primary context with a possible on-site raw material procurement, as all artefacts were made on the same raw material.

The Khempur site is approximately 1.8 km from the nearest raw material outcrop. The site was dominated by the prepared core technology. The artefacts found here were less (n = 153) than Doma (n = 820). The average size of the cores was also reduced at the site. The probable reason for this could be transporting raw material from ~ 2 km. Almost all raw material clasts were used extensively. Only one flake made on chalcedony was observed at the site; otherwise, all artefacts were made on porcellanite.

The Bagia site is approximately 4.2 km from the source of the raw material. The prepared core technology dominates the site. The number of artefacts here was greater (n = 163) compared to Khempur but less than Doma. The mean core size was also smaller at the site, except for multi-platform cores, which show a higher level of exploitation. All the artefacts were made on porcellanite. It is generally observed that there was a constant decrease in the number and size of the artefacts as the distance between the sites and the raw material outcrops increased. The dominant use of porcellanite was observed at sites from the Late Acheulean and Middle Palaeolithic periods.

4.11.2 Mixed technologies site (Middle/Upper/ Microlithic)

The Kargara site exhibits a mixture of various technologies, including prepared and laminar (blade and microlithic). Since the assemblage was discovered on the surface, it is possible that different hominin groups may have occupied the site at different times. The site is approximately 34 km from the porcellanite outcrop, which is believed to be the primary raw material source for the Late Acheulean/Middle Palaeolithic sites mentioned earlier. Porcellanite was the primary raw material used at Kargara, although other materials such as chert, quartz, chalcedony, agate, and quartzite were also utilised. Despite the considerable distance to the nearest raw material source, porcellanite remains the most commonly used material at the site.

4.11.3 Microlithic sites

After the Middle Palaeolithic period, there was a visible change in raw material utilisation. The site of Kone is only 4 km away from the nearest raw material source, but it is mainly dominated by microlithic technology. However, near the raw material source and at least the same distance as Bagia, no prepared cores were found at the site. However, the predominance of porcellanite continues at the site. The site is on the sandstone bedrock near the main road, and the villagers herd their animals in this area. Hence most of the artefacts, especially microblades, were broken. It is important to note that the blade cores and microblade cores are made predominantly on porcellanite, possibly because of the proximity of the raw material source. At the same time, other raw materials, such as chert, quartz, and chalcedony, are used at the site but in less quantity than porcellanite. The possible reduced use of other raw materials is due to the large distance transport, as, in the nearest Panda River, no quartz, chalcedony, or chert pebbles were observed. Therefore, it is assumed that these raw materials

were collected from the riverbed of Son, which is a minimum of 8-10 km north of the site, and one has to cross the porcellanite outcrop to reach there.

Parva Chinguri is further away from the raw material source than the other analysed sites, which is 51 km. It is important to note that the site is on the Kaimur Plateau at an elevation of 300 – 600 MSL. Here, no sign of prepared core technology was observed. The site preserves blade and microblade cores and their artefacts. Despite its distance from the outcrop of raw material, porcellanite was the raw material that was used extensively here. It suggests hominins could transport raw material long distances and were familiar with the geology/rock formations of the valley. In addition to porcellanite, other raw materials such as chert, quartz, limestone, and quartzite were also exploited at the site. The use of limestone was unique to the site. Despite its abundant availability in the valley, it was hardly used for artefact production. Other raw materials used at the site were probably collected from the riverbed of Son River. However, to collect those raw materials clasts, one must go down 300-600 metres and at least 3-4 km south towards the river.

Newari is unique, representing the minimum use of porcellanite (only three porcellanite artefacts) and a dominant use of chert. The site was dominated by laminar technology with the presence of (n = 32) microblade cores. Various raw materials were used on site, but 84% of the artefacts were made on chert. Other materials such as quartz, agate, porcellanite, and chalcedony were also utilised. The site is on the hilltop with a seasonal stream flowing in its foothill and is only ~1 km south of the Son River. It is assumed that the raw material at the site was collected from the riverbed of Son in prehistoric times.

4.12 Box Plot comparison of flakes, blades, microblades and cores

4.12.1 Flakes

Flakes are divided into four categories 1) regular flakes, 2) end flakes, 3) oblique flakes and 4) side flakes *(Figure 52,53)*.

4.12.1.1 Regular flakes

All four categories in box and whisker plots show that the site of Doma, Bagia and Khempur forms a cluster. The mean length for the regular flakes at Doma (n = 35, mean = 44.17, range = 21 – 83), Bagia (n = 2, mean = 45.5, range = 41 – 50) and Khempur (n = 12, mean = 42.41, range = 32 – 66) are between 42.41 and 45.5 mm. The other four sites form a cluster with a mean length between 25.8 and 37 mm (Parva Chinguri (n = 2, mean = 25.8, range = 18 – 33), Kargara (n = 2, mean = 37, range = 27 – 47), Newari (n = 3, mean = 26.33, range = 22 – 37) and Kone (n = 6, mean = 31.66, range = 25 – 43)).

4.12.1.2 End flakes

Similar to regular flakes, the end flakes show a similar pattern with Doma (n = 166, mean = 59.53, range = 25 – 112) and Khempur (n = 29, mean = 55.30, range = 40 – 64) clustering together with the mean length of 59.53 and 55.30 mm, except for Bagia (n = 25, mean = 74.90, range = 36 – 125) showing the highest mean length of 74.90 mm for end flakes among all sites. Parva Chinguri (n =25, mean = 35.22, range = 18 – 55), Kargara (n =39, mean = 35.86, range = 15 – 60), Newari (n = 79, mean = 29.30, range = 15 – 55) and Kone (n = 53, mean = 39.82, range = 16 – 84) cluster together with the mean length between 29.30 and 39.82 mm.

4.12.1.3 Oblique flakes

Similar to end flakes, oblique flakes show a similar pattern with Doma (*n* = 66, mean = 56.12, range = 27 – 115) and Khempur (*n* = 10, mean = 50.6, range = 37 – 68) clustering together with average length of 56.12 and 50.6 mm, respectively. Again, Bagia (*n* = 4, mean = 70, range = 57 – 107) shows the highest mean length of 70 mm among all sites. Additionally, Parva Chinguri (*n* =3, mean = 33, range = 29 – 38), Kargara (*n* =4, mean = 37, range = 21 – 68), Newari (*n* = 25, mean = 35.24, range = 19 – 56) and Kone (*n* =8, mean = 41.25, range = 26 – 60) cluster together with the mean length of 33 to 41.25 mm.

4.12.1.4 Side flakes

Similar to regular flakes, side flakes show a similar pattern with Doma (*n* = 73, mean = 41.30, range = 17 – 126), Bagia (*n* = 9, mean = 48.22, range = 22 – 90) and Khempur (*n* =9, mean = 47.11, range = 27 – 66) clustering together with average width between 41 and 48.22 mm. The four sites, Parva Chinguri (*n* = 15, mean = 23.26, range = 14 – 31), Kargara (*n* = 40, mean = 30.86, range = 8 – 61), Newari (*n* = 32, mean = 22.96, range = 14 – 44) and Kone (*n* = 28, mean = 30.32, range = 14 – 52) cluster together with mean width between 22.96 – 30.32 mm.

4.12.2 Blades

Blades were found at six sites out of seven; at Bagia, no complete blades were reported. The length of the blades at Doma (*n* = 14, mean = 77.35, range = 59 – 105) stands out at a mean length of 77.35 mm. Khempur (*n* = 2, mean = 49, range = 48 – 50), Parva Chinguri (*n* = 15, mean = 39.8, range = 32 – 60), Kargara (*n* = 4, mean = 41.25, range = 32 51), Newari (*n* = 10, mean = 39.3, range = 31 54) and Kone (*n* =4, mean = 47.33, range = 37 – 60) cluster together with mean length ranging from 39.3 to 49 mm.

4.12.3 Microblades

The microliths were only found at Parva Chinguri, Kargara, Newari and Kone; of these sites, Kone (mean = 27.33, range = 25 – 30) and Kargara (mean = 27, range = 25 – 29) seem to cluster together with mean length 27 - 27.33 mm. Newari (mean = 24.66, range = 19 – 30) and Parva Chinguri (mean = 23.5, range = 17 – 29) cluster together with a mean length of 23.5 - 24.66 mm.

4.12.4 Cores

4.12.4.1 Prepared core

No prepared cores were observed at Kone. The size of the prepared cores at Doma (*n* = 14, mean = 92.35, range = 56 – 175) stands out with a mean length of 92.35 mm. It is possibly due to the site's proximity to the raw material source. The prepared cores at Bagia (*n* = 16, mean = 74.25, range = 35 – 103) and Khempur (*n* = 6, mean = 76.33, range = 61 – 102) show average lengths of 74.25 and 76.33 mm, respectively. The respective decrease in size compared to Doma could be due to the distance from the raw material source since Bagia is almost 4 km and Khempur is 2 km from the possible nearby raw material source. Very few prepared cores were observed at Parva Chinguri (*n* = 1, mean = 30), Kargara (*n* = 2, mean = 50, range = 45 – 55) and Newari (*n* = 1, mean = 25).

4.12.4.2 Multi-platform core

Bagia (*n* = 5, mean = 95.2, range = 52 – 143) stand out in multi-platform cores with a mean length of 95.2 mm. No multi-platform cores were found at Parva Chinguri. Other remaining sites, Doma (*n* = 2, mean = 55, range = 55 – 65), Khempur (*n* = 14, mean = 53.07, range = 41 – 85), Kargara (*n* = 4, mean = 60, range = 50 – 76), Newari (*n* = 2, mean = 62.5, range = 41 – 84) and Kone (*n* = 2, mean = 49, range = 44 – 54) have average length between 49- 62.5 mm.

4.12.4.3 Exhausted core

Doma (*n* = 7, mean = 69.85, range = 47 – 99), Bagia (*n* = 2, mean = 64, range = 50 – 78), Khempur (*n* = 2, mean = 65, range = 55 – 75) make a cluster with a mean length between 64 and 69.85 mm. The Parva Chinguri (*n* = 4, mean = 37.5, range = 27 – 64), Kargara (*n* = 5, mean = 39, range = 24 – 56), Newari (*n* = 11, mean = 33.27, range = 24 – 46) and Kone (*n* = 1, mean = 37) form another group with a mean length below 40 mm. The size decrease in the latter could be due to technological change and the distance from the raw material source.

4.12.4.4 Blade core

Similar to the length of the blade at Doma, the size of the blade core at Doma (*n* = 8, mean = 84.37, range = 49 – 122) was also the highest at the site, with a mean length of 84.37 mm and a maximum blade core length reaching 122 mm. The rest of the sites show a slight decrease in the length of the blade core. The mean blade core length of Bagia (*n* = 6, mean = 55.16, range = 31 – 95) and Khempur (*n* = 3, mean = 61.33, range = 46 – 78) was above 55mm. The site of Parva Chinguri (*n* = 12, mean = 47.4, range = 37 – 66) and Kone (*n* = 19, mean = 43.2, range = 31 – 62) show a mean length of 47.4 and 43.2 mm, respectively. Kargara (*n* = 8, mean = 42.3, range = 35 – 67) shows a mean length of 42.3 mm, and Newari (*n* =38, mean = 40.7, range = 30 – 61) shows a minimum mean length of 40.7 mm.

4.12.4.5 Microblade core

Similar to microblades, microblade cores are also found only at Kone (*n* = 3, mean = 24.7, range = 21 – 29), Parva Chinguri (*n* = 4, mean = 25, range = 24 – 26), Kargara (*n* = 4, mean = 27, range = 25 – 29) and Newari (*n* = 32, mean = 24.9, range = 9 – 29). Kargara shows the highest average length of 27 mm, followed by Parva Chinguri with 25 mm and Newari with 24.9 mm, while Kone shows the lowest mean length of 24.7 mm.

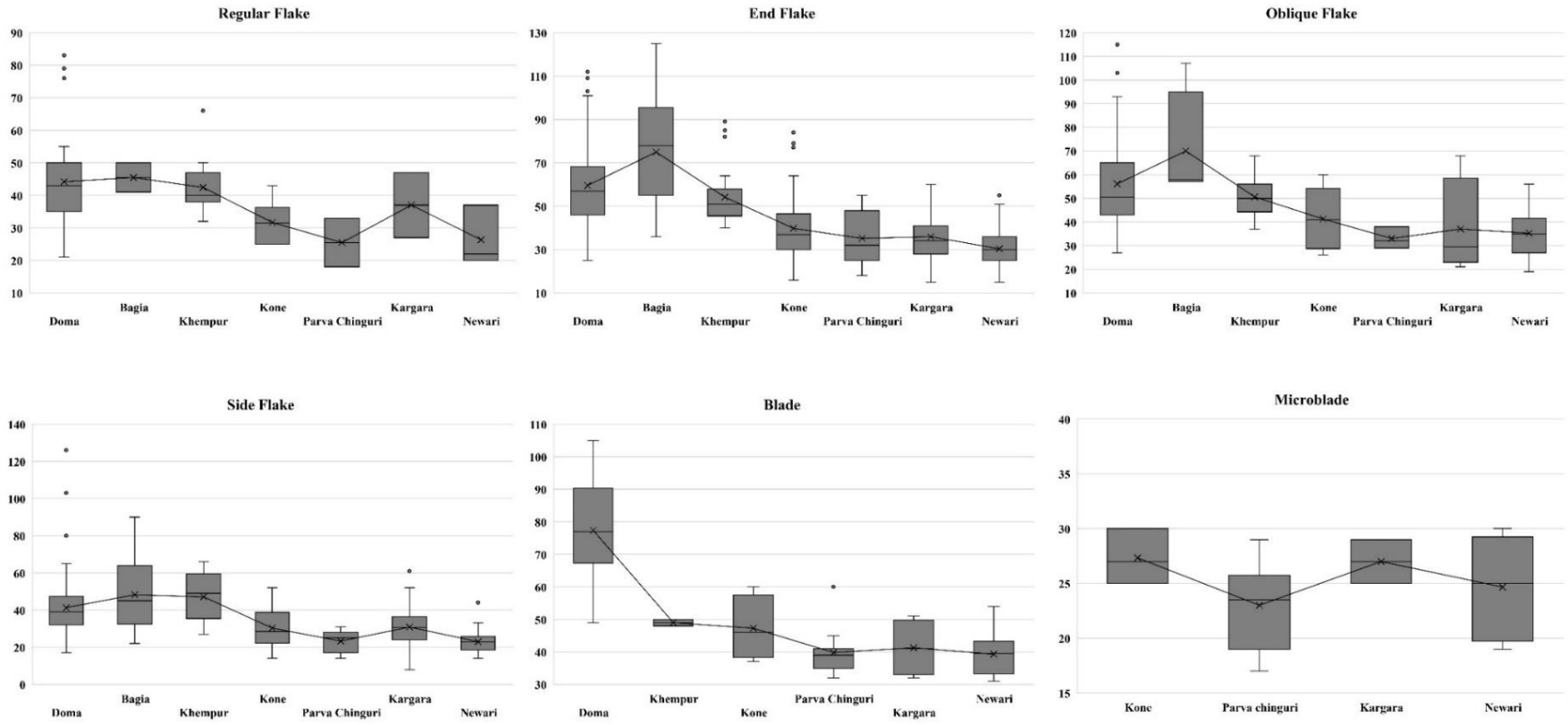

Figure 52. Box and whiskers plot showings mean value and line for various flakes, blades and microblades.

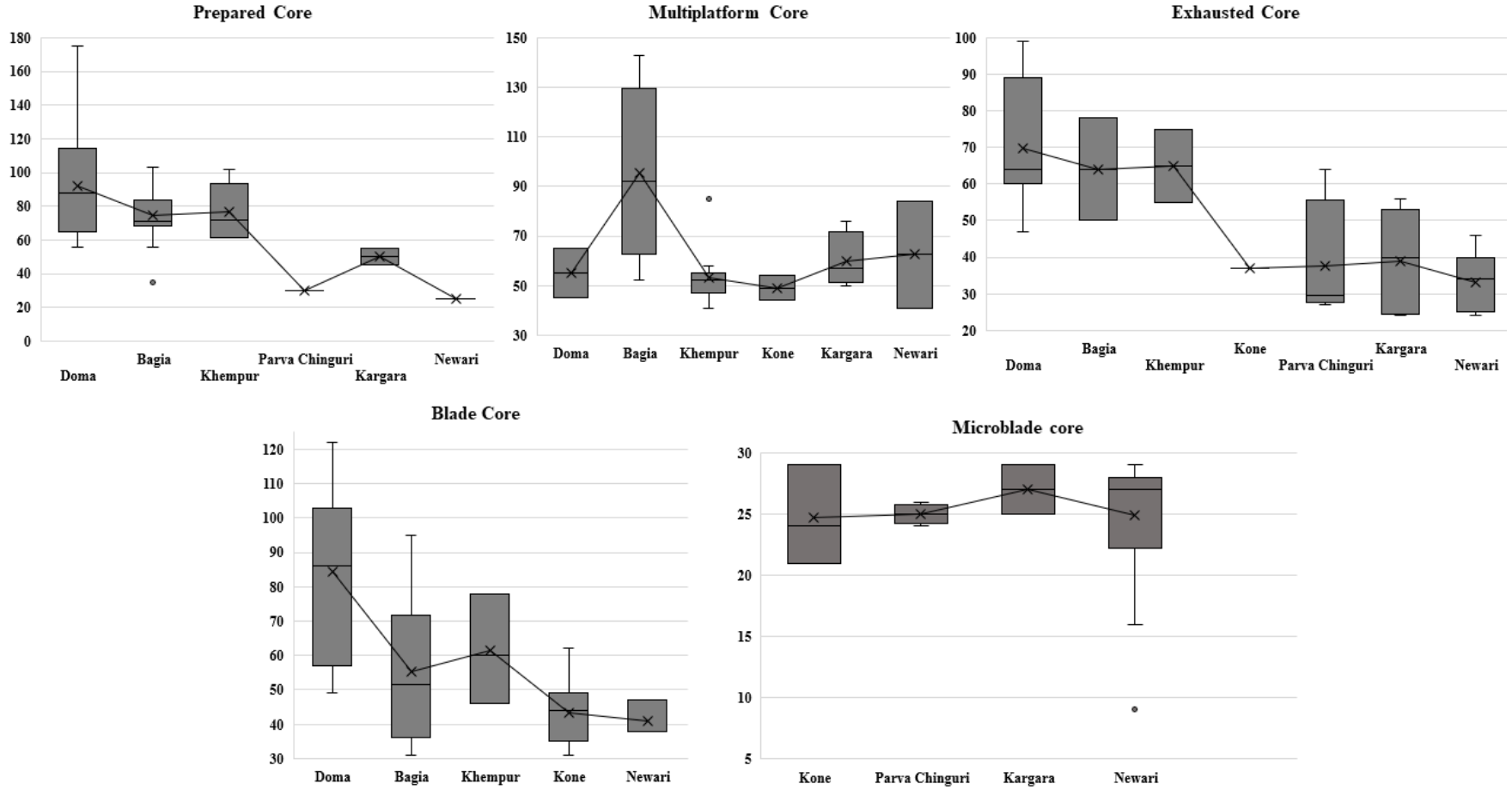

Figure 53. Box and whiskers plot showings mean value and line for various cores.

4.13 Blades, microblades and their blank type correlation

The microblades were only found at four sites and ranges from 17-29 mm in length. The microblades of all the sites show a random scatter plot (*Figure 54*). Compared to microblades, the blades were found at six sites in the study area. These blades range from 30 to 105 mm in length. Doma blades range from 49 to 105 mm in length and generally form a different cluster than the rest of the blade assemblages (*Figure 55*). The remaining blades from different sites range between 30 – 50 mm and form another cluster.

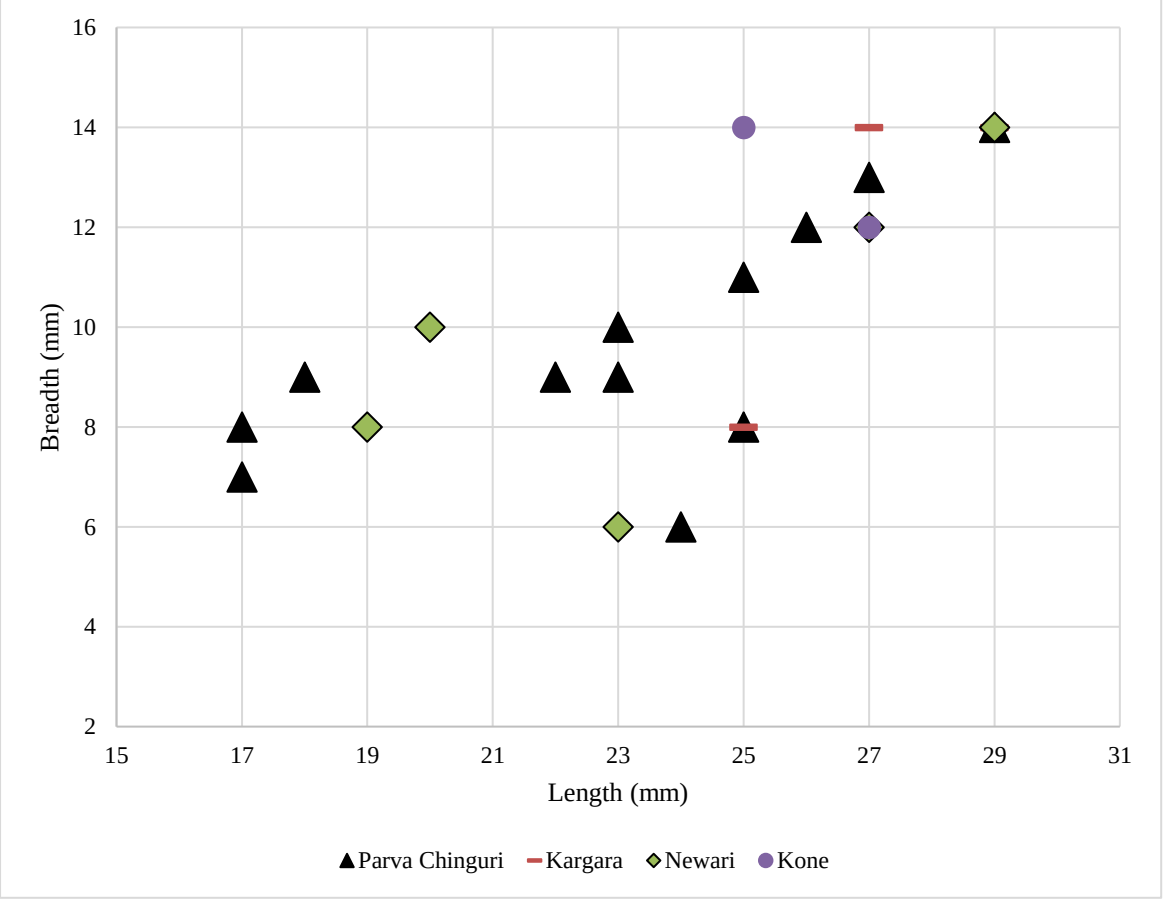

Figure 54. Microblades scatter plot of the LSV.

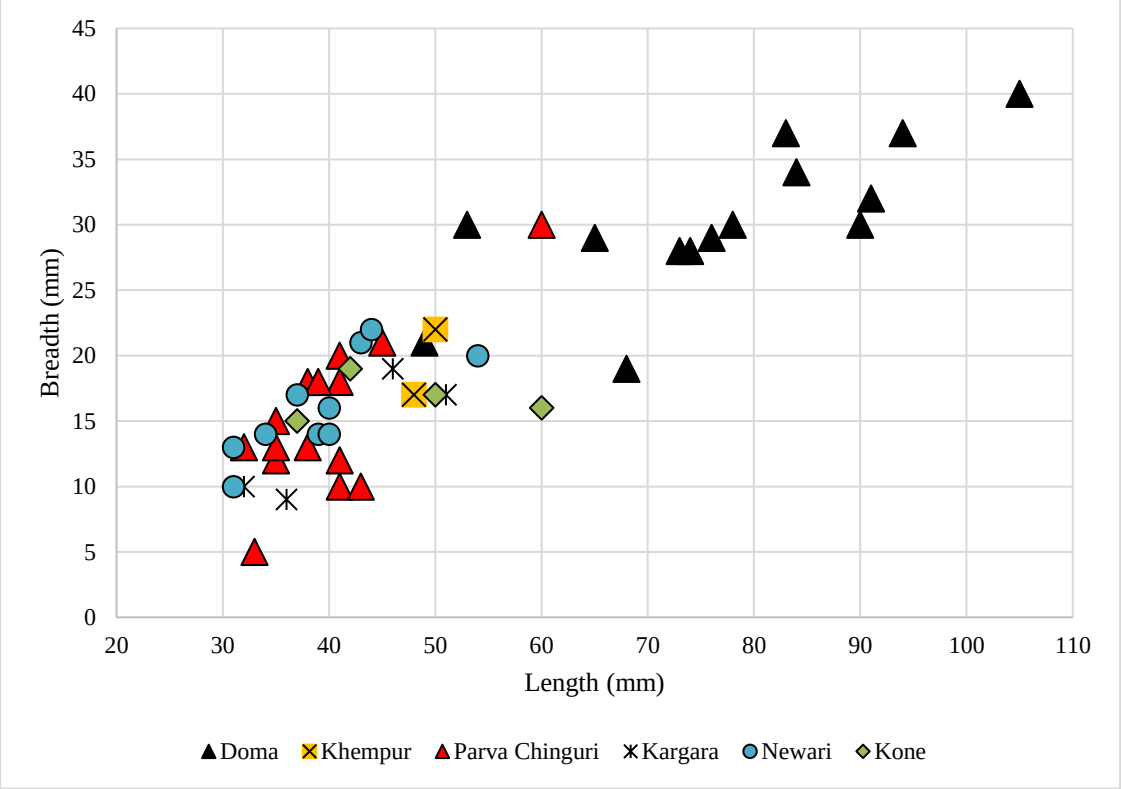

Figure 55. Blades scatter plot of the LSV.

Most of the blades and microblades show similar blank type utilisation. For microblade production, angular clasts (*n* = 3) and indeterminate clasts (*n* = 18) were utilised (*Figure 56 b*). For blade production, angular clasts (*n* = 18) and indeterminate clasts (*n* = 31) and a pebble (*n* = 1) were utilised (*Figure 56 a*).

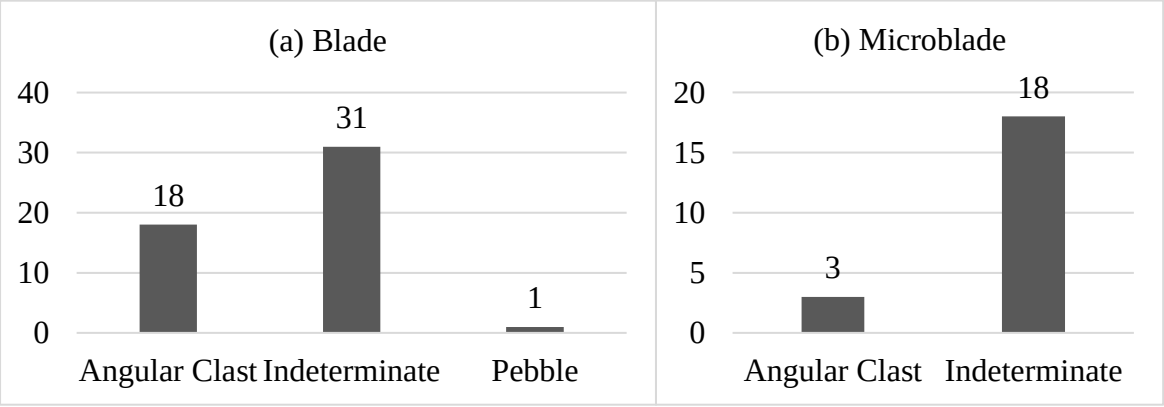

Figure 56. Blank type distribution for blades (a) and microblades (b).

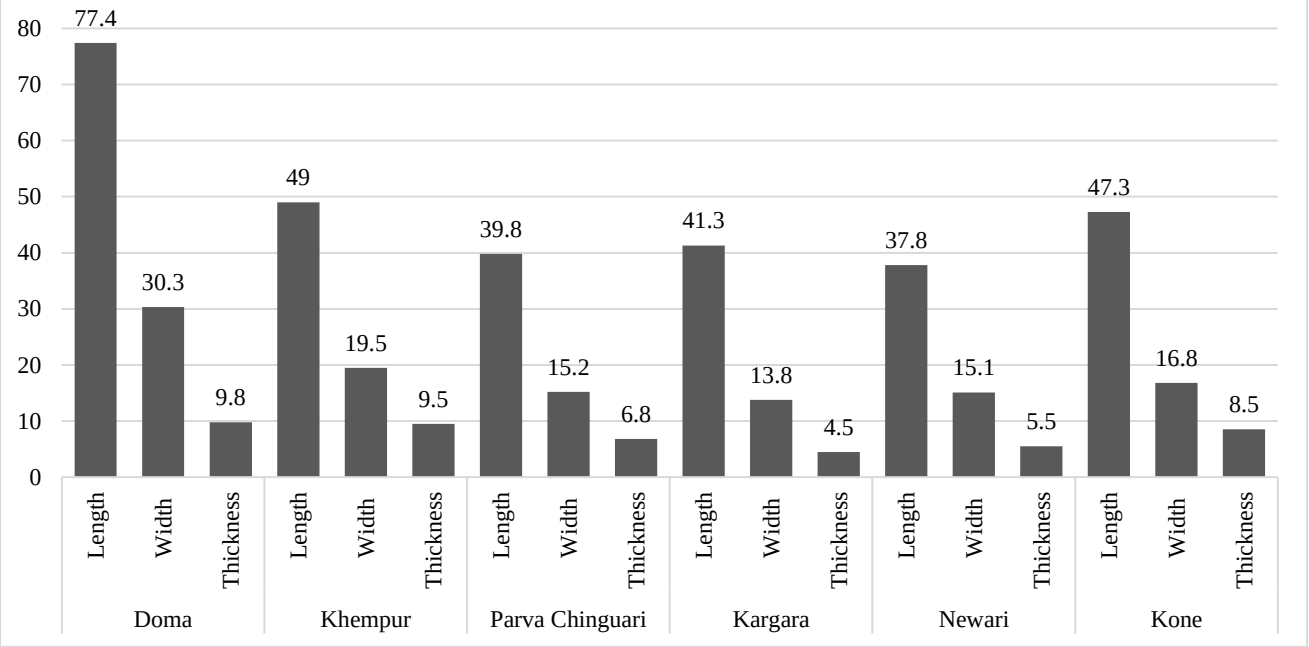

Figure 57. Blade dimensions at different sites in the LSV.

When comparing the blade dimensions of different sites in the LSV (*Figure 57*), it is observed that the blades at Doma were significantly larger than the rest of the blade assemblages, where the mean length, width and thickness are (77.4 × 30.3 × 9.8) mm, and the thickness of the blades at Doma is approximately 1/3 of their width.

After Doma, no other sites show a mean length of more than 49 mm. Khempur and Kone show average dimensions of (49 × 19.5 × 9) mm and (47.3 × 16.8 × 8.5) mm. The average length of the remaining sites was below 42 mm, with Kargara, Parva Chinguri, and Newari exhibiting average dimensions of (41.3 × 13.8 × 4.5) mm, (39.8 × 15.2 × 6.8) mm, and (38.5 × 15.5 × 5.5 mm) mm, respectively.

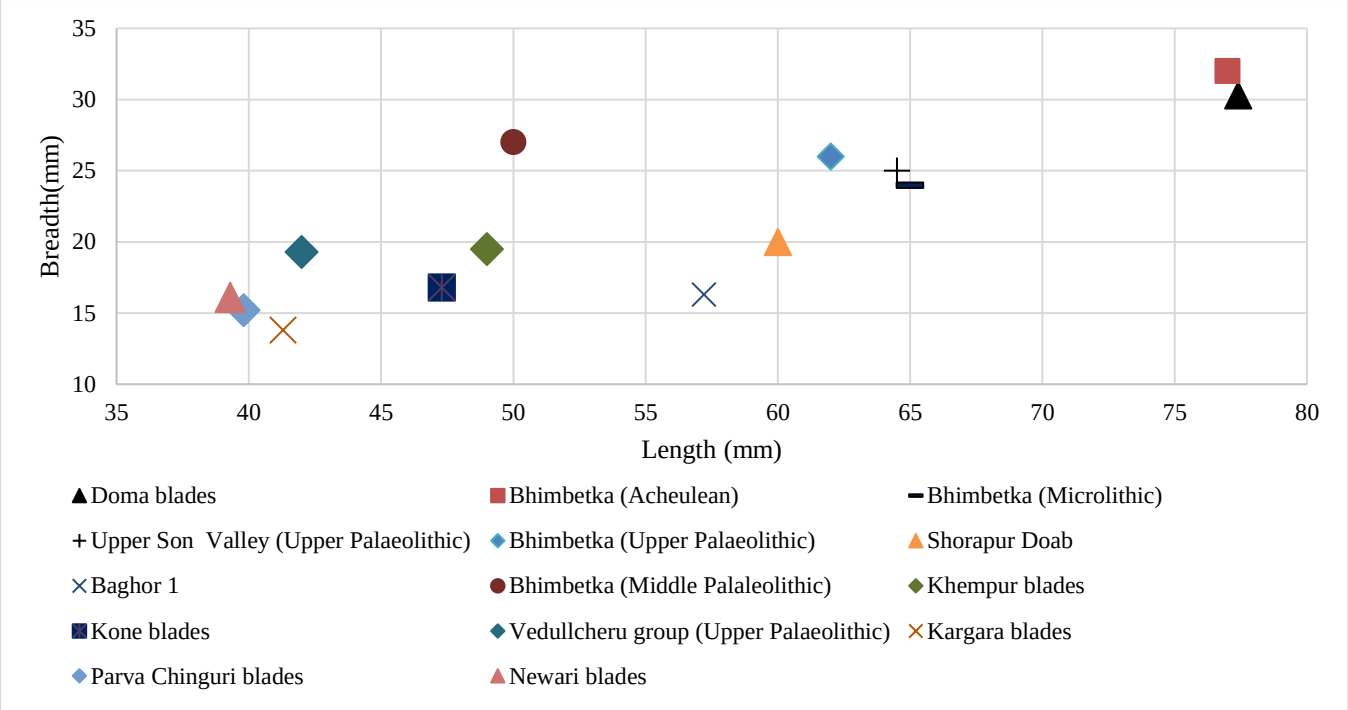

Figure 58. Blades distribution of the LSV in comparison to other Indian assemblages.

When comparing the blade assemblages of the LSV with the other well-known blade assemblages in India (*Figure 58*), it was observed that the blades at Doma lie close to the Acheulean blades found at Bhimbetka. Upper Palaeolithic and microlithic Bhimbetka blades cluster with Upper Palaeolithic blades of the Upper Son Valley, Shorapur Doab and Bahgor 1. Interestingly, the Bhimbetka Middle Palaeolithic blades cluster with Kone and Khempur blades. Furthermore, the Vedullcheru group, Karagara, Newari, and Parva Chinguri blades cluster together.

4.14 Blank type distribution

The knapping process in this study utilised five distinct types of blanks: angular clast, large rounded clast (cobble), small rounded clast (pebble), subangular clast, and indeterminate blanks. Of 1196 artefacts, 48.4% or 579 specimens were made on angular clasts. Following the use of angular clasts, most of the artefacts were devoid of any cortex, making it challenging to identify the original blank type. The original blank type could not be determined for 40.6% (*n* = 485) of the studied assemblages. (*Figure 59,60; Table 29*)

Table 29. Site and artefact specific blank type distribution in the LSV.

Site/Blank type		**Angular Clast**	**Indeterminate**	**Rounded clast (Cobble)**	**Rounded clast (Pebble)**	**Subangular**
Doma	Flake	175 (14.63)	165 (13.79)			
	Core	51 (4.26)	8 (0.66)	1 (0.08)		
	Biface	2 (0.16)	1 (0.08)			
	Blade	7 (0.58)	7 (0.58)			
	Blade flake	6 (0.50)	6 (0.50)			
Bagia	Flake	25 (2.09)	15 (1.25)			
	Core	33 (2.75)	2 (0.16)			
Kargara	Flake	32 (2.67)	25 (2.09)		18 (1.50)	
	Core	21 (1.75)	7 (0.58)		3 (0.25)	
	Blade	3 (0.25)	1 (0.08)			
	Microblade		2 (0.16)		1 (0.08)	
	Hammerstone			2 (0.16)		
Khempur	Flake	20 (1.67)	39 (3.26)	1 (0.08)		
	Core	28 (2.34)	2 (0.16)			
	Blade		2 (0.16)			
Kone	Flake	38 (3.17)	32 (3.17)			25 (2.09)
	Core	16 (1.33)	14 (1.17)	1(0.08)		
	Blade		4 (0.33)			
	Microblade	3 (0.25)				
Newari	Flake	7 (0.58)	55 (4.59)		77 (6.43)	
	Core	81	20 (1.67)			
	Blade	2 (0.16)	8 (0.66)		1 (0.08)	
	Microblade		5 (0.41)			
Parva Chinguri	Flake	14 (1.17)	30		1 (0.08)	
	Core	9 (0.75)	14 (1.17)		1 (0.08)	
	Blade	6 (0.50)	9 (0.75)			
	Microblade		12 (1)			
Total		579 (48.41)	485 (40.55)	5 (0.41)	102 (8.52)	25 (2.09)
Total		1196				

Following the indeterminate clasts, rounded pebbles were utilised, resulting in a total of (n = 102) artefacts, constituting 8.5% of the entire assemblage. Subsequently, subangular and rounded clasts (cobbles) were used, resulting in 2.1% and 0.4% of the total collection, respectively.

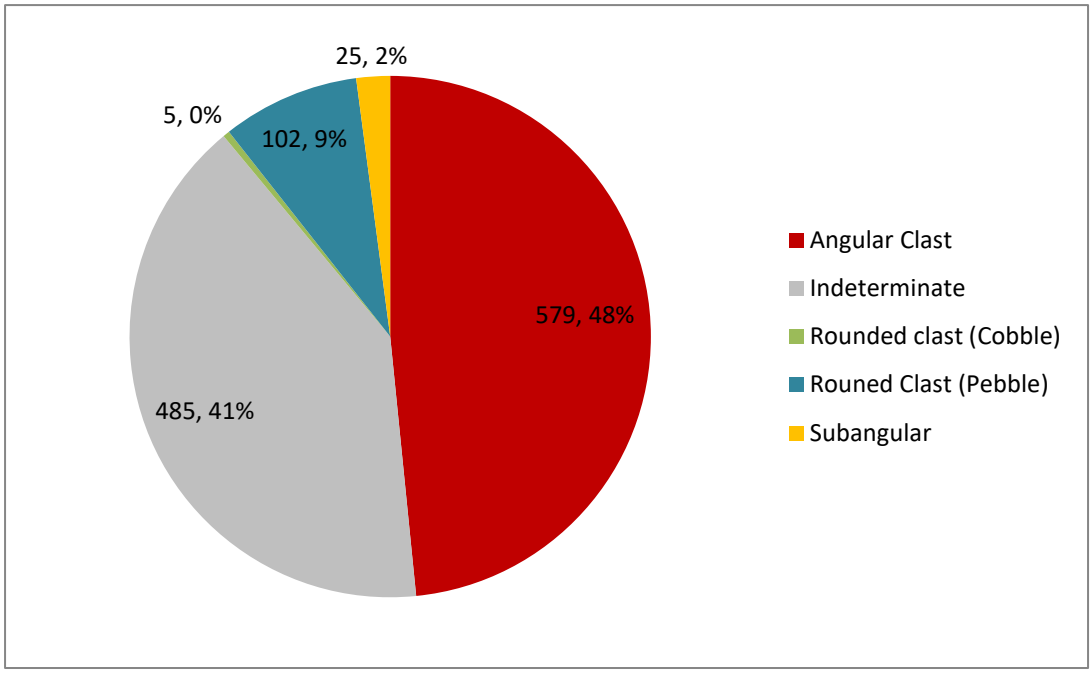

Figure 59. Overall blank type distribution in the LSV.

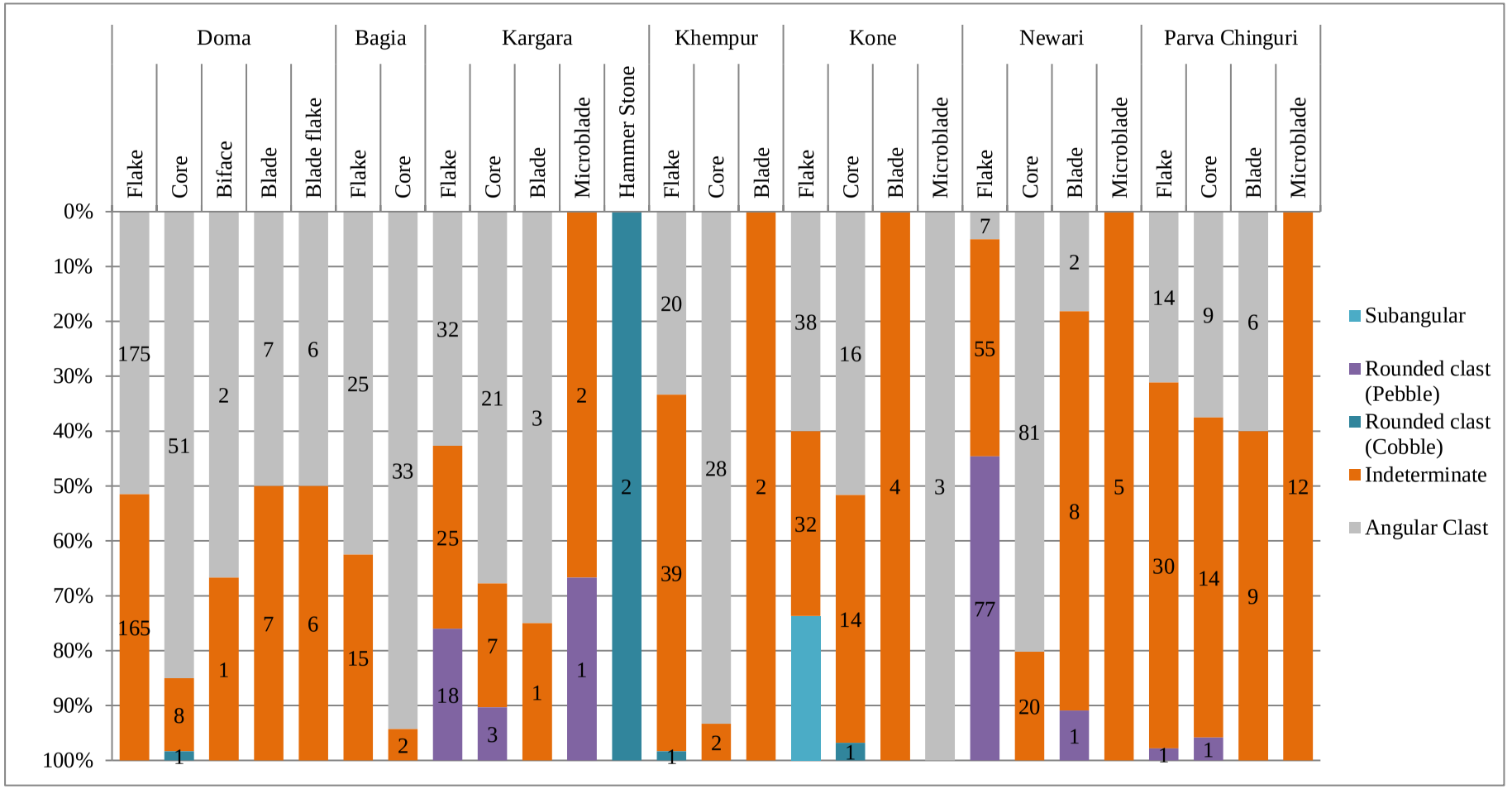

Figure 60. Site and artefact specific blank type distribution in the LSV.

4.15 Striking platform

The striking platforms (*Figure 61-63*) were plain (*n* = 499, 56%), cortical (*n* = 161, 18%), facetted (*n* = 68, 8%), abraded (*n* = 100, 11%), semi-cortical (*n* = 18, 2%), dihedral flat (*n* = 14, 2%), dihedral convex (*n* = 9, 1%), NA (not available) (*n* = 16, 2%), and indeterminate (*n* = 4, 0.4%).

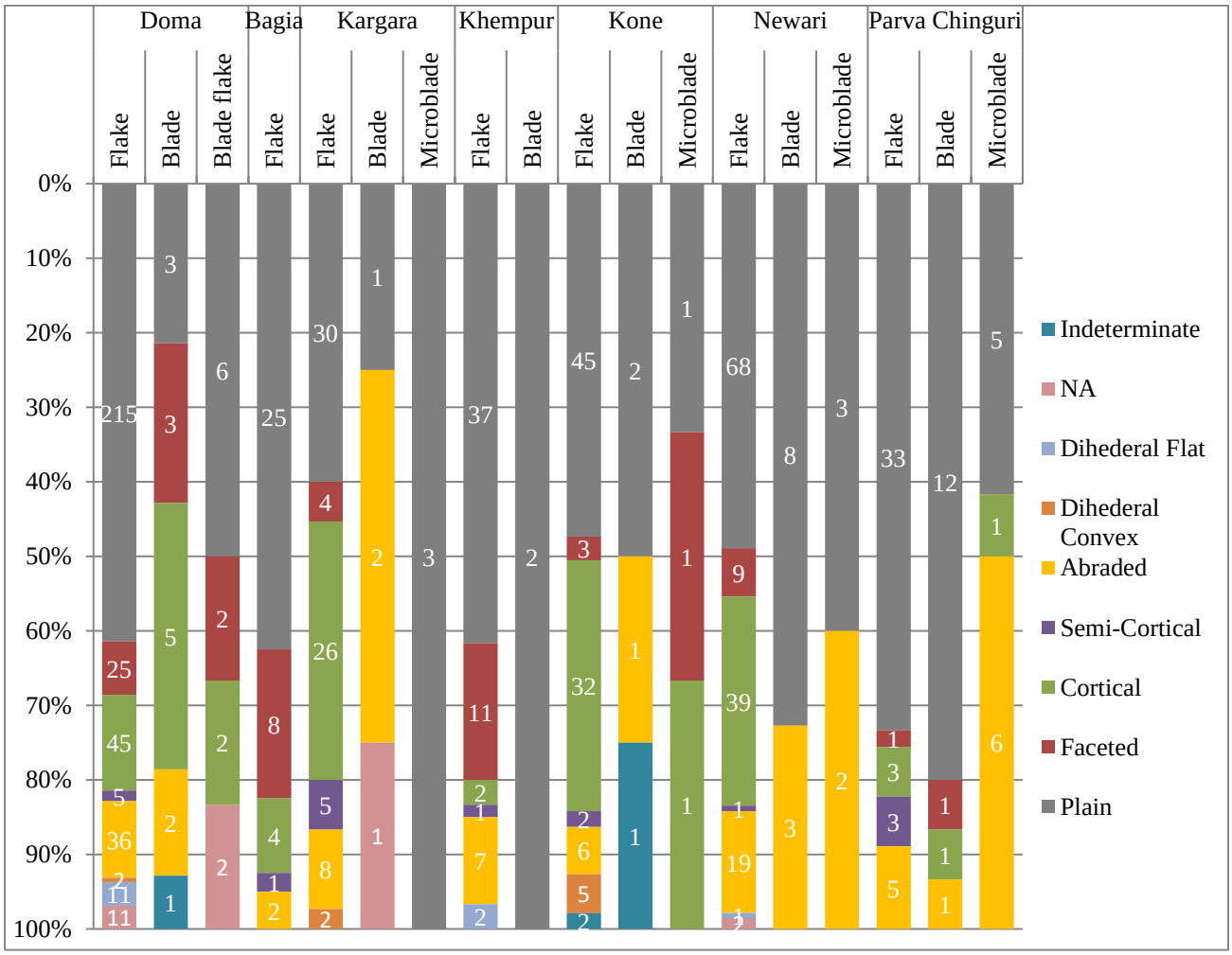

Figure 61. Site and artefact specific striking platform frequency in the LSV.

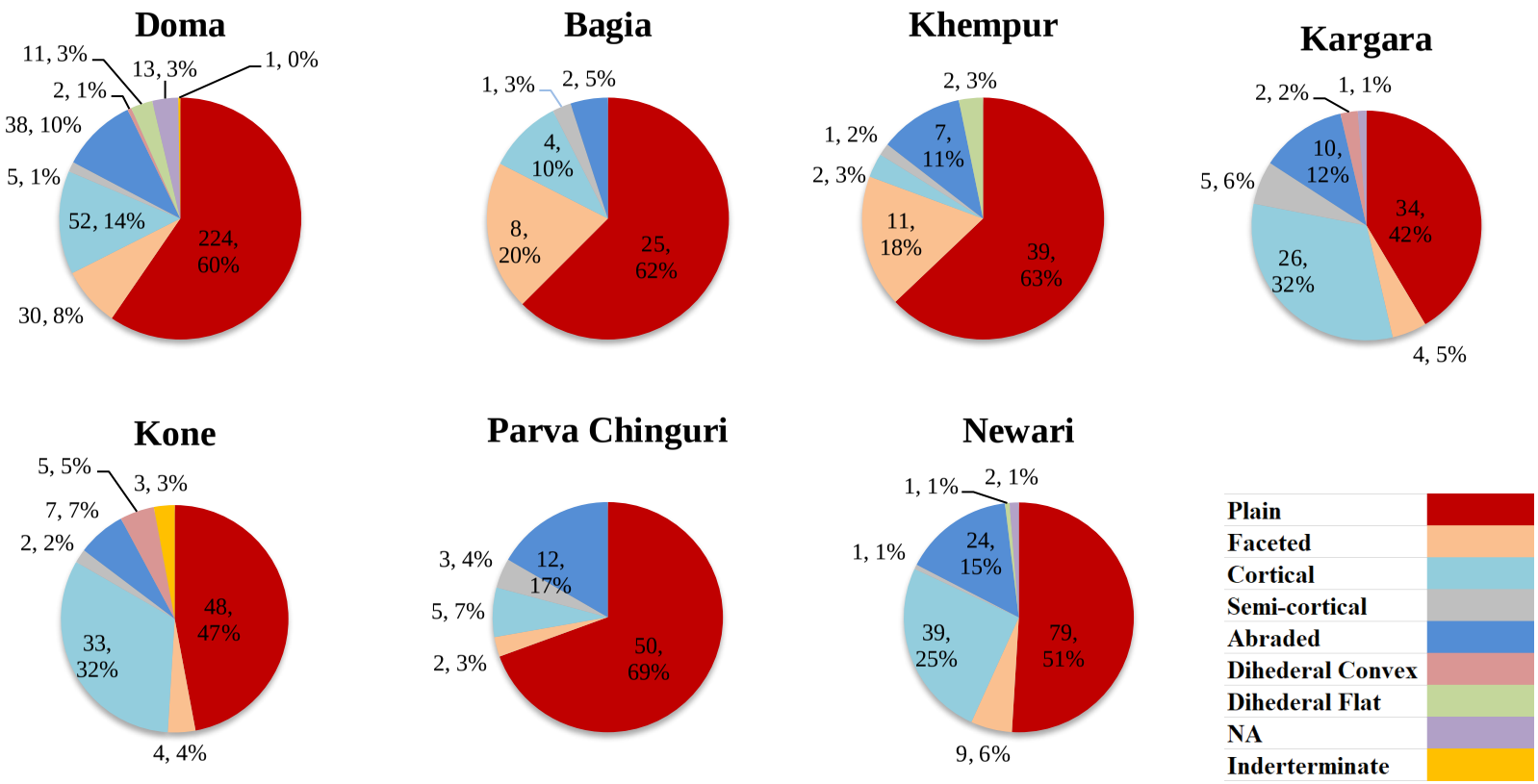

Figure 62. Site-wise striking platform frequency in the LSV.

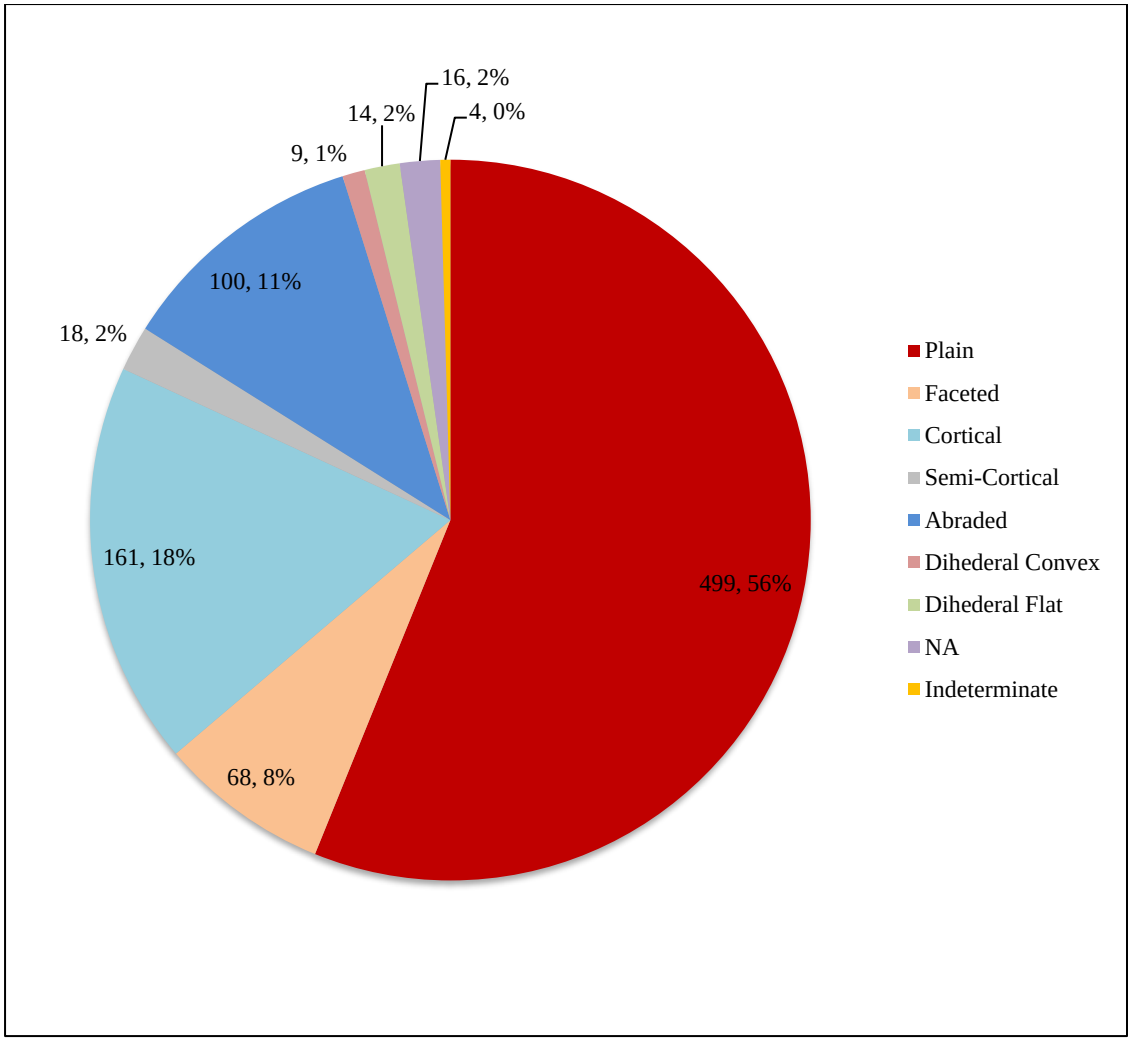

Figure 63. Overall striking platform frequency in the LSV.

4.15.1 Striking Platform frequency site-wise

At Doma, a total of (*n* =376) artefacts, including flakes, blades and blade flakes, show plain (*n* = 224, 60%), facetted (*n* = 30, 8%), cortical (*n* = 52, 14%), semi-cortical (*n* = 5, 1%), abraded (*n* = 38, 10%), dihedral convex (*n* = 2, 1%), dihedral flat (*n* = 11, 3%), NA (not available) (*n* = 13, 3%), and indeterminate (*n* = 1, 0.2%) striking platforms.

At Bagia, a total of (*n* =40) artefacts, including flakes, show plain (*n* = 25, 62%), facetted (*n* = 8, 20%), cortical (*n* = 4, 10%), semi-cortical (*n* = 1, 3%) and abraded (*n* = 2, 5%) striking platforms.

At Kargara, a total of (*n* =82) artefacts, including flakes, blades and microblade, shows plain (*n* = 34, 42%), facetted (*n* = 4, 5%), cortical (*n* = 26, 32%), semi-cortical (*n* = 5, 6%), abraded (*n* = 10, 12%), dihedral convex (*n* = 2, 3%) and NA (not available) (*n* = 1, 1%), striking platforms.

At Khempur, a total of (*n* =62) artefacts, including flakes and blades, show plain (*n* = 39, 63%), facetted (*n* = 11, 18%), cortical (*n* = 2, 3%), semi-cortical (*n* = 1, 2%), abraded (*n* = 7, 11%), and dihedral flat (*n* = 2, 3%) striking platforms.

At Kone, a total of (*n* =99) artefacts, including flakes, blades and microblades, show plain (*n* = 48, 47%), facetted (*n* = 4, 4%), cortical (*n* = 33, 32%), Semi-cortical (*n* = 2, 2%), abraded (*n* = 7, 7%), dihedral convex (*n* = 5, 5%), and indeterminate (*n* = 3, 3%) striking platforms.

At Newari, a total of (*n* =155) artefacts, including flakes, blades and microblade, shows plain (*n* = 79, 51%), facetted (*n* = 9, 6%), cortical (*n* = 39, 25%), semi-cortical (*n* = 1, 1%), abraded (*n* = 24, 15%), dihedral flat (*n* = 1, 1%) and NA (not available) (*n* = 2, 1%) striking platforms.

At Parva Chinguri, a total of (*n* = 72) artefacts, including flakes, blades and microblade, show plain (*n* = 50, 69%), facetted (*n* = 2, 8%), cortical (*n* = 5, 7%), semi-cortical (*n* = 3, 4%) and abraded (*n* = 12, 17%) striking platforms.

4.16 Biface refinement index

The thickness-to-width ratio of a biface is frequently employed as a refinement indicator (Roe 1994). Producing thin specimens is one of the most challenging aspects of biface production (Callahan, 1979; Edwards, 2001). Shipton (2016) proposes that Patpara and Bhimbetka have the thinnest bifaces in India due to the transitional nature of these assemblages. Doma displays some of the thinnest bifaces in South Asia, along with those

from Chakuria, Senraynpalayam, Morgara and Damodarpur (Chauhan, 2010) *(Figure 65-68)*. However, it should be noted that the handaxes of Doma and the Middle Son Valley (e.g., Patpara, Bamburi) are similar in morphology *(Figure 64)*. The Middle Son Valley bifaces were associated with other elements, including Levallois elements and blades. It could imply that many (if not all) of the Middle Son Valley bifaces are part of the regional Middle Palaeolithic record, as Blumenschine et al. (1983) first suggested. The Doma biface assemblage lacks other technological elements; additional regional research is necessary to determine their exact age and techno-cultural affinities with the Middle Son Valley record. Different variables, such as blank type, rock type, and reduction intensity, can all affect thinness.

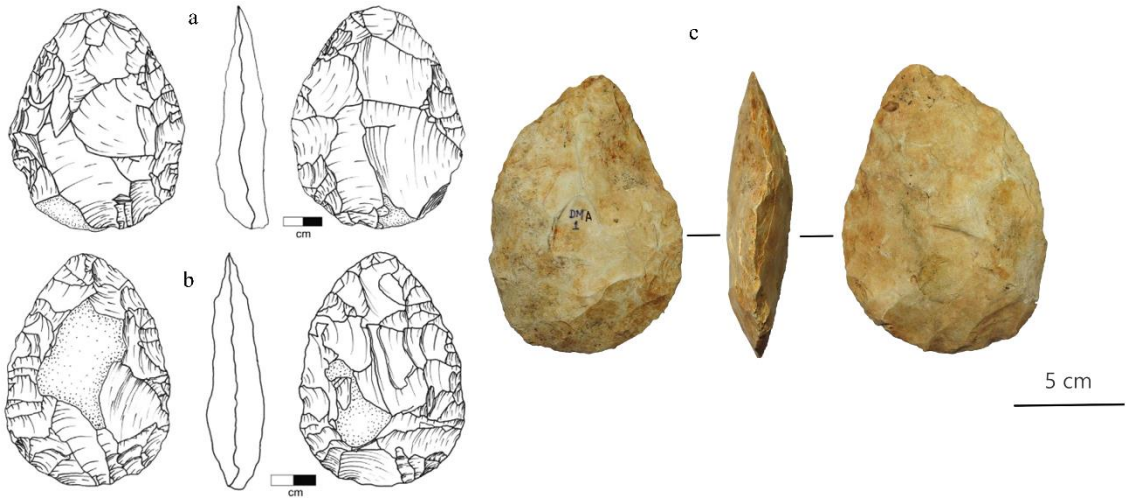

Figure 64. Refined, symmetrical chert handaxe recovered in-situ from Patpara (a), Bamburi (b) in Middle Son Valley and Doma (c) from the LSV.

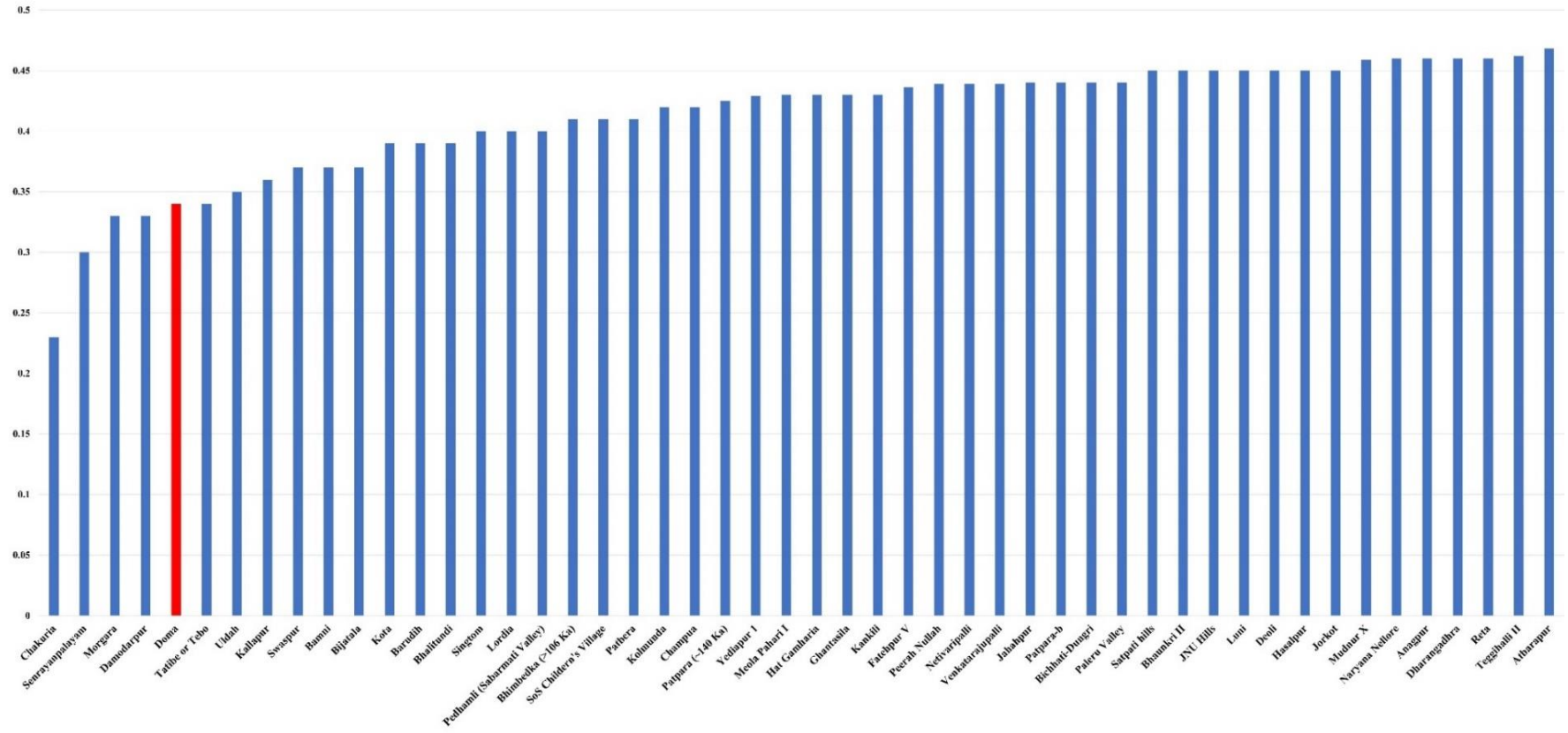

Figure 65. Biface refinement index of sites in South Asia highlighting Doma (a).

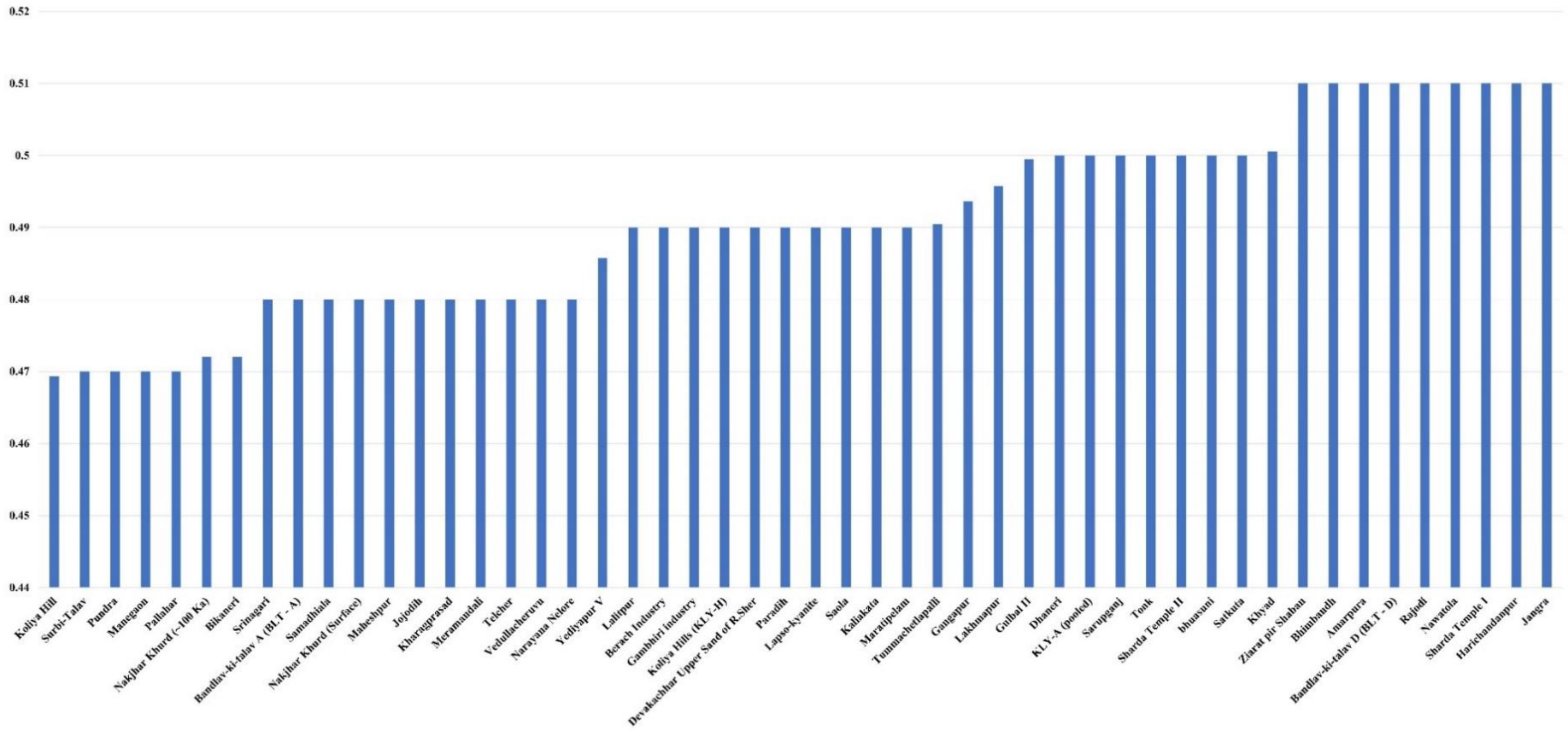

Figure 66. Biface refinement index of sites in South Asia (b).

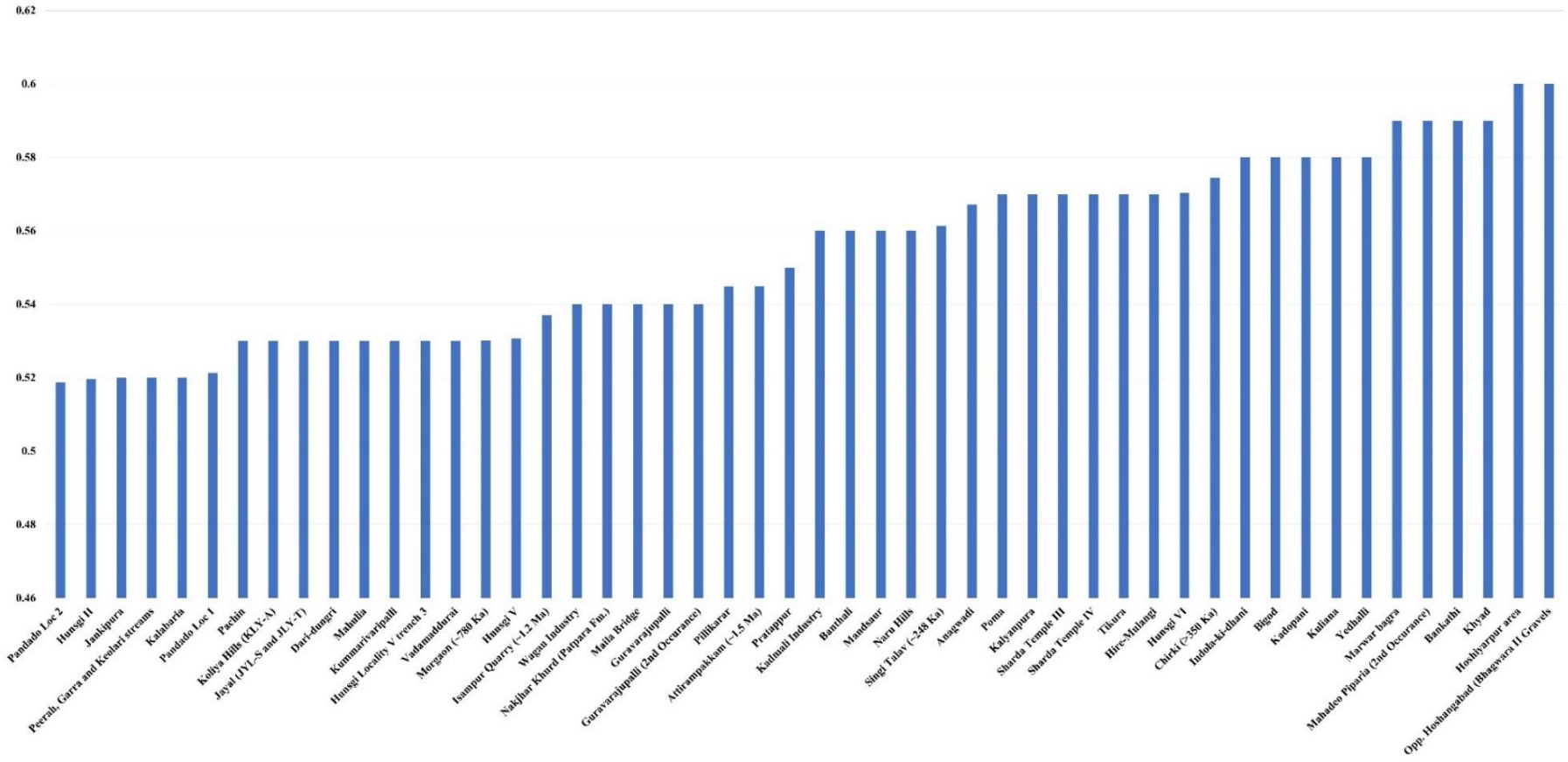

Figure 67. Biface refinement index of sites in South Asia (c).

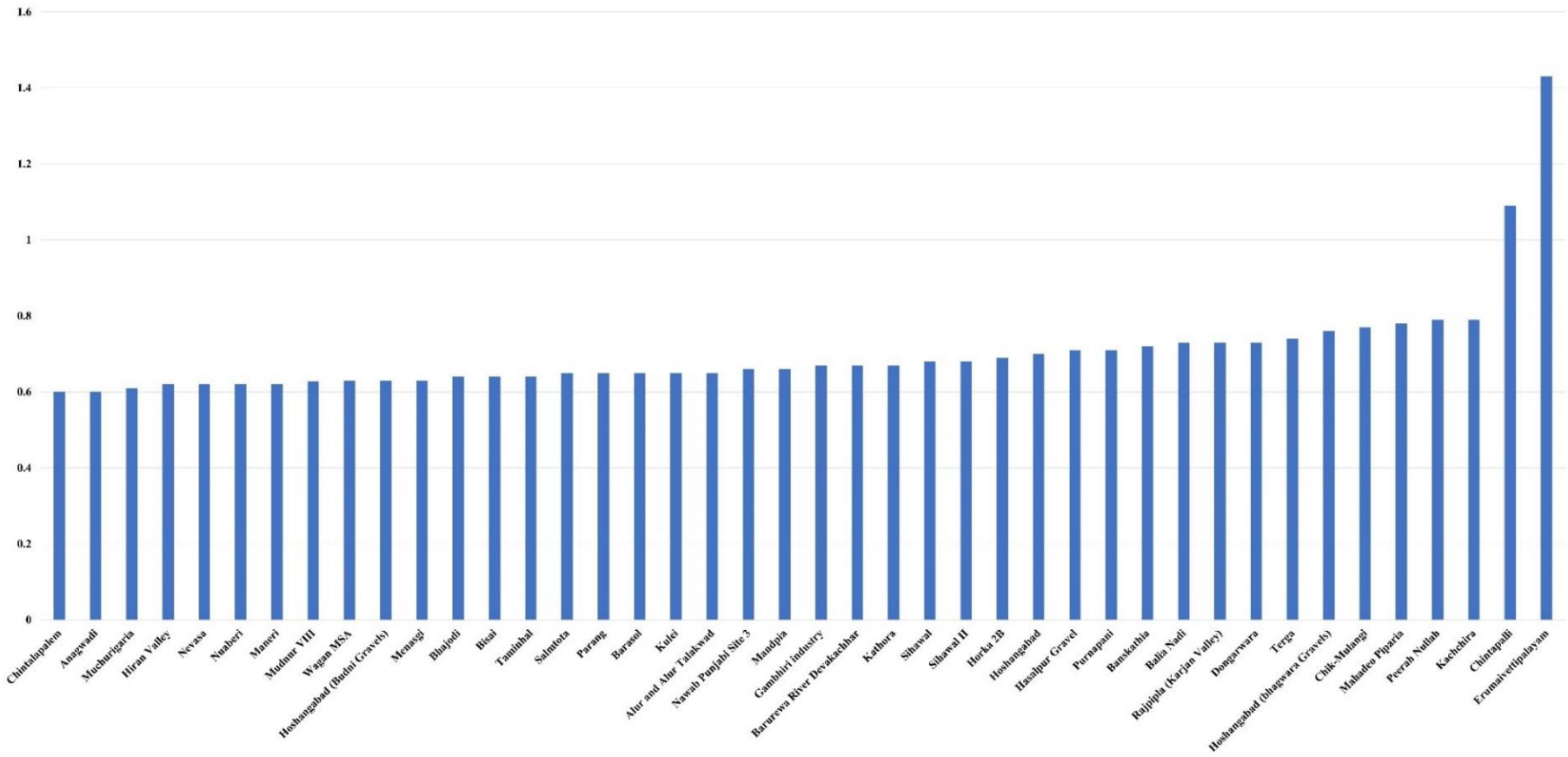

Figure 68. Biface refinement index of sites in South Asia (d).

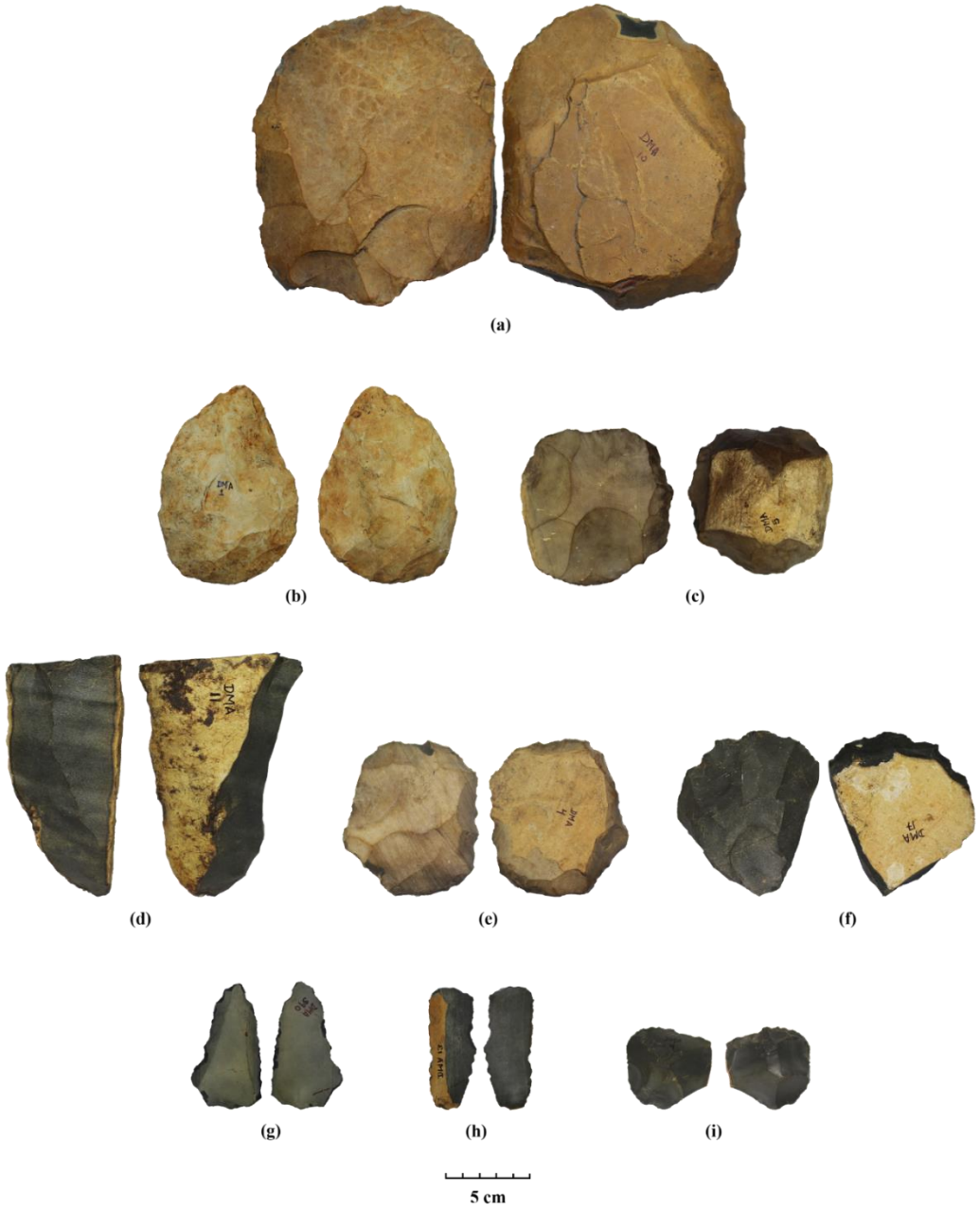

Plate 1. Site – Doma: a) prepared core; b) refined handaxe; c, e) Levallois core; d, f) blade core; g) Levallois point; h) blade; i) discoid core.

Plate 2. Site- Bagia: a,c,d) prepared core; b) Levallois core; e,f,g) flake.

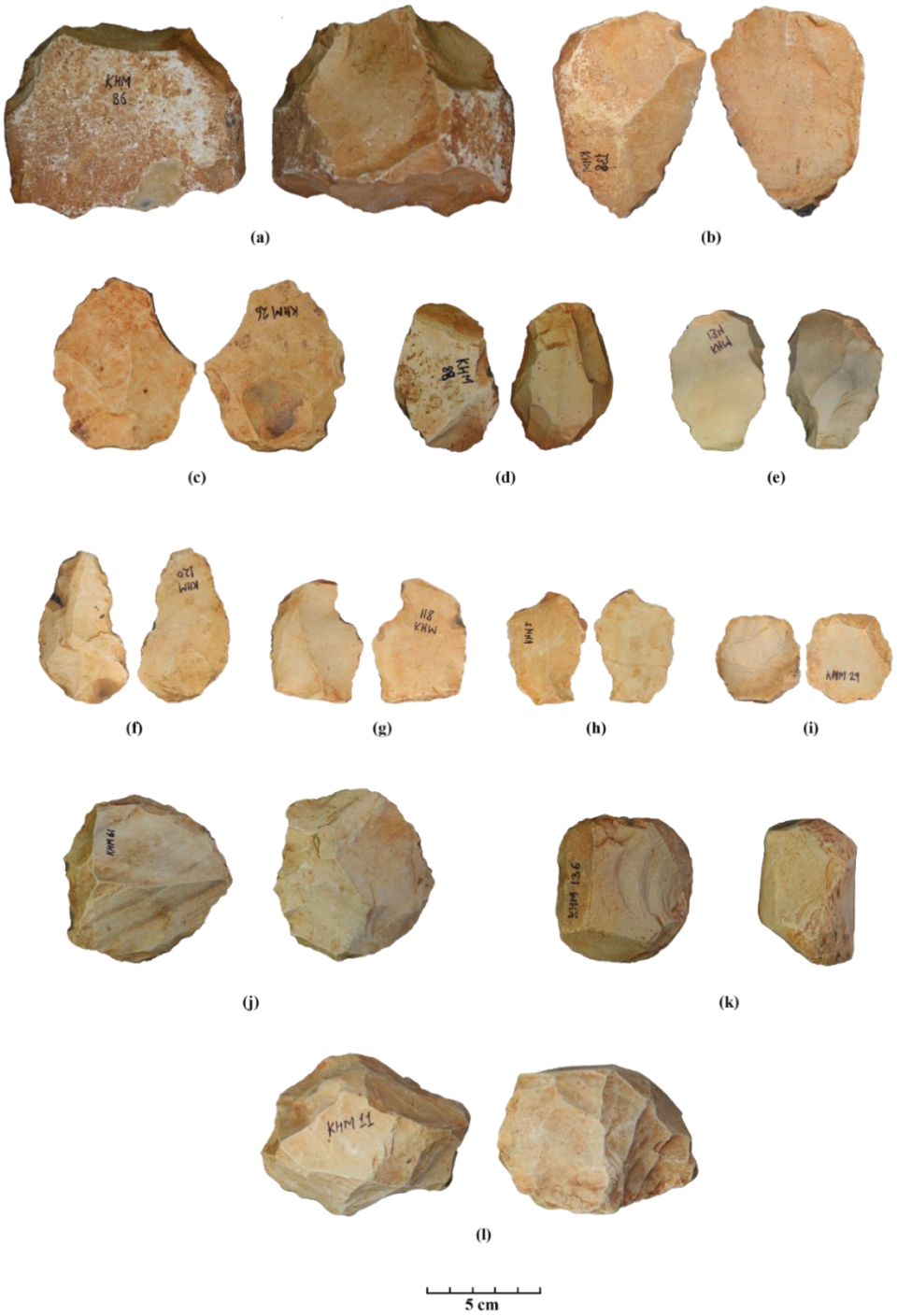

Plate 3. Site- Khempur: a, j) prepared core; b, c) prepared flakes; d) blade core; e, f, g, h, i) flake; k, l) multi-platform core.

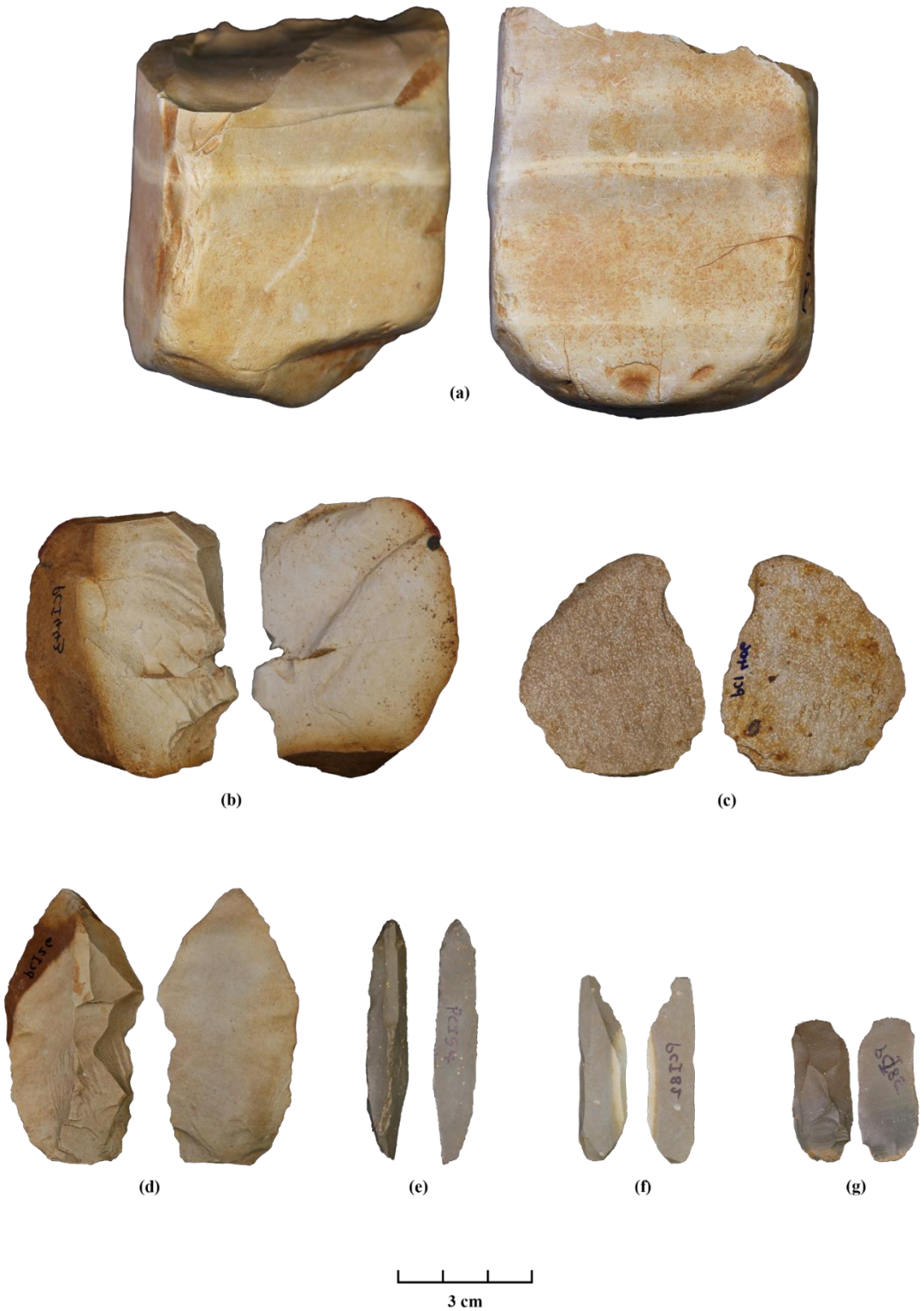

Plate 4. Site- Parva Chinguri: a) single platform unifacial core; b, c) flake; d, e, f, g) blade.

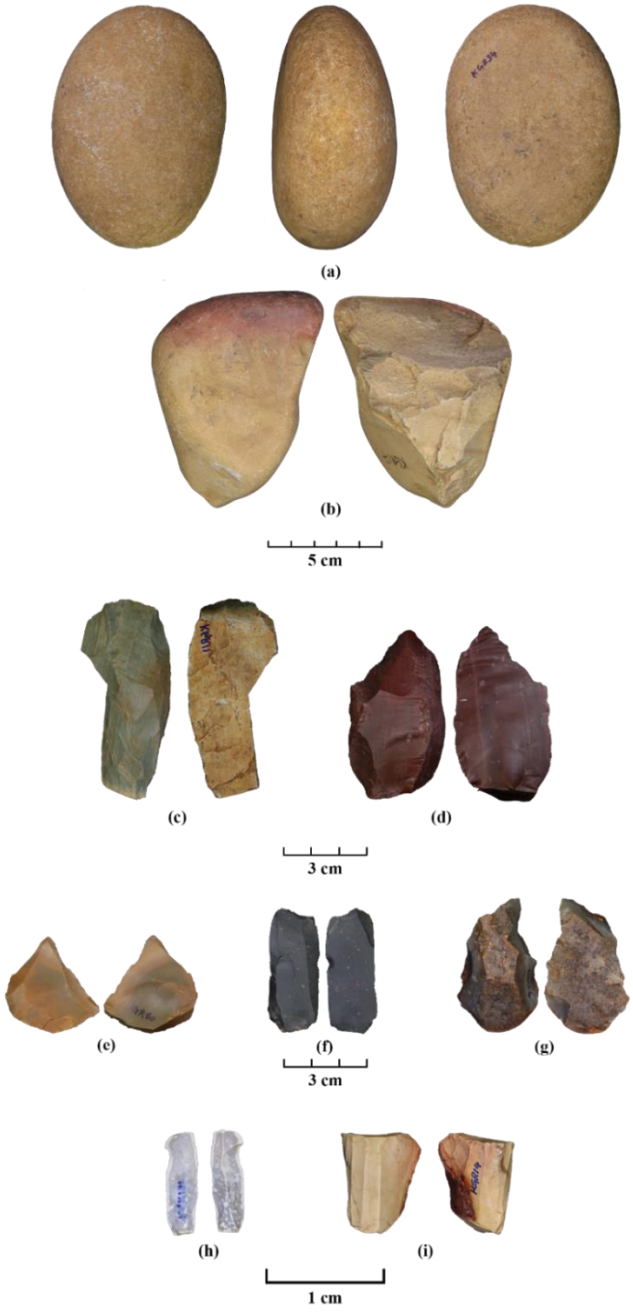

Plate 5. Site- Kargara: a) hammerstone; b) single platform unifacial core; c) blade core; d, e) flake; f) blade; g) multi-platform core; h) microblade; i) microblade core

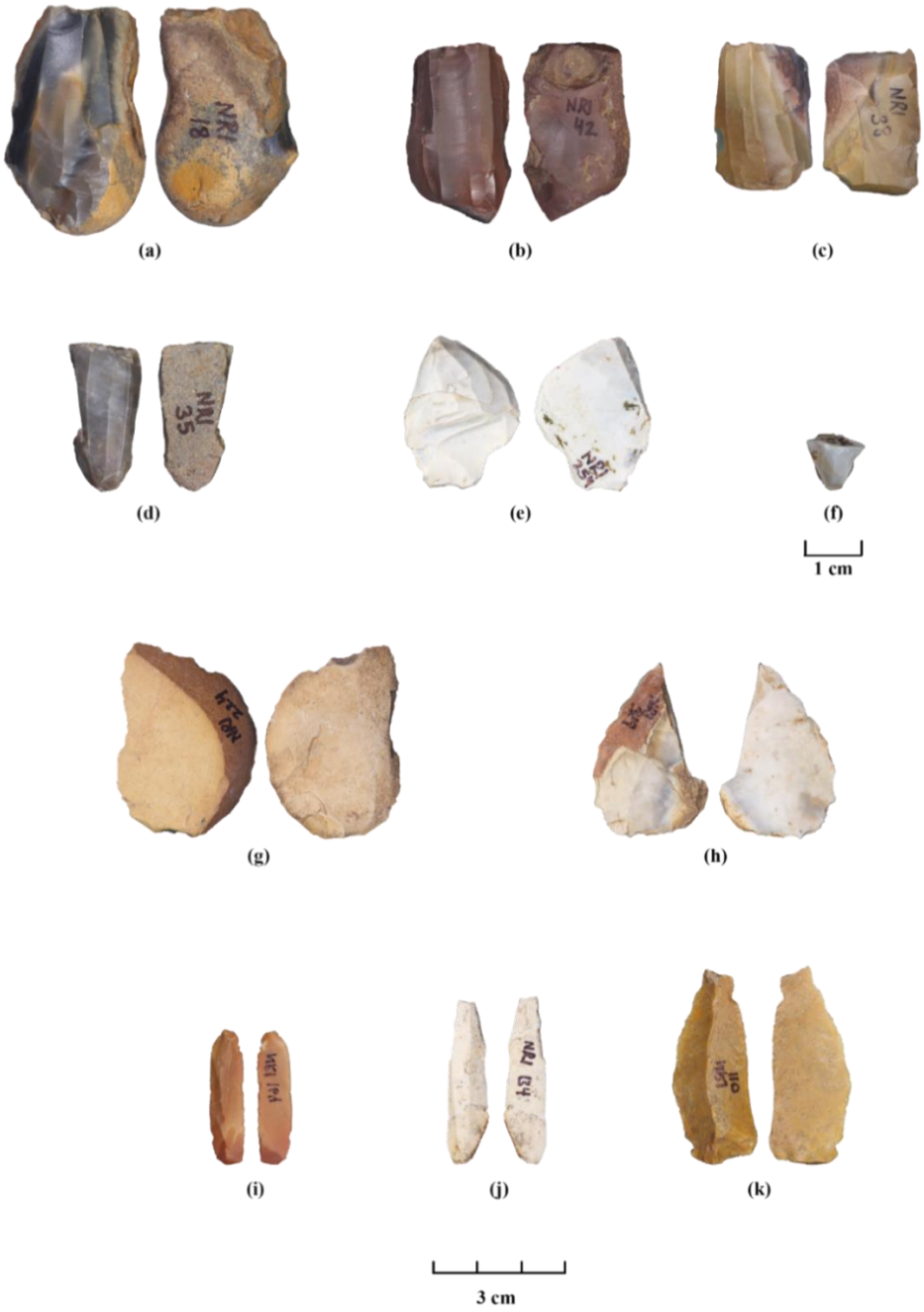

Plate 6. Site- Newari: a, b, c, d, f) microblade core; e, g, h) flake; i) microblade; j, k) blade.

Plate 7. Site- Kone: a,b,e) flake; c) blade core; d) microblade core; f, g) blade; h) single platform unifacial core.

4.17 3D Scanning

One of the primary benefits of using 3D models of stone artefacts for the study of lithic assemblages is quantitative access to previously inaccessible morphological characteristics. Quantification allows the morphological and technological variability of assemblages to be considered in extensive detail (*Figure A1* in appendix), allowing changes in archaeological sequences to be identified. This approach is a supplement to traditional qualitative and semi-quantitative approaches (Bretzke and Connard 2012, Maida et al., 2023). Additionally, this approach allows for the digital storage of data, making it more easily accessible and ensuring its longevity.

5 Geological excavation and various laboratory analyses (geochronology, sedimentology, and stable isotopes)

5.1 Excavation

In March 2021, a geological excavation was conducted at Kargara, located on the right bank of the Son River in the LSV, with the primary goal of understanding the sediment depositional and palaeoenvironmental history of the region. Kargara was selected due to its thicker sedimentation compared to other areas in the valley. A trench with ten steps (AS1, BS2, CS3, DS4, ES5, FS6, GS7, HS8, IS9 and JS10) was dug to a depth of 10.9 meters, and five lithostratigraphic units (LS1, LS2, LS3, LS4, and LS5) were identified (*Figure 69*). The bedrock was not reached during excavation, and the trench could not be expanded due to its proximity to the forest boundary. The excavation was conducted from 15th – 21st March 2021, and 4-6 labourers were hired. A detailed description of each identified unit is presented below.

5.1.1 Lithostratigraphic units:

LS1 – This unit consists of mainly loosely concentrated yellowish-red/brown coloured silty sediments with calcrete nodules extending from the top of the trench (AS1) to the middle of step CS3 (~ 2.6 m).

LS2 – This unit contains rugged and compact brown coloured silty sediments extending from the middle of step CS3 to the middle of step DS4 (~1 m).

LS3 – This unit represents a hard calcrete layer present at the end of step DS4 (~ 0.5 m). It consists of mostly calcrete with dark brown silty sediments.

LS4 – This unit contains brown-coloured silty sediments extending from step ES5 to the middle of step FS6 (~ 0.75 m). A high concentration of calcrete is observed at the upper middle part of step FS6.

LS5 – The unit is the thickest (~ 5 m) in the step trench, occupying steps FS6, GS7, HS8, IS9 and JS10. This unit primarily consists of yellowish-brown coloured silty sediments with two patches of calcretised root casts in steps GS7 and IS9.

5.1.2 Sediment and calcrete collection

A continuous collection of sediments (~100 g) at every 5 cm was made throughout the trench (n=216 samples were collected), and calcrete nodules were collected according to availability. Sediment samples were processed for grain size analysis and geochemical analysis (results discussed below). These sediments will be further considered for pollen analysis, and calcrete samples will be processed for stable isotope analysis in future. A total of nine OSL samples were collected for dating (results discussed below).

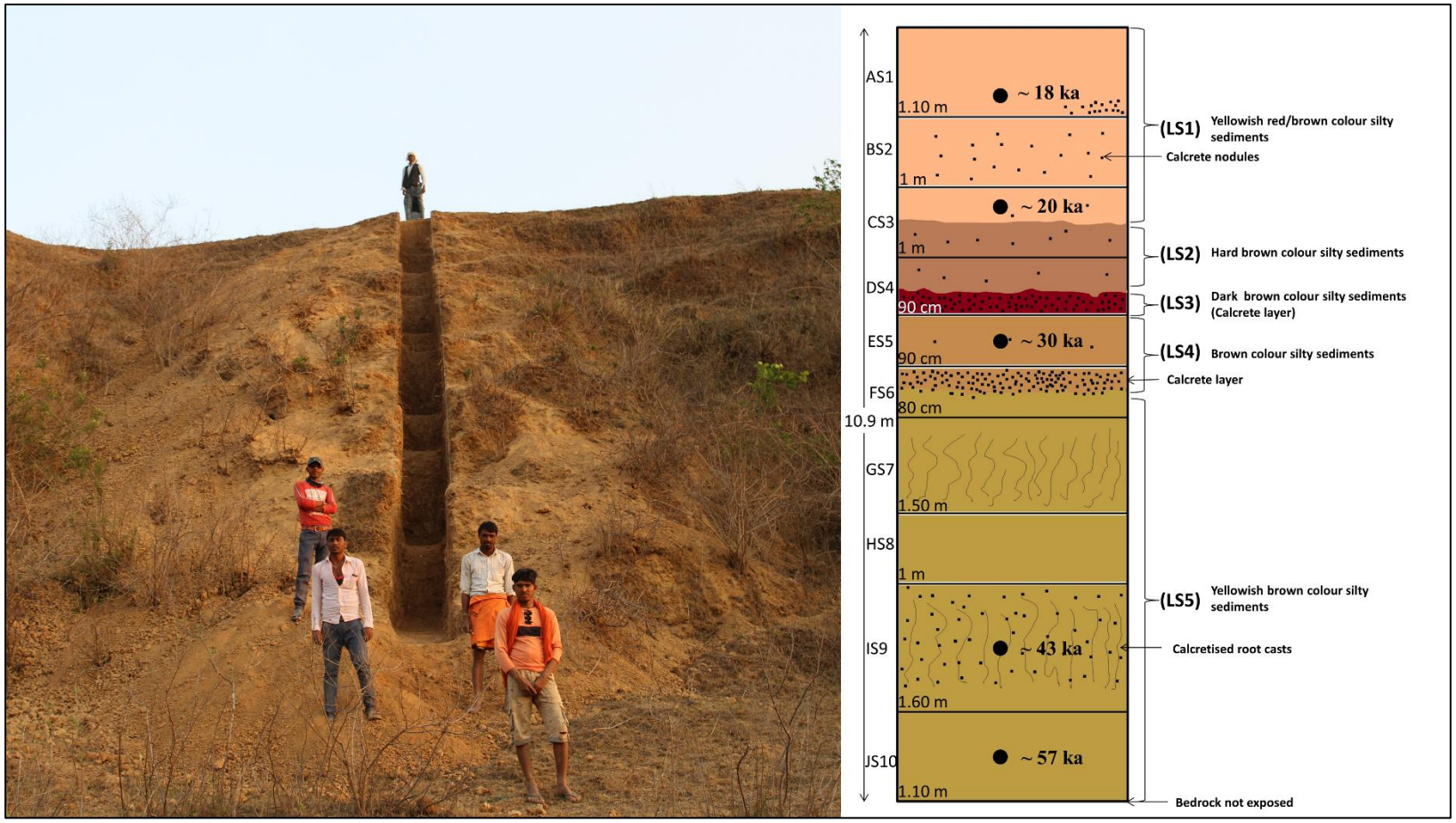

Figure 69. Geological excavation and stratigraphic profile at Kargara, the LSV, Sonbhadra, Uttar Pradesh.

5.2 Laboratory Analyses

5.2.1 OSL Dating

From the Kargara geological excavation, a total of nine samples were collected for OSL analysis. Preliminary dates were obtained from five of nine samples at steps JS10 (10.5 m), IS9 (9.5 m), ES5 (4.5 m), CS3(2.4 m), and AS1 (0.6 m) (*Table 30*).

*Table 30. Summary of sampling depth, stratigraphic unit and dosimetry data for the samples. *Depth of the OSL sample from Datum.*

Sample	Step (Depth*)	Dose (Gy)	err	dose rate (Gy/ka)	err	age (ka)	err	OD (%)	fading (% per dec)
OSL-1	AS1 (0.6 m)	83.3	6.1	4.5	0.2	18.5	1.5	14	0.9 ± 0.4
OSL-2	CS3 (2.4 m)	96.3	10.0	4.7	0.2	20.5	2.2	21	1.8 ± 0.6
OSL-5	ES5 (4.5 m)	147.3	14.0	4.9	0.2	30.3	2.3	20	2.3 ± 0.6
OSL-8	IS9 (9.5 m)	205.3	11.0	4.7	0.2	43.6	2.8	15	1.0 ± 0.4
OSL-9	JS10 (10.5 m)	264.3	13.0	4.6	0.2	57.5	3.5	13	1.1 ± 0.3

The oldest date from the excavation is 57 ka from step JS10, followed by 43 ka from step IS9, 30 ka from step ES 5, 20 ka from step CS 3, and 18 ka from step AS1.

5.2.2 Grain Size[9]

The volume-weighted mean grain size (D [4,3]), clay% (<4 μm), silt% (4–63 μm) and sand% (>63 μm) were calculated from the cumulative grain-size distribution.

The sediment grain size analysis revealed that silt particles dominate the sediment, followed by clay particles. The sand content ranges from 3.12% to 40.86%, with an average of

[9] Grain size data was primarily interpreted and written by the author, the final version was interpreted and modified by Dr. Anoop Ambili (Department of ESS, IISER Mohali)

12.77%, while the silt content ranges from 55.27% to 82.29%, with an average of 72.05%. The clay content ranges from 3.69% to 31.48%, with an average of 15.87%.

The two distinctive periods between 57 to 43 kyr and 20 to 18 kyr exhibited high median grain sizes that corresponded to the increase in sand content (*Figure 70,71*). On the other hand, the period between 43 to 20 kyr is characterised by a general declining trend in the D [4,3] values.

Temporal variation of grain size in sediments from the fluvial sequence may reflect past changes in the energy conditions (Behera et al., 2022). In fluvial landforms, the finer fraction of the grains represents a decrease in the hydrodynamic conditions during the sedimentation process (Mishra et al., 2014; Ankit et al., 2022). Consequently, a coarser mean grain size reflects higher discharge in river systems generally associated with a heavier and increased amount of rainfall, whereas a finer fraction indicates reduced rainfall. The increase in coarser grain size during the 57 to 43 kyr and 20 to 18 kyr periods reflects high energy conditions, while declining energy conditions characterise the 43 -20 kyr period.

5.2.3 XRF analysis

The geochemical data of the Kargara section indicates the variation in major oxides. The oxides in these sequences demonstrate the following order of abundance: SiO_2 > Al_2O_3 > Fe_2O_3 > CaO > MgO > K_2O >Na_2O > TiO_2 > P_2O_5 > MnO. The SiO_2% shows maximum content, which ranges from 42.65 % to 66.73%, followed by Al_2O_3 concentration (9.34 to 14.62) (*Figure 71*).

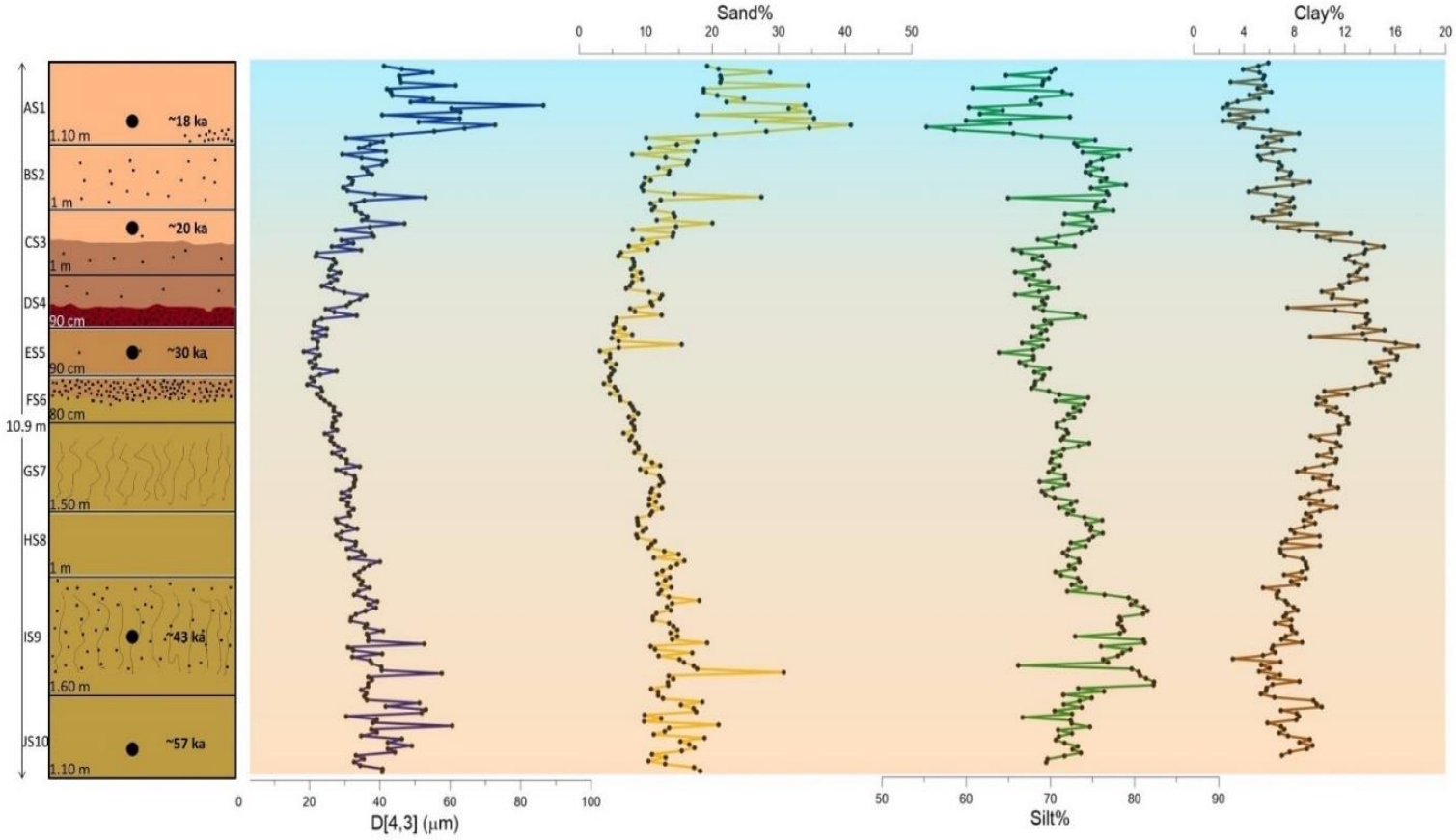

Figure 70. Vertical distribution of D [4,3], Sand, Silt and Clay (%) values of Kargara profile with OSL dates.

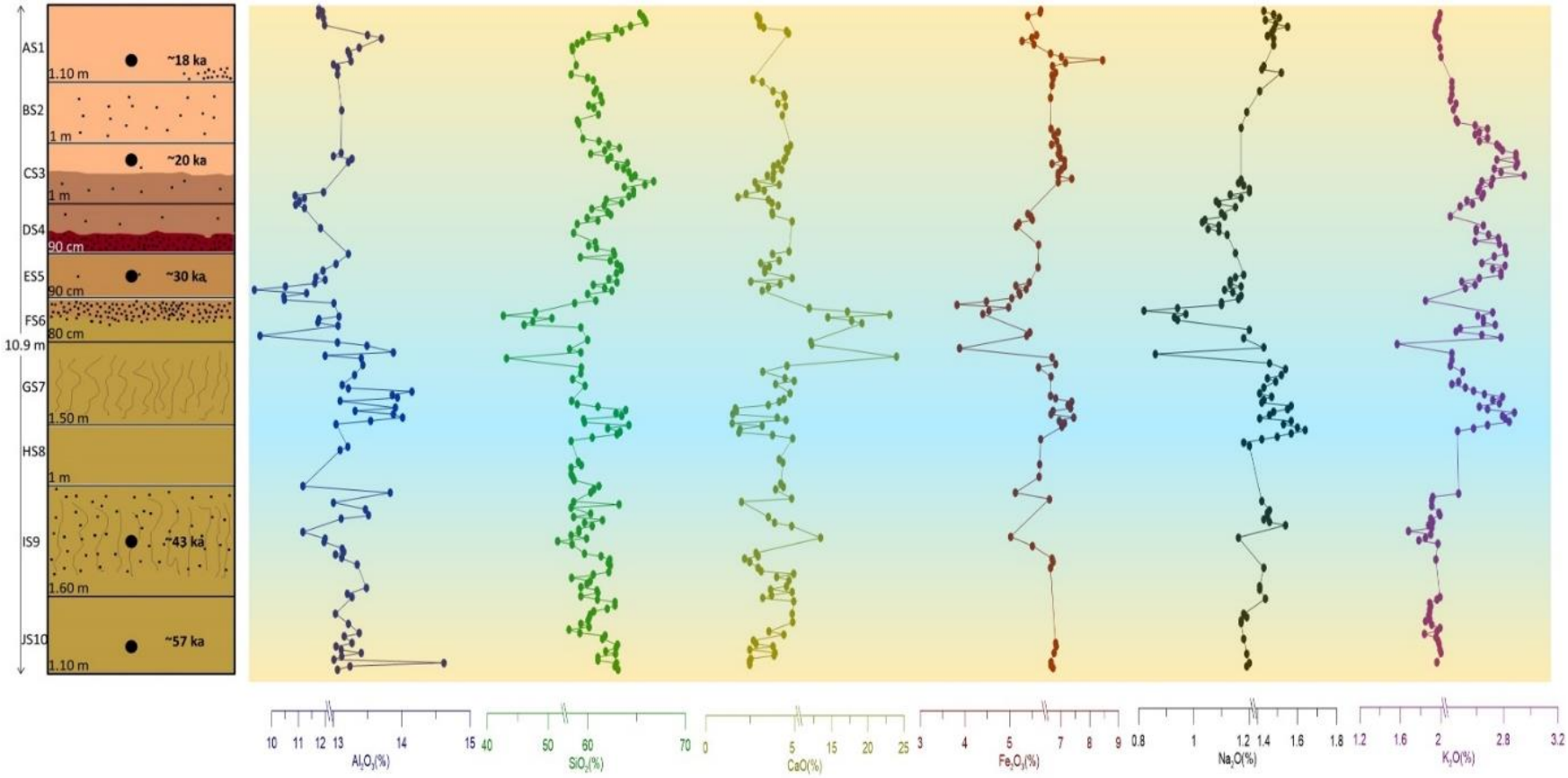

Figure 71. Vertical distribution of major oxides (%) values of Kargara profile with OSL dates.

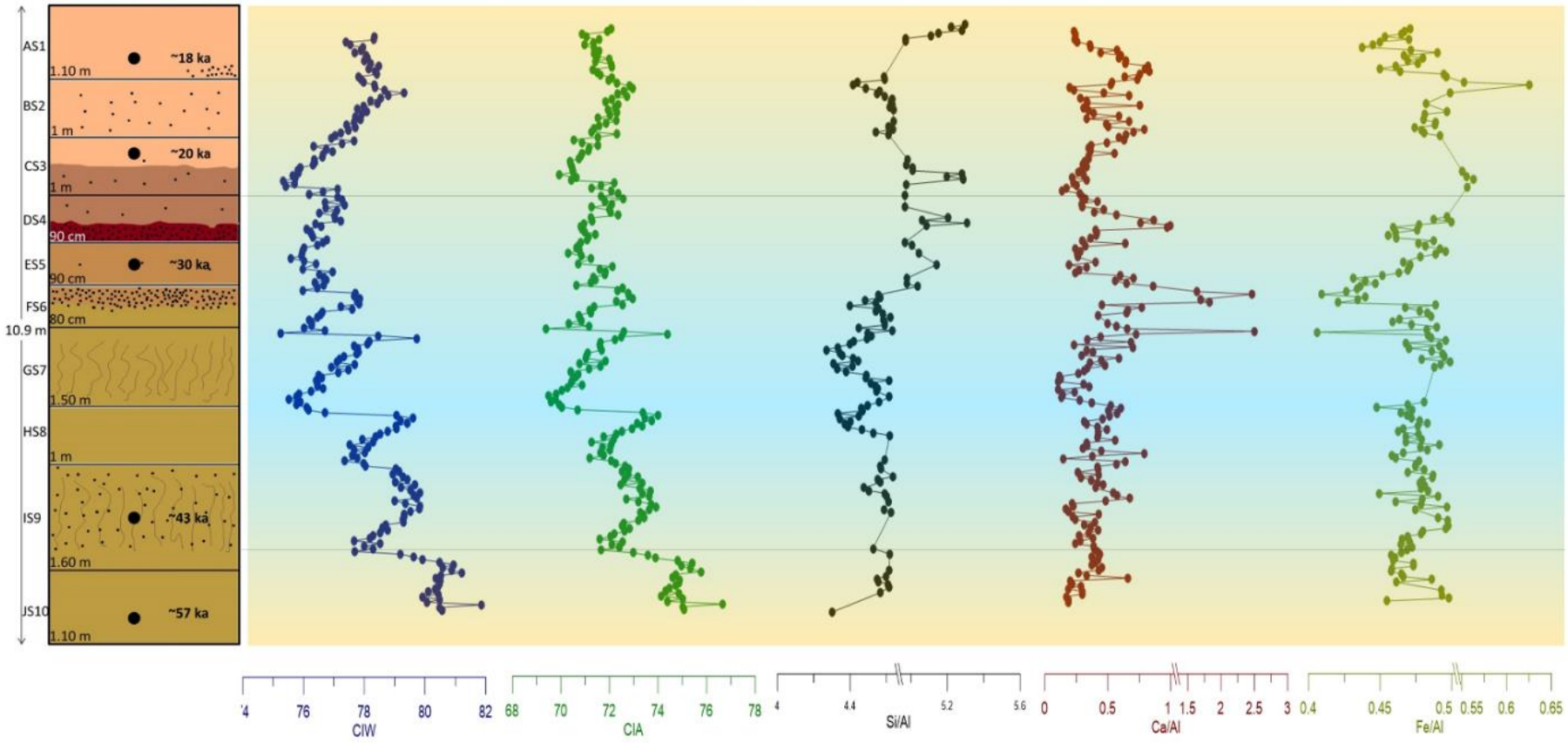

Figure 72. Vertical distribution CIW, CIA values and the elemental ratio of Si/Al, Ca/Al, Fe/Al of Kargara profile with OSL dates.

The major oxide concentration in the Kargara section varied as follows: CaO (1.49% to 23.93%) mean =59.50; Fe_2O_3 (3.82 % to 8.44%), mean =6.16; K_2O (1.57 % to 2.95%), mean =2.31, MgO (1.55 % to 6.85%), mean =2.60; Na_2O (0.82 % to 1.64%), mean =1.29; P_2O_5 (0.055 % to 0.255%), mean =0.11; TiO_2 (0.59 % to 1.45 %), mean =1.05; ZrO_2 (163 to 409), mean = 222.84; MnO (0.07 % to 0.14%), mean =0.096.

The geochemical signature of sediments has been commonly utilized to understand the dominant environmental process and provenance during sediment deposition (Gebregiorgis et al., 2020; Minyuk et al., 2006; Mishra et al., 2019). The elemental ratios (Si/Al and Ca/Al) provide information on the factors controlling the sediment deposition in the basin (Buggle et al., 2011; Lopez et al., 2006; Mishra et al., 2014). The Si/Al ratio provides information on the grain size distribution in the sediments (Behera et al., 2022). The variations in Si/Al values in the Kargara section primarily reflect the changes in grain size. Furthermore, the ratio Ca/Al is commonly used as a proxy for increased salinity and reflects reduced precipitation (Liu et al., 2017). The higher Ca/Al values during 43-30 kyr indicate increased aridity.

Furthermore, the major elemental data was used to calculate the chemical weathering intensities related to changes in precipitation. The Chemical Index of Alteration (CIA) and the Chemical Index of Weathering (CIW) were calculated using the molecular proportion of the oxides following Nesbitt and Young (1982) and Sun et al. (2010). The index of weathering formula applied for calculating the CIA is given below (Reshmi and Achyutan, 2018).

$$CIA = \{Al_2O_3 /(Al_2O_3 + CaO + Na_2O + K_2O)\}\times 100 \text{ ------(1)}$$

The molar ratio of CaO/Na_2O, as proposed by McLennan et al. (1993), has been used to calculate CaO. The CIA values below 50 are considered un-weathered samples; however, the

increased value (> 50 up to 100) indicates a progressive increase in the intensity of weathering with the removal of alkali and alkaline earth elements (Fedo et al., 1995; Nesbitt and Young, 1989). The CIA values (*Figure 72*) in the Kargara section ranged from 69.39 to 76.66 (average=72.04), signifying moderately to highly weathered sediments, while the CIW values varied from 75.23 to 81.85 (average= 77.79). The increasing CIA values from 57 to 43 kyr and 20 to 18 kyr indicate a progressive increase in chemical weathering, while the reduced CIA values from 43 to 20 kyr show reduced precipitation. The elemental ratio also corroborates the result (Ca/Al) and variations in the grain size data.

Overall, the grain size and XRF analysis indicate an increase in the Chemical Index of Alteration (CIA) between 57-43ka and again between 20-18 ka, which likely suggests an increase in precipitation. Conversely, between 43-20 ka, there appears to be a decrease in precipitation.

5.2.4 Stable Isotope Analysis

5.2.4.1 Fossil teeth

The stable carbon isotope composition ($\delta^{13}C$ value) of the body tissue of extant herbivores reflects the type of flora/vegetation (C_3 vs C_4) they ingest (Lee-Thorp et al., 1989). The tooth enamel, the hardest biological tissue, is thick and less prone to diagenetic alteration than bone, making it suitable for reconstructing ancient diets, environments, and climate changes (Cerling et al., 1997a, b; Lee-Thorp et al., 1989).

Terrestrial plants are commonly categorised into three types based on their photosynthetic pathways: C_3 (Calvin cycle), C_4 (hatch slack cycle), and CAM (Crassulacean acid metabolic acid), which generate variances in carbon isotope fractionation during carbon fixation processes (Bender, 1971; Ehleringer et al., 1991). Therefore, these plants are characterized by contrasting $\delta^{13}C$ values. C_3 plants, which include trees, shrubs, and cold-tolerant herbs (Deng

et al., 2001), have more negative $\delta^{13}C$ values ranging from -34‰ to -22‰, whereas those of C_4 plants, which are typical of drier and warmer habitats (Raven et al., 1999; Agrawal et al., 2012) are characterized by relatively higher values which range from -14‰ to -9‰ (Agrawal et al., 2012; Farquhar et al., 1989; O'Leary, 1988). It has been shown that factors like precipitation mainly control the δ13C values of plants, light intensity, atmospheric carbon dioxide concentration, elevation, and canopy effect (Basu et al., 2015; Farquhar et al., 1989; Kohn, 2010; Rao et al., 2017). The $\delta^{13}C$ values of C_3 plants become increasingly negative as precipitation, altitude, and latitude increase (Kohn, 2010). When plants are ingested by herbivores and herbivores are consumed by predators, isotopic fractionation occurs from meals to the tooth enamel. The $\delta^{13}C$ values of the tooth enamel of large herbivores and carnivores are 14‰ and 9‰ higher than those of plants (Cerling and Harris, 1999; Tejada-Lara et al., 2018). Following previous research (Biasatti et al., 2010; Cerling et al., 1997; Janssen et al., 2016; Uno et al., 2018; Wang et al., 2008; Xu et al., 2021), this study attributes $\delta^{13}C$values in tooth enamel lower than -8 to animals consuming only C_3 food, from -8‰ to -2‰ to those consuming a C_3-C_4 mixed diet, and greater than -2 to those consuming primarily C_4 plants.

Because of the complexities of oxygen flux in mammals, palaeoecological and palaeoenvironmental interpretation based on $\delta^{18}O$ values of dental enamel is not straightforward (Ayliffe and Chivas, 1990; Kohn et al., 1996; Levin et al., 2006). However, it is instrumental in reconstructing diet, habitat preferences, and seasonality conditions (Fricke and O'Neil, 1996; Longinelli, 1984). The $\delta^{18}O$ value of tooth enamel is controlled by the $\delta^{18}O$ value of ingested water, which is controlled by the $\delta^{18}O$ of body water. Precipitation, latitude, altitude, aridity, and evaporative processes, as well as physiological and behavioural water

conservation factors and mammalian metabolic processes, all influence the $\delta^{18}O$ value of ingested water (Kohn, 1996; Kohn et al., 1996; Luz and Kolodony, 1985; Luz et al., 1984).

The $\delta^{18}O$ of mammals that frequently drink water depends on the $\delta^{18}O$ value of rainfall; drought-tolerant animals usually have relatively higher $\delta^{18}O$ values because of ^{18}O enrichment of reservoir water due to evaporation (Ayliffe and Chivas, 1990; Kohn et al., 1996; Levin et al., 2006). The variation in $\delta^{18}O$ of water has been attributed to environmental temperature changes, leading to the enrichment of ^{18}O in warmer conditions and relative depletion in cooler conditions (Bryant et al., 1996). Thus, summer is characterized by higher $\delta^{18}O$ values of water, whereas winter has lower $\delta^{18}O$ values in temperate regions. However, in tropical regions, where the environmental temperatures remain above 20º C, the "amount effect" dominates, whereby a lower $\delta^{18}O$ of water indicates periods of increased rainfall compared to higher values during drier periods (Dansgaard, 1964; Feranec and MacFadden, 2000; Higgins and MacFadden, 2004). Amphibious mammals such as hippopotamus generally have lower $\delta^{18}O$ values than their terrestrial counterparts (Bocherens et al., 1996; Cerling et al., 2003b; Clementz et al., 2008). Warm season C_4 grasses growing in open areas would generally have higher $\delta^{18}O$ values due to the loss of ^{16}O by transpiration compared to C_3 plants growing in wetter and closed areas. Therefore, grazers adapted to feeding on water-stressed grasses growing in drier conditions may yield higher $\delta^{18}O$ values than forest-dwelling browsers (Bocherens et al., 1996; Sternberg et al., 1989).

5.2.4.2 Results (Fossil teeth)

The $\delta^{18}O$ and $\delta^{13}C$ values of bioapatite from fossil dental elements of fossil mammals are well-established proxies for reconstructing climatic conditions and dietary patterns (Gehler et al., 2012). The present study analysed a total of 24 mammalian teeth (*Figure 73, Table 31*) from Gopnath in Gujarat and eight different localities in the Narmada Basin (Sher River,

Maua Khera, Luknu Nala, Barman Ghat, Gehra Nala, Amonda, Sokalpur Ghat, Raja Nala, Devakchar – in Narsinghpur District, Nehlai – in Sehore District) in Madhya Pradesh, as well as Doma in Sonbhadra District of Uttar Pradesh. These teeth belong to species of Cervid, Bovid, Suid, Hippopotamid, Canid, and Equid and are presumed to be from the Late Pleistocene, with possible exceptions such as Gopnath. The teeth were analysed for $\delta^{13}C$ and $\delta^{18}O$ values to understand the associated dietary habits and palaeoclimatic conditions during ~MIS 3 – 5, based on indirect stratigraphic and archaeological evidence of their age range.

5.2.4.2.1 Different localities in Narsinghpur, Madhya Pradesh

In eight different localities in Narsinghpur, 14 specimens were collected. Out of these, five were identified to family/genera (cervid, bovid, hippopotamid, equid and suid), and two specimens remain unidentified. The $\delta^{13}C$ values of bovid specimens range from 0.2 to 1.3 ‰, and their $\delta^{18}O$ values range from -0.47 to 0.76 ‰, with the Amonda outlier specimen having $\delta^{13}C$ values of -0.9 ‰ and the $\delta^{18}O$ value of -3.2 ‰.

Two cervid specimens have $\delta^{13}C$ values ranging from -0.2 to 1.1‰ and $\delta^{18}O$ values ranging from 1.6 to 1.9‰, and two hippo specimens have $\delta^{13}C$ values ranging from -3.2 to -1.2 ‰ and $\delta^{18}O$ value ranging from -6.8 to -4.0 ‰. A single equid has a $\delta^{13}C$ value of -2.0‰ and $\delta^{18}O$ value of -2.1‰ and a single suid specimen shows a $\delta^{13}C$ value of -2.4‰ and $\delta^{18}O$ value of -0.6‰. All bovids, cervids, and one hippo predominantly show a pure C_4 diet with water stress in the region with drier conditions except for the Narsinghpur hippo, which shows high rainfall / humid conditions, as hippos are mostly amphibian mammals with a different $\delta^{18}O$ value than other terrestrial animals.

The hippo specimen from Amonda and the suid specimen from Narsinghpur show mixed diets C_3 and C_4. Suids are omnivorous animals that can eat a variety of foods, whereas herbivores generally have a more restricted or specialized diet (Harris and Cerling, 2002).

The $\delta^{18}O$ values of suid specimens indicate the drier conditions. Similar to the Narsinghpur hippo, the Amonda hippo also shows a more negative value of $\delta^{18}O$.

Broadly, the fauna from the Nasinghpur region shows a C_4 diet with mostly grassland type environments with drier conditions.

5.2.4.2.2 Nehlai, Sehore, Gujarat

The author collected a total of five specimens of two species, bovid and suid, from the Nehlai site in the Sehore District. The four bovids specimens have $\delta^{13}C$ values ranging from -7.5 to -3.4‰ and $\delta^{18}O$ values ranging from -2.8 to -2.1‰. A single suid specimen had a $\delta^{13}C$ value of -11.14‰ and an $\delta^{18}O$ range of -4.74‰. The fauna of Nehlai was characterised by a preference for a C_3 diet and the predominance of humid climatic conditions.

5.2.4.2.3 Gopnath, Bhavnagar, Gujarat

The Gopnath palaeontological site is situated on the southern coast of Gujarat state along the Arabian Sea. Four samples of fossil teeth were collected for stable isotope analysis. Three of these four specimens are bovids, and one is canid. The $\delta^{13}C$ values of the bovids range from -3.1 to 2.3 ‰ where two specimens show -3.1‰ and one show 2.3‰ values. The $\delta^{18}O$ ranges from -4.1 to -3.1‰. The canid specimen shows $\delta^{13}C$ value of -2.5‰ and $\delta^{18}O$ value of -4‰.

The $\delta^{13}C$ values primarily indicate C_3-C_4 mix vegetation, with a preference for C_4 diets. The $\delta^{18}O$ value shows relatively humid climatic conditions.

5.2.4.2.4 Doma, the LSV, Uttar Pradesh,

Only one cervid specimen was found and analysed for stable isotope analysis from Doma. The $\delta^{13}C$ value is -2.0 ‰, and $\delta^{18}O$ value is -5.8 ‰. This shows that this cervid primarily grazed on C_4 plants growing in humid climatic conditions.

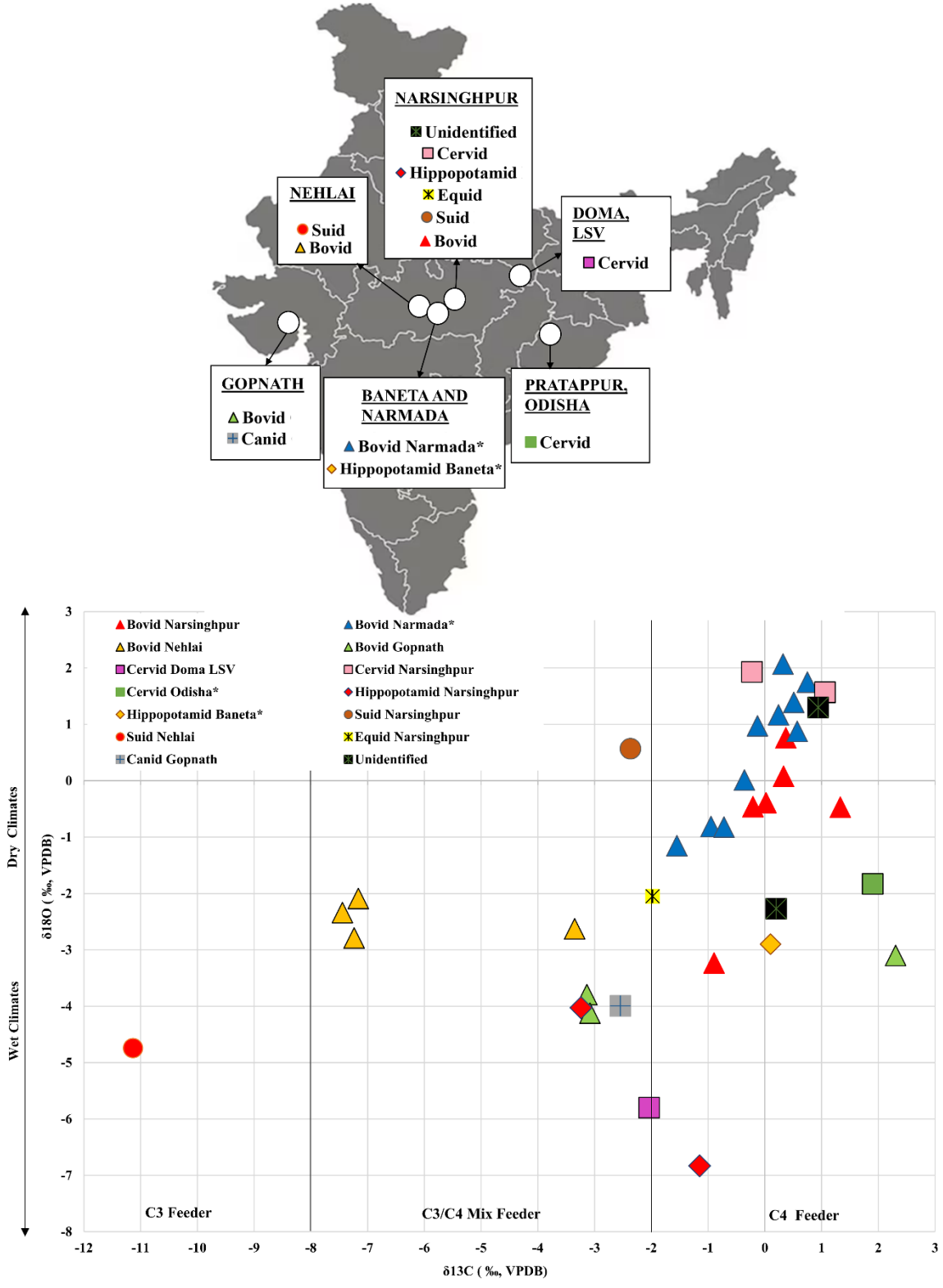

Figure 73. Map of India showing location of the sites/areas of fossil teeth enamel collection and graph showing $\delta^{13}C$ and $\delta^{18}O$ values of fossil enamels, region, and species–wise (data from published sources).*

Table 31. $\delta^{13}C$ and $\delta^{18}O$ values of fossil enamel, region, and species–wise.

Sr. No.	Specimen no.	Probable Family/genera	Location	Location	$\delta^{13}C$ values (‰; VPDB)	$d^{18}O$ values (‰; VPDB)	Probable Age
1	137	Bovid	Sher River	Narsinghpur, M. P.	0.37	0.76	Late Pleistocene
2	1	Suid	Sher River	Narsinghpur, M. P.	-2.37	0.57	Late Pleistocene
3	331	Tooth (unidentified)	Sher River	Narsinghpur, M. P.	0.2	-2.3	Late Pleistocene
4	155	Hippopotamid	Sher River	Narsinghpur, M. P.	-1.2	-6.8	Late Pleistocene
5	217	Cervid	Maua Khera	Narsinghpur, M. P.	-0.2	1.9	Late Pleistocene
6	234	Bovid	Maua Khera	Narsinghpur, M. P.	0.3	0.1	Late Pleistocene
7	152	Tooth (unidentified)	Luknu Nala	Narsinghpur, M. P.	0.94	1.3	Late Pleistocene
8	151	Bovid	Luknu Nala	Narsinghpur, M. P.	1.33	-0.57	Late Pleistocene
9	166	Bovid	Barman Ghat	Narsinghpur, M. P.	-0.2	-0.5	Late Pleistocene
10	120	Bovid	Gehra Nala	Narsinghpur, M. P.	0.0	-0.39	Late Pleistocene
11	206	Equid	Sokalpur Ghat	Narsinghpur, M. P.	-1.98	-2.1	Late Pleistocene
12	291	Cervid	Raja Nala, Piparha	Narsinghpur, M. P.	1.06	1.6	Late Pleistocene
13	NMD 1341	Bovid	Amonda	Narsinghpur, M. P.	-0.9	-3.2	Late Pleistocene
14	NMD 1331	Hippo	Amonda	Narsinghpur, M. P.	-3.2	-4.0	Late Pleistocene
15	NLI 1	Bovid	Nehlai	Sehore, M. P.	-7.24	-2.79	Late Pleistocene
16	NLI 2	Bovid	Nehlai	Sehore, M. P.	-3.35	-2.63	Late Pleistocene
17	NLI 3	Bovid	Nehlai	Sehore, M. P.	-7.16	-2.09	Late Pleistocene
18	NLI 4	Bovid	Nehlai	Sehore, M. P.	-7.45	-2.34	Late Pleistocene
19	NLI 5	Suid	Nehlai	Sehore, M. P.	-11.14	-4.74	Late Pleistocene
20	GPN 1	Canid	Gopnath	Bhavnagar, Gujarat	-2.5	-4.0	156 kyr
21	GPN 14	Bovid	Gopnath	Bhavnagar, Gujarat	-3.1	-3.8	156 kyr
22	GPN 79	Bubalus Sp./bovid	Gopnath	Bhavnagar, Gujarat	2.3	-3.1	156 kyr
23	GPN 96	Bovid	Gopnath	Bhavnagar, Gujarat	-3.1	-4.1	156 kyr
24	DMA CR1	Cervid	Doma	Sonbhadra, U. P.	-2.0	-5.8	Late Pleistocene
25	UNMD1	Bovid*	Narmada Valley	Hathnora, M.P.	-0.13	0.97	Late Pleistocene
26	UNMD2	Bovid*	Narmada Valley	Hathnora, M.P.	-0.36	0.01	Late Pleistocene
27	UNMD3	Bovid*	Narmada Valley	Hathnora, M.P.	-0.95	-0.81	Late Pleistocene
28	UNMD4	Bovid*	Narmada Valley	Hathnora, M.P.	-0.72	-0.82	Late Pleistocene
29	UNMD5	Bovid*	Narmada Valley	Hathnora, M.P.	-1.55	-1.15	Late Pleistocene
30	UNMD6	Bovid*	Narmada Valley	Hathnora, M.P.	0.75	1.75	Late Pleistocene
31	UNMD7	Bovid*	Narmada Valley	Hathnora, M.P.	0.24	1.17	Late Pleistocene
32	UNMD8	Bovid*	Narmada Valley	Hathnora, M.P.	0.51	1.39	Late Pleistocene

33	UNMD9	Bovid*	Narmada Valley	Hathnora, M.P.	0.57	0.88	Late Pleistocene
34	UNMD10	Bovid*	Narmada Valley	Hathnora, M.P.	0.32	2.07	Late Pleistocene
35	BNF-2-1	Hippo*	Baneta	Sehore, M.P.	0.1	-2.9	16 kyr
36	NTUAMS - 4278-1 (BBP)	Cervid*	Pratappur	Mayurbhanj, Odisha	1.9	-1.83	17 kyr

For Narmada Valley fossils: district information was not recovered due to the unavailability of the original thesis, but most likely, these are from Hathnora (Per. Comm. Dr. Sonika Sandhu). M.P. = Madhya Pradesh, U.P. = Uttar Pradesh.

5.2.4.3 Calcrete

Based on the photosynthetic pathway, terrestrial plants are divided into two groups, C_3 (Calvin cycle) and C_4 (Hatch–Slack cycle) plants. The $\delta^{13}C$ values of C_3 plants range from −34 to −19‰ and averages −26.7‰; whereas for C_4 plants it ranges from −18 to −10‰ and averages −12.5‰ (Cerling, et al., 1997). Plants using C_3 photosynthesis have $\delta^{13}C$ values ranging from about -20 to -35‰ (as compared to plants using C_4 photosynthesis that have $\delta^{13}C$ values ranging from about -10‰o to -14‰ (Cerling, 1999). Pedogenic carbonate formed in a pure C_3 ecosystem has $\delta^{13}C$ values of around -9‰ to -12‰ in contrast to pedogenic carbonate formed under pure C_4 vegetation which has $\delta^{13}C$ values of around l‰ to 3‰ (Cerling, 1999, Monger et al., 2009).

5.2.4.4 Results (Calcrete)

Carbonates are widely used as proxy records of palaeoclimatic change. Oxygen ($\delta^{18}O$) and carbon ($\delta^{13}C$) isotopic signatures are indicative of temperature, aridity or vegetation at the time of calcrete formation. This study analysed a total of 162 calcrete nodules for stable isotope analysis. These nodules were collected from the trenches placed at Pilikarar, Talayaghat and Devakachar in Madhya Pradesh (the details of the trenches such as location and stratigraphy is mentioned in Chapter 3, section 3.9).

5.2.4.4.1 Pilikarar, Sehore, Madhya Pradesh

A 3.5-meter step trench was excavated at Pilikarar, and calcrete was collected based on availability. This Pilikarar layer is part of the Baneta formation, which can be broadly dated between ~ 84 to 8 kyr (Kale et al., 2020; Patnaik et al., 2009; Tiwari and Bhai, 1997; Pers. Comm. with Dr. Vivek Singh)

The $\delta^{13}C$ values are Pilikarar ranges from -8.81 to 0.61‰. From depth 350 to 250 cm a linear trend is observed with C4 vegetation with $\delta^{13}C$ value ranging from -1.9 to 0.6‰ with average

of -0.2‰. From 240 to 150 cm depth a quick decrease in the $\delta^{13}C$ value is observed ranging from -8.5 to -5.4‰ with average of -7‰ suggesting C_3/C_4 vegetation with more dominance toward C_3. Following this, a linear trend is observed in the $\delta^{13}C$ value from depth (140 cm to top of the trench), with range of -2-6 o -1.5‰ with average of -1.9‰ suggesting C_4 vegetation.

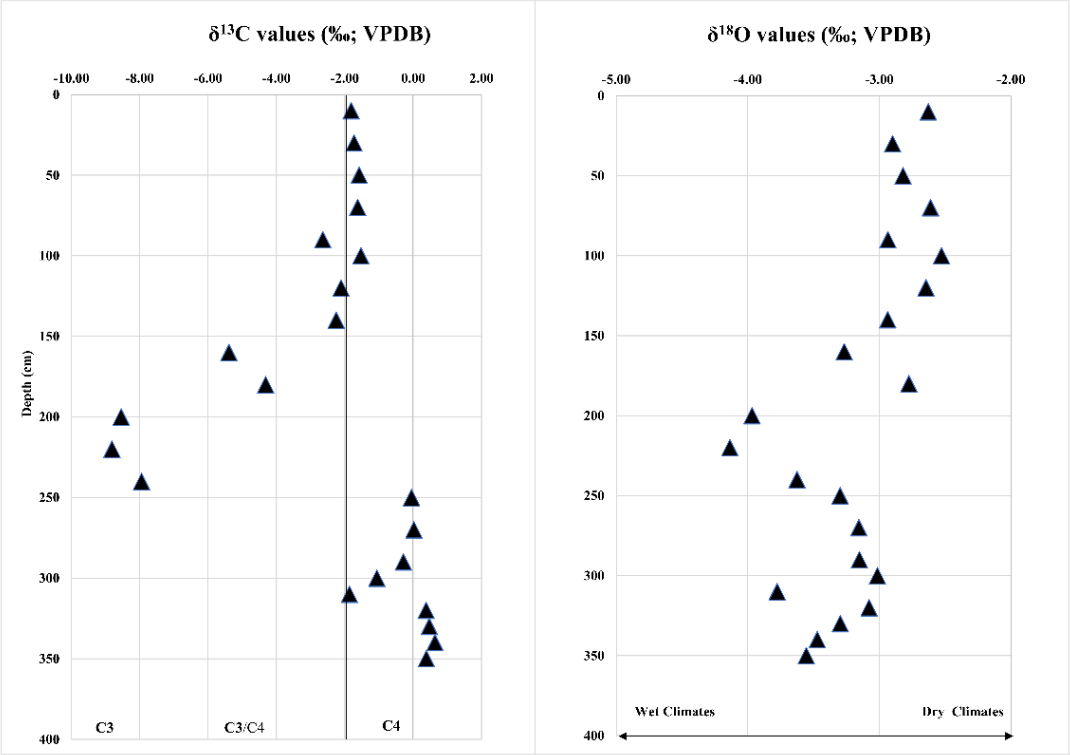

Figure 74. $\delta^{13}C$ and $\delta^{18}O$ values of calcrete at Pilikarar along with depth.

At Pilikarar, $\delta^{18}O$ values range from -4.1 to -2.5 ‰. A nearly linear trend is observed throughout the 3.5 meters, with the highest decrease in $\delta^{18}O$ value occurring around depth (200cm) with -4.1‰ (*Figure 74, Table A 22*). The more negative values of $\delta^{18}O$ indicate humid climates, which is supported by the $\delta^{13}C$ values, which indicate that most of the carbon was derived from mixed C_3-C_4 vegetation. On the other hand, higher $\delta^{18}O$ values indicate

relatively dry climatic condition. During this time higher $\delta^{13}C$ values indicate C_4 dominant vegetation in the study area.

5.2.4.4.2 *Talayaghat, Narsinghpur, Madhya Pradesh*

Calcrete nodules were collected every 10 cm in a 6.3-meter trench at Talayaghat. The $\delta^{13}C$ values range from -9.4 to 0.1 ‰. At depth 640 to 610 cm, a relative higher $\delta^{13}C$ values are observed ranging from -1.6 to 0.9‰. From depth 600-550 cm a quick drop in $\delta^{13}C$ values is observed ranging from -9.4 to -6.8‰ with average of -7.8‰. From depth 540 to 280 cm a linear trend with higher $\delta^{13}C$ values ranging from -3.2 to 0.1‰ with average of -1.2 ‰ is observed. From depth 270 cm to top, mix $\delta^{13}C$ values ranging from -7.5 to -2.1‰ with average of -4.4 ‰ is observed. $\delta^{18}O$ has a range of -5.9 to -2.5‰. There is a gradual increasing trend in the $\delta^{18}O$ values is observed from bottom to top of the trench (*Figure 75, Table A23*).

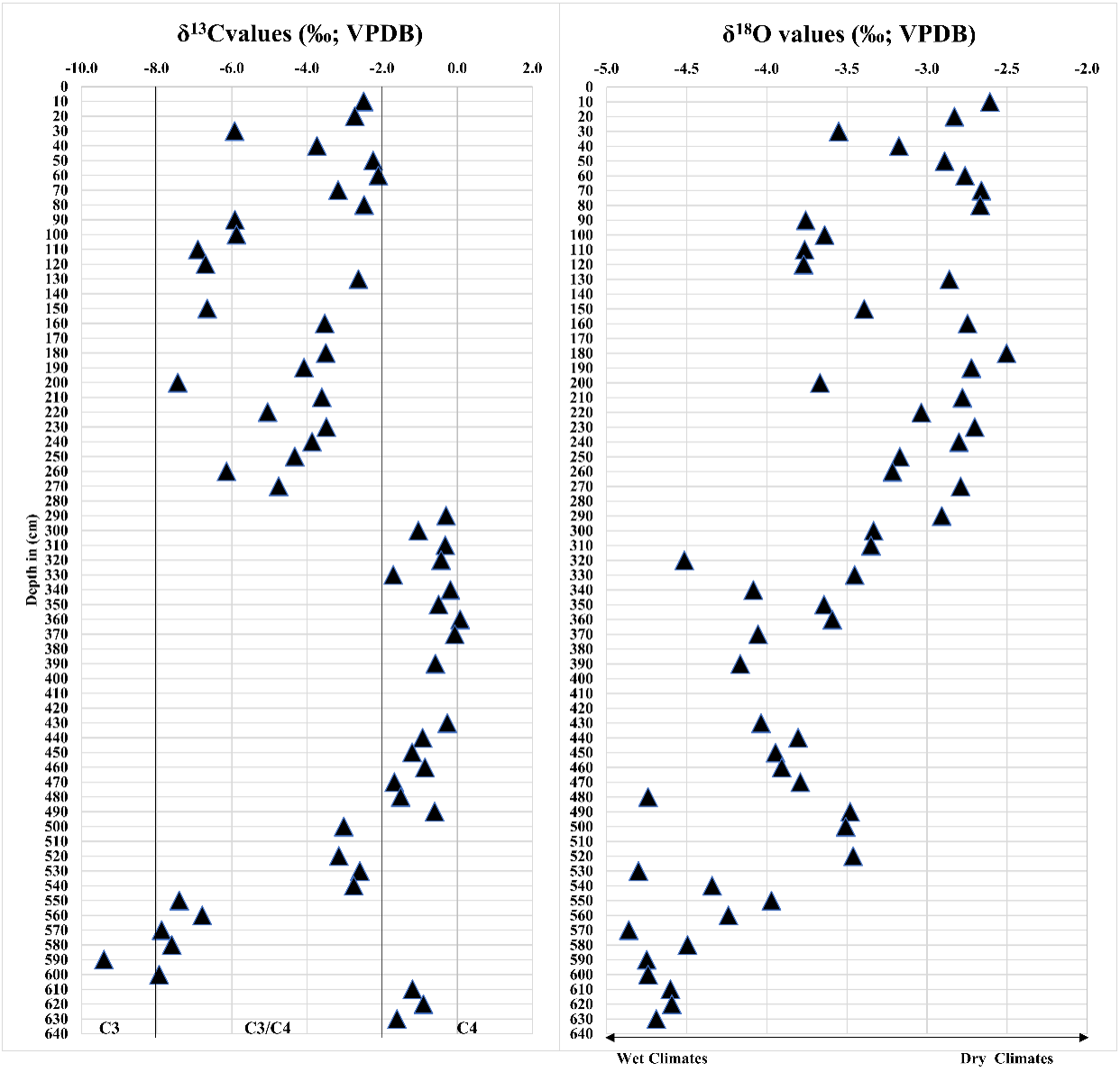

Figure 75. $\delta^{13}C$ and $\delta^{18}O$ values of calcrete Talayaghat along with depth.

5.2.4.4.3 Devakachar, Narsinghpur, Madhya Pradesh

Two trenches were placed at Devakachar (Sher River). Trench 1, conducted in 2018, reached a depth of `13 meters. Trench 2 was an extension of Trench 1, excavated to a depth of around 23 meters. Calcrete samples were systematically collected from both trenches at 10 cm intervals. In the initial 13 meters, a small quantity of calcrete was observed. However, from the 13 to 23-meter trench, a substantial amount of calcrete was collected and subsequently analysed for stable isotope analysis.

The $\delta^{13}C$ values in the trench range from -7.5 to 0.5 ‰. The lowest $\delta^{13}C$ values are observed between 23 and 21 meter, ranging from -7.5 to 0.2 ‰, with an average value of -3.1 ‰. From 20 to 13 meters, the $\delta^{13}C$ values range from -5.8 to 0.5 ‰, with an average value of -2.4 ‰. Generally, there is a gradual increase towards more positive values, and the highest relative positive range is observed at a depth of 20 to 19 meters, with $\delta^{13}C$ values ranging from -2.6 to 0.6 ‰ (*Figure 76, Table A24*).

At Devakachar, the $\delta^{18}O$ values range from -7.1 ‰ to -3 ‰, with an average value of -4.3 ‰. A linear trend is observed throughout the 10-meter depth with relative shift towards drier environments towards the top . The highly negative $\delta^{18}O$ values indicate a humid climatic condition

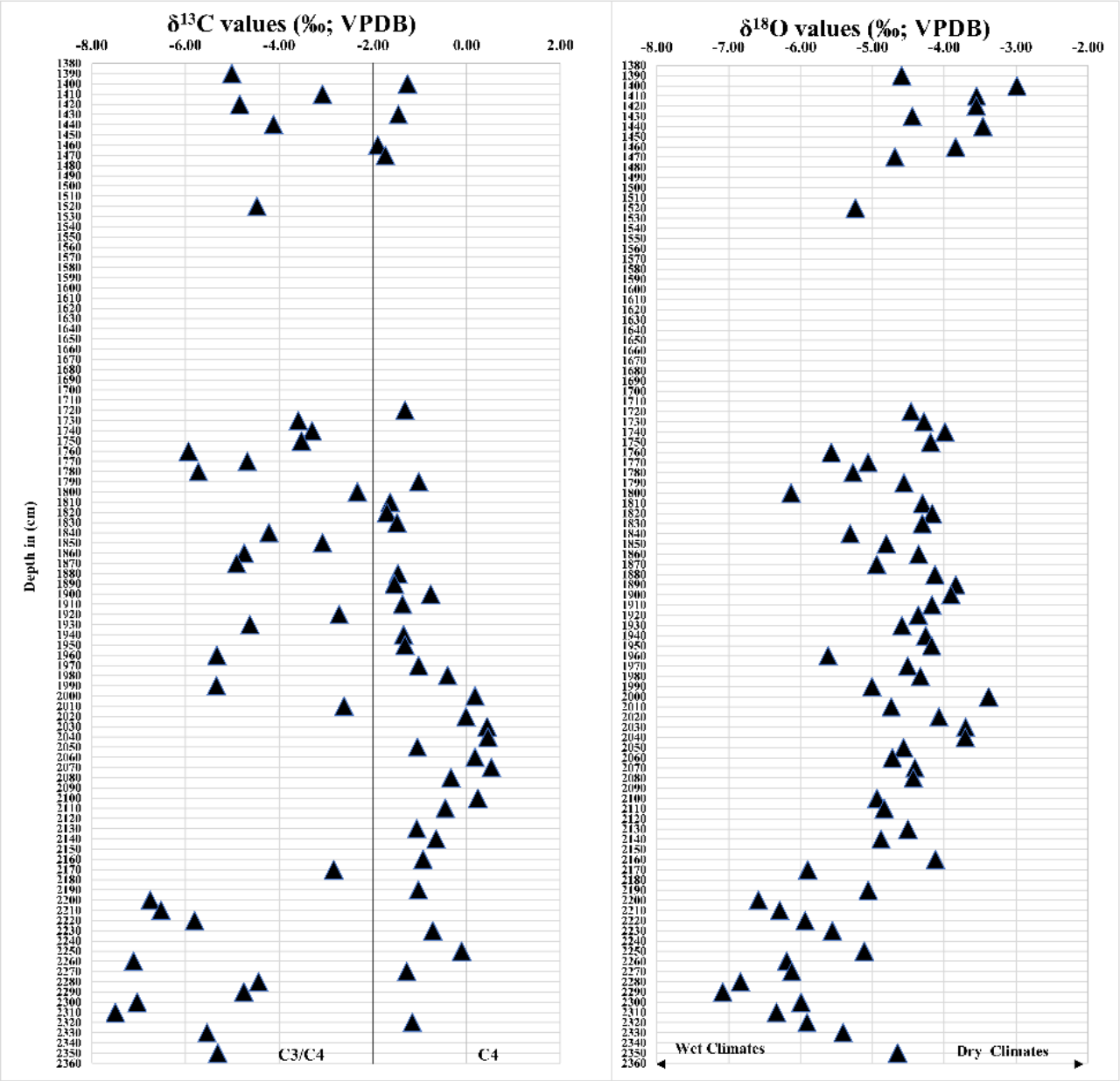

Figure 76. $\delta^{13}C$ and $\delta^{18}O$ values of calcrete Devakachar along with depth.

6 Discussion and Conclusion

This project has focused on reconstructing the Late Pleistocene palaeoenvironments and investigating the prehistoric evidence of north-central India, with an emphasis on the LSV, Sonbhadra District, Uttar Pradesh. The LSV has yielded various Palaeolithic and microlithic evidence from Late Acheulean to microlithic periods. The study region can be classified into two distinct areas: 1) Kaimur Plateau, present to the north of Son River and 2) River valleys, ravines, and hills present to the south of Son River. The sites on the Kaimur Plateau were mostly Upper Palaeolithic/microlithic and were found mainly on the bedrock with very little sedimentation. The sites on the south side mostly were Middle Palaeolithic/Upper Palaeolithic and microlithic; with one Late Acheulean site, the sedimentation appears to be relatively thicker, resulting in artefacts being *in-situ*, eroding out of sediments. The sites discovered in the south were mainly in the foothills and were associated with fine-grain sediments or exposed bedrock outcrops. Although most of the sites were on the surface or had eroded from sediments, two main stratigraphic findings have been made:1) artefacts eroding just a few millimetres above the bedrock from sediments/weathered bedrock; 2) artefacts eroding from fine sediments/fine sediments with calcrete where the bedrock was not visible.

One of the possible reasons for the differentiation of sites at the landscape level between the north and south regions is the availability of raw materials, particularly porcellanite. As discussed in Chapter 4, approximately 70% of the assemblages were made on porcellanite, locally available in the Semri Group of the Vindhyan Supergroup and located in the south of Son River.

When comparing elevations in the northern and southern zones of the study area, the Kaimur Plateau has a vertical 300–600 meters steep elevation, so transporting raw material in that

direction would have been comparatively difficult for Late Acheulean and Middle Palaeolithic populations. Therefore, this spatial barrier to raw material sources would have indirectly affected/limited subsistence strategies during Palaeolithic times (for Late Acheulean and Middle Palaeolithic populations. The north side is dominated by microlithic assemblages, suggesting that the subsistence strategies had changed during that time as compared to Late Acheulean and Middle Palaeolithic time period, hence the preference for technology and raw material. During the microlithic period, there was a shift towards more silicious raw materials such as chert, agate, chalcedony and quartz. As described above, the Late Acheulean to Upper Palaeolithic assemblages were made exclusively on porcellanite. While the use of porcellanite continues for the subsequent production of microliths, its overall frequency significantly decreased. Furthermore, it is observed that raw material transportation and population have increased with the introduction of microlithic technology.

6.1 Context and Behavioural Significance of the Late Acheulean

Identification of Acheulean is generally recognised by the manufacture of large flake blanks for biface production in India and other regions of the Old World (Gaillard et al., 2010; Mishra et al., 2010; Sharon, 2007). The Late Acheulean in the valley is identified only at the Doma site and was predominantly represented by the presence of handaxes. These artefacts were located in Unit III, mostly colluvial rubble, with angular to subangular clasts. At the same time, Doma has also preserved Middle Palaeolithic and laminar elements from Unit II, which overlies Unit III (Mehra, 2022).

Recently, it has become contentious whether bifaces are exclusive cultural markers for the Indian Acheulean (Haslam et al., 2011; Shipton et al., 2013) or are also an integral part of the Indian Middle Palaeolithic (Akhilesh et al., 2018 and references therein). Doma preserves refined bifacial elements and large flakes exclusively in Unit III, without any prepared core

or blade elements. The bifaces in the Middle Son valley were associated with other components, such as Levallois and blade elements. The refinement and morphological similarity of these Doma handaxes with Bamburi and Patpara (Haslam et al., 2011) in the Middle Son Valley is significant and, perhaps, indicates a broad comparable age range of 140 to 120 kyr for the assemblage (*Figure 64).*

The site is contextualised in the Semri Group of the Vindhyan Supergroup. Although the artefacts were found in a colluvial deposit, handaxes were without edge damage, and Unit III was exposed due to anthropogenic activities (agricultural). The recently exposed artefacts were fresh compared to the artefacts that had been exposed earlier.

6.1.1 Behavioural Significance

As the Acheulean artefacts were very low in number and only refined handaxes and large flakes were found, the Acheulean reduction sequence is marked by the absence of primary stages of reduction seen in large to giant cores and associated waste. Acheulean hominins preferred locally available porcellanite, the primary raw material in the valley. Possibly due to the lack of exposure of the Acheulean surface, no waste products and large cores were observed. As the colluvium and hill are exclusively porcellanite, the Late Acheulean hominin population did not transport the raw material but made the desired artefacts at the place of raw material provenance. The handaxes were made on angular clasts, locally available at the site. As the site is on the left bank of the Panda River (seasonal now), it can be suggested to be a prime location for artefact manufacturing and the availability of various food resources.

6.2 Context and Behavioural Significance of Middle Palaeolithic

The Middle Palaeolithic in South Asia is generally defined by the presence of prepared core and flake-based technologies (e.g., Akhilesh et al., 2018; Ajithprasad, 2005; Misra and

Rajaguru, 1978; Pappu, 2001; Sankalia, 1964). Out of the 61 sites found, a total of 9 sites have been provisionally classified as Middle Palaeolithic, and out of the seven analysed assemblages, two sites have been classified as Middle Palaeolithic.

Both Khempur and Bagia sites show the presence of prepared core and flake-based technologies. The site of Khempur is at the foothills of a shale and sandstone hill. The artefacts at the site were found eroding from a shale surface disturbed by ploughing and digging. Artefacts were also observed *in-situ* on the surface of shale bedrock, suggesting a contemporary development of both shale and Middle Palaeolithic artefacts. The Bagia site is also found on the sandstone foothills of the Vindhyan Supergroup. Artefacts have been found eroded from the fine sediment and colluvial rubble of a nearby sandstone hill.

6.2.1 Behavioural Significance

The Middle Palaeolithic sites were found in the foothills and generally away from porcellanite outcrops compared to the Late Acheulean site. The sites were almost exclusively to the south of the Son River, generally away from water sources. For example, the Khempur site is approximately 2.5 km from the assumed raw material source and approximately 5 km from the nearest water sources, suggesting possible population expansion and transportation of raw material and subsistence resources. At Khempur, cores were relatively smaller than flakes, and multi-platform cores were found most frequently at the site, suggesting extensive use of the available raw material. Additionally, the site lacks evidence of primary flakes or the original raw material clast, indicating that the raw material was initially trimmed elsewhere and brought to the site.

The Bagia site, located on the right bank of the Panda River, was most likely selected for its abundant natural resources, particularly water. Compared to the Late Acheulean site, this site

is farther from the raw materials source and shows the dominant presence of prepared cores and flakes. In addition, the site contains unflaked raw material clasts and primary flakes, which imply that the raw material was transported over long distances.

Overall, the use of manuports appears to be a prevalent phenomenon in the LSV. The Middle Palaeolithic assemblages show predominantly single reduction strategies – flake reduction sequence including prepared cores, Levallois cores, other flake cores, and blade reduction sequence. The centripetal prepared cores were prominent at the sites along with the Levallois core; other cores, such as multi-platform and discoid, were also present, and most tools were scrapers of various types, along with points.

In general, porcellanite was a clear preference for artefact production; other materials such as chert (small nodules), quartz, chalcedony, and agate were also present in the Son River gravel and used in subsequent technologies, i.e. laminar, porcellanite remained preferred for the Late Acheulean and Middle Palaeolithic.

6.3 Context and Behavioural Significance of Mixed technologies

In the valley, it is essential to note that most Middle Palaeolithic sites show a notable presence of blade elements, whether it is the presence of blade cores or blades in general. However, the blade quantity was generally much smaller (<5-10 artefacts) than the sites dominated by laminar technology. Further research is required to confirm the status of these sites: whether these sites are genuinely transitional or the same localities were occupied at different times by different or the same populations.

However, out of the 61 sites found, 35 show the presence of different technologies or a mix of different technologies. One such example is the site of Kargara which shows prominent evidence of mixed technologies. The site of Kargara shows the presence of prepared core

technology and laminar technology with the production of blades and microblades. The site is located at the foothills on the right bank of the Son River. Artefacts were found on the surface and were also eroding from sediments. The site could have been a prime location, with nearby water sources and presumably the forested area at the time of occupation full of food resources for hominin populations.

6.3.1 Behavioural Significance

Similar to the Middle Palaeolithic sites, these sites with mixed technologies are also located at the foothills, and the distance from the primary raw material source has also increased. As the distance from the primary raw material source increases, the utilisation of other raw materials such as chert, chalcedony and quartz increases. Although there was an increase in the use of other raw materials, the primary raw material remained porcellanite. This suggests a possible long-distance transport of the raw material as the presumably closest raw material source is approximately 34 km away. Although porcellanite might have been transported long distances, other types of raw materials may have been collected from the nearby riverbed of Son. At Kargara, flakes were found in almost double the quantity of cores; the blade cores were in high quantity, indicating the prominent presence of laminar technology. The site also includes microblade cores and microblades, suggesting a marked change in the subsistence strategies as compared to the Middle Palaeolithic sites.

The assemblages with mixed technologies display predominately three reduction strategies: 1) prepared core reduction strategy, 2) blade and microblade core reduction strategy 3) direct use of natural chunks, nodules, pebbles, and cobbles with retouch. Two major blade reduction technologies ranged from direct percussion of larger cores resulting in thick and broad laminar elements to the potential use of pressure flaking to produce microblades. Crested ridge formation and core rejuvenation were also observed at the site. The utilisation of

quartzite is also unique to the site; a quartzite angular clast has been utilised for producing flakes. The site has also yielded an anvil, suggesting the use of the bipolar technique to open up cores or possibly carry out other percussion activities.

6.4 Context and Behavioural Significance of Microlithic technology

In contrast, there are different debates about the presence of microlithic technology in the region, whether they developed indigenously in the subcontinent or were introduced with the arrival of modern humans in the subcontinent. Irrespective of that, the definition of Indian microlithic technology is somewhat ambiguous, sometimes mixed with Mesolithic and sometimes labelled as *'Late Palaeolithic'*. The Microlithic sites have been located almost in all terrains in the study area. However, out of the 61 sites, 28 sites show the presence of microlithic elements, and some show a mix of blade and microblade elements. Out of the seven analysed sites, three sites, namely Kone, Parva Chinguri and Newari show the dominance of laminar microlithic technology and Newari and Parva Chinguri also show the presence of a single prepared core each.

6.4.1 Behavioural Significance

There was a significant population increase and landscape utilisation expansion during the microlithic period. There was a clear-cut increase in raw material utilisation, as microlith producing populations also added chert, chalcedony, agate, limestone and quartz exploitation to their tool-kits, while Middle the Palaeolithic populations were confined to the use of porcellanite.

Parva Chinguri is located on the Kaimur Plateau (with an elevation of 300 – 600 MSL) and is far from the closest visual raw material (porcellanite) source, ~ 50 km. The site preserves blade and microblade core types and their products in large quantities, and a single prepared

core was also observed. Despite the site's distance from the raw material outcrop, porcellanite was extensively utilised. It shows that hominin populations transported raw material from long distances and were familiar with the geology and rock formations of the valley. In addition, other raw materials such as chert, quartz, limestone, and quartzite were also exploited at the site. The use of limestone is unique to the site; despite its abundance in the valley, it was hardly used for artefact production. Other raw materials used at the site were probably collected from the riverbed of the Son. However, for collecting those raw materials, one has to go 300-600 meters down from the top of the plateau and into the valley.

The Newari site is unique as it represents the minimal use of porcellanite (n = 3) and a dominant use of chert. It is assumed that the raw material at the site was collected from the riverbed of Son in prehistoric times. As the site shows a predominant microblade reduction sequence, it is assumed that the site might have been the youngest of the analysed sites of the study area, and it might have been used for specific subsistence strategies different from the later Palaeolithic sites. Interestingly, the smallest microlithic core was only ~1 cm long and was made on quartz.

The Kone site is only 4 km from the presumed raw material source and is mainly dominated by microlithic technology. However, no prepared cores were found at the site despite its proximity to raw materials and at roughly the same distance from Bagia (Middle Palaeolithic site). However, the predominance of porcellanite continued at the site. The site is on the sandstone bedrock near the main road, and the villagers herd their animals in this area. Hence, most of the artefacts, especially the microblades, were broken. The blade cores and microblade cores were made predominantly on porcellanite, possibly because of the proximity of the source. At the same time, other raw materials, such as chert, quartz, and chalcedony, were used at the site but in less quantity than porcellanite. The blade cores were

exclusively made on porcellanite, while chert and chalcedony were also utilised for microblade cores. The possible reduced use of other raw materials was due to the large distances of raw material sources; for example, in the nearby Panda River, no quartz, chalcedony or chert pebbles were observed. Therefore, it can be safely assumed that these raw materials were collected from the riverbed of Son, which is a minimum of 8-10 km north of the site, and one has to cross the porcellanite outcrop to reach there.

6.5 Understanding the Transitions

What is a transition? It is a brief period of change from one steady state to another. The transitions in prehistory, especially in the Indian subcontinent, are highly misunderstood. The Indian subcontinent has diverse and overlapping Palaeolithic records starting at least from 1.5 Ma onwards (Pappu et al., 2011). These overlaps include Middle Palaeolithic ranging from 385 to 38 kyr (Akhilesh et al., 2018; Blinkhorn et al., 2019; Blinkhorn et al., 2013; Clarkson et al., 2020; Groucutt and Blinkhorn, 2013; Petraglia et al., 2007); the youngest Late Acheulean overlapping and extending up to 140–120 kyr in the Middle Son Valley (Haslam et al., 2011) and 85 kyr in Rajasthan (Blikhorn et al., 2021). Again, the overlap continues with the oldest Upper Palaeolithic (Site 55 in Pakistan) and microlithic phases dating to 48–45 kyr (Clarkson et al., 2020; Dennell et al., 1992; Mishra et al., 2013; Wedage et al., 2019). Thus, these overlaps need to be considered in order to better understand the spatial and temporal variability stemming from hominin behavioural adaptations during this period.

6.5.1 Late Acheulean to Middle Palaeolithic

The transition from Late Acheulean to Middle Palaeolithic is not straightforward. The use of cultural markers such as the presence of bifaces has been alternatively used to define the assemblage as exclusive Late Acheulean (Haslam et al., 2011; Shipton et al., 2013) and

Middle Palaeolithic (Akhilesh et al., 2018 and references therein). This lack of a clear definition in the subcontinent is highlighted by Pardiwalla and Chauhan (in press), that suggests up to 19 previously identified sites with both bifaces and Levallois/prepared core that are considered Late Acheulean and a minimum of 14 sites with almost identical compositions were classified as Middle Palaeolithic. The principal features distinguishing such sites from the preceding Acheulean include the gradual/abrupt discontinuance of LCTs, a drastic reduction in biface frequency, a preference for smaller bifaces, and coexistence with Levallois reduction strategies aiming for small flake production. A distinction has been made between Middle Palaeolithic sites with high and low biface frequencies and based on the proportion of Levallois artefacts (Jayaswal, 1978). Several assemblages spanning the transition to Middle Palaeolithic have been identified in various regions of the Indian subcontinent. For instance, in Gujarat, the Orsang Valley has such assemblages (Ajitprasad, 2005), and the Kaladgi and Hunsgi basins in Karnataka show similar findings (Paddayya, 1982; Petraglia et al., 2003). The Renigunta region in Andhra Pradesh (Murty 1966) and the Dang-Deokhuri valleys in Nepal (Corvinus, 2002) have also produced such assemblages.

A similar pattern was observed at Middle Palaeolithic sites in the Luni basin (Misra, 1968), at Katoati (Blinkhorn et al., 2013), Bhimbetka (Misra, 1985), and in the Sukhi Valley (Ajithprasad, 2005). These sites display handaxes, cleavers, or both, indicating the use of bifacial technology during the Middle Palaeolithic period. In the Middle Son Valley, at the site of Patpara, Blumenschine et al. (1983) classified the assemblage as Middle Palaeolithic based on various assemblage characteristics, including low biface counts, while the same assemblage was interpreted as Late Acheulean because of the presence of bifaces (Shipton et al., 2013).

The present scenario regarding the transition from Late Acheulean to Middle Palaeolithic in the Indian subcontinent is characterised by different schools of thought. A possible transitional phase is the presence of bifaces (including diminutive), and Levallois together can be considered. However, due to the lack of absolute dates for the known stratified sites and the difficulty in classifying surface assemblages, it is challenging to make conclusive statements about this transition.

Therefore, to better understand this transition, more excavations and the collection of technological and chronological data from different parts of the Subcontinent are necessary. While some possible transitional assemblages have been identified, a more comprehensive understanding of the transition from Late Acheulean to Middle Palaeolithic in the Indian subcontinent requires further research and investigation.

6.5.2 Middle Palaeolithic to Upper Palaeolithic or microlithic? (Late Palaeolithic)

As mentioned above, the Indian subcontinent presents a challenge in understanding technological development due to spatial and temporal overlaps of different technologies. This includes the labelling of Upper Palaeolithic and microlithic assemblages together under the "*Late Palaeolithic*" term, the direct development of microliths from Middle Palaeolithic because of climatic deterioration, and the absence of direct in-situ development of microliths in India, with dispersal from Africa instead.

Furthermore, sites with bone tools, engraved ostrich eggshells, and stratigraphic change from the Middle to late Upper Palaeolithic sequence complicate matters, making it challenging to comprehend what is happening at a site or a regional level.

The sites classified as Upper Palaeolithic are present in India; these Upper Palaeolithic assemblages may be confined to specific locations because of the vast and diverse ecological

landscapes and the limited presence of suitable silicious raw materials such as chert, chalcedony, quartz and agate as suggested by Chauhan (2009).

Most of the Indian landscape is abundant in quartzite, so many Lower (1560) to Middle Palaeolithic (750) sites are reported in India. We have a minimum of 530 Upper Palaeolithic/Late Palaeolithic sites. Even out of these 530 sites, all are not exclusively Upper Palaeolithic but include microlithic assemblages (Chauhan, 2020).

It is widely accepted that population growth and dispersals increased during the Late Pleistocene (Atkinson et al., 2008; Petraglia et al., 2009; Timmermann and Friedrich, 2016). Hence, the low number of Upper Palaeolithic/Late Palaeolithic sites might hint at a lack of suitable raw material or its confinement in specific regions. Simultaneously we may have a small population continuing to produce late Middle Palaeolithic artefacts in pockets which could explain the later survival of the Middle Palaeolithic in the subcontinent.

Three categories comprise the Indian Upper Palaeolithic 1) flake-blade assemblages, 2) blade-tool assemblages, and 3) blade-burin assemblages.

1) Flake-blade assemblages comprise relatively broad blades that hint at an early stage of blade tool technology. Along with points and borers made on flakes and flake blades, scrapers constitute most of the assemblage. These assemblages were identified in Bihar and Jharkhand; Singhbhum and other site complexes in Jharkhand are the best representatives of this category (*India Archaeological Review* 1965-66; Ghosh, 1970). The average blade length here is over 4 cm (Ghosh, 1970). It was also suggested that flake-blade assemblages succeeded the flake-based Middle Palaeolithic assemblages.

2) Blade-tool assemblages comprise large to small blades, backed blades, scraper, points, awls, and burin on flakes and flake blades. These assemblages were found in different parts

of India, including Madhya Pradesh, Maharashtra, Karnataka, Andhra Pradesh, Rajasthan, and Uttar Pradesh, as possibly other regions. The average size of the blades and blade tools in the assemblages is greater than 4 cm (Murthy and Reddy, 1975).

3) Blade-Burin industries are distinguished by the prevalence of blades, backed blades and burin elements, even though tools on flakes and flake blades are also included in the assemblages. This group is best represented by Reningunta, where the blade elements range in size from 21 to 105 mm and have an average length of more than 40 mm. These are notably distinct from microlithic assemblages. Upper Palaeolithic and microlithic/Mesolithic are based on laminar/fluted core technology, one of the most significant parallels between the two; the major difference between the two industries is the size of their respective artefacts (Murthy, 1979).

Currently, scholars working in India mainly consider the term Late Palaeolithic (especially in some specific regions like Rajasthan) (Blinkhorn, 2018; Chatterjee et al., 2017; James and Petraglia, 2005). However, as microliths date to 48 kyr now from multiple sites, it is suggested by the author to use the term Upper Palaeolithic and microlithic separately. Although the Upper Palaeolithic is not well-dated or recognised, the presence of the Upper Palaeolithic is reported from associated sites and lithic assemblages from various parts of the Subcontinent (Sankalia, 1974). The richest and best-known sites and site complexes include the Son Valley, the Bhimbetka rock shelters in Madhya Pradesh, Kurnool caves in Andhra Pradesh, the Belan Valley sites in Uttar Pradesh, the Singhbhum region of Bihar, Patne in Maharashtra, Visadi in Gujarat, the Budha Pushkar region in Rajasthan, the Rohri Hills in Pakistan, the Chota Nagpur region in Bihar, the Sanghao rock shelter and Site 55 also in Pakistan (see Chauhan, 2009; Murthy, 1979).

Furthermore, as described above, with different scenarios and a current understanding of the transitional assemblages, the study area provides a great scope of understanding of the topic. The currently suggested multicultural site of Doma shows the presence of bifaces and large flakes, but subsequently, from a different unit (Unit III) than the prepared core and blade elements. Further study at the site might produce a potential understanding of the Late Acheulean to Middle Palaeolithic transition. Furthermore, we have ample evidence of prepared core (Middle Palaeolithic) and laminar technologies (Upper Palaeolithic with large blades and microliths with small blades and flakes) in the valley. As observed in Chapter four, blade size constantly decreased from Middle Palaeolithic to microlithic assemblages. Hence, the study area has excellent potential for transitional studies from Late Acheulean to microlithic.

6.6 The LSV and South Asian parallels, distinctive characteristics, and shortfalls

The LSV assemblages present a broad congruence with other Palaeolithic and microlithic assemblages[10] of South Asia, along with some unique features and shortfalls.

6.6.1 South Asian parallels

6.6.1.1 Late Acheulean

The Late Acheulean assemblage of the LSV, represented by Doma, has yielded three bifaces (handaxes) and large flakes. Similar Late Acheulean assemblages were observed in other

[10] It is important to note that the terms "microblade" and "microlith" are relative and refer to the size of artefacts. In South Asia, these artefacts are sometimes also referred to as "Late Palaeolithic," and definitions can vary widely in the literature depending on the region and the individual researcher. Furthermore, these terms are often used interchangeably in literature.
One more challenge is that complete data, such as detailed artefact measurements, is not always provided. This can sometimes hinder comparisons between different sites and artefacts.

parts of the subcontinent. The Late Acheulean assemblages in the Middle Son Valley, Madhya Pradesh, represented by Patpara (26 bifaces), form only 1% of the total assemblage (*n*= 2284) and Bamburi (*n*= 2, bifaces), comprising only 4% of the complete assemblage (*n*= 47) (Shipton et al., 2013).

The nearest recognised, well-known Late Acheulean Palaeolithic site outside Son Valley is Paisra in the Munger District of Bihar. The site has produced mainly Middle Palaeolithic tool types and large numbers of Levallois flakes and cores. There is a dominance of prepared non-Levallois flakes, and due to the presence of handaxes and cleavers, the site was initially classified as Acheulean. The structural remains of post-holes for temporary shelters and several stone alignments of various sizes form significant features of the Acheulean floors at Paisra. On typo-technological grounds, the site at Paisra belongs to an advanced Acheulean stage, possibly covering a period between 100 and 50 ka BP (Pappu, 2001).

The assemblage from Layer 3 at Singi Talav, Rajasthan, dated to 85 kyr, was defined as Late Acheulean, here only (n = 3) handaxes without any cleavers were reported, and these handaxes form only 0.75% of the total assemblage (n = 401) of Layer 3 (Blinkhorn et al., 2021; Gaillard and Rajaguru, 2017; Gaillard et al., 1985).

In the Kaladgi basin of Karnataka, the site of Lakhampur West was assigned to Late Acheulean. The site consists of 1701 artefacts, most of which were flakes (*n*=1593, 93.6%) and 11 handaxes forming 0.7% and three cleavers forming 0.2% of total complete assemblages. These bifaces at the site were highly refined and symmetrical (Petraglia et al., 2003).

In Orsang Valley, Gujarat, different sites: Sadhara (Loc. II and IV), Ucnhet (Loc. I-II), Baskario (Loc. I & III), Pipiya (Loc. I-III) and Dori-Dunger (Loc. II) show the dominance of

Late Acheulean artefacts. These artefacts mainly include handaxes and scrapers, and the handaxes show high refinement and have a mean length of 90 mm (Ajithprasad, 2005b).

The frequency of handaxes from Doma, Lakhampur West and Singi Talav remains the same, showing 0.7% of the respective total assemblage.

6.6.1.2 Middle Palaeolithic

The Middle Palaeolithic assemblages of the LSV can be broadly compared with the different sites in the subcontinent. A few of the examples are follows as:

The Kortallayar Basin sites contain various artefacts such as cores, scrapers, flakes and debitage. Within the sites, Aryathur consists of 13 cores, including Levallois (*n*=3) and flake blade (*n*=2), out of 508 artefacts. At Nambakkam, two cores comprising Levallois (*n*=1) and discoid (*n*=1) were found among 108 total artefacts. Similarly, Neyvclli exhibited one Levallois core (*n*=1) out of 57 total artefacts. Mailapur site produced a total of 163 artefacts, which includes 19 cores containing Levallois (*n*=2), discoid (*n*=5) and flake (*n*=3), flake blade (*n*=1), and exhausted (*n*=6) artefacts. Gunipalayani site consists of 12 cores, which include Levallois (*n*=5), discoid (*n*=1), flake blade (*n*=1), and exhausted (*n*=2) cores out of 200 total artefacts. Placepalayam displays Levallois (*n*=3), discoid (*n*=2) and flake blade (*n*=1) cores out of 200 total artefacts (Pappu, 2000).

The site of Hanumanthunipadu from Andhra Pradesh has a total of 305 artefacts; out of these, 17 were cores, and these cores include multi-platform cores (*n*=6), Levallois (*n*=3) and core fragments (*n*=8). Other artefacts include diminutive handaxes (*n*=2) and, handaxe (*n*=1), scraper (*n*=4). The Levallois cores from this site were relatively similar to those found in the LSV with flat backs (Anil et al., 2022).

Katoati is a site in western Rajasthan; a total of 1519 artefacts have been reported from the site, and out of these, 275 (18.10 %) were cores. These cores include prepared (*n*=28), multi-platform (*n*=73), Single Platform (*n*=154) and bidirectional core (*n*=12) (Blinkhorn, 2012). A similar type of artefacts has also been reported from the LSV.

The Middle Palaeolithic assemblage of Dhaba in Middle Son Valley also shows similarities to the LSV; at Dhaba, artefacts include core such as Levallois (*n*=10), multi-platform (*n*=5), single platform (*n*=1) discoid (*n*=1) (Haslam et al., 2011). Like the specimen from Hanumanthunipadu and the LSV, the prepared cores at Dhaba also show a flat back ventral surface *(Figure 77)*

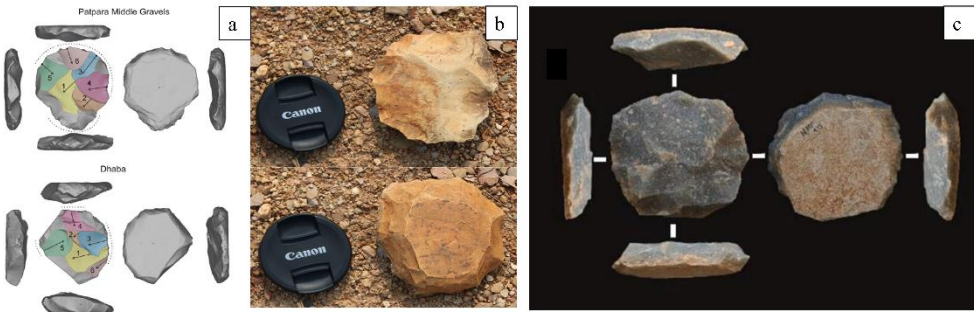

Figure 77. Flatback prepared core from a) Patpara, Dhaba (Haslam et al., 2012); b) the LSV; c) Hanumanthunipadu (Anil et al., 2022).

The site of Jwalapuram Locality 3, Andhra Pradesh, has been famous due to the debate over Middle Palaeolithic assemblages below and above Toba ash. Various artefacts (*n*=108) were found at the site, out of which only 12% were cores, which include Levallois (*n*=1), multi-platform (*n*=11) and single platform (*n*=2) and various scrapers (*n*=19) (Haslam et al., 2010a).

6.6.1.3 Upper Palaeolithic

In comparing the LSV blade assemblages with other well-known blade assemblages in India (as shown in *Figure 58* and *Table 32*), the blades found at Doma are closely related to the Acheulean blades discovered at Bhimbetka (Misra, 1982). The Upper Palaeolithic and microlithic blades at Bhimbetka are grouped with Upper Palaeolithic blades found in regions such as the Upper Son Valley, Shorapur Doab, and Bahgor 1 (Ahmad, 1984; Kenoyer et al., 1983; Paddayya 1968).

Interestingly, the Middle Palaeolithic blades at Bhimbetka are closely related to the Kone and Khempur blades of the LSV. The Vedullcheru group, Kargara, Newari, and Parva Chinguri blades are also clustered together (Murthy, 1968; 1970).

These findings suggest that the blade assemblages found in the LSV share similarities with other well-known blade assemblages in India. Overall, this provides valuable insights into the blade technologies of different regions in India and their evolutionary trajectories.

Table 32. Well-known blade assemblages in India with blades from the LSV.

Sites	**Length (mm)**	**Width (mm)**
Doma blade (LSV)	77.4	30.3
Bhimbetka (Acheulean)	77	32
Bhimbetka (Microlithic)	65	24
Upper Son Valley (Upper Palaeolithic)	64.5	25
Bhimbetka (Upper Palaeolithic)	62	26
Bhimbetka (Middle Palaeolithic)	50	27
Khempur blade (LSV)	49	19.5
Kone blade (LSV)	47.3	16.8
Vedullcheru group (Upper Palaeolithic)	42	19.3
Kargara blade (LSV)	41.3	13.8
Parva Chinguri blade (LSV)	39.8	15.2
Newari blade (LSV)	39.3	16.1

6.6.1.4 Microlithic

The microlithic assemblages in the LSV display similar features to those in other prominent microlithic sites across the Indian subcontinent. For instance, the Mehtakheri site in Madhya Pradesh has yielded a total of 901 artefacts, including 50 microblades, 12 microblade cores, and 634 flakes (Mishra et al., 2013). At the Bhalugarh site in Odisha, out of a total of 1518 artefacts, cores comprise 27%, flakes 51%, blades only 2% of the assemblage, and bladelets are 4%, some of which were backed tools (Menedaly and Hussain, 2015). The average size of these bladelets is approximately 22 mm, similar to the microblades found in the LSV. Another site in the Middle Ong Basin, Odisha, out of a total of 6302 artefacts, cores comprise (*n*=1159, 14.02%), flake number (*n*=3621, 43.81%), while blade and bladelets represent 8.90% (*n*= 736) and 8.23% (*n*=680) of the total assemblage respectively (Barik and Sabale, 2021).

Other well-known microlithic sites such as Jwalapuram (Andhra Pradesh, India), Batadombalena (Sri Lanka), Budha Pushkar (Rajasthan, India), Mahadebbera (West Bengal, India) also contain important artefacts such as microblades and microblade cores (Basak et al., 2014; Blinkhorn, 2018; Clarkson et al., 2009; Clarkson et al., 2017; Perera et al., 2011; Mishra et al., 2013), which were also observed in the LSV.

6.6.2 Unique features and shortfalls

The unique characteristic of the LSV lithic assemblages is the high frequency of blades, which have been discovered at multiple sites throughout India. However, the blades found at Doma in the LSV have an average length of ~ 77mm and were morphometrically similar to those discovered at Bhimbetka from the Acheulean layer. Additionally, Upper Palaeolithic laminar elements have been observed in 73% of the sites within the LSV. Porcellanite is not only present but is the primary raw material that persists from Late Acheulean to microlithic

assemblages. This highlights the versatile nature of porcellanite that allowed the hominins to exploit it for a more extended period. This puts into perspective the hypothesis that Upper Palaeolithic assemblages were limited to specific geographical locations and made from crypto-crystalline materials (in the case of the LSV, porcellanite acted as a suitable substitute for producing laminar element otherwise made on crypto-crystalline materials).

Another characteristic of the LSV is the presence of fossils with the lithic assemblages. The fossils were associated with the prepared core and laminar elements at the Doma site (Mehra, 2022) and with laminar elements at Parva Chinguri *(Figure 78*). The multiproxy approaches (e.g., stable isotope, dating) at these sites will further highlight the hominin landscape and environment interactions. Palaeoenvironmental conditions at Doma suggests humid climatic condition (see section 6.7.1); developing the same for the microlithic site of Parva Chinguri would be interesting to further add to our technology and understanding human-environment interaction.

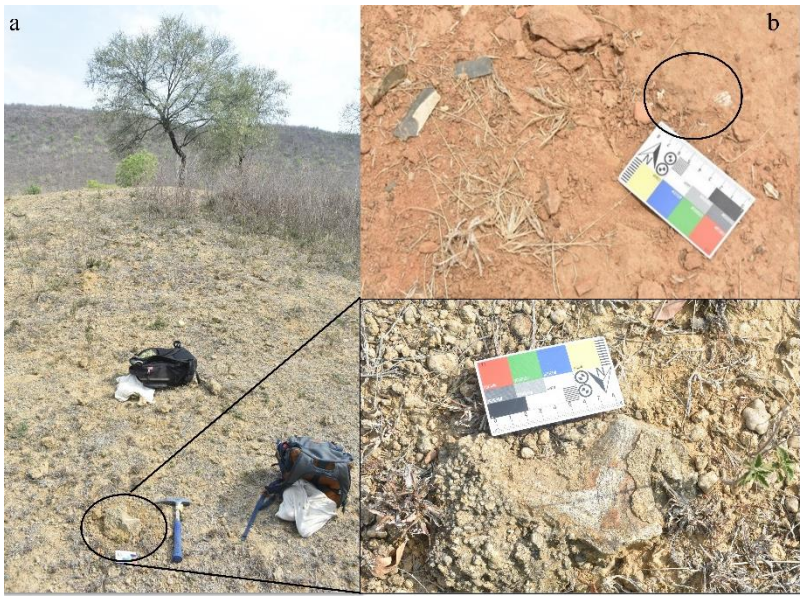

Figure 78. a) Fossilised antler at Doma; b) fossilised teeth (in black circle) with laminar elements at Parva Chinguri.

The LSV lacks Early Acheulean and has a low representation of Late Acheulean. This could be attributed to the absence of suitable raw materials, such as quartzite, which is required for producing large flake Acheulean. Previous studies have shown that Early Acheulean or Lower Palaeolithic sites in India are primarily made on coarse grain material (especially quartzite) (e.g., Blinkhorn et al., 2021; Cornivus, 2001; Gaillard et al., 1985; Misra, 1985; Pappu et al., 2011; Singh and Katiyar, 2022), with few exceptions, such as Hunsgi, where limestone was utilised (Paddayya, 2001). Even in the nearby Middle Son Valley, Late Acheulean handaxes were made using quartzite and limestone (Haslam et al., 2011). Therefore, the lack of quartzite could be a possible reason for the absence of Early Acheulean in the LSV.

Another possible explanation for the absence of Early Acheulean could be sedimentation, as the Late Acheulean handaxes discovered at Doma were buried beneath colluvium and Quaternary sediments and were only unearthed due to anthropogenic activities. Overall, the Son Valley lithic assemblages present a unique combination of lithic elements, indicating the prevalence of blades and the absence of Early Acheulean, which could be attributed to the lack of suitable raw materials or sedimentation.

6.7 Hominins and environments

Due to the unavailability of absolute dating from the faunal sites under investigation, a broad correlation methodology was employed, using stratigraphy and archaeology to estimate their temporal contexts. On a broader level, we can bracket the various sites under study into the following *(Table 33).*

6.7.1 The LSV, Sonbhadra, Uttar Pradesh

In the LSV, Doma has yielded Late Acheulean, Middle Palaeolithic and Upper Palaeolithic artefacts along with vertebrate fossils. The Middle Palaeolithic[11] and Upper Palaeolithic artefacts were stratigraphically in the same layer as vertebrate fossils. Based on morphology and technology, these Middle Palaeolithic artefacts can be compared to those found in Middle Son Valley dated to 80-60 kyr *(Figure 77).* Geological trench sediments at Kargara provide dates between ~57-18 kyr. Overall, correlations suggest that the fossils recovered from Doma can be attributed to the period of 80-60 kyr, and dates of the LSV can be tentatively bracketed to at least 80-18 kyr. During this time, Middle Palaeolithic, Upper Palaeolithic and microlithic assemblages were dominant (Basak and Srivastava, 2017; Blinkhorn, 2013; Blinkhorn et al., 2019; Clarkson et al., 2020; Dennell et al., 1992; Mellars et al., 2013; Mishra et al., 2013; Perera et al., 2011; Petraglia, 2007).

The faunal palaeoenvironmental reconstruction from the LSV suggests that mostly C_4 vegetation was present in the region with humid/wetter climatic conditions. Similar conditions were observed in the compiled data of the subcontinent (Achyuthan et al., 2007; 2019; Alam et al., 1997; Allu et al., 2015; Bolton et al., 2013; Caley et al., 2011; Jain et al., 2005; Juyal et al., 2000, 2006; Kathayat et al., 2016; Prabhu et al., 2004; (select references in Sinha et al., 2020); Thokchom et al., 2017) and at the Palaeolithic sites of Sandhav (Blinkhorn et al., 2019), 16R (Achyuthan et al., 2007), Katoati (Blinkhorn et al., 2017), and Singi Talav (Blinkhorn et al., 2021). The climatic conditions in the LSV at Kargara have been observed to be humid from 57-43 kyr, similar to those observed by (Andrews et al., 1998;

[11] The Middle Palaeolithic in India has a broad age range of 385-38 ka, in the Middle Son Valley it is dated to 80-60 kyr, and microliths start at 48 ka. As Patpara, Dhaba and Doma sites are found along the Son River and with almost similar raw material, it is possible that Middle-Upper Palaeolithic artefacts at Doma may range from 80 – 48 kyr, but we cannot deny the lack of an absolute date for the site; it can be older or younger as well.

Bhandari et al., 2009; Blinkhorn et al., 2017; Bolton et al., 2013; Bronger et al., 1987; Caley et al., 2011; Farooqui et al., 2010; Jain et al., 2005; Juyal et al., 2000; Juyal et al., 2000; 2006; Kar et al., 2001; Kathayat et al., 2016; Pal et al., 2005; Prabhu et al., 2004; Singh, 2005; Srivastava et al., 2001). A dry spell around 50 kyr (Bhattacharyya, 1983; Singh, 2005) (from geochemical and Grain-size analysis) may have influenced the emergence of microlithic technology, but more research is required to confirm this. The environment from 43 – 20 ka is marked by low precipitation; similar conditions were observed from compiled data (Trivedi et al., 2012). From 20 kyr onwards, climatic conditions ameliorated, suggesting the impact of LGM in the region.

6.7.2 Nehlai, Sehore, Madhya Pradesh

The lithic assemblage is provisionally interpreted to be of Late Pleistocene age based on regional stratigraphic correlation, association with the Baneta Formation and general condition of the associated faunal specimens. It has been classified as core-and-flake technology (Pers. Comm. with Dr. Vivek Singh). The fossils and tools were discovered in the same geological trench, but no cut marks were discovered. According to Singh (2022), the site belongs to the Baneta Formation and dates to 84 - 8 kyr. This corresponds to our compiled climatic data, which indicates 125-80 kyr as a generally humid phase. The fauna here is adapted to C_3 /C_4 mix diets with a preference for C_3, with comparable semi-humid climatic conditions to the Narsinghpur region (discussed below). This inference is consistent with our compiled data, where we have mixed climate interpretations from 79-70 kyr and semi-arid conditions (Jha et al., 2020; Reddy et al., 2013). This is also supported by the Middle Palaeolithic site of Jwalapuram and Belan Valley, where similar C_3/C_4 vegetation was observed before ~74 kyr (Toba supereruption), followed by a shift to C_4 vegetation around and after 74 kyr (Haslam et al., 2010a; Jha et al., 2020; Williams et al., 2009). This is seen in

the Narsinghpur region, which is dominated by Middle and Upper Palaeolithic assemblages (Badam 1979; Lal et al., 2023; Patnaik 1995) as well as arid climatic conditions from 69-60 kyr (Bolton et al., 2013; Caley et al., 2011; Kathayat et al., 2016; Prabhu et al., 2004; Singh 2005) as seen from the isotope data presented in this thesis.

6.7.3 Different localities in Narsinghpur, Madhya Pradesh

Most of these fossils from the Narsinghpur region can be provisionally attributed to the Hirdepur and Baneta Formations, and they are generally associated with Middle Palaeolithic assemblages without any bifaces[12] (Badam, 1998; Lal et al., 2023; Patnaik, 1995). A bone collagen test on these fossils revealed no retrievable bone collagen, indicating that they are older than 50 kyr[13]. Therefore, the Narsinghpur region can be bracketed between 74 to 30 kyr on broad geoarchaeological understanding (Kotlia and Joshi, 2011; IAR 1985-86, p. 53, Tewari and Bhai 1997).

Broadly, the fauna from the Nasinghpur region shows a C_4 diet with mostly grassland type environments with drier conditions. Similar conditions were also observed in bovids from elsewhere in the Narmada Valley (Sandhu et al., 2021; Kalwanker, 2013) during the Late Pleistocene. These values are similar to those of the hippo from Baneta in the Sehore District of Madhya Pradesh and the cervid from Pratappur in the Mayurbhanj District of Odisha; however, these were dated to 16,467–15,660 cal BP and 17,875 cal BP, respectively.

[12] The absence of bifaces does not necessarily reflect age, but such assemblages are generally younger than 100 ka.

[13] Some of the fossils were tested for the radiocarbon dating but due to the lack of bone collagen in the fossil, dates were not obtained suggesting that the fossils are older than 50 kyr (Pers. Comm. with Prof. Rajeev Patnaik)

6.7.4 Gopnath, Bhavnagar, Gujarat

The site of Gopnath is stratigraphically dated to 57 kyr (Costa, 2017), but another geological date suggests it is dated to 156 kyr (Sharma et al., 2017). The climatic data from Gopnath suggested C_3/C_4 vegetation with humid climatic conditions before the Late Pleistocene, which is also observed at Singi Talav (~177 ka) but with a predominance of C_4 vegetation (Blinkhorn et al., 2021).

6.7.5 Pilikarar (Sehore), Talayaghat and Devakachar (Narsinghpur), Madhya Pradesh

Specifically, the stable isotope values obtained from the Baneta formation on Pilikarar site indicate a period with C_3 vegetation at a depth of 250-150 cm, despite the overall prevalence of C_4 vegetation. This correlation suggests that this phase could potentially be dated to 79-70 kyr, as similar findings have been observed in faunal (specially from Nehlai which is in the same district) and compiled data from various studies in the subcontinent (Haslam et al., 2010a; Jha et al., 2020; Williams et al., 2009).

At Talayaghat, a similar situation to Nahlai and Pilikarar is observed, where the transition from a C_3/C_4 mixed vegetation to predominantly C_4 vegetation occurred around and after 74 kyr. In the Devakachar area, Middle Palaeolithic artefacts and fossils were discovered at a depth of 17-18 meters. The stable isotope values indicate a mixture of C_3/C_4 vegetation at these levels, with a predominance of C_4 vegetation during humid climates.

Overall, the data derived from carbonate nodules collected from Pilikarar, Talayaghat, and Devakachar suggest a combination of C_3 and C_4 vegetation, with prevalence of C_4 vegetation. The climate also exhibits a mixed nature, with a tendency towards humid environments. These are preliminary comparisons, and a complete correlation can only be established once absolute dates, currently in the process, are available.

Table 33. Late Pleistocene climatic interpretations from compiled and new data.

Age	Compiled data	LSV	Narsinghpur Region	Nehlai
10-20 ka	Arid	Humid		Humid
20-30 ka	Mixed	Arid		Humid
30-40 ka	Humid	Arid	Arid	Humid
40-50ka	Humid	Humid	Arid	Humid
50-60 ka	Humid	Humid (Arid before 50 ka?)	Arid	Humid
60-70 ka	Arid	Humid	Arid	Humid
70-80 ka	Mixed	Humid	Arid	Humid
80-90 ka	Humid	Humid		Humid
90-100 ka	Humid			
100-110 ka	Humid			
110-120 ka	Humid			
120- 130ka	Humid			

6.7.6 Discussion

Understanding how *H. sapiens* spread from Africa to the rest of the world is one of the most contentious topics in human evolution (Bae et al., 2017; Groucutt et al., 2015a; Mellars et al., 2013). Several disciplines have conducted extensive research on the dispersal of *Homo sapiens* from Africa with two prominent hypotheses: 1) that a single successful dispersal occurred 60-50 kyr with microlithic technologies (Mellars, 2006; Mellars et al., 2013), and 2) that multiple dispersals occurred, beginning much earlier during MIS 5, as evidenced by the spread of Middle Palaeolithic technology (Armitage et al., 2011; Blinkhorn and Petraglia, 2014; Boivin et al., 2013; Dennell and Petraglia, 2012; Groucutt and Blinkhorn, 2013; Groucutt and Petraglia, 2014; Petraglia, 2007; Petraglia et al., 2010).

Research into Late Pleistocene human dispersals over the last two decades has put a question on modern arid environments like those encountered in the Arabian Peninsula and the Thar

Desert of northwestern India, and high-altitude regions, as being barriers for population movements (Blinkhorn et al., 2013; Boivin et al., 2013; Breeze et al., 2016; Gamble et al., 2004; Groucutt et al., 2015; Mellars et al., 2006; Stewart et al., 2012). The appearance of periodic pathways has been confirmed by palaeoclimatic and terrain modelling research, while new archaeological research has revealed significant hominin presence in the past (Blinkhorn et al., 2013; Boivin et al., 2013; Breeze et al., 2016; Field et al., 2007; Gamble et al., 2004; Stewart et al., 2012). Furthermore, compared to other hominins, our species demonstrate distinct adaptive plasticity in changing habitats and climates (Groove, 2015; Roberts and Steward, 2018; Roberts et al., 2016).

Overall, it is evident that human dispersals were favoured during humid climate conditions, whether during MIS 5 or 3. The Middle Palaeolithic technologies were prevalent during the Late Pleistocene before the emergence of microliths around 70 kyr in Africa and 48 kyr in South Asia. The end of the Acheulean is also an important feature of the Late Pleistocene, probably lasting up to 29 kyr based on computer modelling (Keys et al., 2021). Moreover, Africa's Middle Palaeolithic (or Middle Stone Age) continued till the Holocene (Scerri et al., 2021).

Also, South Asia presents one of the earliest occurrences of the Middle Palaeolithic (Akhilesh et al., 2018; Anil et al., 2022) and the youngest Late Acheulean (Blinkhorn et al., 2021; Haslam et al., 2011) in the world. Overall, humid conditions have favoured the spread of Palaeolithic technologies globally, and South Asia is no exception. However, due to the lack of hominin fossils and the overlap of different technologies during the Late Pleistocene in South Asia, it is hard to pinpoint the impact of the environment on specific technological adaptation or dispersal (e.g., as the origin of microlithic technology in Africa at Pinnacle Point (71 kyr) is associated with climate change (Brown et al., 2012; Wilkins et al., 2017) and

at Howiesons Poort (65-60 kyr) it was not (Guerin et al., 2013; Roberts et al., 2016; Tribolo et al., 2009)).

The South Asian climate may have facilitated technological and species dispersals and adaptation within or into South Asia, as the climates were generally humid during the Late Pleistocene, with exceptions from 69-60 kyr and 19-10 kyr. Based on comparisons between compiled climatic reconstructions, palaeoclimatic data generated in the thesis and archaeological data, it can be concluded that Late Pleistocene environments did not cause any significant changes in technological turnover with Middle Palaeolithic technology persisting throughout most of the period *(Figure 79).*

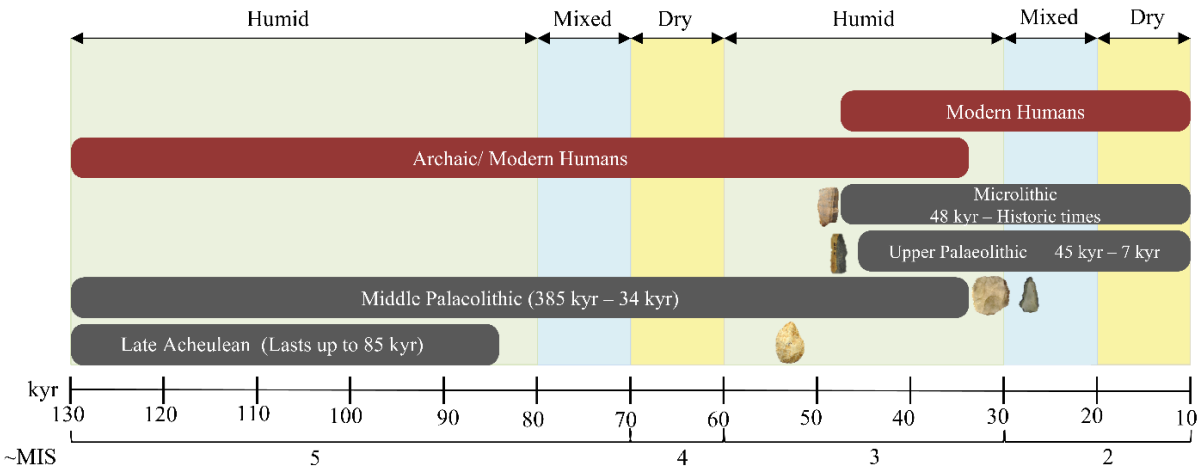

Figure 79. Late Pleistocene technological and human evolution dynamics in the Indian subcontinent.

Additionally, important climatic events impacted overall vegetation, such as the Toba supereruption after ~74 kyr, but technology remained constant. Similarly, the climate became more arid during the Last Glacial Maximum, but microlithic technologies remained constant.

Regardless of the overall consistency of technology, independent innovation or adaptation at the site level is always possible.

6.8 Concluding remarks, limitations, and future directions

This section summarises research objectives and their outcome, study limitations, future direction, and suggestions for scholars working on similar topics.

6.8.1 Research objectives and outcome summary

a} To conduct surveys to locate new Palaeolithic and microlithic sites in the LSV, Sonbhadra District, Uttar Pradesh, b} To collect sediment samples from a geological excavation to characterise the stratigraphy and palaeoenvironment of the study area.

- Landscape-level comparison between Late Acheulean to microlithic sites from the LSV (raw material variability and selection, regional adaptations, site formation differences, lithic typo-technology)
- Optical Luminescence (OSL) dating of a part of the LSV to understand the chronology and link the paleoenvironmental data with lithic occurrences

The surveys in the LSV have yielded 61 new sites, which belong to Late Acheulean to microlithic period. The Late Acheulean and Middle Palaeolithic sites were found mainly in the south of the Son, while Upper Palaeolithic and microlithic sites were found across the region. Porcellanite is the primary raw material utilised in the study area from the Late Acheulean to Upper Palaeolithic period, while the inclusion of more silicious raw materials like chert, chalcedony, agate was observed in microlithic assemblages.

The sediment depositional history of the LSV goes back to at least 57 kyr; the period from 57 – 43 kyr suggests mostly humid climatic conditions, with a possible drier spell at 55 kyr. The

period from 43-20 kyr suggests reduced precipitation and 20-18 kyr seeing an amelioration in climatic conditions.

2) Compile published sources for the Late Pleistocene palaeoenvironmental reconstruction of South Asia.

According to the compilation, the Late Pleistocene environmental records show that the period from 125-80 kyr was dominated by humid environments, followed by varied climatic conditions at 79-70 kyr and arid environments at 69-60 kyr. South Asia's environmental conditions were generally humid between 59 and 30 kyr. The period from 29 to 20 (LGM) has yielded mixed results, followed by arid conditions from 19 to 11 kyr.

3) To visit the previously reported Late Pleistocene Palaeolithic and fossil sites or museum/university collections to collect enamel samples of fossil teeth and carbonates to reconstruct Late Pleistocene paleoenvironments.

The faunal palaeoenvironmental reconstruction from the LSV suggests that mostly C_4 vegetation was present in the region with humid/wetter climatic conditions. The fauna at Nehlai is adapted to C_3 /C_4 mix diets with a preference for C_3, with comparable semi-humid climatic conditions. Broadly, the fauna from the Nasinghpur region shows a C_4 diet with mostly grassland type environments with drier conditions. The climatic data from Gopnath suggested C_3/C_4 vegetation with humid climatic conditions before the Late Pleistocene *(Table 34).*

6.8.2 Limitations of the study

The study is limited primarily due to the lack of absolute dating for the analysed sites. This limitation makes it challenging to identify climate changes specific to a particular time and their impact on technology. Additionally, the ages of different technologies in the LSV

remain unclear. A secondary limitation of the study is that only a single proxy has been used to establish palaeoenvironmental reconstruction in north-central India. Although calcrete samples were collected from various sites, data analysis was hindered by the pandemic and inadequate equipment functionality. A critical constraint is the absence of archaeological excavations in the LSV due to a lack of suitable permits from the Archaeological Survey of India for various reasons.

6.8.3 Future directions

This study lays the groundwork for Late Pleistocene paleoenvironmental research in India and serves as a reference for scholars in the field. The author also intends to establish a comprehensive database of Late Pleistocene studies, including archaeological data, in the near future. While many environmental reconstructions for this period have been conducted in the Himalayan zone, the Thar Desert and Ganga plain, along with other regions in central, western, northeastern, and southern India, Sri Lanka and deep-sea cores in the Arabian Sea, have been relatively understudied. It is, therefore, critical to address these geographic gaps through future multidisciplinary research across India, Pakistan, Nepal, Bhutan, Bangladesh, and Sri Lanka. In particular, central, northeastern, and peninsular India offer vast areas for focused attention in problem-oriented research projects.

This study also highlights the lack of environmental reconstructions for Palaeolithic sites in India and suggests that scholars incorporate a multidisciplinary approach to better understand the interactions between hominins and their environment. Chapter 2 identifies a gap in reconstructions for the 125-50 kyr period, emphasising the need for unbiased data collection from understudied regions and periods.

Finally, the thesis's contribution is as follows: 1) it provides first-hand information on Late Pleistocene environmental studies in South Asia. 2) Suggest the use of consistent terminology and addresses significant spatial and temporal gaps in archaeological and palaeoenvironmental studies. 3) A window into the Late Pleistocene environments that suggest general humidity during the period (while calling for more site-specific research). 4) The overall status of Acheulean in the LSV, with the earlier phase completely absent and the only indication of a Late Acheulean without any extensive evidence. 5) Throws light on the distribution of sites from different techno-cultural periods (e.g., Middle and Upper Palaeolithic only restricted to the south of Son) while suggesting a gradual growth in populations in later periods (based on number and distribution of microlithic sites. 6) Shifts in subsistence and economy evidenced by the technological developments in blade technologies (interpreted by the gradual decrease in their size). 7) Overall understanding of prehistoric technological transitions due to overlap and extensive presence of sites from Late Acheulean to microlithic.

In the future, the author aims to produce absolute dates for the lithic assemblages in the LSV. Once this has been accomplished, various approaches can be utilised to understand better the palaeoenvironment and hominin adaptations (e.g., pollen studies, stable isotope analysis, in addition to carbon and oxygen), biomarkers, and taphonomy. In addition, use-wear analysis and experimental archaeology can be utilised to understand hominin adaptations. A more comprehensive understanding of the archaeological site can be achieved by employing various approaches.

Table 34. Prehistoric archaeological sites with palaeoenvironment reconstructions, including sites from this study

Sr. No.	Site	Age	Technology	Palaeoclimate	References
1	16 R, Rajasthan	126-70 kyr	Late Acheulean?/Middle Palaeolithic	C_4 vegetation Wetter climate	Achyuthan et al., 2007; Blinkhorn et al., 2013
2	Sandhav, Gujarat	114 kyr	Middle Palaeolithic	C_4 vegetation with enhanced monsoon	Blinkhorn et al., 2019
3	Katoti, Rajasthan	96-60 kyr	Middle Palaeolithic	Humid environments	Blinkhorn et al., 2017
4	Jwalapuram, Andhra Pradesh	80-38 kyr	Middle Palaeolithic	Mixed C_3/ C_4 environment, Variable rainfall	Haslam et al., 2010a
5	Fa Hien-Lena, Sri Lanka	36 kyr	Microlithic	Wet Climate	Roberts et al., 2017
6	Pratappur, Odisha	17875 Cal BP	Microlithic	C_4 arid environments	Patnaik et al., 2019
7	Doma, LSV, Uttar Pradesh	~ 80 kyr	Middle Palaeolithic	C_4 vegetation with humid environments	This study
8	Nehlai, Madhya Pradesh	~84 to 8 kyr	Core and flake assemblage? Middle Palaeolithic	Mixed C_3/ C_4 vegetation with a dominance towards C_3. Semi-humid climate	Kotlia and Joshi 2011; IAR 1985-86, p. 53, Tewari and Bhai, 1997
9	Different localities in Narsinghpur, Madhya Pradesh	~74 kyr to 30 kyr	Middle Palaeolithic	C_4 vegetation with drier conditions	Kotlia and Joshi 2011; IAR 1985-86, p. 53, Tewari and Bhai, 1997
10	Singi Talav, Rajasthan	177 – 65 kyr	Late Acheulean – Middle Palaeolithic	C_4 vegetation with a warm and humid climate	Blinkhorn et al., 2021

7 References

Achyuthan, H., Quade, J., Roe, L. and Placzek, C., 2007. Stable isotopic composition of pedogenic carbonates from the eastern margin of the Thar Desert, Rajasthan, India. *Quaternary International*, *162*, pp.50-60.

Achyuthan, H., Shankar, N., Braida, M. and Ahmad, S.M., 2012. Geochemistry of calcretes (calcic palaeosols and hardpan), Coimbatore, Southern India: Formation and Paleoenvironment. *Quaternary International*, *265*, pp.155-169.

Adamson, K., Candy, I. and Whitfield, L., 2015, April. High-resolution analysis of Quaternary calcretes: a coupled stable isotope and micromorphological approach. In *EGU General Assembly Conference Abstracts* (p. 12267).

Agrawal, D. P., R.P. Dhir, R.V. Krishnamurthy, V.N. Misra, C. Nanda, and S.N. Rajaguru 1980. Multiple Evidence for Climatic Change in Rajasthan, in *Arid Zone Research and Development* CAZRI, (H.S. Mann Ed.), pp. 1-18. Jodhpur: Scientific Publishers.

Agrawal, D.P. and Kusumgar, S., 1974. On the calibration of C-14 dates. *Puratattva*, *7*, pp.70-73.

Agrawal, D.P., Juyal, N., Sharma, P., Gardner, R. and Rendell, H., 1988. Palaeogeography of the loess deposits of Kashmir. *Proceedings of the Indian National Science Academy, Part A. Physical sciences*, *54*(3), pp.383-389.

Agrawal, S., Sanyal, P., Balakrishnan, S. and Dash, J.K., 2013. Exploring the temporal change in provenance encoded in the late Quaternary deposits of the Ganga Plain. *Sedimentary Geology*, *293*, pp.1-8.

Agrawal, S., Sanyal, P., Bera, M.K., Dash, J.K. and Balakrishnan, S., 2013. Paleoclimatic, paleovegetational and provenance change in the Ganga Plain during the late Quaternary. *Journal of Earth System Science*, *122*(4), pp.1141-1152.

Agrawal, S., Sanyal, P., Sarkar, A., Jaiswal, M.K. and Dutta, K., 2012. Variability of Indian monsoonal rainfall over the past 100 ka and its implication for C3–C4 vegetational change. *Quaternary Research*, *77*(1), pp.159-170.

Ahmad, N., 1984. *The Stone Age Cultures of the Upper Son Valley, Madhya Pradesh* (No. 4). Ramanand Vidya Bhawan.

Aitken, M.J., 1998. Introduction to optical dating: the dating of Quaternary sediments by the use of photon-stimulated luminescence. Clarendon Press.

Ajithprasad, P., 2005. Early middle palaeolithic: a transition phase between the upper acheulian and middle palaeolithic cultures in the Orsang Valley, Gujarat. *Man and Environment*, *30*(2), pp.1-11.

Akhilesh, K., Pappu, S., Rajapara, H.M., Gunnell, Y., Shukla, A.D. and Singhvi, A.K., 2018. Early Middle Palaeolithic culture in India around 385–172 ka reframes Out of Africa models. *Nature*, *554*(7690), pp.97-101.

Alam, M.S., Keppens, E. and Paepe, R., 1997. The use of oxygen and carbon isotope composition of pedogenic carbonates from Pleistocene palaeosols in NW Bangladesh, as palaeoclimatic indicators. *Quaternary Science Reviews*, *16*(2), pp.161-168.

Allu, N.C., M. Tiwari, M.G. Yadava, N.C. Dung, C. Shen, S.P. Belgaonkar, R. Ramesh, and A.H. Laskar 2015. Stalagmite δ18O Variations in Southern India Reveal Divergent Trends of Indian Summer Monsoon and East Asian Summer Monsoon During The Last Interglacial. *Quaternary International* 371: 191-196.

Ambrose, S.H., 1998. Late Pleistocene human population bottlenecks, volcanic winter, and differentiation of modern humans. *Journal of human evolution*, *34*(6), pp.623-651.

Andrefsky, W. and Andrefsky Jr, W., 1998. *Lithics*. Cambridge University Press.

Andrews, J.E., Singhvi, A.K., Kailath, A.J., Kuhn, R., Dennis, P.F., Tandon, S.K. and Dhir, R.P., 1998. Do stable isotope data from calcrete record Late Pleistocene monsoonal climate variation in the Thar Desert of India?. *Quaternary Research*, *50*(3), pp.240-251.

Anil, D., Chauhan, N., Ajithprasad, P., Devi, M., Mahesh, V. and Khan, Z., 2022. An early presence of modern human or convergent evolution? a 247 ka middle palaeolithic assemblage from Andhra Pradesh, India. *Journal of Archaeological Science: Reports*, *45*, p.103565.

Ankit, Y., Mishra, P.K., Mehta, B., Anoop, A., Misra, S. and Jamir, T., 2022. Hydroclimatic variability in Northeast India during the last two millennia: Sedimentological and geochemical record from Shilloi Lake, Nagaland. *Palaeogeography, Palaeoclimatology, Palaeoecology*, *602*, p.111151.

Anoop, A., Prasad, S., Plessen, B., Basavaiah, N., Gaye, B., Naumann, R., Menzel, P., Weise, S. and Brauer, A., 2013. Palaeoenvironmental implications of evaporative gaylussite crystals from Lonar Lake, central India. *Journal of Quaternary Science*, *28*(4), pp.349-359.

Ansari, M.H. and Vink, A., 2007. Vegetation history and palaeoclimate of the past 30 kyr in Pakistan as inferred from the palynology of continental margin sediments off the Indus Delta. *Review of Palaeobotany and Palynology*, *145*(3-4), pp.201-216.

Antón, S.C., 2003. Natural history of Homo erectus. *American Journal of Physical Anthropology: The Official Publication of the American Association of Physical Anthropologists*, *122*(S37), pp.126-170.

Argue, D., Groves, C.P., Lee, M.S. and Jungers, W.L., 2017. The affinities of Homo floresiensis based on phylogenetic analyses of cranial, dental, and postcranial characters. *Journal of human evolution*, *107*, pp.107-133.

Armitage, S.J., Jasim, S.A., Marks, A.E., Parker, A.G., Usik, V.I. and Uerpmann, H.P., 2011. The southern route "out of Africa": evidence for an early expansion of modern humans into Arabia. *Science*, *331*(6016), pp.453-456.

Arnold, L.J., Duval, M., Demuro, M., Spooner, N.A., Santonja, M. and Pérez-González, A., 2016. OSL dating of individual quartz 'supergrains' from the Ancient Middle Palaeolithic site of Cuesta de la Bajada, Spain. *Quaternary Geochronology*, *36*, pp.78-101.

Arsuaga, J.L., Martínez, I., Arnold, L.J., Aranburu, A., Gracia-Téllez, A., Sharp, W.D., Quam, R.M., Falguères, C., Pantoja-Pérez, A., Bischoff, J. and Poza-Rey, E., 2014. Neandertal roots: Cranial and chronological evidence from Sima de los Huesos. *Science*, *344*(6190), pp.1358-1363.

Athreya, S., 2007. Was Homo heidelbergensis in South Asia? A test using the Narmada fossil from central India. *The evolution and history of human populations in South Asia: Inter-disciplinary studies in archaeology, biological anthropology, linguistics and genetics*, pp.137-170.

Athreya, S., 2014. Modern Human Emergence in South Asia. *Emergence and diversity of modern human behavior in Paleolithic Asia*, p.61.

Atkinson, Q.D., Gray, R.D. and Drummond, A.J., 2008. mtDNA variation predicts population size in humans and reveals a major Southern Asian chapter in human prehistory. Molecular biology and evolution, 25(2), pp.468-474.

Aubert, M., Pike, A.W., Stringer, C., Bartsiokas, A., Kinsley, L., Eggins, S., Day, M. and Grün, R., 2012. Confirmation of a late middle Pleistocene age for the Omo Kibish 1 cranium by direct uranium-series dating. *Journal of Human Evolution*, *63*(5), pp.704-710.

Auclair, M., Lamothe, M. and Huot, S., 2003. Measurement of anomalous fading for feldspar IRSL using SAR. *Radiation measurements*, *37*(4-5), pp.487-492.

Auden. 1933. Vindhyan sedimentation in the Son valley, Mirzapur district. *India Geological survey Memoirs,* 62, ii pp, 141-250.

Ayliffe, L.K. and Chivas, A.R., 1990. Oxygen isotope composition of the bone phosphate of Australian kangaroos: potential as a palaeoenvironmental recorder. *Geochimica et Cosmochimica Acta*, *54*(9), pp.2603-2609.

Babeesh, C., Achyuthan, H., Jaiswal, M.K. and Lone, A., 2017. Late Quaternary loess-like paleosols and pedocomplexes, geochemistry, provenance and source area weathering, Manasbal, Kashmir Valley, India. *Geomorphology*, *284*, pp.191-205.

Badam, G. L., 1979a. Quaternary palaeontology of the Central Narmada Valley and its implications in the prehistoric studies. *Geological Survey of India, Miscellaneous Publications*, 45: pp. 311-320.

Badam, G.L. 1984. Pleistocene Faunal Succession of India. *The Evolution of the East Asian Environment Palaeobotany, Palaeogeology and Palaeoanthropology* (WHYTE, R.O. ed. Vol.2), pp. 746–775. University of Hong Kong, Hong Kong.

Badam, G.L., 1988. Quaternary faunal succession of India. *Visesa Prakasana-Bharatiya Bhuvaijñanika Sarveksana*, (11), pp.277-3045.

Badam, G.L., 2002. Quaternary vertebrate paleontology in India: fifty years of research. *Indian Archaeology in Retrospect*, *3*, pp.209-45.

Bae, C.J., Douka, K. and Petraglia, M.D., 2017. On the origin of modern humans: Asian perspectives. *Science*, *358*(6368), p.eaai9067.

Bae, C.J., Wang, W., Zhao, J., Huang, S., Tian, F. and Shen, G., 2014. Modern human teeth from late Pleistocene Luna cave (Guangxi, China). *Quaternary International*, *354*, pp.169-183

Balasse, M. and Ambrose, S.H., 2005. Distinguishing sheep and goats using dental morphology and stable carbon isotopes in C4 grassland environments. *Journal of Archaeological Science*, *32*(5), pp.691-702.

Balasse, M., Ambrose, S.H., Smith, A.B. and Price, T.D., 2002. The seasonal mobility model for prehistoric herders in the south-western Cape of South Africa assessed by isotopic analysis of sheep tooth enamel. *Journal of archaeological science*, *29*(9), pp.917-932.

Balter, M. 2010. News of the Week, Archaeology: of Two Minds about Toba's Impact. *Science* 327, pp.1187–1188.

Band, S., and M. Yadava 2020. Addressing Past Monsoon Variability from Speleothems. *Current Science 119*(2), pp. 244-254.

Baptista, A. 2012, Ostrich in Indian Archaeology, Unpublished M.A. dissertation, Deccan College.

Barik, K. and Sabale, P.D., 2021. A Preliminary Report on Prehistoric Investigation in the Middle Ong River Basin with Particular Reference to the Uttali and the Ghensali Stream, Southern Bargarh Upland, Odisha. *Ancient Asia*, *12*.

Barnosky, A.D., Koch, P.L., Feranec, R.S., Wing, S.L. and Shabel, A.B., 2004. Assessing the causes of late Pleistocene extinctions on the continents. *science*, *306*(5693), pp.70-75.

Basak, B. and Srivastava, P., 2017. Earliest dates of Microlithic industries (42–25 ka) from West Bengal, eastern India: New light on modern human occupation in the Indian subcontinent. *Asian Perspectives*, pp.237-259.

Basak, B., Badam, G.L., Kshirsagar, A. and Rajaguru, S.N., 1998. Late Quaternary Environment, Palaeontology and Culture of Tarafeni Valley, Midnapur District, West Bengal-A Preliminary Study. *Journal-Geological Society of India*, *51*, pp.731-740.

Basak, B., Srivastava, P., Dasgupta, S., Kumar, A. and Rajaguru, S.N., 2014. Earliest dates and implications of Microlithic industries of Late Pleistocene from Mahadebbera and Kana, Purulia district, West Bengal. *Current Science*, pp.1167-1171.

Basavaiah, N., Juyal, N., Pant, R.K., Yadava, M.G., Singhvi, A.K. and Appel, E., 2004. Late Quarternary climate changes reconstructed from mineral magnetic studies from proglacial lake deposits of Higher Central Himalaya. *Journal of Indian Geophysical Union* 8, pp. 27-31.

Baskaran, M., Marathe, A.R., Rajaguru, S.N. and Somayajulu, B.L.K., 1986. Geochronology of palaeolithic cultures in the Hiran Valley, Saurashtra, India. *Journal of Archaeological Science*, *13*(6), pp.505-514.

Basu, S., Agrawal, S., Sanyal, P., Mahato, P., Kumar, S. and Sarkar, A., 2015. Carbon isotopic ratios of modern C3–C4 plants from the Gangetic Plain, India and its implications to paleovegetational reconstruction. *Palaeogeography, Palaeoclimatology, Palaeoecology*, *440*, pp.22-32.

Beck, H.L. and de Planque, G., 1985. Dose rate conversion factors. *Health Phys.;(United States)*, *49*(5).

Bedaso, Z., Wynn, J.G., Alemseged, Z. and Geraads, D., 2010. Paleoenvironmental reconstruction of the Asbole fauna (Busidima Formation, Afar, Ethiopia) using stable isotopes. *Geobios*, *43*(2), pp.165-177.

Behera, D., Mishra, P.K., Sabale, P., Bhattacharya, S. and Anoop, A., 2022. Late Holocene climate variability and its impact on cultural dynamics in central India. *Geological Society, London, Special Publications*, *515*.

Bender, M.M., 1971. Variations in the 13C/12C ratios of plants in relation to the pathway of photosynthetic carbon dioxide fixation. Phytochemistry, 10(6), pp.1239-1244.

Bera, S.K., Gupta H.P. and Anjum F., 1996. 20,000 Years Sequence of Paleofloristics and Paleoenvironment in Palni Hills, South India. *Geophytology*, 26(I), pp. 96-104.

Bhandari, S., Maurya, D.M. and Chamyal, L.S., 2005. Late Pleistocene alluvial plain sedimentation in lower Narmada Valley, Western India: palaeoenvironmental implications. *Journal of Asian Earth Sciences*, *24*(4), pp.433-444.

Bhandari, S., Momohara, A. and Paudayal, K.N., 2009. Late Pleistocene plant macro-fossils from the Gokarna formation of the Kathmandu Valley, Central Nepal. *Bulletin of the Department of Geology*, *12*, pp.75-88.

Bhattacharyya, A. 1996. Recent advances in Vindhyan geology. *Recent advances in Vindhyan geology*, https://doi.org/10.1016/s0301-9268(97)86637-5.

Bhattacharyya, A., 1989. Vegetation and climate during the last 30,000 years in Ladakh. *Palaeogeography, Palaeoclimatology, Palaeoecology*, *73*(1-2), pp.25-38.

Bhattacharyya, A., Mehrotra, N., Shah, S.K., Basavaiah, N., Chaudhary, V. and Singh, I.B., 2014. Analysis of vegetation and climate change during late Pleistocene from Ziro valley, Arunachal Pradesh, eastern Himalaya region. *Quaternary Science Reviews*, *101*, pp.111-123.

Bhattacharyya, A., Ranhotra, P.S. and Gergan, J.T., 2011. Vegetation vis-a-vis climate and glacier history during 12,400 to 5,400 yr BP from Dokriani valley, Garhwal Himalaya, India. *Journal of the Geological Society of India*, *77*(5), pp.401-408.

Biasatti, D., Wang, Y. and Deng, T., 2010. Strengthening of the East Asian summer monsoon revealed by a shift in seasonal patterns in diet and climate after 2–3 Ma in northwest China. *Palaeogeography, Palaeoclimatology, Palaeoecology*, *297*(1), pp.12-25.

Biodiversity Impact Assessment Report for Proposed 400kV D / C Jaunpur Obra Transmission Line passing through Kaimur Wildlife Sanctuary 2019. *Obra-C Badaun Transmission Limited (OCBTL)* Bareilly , Uttar Pradesh.

Biswas, R. H., M.A.J. Williams, R. Raj, N. Juyal, and A.K. Singhvi 2013. Methodological Studies on Luminescence Dating of Volcanic Ashes. *Quaternary Geochronology* 17: pp.14-25.

Biswas, S., 1997. Fossil Mammalia of the Quaternary sequence of the Narmada valley: their affinity, age and ecology. *Quaternary Geology of the Narmada Valley*, pp.91-104.

Blinkhorn, J. (2012). The Palaeolithic occupation of Thar, Published thesis, St. Hugh's College, University of Oxford.

Blinkhorn, J. and Petraglia, M.D., 2017. Environments and cultural change in the Indian subcontinent: implications for the dispersal of Homo sapiens in the Late Pleistocene. *Current Anthropology*, *58*(S17), pp.S463-S479.

Blinkhorn, J., 2013. A new synthesis of evidence for the Upper Pleistocene occupation of 16R Dune and its southern Asian context. *Quaternary International*, *300*, pp.282-291.

Blinkhorn, J., 2018. Buddha Pushkar revisited: Technological variability in Late Palaeolithic stone tools at the Thar Desert margin, India. Journal of Archaeological Science: Reports, 20, pp.168-182.

Blinkhorn, J., Achyuthan, H. and Petraglia, M.D., 2015. Ostrich expansion into India during the Late Pleistocene: Implications for continental dispersal corridors. *Palaeogeography, Palaeoclimatology, Palaeoecology*, *417*, pp.80-90.

Blinkhorn, J., Achyuthan, H., Ditchfield, P. and Petraglia, M., 2017. Palaeoenvironmental dynamics and palaeolithic occupation at Katoati, Thar Desert, India. *Quaternary Research*, *87*(2), pp.298-313.

Blinkhorn, J., Achyuthan, H., Durcan, J., Roberts, P. and Ilgner, J., 2021. Constraining the chronology and ecology of Late Acheulean and Middle Palaeolithic occupations at the margins of the monsoon. *Scientific reports*, *11*(1), pp.1-14.

Blinkhorn, J., Achyuthan, H., Petraglia, M. and Ditchfield, P., 2013. Middle Palaeolithic occupation in the Thar Desert during the Upper Pleistocene: the signature of a modern human exit out of Africa? *Quaternary Science Reviews*, *77*, pp.233-238.

Blinkhorn, J., Ajithprasad, P., Mukherjee, A., Kumar, P., Durcan, J.A. and Roberts, P., 2019. The first directly dated evidence for Palaeolithic occupation on the Indian coast at Sandhav, Kachchh. *Quaternary Science Reviews*, *224*, p.105975.

Blinkhorn, J., Parker, A.G., Ditchfield, P., Haslam, M. and Petraglia, M., 2012. Uncovering a landscape buried by the super-eruption of Toba, 74,000 years ago: A multi-proxy environmental reconstruction of landscape heterogeneity in the Jurreru Valley, south India. *Quaternary International*, *258*, pp.135-147.

Blumenschine, R.J., Brandt, S.A. and Clark, J.D., 1983. Excavations and analysis of middle Palaeolithic artifacts from Patpara, Madhya Pradesh. *Palaeoenvironments and Prehistory in the Middle Son Valley. Abinash Prakashan, Allahabad*, pp.39-99.

Blumenschine, R.J., Peters, C.R., Masao, F.T., Clarke, R.J., Deino, A.L., Hay, R.L., Swisher, C.C., Stanistreet, I.G., Ashley, G.M., McHenry, L.J. and Sikes, N.E., 2003. Late Pliocene Homo and hominid land use from western Olduvai Gorge, Tanzania. *Science*, *299*(5610), pp.1217-1221.

Bocherens, H., Koch, P.L., Mariotti, A., Geraads, D. and Jaeger, J.J., 1996. Isotopic biogeochemistry (13 C, 18 O) of mammalian enamel from African Pleistocene hominid sites. *Palaios*, pp.306-318.

Boëda, E., 1993. Le débitage discoïde et le débitage Levallois récurrent centripède. *Bulletin de la Société préhistorique française*, *90*(6), pp.392-404.

Bohra, A., Kotlia, B.S. and Basavaiah, N., 2017. Palaeoclimatic reconstruction by using the varvite sediments of Bharatpur, Upper Lahaul Valley, NW Himalaya, India. *Quaternary International*, *443*, pp.39-48.

Boivin, N., Fuller, D.Q., Dennell, R., Allaby, R. and Petraglia, M.D., 2013. Human dispersal across diverse environments of Asia during the Upper Pleistocene. *Quaternary International*, *300*, pp.32-47.

Bolton, C.T., Chang, L., Clemens, S.C., Kodama, K., Ikehara, M., Medina-Elizalde, M., Paterson, G.A., Roberts, A.P., Rohling, E.J., Yamamoto, Y. and Zhao, X., 2013. A 500,000 year record of Indian summer monsoon dynamics recorded by eastern equatorial

Indian Ocean upper water-column structure. *Quaternary Science Reviews*, *77*, pp.167-180.

Bookhagen, B., Thiede, R.C. and Strecker, M.R., 2005. Late Quaternary intensified monsoon phases control landscape evolution in the northwest Himalaya. *Geology*, *33*(2), pp.149-152.

Bordes, F., 1961. Typologie du paléolithique ancien et moyen. Bordeaux. *Cahiers du Quaternaire, 108.*

Borgaonkar, H.P., Sikder, A.B. and Ram, S., 2011. High altitude forest sensitivity to the recent warming: a tree-ring analysis of conifers from Western Himalaya, India. *Quaternary International*, *236*(1-2), pp.158-166.

Bretzke, K. and Conard, N.J., 2012. Evaluating morphological variability in lithic assemblages using 3D models of stone artifacts. *Journal of Archaeological Science*, 39(12), pp.3741-3749.

Bronger, A., Pant, R.K. and Singhvi, A.K., 1987. Pleistocene climatic changes and landscape evolution in the Kashmir Basin, India: paleopedologic and chronostratigraphic studies. *Quaternary research*, *27*(2), pp.167-181.

Brown, J.A., 1889. On some small highly specialized forms of stone implements, found in Asia, North Africa, and Europe. *Journal of Anthropological Institute of Great Britain and Ireland*, pp.134-139.

Brown, K.S., Marean, C.W., Jacobs, Z., Schoville, B.J., Oestmo, S., Fisher, E.C., Bernatchez, J., Karkanas, P. and Matthews, T., 2012. An early and enduring advanced technology originating 71,000 years ago in South Africa. *Nature*, *491*(7425), pp.590-593.

Bruggemann, J. Henrich, Richard T. Buffler, Mireille MM Guillaume, Robert C. Walter, Rudo von Cosel, Berhane N. Ghebretensae, and Seife M. Berhe. "Stratigraphy, palaeoenvironments and model for the deposition of the Abdur Reef Limestone: context for an important archaeological site from the last interglacial on the Red Sea coast of Eritrea*." Palaeogeography, Palaeoclimatology, Palaeoecology* 203, no. 3-4 (2004): 179-206.

Brunet, M., Guy, F., Pilbeam, D., Mackaye, H.T., Likius, A., Ahounta, D., Beauvilain, A., Blondel, C., Bocherens, H., Boisserie, J.R. and De Bonis, L., 2002. A new hominid from the Upper Miocene of Chad, Central Africa. *Nature*, *418*(6894), pp.145-151.

Bryant, J.D., Froelich, P.N., Showers, W.J. and Genna, B.J., 1996. A tale of two quarries: biologic and taphonomic signatures in the oxygen isotope composition of tooth enamel phosphate from modern and Miocene equids. *Palaios*, pp.397-408.

Buggle, B., Glaser, B., Hambach, U., Gerasimenko, N. and Marković, S., 2011. An evaluation of geochemical weathering indices in loess–paleosol studies. *Quaternary International*, *240*(1-2), pp.12-21.

Bulbul, M., Ankit, Y., Basu, S. and Anoop, A., 2021. Characterization of sedimentary organic matter and depositional processes in the Mandovi estuary, western India: An integrated lipid biomarker, sedimentological and stable isotope approach. *Applied Geochemistry*, *131*, p.105041.

Burns, S.J., Fleitmann, D., Mudelsee, M., Neff, U., Matter, A. and Mangini, A., 2002. A 780-year annually resolved record of Indian Ocean monsoon precipitation from a speleothem from south Oman. *Journal of Geophysical Research: Atmospheres*, *107*(D20), pp.ACL-9.

Butzer, K.W., 1969. Early Homo sapiens remains from the Omo River region of south-west Ethiopia: Geological interpretation of two Pleistocene hominid sites in the Lower Omo Basin. *Nature*, *222*, pp.1133-1135.

Caley, T., Malaizé, B., Zaragosi, S., Rossignol, L., Bourget, J., Eynaud, F., Martinez, P., Giraudeau, J., Charlier, K. and Ellouz-Zimmermann, N., 2011. New Arabian Sea records help decipher orbital timing of Indo-Asian monsoon. *Earth and Planetary Science Letters*, *308*(3-4), pp.433-444.

Callahan, E., 1979. The basics of biface knapping in the eastern fluted point tradition: a manual for flintknappers and lithic analysts. *Eastern States Archaeological Federation*.

Carto, S.L., Weaver, A.J., Hetherington, R., Lam, Y. and Wiebe, E.C., 2009. Out of Africa and into an ice age: on the role of global climate change in the late Pleistocene

migration of early modern humans out of Africa. *Journal of human evolution*, *56*(2), pp.139-151.

Castañeda, I.S., Mulitza, S., Schefuß, E., dos Santos, R.A.L., Damsté, J.S.S. and Schouten, S., 2009. Wet phases in the Sahara/Sahel region and human migration patterns in North Africa. *Proceedings of the National Academy of Sciences*, *106*(48), pp.20159-20163.

Census of India, Sonbhadra 2011.

Cerling, T. E., Harris, J. M., and MacFadden, B. J. 1997c. "Carbon Isotopes, Diets of North American Equids, and the Evolution ofNorth American C4 Grasslands," in *Stable Isotopes and the Integration of Biological, Ecological, and Geochemical Processes*. Editors H. Griffiths, D. Robinson, and P. van Gardingen (Oxford: Bios Scientific Publishers), pp. 363–379.

Cerling, T.E. and Harris, J.M., 1999. Carbon isotope fractionation between diet and bioapatite in ungulate mammals and implications for ecological and paleoecological studies. *Oecologia*, *120*(3), pp.347-363.

Cerling, T.E., 1999. Paleorecords of C4 plants and ecosystems. *C4 plant biology*, pp.445-469.

Cerling, T.E., Harris, J.M. and Leakey, M.G., 2003. Isotope Paleoecology of the Nawata and Nachukui Formations at Lothagam, Turkana Basin, Kenya. In *Lothagam* (pp. 605-624). Columbia University Press.

Cerling, T.E., Harris, J.M., Ambrose, S.H., Leakey, M.G. and Solounias, N., 1997a. Dietary and environmental reconstruction with stable isotope analyses of herbivore tooth enamel from the Miocene locality of Fort Ternan, Kenya. *Journal of Human Evolution*, *33*(6), pp.635-650.

Cerling, T.E., Harris, J.M., MacFadden, B.J., Leakey, M.G., Quade, J., Eisenmann, V. and Ehleringer, J.R., 1997b. Global vegetation change through the Miocene/Pliocene boundary. *Nature*, *389*(6647), pp.153-158.

Chakrabarti, R., Basu, A.R. and Chakrabarti, A., 2007. Trace element and Nd-isotopic evidence for sediment sources in the mid-Proterozoic Vindhyan Basin, central India. *Precambrian Research*, *159*(3-4), pp.260-274.

Champion, H.G. and Seth, S.K., 1968. *A revised survey of the forest types of India*. Manager of publications.

Channell, J.E.T. and Vigliotti, L., 2019. The role of geomagnetic field intensity in late quaternary evolution of humans and large mammals. *Reviews of Geophysics*, *57*(3), pp.709-738.

Chauhan, M.S., Pokharia, A.K. and Srivastava, R.K., 2015. Late Quaternary vegetation history, climatic variability and human activity in the Central Ganga Plain, deduced by pollen proxy records from Karela Jheel, India. *Quaternary International*, *371*, pp.144-156.

Chauhan, O.S., Borole, O.V., Gujar, A.R., Mascarenhas, A., Mislanker, P.G. and Rao, C.M., 1993. Evidences of climatic variations during Late Pleistocene–Holocene in the eastern Bay of Bengal. *Current Science*, pp.558-562.

Chauhan, P. R., and Patnaik, R. (2017). Pilikarar: An Early Acheulian Site in the Central Narmada Basin, India. In K. Paddayya, and B. Basak (Eds.), *Prehistoric Research in the Indian Subcontinent: A Reappraisal and New Directions,* pp. 117- 143. Delhi: Primus Books.

Chauhan, P.R. 2009. The South Asian Paleolithic Record and its Potential for Transitions Studies. In: *Sourcebook of Paleolithic Transitions* (Camps, M., Chauhan, P.R. Eds.) pp.121-139. Springer, New York

Chauhan, P.R. 2019. Interpretative Shifts in Understanding the Prehistoric Settlement of the Indian Subcontinent, In *Interrogating Human Origins: Decolonisation and the Deep Human Past*. (Martin Porr, Jacqueline Matthews Eds.) pp. 239-256. Routledge, London,

Chauhan, P.R., 2004. A review of the Early Acheulian evidence from South Asia. Assemblage 8. *Avaialble from: http://www. shef. ac. uk/assem/issue8/chauhan. html*.

Chauhan, P.R., 2010. Metrical variability between South Asian handaxe assemblages: preliminary observations. In *New perspectives on old stones* (pp. 119-166). Springer, New York, NY.

Chauhan, P.R., 2020. Human evolution in the center of the old world: An updated review of the South Asian Paleolithic. *Pleistocene Archaeology-Migration, Technology, and Adaptation*. *Intech*, 13.

Chauhan, P.R., 2023. Chrono-contextual issues at open-air Pleistocene vertebrate fossil sites of central and peninsular India and implications for Indian palaeoanthropology. *Geological Society, London, Special Publications*, *515*(1),SP515-2021.

Chauhan, P.R., Ozarkar, S. and Kulkarni, S., 2015. Genes, stone tools, and modern human dispersals in the center of the Old World. *Emergence and diversity of modern human behavior in Paleolithic Asia*, pp.94-113.

Chawla, S., Dhir, R.P. and Singhvi, A.K., 1992. Thermoluminescence chronology of sand profiles in the Thar Desert and their implications. *Quaternary Science Reviews*, *11*(1-2), pp.25-32.

Chen, F., Welker, F., Shen, C.C., Bailey, S.E., Bergmann, I., Davis, S., Xia, H., Wang, H., Fischer, R., Freidline, S.E. and Yu, T.L., 2019. A late middle Pleistocene Denisovan mandible from the Tibetan Plateau. *nature*, *569*(7756), pp.409-412.

Clark, J.D. and Brown, K.S., 2001. The Twin Rivers Kopje, Zambia: stratigraphy, fauna, and artefact assemblages from the 1954 and 1956 excavations. Journal of Archaeological Science, 28(3), pp.305-330.

Clark, J.D. and Williams, M.A.J., 1987. Paleoenvironments and prehistory in north central India: a preliminary report. *Studies in the Archaeology of India and Pakistan. Aris and Phillips Ltd, Warminster*, pp.19-41.

Clark, J.D., Beyene, Y., WoldeGabriel, G., Hart, W.K., Renne, P.R., Gilbert, H., Defleur, A., Suwa, G., Katoh, S., Ludwig, K.R. and Boisserie, J.R., 2003. Stratigraphic, chronological and behavioural contexts of Pleistocene Homo sapiens from Middle Awash, Ethiopia. *Nature*, *423*(6941), pp.747-752.

Clark, P.U. and Mix, A.C., 2002. Ice sheets and sea level of the Last Glacial Maximum. *Quaternary Science Reviews*, *21*(1-3), pp.1-7.

Clarkson, C., Harris, C., Li, B., Neudorf, C.M., Roberts, R.G., Lane, C., Norman, K., Pal, J., Jones, S., Shipton, C. and Koshy, J., 2020. Human occupation of northern India spans the Toba super-eruption~ 74,000 years ago. *Nature communications*, *11*(1), pp.1-10.

Clarkson, C., Jones, S. and Harris, C., 2012. Continuity and change in the lithic industries of the Jurreru Valley, India, before and after the Toba eruption. *Quaternary International*, *258*, pp.165-179.

Clarkson, C., Petraglia, M., Harris, C., Shipton, C. and Norman, K., 2018. The South Asian Microlithic: Homo sapiens dispersal or adaptive response? In *Lithic Technological Organization and Paleoenvironmental Change* (pp. 37-61). Springer, Cham.

Clarkson, C., Petraglia, M., Korisettar, R., Haslam, M., Boivin, N., Crowther, A., Ditchfield, P., Fuller, D., Miracle, P., Harris, C. and Connell, K., 2009. The oldest and longest enduring microlithic sequence in India: 35 000 years of modern human occupation and change at the Jwalapuram Locality 9 rockshelter. *Antiquity*, *83*(320), pp.326-348.

Clemens, S.C. and Prell, W.L., 2003. A 350,000 year summer-monsoon multi-proxy stack from the Owen Ridge, Northern Arabian Sea. *Marine Geology*, *201*(1-3), pp.35-51.

Clementz, M.T., Holroyd, P.A. and Koch, P.L., 2008. Identifying aquatic habits of herbivorous mammals through stable isotope analysis. *Palaios*, *23*(9), pp.574-585.

Cockburn, J., 1883. On the recent existence of Rhinoceros indicus in the North Western Provinces, and a description of a tracing of an archaic rock painting from Mirzapore representing the hunting of this animal. *Journal of the Asiatic Society of Bengal*, *52*(2), pp.56-64.

Cockburn.J. Cave drawings of KaimurRange. North-West Provinces JkaS.1899.

Cohen K.M. and Gibbard, P., 2011 Global chronostratigraphical correlation table for the last 2.7 million years. Subcommission on Quaternary Stratigraphy, *International Commission on Stratigraphy*, Cambridge, England.

Collard, M., Vaesen, K., Cosgrove, R. and Roebroeks, W., 2016. The empirical case against the 'demographic turn'in Palaeolithic archaeology. *Philosophical Transactions of the Royal Society B: Biological Sciences*, *371*(1698), p.20150242.

Cooper, A., Turney, C.S., Palmer, J., Hogg, A., McGlone, M., Wilmshurst, J., Lorrey, A.M., Heaton, T.J., Russell, J.M., McCracken, K. and Anet, J.G., 2021. A global environmental crisis 42,000 years ago. *Science*, *371*(6531), pp.811-818.

Cooper, R.G., Mahrose, K., Horbańczuk, J.O., Villegas-Vizcaíno, R., Kennou Sebei, S. and Faki Mohammed, A.E., 2009. The wild ostrich (Struthio camelus): a review. *Tropical Animal Health and Production*, *41*(8), pp.1669-1678.

Corvinus, G.V., 1983. A Survey of the Pravara River System in Western Maharashtra, India, Vol 2.: The Excavations of the Acheulian Site of Chirki-on-Pravara, India. *Tubingen: Institute for Urgeschichte*.

Costa, A.G., 2017. A new Late Pleistocene fauna from arid coastal India: implications for inundated coastal refugia and human dispersals. *Quaternary International*, *436*, pp.253-269.

Costa, A.G., Ajithprasad, P. and Sharma, B., 2011. Tracking early humans in coastal western India: the Gujarat Palaeoanthropology project. *Antiquity*, *85*, p.327.

d'Errico, F., Gaillard, C. and Misra, V.N., 1989. Collection of non-utilitarian objects by Homo erectus in India. In *Hominidae. Proceedings of the 2nd International Congress of Human Paleontology* (pp. 237-239). Milan: Editoriale Jaca Book.

Dansgaard, W., 1964. Stable isotopes in precipitation. *tellus*, *16*(4), pp.436-468.

Dar, R.A., Chandra, R., Romshoo, S.A., Lone, M.A. and Ahmad, S.M., 2015. Isotopic and micromorphological studies of Late Quaternary loess–paleosol sequences of the Karewa Group: inferences for palaeoclimate of Kashmir Valley. *Quaternary International*, *371*, pp.122-134.

Dart, R.A. and Salmons, A., 1925. Australopithecus africanus: the man-ape of South Africa. *A Century of Nature: Twenty-One Discoveries that Changed Science and the World*, pp.10-20.

Debénath, A. and Dibble, H.L., 1994. *Handbook of Paleolithic Typology: Lower and middle paleolithic of Europe* (Vol. 1). UPenn Museum of Archaeology.

Delson, E. 2019. An early modern human outside Africa. *Nature* 571, pp 487-488.

Demenocal, P.B. and Stringer, C., 2016. Climate and the peopling of the world. *Nature*, *538*(7623), pp.49-50.

Demeter, F., Shackelford, L., Westaway, K., Duringer, P., Bacon, A.M., Ponche, J.L., Wu, X., Sayavongkhamdy, T., Zhao, J.X., Barnes, L. and Boyon, M., 2015. Early modern humans and morphological variation in Southeast Asia: fossil evidence from Tam Pa Ling, Laos. *PloS one*, *10*(4), p.e0121193.

Deng, T., Dong, J.S. and Wang, Y., 2001. Quaternary Terrestrial Ecosystem Evolution of North China Recorded by Fossil Stable Carbon Isotope. *Chin. Sci. Bull*, *46*, pp.1213-1215.

Dennell, R. and Petraglia, M.D., 2012. The dispersal of Homo sapiens across southern Asia: how early, how often, how complex?. *Quaternary Science Reviews*, *47*, pp.15-22.

Dennell, R. and Roebroeks, W., 2005. An Asian perspective on early human dispersal from Africa. *Nature*, *438*(7071), pp.1099-1104.

Dennell, R., 2021. Geoarchaeology in India in the 21st century: an outsider's perspective. *Geological Society, London, Special Publications*, *515*.

Dennell, R.W., Rendell, H.M., Halim, M. and Moth, E., 1992. A 45,000-year-old open-air Paleolithic site at Riwat, northern Pakistan. *Journal of Field Archaeology*, pp.17-33.

Deo, S., Mishra, S. and Rajaguru, S.N., 2004. Palaeoclimatic studies at the Deccan College (1940-2005): a geoarchaeological approach. *Bulletin of the Deccan College Research Institute*, *64*, pp.209-228.

Deotare, B.C. and Kajale, M.D., 1996. Quaternary pollen analysis and palaeoenvironmental studies on the salt basins at Pachpadra and Thob western Rajasthan India preliminary observations. *Man and Environment*, *21*(1), pp.24-31.

Deotare, B.C., Kajale, M.D., Rajaguru, S.N., Kusumgar, S., Jull, A.J.T. and Donahue, J.D., 2004. Palaeoenvironmental history of Bap-Malar and Kanod playas of western Rajasthan, Thar desert. *Journal of Earth System Science*, *113*(3), pp.403-425.

Deraniyagala, S.U. 1992. *The Prehistory Of Sri Lanka: An Ecological Perspective*, Parts I and II. Colombo: Department of Archaeological Survey, Government of Sri Lanka.

Deraniyagala, S.U., 1988. *The prehistory of Sri Lanka: an ecological perspective*. Harvard University.

Détroit, F., Mijares, A.S., Corny, J., Daver, G., Zanolli, C., Dizon, E., Robles, E., Grün, R. and Piper, P.J., 2019. A new species of Homo from the Late Pleistocene of the Philippines. *Nature*, *568*(7751), pp.181-186.

Dhir, R.P., Singhvi, A.K., Andrews, J.E., Kar, A., Sareen, B.K., Tandon, S.K., Kailath, A. and Thomas, J.V., 2010. Multiple episodes of aggradation and calcrete formation in Late Quaternary aeolian sands, Central Thar Desert, Rajasthan, India. *Journal of Asian Earth Sciences*, *37*(1), pp.10-16.

Dhir, R.P., Tandon, S.K., Sareen, B.K., Ramesh, R., Rao, T.K.G., Kailath, A.J. and Sharma, N., 2004. Calcretes in the Thar desert: genesis, chronology and palaeoenvironment. *Journal of Earth System Science*, *113*(3), pp.473-515.

Di Maida, G., Hattermann, M. and Delpiano, D., 2023. 3D models of lithic artefacts: A test on their efficacy. Digital Applications in Archaeology and Cultural Heritage, p.e00279.

District Survey report, Sonbhadra, Directorate of Geology and Mining, 2016.

Dixit, S. and Bera, S.K., 2013. Pollen-inferred vegetation vis-à-vis climate dynamics since Late Quaternary from Western Assam, Northeast India: Signal of global climatic events. *Quaternary International*, *286*, pp.56-68.

Duplessy, J.C., 1982. Glacial to interglacial contrasts in the northern Indian Ocean. *Nature*, *295*(5849), pp.494-498.

Dutt, S., Gupta, A.K., Clemens, S.C., Cheng, H., Singh, R.K., Kathayat, G. and Edwards, R.L., 2015. Abrupt changes in Indian summer monsoon strength during 33,800 to 5500 years BP. *Geophysical Research Letters*, *42*(13), pp.5526-5532.

Dutta, P.C., 1984. Sarai Nahar Rai man: The first and oldest human fossil record in South Asia. *Anthropologie*, pp.35-50.

Dutta, S., Suresh, N. and Kumar, R., 2012. Climatically controlled Late Quaternary terrace staircase development in the fold-and-thrust belt of the Sub Himalaya. *Palaeogeography, Palaeoclimatology, Palaeoecology*, *356*, pp.16-26.

Duval, M., Guilarte, V., Campaña, I., Arnold, L., Miguens, L., Iglesias, J., González-Sierra, S., 2018. Quantifying hydrofluoric acid etching of quartz and feldspar coarse grains based on weight loss estimates: implication for ESR and luminescence dating studies, *Ancient TL*, *36*, pp. 1-14.

Edwards, S.W., 2001. A modern knapper's assessment of the technical skills of the Late Acheulean biface workers at Kalambo Falls. *Kalambo Falls prehistoric site*, *3*, pp.605-611.

Ehleringer, J.R., Sage, R.F., Flanagan, L.B. and Pearcy, R.W., 1991. Climate change and the evolution of C4 photosynthesis. Trends in ecology & evolution, 6(3), pp.95-99.

Eriksson, M., 2012. Early warning systems for water in agriculture. *Feeding a Thirsty World*, p.39.

Farooqui, A., Pattan, J.N., Parthiban, G. and Srivastava, J., 2014. Palynological record of tropical rain forest vegetation and sea level fluctuations since 140 ka from sediment core, south-eastern Arabian Sea. *Palaeogeography, Palaeoclimatology, Palaeoecology*, *411*, pp.95-109.

Farooqui, A., Ray, J.G., Farooqui, S.A., Tiwari, R.K. and Khan, Z.A., 2010. Tropical rainforest vegetation, climate and sea level during the Pleistocene in Kerala, India. *Quaternary International*, *213*(1-2), pp.2-11.

Farquhar, G.D., Ehleringer, J.R. and Hubick, K.T., 1989. Carbon isotope discrimination and photosynthesis. *Annual review of plant physiology and plant molecular biology*, *40*(1), pp.503-537.

Faurby, S. and Svenning, J.C., 2015. Historic and prehistoric human-driven extinctions have reshaped global mammal diversity patterns. *Diversity and Distributions*, *21*(10), pp.1155-1166.

Fedo, C.M., Wayne Nesbitt, H. and Young, G.M., 1995. Unraveling the effects of potassium metasomatism in sedimentary rocks and paleosols, with implications for paleoweathering conditions and provenance. *Geology*, *23*(10), pp.921-924.

Feranec, R.S. and MacFadden, B.J., 2000. Evolution of the grazing niche in Pleistocene mammals from Florida: evidence from stable isotopes. *Palaeogeography, Palaeoclimatology, Palaeoecology*, *162*(1-2), pp.155-169.

Fewlass, H., Talamo, S., Wacker, L., Kromer, B., Tuna, T., Fagault, Y., Bard, E., McPherron, S.P., Aldeias, V., Maria, R. and Martisius, N.L., 2020. A 14C chronology for the Middle to Upper Palaeolithic transition at Bacho Kiro cave, Bulgaria. *Nature ecology & evolution*, *4*(6), pp.794-801.

Foley, R., 1981. Off-site archaeology and human adaptation in Eastern Africa: an analysis of regional artefact density in the Amboseli, southern Kenya. *BAR Publishing*.

Foote, R.B., 1885. Notes on the results of Mr HB Foote's further excavations in the Billa Surgam caves. *Records of the Geological Survey of India*, *18*(4), pp.227-35.

Franco, N.V., Brook, G.A., Mancini, M.V. and Vetrisano, L., 2016. Changes in lithic technology and environment in southern continental Patagonia: the Chico and Santa Cruz River basins. *Quaternary International*, *422*, pp.57-65.

Freidline, S.E., Gunz, P., Janković, I., Harvati, K. and Hublin, J.J., 2012. A comprehensive morphometric analysis of the frontal and zygomatic bone of the Zuttiyeh fossil from Israel. *Journal of Human Evolution*, *62*(2), pp.225-241.

Freidline, S.E., Westaway, K.E., Joannes-Boyau, R., Duringer, P., Ponche, J.L., Morley, M.W., Hernandez, V.C., McAllister-Hayward, M.S., McColl, H., Zanolli, C. and Gunz, P., 2023. Early presence of Homo sapiens in Southeast Asia by 86–68 kyr at Tam Pà Ling, Northern Laos. *Nature Communications*, 14(1), pp.3193.

Fricke, H.C. and O'Neil, J.R., 1996. Inter-and intra-tooth variation in the oxygen isotope composition of mammalian tooth enamel phosphate: implications for

palaeoclimatological and palaeobiological research. *Palaeogeography, Palaeoclimatology, Palaeoecology*, *126*(1-2), pp.91-99.

Funaki, T., Sato, H., Korisettar, R., Shitaoka, Y., Noguchi, A. and Nagasaki, J.I., 2022. New Chronometric Dating of Indian Middle/Upper Palaeolithic Sites at Jwalapuram, Andhra Pradesh, Southern India. *Journal of Archaeological Studies in India*, 2(2), pp. 101-113.

Gaillard, C. and Rajaguru, S. N., 2017. Revisiting the Acheulian site of Singi Talav at Didwana (Rajasthan) 35 years. in *Rethinking the Past: A Tribute to Professor V. N. Misra* (ed. Deo, S. G.) 25–39 (Indian Society for Prehistoric and Quaternary Studies,). doi:10.7765/9780719098451.00013.

Gaillard, C., Mishra, S., Singh, M., Deo, S. and Abbas, R., 2010. Lower and early Middle Pleistocene Acheulian in the Indian sub-continent. *Quaternary International*, *223*, pp.234-241.

Gaillard, C., Misra, V.N., Rajaguru, S.N., Raju, D.R. and Raghavan, H., 1985. Acheulian occupation at Singi Talav in the Thar Desert: A preliminary report on 1981 excavation. *Bulletin of the Deccan College Research Institute,* pp.141-152.

Gebregiorgis, D., Deocampo, D.M., Longstaffe, F.J., Simpson, A., Ashley, G.M., Beverly, E.J., Delaney, J.S. and Cuadros, J., 2020. Oxygen isotopes in authigenic clay minerals: Toward building a reliable salinity proxy. *Geophysical research letters*, *47*(3), p.e2019GL085576.

Gehler, A., Tütken, T. and Pack, A., 2012. Oxygen and carbon isotope variations in a modern rodent community–implications for palaeoenvironmental reconstructions. *PLoS One*, *7*(11), p.e49531.

Ghosh, P. and Bhattacharya, S.K., 2003. Sudden warming epochs during 42 to 28 ky bp in the Himalayan region from stable iso-tope record of sediment column from a relict lake in Goting, Garhwal, North India. *Current Science*, *85*(1), pp.101-108.

Ghosh, R., Bera, S., Sarkar, A., Paruya, D.K., Yao, Y.F. and Li, C.S., 2015. A∼ 50 ka record of monsoonal variability in the Darjeeling foothill region, eastern Himalayas. *Quaternary Science Reviews*, *114*, pp.100-115.

Ghosh, R., Paruya, D.K., Khan, M.A., Chakraborty, S., Sarkar, A. and Bera, S., 2014. Late Quaternary climate variability and vegetation response in Ziro Lake Basin, Eastern Himalaya: A multiproxy approach. *Quaternary International*, *325*, pp.13-29.

Ghosh, S., Sanyal, P. and Kumar, R., 2017. Evolution of C4 plants and controlling factors: Insight from n-alkane isotopic values of NW Indian Siwalik paleosols. *Organic Geochemistry*, *110*, pp.110-121.

Ghosh, S.K. 1971. Petrology of the Porcellanite Rocks of the Samaria Area, Sidhi District, Madhya Pradesh. *The Quarterly journal of the Geological, Mining, and Metallurgical Society of India*, *43*, pp. 153–164.

Green, R.E., Krause, J., Briggs, A.W., Maricic, T., Stenzel, U., Kircher, M., Patterson, N., Li, H., Zhai, W., Fritz, M.H.Y. and Hansen, N.F., 2010. A draft sequence of the Neandertal genome. *science*, *328*(5979), pp.710-722.

Groucutt, H.S., Scerri, E.M., Lewis, L., Clark-Balzan, L., Blinkhorn, J., Jennings, R.P., Parton, A. and Petraglia, M.D., 2015. Stone tool assemblages and models for the dispersal of Homo sapiens out of Africa. *Quaternary International*, *382*, pp.8-30.

Groucutt, H.S., Scerri, E.M., Stringer, C. and Petraglia, M.D., 2019. Skhul lithic technology and the dispersal of Homo sapiens into Southwest Asia. *Quaternary International*, *515*, pp.30-52.

Groucutt, H.S., White, T.S., Clark-Balzan, L., Parton, A., Crassard, R., Shipton, C., Jennings, R.P., Parker, A.G., Breeze, P.S., Scerri, E.M. and Alsharekh, A., 2015. Human occupation of the Arabian empty quarter during MIS 5: evidence from Mundafan Al-Buhayrah, Saudi Arabia. *Quaternary Science Reviews*, *119*, pp.116-135.

Guérin, G., Murray, A.S., Jain, M., Thomsen, K.J. and Mercier, N., 2013. How confident are we in the chronology of the transition between Howieson's Poort and Still Bay. *Journal of human evolution*, *64*(4), pp.314-317.

Gupta, A., Kale, V.S., Owen, L.A. and Singhvi, A.K., 2007. Late Quaternary bedrock incision in the Narmada river at Dardi Falls. *Current Science*, pp.564-567.

Gupta, A.K., Anderson, D.M. and Overpeck, J.T., 2003. Abrupt changes in the Asian southwest monsoon during the Holocene and their links to the North Atlantic Ocean. *Nature*, *421*(6921), pp.354-357.

Gupta, H.P. and C. Sharma 1982. Quaternary Palynostrati-graphy in India-A critical review. *Journal of Palaeontological Society of India 1*, pp. 130-138.

Gupta, S.K., 1988. Recent Palaeoclimatic Data from Indian Region with Reference to Climatic Modelling and Environmental Studies. *Proceedings of the Indian National Science Academy, Part A. Physical Sciences 54(3),* pp. 343-353.

Gupta, S.K., Sharma, P., Juyal, N. and Agrawal, D.P., 1991. Loess—palaeosol sequence in Kashmir: correlation of mineral magnetic stratigraphy with the marine palaeoclimatic record. *Journal of Quaternary Science*, *6*(1), pp.3-12.

Hait, A.K., Das, H.K., Ghosh, S., Ray, A.K. and Chanda, S., 1996. Environmental variations in Late Quaternary sequence of Kolaghat, West Bengal, India. *Current Science*, pp.1089-1093

Harmand, S., Lewis, J.E., Feibel, C.S., Lepre, C.J., Prat, S., Lenoble, A., Boës, X., Quinn, R.L., Brenet, M., Arroyo, A. and Taylor, N., 2015. 3.3-million-year-old stone tools from Lomekwi 3, West Turkana, Kenya. *Nature*, *521*(7552), pp.310-315.

Harmon, K., 2012. New DNA analysis shows ancient humans interbred with Denisovans. *Scientific American.*

Harris, J.M. and Cerling, T.E., 2002. Dietary adaptations of extant and Neogene African suids. *Journal of Zoology*, *256*(1), pp.45-54.

Harvati, K., Röding, C., Bosman, A.M., Karakostis, F.A., Grün, R., Stringer, C., Karkanas, P., Thompson, N.C., Koutoulidis, V., Moulopoulos, L.A. and Gorgoulis, V.G., 2019. Apidima Cave fossils provide earliest evidence of Homo sapiens in Eurasia. *Nature*, *571*(7766), pp.500-504.

Haslam, M. and Petraglia, M., 2010. Comment on "Environmental impact of the 73 ka Toba super-eruption in South Asia" by MAJ Williams, SH Ambrose, S. van der Kaars, C. Ruehlemann, U. Chattopadhyaya, J. Pal and PR Chauhan [Palaeogeography, Palaeoclimatology, Palaeoecology 284 (2009) 295–314]. *Palaeogeography,*

Palaeoclimatology, Palaeoecology, *296*(1-2), pp.199-203.

Haslam, M., Clarkson, C., Petraglia, M., Korisettar, R., Jones, S., Shipton, C., Ditchfield, P. and Ambrose, S.H., 2010a. The 74 ka Toba super-eruption and southern Indian hominins: archaeology, lithic technology and environments at Jwalapuram Locality 3. *Journal of Archaeological Science*, *37*(12), pp.3370-3384.

Haslam, M., Clarkson, C., Roberts, R.G., Bora, J., Korisettar, R., Ditchfield, P., Chivas, A.R., Harris, C., Smith, V., Oh, A. and Eksambekar, S., 2012a. A southern Indian Middle Palaeolithic occupation surface sealed by the 74 ka Toba eruption: further evidence from Jwalapuram Locality 22. *Quaternary International*, *258*, pp.148-164.

Haslam, M., Harris, C., Clarkson, C., Pal, J.N., Shipton, C., Crowther, A., Koshy, J., Bora, J., Ditchfield, P., Ram, H.P. and Price, K., 2012b. Dhaba: an initial report on an Acheulean, Middle Palaeolithic and microlithic locality in the Middle Son Valley, north-central India. *Quaternary International*, *258*, pp.191-199.

Haslam, M., Korisettar, R., Petraglia, M., Smith, T., Shipton, C. and Ditchfield, P., 2010b. In Foote's steps: the history, significance and recent archaeological investigation of the Billa Surgam Caves in southern India. *South Asian Studies*, *26*(1), pp.1-19.

Haslam, M., Roberts, R.G., Shipton, C., Pal, J.N., Fenwick, J.L., Ditchfield, P., Boivin, N., Dubey, A.K., Gupta, M.C. and Petraglia, M., 2011. Late Acheulean hominins at the Marine Isotope Stage 6/5e transition in north-central India. *Quaternary Research*, *75*(3), pp.670-682.

Hershkovitz, I., May, H., Sarig, R., Pokhojaev, A., Grimaud-Hervé, D., Bruner, E., Fornai, C., Quam, R., Arsuaga, J.L., Krenn, V.A. and Martinón-Torres, M., 2021. A middle pleistocene homo from Nesher Ramla, Israel. *Science*, *372*(6549), pp.1424-1428.

Hershkovitz, I., Weber, G.W., Quam, R., Duval, M., Grün, R., Kinsley, L., Ayalon, A., Bar-Matthews, M., Valladas, H., Mercier, N. and Arsuaga, J.L., 2018. The earliest modern humans outside Africa. *Science*, *359*(6374), pp.456-459.

Higgins, P. and MacFadden, B.J., 2004. “Amount Effect” recorded in oxygen isotopes of Late Glacial horse (Equus) and bison (Bison) teeth from the Sonoran and Chihuahuan

deserts, southwestern United States. *Palaeogeography, Palaeoclimatology, Palaeoecology*, *206*(3-4), pp.337-353.

Higham, T., Compton, T., Stringer, C., Jacobi, R., Shapiro, B., Trinkaus, E., Chandler, B., Gröning, F., Collins, C., Hillson, S. and O'Higgins, P., 2011. The earliest evidence for anatomically modern humans in northwestern Europe. *Nature*, *479*(7374), pp.521-524.

Högberg, A., 2016. A lithic attribute analysis on blades from the middle stone age site, hollow rock shelter, western Cape Province, South Africa. *Lithic Technology*, *41*(2), pp.93-113.

Hublin, J.J., 2009. The origin of Neandertals. *Proceedings of the National Academy of Sciences*, *106*(38), pp.16022-16027.

Hublin, J.J., Ben-Ncer, A., Bailey, S.E., Freidline, S.E., Neubauer, S., Skinner, M.M., Bergmann, I., Le Cabec, A., Benazzi, S., Harvati, K. and Gunz, P., 2017. New fossils from Jebel Irhoud, Morocco and the pan-African origin of Homo sapiens. *Nature*, *546*(7657), pp.289-292.

Hublin, J.J., Sirakov, N., Aldeias, V., Bailey, S., Bard, E., Delvigne, V., Endarova, E., Fagault, Y., Fewlass, H., Hajdinjak, M. and Kromer, B., 2020. Initial upper palaeolithic Homo sapiens from Bacho Kiro cave, Bulgaria. *Nature*, *581*(7808), pp.299-302.

Huntley, D.J. and Lamothe, M., 2001. Ubiquity of anomalous fading in K-feldspars and the measurement and correction for it in optical dating. *Canadian Journal of Earth Sciences*, *38*(7), pp.1093-1106.

Huntley, D.J., Godfrey-Smith, D.I. and Thewalt, M.L., 1985. Optical dating of sediments. *Nature*, *313*(5998), pp.105-107.

Hurcombe, L., 2004. The stone artefacts from the Pabbi Hills. *Early Hominin Landscapes in Northern Pakistan: Investigations in the Pabbi Hills. British Archaeological Reports International Series*, *1265*, pp.222-292.

Imbrie, J., Hays, J.D., Martinson, D.G., McIntyre, A., Mix, A.C., Morley, J.J., Pisias, N.G., Prell, W.L. and Shackleton, N.J., 1984. The orbital theory of Pleistocene climate: support from a revised chronology of the marine d18O record. in Berger, A. L. et al., (eds.), Milankovitch and Climate, Part I, D. Reidel Publication, pp. 269.

India Archaeological Review 1965-66, pp 8.

India State of Forest Report, Uttar Pradesh, Forest Survey of India (*Ministry of Environment, Forest and Climate Change*), 2021.

Indian Archaeology A Review – IAR 1956-57, pp. 48.

Indian Archaeology A Review – IAR 1962-63, pp. 33 and 37.

Indian Archaeology A Review – IAR 1977-78, pp. 56 and 58.

Indian Archaeology A Review – IAR 1980-81, pp. 73.

Indian Archaeology A Review – IAR 1982-83, pp. 145.

Indian Archaeology A Review – IAR 1985-86, pp 53.

Inizan, M.L., Reduron-Ballinger, M., Roche, H. and Tixier, J., 1999. Technology and terminology of knapped stone. *Crep, Nanterre*, p.189.

Isaac, G.L., 1972. Early phases of human behaviour: models in Lower Palaeolithic archaeology. *Models in archaeology*, pp.167-199.

Jacobs, Z., Jankowski, N.R., Dibble, H.L., Goldberg, P., McPherron, S.J., Sandgathe, D. and Soressi, M., 2016. The age of three Middle Palaeolithic sites: single-grain optically stimulated luminescence chronologies for Pech de l'Azé I, II and IV in France. *Journal of human evolution*, *95*, pp.80-103.

Jagtap, S. and Deo, S.G., 2016. Absolute Chronology of the Quaternary Period from the Deccan Trap region, Maharashtra. *Man and Environment*, *41*(1), pp.88-113.

Jain, M., Tandon, S.K., Singhvi, A.K., Mishra, S. and Bhatt, S.C., 2005. Quaternary alluvial stratigraphical development in a desert setting: a case study from the Luni River basin, Thar Desert of western India. *Fluvial Sedimentology VII, International Association of Sedimentologists. Special Publication*, *35*, pp.349-371.

James, H.A. and Petraglia, M., 2005. Modern human origins and the evolution of behavior in the later Pleistocene record of South Asia. *Current anthropology*, *46*(S5), pp.S3-S27.

Jamir, T., M. Mitri and T. Thakuria. (nd). *Rethinking Northeast Indian Prehistory: reappraisal to an old problem*. In Prof. K. Paddayya Festschrift, eds. V. Selvakumar, S.K. Aruni and H. Dave

Janssen, R., Joordens, J.C., Koutamanis, D.S., Puspaningrum, M.R., de Vos, J., Van Der Lubbe, J.H., Reijmer, J.J., Hampe, O. and Vonhof, H.B., 2016. Tooth enamel stable isotopes of Holocene and Pleistocene fossil fauna reveal glacial and interglacial paleoenvironments of hominins in Indonesia. *Quaternary Science Reviews*, *144*, pp.145-154.

Jayaswal, V., 1978. Palaeohistory of India:(a study of the prepared core technique). Agam Kala Prakashan, New Delhi.

Jha, D.K., Sanyal, P. and Philippe, A., 2020. Multi-proxy evidence of Late Quaternary climate and vegetational history of north-central India: Implication for the Paleolithic to Neolithic phases. *Quaternary Science Reviews*, *229*, p.106121.

John, S.K., 2018. Rainfall Pattern Analysis over India in Relation to the State of Kerala. *Engineering and Mathematical Topics in Rainfall*, p.17, IntechOpen.

Jones, S.C. and Pal, J.N., 2009. The Palaeolithic of the Middle Son valley, north-central India: changes in hominin lithic technology and behaviour during the Upper Pleistocene. *Journal of Anthropological Archaeology*, *28*(3), pp.323-341.

Jones, S.C., 2010. Palaeoenvironmental response to the∼ 74 ka Toba ash-fall in the Jurreru and Middle Son valleys in southern and north-central India. *Quaternary Research*, *73*(2), pp.336-350.

Jones, S.C., 2012. Local-and regional-scale impacts of the∼ 74 ka Toba supervolcanic eruption on hominin populations and habitats in India. *Quaternary International*, *258*, pp.100-118.

Jourdan, F., Moynier, F., Koeberl, C. and Eroglu, S., 2011. 40Ar/39Ar age of the Lonar crater and consequence for the geochronology of planetary impacts. *Geology*, *39*(7), pp.671-674.

Jouzel, J., Masson-Delmotte, V., Cattani, O., Dreyfus, G., Falourd, S., Hoffmann, G., Minster, B., Nouet, J., Barnola, J.M., Chappellaz, J. and Fischer, H., 2007. Orbital and

millennial Antarctic climate variability over the past 800,000 years. *science*, *317*(5839), pp.793-796.

Jukar, A.M., Lyons, S.K., Wagner, P.J. and Uhen, M.D., 2021. Late Quaternary extinctions in the Indian subcontinent. *Palaeogeography, Palaeoclimatology, Palaeoecology*, *562*, p.110137.

Jukar, A.M., Patnaik, R., Chauhan, P.R., Li, H.C. and Lin, J.P., 2019. The youngest occurrence of Hexaprotodon Falconer and Cautley, 1836 (Hippopotamidae, Mammalia) from South Asia with a discussion on its extinction. *Quaternary International*, *528*, pp.130-137.

Juyal, N., Chamyal, L.S., Bhandari, S., Bhushan, R. and Singhvi, A.K., 2006. Continental record of the southwest monsoon during the last 130 ka: evidence from the southern margin of the Thar Desert, India. *Quaternary Science Reviews*, *25*(19-20), pp.2632-2650.

Juyal, N., Kar, A., Rajaguru, S.N. and Singhvi, A.K., 2003. Luminescence chronology of aeolian deposition during the Late Quaternary on the southern margin of Thar Desert, India. *Quaternary International*, *104*(1), pp.87-98.

Juyal, N., Pant, R.K., Basavaiah, N., Yadava, M.G., Saini, N.K. and Singhvi, A.K., 2004. Climate and seismicity in the higher Central Himalaya during 20–10 ka: evidence from the Garbayang basin, Uttaranchal, India. *Palaeogeography, Palaeoclimatology, Palaeoecology*, *213*(3-4), pp.315-330.

Juyal, N., Raj, R., Maurya, D.M., Chamyal, L.S. and Singhvi, A.K., 2000. Chronology of Late Pleistocene environmental changes in the lower Mahi basin, western India. *Journal of Quaternary Science: Published for the Quaternary Research Association*, *15*(5), pp.501-508.

Kaifu, Y., Izuho, M. and Goebel, T., 2015. Modern human dispersal and behavior in Paleolithic Asia. *Emergence and diversity of modern human behavior in Paleolithic Asia*, pp.535-566.

Kajale M.D. 1979. Bioarchaeology of the Ghod Valley, Maharashtra. Unpublished Ph.D. thesis, Pune: University of Poona.

Kajale, M.D. and Rajaguru, S.N., 1989. A Preliminary Palynological study of Alluvial sediments around Nirgudsar in the Ghod Valley, Upland Maharashtra. *Man and Environment*, *14*(1), pp.117-121.

Kale, M.G., Pundalik, A.S. and Kumar, D., 2020. Fluvial facies and petrography of Late Pleistocene Baneta sediments, Central Narmada Basin, Madhya Pradesh, India. *Journal of Earth System Science*, *129*(1), pp.1-24.

Kale, V.S. and Rajaguru, S.N., 1987. Late Quaternary alluvial history of the northwestern Deccan upland region. *Nature*, *325*(6105), pp.612-614.

Kale, V.S., 2014. Geomorphic history and landscapes of India. In *Landscapes and landforms of India* (pp. 25-37). Springer, Dordrecht.

Kale, V.S., Mishra, S. and Baker, V.R., 2003. Sedimentary records of palaeofloods in the bedrock gorges of the Tapi and Narmada rivers, central India. *Current Science*, pp.1072-1079.

Kalwankar, C. 2013. Stable Isotopes and Bovine Taxonomy. Unpublished M.A. dissertation. Deccan College.

Kar, A., Singhvi, A.K., Rajaguru, S.N., Juyal, N., Thomas, J.V., Banerjee, D. and Dhir, R.P., 2001. Reconstruction of the late Quaternary environment of the lower Luni plains, Thar Desert, India. *Journal of Quaternary Science: Published for the Quaternary Research Association*, *16*(1), pp.61-68.

Kar, R. and Quamar, M.F., 2020. Late Pleistocene-Holocene vegetation and climate change from the Western and Eastern Himalaya (India): palynological perspective. *Current Science*, *119*(2), pp.195-218.

Kathayat, G., Cheng, H., Sinha, A., Spötl, C., Edwards, R.L., Zhang, H., Li, X., Yi, L., Ning, Y., Cai, Y. and Lui, W.L., 2016. Indian monsoon variability on millennial-orbital timescales. *Scientific reports*, *6*(1), pp.1-7.

Katupotha, K.N.J. 2012. Palaeoenvironmental Evidence in Northwest Sri Lanka: Evidence from Mundal Lake and its Environs. *National Conference on Palaeobiodiversity*, pp. 98-109.

Kelkar, R.R., 2009. Monsoon prediction. *BS Publications*, Hyderabad.

Kelly, R.L., 1988. The three sides of a biface. *American antiquity*, *53*(4), pp.717-734.

Kennedy, K.A. and Deraniyagala, S.U., 1989. Fossil remains of 28,000-year-old hominids from Sri Lanka. *Current Anthropology*, *30*(3), pp.394-399.

Kennedy, K.A., 1999. Paleoanthropology of south Asia. *Evolutionary Anthropology: Issues, News, and Reviews: Issues, News, and Reviews*, *8*(5), pp.165-185.

Kennedy, K.A., 2000. *God-apes and fossil men: Paleoanthropology of South Asia*. Ann Arbor: University of Michigan Press.

Kennedy, K.A., Deraniyagala, S.U., Roertgen, W.J., Chiment, J. and Disotell, T., 1987. Upper pleistocene fossil hominids from Sri Lanka. *American Journal of Physical Anthropology*, *72*(4), pp.441-461.

Kenoyer, J.M., 1983. An upper palaeolithic shrine in India? *Antiquity*, *57*(220), p.88.

Kenoyer, J.M., Mandal, D., Misra, V.D. and Pal, J.N., 1983. Preliminary report on excavations at the late Palaeolithic occupation site at Baghor I locality. *Palaeoenvironments and Prehistory in the Middle Son Valley. Abinash Prakashan, Allahabad*, pp.117-142.

Kenoyer, M. and Pal, J.N., 1983. Report on the excavation and analysis of an Upper Acheulean assemblage from Sihawal II. *Palaeoenvironments and Prehistory in the Middle Son Valley. Abinash Prakashan, Allahabad*, pp.23-38.

Key, A.J., Jarić, I. and Roberts, D.L., 2021. Modelling the end of the Acheulean at global and continental levels suggests widespread persistence into the Middle Palaeolithic. *Humanities and Social Sciences Communications*, *8*(1), pp.1-12.

Khadkikar, A.S. and Basavaiah, N., 2004. Morphology, mineralogy and magnetic susceptibility of epikarst-Terra Rossa developed in late Quaternary aeolianite deposits of southeastern Saurashtra, India. *Geomorphology*, *58*(1-4), pp.339-355.

Khadkikar, A.S., Chamyal, L.S. and Ramesh, R., 2000. The character and genesis of calcrete in Late Quaternary alluvial deposits, Gujarat, western India, and its bearing on

the interpretation of ancient climates. *Palaeogeography, Palaeoclimatology, Palaeoecology*, *162*(3-4), pp.239-261.

Khan, I., Trivedi, A., Ali, S.N., Bali, R., Sangode, S.J. and Deepak, O., 2022. Late Pleistocene-Holocene vegetation and climate variability of the western Himalaya, India. *Journal of Asian Earth Sciences*, *233*, p.105245.

Khonde, N.N., Maurya, D.M. and Chamyal, L.S., 2017. Late Pleistocene–Holocene clay mineral record from the Great Rann of Kachchh basin, Western India: implications for palaeoenvironments and sediment sources. *Quaternary International*, *443*, pp.86-98.

Kim, B.Y. and Lohmueller, K.E., 2015. Selection and reduced population size cannot explain higher amounts of Neandertal ancestry in East Asian than in European human populations. *The American Journal of Human Genetics*, *96*(3), pp.454-461.

Kimbel, W.H., Johanson, D.C. and Rak, Y., 1997. Systematic assessment of a maxilla of Homo from Hadar, Ethiopia. *American Journal of Physical Anthropology: The Official Publication of the American Association of Physical Anthropologists*, *103*(2), pp.235-262.

Klein, R.G., 2008. Out of Africa and the evolution of human behavior. *Evolutionary Anthropology: Issues, news, and reviews*, *17*(6), pp.267-281.

Kohn, M.J., 1996. Predicting animal d18O: accounting for diet and physiological adaptation. *Geochem. Cosmochim. Acta* 60, 3889e3896.

Kohn, M.J., 2010. Carbon isotope compositions of terrestrial C3 plants as indicators of (paleo) ecology and (paleo) climate. *Proceedings of the National Academy of Sciences*, *107*(46), pp.19691-19695.

Kohn, M.J., Schoeninger, M.J. and Valley, J.W., 1996. Herbivore tooth oxygen isotope compositions: effects of diet and physiology. *Geochimica et Cosmochimica Acta*, *60*(20), pp.3889-3896.

Kolbert, E., 2014. *The sixth extinction: An unnatural history*. A&C Black

Korisettar, R. 2014. Antiquity of Modern Humans and Behavioral Modernity in the Indian Subcontinent. Emergence and Diversity of Modern Human Behavior in Paleolithic

Asia. *Modern Humans: Their African Origin and Global Dispersal*, pp.80-93. New York: Columbia University Press.

Kotlia, B.S. and Joshi, M., 2011. Taphonomy of Late Pleistocene micromammalian fauna of Narmada valley, Central India. *Palaeoworld*, *20*(1), pp.84-91.

Kotlia, B.S., Bhalla, M.S., Sharma, C., Rajagopalan, G., Ramesh, R., Chauhan, M.S., Mathur, P.D., Bhandari, S. and Chacko, S.T., 1997. Palaeoclimatic conditions in the upper Pleistocene and Holocene Bhimtal-Naukuchiatal lake basin in south-central Kumaun, North India. *Palaeogeography, Palaeoclimatology, Palaeoecology*, *130*(1-4), pp.307-322.

Kotlia, B.S., Hinz-Schallreuter, I., Schallreuter, R. and Schwarz, J., 1998. Evolution of Lamayuru palaeolake in the Trans Himalaya: palaeoecological implications. *E&G Quaternary Science Journal*, *48*(1), pp.177-191.

Kotlia, B.S., Singh, A.K., Joshi, L.M. and Dhaila, B.S., 2015. Precipitation variability in the Indian Central Himalaya during last ca. 4,000 years inferred from a speleothem record: Impact of Indian Summer Monsoon (ISM) and Westerlies. *Quaternary International*, *371*, pp.244-253.

Krause, J., Fu, Q., Good, J.M., Viola, B., Shunkov, M.V., Derevianko, A.P. and Pääbo, S., 2010. The complete mitochondrial DNA genome of an unknown hominin from southern Siberia. *Nature*, *464*(7290), pp.894-897.

Krings, M., Stone, A., Schmitz, R.W., Krainitzki, H., Stoneking, M. and Pääbo, S., 1997. Neandertal DNA sequences and the origin of modern humans. *cell*, *90*(1), pp.19-30.

Kroon, D. and Ganssen, G., 1989. Northern Indian Ocean upwelling cells and the stable isotope composition of living planktonic foraminifers. *Deep Sea Research Part A. Oceanographic Research Papers*, *36*(8), pp.1219-1236.

Kukla, G.J., 2000. The last interglacial. *Science*, *287*(5455), pp.987-988.

Kumar, B., Venkatesh, M. and Triphati, A., 2018. A GIS-based approach in drainage morphometric analysis of Rihand River Basin, Central India. *Sustainable Water Resources Management*, *4*(1), pp.45-54.

Kumar, M., Saikia, K., Agrawal, S., Ghosh, R., Ali, S.N., Arif, M., Singh, D.S., Sharma, A., Phartiyal, B. and Bajpai, S., 2022. Climatic control on the C3 and C4 plant abundance during the late Pleistocene–Holocene in the northern Gangetic Plain, India. *Palaeogeography, Palaeoclimatology, Palaeoecology*, *591*, p.110890.

Kumar, O., Devrani, R. and Ramanathan, A.L., 2017. Deciphering the past climate and monsoon variability from lake sediment archives of India: a review. *Journal of Climate Change*, *3*(2), pp.11-23.

Kumar, S. and Sharma, M., 2012. *Vindhyan Basin, Son Valley Area Central India*. Palaeontological Society of India.

Lal, R., Padhan, T., Jangra, B., Chauhan, P.R., Sahu, S. and Patnaik, R., 2023. New field observations on the Quaternary geology and vertebrate palaeontological occurrences in the Narsinghpur region of Narmada valley (central India). *Geological Society, London, Special Publications*, *515*(1), pp.SP515-2020.

Lambeck, K., Esat, T.M. and Potter, E.K., 2002. Links between climate and sea levels for the past three million years. *Nature*, *419*(6903), pp.199-206.

Langgut, D., Almogi-Labin, A., Bar-Matthews, M., Pickarski, N. and Weinstein-Evron, M., 2018. Evidence for a humid interval at∼ 56–44 ka in the Levant and its potential link to modern humans dispersal out of Africa. *Journal of Human Evolution*, *124*, pp.75-90.

Langley, M.C., Amano, N., Wedage, O., Deraniyagala, S., Pathmalal, M.M., Perera, N., Boivin, N., Petraglia, M.D. and Roberts, P., 2020. Bows and arrows and complex symbolic displays 48,000 years ago in the South Asian tropics. *Science Advances*, *6*(24), p.eaba3831.

Laskar, A.H. and Bohra, A., 2021. Impact of indian summer monsoon change on ancient indian civilizations during the holocene. *Frontiers in Earth Science*, *9*, p.709455.

Laskar, A.H., Sharma, N., Ramesh, R., Jani, R.A. and Yadava, M.G., 2010. Paleoclimate and paleovegetation of Lower Narmada Basin, Gujarat, Western India, inferred from stable carbon and oxygen isotopes. *Quaternary International*, *227*(2), pp.183-189.

Law, Y.D., 1954. Contributions to the geology of Son Valley in Vindhya Pradesh. *The Quarterly Journal of the Geological, Mining and Metallurgical Society of India*, *26*(2), pp.65-79.

Lee, H.W., 2013. The persistence of Mode 1 technology in the Korean Late Paleolithic. *Plos one*, 8(5), p.e64999.

Lee-Thorp, J.A., Sealy, J.C. and Van Der Merwe, N.J., 1989. Stable carbon isotope ratio differences between bone collagen and bone apatite, and their relationship to diet. *Journal of archaeological science*, *16*(6), pp.585-599.

Levin, N.E., Cerling, T.E., Passey, B.H., Harris, J.M. and Ehleringer, J.R., 2006. A stable isotope aridity index for terrestrial environments. *Proceedings of the National Academy of Sciences*, *103*(30), pp.11201-11205.

Lewis, L. Early microlithic technologies and behavioural variability in Southern Africa and South Asia. Ph.D. thesis, University of Oxford.

Lewis, L., Perera, N. and Petraglia, M., 2014. First technological comparison of Southern African Howiesons Poort and South Asian Microlithic industries: An exploration of inter-regional variability in microlithic assemblages. *Quaternary International*, *350*, pp.7-25.

Li, H., Li, Z.Y., Gao, X., Kuman, K. and Sumner, A., 2019. Technological behavior of the early Late Pleistocene archaic humans at Lingjing (Xuchang, China). *Archaeological and Anthropological Sciences*, 11, pp.3477-3490.

Li, Y., Zhou, Y., Sun, X. and Li, H., 2018. New evidence of a lithic assemblage containing in situ Late Pleistocene bifaces from the Houfang site in the Hanshui River Valley, Central China. *Comptes Rendus Palevol*, 17(1-2), pp.131-142.

Liu, S., Krijgsman, W., Dekkers, M.J. and Palcu, D., 2017. Early diagenetic greigite as an indicator of paleosalinity changes in the middle M iocene P aratethys S ea of central E urope. *Geochemistry, Geophysics, Geosystems*, *18*(7), pp.2634-2645.

Liu, W., Jin, C.Z., Zhang, Y.Q., Cai, Y.J., Xing, S., Wu, X.J., Cheng, H., Edwards, R.L., Pan, W.S., Qin, D.G. and An, Z.S., 2010. Human remains from Zhirendong, South China, and modern human emergence in East Asia. *Proceedings of the National Academy of Sciences*, *107*(45), pp.19201-19206.

Liu, W., Martinón-Torres, M., Cai, Y.J., Xing, S., Tong, H.W., Pei, S.W., Sier, M.J., Wu, X.H., Edwards, R.L., Cheng, H. and Li, Y.Y., 2015. The earliest unequivocally modern humans in southern China. *Nature*, *526*(7575), pp.696-699.

Lombard, M., 2012. Thinking through the Middle Stone Age of sub-Saharan Africa. *Quaternary International*, *270*, pp.140-155.

Longinelli, A., 1984. Oxygen isotopes in mammal bone phosphate: a new tool for paleohydrological and paleoclimatological research. *Geochimica et cosmochimica Acta*, *48*(2), pp.385-390.

López Laseras, P., Navarro, E., Marce Romero, R., Ordóñez Salinas, J., Caputo Galarce, L. and Armengol, J., 2006. Elemental ratios in sediments as indicators of ecological processes in Spanish reservoirs. *Limnetica*, *25*(1-2), pp.499-512.

Lorius, C., Jouzel, J., Ritz, C., Merlivat, L., Barkov, N.I., Korotkevich, Y.S. and Kotlyakov, V.M., 1985. A 150,000-year climatic record from Antarctic ice. *nature*, *316*(6029), pp.591-596.

Luz, B. and Kolodny, Y., 1985. Oxygen isotope variations in phosphate of biogenic apatites, IV. Mammal teeth and bones. *Earth and planetary science letters*, *75*(1), pp.29-36.

Luz, B., Kolodny, Y. and Horowitz, M., 1984. Fractionation of oxygen isotopes between mammalian bone-phosphate and environmental drinking water. *Geochimica et Cosmochimica Acta*, *48*(8), pp.1689-1693.

Macaulay, V., Hill, C., Achilli, A., Rengo, C., Clarke, D., Meehan, W., Blackburn, J., Semino, O., Scozzari, R., Cruciani, F. and Taha, A., 2005. Single, rapid coastal settlement of Asia revealed by analysis of complete mitochondrial genomes. *Science*, *308*(5724), pp.1034-1036.

Mackay, A., 2008. On the production of blades and its relationship to backed artefacts in the Howiesons Poort at Diepkloof, South Africa. *Lithic Technology*, *33*(1), pp.87-99.

Maharana, C. and Tripathi, J.K. 2018. The Son, A Vindhyan River. 191–197, https://doi.org/10.1007/978-981-10-2984-4_15.

Malaspinas, A.S., Westaway, M.C., Muller, C., Sousa, V.C., Lao, O., Alves, I., Bergström, A., Athanasiadis, G., Cheng, J.Y., Crawford, J.E. and Heupink, T.H., 2016. A genomic history of Aboriginal Australia. *Nature*, *538*(7624), pp.207-214.

Mallick, S., Li, H., Lipson, M., Mathieson, I., Gymrek, M., Racimo, F., Zhao, M., Chennagiri, N., Nordenfelt, S., Tandon, A. and Skoglund, P., 2016. The Simons genome diversity project: 300 genomes from 142 diverse populations. *Nature*, *538*(7624), pp.201-206.

Martin, P. S., 1984. Catastrophic extinctions and Late Pleistocene blitzkrieg: Two radiocarbon tests. In Extinctions, ed. M. H. Niteki. Chicago University Press, Chicago, pp. 153-89.

Martin, P.S., 2005. Twilight of the mammoths: Ice Age extinctions and the rewilding of America (Vol. 8). University of California Press.

Maya, K., Limaye, R.B., Padmalal, D. and Kumaran, N.K., 2017. Geomorphic response to sea level and climate changes during Late Quaternary in a humid tropical coastline: Terrain evolution model from Southwest India. *PloS one*, *12*(5), p.e0176775.

McCall, G.S., 2007. Behavioral ecological models of lithic technological change during the later Middle Stone Age of South Africa. *Journal of Archaeological Science*, *34*(10), pp.1738-1751.

McLaren, S.J., Leng, M.J., Knowles, T. and Bradley, A.V., 2012. Evidence of past environmental conditions during the evolution of a calcretised Wadi System in Southern Jordan using stable isotopes. *Palaeogeography, Palaeoclimatology, Palaeoecology*, *348*, pp.1-12.

Mehra, S.B., 2022. Doma: a new multi-technological lithic occurrence in the Lower Son Valley (north-central India) and its regional context. *Geological Society, London, Special Publications*, *515*(1), pp.SP515-2020.

Mehra, S.B., and Chauhan, P.R., 2021. Late Pleistocene Environments of South Asia: A Review of Multidisciplinary Research and Relevance for Understanding Hominin Environmental Adaptations *Man and Environment*, XLVI(1): pp13-44.

Mehrotra, M. and Banerjee, R., 1983. A study of the Son Porcellanite Formation (lower Vindhyan) around Kunjhur, District Sidhi, Madhya Pradesh. *Bulletin of Geological Assosiation*, *16*, pp. 13–20.

Mehrotra, N.C., Pal, D., and Srivastava, R.K., 1979. Aspects and Prospects of Palynology in Solving the Quaternary Geology Problems of Himalaya with Special Reference to the Karewa Sediments of Kashmir Valley. *Himalyan Geology* 9(1), pp. 371-384.

Mellars, P., 2006. Going east: new genetic and archaeological perspectives on the modern human colonization of Eurasia. *Science*, *313*(5788), pp.796-800.

Mellars, P., Gori, K.C., Carr, M., Soares, P.A. and Richards, M.B., 2013. Genetic and archaeological perspectives on the initial modern human colonization of southern Asia. *Proceedings of the National Academy of Sciences*, *110*(26), pp.10699-10704.

Mendaly, S. and Hussain, S., 2015. Microlithic Industry of Odisha with Particular Reference to Bhalugarh, District-Jharsuguda, Odisha: A Preliminary Report. *Heritage: Journal of Multidisciplinary Studies in Archaeology*, *3*, pp.346-369.

Merh, S.S. and Chamyal, L.S., 1993. The quaternary sediments in Gujarat. *Current Science*, pp.823-827.

Michel, V., Shen, G., Valensi, P. and de Lumley, H., 2009. ESR dating of dental enamel from Middle Palaeolithic levels at Lazaret Cave, France. *Quaternary Geochronology*, 4(3), pp.233-240.

Michel, V., Valladas, H., Shen, G., Wang, W., Zhao, J.X., Shen, C.C., Valensi, P. and Bae, C.J., 2016. The earliest modern Homo sapiens in China. *Journal of Human Evolution*, *101*(10), p.1e104.

Mijares, A.S., Détroit, F., Piper, P., Grün, R., Bellwood, P., Aubert, M., Champion, G., Cuevas, N., De Leon, A. and Dizon, E., 2010. New evidence for a 67,000-year-old human presence at Callao Cave, Luzon, Philippines. *Journal of human evolution*, *59*(1), pp.123-132.

Miller, A.V., Fernandes, R., Janzen, A., Nayak, A., Swift, J., Zech, J., Boivin, N. and Roberts, P., 2018. Sampling and pretreatment of tooth enamel carbonate for stable carbon and oxygen isotope analysis. *JoVE (Journal of Visualized Experiments)*, (138), p.e58002.

Minyuk, P.S., Brigham-Grette, J., Melles, M., Borkhodoev, V.Y. and Glushkova, O.Y., 2007. Inorganic geochemistry of El'gygytgyn Lake sediments (northeastern Russia) as an indicator of paleoclimatic change for the last 250 kyr. *Journal of Paleolimnology*, *37*(1), pp.123-133.

Mishra, M., Srivastava, V. and Srivastava, H.B., 2017. A report on the occurrence of ferruginous breccia in Chopan porcellanite formation from Semri group, Sonbhadra district (UP). *Journal of Scientific Research. Banaras Hindu University*, *61*, pp.1-11.

Mishra, P., Pradhan, U.K., Panda, U.S., Patra, S.K., RamanaMurthy, M.V., Seth, B. and Mohanty, P.K., 2014. Field measurements and numerical modeling of nearshore processes at an open coast port on the east coast of India. *Indian Journal of Geo-Marine Sciences 43(7),* pp 1272 – 1280.

Mishra, P.K., Anoop, A., Jehangir, A., Prasad, S., Menzel, P., Schettler, G., Naumann, R., Weise, S., Andersen, N., Yousuf, A.R. and Gaye, B., 2014. Limnology and modern sedimentation patterns in high altitude Tso Moriri Lake, NW Himalaya–implications for proxy development. *Fundamental and Applied Limnology*, *185*(3-4), pp.329-348.

Mishra, P.K., Parth, S., Ankit, Y., Kumar, S., Ambili, V., Kumar, V.V., Singh, S. and Anoop, A., 2019. Geochemical and sedimentological characteristics of surface sediments from Ashtamudi Estuary, Southern India: implications for provenance and modern sedimentary dynamics. *Environmental Earth Sciences*, *78*(14), pp.1-11.

Mishra, S., and Rajaguru, S.N., 2001. Late Quaternary Palaeoclimates of Western India: A Geoarchaeological Approach. *Mausam* 52, pp. 285-296.

Mishra, S., Chauhan, N. and Singhvi, A.K., 2013. Continuity of microblade technology in the Indian Subcontinent since 45 ka: implications for the dispersal of modern humans. *PLoS One*, *8*(7), p.e69280.

Mishra, S., Deo, S., Sangode, S., Chen, C.H., Abbas, R. and Naik, S., 2005. Hominid response to the catastrophic OTT eruption at Bori and Morgaon in Western India. In *International Symposium on Migration and Evolution of Early Humans in the Old World. Bose, Guangxi Zhuang Autonomous Region, China*.

Mishra, S., Gaillard, C., Deo, S., Singh, M., Abbas, R. and Agrawal, N., 2010. Large Flake Acheulian in India: Implications for understanding lower Pleistocene human dispersals. *Quaternary International*, *223*(224), pp.271-272.

Mishra, S., Naik, S., Rajaguru, S.N., Deo, S. and Ghate, S., 2003. Fluvial Response to Late Quaternary Climatic Change: Case Studies from Upland Western India. *Proceedings of Indian National Science Academy* 69(2), pp. 185-200.

Mishra, V. D., 2002. Mesolithic Culture in India. in (eds.Misra, V. D. and Pal, J. N.). *Mesolithic India*. Department of ancient history, culture and archaeology. University of Allahabad

Misra, O.P., 2003. *Archaeological Excavations in Central India: Madhya Pradesh and Chhattisgarh*. Mittal Publications.

Misra, V.D., 1977. Some aspects of Indian archaeology. pp 45

Misra, V.D., Rana, R.S., Clark, J.D., Blumenschine, R.J. and Sharma, G.R., 1983. Preliminary excavations at the Son River section at Nakjhar Khurd. *Palaeoenvironments and Prehistory in the Middle Son Valley. Abinash Prakashan, Allahabad*, pp.101-115.

Misra, V.N. and Kanungo, A.K., 2019. *The Mesolithic Age in South Asia: Tradition and Transition*. Aryan Books International.

Misra, V.N. and Rajaguru, S.N., 1978. The Acheulian Industry of Rock Shelter IIIF-23 at Bhimbetka, Central India-A Preliminary Study1. *Australian Archaeology*, *8*(1), pp.63-106.

Misra, V.N., 1968. Middle Stone Age in Rajasthan. La Préhistoire, Problèmes et Tendancies. Paris: Centre National de la Recherché Scientifique, pp.295-305.

Misra, V.N., 1982. Evolution of the blade element in the stone industries of the rock shelter III F-23, Bhimbetka. *Indian Archaeology, New Perspectives*, pp.7-13.

Misra, V.N., 1985. The Acheulian succession at Bhimbetka, Central India. *Recent advances in Indo-Pacific prehistory (New Delhi 1985)*, pp.35-47.

Misra, V.N., 1987. Evolution of the landscape and human adaptations in the Thar desert, Presidential Address (Anthropology and Archaeology Section). In *74th Session of the Indian Science Congress. Calcutta*.

Misra, V.N., 1989. Stone Age India: an ecological perspective. *Man and Environment*, *14*(1), pp.17-64.

Misra, V.N., 2001. Prehistoric human colonization of India. *Journal of Biosciences*, *26*(4), pp.491-531.

Misra, V.N., 2002. The Mesolithic Age in India. *Indian archaeology in retrospect*, *1*, pp.111-126.

Mondal, M., Casals, F., Xu, T., Dall'Olio, G.M., Pybus, M., Netea, M.G., Comas, D., Laayouni, H., Li, Q., Majumder, P.P. and Bertranpetit, J., 2016. Genomic analysis of Andamanese provides insights into ancient human migration into Asia and adaptation. *Nature Genetics*, *48*(9), pp.1066-1070.

Morwood, M.J., Soejono, R.P., Roberts, R.G., Sutikna, T., Turney, C.S., Westaway, K.E., Rink, W.J., Zhao, J.X., Van Den Bergh, G.D., Due, R.A. and Hobbs, D.R., 2004. Archaeology and age of a new hominin from Flores in eastern Indonesia. *Nature*, *431*(7012), pp.1087-1091.

Mosimann, J.E. and Martin, P.S., 1975. Simulating overkill by Paleoindians: did man hunt the giant mammals of the New World to extinction? Mathematical models show that the hypothesis is feasible. *American Scientist*, *63*(3), pp.304-313.

Murali, R., Murthy, C.N. and Chamyal, L.S., 2012. Characterization of colloids in the late Quaternary sediment sequences of Mahi river basin, Gujarat, India. *Current Science*, pp.1209-1215.

Murata, F., Hayashi, T., Matsumoto, J. and Asada, H., 2007. Rainfall on the Meghalaya plateau in northeastern India—one of the rainiest places in the world. *Natural Hazards*, *42*(2), pp.391-399.

Murty, M. L. K. Stone Age Cultures of Chittoor District, Andhra Pradesh (University of Poona, Pune, 1966).

Murty, M.L.K., 1969, February. Blade and burin industries near Renigunta on the South-East Coast of India. In Proceedings of the Prehistoric Society (Vol. 34, pp. 83-101). Cambridge University Press.

Murty, M.L.K., 1970. Blade-and-Burin and Late Stone Age industries around Renigunta, Chitoor District. Studies in Indian Archaeology. Professor HD Sankalia Felicitation Volume, pp.106-128.

Murty, M.L.K., 1979. Recent research on the Upper Palaeolithic phase in India. *Journal of Field Archaeology*, *6*(3), pp.301-320.

Nag, D. and Phartiyal, B., 2015. Climatic variations and geomorphology of the Indus River valley, between Nimo and Batalik, Ladakh (NW trans Himalayas) during late quaternary. *Quaternary International*, *371*, pp.87-101.

Narain, A. K., & Pant, P. C. A Summary Account of Archaeological Explorations in East UP 1962-63', Bharati. *Bulletin of the College of Indology, Banaras Hindu University*, (8 Part I), 1964-65.

Nesbitt, H. and Young, G.M., 1982. Early Proterozoic climates and plate motions inferred from major element chemistry of lutites. *nature*, *299*(5885), pp.715-717.

Nesbitt, H.W. and Young, G.M., 1989. Formation and diagenesis of weathering profiles. *The Journal of Geology*, *97*(2), pp.129-147.

Newbold, T.J., 1844. Notes on the osseous breccia and deposit in the caves of Billa Soorgum, Lat 15◦ 25', Long 78◦ 15', southern India. *Journal of the Asiatic Society of Bengal*, *13*(2), pp.610-15.

Ni, X., Ji, Q., Wu, W., Shao, Q., Ji, Y., Zhang, C., Liang, L., Ge, J., Guo, Z., Li, J. and Li, Q., 2021. Massive cranium from Harbin in northeastern China establishes a new Middle Pleistocene human lineage. *The Innovation*, *2*(3), p.100130.

Nicholson, S.L., Hosfield, R., Groucutt, H.S., Pike, A.W., Burns, S.J., Matter, A. and Fleitmann, D., 2022. A climatic evaluation of the southern dispersal route during MIS 5e. *Quaternary Science Reviews*, *279*, p.107378.

Nisha, N.R. and Singh, A.D., 2012. Benthic foraminiferal biofacies on the shelf and upper continental slope off North Kerala (Southwest India). *Journal of the Geological Society of India*, *80*(6), pp.783-801.

Norton, C.J. and Jin, J.J., 2009. The evolution of modern human behavior in East Asia: current perspectives. *Evolutionary Anthropology: Issues, News, and Reviews: Issues, News, and Reviews*, *18*(6), pp.247-260.

Nowell, A., 2010. Defining behavioral modernity in the context of Neandertal and anatomically modern human populations. *Annual review of anthropology*, *39*, pp.437-452.

O'Leary, M.H., 1988. Carbon isotopes in photosynthesis. *Bioscience*, *38*(5), pp.328-336.

Oppenheimer, S., 2003. Out of Eden: The Peopling of the World. Constable, London (revised paperback edition 2004a).

Oppenheimer, S., 2009. The great arc of dispersal of modern humans: Africa to Australia. *Quaternary International*, *202*(1-2), pp.2-13.

Oppenheimer, S., 2012. A single southern exit of modern humans from Africa: Before or after Toba? *Quaternary International*, *258*, pp.88-99.

Osborne, C.P., 2008. Atmosphere, ecology and evolution: what drove the Miocene expansion of C4 grasslands? *Journal of Ecology*, *96*(1), pp.35-45.

O'Shea, N. and Delson, E., 2018. The Origin of Us Archaeological and fossil finds shed light on the emergence and spread of modern humans. *Natural History*, *126*(8), pp.19-22.

Overpeck, J., Anderson, D., Trumbore, S. and Prell, W., 1996. The southwest Indian Monsoon over the last 18 000 years. *Climate Dynamics*, *12*(3), pp.213-225.

Owen, L.A., Bailey, R.M., Rhodes, E.J., Mitchell, W.A. and Coxon, P., 1997. Style and timing of glaciation in the Lahul Himalaya, northern India: a framework for reconstructing late Quaternary palaeoclimatic change in the western Himalayas. *Journal of Quaternary Science: Published for the Quaternary Research Association*, *12*(2), pp.83-109.

Paddayya, K., 1982. in Transition from Lower to Middle Palaeolithic and the Origin of Modern Man (ed. Ronen, A.) 257–264 (BAR).

Pagani, L., Lawson, D.J., Jagoda, E., Mörseburg, A., Eriksson, A., Mitt, M., Clemente, F., Hudjashov, G., DeGiorgio, M., Saag, L. and Wall, J.D., 2016. Genomic analyses inform on migration events during the peopling of Eurasia. *Nature*, *538*(7624), pp.238-242.

Pal, D.K., Bhattacharyya, T., Sinha, R., Srivastava, P., Dasgupta, A.S., Chandran, P., Ray, S.K. and Nimje, A., 2012. Clay minerals record from Late Quaternary drill cores of the Ganga Plains and their implications for provenance and climate change in the Himalayan Foreland. *Palaeogeography, Palaeoclimatology, Palaeoecology*, *356*, pp.27-37.

Pal, J.N., 2002. The Middle Palaeolithic Culture of South Asia. In *Indian Archaeology in Retrospect- Archaeology and Interactive Disciplines (Volume 1)*, edited by S. Settar and R. Korisettar, pp. 67–83. Manohar and Indian Council of Historical Research, New Delhi.

Pal, J.N., Williams, M.A.J., Jaiswal, M. and Singhvi, A.K., 2005. Infra red stimulated luminescence ages for prehistoric cultures in the Son and Belan valleys, north central India. *Journal of Interdisciplinary Studies in History and Archaeology*, *1*, pp.51-62.

Pandarinath, K., Prasad, S. and Gupta, S.K., 1999. A 75 ka record of palaeoclimatic changes inferred from crystallinity index of Illite from Nal Sarovar, western India. *Journal of the Geological Society of India*, *54*(5), pp.515-522.

Pandey, A.K., Pandey, P., Singh, G.D. and Juyal, N., 2014. Climate footprints in the Late Quaternary–Holocene landforms of Dun Valley, NW Himalaya, India. *Current Science*, pp.245-253.

Pandey, J.N. and Pal, J.N., 1988. Acheulian occupation at Maihar. *Man and Environment*, *12*(20), pp.1-202.

Pant, P.C. and Jayaswal, V., 1991. *Paisra, the Stone Age Settlement of Bihar*. Agam Kala Prakashan.

Pant, P.C., 1982. *Prehistoric Uttar Pradesh: A Study of Old Stone Age*. Agam Kala Prakashan.

Pappu, R.S., 2001. *Acheulian culture in peninsular India: an ecological perspective*. DK Printworld.

Pappu, S., Gunnell, Y., Akhilesh, K., Braucher, R., Taieb, M., Demory, F. and Thouveny, N., 2011. Early Pleistocene presence of Acheulian hominins in south India. *science*, *331*(6024), pp.1596-1599.

Patnaik, R., 1995. Narmada Valley microvertebrates: systematics, taphonomy and palaeoecology. *Man and Environment*, *20*(2), pp.75-90.

Patnaik, R., Chauhan, P.R., Rao, M.R., Blackwell, B.A., Skinner, A.R., Sahni, A., Chauhan, M.S. and Khan, H.S., 2009. New geochronological, paleoclimatological, and archaeological data from the Narmada Valley hominin locality, central India. *Journal of Human Evolution*, *56*(2), pp.114-133.

Patnaik, R., Li, H.C., Lin, J.P., Bansal, M. and Chauhan, P.R., 2019. Microlithic, faunal, floral and isotopic data from an archaeological site 14C dated to LGM in the eastern state of Odisha, India. *Quaternary International*, *528*, pp.138-146.

Peregrine, P.N., 2018. Sampling theory. *The Encyclopedia of Archaeological Sciences*, pp.1-3.

Perera, H.N., 2010. Prehistoric Sri Lanka: Late Pleistocene Rockshelters and an Open Air Site. BAR International Series. Archaeopress, Oxford.

Perera, N., Kourampas, N., Simpson, I.A., Deraniyagala, S.U., Bulbeck, D., Kamminga, J., Perera, J., Fuller, D.Q., Szabó, K. and Oliveira, N.V., 2011. People of the ancient rainforest: Late Pleistocene foragers at the Batadomba-lena rockshelter, Sri Lanka. *Journal of human evolution*, *61*(3), pp.254-269.

Petit, J.R., Jouzel, J., Raynaud, D., Barkov, N.I., Barnola, J.M., Basile, I., Bender, M., Chappellaz, J., Davis, M., Delaygue, G. and Delmotte, M., 1999. Climate and atmospheric history of the past 420,000 years from the Vostok ice core, Antarctica. *Nature*, *399*(6735), pp.429-436.

Petraglia, M., Clarkson, C., Boivin, N., Haslam, M., Korisettar, R., Chaubey, G., Ditchfield, P., Fuller, D., James, H., Jones, S. and Kivisild, T., 2009. Population increase and environmental deterioration correspond with microlithic innovations in South Asia

ca. 35,000 years ago. *Proceedings of the National Academy of Sciences*, *106*(30), pp.12261-12266.

Petraglia, M., Korisettar, R., Boivin, N., Clarkson, C., Ditchfield, P., Jones, S., Koshy, J., Lahr, M.M., Oppenheimer, C., Pyle, D. and Roberts, R., 2007. Middle Paleolithic assemblages from the Indian subcontinent before and after the Toba super-eruption. *science*, *317*(5834), pp.114-116.

Petraglia, M.D., Ditchfield, P., Jones, S., Korisettar, R. and Pal, J.N., 2012. The Toba volcanic super-eruption, environmental change, and hominin occupation history in India over the last 140,000 years. *Quaternary International*, *258*, pp.119-134.

Petraglia, M.D., Haslam, M., Fuller, D.Q., Boivin, N. and Clarkson, C., 2010. Out of Africa: new hypotheses and evidence for the dispersal of Homo sapiens along the Indian Ocean rim. *Annals of human biology*, *37*(3), pp.288-311.

Petraglia, M.D., Korisettar, R. and Schuldenrein, J., 2003. Landscapes, activity, and the Acheulean to Middle Paleolithic transition in the Kaladgi Basin, India. Eurasian Prehistory, 1(2), pp.3-24.

Petraglia, M.D., Korisettar, R., Bai, M.K., Boivin, N., Janardhana, B., Clarkson, C., Cunningham, K., Ditchfield, P., Fuller, D., Hampson, J. and Haslam, M., 2009. Pleistocene and Holocene occupations of the Kurnool District India: Cave and rockshelter records, the Toba super-eruption and forager-farmer interactions. *Journal of Eurasian Prehistory*, *6*(1-2), pp.119-166.

Petraglia, M.D., Korisettar, R., Noll, M. and Schuldenrein, J., 2003. An Extensive Middle Palaeolithic Quarry Landscape in the Kaladgi Basin, Southern India. *Antiquity*, *77*(295).

Phartiyal, B., Sharma, A., Upadhyay, R. and Sinha, A.K., 2005. Quaternary geology, tectonics and distribution of palaeo-and present fluvio/glacio lacustrine deposits in Ladakh, NW Indian Himalaya—a study based on field observations. *Geomorphology*, *65*(3-4), pp.241-256.

Ponton, C., Giosan, L., Eglinton, T.I., Fuller, D.Q., Johnson, J.E., Kumar, P. and Collett, T.S., 2012. Holocene Aridification of India. *Geophysical Research Letters 39(3)*, pp. 1-6.

Porat, N., Chazan, M., Grün, R., Aubert, M., Eisenmann, V. and Horwitz, L.K., 2010. New radiometric ages for the Fauresmith industry from Kathu Pan, southern Africa: implications for the Earlier to Middle Stone Age transition. *Journal of Archaeological Science*, *37*(2), pp.269-283.

Potts, R., 2013. Hominin evolution in settings of strong environmental variability. *Quaternary Science Reviews*, *73*, pp.1-13.

Powar, K.B., 1993. Geomorphological evolution of Konkan Coastal Belt and adjoining Sahyadri Uplands with reference of Quaternary uplift. *Current science (Bangalore)*, *64*(11-12), pp.793-796.

Prabhu, C.N., Shankar, R., Anupama, K., Taieb, M., Bonnefille, R., Vidal, L. and Prasad, S., 2004. A 200-ka pollen and oxygen-isotopic record from two sediment cores from the eastern Arabian Sea. *Palaeogeography, Palaeoclimatology, Palaeoecology*, *214*(4), pp.309-321.

Prasad, S. 1996. Late Quaternary Palaeoenvironment and Evolution of Nal region, Gujarat, India. Unpublished Ph.D. thesis, M.S. University of Baroda.

Premathilake, R. and Gunatilaka, A., 2013. Chronological framework of Asian Southwest Monsoon events and variations over the past 24,000 years in Sri Lanka and regional correlations. *Journal of the National Science Foundation of Sri Lanka*, *41*(3).

Premathilake, R. and Risberg, J., 2003. Late Quaternary climate history of the Horton plains, central Sri Lanka. *Quaternary Science Reviews*, *22*(14), pp.1525-1541.

Premathilake, R., 2012. Human used upper montane ecosystem in the Horton Plains, central Sri Lanka–a link to Lateglacial and early Holocene climate and environmental changes. *Quaternary Science Reviews*, *50*, pp.23-42.

Prüfer, K., Racimo, F., Patterson, N., Jay, F., Sankararaman, S., Sawyer, S., Heinze, A., Renaud, G., Sudmant, P.H., De Filippo, C. and Li, H., 2014. The complete genome sequence of a Neanderthal from the Altai Mountains. *Nature*, *505*(7481), pp.43-49.

Quamar, M.F. and Bera, S.K., 2017. Do the common natural pollen trapping media behave similarly? A comparative study of modern palynoassemblages from Chhattisgarh, central India. *Quaternary International*, *444*, pp.217-226.

Quamar, M.F. and Chauhan, M.S., 2012. Late Quaternary vegetation, climate as well as lake-level changes and human occupation from Nitaya area in Hoshangabad District, southwestern Madhya Pradesh (India), based on pollen evidence. *Quaternary International*, *263*, pp.104-113.

Quamar, M.F., 2015. Non-pollen palynomorphs from the late Quaternary sediments of southwestern Madhya Pradesh (India) and their palaeoenvironmental implications. *Historical Biology*, *27*(8), pp.1070-1078.

Rafferty J. P., 2011. "Tarantian Stage". *Encyclopaedia Britannica*.

Raghavan, H., 1987. Quaternary Geology of Naguar District, Rajasthan. Unpublished Ph.D. thesis, University of Poona.

Rai, P.K., Mishra, V.N. and Mohan, K., 2017. A study of morphometric evaluation of the Son basin, India using geospatial approach. *Remote Sensing Applications: Society and Environment*, *7*, pp.9-20.

Raj, R. 1999. Tectonic Geomorphology and Late Quaternary Palaeoenvironment of Mahi Basin Western India. Unpublished Ph.D. thesis, M.S. University of Baroda.

Raj, R., Chamyal, L.S., Juyal, N., Phartiyal, B., Ali, S.N. and Thakur, B., 2016. Late Quaternary fluvio-aeolian interaction: palaeoenvironment and palaeoclimatic conditions in the pediment zone of Vatrak River basin, western India. *Zeitschrift für Geomorphologie*, *60*(2), pp.151-169.

Rajagopalan, G., Sukumar, R., Ramesh, R., Pant, R.K. and Rajagopalan, G., 1997. Late Quaternary vegetational and climatic changes from tropical peats in southern India–an extended record up to 40,000 years BP. *Current Science*, pp.60-63.

Rajaguru, S.N., Deo, S. and Mishra, S., 2011. Pleistocene climatic changes in western India: a geoarchaeological approach. *Abstract "Future of the Past", Manglore, India*.

Rajaguru, S.N., Kale, V.S. and Badam, G.L., 1993. Quaternary fluvial systems in Upland Maharashtra. *Current Science*, pp.817-822.

Rajendran, P. 1979. Environment and Stone Age Cultures of North Kerala. Unpublished Ph.D. thesis, University of Poona.

Raju, D.R. and Venkatasubbaiah, P.C., 2002. The archaeology of the Upper Palaeolithic phase in India. *Indian archaeology in retrospect. Prehistory. Archaeology of South Asia (New Delhi 2002)*, pp.85-109.

Raju, N.J., Dey, S., Gossel, W. and Wycisk, P., 2012. Fluoride hazard and assessment of groundwater quality in the semi-arid Upper Panda River basin, Sonbhadra district, Uttar Pradesh, India. *Hydrological Sciences Journal*, *57*(7), pp.1433-1452.

Ranhotra, P.S., Bhattacharyya, A. and Kotlia, B.S., 2007. Vegetation and Climatic Changes around Lamayuru, Trans-Himalaya during the Last 35 Kyr BP. *Palaeobotanist* 56(1-3), pp. 117-126

Ranhotra, P.S., Sharma, J., Bhattacharyya, A., Basavaiah, N. and Dutta, K., 2018. Late Pleistocene-Holocene vegetation and climate from the palaeolake sediments, Rukti valley, Kinnaur, Himachal Himalaya. *Quaternary International*, *479*, pp.79-89.

Rao, K.L., 1975. India's Water Wealth Orient Longman Ltd. *New Delhi, 255pp*.

Rao, Z., Guo, W., Cao, J., Shi, F., Jiang, H. and Li, C., 2017. Relationship between the stable carbon isotopic composition of modern plants and surface soils and climate: A global review. *Earth-Science Reviews*, *165*, pp.110-119.

Rashid, H., England, E., Thompson, L. and Polyak, L., 2011. Late glacial to Holocene Indian summer monsoon variability based upon sediment records taken from the Bay of Bengal. *TAO: Terrestrial, Atmospheric and Oceanic Sciences*, *22*(2), p.2.

Rasmussen, M., Guo, X., Wang, Y., Lohmueller, K.E., Rasmussen, S., Albrechtsen, A., Skotte, L., Lindgreen, S., Metspalu, M., Jombart, T. and Kivisild, T., 2011. An Aboriginal Australian genome reveals separate human dispersals into Asia. *Science*, *334*(6052), pp.94-98.

Raven, P.H., Evert, R.F. and Eichhorn, S.E., 1999. *Biology of Plants*, WH Freedman and Company Worth Publishers.

Reddy, D.V., Singaraju, V., Mishra, R., Kumar, D., Thomas, P.J., Rao, K.K. and Singhvi, A.K., 2013. Luminescence chronology of the inland sand dunes from SE India. *Quaternary Research*, *80*(2), pp.265-273.

Reich, D., Green, R.E., Kircher, M., Krause, J., Patterson, N., Durand, E.Y., Viola, B., Briggs, A.W., Stenzel, U., Johnson, P.L. and Maricic, T., 2010. Genetic history of an archaic hominin group from Denisova Cave in Siberia. *Nature*, *468*(7327), pp.1053-1060.

Reich, D., Patterson, N., Kircher, M., Delfin, F., Nandineni, M.R., Pugach, I., Ko, A.M.S., Ko, Y.C., Jinam, T.A., Phipps, M.E. and Saitou, N., 2011. Denisova admixture and the first modern human dispersals into Southeast Asia and Oceania. *The American Journal of Human Genetics*, *89*(4), pp.516-528.

Rendell, H., 1988. Environmental changes during the Pleistocene in the Potwar Plateau and Peshawar Basin, northern Pakistan. *Proceedings of the Indian National Science Academy, Part A. Physical sciences*, *54*(3), pp.390-398.

Rendell, H.M., Hailwood, E.A. and Dennell, R.W., 1987. Magnetic polarity stratigraphy of Upper Siwalik Sub-Group, Soan Valley, Pakistan: implications for early human occupance of Asia. *Earth and Planetary Science Letters*, *85*(4), pp.488-496.

Renfrew, C. and Bahn, P., 2012. *Archaeology: Theories, Methods and Practice*. Thames and Hudson.

Renfrew, C. and Bahn, P., 2016. *Archaeology: Theories, Methods and Practice*. Revised & Updated.

Resmi, M.R. and Achyuthan, H., 2018. Northeast monsoon variations during the Holocene inferred from palaeochannels and active channels of the Palar River basin, Southern Peninsular India. *The Holocene*, *28*(6), pp.895-913.

Retallack, G.J., Bajpai, S., Liu, X., Kapur, V.V. and Pandey, S.K., 2018. Advent of strong South Asian monsoon by 20 million years ago. *The Journal of Geology*, *126*(1), pp.1-24.

Reyes-Centeno, H., Ghirotto, S., Détroit, F., Grimaud-Hervé, D., Barbujani, G. and Harvati, K., 2014. Genomic and cranial phenotype data support multiple modern human dispersals from Africa and a southern route into Asia. *Proceedings of the National Academy of Sciences*, *111*(20), pp.7248-7253.

Rhodes, E.J., 2011. Optically stimulated luminescence dating of sediments over the past 200,000 years. *Annual Review of Earth and Planetary Sciences*, *39*(1), pp.461-488.

Richards, B.W., Owen, L.A. and Rhodes, E.J., 2000. Timing of Late Quaternary glaciations in the Himalayas of northern Pakistan. *Journal of Quaternary Science: Published for the Quaternary Research Association*, *15*(3), pp.283-297.

Rightmire, G.P., 2009. Middle and later Pleistocene hominins in Africa and Southwest Asia. *Proceedings of the National Academy of Sciences*, *106*(38), pp.16046-16050.

Roberts, D.L., Jarić, I., Lycett, S.J., Flicker, D. and Key, A., 2023. Homo floresiensis and Homo luzonensis are not temporally exceptional relative to Homo erectus. Journal of Quaternary Science.

Roberts, P. and Petraglia, M., 2015. Pleistocene rainforests: barriers or attractive environments for early human foragers? *World Archaeology*, *47*(5), pp.718-739.

Roberts, P., Blinkhorn, J. and Petraglia, M.D., 2018. A transect of environmental variability across South Asia and its influence on Late Pleistocene human innovation and occupation. *Journal of Quaternary Science*, *33*(3), pp.285-299.

Roberts, P., Delson, E., Miracle, P., Ditchfield, P., Roberts, R.G., Jacobs, Z., Blinkhorn, J., Ciochon, R.L., Fleagle, J.G., Frost, S.R. and Gilbert, C.C., 2014. Continuity of mammalian fauna over the last 200,000 years in the Indian subcontinent. *Proceedings of the National Academy of Sciences*, *111*(16), pp.5848-5853.

Roberts, P., Henshilwood, C.S., van Niekerk, K.L., Keene, P., Gledhill, A., Reynard, J., Badenhorst, S. and Lee-Thorp, J., 2016. Climate, environment and early human innovation: stable isotope and faunal proxy evidence from archaeological sites (98-59ka) in the southern Cape, South Africa. *PLoS One*, *11*(7), p.e0157408.

Roberts, P., Perera, N., Wedage, O., Deraniyagala, S., Perera, J., Eregama, S., Gledhill, A., Petraglia, M.D. and Lee-Thorp, J.A., 2015. Direct evidence for human reliance on rainforest resources in late Pleistocene Sri Lanka. *Science*, *347*(6227), pp.1246-1249.

Roberts, P., Perera, N., Wedage, O., Deraniyagala, S., Perera, J., Eregama, S., Petraglia, M.D. and Lee-Thorp, J.A., 2017. Fruits of the forest: human stable isotope ecology and rainforest adaptations in Late Pleistocene and Holocene (∼ 36 to 3 ka) Sri Lanka. *Journal of human evolution*, *106*, pp.102-118.

Rodgers, W.A., 2000. Wildlife protected area network in India: A review executive summary. Wildlife Institute of India, Dehradun

Rodríguez, J., Burjachs, F., Cuenca-Bescós, G., García, N., Van der Made, J., González, A.P., Blain, H.A., Expósito, I., López-García, J.M., Antón, M.G. and Allué, E., 2011. One million years of cultural evolution in a stable environment at Atapuerca (Burgos, Spain). *Quaternary Science Reviews*, *30*(11-12), pp.1396-1412.

Roe, D.A., 1994. A metrical analysis of selected sets of handaxes and cleavers from Olduvai Gorge. *Olduvai Gorge*, *5*, pp.1968-1971.

Rosenmeier, M.F., Hodell, D.A., Brenner, M., Curtis, J.H., Martin, J.B., Anselmetti, F.S., Ariztegui, D. and Guilderson, T.P., 2002. Influence of vegetation change on watershed hydrology: implications for paleoclimatic interpretation of lacustrine δ18O records. *Journal of Paleolimnology*, *27*(1), pp.117-131.

Roy, N.G., Sinha, R. and Gibling, M.R., 2012. Aggradation, incision and interfluve flooding in the Ganga Valley over the past 100,000 years: testing the influence of monsoonal precipitation. *Palaeogeography, Palaeoclimatology, Palaeoecology*, *356*, pp.38-53.

Sadakata, N., Maemoku, H., Rajaguru, S.N., Mishra, S. and Fujiwara, K., 1995. Late Quaternary environmental change in the Pravara Basin, northwestern Deccan upland, India. In *Proceedings of the International Symposium on Palaeoenvironmental Change in Tropical-Subtropical Monsoon Asia* (pp. 43-56).

Sali, S., 1989. The Upper Palaeolithic and Mesolithic Cultures of Maharashtra (Deccan College Postgraduate Research Institute, Pune, India).

Sandhu, S., Sathe, V., Chakarborty, K.S., Chakraborty, S. and Chauhan, P.R., 2021. Carbon and Oxygen Isotope Analysis of Modern Cattle (Bos indicus) Molars from the Central Narmada Valley, India. *Ancient Asia*, *12*.

Sandom, C., Faurby, S., Sandel, B. and Svenning, J.C., 2014. Global late Quaternary megafauna extinctions linked to humans, not climate change. *Proceedings of the Royal Society B: Biological Sciences*, *281*(1787), pp.20133254.

Sankalia, H.D., 1956. Animal fossils and Palaeolithic industries from the Pravara basin at Nevasa, district Ahmednagar. *Ancient India*, *12*, pp.35-52.

Sankalia, H.D., 1964. Middle Stone Age Culture in India and Pakistan: Recent investigations show a distinct culture intermediate between the Early and Late stone ages. *Science*, *146*(3642), pp.365-375.

Sankararaman, S., Mallick, S., Patterson, N. and Reich, D., 2016. The combined landscape of Denisovan and Neanderthal ancestry in present-day humans. Current Biology, 26(9), pp.1241-1247.

Sankhyan, A.R., Dewangan, L.N., Chakraborty, S., Kundu, S., Prabha, S., Chakravarty, R. and Badam, G.L., 2012. New human fossils and associated findings from the Central Narmada Valley, India. *Current Science*, pp.1461-1469.

Sanwal, J., Rajendran, C.P. and Sheshshayee, M.S., 2019. Reconstruction of late Quaternary climate from a Paleo-lacustrine profile in the Central (Kumaun) Himalaya: Viewing the results in a regional context. *Frontiers in Earth Science*, *7*, pp.2.

Sarkar, A., Mukherjee, A.D., Bera, M.K., Das, B., Juyal, N., Morthekai, P., Deshpande, R.D., Shinde, V.S. and Rao, L.S., 2016. Oxygen isotope in archaeological bioapatites from India: Implications to climate change and decline of Bronze Age Harappan civilization. *Scientific Reports*, *6*(1), p.26555.

Scally, A. and Durbin, R., 2012. Revising the human mutation rate: implications for understanding human evolution. *Nature Reviews Genetics*, *13*(10), pp.745-753.

Scerri, E.M., Niang, K., Candy, I., Blinkhorn, J., Mills, W., Cerasoni, J.N., Bateman, M.D., Crowther, A. and Groucutt, H.S., 2021. Continuity of the Middle Stone Age into the holocene. *Scientific Reports*, *11*(1), pp.1-11.

Scerri, E.M., Thomas, M.G., Manica, A., Gunz, P., Stock, J.T., Stringer, C., Grove, M., Groucutt, H.S., Timmermann, A., Rightmire, G.P. and d'Errico, F., 2018. Did our species evolve in subdivided populations across Africa, and why does it matter?. *Trends in ecology & evolution*, *33*(8), pp.582-594.

Schmidt, S., Tsukamoto, S., Salomon, E., Frechen, M. and Hetzel, R., 2012. Optical dating of alluvial deposits at the orogenic front of the Andean Precordillera (Mendoza, Argentina). *Geochronometria*, *39*(1), pp.62-75.

Sengupta, D., Bhandari, N. and Watanabe, S., 1997. Formation age of Lonar meteor crater, India. *Revista de Fisica Aplicada e Instrumentacao*, *12*(1), pp.1-7.

Senut, B., Pickford, M., Gommery, D., Mein, P., Cheboi, K. and Coppens, Y., 2001. First hominid from the Miocene (Lukeino formation, Kenya). *Comptes Rendus de l'Académie des Sciences-Series IIA-Earth and Planetary Science*, *332*(2), pp.137-144.

Shah, R.A., Achyuthan, H., Lone, A.M., Jaiswal, M.K. and Paul, D., 2021. Constraining the timing and deposition pattern of loess-palaeosol sequences in Kashmir Valley, Western Himalaya: Implications to paleoenvironment studies. *Aeolian Research*, *49*, p.100660.

Sharma, G.R. and Clark, J.D. eds., 1983. *Palaeoenvironments and Prehistory in the Middle Son Valley, Madhya Pradesh, North-Central India* (Vol. 7). Abinash Prakashan.

Sharma, G.R. and Clark, J.D., 1982. Palaeo-environments and prehistory in the Middle Son Valley, northern Madhya Pradesh. *Man and Environment*, *6*, pp.56-62.

Sharma, K., Bhatt, N., Shukla, A.D., Cheong, D.K. and Singhvi, A.K., 2017. Optical dating of late Quaternary carbonate sequences of Saurashtra, western India. *Quaternary Research*, *87*(1), pp.133-150.

Sharma, S. 2001.Cultural Affinities between Southeast Asia and Northeast India during Prehistoric Times with Special Reference to Ganol and Rongraam Valleys in Meghalyala. Unpublished Ph.D. thesis, University of Poona.

Sharma, S., Joachimski, M., Sharma, M., Tobschall, H.J., Singh, I.B., Sharma, C., Chauhan, M.S. and Morgenroth, G., 2004. Lateglacial and Holocene environmental changes in Ganga plain, Northern India. *Quaternary Science Reviews*, *23*(1-2), pp.145-159.

Sharma, S., Joachimski, M.M., Tobschall, H.J., Singh, I.B., Sharma, C. and Chauhan, M.S., 2006. Correlative evidences of monsoon variability, vegetation change and human inhabitation in Sanai lake deposit: Ganga Plain, India. *Current Science*, pp.973-978.

Sharon, G. (2006) Acheulian Large Flake Industries Technology, Chronology, Distribution and Significance, Published Ph.d. thesis, Hebrew University of Jerusalem.

Sharon, G., 2007. *Acheulian large flake industries: technology, chronology, and significance* (Vol. 1701). British Archaeological Reports Limited.

Shea, J.J., 2016. *Stone tools in human evolution: behavioral differences among technological primates*. Cambridge University Press.

Shen, G., Wang, W., Wang, Q., Zhao, J., Collerson, K., Zhou, C. and Tobias, P.V., 2002. U-Series dating of Liujiang hominid site in Guangxi, Southern China. *Journal of Human Evolution*, *43*(6), pp.817-829.

Shi, Y., Yu, G., Liu, X., Li, B. and Yao, T., 2001. Reconstruction of the 30–40 ka BP enhanced Indian monsoon climate based on geological records from the Tibetan Plateau. *Palaeogeography, Palaeoclimatology, Palaeoecology*, *169*(1-2), pp.69-83.

Shipton, C., 2016. Hierarchical organization in the Acheulean to Middle Palaeolithic transition at Bhimbetka, India. *Cambridge Archaeological Journal*, *26*(4), pp.601-618.

Shipton, C., Clarkson, C., Pal, J.N., Jones, S.C., Roberts, R.G., Harris, C., Gupta, M.C., Ditchfield, P.W. and Petraglia, M.D., 2013. Generativity, hierarchical action and recursion in the technology of the Acheulean to Middle Palaeolithic transition: a perspective from Patpara, the Son Valley, India. *Journal of Human Evolution*, *65*(2), pp.93-108.

Shipton, C., Roberts, P., Archer, W., Armitage, S.J., Bita, C., Blinkhorn, J., Courtney-Mustaphi, C., Crowther, A., Curtis, R., d'Errico, F. and Douka, K., 2018. 78,000-year-old record of Middle and Later stone age innovation in an East African tropical forest. *Nature communications*, *9*(1), pp.1832.

Sikora, M., 2017. A genomic view of the Pleistocene population history of Asia. *Current Anthropology*, *58*(S17), pp. S397-S405.

Singh V., 2022. Acheulean landscape and technological adaptation in the Central Narmada Valley, Madhya Pradesh (India). Unpublished thesis, Indian Institute of Science Education and Research, Mohali, Punjab.

Singh, A. and A. K. Srivastava, 2022. Had Youngest Toba Tuff (YTT, ca. 75 ka) eruption really destroyed living media explicitly in entire Southeast Asia or just a theoretical debate? an extensive review of its catastrophic event. *Journal of Asian Earth Sciences: X*, pp.100083.

Singh, A., Paul, D., Sinha, R., Thomsen, K.J. and Gupta, S., 2016. Geochemistry of buried river sediments from Ghaggar Plains, NW India: Multi-proxy records of variations in provenance, paleoclimate, and paleovegetation patterns in the Late Quaternary. *Palaeogeography, Palaeoclimatology, Palaeoecology*, *449*, pp.85-100.

Singh, I.B., 2005. Quaternary palaeoenvironments of the Ganga Plain and anthropogenic activity. *Man and Environment*, *30*(1), pp.1-35.

Singh, K.N. and Srivastava, R.N., 1982. On the occurrence of ash-tuff cone structures from the Porcellanite Formation, Chopan area, Mirzapur District, Uttar Pradesh. *Indian Journal Earth Science*, *10*, pp.107-109.

Singh, S., Kar, R. and Khandelwal, A., 2010. Impact of modern pollen rain studies from South and Little Andaman Islands, India, to interpret present and past vegetation. *Current Science*, *99*(9), pp.1251-1256.

Singhvi AK, Bhatt N, Glennie KW, Srivastava P., 2012. India, Arabia and adjacent regions. In: Metcalfe SE, Nash DJ (eds) *Quaternary environmental change in the tropics*. Wiley, New York, pp 151–206.

Singhvi, A.K. and V.S. Kale 2010. Paleoclimate Studies in India: Last Ice Age to the Present. New Delhi, *INSA.*

Singhvi, A.K., and Kale, V.S., (2009) Paleoclimate studies in India: last ice age to the present. *Indian National Science Academy*, Report Ser. 4, New Delhi.

Singhvi, A.K., Deraniyagala, S.U. and Sengupta, D., 1986. Thermoluminescence dating of Quaternary red-sand beds: a case study of coastal dunes in Sri Lanka. *Earth and Planetary Science Letters*, *80*(1-2), pp.139-144.

Singhvi, A.K., Williams, M.A.J., Rajaguru, S.N., Misra, V.N., Chawla, S., Stokes, S., Chauhan, N., Francis, T., Ganjoo, R.K. and Humphreys, G.S., 2010. A∼ 200 ka record of

climatic change and dune activity in the Thar Desert, India. *Quaternary Science Reviews*, *29*(23-24), pp.3095-3105.

Sinha, R., Singh, A. and Tandon, S.K., 2020. Fluvial archives of north and northwestern India as recorders of climatic signatures in the late Quaternary: review and assessment. *Current Science*, *119*(2), pp.232-243.

Sinha, R., Smykatz-Kloss, W., Stüben, D., Harrison, S.P., Berner, Z. and Kramar, U., 2006. Late Quaternary palaeoclimatic reconstruction from the lacustrine sediments of the Sambhar playa core, Thar Desert margin, India. *Palaeogeography, Palaeoclimatology, Palaeoecology*, *233*(3-4), pp.252-270.

Smith, F.A., Elliott Smith, R.E., Lyons, S.K. and Payne, J.L., 2018. Body size downgrading of mammals over the late Quaternary. *Science*, *360*(6386), pp.310-313.

Soares, P., Alshamali, F., Pereira, J.B., Fernandes, V., Silva, N.M., Afonso, C., Costa, M.D., Musilová, E., Macaulay, V., Richards, M.B. and Černý, V., 2012. The expansion of mtDNA haplogroup L3 within and out of Africa. *Molecular biology and evolution*, *29*(3), pp.915-927.

Sonakia, A. and Biswas, S., 1998. Antiquity of the Narmada Homo erectus, the early man of India. *Current Science*, pp.391-393.

Sonakia, A. and Biswas, S., 2011. *Fossil Mammals Including Early Man from the Quaternary Deposits of the Narmada and Son Basins of Madhya Pradesh India*. Geological Survey of India.

Sonakia, A., 1984. The skull cap of early man and associated mammalian fauna from Narmada Valley alluvium, Hoshangabad area, Madhya Pradesh, India. *Records of the Geological survey of India*, *113*(6), pp.159-172.

Srivastava, G., Trivedi, A., Mehrotra, R.C., Paudayal, K.N., Limaye, R.B., Kumaran, K.P.N. and Yadav, S.K., 2016. Monsoon variability over Peninsular India during Late Pleistocene: Signatures of vegetation shift recorded in terrestrial archive from the corridors of Western Ghats. *Palaeogeography, Palaeoclimatology, Palaeoecology*, *443*, pp.57-65.

Srivastava, P., Juyal, N., Singhvi, A.K., Wasson, R.J. and Bateman, M.D., 2001. Luminescence chronology of river adjustment and incision of Quaternary sediments in the alluvial plain of the Sabarmati River, north Gujarat, India. *Geomorphology*, *36*(3-4), pp.217-229.

Srivastava, P., Singh, I.B., Sharma, M. and Singhvi, A.K., 2003. Luminescence chronometry and Late Quaternary geomorphic history of the Ganga Plain, India. *Palaeogeography, Palaeoclimatology, Palaeoecology*, *197*(1-2), pp.15-41.

Srivastava, R.N., Srivastava, A.K., Singh, K.N. and Redcliffe, R.P., 2003. Sedimentation and depositional environment of the Chopan porcellanite formation, Semri group, Vindhyan supergroup in parts of Sonbhadra district, Uttar Pradesh. *J. Palaeontol. Soc. India*, *48*, pp.167-179.

Stager, J.C., Ryves, D.B., Chase, B.M. and Pausata, F.S., 2011. Catastrophic drought in the Afro-Asian monsoon region during Heinrich event 1. *science*, *331*(6022), pp.1299-1302.

Sternberg, L.S.L., Mulkey, S.S. and Joseph Wright, S., 1989. Oxygen isotope ratio stratification in a tropical moist forest. *Oecologia*, *81*(1), pp.51-56.

Stringer, C., 2016. The origin and evolution of Homo sapiens. *Philosophical Transactions of the Royal Society B: Biological Sciences*, *371*(1698), p.20150237.

Stringer, C.B. and Andrews, P., 1988. Genetic and fossil evidence for the origin of modern humans. *Science*, *239*(4845), pp.1263-1268.

Sun, Q., Wang, S., Zhou, J., Chen, Z., Shen, J., Xie, X., Wu, F. and Chen, P., 2010. Sediment geochemistry of Lake Daihai, north-central China: implications for catchment weathering and climate change during the Holocene. *Journal of Paleolimnology*, *43*(1), pp.75-87.

Sunita, M. and Meenal, M., 2013. Role of Biofertilizers in Maintaining Nutritional Status Of Soil In Sonbhadra And Mirzapur Districts Of Eastern Uttar Pradesh, India. *International Journal of Humanities and Social Science Invention* 2 (5) pp.23-30.

Tejada-Lara, J.V., MacFadden, B.J., Bermudez, L., Rojas, G., Salas-Gismondi, R. and Flynn, J.J., 2018. Body mass predicts isotope enrichment in herbivorous mammals. *Proceedings of the Royal Society B, 285*(1881), p.20181020.

Tewari, R., P.K. Singh, R.K. Srivastava and G.C. Singh 1995. Archaeological investigations in District Sonbhadra, Uttar Pradesh, *Pragdhara.5*:55-132, journal of the UP State Archaeological Organization.

Tewari, R., Pant, P.C., Singh, I.B., Sharma, S., Sharma, M., Srivastava, P., Singhvi, A.K., Mishra, P.K. and Tobschall, H.J., 2002. Middle Palaeolithic human activity and palaeoclimate at Kalpi in Yamuna valley, Ganga plain. *Man and Environment*, *27*(2), pp.1-13.

Tewari, R., Singh, G.C. and Trivedi, R.K., 2013. Report of the excavations at Raja-Nal-ka-Tila, district Sonbhadra, Uttar Pradesh (India): 1995-96-97. *Pragdhara 21e22, 1e226.*

Thapar, B.K., 1979. Indian Archaeology 1975-76-a Review. Archaeological Survey of India, New Delhi

Thokchom A.S. 1987. Quaternary Studies in the Manipur Valley. Unpublished Ph.D. thesis, University of Poona.

Thokchom, S., Bhattacharya, F., Prasad, A.D., Dogra, N.N. and Rastogi, B.K., 2017. Paleoenvironmental implications and drainage adjustment in the middle reaches of the Sabarmati river, Gujarat: Implications towards hydrological variability. *Quaternary International*, *454*, pp.1-14.

Thompson, J.C., Mackay, A., De Moor, V. and Gomani-Chindebvu, E., 2014. Catchment survey in the Karonga District: A landscape-scale analysis of Provisioning and core reduction strategies during the Middle Stone Age of northern Malawi. *African Archaeological Review*, *31*(3), pp.447-478.

Thomsen, K.J., Murray, A.S. and Jain, M., 2011. Stability of IRSL signals from sedimentary K-feldspar samples. *Geochronometria*, *38*(1), pp.1-13.

Thorne, A., Grün, R., Mortimer, G., Spooner, N.A., Simpson, J.J., McCulloch, M., Taylor, L. and Curnoe, D., 1999. Australia's oldest human remains: age of the Lake Mungo 3 skeleton. *Journal of human evolution*, *36*(6), pp.591-612.

Tiju, V.I., T.N. Prakash, L.S. Nair, G. Sreenivasulu and R. Nagendra 2021. Reconstruction of the paleoenvironment of the late Quaternary sediments of the Kerala coast, SW India. *Journal of Asian Earth Sciences*, *222*, p.104952.

Timmermann, A. and Friedrich, T., 2016. Late Pleistocene climate drivers of early human migration. *nature*, *538*(7623), pp.92-95.

Tiwari, M.P. and Bhai, H.Y., 1997. Quaternary stratigraphy of the Narmada Valley. *Geological Survey of India Special Publication*, *46*, pp.33-63.

Tribolo, C., Mercier, N., Valladas, H., Joron, J.L., Guibert, P., Lefrais, Y., Selo, M., Texier, P.J., Rigaud, J.P., Porraz, G. and Poggenpoel, C., 2009. Thermoluminescence dating of a Stillbay–Howiesons Poort sequence at Diepkloof Rock Shelter (Western Cape, South Africa). *Journal of Archaeological Science*, *36*(3), pp.730-739.

Trivedi, A., Chauhan, M.S., Sharma, A., Nautiyal, C.M. and Tiwari, D.P., 2012. Late Pleistocene–Holocene vegetation and climate change in the Central Ganga Plain: a multiproxy study from Jalesar Tal, Unnao District, Uttar Pradesh. *Current Science*, pp.555-562.

Tucci, S. and Akey, J.M., 2016. A map of human wanderlust. *Nature*, *538*(7624), pp.179-180.

Umarjikar S.V. 1984. Quaternary Geology of the Upper Krishna Basin. Unpublished Ph.D. thesis, University of Poona.

Uno, K.T., Rivals, F., Bibi, F., Pante, M., Njau, J. and de la Torre, I., 2018. Large mammal diets and paleoecology across the Oldowan–Acheulean transition at Olduvai Gorge, Tanzania from stable isotope and tooth wear analyses. *Journal of human evolution*, *120*, pp.76-91.

Vaidyanadhan, R. and Ghosh, R.N., 1993. Quaternary of the east coast of India. *Current science*, pp.804-816.

Valdiya, K.S., 2016. Physiographic layout of Indian subcontinent. In *The Making of India* (pp. 1-19). Springer, Cham.

Van Campo, E., 1986. Monsoon Fluctuations in Two 20,000-Yr BP Oxygen-Isotope/Pollen Records Off Southwest India1. *Quaternary Research*, *26*(3), pp.376-388.

Van den Bergh, G.D., Kaifu, Y., Kurniawan, I., Kono, R.T., Brumm, A., Setiyabudi, E., Aziz, F. and Morwood, M.J., 2016. Homo floresiensis-like fossils from the early Middle Pleistocene of Flores. *Nature*, *534*(7606), pp.245-248.

Verma, N. and Patel, R.K., 2021. Delineation of groundwater potential zones in lower Rihand River Basin, India using geospatial techniques and AHP. *The Egyptian Journal of Remote Sensing and Space Science*, *24*(3), pp.559-570.

Verma, P., and M.R. Rao 2011. Quaternary Vegetation and Climate Change in Central Narmada Valley: Palynological Records from Hominin Bearing Sedimentary Successions, in Geological Processes and Climate Change (Singh DN and Chabbra L S Eds.), pp.71-84. Chennai, Macmillan Publishers India Pvt. Ltd.

Vernot, B. and Akey, J.M., 2015. Complex history of admixture between modern humans and Neandertals. *The American Journal of Human Genetics*, *96*(3), pp.448-453.

Villa, P., Pollarolo, L., Conforti, J., Marra, F., Biagioni, C., Degano, I., Lucejko, J.J., Tozzi, C., Pennacchioni, M., Zanchetta, G. and Nicosia, C., 2018. From Neandertals to modern humans: New data on the Uluzzian. *PloS one*, *13*(5), p.e0196786.

Vrba, E.S., Bibi, F. and Costa, A.G., 2015. First Asian record of a late Pleistocene reduncine (Artiodactyla, Bovidae, Reduncini), Sivacobus sankaliai, sp. nov., from Gopnath (Miliolite Formation) Gujarat, India, and a revision of the Asian genus Sivacobus Pilgrim, 1939. *Journal of Vertebrate Paleontology*, *35*(4), p.e943399.

Wakankar, V.S., 1973. Bhimbetka excavations. *Journal of Indian History*, *51*(151), pp.23-32.

Wang, Y., Kromhout, E., Zhang, C., Xu, Y., Parker, W., Deng, T. and Qiu, Z., 2008. Stable isotopic variations in modern herbivore tooth enamel, plants and water on the Tibetan Plateau: Implications for paleoclimate and paleoelevation reconstructions. *Palaeogeography, Palaeoclimatology, Palaeoecology*, *260*(3-4), pp.359-374.

Ward, C.V., Kimbel, W.H. and Johanson, D.C., 2011. Complete fourth metatarsal and arches in the foot of Australopithecus afarensis. *Science*, *331*(6018), pp.750-753.

Wedage, O., Amano, N., Langley, M.C., Douka, K., Blinkhorn, J., Crowther, A., Deraniyagala, S., Kourampas, N., Simpson, I., Perera, N. and Picin, A., 2019. Specialized rainforest hunting by Homo sapiens~ 45,000 years ago. *Nature Communications*, *10*(1), pp.1-8.

Wedage, O., Picin, A., Blinkhorn, J., Douka, K., Deraniyagala, S., Kourampas, N., Perera, N., Simpson, I., Boivin, N., Petraglia, M. and Roberts, P., 2019. Microliths in the South Asian rainforest~ 45-4 ka: New insights from Fa-Hien Lena Cave, Sri Lanka. *Plos One*, *14*(10), p.e0222606.

Westaway, K.E., Louys, J., Awe, R., Morwood, M.J., Price, G.J., Zhao, J.X., Aubert, M., Joannes-Boyau, R., Smith, T.M., Skinner, M.M. and Compton, T., 2017. An early modern human presence in Sumatra 73,000–63,000 years ago. *Nature*, *548*(7667), pp.322-325.

White, M., Ashton, N. and Scott, B., 2011. The emergence, diversity and significance of Mode 3 (prepared core) technologies. In *Developments in quaternary sciences* (Vol. 14, pp. 53-65). Elsevier.

White, T.D., Asfaw, B., DeGusta, D., Gilbert, H., Richards, G.D., Suwa, G. and Clark Howell, F., 2003. Pleistocene homo sapiens from middle awash, ethiopia. *Nature*, *423*(6941), pp.742-747.

Wilkins, J., Brown, K.S., Oestmo, S., Pereira, T., Ranhorn, K.L., Schoville, B.J. and Marean, C.W., 2017. Lithic technological responses to Late Pleistocene glacial cycling at pinnacle point site 5-6, South Africa. *PloS one*, *12*(3), p.e0174051.

Wilkins, J., Schoville, B.J., Pickering, R., Gliganic, L., Collins, B., Brown, K.S., von der Meden, J., Khumalo, W., Meyer, M.C., Maape, S. and Blackwood, A.F., 2021. Innovative Homo sapiens behaviours 105,000 years ago in a wetter Kalahari. *Nature*, *592*(7853), pp.248-252.

Williams, M., 2012a. Did the 73 ka Toba super-eruption have an enduring effect? Insights from genetics, prehistoric archaeology, pollen analysis, stable isotope geochemistry, geomorphology, ice cores, and climate models. *Quaternary International*, *269*, pp.87-93.

Williams, M., 2012b. The~ 73 ka Toba super-eruption and its impact: History of a debate. *Quaternary International*, *258*, pp.19-29.

Williams, M.A. and Clarke, M.F., 1984. Late Quaternary environments in north-central India. *Nature*, *308*(5960), pp.633-635.

Williams, M.A. and Royce, K., 1982. Quaternary geology of the Middle Son valley, north central India: implications for prehistoric archaeology. *Palaeogeography, Palaeoclimatology, Palaeoecology*, *38*(3-4), pp.139-162.

Williams, M.A., Ambrose, S.H., van der Kaars, S., Ruehlemann, C., Chattopadhyaya, U., Pal, J. and Chauhan, P.R., 2009. Environmental impact of the 73 ka Toba super-eruption in South Asia. *Palaeogeography, Palaeoclimatology, Palaeoecology*, *284*(3-4), pp.295-314.

Williams, M.A.J. and Clarke, M.F., 1995. Quaternary geology and prehistoric environments in the Son and Belan Valleys, north-central India, *Quaternary environmentsand geoarchaeology of India*. Bangalore, Geological Society of India.

Williams, M.A.J. and Royce, K., 1983. Alluvial history of the Middle Son Valley, north central India. *Palaeoenvironments and Prehistory in the Middle Son Valley. Abinash Prakashan, Allahabad*, pp.9-21.

Williams, M.A.J., Pal, J.N., Jaiswal, M. and Singhvi, A.K., 2006. River response to Quaternary climatic fluctuations: evidence from the Son and Belan valleys, north-central India. *Quaternary Science Reviews*, *25*(19-20), pp.2619-2631.

Wintle, A.G., 1997. Luminescence dating: laboratory procedures and protocols. *Radiation measurements*, *27*(5-6), pp.769-817.

Wojtczak, D. (2014). The early middle palaeolithic blade industry from Hummal, Central Syria, Published Ph.d. thesis, University of Basel.

Wünnemann, B., Demske, D., Tarasov, P., Kotlia, B.S., Reinhardt, C., Bloemendal, J., Diekmann, B., Hartmann, K., Krois, J., Riedel, F. and Arya, N., 2010. Hydrological evolution during the last 15 kyr in the Tso Kar lake basin (Ladakh, India), derived from geomorphological, sedimentological and palynological records. *Quaternary Science Reviews*, *29*(9-10), pp.1138-1155.

Xu, Z., Pei, S., Hu, Y., de la Torre, I. and Ma, D., 2021. Stable Isotope Analysis of Mammalian Enamel From the Early Pleistocene Site of Madigou, Nihewan Basin: Implications for Reconstructing Hominin Paleoenvironmental Adaptations in North China. *Frontiers in Earth Science*, *9*, p.789781.

Yadav, R.R., Braeuning, A. and Singh, J., 2011. Tree ring inferred summer temperature variations over the last millennium in western Himalaya, India. *Climate Dynamics*, *36*(7), pp.1545-1554.

Zhao, Y., Zhou, J., Chen, F., Wang, X., Ge, J., Gao, X., Stewart, B.A. and Li, F., 2021. Lithic technological responses to environmental change during the penultimate glacial cycle (MIS 7–6) at the Yangshang site, western Chinese Loess Plateau. *Quaternary Research*, *103*, pp.148-159.

Ziegler, M., Simon, M.H., Hall, I.R., Barker, S., Stringer, C. and Zahn, R., 2013. Development of Middle Stone Age innovation linked to rapid climate change. *Nature communications*, *4*(1), pp.1-9.

8 Appendix

Select lithic analysis

Table A 1. Doma flake measurements and other select attributes.

Code	Typological classification	Length (mm)	Width (mm)	Thickness (mm)	Weight(g)	Bulb of percussion	Platform width (mm)	Platform thickness (mm)	Platform preparation	No. of dorsal flake scars	Dorsal flakescar pattern	Flake termination	Raw material	Blank type
DMA 12	flake oblique	93	68	30	199	prominent	43	17	plain	10	bidirectional	feather	porcellanite	angular clast
DMA 14	flake end	50	44	22	47	flat	39	25	plain	4	bidirectional	feather	porcellanite	angular clast
DMA 15	flake oblique	60	57	14	48	prominent	30	14	cortical	3	unidirectional	feather	porcellanite	angular clast
DMA 18	flake end	85	52	11	49	broken	na	na	abraded	0	na	feather	porcellanite	angular clast
DMA 19	flake oblique	62	48	21	76	flat	26	19	plain	1	unidirectional	feather	porcellanite	angular clast
DMA 20	flake end	45	33	9	16	flat	20	9	plain	5	unidirectional	feather	porcellanite	indeterminate
DMA 22	flake oblique	62	55	13	30	prominent	11	6	plain	3	centripetal	feather	porcellanite	indeterminate
DMA 24	flake side	34	35	7	10	flat	16	6	dihedral flat	3	unidirectional	feather	porcellanite	indeterminate
DMA 27	flake oblique	65	32	15	27	flat	8	4	abraded	2	unidirectional	feather	porcellanite	angular clast
DMA 29	flake side	34	40	15	15	flat	21	9	plain	1	unidirectional	feather	porcellanite	angular clast
DMA 30	flake end	36	34	11	17	flat	20	9	plain	3	unidirectional	feather	porcellanite	indeterminate
DMA 32	flake end	46	41	7	15	prominent	23	6	cortical	2	unidirectional	feather	porcellanite	indeterminate
DMA 33	flake end	59	25	15	22	flat	18	14	cortical	3	unidirectional	feather	porcellanite	angular clast
DMA 35	flake oblique	103	99	20	307	flat	16	9	abraded	2	unidirectional	feather	porcellanite	angular clast
DMA 36	flake side	126	136	36	621	prominent	86	35	plain	2	unidirectional	feather	porcellanite	angular clast
DMA 37	flake end	82	56	26	130	broken	na	na	na	12	centripetal	feather	porcellanite	angular clast
DMA 40	flake oblique	44	34	12	16	flat	6	4	cortical	2	unidirectional	feather	porcellanite	indeterminate
DMA 43	flake oblique	44	30	13	15	prominent	18	9	plain	2	unidirectional	feather	porcellanite	angular clast
DMA 44	flake side	23	35	9	7	flat	11	4	plain	3	bidirectional	feather	porcellanite	indeterminate
DMA 49	flake side	22	33	6	5	flat	18	4	plain	5	bidirectional	feather	porcellanite	indeterminate
DMA 57	flake oblique	78	61	32	120	flat	17	19	plain	2	unidirectional	feather	porcellanite	angular clast
DMA 60	flake side	31	43	6	6	prominent	20	8	plain	2	unidirectional	feather	porcellanite	indeterminate
DMA 61	flake side	38	83	63	142	prominent	47	43	plain	6	irregular	indeterminate	porcellanite	angular clast
DMA 63	flake end	37	30	11	15	prominent	26	12	plain	3	unidirectional	feather	porcellanite	angular clast
DMA 65	flake end	61	33	20	39	flat	26	14	plain	2	unidirectional	feather	porcellanite	indeterminate
DMA 67	flake end	44	35	10	13	flat	na	na	abraded	5	centripetal	feather	porcellanite	indeterminate
DMA 69	flake end	60	43	12	22	flat	11	5	plain	4	centripetal	feather	porcellanite	indeterminate
DMA 70	flake end	39	34	10	13	flat	19	9	abraded	3	unidirectional	feather	porcellanite	angular clast
DMA 71	flake side	24	26	7	4	prominent	11	4	cortical	3	unidirectional	feather	porcellanite	angular clast
DMA 75	flake end	50	22	11	11	flat	18	10	cortical	4	bidirectional	feather	porcellanite	indeterminate
DMA 76	flake end	37	29	12	12	flat	28	12	plain	2	unidirectional	feather	porcellanite	angular clast
DMA 77	flake oblique	55	55	22	91	flat	38	18	plain	3	unidirectional	feather	porcellanite	angular clast
DMA 78	flake side	18	46	10	10	prominent	21	11	plain	1	unidirectional	feather	porcellanite	indeterminate
DMA 82	flake side	37	52	25	50	flat	31	17	plain	4	unidirectional	feather	porcellanite	angular clast
DMA 83	flake regular	41	27	14	15	flat	16	15	cortical	2	bidirectional	step	porcellanite	angular clast

DMA 87	flake end	35	32	10	13	prominent	24	8	dihedral convex	2	indeterminate	step	porcellanite	angular clast
DMA 90	flake side	24	54	28	30	broken	na	na	na	2	unidirectional	indeterminate	porcellanite	angular clast
DMA 95	flake end	55	31	8	16	flat	21	5	plain	3	unidirectional	feather	porcellanite	indeterminate
DMA 96	flake end	47	30	10	15	prominent	20	11	plain	3	unidirectional	feather	porcellanite	indeterminate
DMA 100	flake oblique	33	24	10	14	prominent	12	6	plain	3	unidirectional	feather	porcellanite	indeterminate
DMA 102	flake end	38	23	7	4	prominent	14	6	cortical	2	unidirectional	feather	porcellanite	angular clast
DMA 107	flake oblique	44	40	10	16	prominent	24	8	facetted	3	unidirectional	step	porcellanite	angular clast
DMA 109	flake end	43	30	9	11	prominent	14	9	plain	3	unidirectional	feather	porcellanite	indeterminate
DMA 110	flake side	53	71	15	44	flat	18	7	plain	3	bidirectional	feather	porcellanite	indeterminate
DMA 112	flake end	44	30	7	9	prominent	30	7	plain	2	unidirectional	feather	porcellanite	indeterminate
DMA 113	flake end	49	30	10	11	flat	5	3	abraded	3	unidirectional	feather	porcellanite	angular clast
DMA 116	flake side	41	51	15	22	flat	46	21	plain	2	unidirectional	step	porcellanite	indeterminate
DMA 117	flake oblique	43	31	8	11	prominent	21	8	plain	2	unidirectional	feather	porcellanite	indeterminate
DMA 126	flake end	87	43	25	112	flat	20	12	plain	3	unidirectional	feather	porcellanite	angular clast
DMA 127	flake end	68	47	15	47	prominent	48	14	facetted	2	unidirectional	feather	porcellanite	angular clast
DMA 132	flake end	98	53	19	78	prominent	35	11	plain	3	unidirectional	step	porcellanite	angular clast
DMA 133	flake end	109	54	21	123	flat	26	8	cortical	1	unidirectional	feather	porcellanite	angular clast
DMA 138	flake oblique	45	39	10	20	prominent	19	9	plain	6	bidirectional	feather	porcellanite	indeterminate
DMA 140	flake end	81	64	25	96	prominent	63	25	plain	3	bidirectional	feather	porcellanite	angular clast
DMA 149	flake side	39	55	22	52	flat	40	22	plain	4	centripetal	feather	porcellanite	angular clast
DMA 150	flake end	68	49	10	32	prominent	23	10	facetted	5	centripetal	feather	porcellanite	indeterminate
DMA 151	flake side	48	52	11	38	prominent	34	12	facetted	2	unidirectional	feather	porcellanite	indeterminate
DMA 155	flake end	69	47	12	41	prominent	28	12	plain	4	bidirectional	feather	porcellanite	angular clast
DMA 156	flake side	103	160	31	628	prominent	45	23	cortical	10	unidirectional	feather	porcellanite	angular clast
DMA 158	flake oblique	49	36	13	23	flat	na	na	cortical	7	bidirectional	feather	porcellanite	indeterminate
DMA 160	flake end	54	45	19	61	flat	25	19	plain	6	irregular	feather	porcellanite	angular clast
DMA 161	flake oblique	69	55	18	57	flat	7	5	plain	3	centripetal	feather	porcellanite	angular clast
DMA 162	flake end	63	42	14	54	flat	26	16	cortical	4	unidirectional	feather	porcellanite	angular clast
DMA 164	flake oblique	83	75	22	142	prominent	21	12	plain	3	unidirectional	feather	porcellanite	angular clast
DMA 165	flake side	40	40	10	13	prominent	15	11	plain	6	bidirectional	feather	porcellanite	indeterminate
DMA 168	flake end	65	21	20	32	prominent	24	23	plain	2	unidirectional	feather	porcellanite	angular clast
DMA 169	flake end	57	24	10	19	prominent	11	5	plain	1	unidirectional	feather	porcellanite	angular clast
DMA 172	flake end	73	30	16	33	prominent	18	15	cortical	4	unidirectional	feather	porcellanite	angular clast
DMA 175	flake side	32	62	20	51	prominent	38	25	plain	2	unidirectional	feather	porcellanite	angular clast
DMA 176	flake end	84	39	20	81	broken	21	15	plain	4	unidirectional	feather	porcellanite	angular clast
DMA 177	flake oblique	42	29	10	13	broken	10	4	plain	15	centripetal	feather	porcellanite	indeterminate
DMA 180	flake oblique	45	26	8	13	prominent	15	9	plain	3	bidirectional	feather	porcellanite	indeterminate
DMA 185	flake oblique	50	26	20	34	flat	18	18	plain	3	indeterminate	feather	porcellanite	angular clast
DMA 187	flake end	64	45	15	52	prominent	34	10	plain	6	unidirectional	feather	porcellanite	angular clast
DMA 188	flake end	52	49	13	36	prominent	32	14	plain	2	unidirectional	feather	porcellanite	angular clast
DMA 189	flake oblique	76	57	24	94	prominent	15	12	plain	8	unidirectional	feather	porcellanite	angular clast
DMA 191	flake end	73	34	16	45	flat	5	4	plain	5	unidirectional	feather	porcellanite	indeterminate
DMA 192	flake oblique	52	48	12	39	flat	12	8	plain	9	unidirectional	feather	porcellanite	angular clast
DMA 194	flake end	70	63	38	239	prominent	68	26	abraded	7	bidirectional	feather	porcellanite	angular clast
DMA 195	flake oblique	62	35	18	47	flat	14	15	plain	2	unidirectional	feather	porcellanite	indeterminate
DMA 198	flake oblique	74	51	20	55	flat	13	5	cortical	4	centripetal	feather	porcellanite	angular clast
DMA 199	flake end	38	28	6	6	flat	16	7	plain	3	unidirectional	feather	porcellanite	indeterminate
DMA 200	flake side	34	50	8	17	prominent	23	10	plain	1	unidirectional	feather	porcellanite	indeterminate

DMA 201	flake side	25	27	16	12	flat	18	16	plain	3	irregular	feather	porcellanite	indeterminate
DMA 202	flake oblique	30	24	6	5	prominent	15	6	plain	4	crossed	feather	porcellanite	indeterminate
DMA 206	flake oblique	44	64	14	36	flat	20	8	plain	3	unidirectional	feather	porcellanite	indeterminate
DMA 208	flake oblique	32	15	5	2	prominent	13	4	plain	3	bidirectional	feather	porcellanite	indeterminate
DMA 217	flake end	54	32	13	17	flat	8	3	plain	2	unidirectional	feather	porcellanite	angular clast
DMA 221	flake side	22	48	8	9	flat	21	7	plain	0	na	feather	porcellanite	angular clast
DMA 223	flake end	47	32	10	12	flat	na	na	abraded	2	unidirectional	feather	porcellanite	indeterminate
DMA 224	flake oblique	36	16	6	2	prominent	9	4	abraded	1	unidirectional	feather	porcellanite	indeterminate
DMA 238	flake end	44	21	8	6	prominent	9	3	cortical	4	unidirectional	hinge	porcellanite	indeterminate
DMA 239	flake regular	31	29	5	4	flat	20	5	plain	4	unidirectional	feather	porcellanite	indeterminate
DMA 242	flake end	43	33	7	10	prominent	18	6	facetted	2	unidirectional	feather	porcellanite	indeterminate
DMA 243	flake end	55	25	10	18	flat	na	na	abraded	5	crossed	feather	porcellanite	indeterminate
DMA 250	flake end	25	17	4	2	prominent	10	3	dihedral flat	5	unidirectional	feather	porcellanite	indeterminate
DMA 254	flake end	31	26	6	6	flat	23	7	plain	2	unidirectional	feather	porcellanite	indeterminate
DMA 259	flake side	17	30	4	1	prominent	15	4	dihedral flat	2	unidirectional	feather	porcellanite	indeterminate
DMA 260	flake side	23	51	27	21	prominent	43	12	plain	1	unidirectional	feather	porcellanite	angular clast
DMA 265	flake oblique	115	104	30	411	prominent	na	na	plain	17	centripetal	feather	porcellanite	angular clast
DMA 269	flake end	72	40	14	39	flat	23	8	plain	5	centripetal	feather	porcellanite	angular clast
DMA 270	flake end	101	52	20	101	prominent	17	9	cortical	4	unidirectional	feather	porcellanite	angular clast
DMA 271	flake side	60	60	20	65	flat	27	9	plain	5	crossed	feather	porcellanite	angular clast
DMA 272	flake end	61	34	11	25	prominent	31	11	dihedral flat	5	bidirectional	feather	porcellanite	indeterminate
DMA 273	flake oblique	36	32	10	12	prominent	12	5	plain	2	unidirectional	feather	porcellanite	indeterminate
DMA 274	flake end	85	61	14	80	flat	23	11	plain	4	bidirectional	feather	porcellanite	indeterminate
DMA 275	flake oblique	50	35	6	9	flat	10	5	plain	2	unidirectional	feather	porcellanite	indeterminate
DMA 276	flake oblique	78	43	18	67	prominent	11	6	plain	8	unidirectional	feather	porcellanite	angular clast
DMA 279	flake side	38	50	8	20	prominent	10	7	plain	1	unidirectional	feather	porcellanite	indeterminate
DMA 280	flake oblique	52	40	12	33	prominent	22	10	cortical	2	unidirectional	feather	porcellanite	angular clast
DMA 282	flake end	35	23	8	7	prominent	19	7	plain	1	unidirectional	feather	porcellanite	indeterminate
DMA 285	flake side	47	70	10	51	prominent	50	11	plain	1	unidirectional	feather	porcellanite	angular clast
DMA 288	flake oblique	62	39	14	31	flat	21	11	cortical	7	unidirectional	feather	porcellanite	angular clast
DMA 289	flake end	65	39	8	19	flat	15	8	plain	5	centripetal	feather	porcellanite	indeterminate
DMA 295	flake oblique	76	45	17	50	flat	na	na	abraded	5	unidirectional	feather	porcellanite	angular clast
DMA 296	flake side	41	34	10	19	flat	41	12	cortical	4	bidirectional	feather	porcellanite	angular clast
DMA 300	flake regular	43	42	9	23	prominent	17	8	facetted	5	centripetal	feather	porcellanite	indeterminate
DMA 303	flake side	55	56	12	39	flat	16	6	plain	4	bidirectional	feather	porcellanite	indeterminate
DMA 304	flake end	40	29	7	12	flat	15	8	plain	2	unidirectional	step	porcellanite	angular clast
DMA 307	flake side	30	33	8	8	prominent	29	7	plain	3	unidirectional	feather	porcellanite	angular clast
DMA 309	flake end	65	47	12	44	flat	28	11	facetted	5	unidirectional	feather	porcellanite	indeterminate
DMA 313	flake end	52	35	9	20	prominent	13	7	cortical	5	unidirectional	hinge	porcellanite	angular clast
DMA 314	flake end	50	45	10	28	prominent	22	9	plain	7	bidirectional	feather	porcellanite	angular clast
DMA 316	flake end	57	43	11	23	prominent	10	6	plain	5	unidirectional	feather	porcellanite	indeterminate
DMA 317	flake end	40	31	8	11	prominent	22	9	plain	1	unidirectional	feather	porcellanite	angular clast
DMA 318	flake end	37	34	10	12	flat	17	6	plain	3	bidirectional	feather	porcellanite	indeterminate
DMA 320	flake oblique	35	31	15	22	prominent	27	10	plain	4	centripetal	feather	porcellanite	indeterminate
DMA 321	flake end	59	32	16	32	prominent	15	14	plain	2	unidirectional	feather	porcellanite	angular clast
DMA 325	flake end	50	34	9	18	flat	16	9	plain	1	unidirectional	feather	porcellanite	angular clast
DMA 326	flake end	43	29	7	10	prominent	15	6	plain	2	unidirectional	feather	porcellanite	indeterminate
DMA 328	flake end	33	25	9	8	flat	21	9	plain	4	unidirectional	hinge	porcellanite	indeterminate

DMA 333	flake end	94	69	24	161	prominent	41	21	plain	2	unidirectional	feather	porcellanite	angular clast
DMA 335	flake side	80	113	48	625	prominent	75	38	plain	3	unidirectional	feather	porcellanite	angular clast
DMA 338	flake end	36	25	6	6	flat	11	5	dihedral flat	6	bidirectional	feather	porcellanite	angular clast
DMA 344	flake side	55	62	14	41	prominent	18	8	dihedral flat	6	bidirectional	feather	porcellanite	indeterminate
DMA 345	flake side	42	70	11	41	flat	46	11	plain	1	unidirectional	feather	porcellanite	angular clast
DMA 348	flake side	56	62	25	100	prominent	20	13	plain	11	centripetal	feather	porcellanite	angular clast
DMA 349	flake oblique	67	45	14	46	broken	na	na	na	6	bidirectional	feather	porcellanite	angular clast
DMA 350	flake end	45	33	8	15	flat	27	6	plain	2	unidirectional	feather	porcellanite	angular clast
DMA 352	flake end	50	29	11	15	broken	na	na	na	3	unidirectional	feather	porcellanite	indeterminate
DMA 358	flake end	57	39	11	26	prominent	24	9	plain	7	centripetal	feather	porcellanite	indeterminate
DMA 360	flake end	62	20	8	10	prominent	20	9	plain	2	unidirectional	feather	porcellanite	angular clast
DMA 361	flake side	44	47	10	25	prominent	29	9	plain	3	bidirectional	feather	porcellanite	angular clast
DMA 362	flake end	81	42	12	45	flat	11	5	abraded	3	unidirectional	feather	porcellanite	angular clast
DMA 366	flake side	62	66	11	57	flat	20	5	cortical	0	na	feather	porcellanite	angular clast
DMA 367	flake end	67	52	12	62	flat	29	16	plain	8	centripetal	feather	porcellanite	angular clast
DMA 369	flake oblique	43	34	11	24	flat	na	na	abraded	4	bidirectional	feather	porcellanite	indeterminate
DMA 370	flake end	67	64	15	61	prominent	24	10	plain	6	centripetal	feather	porcellanite	indeterminate
DMA 372	flake side	35	66	16	42	flat	16	11	plain	1	unidirectional	feather	porcellanite	angular clast
DMA 373	flake side	50	71	18	55	prominent	20	11	plain	3	unidirectional	feather	porcellanite	angular clast
DMA 376	flake end	60	35	15	33	flat	19	9	plain	3	unidirectional	feather	porcellanite	indeterminate
DMA 378	flake end	61	45	14	40	flat	20	9	plain	1	unidirectional	feather	porcellanite	angular clast
DMA 384	flake oblique	47	34	12	21	prominent	18	9	cortical	3	unidirectional	feather	porcellanite	angular clast
DMA 385	flake side	32	43	12	19	prominent	11	7	cortical	1	unidirectional	feather	porcellanite	angular clast
DMA 388	flake side	32	43	8	12	flat	27	7	abraded	4	bidirectional	feather	porcellanite	angular clast
DMA 389	flake end	53	35	4	22	prominent	20	14	plain	4	unidirectional	feather	porcellanite	angular clast
DMA 394	flake end	39	25	8	8	prominent	19	8	facetted	3	unidirectional	feather	porcellanite	angular clast
DMA 395	flake end	53	28	7	10	flat	16	6	plain	5	centripetal	feather	porcellanite	indeterminate
DMA 402	flake oblique	43	36	12	19	prominent	16	12	plain	3	centripetal	feather	porcellanite	indeterminate
DMA 405	flake oblique	42	30	14	14	flat	14	9	cortical	4	crossed	feather	porcellanite	angular clast
DMA 407	flake end	90	76	28	193	prominent	28	13	plain	13	centripetal	hinge	porcellanite	indeterminate
DMA 408	flake oblique	45	31	11	15	prominent	13	5	plain	11	unidirectional	feather	porcellanite	angular clast
DMA 410	flake side	34	41	9	11	prominent	19	6	plain	5	unidirectional	feather	porcellanite	angular clast
DMA 412	flake oblique	27	21	5	3	broken	na	na	abraded	4	crossed	feather	porcellanite	indeterminate
DMA 414	flake end	60	45	7	21	prominent	12	4	facetted	3	centripetal	feather	porcellanite	indeterminate
DMA 416	flake end	40	20	12	9	prominent	na	na	plain	2	crossed	indeterminate	porcellanite	indeterminate
DMA 417	flake oblique	29	20	6	4	prominent	21	5	facetted	2	unidirectional	feather	porcellanite	indeterminate
DMA 418	flake side	47	50	9	27	prominent	21	6	plain	10	irregular	feather	porcellanite	indeterminate
DMA 422	flake oblique	32	30	7	5	prominent	12	5	plain	6	irregular	feather	porcellanite	angular clast
DMA 426	flake side	30	38	8	8	prominent	17	8	plain	3	centripetal	feather	porcellanite	indeterminate
DMA 432	flake side	37	49	10	18	broken	28	10	cortical	6	crossed	feather	porcellanite	angular clast
DMA 433	flake end	39	17	7	3	broken	na	na	abraded	2	crossed	feather	porcellanite	indeterminate
DMA 435	flake regular	21	24	5	2	prominent	9	3	abraded	5	irregular	feather	porcellanite	indeterminate
DMA 440	flake oblique	63	46	21	63	flat	23	9	cortical	3	irregular	feather	porcellanite	angular clast
DMA 441	flake side	33	40	10	15	prominent	21	7	cortical	10	unidirectional	feather	porcellanite	angular clast
DMA 442	flake side	43	54	7	18	prominent	18	7	cortical	4	crossed	feather	porcellanite	angular clast
DMA 444	flake regular	41	41	9	14	prominent	22	6	plain	4	crossed	feather	porcellanite	indeterminate
DMA 448	flake end	59	50	12	42	prominent	24	13	plain	7	centripetal	feather	porcellanite	indeterminate
DMA 451	flake end	50	45	14	33	flat	28	10	plain	5	centripetal	feather	porcellanite	indeterminate

DMA 453	flake end	43	34	9	11	prominent	31	10	plain	5	bidirectional	feather	porcellanite	indeterminate
DMA 454	flake end	46	35	9	17	prominent	15	5	plain	4	unidirectional	feather	porcellanite	indeterminate
DMA 455	flake end	67	35	11	31	prominent	23	10	dihedral flat	6	centripetal	feather	porcellanite	indeterminate
DMA 456	flake end	67	38	14	30	prominent	15	6	plain	9	irregular	feather	porcellanite	indeterminate
DMA 470	flake end	55	27	9	11	flat	11	3	plain	4	bidirectional	feather	porcellanite	indeterminate
DMA 472	flake oblique	34	30	9	11	prominent	14	9	plain	1	unidirectional	feather	porcellanite	indeterminate
DMA 474	flake end	86	35	17	44	prominent	25	17	semi-cortical	2	unidirectional	feather	porcellanite	indeterminate
DMA 476	flake side	48	71	20	64	prominent	27	10	plain	4	unidirectional	feather	porcellanite	angular clast
DMA 477	flake oblique	47	40	15	25	broken	na	na	na	4	unidirectional	feather	porcellanite	angular clast
DMA 479	flake end	54	27	6	13	broken	na	na	na	1	unidirectional	feather	porcellanite	angular clast
DMA 480	flake regular	43	47	9	23	prominent	25	8	cortical	5	irregular	feather	porcellanite	angular clast
DMA 488	flake end	75	38	21	52	broken	na	na	na	8	centripetal	feather	porcellanite	indeterminate
DMA 489	flake end	103	50	26	133	prominent	24	12	cortical	5	irregular	feather	porcellanite	angular clast
DMA 491	flake end	46	40	10	20	prominent	10	8	plain	4	unidirectional	feather	porcellanite	angular clast
DMA 493	flake end	92	25	16	41	flat	12	6	plain	17	bidirectional	feather	porcellanite	indeterminate
DMA 495	flake oblique	63	50	18	57	prominent	30	20	plain	4	bidirectional	feather	porcellanite	angular clast
DMA 496	flake end	112	60	38	261	prominent	55	25	plain	3	unidirectional	feather	porcellanite	angular clast
DMA 498	flake side	46	63	11	38	flat	19	6	plain	4	unidirectional	feather	porcellanite	indeterminate
DMA 500	flake end	84	65	25	202	prominent	30	17	cortical	9	unidirectional	feather	porcellanite	angular clast
DMA 501	flake side	44	68	20	54	flat	13	8	plain	3	unidirectional	feather	porcellanite	angular clast
DMA 510	flake end	65	43	17	52	prominent	38	18	plain	3	unidirectional	feather	porcellanite	angular clast
DMA 512	flake end	65	57	11	42	flat	30	8	plain	5	crossed	feather	porcellanite	indeterminate
DMA 513	flake side	34	43	8	12	prominent	11	8	plain	3	unidirectional	feather	porcellanite	indeterminate
DMA 514	flake side	53	64	8	31	prominent	23	9	cortical	0	NA	feather	porcellanite	angular clast
DMA 515	flake end	51	29	10	17	flat	16	5	abraded	2	unidirectional	feather	porcellanite	angular clast
DMA 516	flake oblique	66	50	14	51	prominent	13	6	plain	14	irregular	feather	porcellanite	indeterminate
DMA 519	flake oblique	64	55	13	54	prominent	18	11	plain	8	unidirectional	feather	porcellanite	angular clast
DMA 524	flake end	60	35	14	28	broken	na	na	na	3	unidirectional	feather	porcellanite	indeterminate
DMA 527	flake side	29	39	7	9	prominent	23	8	plain	1	unidirectional	feather	porcellanite	indeterminate
DMA 528	flake end	42	30	8	9	flat	12	5	plain	4	crossed	feather	porcellanite	indeterminate
DMA 531	flake side	52	74	11	46	prominent	na	na	na	1	unidirectional	feather	porcellanite	angular clast
DMA 532	flake regular	47	47	15	35	prominent	47	15	plain	2	unidirectional	feather	porcellanite	angular clast
DMA 541	flake end	64	41	10	27	prominent	na	na	abraded	3	unidirectional	feather	porcellanite	angular clast
DMA 542	flake oblique	48	41	9	18	prominent	29	9	semi-cortical	1	unidirectional	feather	porcellanite	angular clast
DMA 547	flake regular	55	59	22	67	flat	33	18	plain	2	unidirectional	feather	porcellanite	angular clast
DMA 548	flake end	49	23	9	12	flat	18	10	plain	4	bidirectional	feather	porcellanite	indeterminate
DMA 551	flake regular	35	35	7	10	flat	12	6	plain	3	unidirectional	feather	porcellanite	indeterminate
DMA 553	flake end	54	33	8	17	prominent	15	10	cortical	2	unidirectional	feather	porcellanite	angular clast
DMA 555	flake regular	40	40	9	17	prominent	16	6	plain	1	unidirectional	feather	porcellanite	angular clast
DMA 556	flake end	53	32	6	12	flat	na	na	abraded	3	unidirectional	feather	porcellanite	indeterminate
DMA 557	flake end	73	40	17	45	prominent	27	8	dihedral flat	5	bidirectional	feather	porcellanite	angular clast
DMA 559	flake oblique	42	34	11	17	flat	17	9	plain	2	unidirectional	feather	porcellanite	indeterminate
DMA 560	flake end	46	36	13	26	prominent	23	10	plain	0	na	feather	porcellanite	angular clast
DMA 562	flake oblique	90	60	13	82	flat	25	10	plain	2	unidirectional	feather	porcellanite	angular clast
DMA 564	flake end	75	59	14	66	prominent	26	9	semi-cortical	7	centripetal	feather	porcellanite	angular clast
DMA 567	flake end	85	45	16	73	flat	26	7	facetted	6	bidirectional	feather	porcellanite	indeterminate
DMA 568	flake side	41	51	10	25	prominent	40	11	plain	1	unidirectional	feather	porcellanite	indeterminate
DMA 574	flake end	43	30	10	9	prominent	17	10	plain	2	unidirectional	feather	porcellanite	indeterminate

DMA 577	flake oblique	46	37	12	19	flat	13	5	cortical	2	unidirectional	feather	porcellanite	angular clast
DMA 578	flake end	67	47	10	31	flat	32	8	facetted	3	bidirectional	feather	porcellanite	indeterminate
DMA 580	flake end	36	29	7	5	flat	22	9	plain	3	bidirectional	feather	porcellanite	indeterminate
DMA 584	flake end	98	51	12	69	flat	15	7	abraded	2	unidirectional	feather	porcellanite	angular clast
DMA 588	flake end	61	37	11	26	prominent	27	10	dihedral flat	7	centripetal	feather	porcellanite	indeterminate
DMA 591	flake end	67	36	9	18	flat	17	9	plain	2	unidirectional	feather	porcellanite	indeterminate
DMA 592	flake end	59	38	16	32	flat	38	13	plain	3	unidirectional	feather	porcellanite	angular clast
DMA 594	flake regular	54	57	16	40	flat	11	4	plain	1	unidirectional	feather	porcellanite	angular clast
DMA 596	flake side	38	58	9	25	prominent	18	8	plain	3	unidirectional	feather	porcellanite	indeterminate
DMA 604	flake side	18	47	11	14	flat	30	22	plain	0	na	feather	porcellanite	angular clast
DMA 607	flake end	50	40	13	25	prominent	22	14	plain	2	unidirectional	feather	porcellanite	indeterminate
DMA 610	flake oblique	42	39	25	29	prominent	32	5	semi-cortical	1	indeterminate	feather	porcellanite	indeterminate
DMA 611	flake end	47	38	9	16	prominent	13	7	plain	3	unidirectional	feather	porcellanite	angular clast
DMA 613	flake end	37	26	10	8	prominent	24	10	dihedral co	2	unidirectional	feather	porcellanite	indeterminate
DMA 614	flake end	53	47	15	30	prominent	24	8	plain	3	bidirectional	feather	porcellanite	indeterminate
DMA 615	flake end	48	33	8	11	flat	11	4	plain	3	unidirectional	feather	porcellanite	angular clast
DMA 617	flake regular	28	29	8	9	prominent	19	7	semi-cortical	2	unidirectional	feather	porcellanite	angular clast
DMA 622	flake end	60	38	15	34	prominent	7	3	plain	8	unidirectional	feather	porcellanite	indeterminate
DMA 625	flake end	99	49	14	64	flat	37	9	facetted	5	bidirectional	feather	porcellanite	angular clast
DMA 629	flake end	71	42	14	40	flat	na	na	abraded	3	bidirectional	feather	porcellanite	angular clast
DMA 630	flake side	37	51	12	24	prominent	22	11	plain	6	unidirectional	feather	porcellanite	angular clast
DMA 631	flake regular	76	67	31	150	prominent	23	7	cortical	3	bidirectional	feather	porcellanite	angular clast
DMA 633	flake end	46	32	10	19	flat	22	10	facetted	5	unidirectional	feather	porcellanite	indeterminate
DMA 635	flake end	79	41	10	35	prominent	18	11	plain	6	bidirectional	feather	porcellanite	indeterminate
DMA 636	flake side	65	81	23	132	flat	37	31	plain	8	irregular	feather	porcellanite	angular clast
DMA 640	flake end	51	34	9	15	flat	20	7	abraded	3	unidirectional	feather	porcellanite	indeterminate
DMA 643	flake regular	43	46	17	37	prominent	20	12	plain	4	bidirectional	feather	porcellanite	angular clast
DMA 644	flake end	70	44	13	37	broken	na	na	na	12	crossed	feather	porcellanite	angular clast
DMA 647	flake side	49	55	13	45	prominent	25	10	plain	4	unidirectional	feather	porcellanite	indeterminate
DMA 648	flake end	64	56	13	54	prominent	30	12	facetted	11	crossed	feather	porcellanite	indeterminate
DMA 649	flake end	55	30	11	21	flat	20	10	facetted	4	bidirectional	feather	porcellanite	angular clast
DMA 650	flake side	45	67	24	68	prominent	48	21	plain	3	bidirectional	feather	porcellanite	angular clast
DMA 651	flake end	63	35	13	25	prominent	17	9	plain	6	crossed	feather	porcellanite	indeterminate
DMA 653	flake end	76	31	22	35	flat	19	8	cortical	6	centripetal	feather	porcellanite	indeterminate
DMA 654	flake oblique	65	35	13	37	flat	20	9	cortical	2	unidirectional	feather	porcellanite	angular clast
DMA 655	flake regular	50	46	9	15	prominent	7	3	plain	7	centripetal	step	porcellanite	indeterminate
DMA 656	flake side	40	62	10	25	prominent	19	7	plain	6	irregular	feather	porcellanite	indeterminate
DMA 658	flake oblique	59	39	14	34	prominent	20	10	cortical	10	centripetal	feather	porcellanite	angular clast
DMA 659	flake side	42	55	13	24	flat	23	8	cortical	8	centripetal	feather	porcellanite	indeterminate
DMA 660	flake end	85	50	24	79	flat	15	9	plain	9	centripetal	feather	porcellanite	indeterminate
DMA 662	flake end	47	39	14	24	prominent	11	3	plain	4	bidirectional	feather	porcellanite	indeterminate
DMA 663	flake regular	39	40	8	14	prominent	32	9	plain	6	unidirectional	feather	porcellanite	indeterminate
DMA 666	flake end	69	40	8	30	flat	11	5	cortical	7	unidirectional	feather	porcellanite	indeterminate
DMA 671	flake side	35	77	24	79	flat	57	20	plain	7	centripetal	feather	porcellanite	indeterminate
DMA 672	flake oblique	64	56	26	108	prominent	46	26	plain	0	na	feather	porcellanite	angular clast
DMA 676	flake end	45	25	12	15	flat	19	8	plain	2	unidirectional	feather	porcellanite	angular clast
DMA 680	flake end	80	42	16	69	prominent	25	11	plain	6	bidirectional	feather	porcellanite	indeterminate
DMA 681	flake end	60	42	5	22	prominent	11	4	plain	3	unidirectional	feather	porcellanite	indeterminate

DMA 682	flake end	59	47	16	35	prominent	31	15	plain	6	unidirectional	feather	porcellanite	indeterminate
DMA 687	flake regular	83	72	18	77	prominent	19	9	plain	6	centripetal	feather	porcellanite	indeterminate
DMA 689	flake end	76	41	12	46	flat	20	10	plain	4	unidirectional	feather	porcellanite	angular clast
DMA 694	flake end	59	24	13	20	flat	16	9	facetted	7	centripetal	feather	porcellanite	angular clast
DMA 695	flake end	34	28	7	7	prominent	24	6	plain	2	unidirectional	feather	porcellanite	indeterminate
DMA 697	flake end	56	26	18	18	flat	6	3	plain	2	unidirectional	feather	porcellanite	angular clast
DMA 698	flake end	35	22	15	10	flat	17	8	plain	2	bidirectional	feather	porcellanite	angular clast
DMA 704	flake end	84	60	20	124	prominent	26	14	plain	1	unidirectional	feather	porcellanite	angular clast
DMA 705	flake side	42	59	14	37	flat	41	12	cortical	4	unidirectional	hinge	porcellanite	angular clast
DMA 706	flake side	52	68	20	95	prominent	48	12	plain	2	unidirectional	feather	porcellanite	angular clast
DMA 708	flake end	88	52	14	69	prominent	30	10	plain	6	centripetal	feather	porcellanite	indeterminate
DMA 709	flake end	67	39	13	29	flat	21	11	facetted	2	unidirectional	feather	porcellanite	indeterminate
DMA 711	flake regular	49	50	16	35	prominent	39	19	plain	1	unidirectional	feather	porcellanite	angular clast
DMA 712	flake end	57	38	7	15	prominent	12	6	plain	3	unidirectional	feather	porcellanite	indeterminate
DMA 714	flake end	56	30	8	13	flat	8	4	plain	3	bidirectional	feather	porcellanite	indeterminate
DMA 718	flake regular	45	35	18	35	flat	28	8	plain	3	unidirectional	feather	porcellanite	angular clast
DMA 721	flake regular	45	33	11	22	flat	28	10	facetted	4	unidirectional	hinge	porcellanite	indeterminate
DMA 722	flake regular	32	30	19	16	flat	25	14	plain	2	unidirectional	indeterminate	porcellanite	indeterminate
DMA 723	flake regular	37	43	9	17	prominent	30	10	facetted	3	unidirectional	feather	porcellanite	angular clast
DMA 726	flake oblique	116	58	29	264	prominent	32	15	plain	2	bidirectional	feather	porcellanite	angular clast
DMA 728	flake regular	79	94	15	123	prominent	29	12	plain	4	crossed	feather	porcellanite	angular clast
DMA 729	flake oblique	43	31	7	8	flat	10	4	plain	2	bidirectional	feather	porcellanite	angular clast
DMA 730	flake end	53	35	6	12	flat	4	2	plain	4	centripetal	feather	porcellanite	angular clast
DMA 731	flake regular	35	22	6	4	prominent	16	6	plain	4	bidirectional	feather	porcellanite	indeterminate
DMA 732	flake end	38	31	10	12	prominent	25	8	cortical	2	unidirectional	feather	porcellanite	angular clast
DMA 734	flake regular	44	41	11	20	flat	25	11	plain	1	unidirectional	feather	porcellanite	indeterminate
DMA 737	flake regular	47	45	8	17	prominent	19	10	plain	2	unidirectional	feather	porcellanite	indeterminate
DMA 738	flake regular	53	44	13	32	prominent	36	14	plain	2	unidirectional	feather	porcellanite	indeterminate
DMA 740	flake oblique	61	42	8	24	flat	10	4	plain	2	unidirectional	feather	porcellanite	angular clast
DMA 741	flake regular	28	34	15	22	prominent	34	18	plain	3	unidirectional	hinge	porcellanite	indeterminate
DMA 742	flake regular	35	22	7	6	flat	14	5	plain	1	unidirectional	feather	porcellanite	indeterminate
DMA 743	flake side	54	68	20	64	prominent	14	9	plain	2	bidirectional	feather	porcellanite	angular clast
DMA 744	flake oblique	76	55	15	73	flat	20	9	plain	5	centripetal	feather	porcellanite	indeterminate
DMA 745	flake end	90	75	20	107	flat	na	na	na	2	bidirectional	feather	porcellanite	angular clast
DMA 747	flake regular	26	26	7	5	prominent	14	6	plain	1	unidirectional	feather	porcellanite	indeterminate
DMA 748	flake regular	55	48	12	28	prominent	35	13	facetted	2	unidirectional	feather	porcellanite	angular clast
DMA 749	flake side	28	36	26	19	prominent	23	12	plain	3	bidirectional	feather	porcellanite	angular clast
DMA 750	flake side	39	45	13	25	flat	34	13	cortical	2	unidirectional	feather	porcellanite	indeterminate
DMA 751	flake end	65	48	11	32	prominent	31	8	dihedral flat	6	bidirectional	feather	porcellanite	indeterminate
DMA 753	flake side	45	58	17	54	flat	38	10	cortical	5	bidirectional	feather	porcellanite	angular clast
DMA 754	flake end	52	37	11	21	flat	33	11	plain	2	unidirectional	feather	porcellanite	indeterminate
DMA 760	flake end	66	40	15	34	prominent	39	16	plain	3	unidirectional	feather	porcellanite	indeterminate
DMA 762	flake regular	50	51	14	36	flat	16	7	plain	4	centripetal	hinge	porcellanite	indeterminate
DMA 764	flake regular	38	34	10	11	prominent	25	12	plain	3	unidirectional	feather	porcellanite	indeterminate
DMA 766	flake end	54	38	13	27	flat	22	11	abraded	2	unidirectional	feather	porcellanite	angular clast
DMA 767	flake end	30	23	7	6	prominent	19	8	plain	1	unidirectional	feather	porcellanite	angular clast
DMA 768	flake end	41	42	8	20	prominent	23	10	abraded	5	centripetal	hinge	porcellanite	indeterminate
DMA 770	flake regular	42	44	10	14	prominent	18	7	facetted	3	unidirectional	feather	porcellanite	indeterminate

DMA 771	flake side	42	51	14	31	prominent	17	10	plain	5	bidirectional	feather	porcellanite	indeterminate
DMA 773	flake side	26	52	11	15	prominent	39	8	cortical	4	bidirectional	feather	porcellanite	angular clast
DMA 775	flake oblique	51	46	14	26	prominent	21	11	plain	4	unidirectional	feather	porcellanite	indeterminate
DMA 777	flake oblique	63	46	15	57	prominent	12	9	plain	15	unidirectional	feather	porcellanite	angular clast
DMA 778	flake end	61	33	18	34	prominent	21	12	plain	7	unidirectional	feather	porcellanite	angular clast
DMA 786	flake oblique	47	41	12	24	prominent	12	7	plain	3	bidirectional	feather	porcellanite	angular clast
DMA 788	flake regular	36	36	12	17	prominent	24	11	plain	6	bidirectional	feather	porcellanite	indeterminate
DMA 790	flake side	21	36	9	7	flat	32	11	facetted	2	centripetal	feather	porcellanite	indeterminate
DMA 791	flake end	48	26	7	8	flat	16	7	plain	2	unidirectional	feather	porcellanite	indeterminate
DMA 793	flake end	43	25	6	4	prominent	13	7	plain	4	crossed	feather	porcellanite	indeterminate
DMA 803	flake end	57	29	11	15	prominent	29	15	dihedral flat	5	crossed	feather	porcellanite	indeterminate
DMA 805	flake side	46	61	12	37	prominent	38	5	plain	6	bidirectional	feather	porcellanite	indeterminate
DMA 809	flake end	40	25	11	11	flat	na	na	abraded	2	irregular	step	porcellanite	angular clast
DMA 810	flake end	110	82	17	177	prominent	37	15	facetted	4	irregular	feather	porcellanite	angular clast
DMA 816	flake end	78	50	16	75	prominent	22	10	plain	3	bidirectional	feather	porcellanite	angular clast
DMA 817	flake end	67	48	9	25	prominent	7	6	facetted	3	bidirectional	feather	porcellanite	indeterminate
DMA 821	flake side	33	61	16	31	prominent	22	8	plain	1	unidirectional	feather	porcellanite	angular clast

Table A 2. Doma core measurements and other recorded attributes (select).

Code	Typological classification	Length (mm)	Width(mm)	Thickness(mm)	Weight(g)	No. of striking platform	Method ofFlaking	Flaking Pattern	Type of Core	Raw material	Blank type
DMA 4	core	90	80	24	214	1	Levallois	centripetal	Levallois	porcellanite	angular clast
DMA 5	core	86	82	42	326	1	Levallois	centripetal	Levallois	porcellanite	rounded clast
DMA 7	core	114	91	31	416	1	prepared	bidirectional	prepared	porcellanite	angular clast
DMA 8	core	114	98	30	377	1	prepared	bidirectional	prepared	porcellanite	angular clast
DMA 9	core	54	46	35	73	2	discoid	centripetal	discoid	porcellanite	angular clast
DMA 10	core	175	142	36	1263	1	prepared	centripetal	prepared	porcellanite	angular clast
DMA 11	core	122	92	56	654	1	regular	unidirectional	blade	porcellanite	angular clast
DMA 17	core	92	75	40	311	2	prepared	unidirectional	blade	porcellanite	angular clast
DMA 26	core	66	56	31	113	2	regular	multidirectional	amorphous	porcellanite	angular clast
DMA 52	core	83	72	54	255	2	regular	centripetal	prepared	porcellanite	angular clast
DMA 53	core	88	78	26	210	1	regular	core on flak	amorphous	porcellanite	angular clast
DMA 73	core	47	39	33	46	4	regular	multidirectional	exhausted	porcellanite	indeterminate
DMA 178	core	123	102	37	629	2	regular	centripetal	amorphous	porcellanite	angular clast
DMA 184	core	78	43	37	181	2	prepared	unidirectional	blade	porcellanite	angular clast
DMA 186	core	45	53	25	76	4	regular	multidirectional	multi-platform	porcellanite	angular clast
DMA 267	core	99	76	34	277	1	regular	multidirectional	exhausted	porcellanite	angular clast
DMA 290	core	60	59	25	97	2	centripetal	centripetal	exhausted	porcellanite	angular clast
DMA 292	core	56	47	40	109	1	prepared	centripetal	prepared	porcellanite	indeterminate
DMA 319	core	69	51	15	60	1	regular	bidirectional	core-on-flake	porcellanite	indeterminate
DMA 323	core	56	54	24	99	1	regular	orthogonal	amorphous	porcellanite	indeterminate
DMA 331	core	111	97	33	366	1	prepared	centripetal	prepared	porcellanite	angular clast
DMA 332	core	104	53	46	344	1	laminar	unidirectional	blade	porcellanite	angular clast
DMA 341	core	89	80	44	302	1	regular	multidirectional	amorphous	porcellanite	angular clast
DMA 342	core	115	77	40	432	3	regular	unidirectional	prepared	porcellanite	angular clast
DMA 343	core	64	61	38	138	1	regular	centripetal	exhausted	porcellanite	indeterminate
DMA 359	core	74	63	25	128	1	centripetal	centripetal	core-on-flake	porcellanite	indeterminate
DMA 391	core	65	60	39	147	1	prepared	centripetal	prepared	porcellanite	indeterminate
DMA 400	core	100	69	20	213	1	laminar	bidirectional	blade	porcellanite	angular clast
DMA 401	core	96	80	44	315	1	regular	centripetal	amorphous	porcellanite	angular clast
DMA 447	core	92	63	40	281	1	regular	bidirectional	amorphous	porcellanite	angular clast
DMA 449	core	149	95	30	530	1	regular	unidirectional	core-on-flake	porcellanite	angular clast
DMA 462	core	66	65	25	145	1	centripetal	centripetal	prepared	porcellanite	angular clast
DMA 467	core	78	55	25	98	1	centripetal	centripetal	centripetal	porcellanite	angular clast
DMA 475	core	57	80	30	186	1	regular	multidirectional	core-on-flake	porcellanite	angular clast
DMA 478	core	61	48	25	95	1	centripetal	centripetal	centripetal	porcellanite	angular clast
DMA 486	core	94	93	61	497	2	regular	bidirectional	amorphous	porcellanite	angular clast
DMA 504	core	77	64	24	127	1	centripetal	centripetal	prepared	porcellanite	angular clast
DMA 509	core	80	74	43	232	1	centripetal	centripetal	discoid	porcellanite	angular clast
DMA 517	core	100	77	34	311	1	centripetal	centripetal	prepared	porcellanite	angular clast
DMA 518	core	92	70	50	258	2	regular	unidirectional	amorphous	porcellanite	angular clast
DMA 569	core	81	79	36	312	1	regular	centripetal	amorphous	porcellanite	angular clast
DMA 571	core	70	61	17	72	1	centripetal	centripetal	exhausted	porcellanite	angular clast
DMA 582	core	89	73	34	225	1	regular	multidirectional	exhausted	porcellanite	angular clast

DMA 600	core	64	60	33	122	1	discoid	centripetal	discoid	porcellanite	indeterminate
DMA 618	core	97	82	51	383	1	centripetal	centripetal	centripetal	porcellanite	angular clast
DMA 624	core	109	61	42	280	1	centripetal	centripetal	centripetal	porcellanite	angular clast
DMA 634	core	50	45	27	70	2	laminar	bidirectional	blade	porcellanite	angular clast
DMA 637	core	78	64	40	226	1	regular	multidirectional	amorphous	porcellanite	angular clast
DMA 665	core	89	89	40	333	1	regular	centripetal	centripetal	porcellanite	angular clast
DMA 667	core	92	86	20	216	1	prepared	centripetal	prepared	porcellanite	angular clast
DMA 692	core	60	57	19	90	1	prepared	centripetal	prepared	porcellanite	angular clast
DMA 700	core	85	78	48	331	1	regular	multidirectional	amorphous	porcellanite	angular clast
DMA 735	core	49	34	28	48	1	laminar	unidirectional	blade	porcellanite	angular clast
DMA 752	core	87	77	23	139	1	regular	centripetal	centripetal	porcellanite	angular clast
DMA 779	core	65	58	33	172	1	prepared	centripetal	prepared	porcellanite	angular clast
DMA 784	core	80	63	22	118	1	laminar	unidirectional	blade	porcellanite	angular clast
DMA 800	core	103	80	28	262	1	centripetal	centripetal	centripetal	porcellanite	angular clast
DMA 801	core	82	76	43	341	2	regular	bidirectional	amorphous	porcellanite	angular clast
DMA 813	core	60	58	30	136	1	regular	multidirectional	exhausted	porcellanite	angular clast
DMA 814	core	65	54	21	92	2	regular	unidirectional	multi-platform core	porcellanite	angular clast

Table A 3. Doma blade and blade flake measurements and other select attributes.

Code	**Typological classification**	**Length (mm)**	**Width (mm)**	**Thickness (mm)**	**Weight(g)**	**Platform width (mm)**	**Platform thickness (mm)**	**Platform preparation**	**Dorsal ridges**	**Axial percussion**	**Termination**	**Shoulders**	**Bulb of percussion**	**Raw material**	**Blank type**
DMA 13	blade	73	28	11	24	16	5	plain	1	left	feather	4	prominent	porcellanite	angular clast
DMA 93	blade	49	21	7	9	12	7	cortical	2	parallel	feather	1	prominent	porcellanite	angular clast
DMA 129	blade	94	37	11	44	16	7	indeterminate	2	left	feather	2	flat	porcellanite	angular clast
DMA 167	blade	53	30	9	13	15	6	cortical	1	parallel	feather	2	prominent	porcellanite	indeterminate
DMA 182	blade	91	32	11	40	20	8	facetted	3	parallel	feather	1	prominent	porcellanite	angular clast
DMA 196	blade	78	30	8	27	17	8	plain	2	parallel	step	1	flat	porcellanite	indeterminate
DMA 268	blade	84	34	9	32	18	5	facetted	2	right	feather	2	flat	porcellanite	indeterminate
DMA 329	blade	76	29	10	26	14	8	abraded	3	parallel	step	1	prominent	porcellanite	angular clast
DMA 374	blade flake	91	25	14	40	10	10	plain	2	parallel	feather	1	flat	porcellanite	angular clast
DMA 377	blade	83	37	8	27	17	7	facetted	3	parallel	feather	4	flat	porcellanite	indeterminate
DMA 380	blade	105	40	18	85	37	18	plain	2	right	feather	1	prominent	porcellanite	indeterminate
DMA 390	blade flake	75	42	10	32	33	7	facetted	2	right	feather	2	prominent	porcellanite	indeterminate
DMA 403	blade	74	28	8	21	27	6	cortical	1	left	feather	2	flat	porcellanite	indeterminate
DMA 413	blade	90	30	14	36	21	11	cortical	1	left	feather	1	prominent	porcellanite	angular clast
DMA 471	blade	68	19	7	10	na	na	abraded	2	na	feather	na	na	porcellanite	angular clast
DMA 530	blade flake	56	25	11	15	27	10	cortical	1	right	feather	2	flat	porcellanite	indeterminate
DMA 543	blade flake	88	38	10	34	17	8	plain	1	parallel	feather	1	prominent	porcellanite	angular clast
DMA 675	blade	65	29	6	16	8	6	cortical	2	parallel	feather	2	flat	porcellanite	indeterminate
DMA 685	blade flake	97	31	12	33	na	na	na	1	na	feather	na	broken	porcellanite	angular clast
DMA 690	blade flake	94	47	15	78	35	12	plain	4	parallel	feather	1	prominent	porcellanite	indeterminate
DMA 693	blade flake	80	32	12	38	na	na	na	1	parallel	feather	na	na	porcellanite	angular clast
DMA 707	blade flake	84	32	13	40	20	9	cortical	1	left	feather	na	prominent	porcellanite	angular clast

DMA 765	blade flake	56	35	10	25	29	12	plain	1	left	hinge	1	flat	porcellanite	indeterminate
DMA 794	blade flake	72	42	11	39	38	10	facetted	2	left	feather	1	flat	porcellanite	angular clast
DMA 797	blade flake	99	47	14	72	41	11	plain	1	parallel	feather	1	flat	porcellanite	indeterminate
DMA 808	blade flake	70	35	13	35	21	14	plain	1	right	feather	1	prominent	porcellanite	indeterminate

Table A 4. Doma biface measurement and other select attributes.

Code	Typological classification	Length (mm)	Width (mm)	Thickness (mm)	Weight (g)	L1	Width at the tip (B1)	Width at the base (B2)	Width at the Mid-Point B3	Thickness at Tip (T1)	Thickness at base (T2)	Thickness at Mid- Point (T3)	Tip angle	No. of flake scars on dorsal	No. of flake scars on ventral	Working edge length	Biface shape	Butt shape	Raw material	Blank type
DMA 1	biface	115	80	27	220	38	45	70	77	17	17	26	20	20	25	290	pear shaped	absent	porcellanite	indeterminate
DMA 2	biface	137	107	36	570	40	60	91	103	23	31	36	38	11	11	324	pear shaped	round	porcellanite	angular clast
DMA 823	biface	97	75	27	188	0	45	68	73	14	19	27	39	17	10	190	point	square	porcellanite	angular clast

Table A 5. Bagia flake measurements and other select attributes.

Code	Typological classification	Length (mm)	Width (mm)	Thickness (mm)	Weight (g)	Bulb of percussion	Platform Width (mm)	Platform Thickness (mm)	Platform preparation	No. of dorsal flake scars	Dorsal flakescar pattern	Flake termination	Raw material	Blank type
BGA 2	flake oblique	107	84	17	159	prominent	38	11	plain	0	na	feather	porcellanite	angular clast
BGA 5	flake side	52	70	15	65	prominent	70	12	plain	4	unidirectional	feather	porcellanite	indeterminate
BGA 13	flake end	96	65	33	202	prominent	57	35	plain	4	irregular	feather	porcellanite	angular clast
BGA 14	Flake oblique	59	54	12	36	prominent	18	8	plain	7	bidirectional	feather	porcellanite	indeterminate
BGA 27	flake end	78	52	19	75	prominent	47	16	facetted	3	bidirectional	feather	porcellanite	angular clast
BGA 29	flake end	52	35	14	27	flat	21	12	plain	2	unidirectional	feather	porcellanite	angular clast
BGA 35	flake oblique	57	49	13	37	prominent	38	9	semi-cortical	2	unidirectional	feather	porcellanite	angular clast
BGA 36	flake end	69	44	14	37	prominent	21	11	cortical	2	unidirectional	feather	porcellanite	angular clast
BGA 38	flake side	45	58	11	33	prominent	27	11	facetted	1	unidirectional	feather	porcellanite	indeterminate
BGA 39	flake oblique	57	42	14	43	prominent	19	10	plain	3	unidirectional	feather	porcellanite	angular clast
BGA 41	flake end	95	61	26	128	prominent	15	12	cortical	2	indeterminate	feather	porcellanite	angular clast
BGA 44	flake end	55	30	15	28	flat	28	13	cortical	3	unidirectional	feather	porcellanite	angular clast
BGA 51	flake side	37	43	14	24	prominent	33	9	plain	6	irregular	feather	porcellanite	angular clast
BGA 57	flake side	47	57	11	33	flat	25	10	facetted	5	bidirectional	feather	porcellanite	indeterminate
BGA 59	flake side	34	45	10	13	prominent	25	9	facetted	4	bidirectional	feather	porcellanite	indeterminate
BGA 69	flake end	47	40	15	29	flat	24	10	cortical	2	unidirectional	feather	porcellanite	angular clast
BGA 79	flake end	36	33	15	16	prominent	11	5	plain	2	unidirectional	feather	porcellanite	angular clast
BGA 86	flake regular	50	47	13	30	prominent	41	12	facetted	6	unidirectional	feather	porcellanite	indeterminate
BGA 94	flake regular	41	41	11	21	prominent	12	6	plain	3	irregular	feather	porcellanite	indeterminate
BGA 95	flake side	31	37	9	13	prominent	14	9	plain	3	unidirectional	feather	porcellanite	indeterminate
BGA 105	flake end	43	31	8	11	flat	13	8	plain	3	unidirectional	feather	porcellanite	indeterminate
BGA 108	flake end	54	20	17	19	flat	19	4	plain	3	irregular	feather	porcellanite	angular clast
BGA 111	flake end	113	74	12	104	flat	15	6	plain	7	bidirectional	feather	porcellanite	angular clast

BGA 113	flake side	22	36	7	8	prominent	18	5	abraded	4	unidirectional	feather	porcellanite	angular clast
BGA 114	flake end	56	32	7	14	prominent	20	7	facetted	3	unidirectional	feather	porcellanite	indeterminate
BGA 115	flake end	55	37	8	19	flat	9	5	plain	3	bidirectional	feather	porcellanite	indeterminate
BGA 116	flake end	60	27	20	28	prominent	25	14	plain	3	irregular	feather	porcellanite	angular clast
BGA 117	flake end	80	35	15	53	prominent	26	8	plain	0	na	feather	porcellanite	angular clast
BGA 127	flake side	90	110	24	127	flat	26	9	plain	6	centripetal	feather	porcellanite	indeterminate
BGA 138	flake side	76	87	28	157	prominent	38	16	plain	1	unidirectional	feather	porcellanite	angular clast
BGA 139	flake end	125	50	22	123	prominent	29	9	plain	4	unidirectional	feather	porcellanite	angular clast
BGA 144	flake end	82	69	26	155	prominent	na	na	abraded	4	irregular	feather	porcellanite	angular clast
BGA 145	flake end	61	45	17	53	flat	16	11	plain	3	unidirectional	feather	porcellanite	angular clast
BGA 146	flake end	81	56	11	53	flat	21	9	plain	2	unidirectional	feather	porcellanite	indeterminate
BGA 148	flake end	100	54	17	89	prominent	33	17	plain	4	bidirectional	feather	porcellanite	indeterminate
BGA 151	flake end	100	53	19	110	prominent	20	13	facetted	1	unidirectional	step	porcellanite	angular clast
BGA 154	flake end	101	74	21	116	prominent	24	8	plain	2	unidirectional	step	porcellanite	angular clast
BGA 158	flake end	84	49	21	86	flat	23	10	plain	5	crossed	feather	porcellanite	angular clast
BGA 160	flake end	62	48	15	41	flat	15	9	plain	1	unidirectional	feather	porcellanite	angular clast
BGA 161	flake end	89	73	17	97	flat	21	7	facetted	4	centripetal	feather	porcellanite	indeterminate

Table A 6. Bagia core measurements and other select attributes

Code	**Typological classification**	**Length (mm)**	**Width (mm)**	**Thickness (mm)**	**Weight(g)**	**Striking platform**	**Method of Flaking**	**Flaking Pattern**	**Type of Core**	**Raw material**	**Blank Type**
BGA 1	core	85	75	39	259	2	discoid	discoid	discoid	porcellanite	angular clast
BGA 15	core	56	48	24	64	1	prepared	bidirectional	prepared	porcellanite	angular clast
BGA 16	core	53	43	28	60	1	regular	unidirectional	single platform unifacial	chalcedony	angular clast
BGA 25	core	69	62	16	82	2	prepared	centripetal	prepared	porcellanite	angular clast
BGA 28	core	72	58	16	90	2	prepared	bidirectional	prepared	porcellanite	angular clast
BGA 30	core	70	55	16	69	2	prepared	centripetal	prepared	porcellanite	angular clast
BGA 31	core	63	60	23	116	2	prepared	centripetal	Levallois	porcellanite	angular clast
BGA 32	core	68	67	16	91	2	prepared	centripetal	prepared	porcellanite	angular clast
BGA 34	core	68	59	17	70	2	prepared	multidirectional	prepared	porcellanite	angular clast
BGA 37	core	78	51	31	113	2	centripetal	centripetal	exhausted	porcellanite	angular clast
BGA 52	core	38	32	22	29	2	laminar	bidirectional	blade	porcellanite	angular clast
BGA 58	core	75	50	19	78	1	prepared	centripetal	prepared	porcellanite	angular clast
BGA 61	core	80	79	27	181	2	centripetal	centripetal	prepared	porcellanite	angular clast
BGA 62	core	50	44	26	61	2	regular	centripetal	exhausted	porcellanite	angular clast
BGA 63	core	68	58	20	97	2	regular	centripetal	prepared	porcellanite	angular clast
BGA 70	core	68	55	21	87	1	prepared	bidirectional	prepared	porcellanite	angular clast
BGA 73	core	54	45	18	50	2	regular	multidirectional	core-on-flake	porcellanite	angular clast
BGA 76	core	57	40	30	63	2	1: laminar; 2: regular	multidirectional	blade	porcellanite	angular clast
BGA 77	core	85	52	14	70	1	centripetal	centripetal	prepared	porcellanite	angular clast
BGA 89	core	46	41	27	41	3	1: laminar; 2: irregular	unidirectional	blade	porcellanite	indeterminate
BGA 103	core	35	30	19	19	2	centripetal	centripetal	prepared	porcellanite	indeterminate
BGA 107	core	73	42	31	117	5	1-2: unidirectional, 3:	multidirectional	multi-platform	porcellanite	angular clast
BGA 119	core	31	30	17	19	3	regular	unidirectional	blade	porcellanite	angular clast

BGA 131	core	92	70	67	768	2	regular	multidirectional	multi-platform	porcellanite	angular clast
BGA 132	core	143	85	68	1110	3	regular	multidirectional	multi-platform	porcellanite	angular clast
BGA 133	core	103	84	19	199	1	centripetal	centripetal	prepared	porcellanite	angular clast
BGA 135	core	116	87	55	602	2	regular	multidirectional	multi-platform	porcellanite	angular clast
BGA 136	core	180	81	51	789	2	regular	unidirectional	single platform bifacial	porcellanite	angular clast
BGA 140	core	78	68	34	194	3	1,3: regular; 2 centripetal	multidirectional	prepared	porcellanite	angular clast
BGA 143	core	64	43	19	80	1	laminar	unidirectional	blade	porcellanite	angular clast
BGA 150	core	96	66	27	197	2	centripetal	centripetal	prepared	porcellanite	angular clast
BGA 152	core	76	63	55	297	2	regular	bidirectional	double platform	porcellanite	angular clast
BGA 155	core	97	84	34	325	2	centripetal	centripetal	prepared	porcellanite	angular clast
BGA 157	core	95	44	22	185	1	laminar	unidirectional	blade	porcellanite	angular clast
BGA 159	core	52	44	40	77	3	regular	multidirectional	multi-platform	porcellanite	angular clast

Table A 7. Khempur flake measurements and other select attributes.

Code	**Typological classification**	**Length(mm)**	**Width(mm)**	**Thickness(mm)**	**Weight(g)**	**Bulb of percussion**	**Platform width (mm)**	**Platform thickness**	**Platform preparation**	**No. of dorsalflake scars**	**Dorsal flake scarpattern**	**Flake termination**	**Raw material**	**Blank type**
KHM 2	flake end	49	35	6	9	flat	17	6	plain	2	unidirectional	feather	porcellanite	indeterminate
KHM 8	flake end	42	31	8	12	flat	28	10	facetted	3	unidirectional	feather	porcellanite	indeterminate
KHM 10	flake oblique	68	45	21	57	prominent	23	12	plain	3	bidirectional	feather	porcellanite	angular clast
KHM 12	flake side	66	55	23	76	flat	33	14	abraded	4	centripetal	feather	porcellanite	indeterminate
KHM 14	flake regular	38	39	14	26	flat	18	9	plain	3	crossed	feather	porcellanite	indeterminate
KHM 15	flake end	42	21	7	7	flat	14	5	plain	1	unidirectional	feather	porcellanite	indeterminate
KHM 16	flake regular	32	31	6	6	prominent	8	3	plain	3	crossed	feather	porcellanite	angular clast
KHM 17	flake end	44	24	7	9	prominent	20	8	facetted	3	bidirectional	feather	porcellanite	indeterminate
KHM 21	flake regular	38	36	9	14	prominent	13	6	plain	5	bidirectional	feather	porcellanite	angular clast
KHM 23	flake end	49	43	9	20	prominent	25	8	plain	2	unidirectional	feather	porcellanite	indeterminate
KHM 24	flake oblique	49	46	11	26	flat	11	6	plain	3	bidirectional	feather	porcellanite	angular clast
KHM 26	flake end	54	46	10	21	flat	30	9	facetted	4	bidirectional	feather	porcellanite	indeterminate
KHM 29	flake regular	39	38	11	21	flat	33	10	dihedral flat	10	centripetal	feather	porcellanite	indeterminate
KHM 36	flake end	41	26	14	15	flat	12	10	plain	3	unidirectional	feather	porcellanite	indeterminate
KHM 38	flake end	40	35	8	15	flat	na	na	abraded	4	unidirectional	feather	porcellanite	indeterminate
KHM 39	flake end	47	28	6	7	flat	4	1	plain	2	unidirectional	feather	porcellanite	angular clast
KHM 42	flake side	54	66	19	65	flat	21	6	abraded	3	unidirectional	feather	porcellanite	indeterminate
KHM 43	flake regular	41	41	7	9	prominent	5	4	plain	1	unidirectional	feather	porcellanite	indeterminate
KHM 44	flake side	27	33	8	5	flat	na	na	plain	2	bidirectional	feather	porcellanite	indeterminate
KHM 49	flake end	60	37	11	22	prominent	16	6	plain	4	unidirectional	feather	porcellanite	angular clast
KHM 50	flake end	49	25	12	15	flat	15	6	plain	4	unidirectional	feather	porcellanite	indeterminate
KHM 52	flake side	36	45	8	13	flat	19	8	plain	2	unidirectional	feather	porcellanite	indeterminate
KHM 53	flake oblique	39	34	13	21	prominent	22	11	plain	3	bidirectional	feather	porcellanite	indeterminate
KHM 57	flake end	89	69	17	121	prominent	69	18	facetted	6	centripetal	feather	porcellanite	indeterminate
KHM 58	flake end	58	36	15	33	flat	35	17	abraded	2	indeterminate	hinge	porcellanite	indeterminate
KHM 60	flake regular	42	46	9	21	prominent	32	8	facetted	3	irregular	feather	porcellanite	indeterminate
KHM 63	flake end	48	38	10	17	prominent	20	6	facetted	3	centripetal	feather	porcellanite	indeterminate

KHM 69	flake end	54	29	12	24	prominent	24	10	plain	3	unidirectional	feather	porcellanite	indeterminate
KHM 70	flake oblique	51	57	13	40	flat	29	13	dihedral flat	6	crossed	feather	porcellanite	indeterminate
KHM 71	flake oblique	51	37	15	25	prominent	15	4	abraded	2	unidirectional	feather	porcellanite	angular clast
KHM 73	flake end	44	27	10	11	prominent	19	10	plain	3	unidirectional	feather	porcellanite	indeterminate
KHM 78	flake side	49	69	22	77	prominent	43	19	plain	1	unidirectional	feather	porcellanite	angular clast
KHM 83	flake end	57	43	14	47	flat	25	7	plain	11	centripetal	feather	porcellanite	indeterminate
KHM 84	flake oblique	62	73	23	106	prominent	38	11	plain	6	unidirectional	feather	porcellanite	angular clast
KHM 85	flake end	58	53	17	47	flat	18	5	plain	5	unidirectional	feather	porcellanite	angular clast
KHM 94	flake side	35	71	20	30	flat	64	20	semi-cortical	2	bidirectional	feather	porcellanite	angular clast
KHM 95	flake end	64	51	17	59	prominent	26	8	plain	2	unidirectional	feather	porcellanite	angular clast
KHM 97	flake side	42	53	10	26	prominent	31	10	plain	7	centripetal	feather	porcellanite	angular clast
KHM 99	flake oblique	46	40	15	33	prominent	29	8	plain	7	centripetal	feather	porcellanite	indeterminate
KHM 101	flake end	46	38	10	17	prominent	17	6	facetted	2	unidirectional	feather	porcellanite	angular clast
KHM 103	flake regular	66	69	27	148	prominent	69	12	plain	4	bidirectional	feather	porcellanite	angular clast
KHM 104	flake end	82	46	16	79	prominent	37	14	facetted	4	unidirectional	feather	porcellanite	indeterminate
KHM 105	flake side	50	58	16	61	prominent	42	12	plain	2	unidirectional	feather	porcellanite	angular clast
KHM 110	flake end	51	46	13	35	prominent	22	8	plain	12	bidirectional	feather	porcellanite	indeterminate
KHM 113	flake regular	48	45	12	24	prominent	23	9	plain	5	bidirectional	feather	porcellanite	indeterminate
KHM 116	flake end	47	34	6	12	prominent	na	na	abraded	4	unidirectional	feather	porcellanite	indeterminate
KHM 117	flake oblique	54	51	14	38	prominent	19	11	plain	4	bidirectional	feather	porcellanite	indeterminate
KHM 118	flake end	51	41	11	25	prominent	34	10	cortical	4	unidirectional	feather	porcellanite	indeterminate
KHM 120	flake end	62	40	11	26	prominent	13	7	plain	4	unidirectional	feather	porcellanite	indeterminate
KHM 124	flake regular	32	32	12	14	prominent	20	13	plain	2	unidirectional	hinge	porcellanite	angular clast
KHM 129	flake regular	39	42	13	19	prominent	22	14	plain	2	unidirectional	feather	porcellanite	indeterminate
KHM 133	flake end	56	30	12	17	prominent	22	7	facetted	1	unidirectional	feather	porcellanite	angular clast
KHM 134	flake end	57	40	12	38	prominent	19	11	facetted	10	unidirectional	feather	porcellanite	indeterminate
KHM 135	flake oblique	49	26	14	23	prominent	15	8	plain	1	unidirectional	feather	chalcedony	rounded clast
KHM 137	flake oblique	37	41	8	10	prominent	17	6	abraded	5	bidirectional	feather	porcellanite	indeterminate
KHM 138	flake end	85	67	16	98	prominent	40	17	facetted	2	unidirectional	feather	porcellanite	angular clast
KHM 141	flake regular	50	27	11	20	prominent	20	6	plain	3	irregular	feather	porcellanite	indeterminate
KHM 148	flake end	45	34	11	15	flat	25	9	plain	5	unidirectional	feather	porcellanite	indeterminate
KHM 152	flake side	65	82	17	109	prominent	35	18	cortical	7	centripetal	feather	porcellanite	angular clast
KHM 153	flake regular	44	43	12	23	prominent	42	10	plain	3	indeterminate	feather	porcellanite	indeterminate

Table A 8. Khempur core measurements and other select attributes.

Code	**Typological classification**	**Length (mm)**	**Width (mm)**	**Thickness (mm)**	**Weight (g)**	**No. of striking platform**	**Method of Flaking**	**Flaking Pattern**	**Type of Core**	**Raw material**	**Blank type**
KHM 1	core	49	45	29	84	1	regular	bidirectional	single platform bifacial	porcellanite	angular clast
KHM 4	core	61	60	30	132	1	prepared	bidirectional	prepared	porcellanite	angular clast
KHM 11	core	85	68	57	371	3	prepared	multidirectional	multi-platform	porcellanite	angular clast
KHM 22	core	35	25	15	18	2	laminar	unidirectional	core-on-flake	porcellanite	indeterminate
KHM 37	core	64	54	18	77	1	prepared	bidirectional	prepared	porcellanite	angular clast
KHM 55	core	54	52	36	111	3	regular	multidirectional	multi-platform	porcellanite	angular clast

KHM 61	core	79	73	32	158	2	prepared	centripetal	prepared	porcellanite	angular clast
KHM 67	core	55	55	30	110	3	regular	multidirectional	exhausted	porcellanite	angular clast
KHM 76	core	75	59	45	266	4	regular	multidirectional	exhausted	porcellanite	angular clast
KHM 77	core	52	39	30	70	3	regular	unidirectional	multi-platform	porcellanite	angular clast
KHM 79	core	91	57	61	324	2	prepared	multidirectional	prepared	porcellanite	angular clast
KHM 80	core	61	52	32	106	2	prepared	1- unidirectional; 2- bidirectional	prepared	porcellanite	angular clast
KHM 81	core	55	43	32	87	3	regular	unidirectional	multi-platform	porcellanite	angular clast
KHM 82	core	46	30	20	30	2	laminar	unidirectional	blade	porcellanite	angular clast
KHM 86	core	102	83	45	472	1	prepared	centripetal	prepared	porcellanite	angular clast
KHM 87	core	47	31	30	59	3	regular	unidirectional	multi-platform	porcellanite	angular clast
KHM 88	core	60	61	17	53	2	laminar	bidirectional opposed	blade	porcellanite	angular clast
KHM 89	core	48	29	23	45	4	regular	unidirectional	multi-platform	porcellanite	angular clast
KHM 92	core	39	41	18	25	2	laminar	bidirectional	core-on-flake	porcellanite	indeterminate
KHM 100	core	75	72	42	298	1	regular	unidirectional	single platform unifacial	porcellanite	angular clast
KHM 102	core	78	60	23	146	7	laminar	unidirectional	blade	porcellanite	angular clast
KHM 109	core	45	29	17	31	2	regular	multidirectional	multi-platform	porcellanite	angular clast
KHM 114	core	48	41	35	96	3	regular	unidirectional	multi-platform	porcellanite	angular clast
KHM 115	core	52	34	30	64	3	regular	unidirectional	multi-platform	porcellanite	angular clast
KHM 121	core	41	29	29	51	3	regular	unidirectional	multi-platform	porcellanite	angular clast
KHM 122	core	47	42	36	87	3	regular	unidirectional	multi-platform	porcellanite	angular clast
KHM 125	core	69	52	43	178	1	regular	unidirectional	single platform unifacial	porcellanite	angular clast
KHM 130	core	58	51	45	196	2	regular	unidirectional	multi-platform	porcellanite	angular clast
KHM 136	core	55	53	37	166	2	regular	multidirectional	multi-platform	porcellanite	angular clast
KHM 150	core	56	56	30	118	2	regular	unidirectional	multi-platform	porcellanite	angular clast

Table A 9. Parva Chinguri flake measurements and other select attributes.

Code	**Typological classification**	**Length (mm)**	**Width (mm)**	**Thickness (mm)**	**Weight(g)**	**Bulb of percussion**	**Platform width (mm)**	**Platform thickness (mm)**	**Platform preparation**	**No. of dorsal flake scars**	**Dorsal flake scar pattern**	**Flake termination**	**Raw material**	**Blank type**
PCI 2	flake end	32	21	7	6	prominent	15	6	plain	5	unidirectional	feather	porcellanite	indeterminate
PCI 12	flake oblique	29	17	7	3	prominent	4	2	plain	0	na	feather	chert	indeterminate
PCI 22	flake end	41	34	12	17	prominent	20	8	plain	3	unidirectional	feather	porcellanite	indeterminate
PCI 37	flake end	31	25	6	4	prominent	21	6	semi-cortical	3	unidirectional	feather	porcellanite	indeterminate
PCI 38	flake end	25	20	5	2	prominent	13	5	plain	1	unidirectional	feather	porcellanite	indeterminate
PCI 39	flake side	17	30	5	2	prominent	11	3	plain	0	na	feather	porcellanite	angular clast
PCI 42	flake side	28	33	7	6	prominent	16	5	plain	2	bidirectional	feather	chert	angular clast
PCI 51	flake side	29	32	7	5	prominent	20	5	abraded	1	unidirectional	feather	chert	angular clast
PCI 61	flake end	24	20	8	4	prominent	15	6	abraded	1	unidirectional	feather	porcellanite	angular clast
PCI 84	flake end	28	18	5	0	flat	17	2	abraded	1	unidirectional	feather	porcellanite	indeterminate
PCI 86	flake end	32	27	11	7	prominent	25	10	plain	2	unidirectional	feather	porcellanite	indeterminate
PCI 106	flake side	15	30	5	0	prominent	17	4	plain	2	unidirectional	feather	porcellanite	indeterminate
PCI 115	flake end	18	11	3	0	prominent	8	3	plain	1	unidirectional	feather	porcellanite	indeterminate
PCI 139	flake side	14	17	4	0	prominent	12	4	plain	0	na	feather	porcellanite	indeterminate

PCI 223	flake end	24	20	9	2	prominent	7	4	plain	2	bidirectional	feather	quartz	indeterminate
PCI 229	flake side	17	22	5	0	prominent	16	5	abraded	1	unidirectional	feather	porcellanite	indeterminate
PCI 234	flake end	19	17	4	0	prominent	7	3	plain	1	unidirectional	feather	quartz	indeterminate
PCI 257	flake side	22	32	12	4	prominent	14	9	plain	2	irregular	feather	porcellanite	angular clast
PCI 298	flake end	50	25	14	9	prominent	6	2	plain	4	irregular	feather	chert	angular clast
PCI 302	flake oblique	32	27	8	4	prominent	8	3	plain	4	irregular	feather	porcellanite	indeterminate
PCI 304	flake oblique	38	29	8	6	prominent	14	6	plain	1	unidirectional	feather	porcellanite	angular clast
PCI 309	flake regular	18	18	6	0	flat	4	1	plain	1	unidirectional	feather	porcellanite	indeterminate
PCI 312	flake end	51	37	15	26	prominent	16	6	plain	4	centripetal	feather	chert	indeterminate
PCI 318	flake side	25	33	11	3	flat	11	2	plain	0	na	feather	porcellanite	indeterminate
PCI 326	flake side	19	23	8	0	prominent	16	8	plain	3	unidirectional	feather	quartz	indeterminate
PCI 332	flake side	31	38	10	9	prominent	20	9	semi-cortical	2	unidirectional	feather	porcellanite	angular clast
PCI 334	flake end	23	17	5	0	prominent	9	4	plain	3	unidirectional	feather	quartz	indeterminate
PCI 338	flake side	29	39	11	8	prominent	23	11	plain	3	crossed	feather	porcellanite	angular clast
PCI 341	flake end	50	36	12	24	prominent	13	8	plain	4	bidirectional	feather	porcellanite	angular clast
PCI 345	flake end	41	27	8	5	prominent	15	6	plain	3	unidirectional	feather	porcellanite	indeterminate
PCI 347	flake side	26	33	10	4	prominent	9	4	semi-cortical	1	unidirectional	feather	porcellanite	angular clast
PCI 348	flake side	28	44	6	7	prominent	17	6	plain	1	unidirectional	feather	porcellanite	indeterminate
PCI 354	flake end	30	20	4	0	prominent	7	3	plain	3	indeterminate	feather	porcellanite	indeterminate
PCI 356	flake end	40	30	5	3	prominent	21	5	facetted	0	na	feather	porcellanite	indeterminate
PCI 371	flake end	25	18	5	0	prominent	14	4	cortical	1	unidirectional	feather	porcellanite	angular clast
PCI 406	flake end	48	40	7	11	prominent	24	7	cortical	0	na	feather	porcellanite	angular clast
PCI 413	flake side	23	37	6	0	prominent	27	6	plain	1	unidirectional	feather	chert	indeterminate
PCI 416	flake end	36	28	11	7	prominent	11	5	plain	1	unidirectional	feather	porcellanite	indeterminate
PCI 422	flake end	48	38	8	11	prominent	26	6	abraded	4	unidirectional	feather	limestone	indeterminate
PCI 425	flake end	30	28	12	7	prominent	13	3	plain	1	unidirectional	feather	quartz	indeterminate
PCI 426	flake end	48	31	8	9	prominent	12	5	plain	2	bidirectional	feather	porcellanite	indeterminate
PCI 429	flake end	30	23	11	3	prominent	11	6	plain	2	unidirectional	feather	quartz	pebble
PCI 431	flake regular	33	33	12	11	prominent	25	7	plain	2	indeterminate	feather	porcellanite	indeterminate
PCI 438	flake side	26	35	8	4	prominent	23	8	plain	1	unidirectional	feather	quartzite	indeterminate
PCI 443	flake end	55	43	17	47	prominent	33	15	cortical	1	unidirectional	feather	porcellanite	angular clast

Table A 10. Parva Chinguri core measurements and other select attributes.

Code	Typological classification	Length (mm)	Width (mm)	Thickness (mm)	Weight (mm)	No. of striking platform	Method of Flaking	Flaking Pattern	Type of Core	Raw material	Blank type
PCI 16	core	53	25	15	23	2	laminar	bidirectional	blade core	porcellanite	indeterminate
PCI 19	core	37	17	14	11	2	laminar	bidirectional	blade core	porcellanite	indeterminate
PCI 24	core	66	32	11	27	1	laminar	unidirectional	blade core	porcellanite	angular clast
PCI 25	core	54	36	23	57	1	laminar	unidirectional	blade core	chert	indeterminate
PCI 29	core	41	26	15	20	1	laminar	unidirectional	blade core	chert	indeterminate
PCI 31	core	43	21	15	13	1	laminar	unidirectional	blade core	chert	indeterminate
PCI 57	core	26	19	11	4	2	laminar	bidirectional	microblade	porcellanite	indeterminate
PCI 58	core	24	14	13	4	1	laminar	unidirectional	microblade	porcellanite	angular clast

PCI 60	core	27	14	11	6	2	regular	orthogonal	exhausted	quartz	pebble
PCI 220	core	41	28	23	39	2	laminar	bidirectional	blade core	porcellanite	angular clast
PCI 306	core	45	43	21	43	1	laminar	unidirectional	blade core	chert	indeterminate
PCI 313	core	64	50	41	130	1	regular	centripetal	exhausted	chert	angular clast
PCI 317	core	42	17	13	10	2	laminar	bidirectional	blade core	porcellanite	indeterminate
PCI 327	core	29	23	17	11	2	regular	bidirectional	exhausted	quartz	indeterminate
PCI 343	core	25	14	12	2	1	laminar	unidirectional	microblade	porcellanite	angular clast
PCI 409	core	30	24	20	11	2	regular	bidirectional	prepared	porcellanite	indeterminate
PCI 410	core	73	57	28	128	1	regular	unidirectional	single platform unifacial	porcellanite	angular clast
PCI 411	core	75	64	60	443	1	regular	unidirectional	single platform unifacial	porcellanite	angular clast
PCI 415	core	30	25	13	8	2	laminar	bidirectional	exhausted	porcellanite	indeterminate
PCI 421	core	72	56	49	250	1	regular	unidirectional	single platform unifacial	quartz	angular clast
PCI 434	core	25	14	9	1	1	laminar	unidirectional	microblade	porcellanite	indeterminate
PCI 435	core	40	19	14	8	1	laminar	unidirectional	blade core	quartz	indeterminate
PCI 441	core	47	36	16	42	1	laminar	bidirectional	blade core	porcellanite	angular clast
PCI 442	core	60	30	24	46	2	laminar	bidirectional	blade core	chert	indeterminate

Table A 11. Parva Chinguri blade and microblade measurements and other select attributes.

Code	Typological classification	Length (mm)	Width (mm)	Thickness (mm)	Weight(g)	Platform width (mm)	Platform thickness (mm)	Platform preparation	Dorsal ridges	Axial percussion	Termination	Shoulders	Bulb of percussion	Raw material	Blank type
PCI 26	blade	60	30	11	20	15	7	plain	1	parallel	feather	2	prominent	porcellanite	angular clast
PCI 36	blade	41	18	11	6	8	3	plain	2	parallel	overshot	1	prominent	porcellanite	indeterminate
PCI 44	blade	35	15	15	6	13	12	cortical	2	parallel	feather	1	prominent	porcellanite	angular clast
PCI 52	blade	35	12	5	1	3	1	plain	1	parallel	feather	2	flat	porcellanite	indeterminate
PCI 65	blade	35	13	3	0	7	3	facetted	1	right	feather	1	prominent	porcellanite	indeterminate
PCI 67	blade	41	12	6	1	8	1	plain	3	parallel	feather	1	flat	porcellanite	indeterminate
PCI 73	microblade	26	12	4	0	9	3	plain	2	parallel	step	1	prominent	chert	indeterminate
PCI 80	blade	38	13	4	0	5	2	plain	2	left	feather	2	prominent	porcellanite	angular clast
PCI 82	blade	41	10	5	0	5	2	plain	1	left	feather	2	flat	porcellanite	angular clast
PCI 85	blade	32	13	3	0	6	1	plain	2	parallel	feather	2	flat	porcellanite	indeterminate
PCI 91	microblade	23	10	4	0	6	2	plain	3	right	feather	1	prominent	porcellanite	indeterminate
PCI 97	microblade	18	9	2	0	5	1	abraded	2	parallel	feather	3	flat	porcellanite	indeterminate
PCI 112	blade	33	5	4	0	3	3	abraded	2	parallel	feather	3	flat	porcellanite	indeterminate
PCI 133	microblade	24	6	2	0	3	1	abraded	1	right	feather	2	prominent	porcellanite	indeterminate
PCI 232	microblade	25	11	3	0	8	2	abraded	2	left	feather	2	flat	porcellanite	indeterminate
PCI 256	blade	43	10	3	0	6	2	plain	2	right	feather	2	flat	porcellanite	angular clast
PCI 310	blade	41	20	10	10	11	10	plain	1	left	feather	1	prominent	porcellanite	angular clast
PCI 322	microblade	29	14	7	0	10	5	abraded	2	left	feather	1	prominent	porcellanite	indeterminate
PCI 333	blade	38	18	8	1	7	4	plain	3	parallel	feather	2	prominent	porcellanite	indeterminate
PCI 336	blade	39	18	6	0	6	2	plain	2	left	hinge	2	prominent	porcellanite	indeterminate
PCI 368	microblade	23	9	3	0	5	1	plain	1	parallel	feather	3	flat	porcellanite	indeterminate
PCI 372	microblade	22	9	4	0	5	2	plain	2	left	feather	3	prominent	porcellanite	indeterminate
PCI 390	microblade	17	7	1	0	6	1	abraded	2	right	feather	4	flat	chert	indeterminate

PCI 391	microblade	17	8	3	0	5	2	plain	2	left	feather	2	prominent	porcellanite	indeterminate
PCI 402	blade	45	21	9	8	18	6	plain	3	left	feather	2	prominent	porcellanite	indeterminate
PCI 428	microblade	25	8	4	0	6	4	abraded	1	left	feather	1	NA	porcellanite	indeterminate
PCI 437	microblade	27	13	7	0	8	4	cortical	0	right	feather	1	prominent	chert	indeterminate

Table A 12. Kargara flake measurements and other select attributes.

Code	**Typological classification**	**Length (mm)**	**Width (mm)**	**Thickness (mm)**	**Weight(g)**	**Bulb of percussion**	**Platform width (mm)**	**Platform thickness (mm)**	**Platform preparation**	**No. of dorsalflake scars**	**Dorsal flake scarpattern**	**Flake termination**	**Raw material**	**Blank type**
KGR 13	flake side	38	47	19	47	prominent	39	11	plain	1	unidirectional	feather	porcellanite	angular clast
KGR 24	flake side	25	26	14	11	prominent	22	15	semi-cortical	1	unidirectional	feather	porcellanite	angular clast
KGR 31	flake side	40	43	19	36	prominent	31	8	plain	3	centripetal	feather	porcellanite	indeterminate
KGR 36	flake oblique	68	69	21	77	prominent	20	9	dihedral convex	3	centripetal	feather	quartzite	indeterminate
KGR 42	flake side	61	41	15	36	prominent	52	15	facetted	5	centripetal	feather	porcellanite	indeterminate
KGR 45	flake end	36	26	16	13	prominent	17	5	semi-cortical	4	bidirectional	feather	chalcedony	pebble
KGR 46	flake end	38	35	12	23	prominent	25	9	cortical	4	irregular	feather	porcellanite	angular clast
KGR 47	flake end	36	35	8	12	prominent	27	9	cortical	2	unidirectional	feather	porcellanite	angular clast
KGR 48	flake side	32	42	13	23	prominent	42	14	cortical	1	unidirectional	feather	porcellanite	angular clast
KGR 49	flake side	27	37	7	6	prominent	19	5	plain	3	bidirectional	feather	porcellanite	angular clast
KGR 50	flake end	55	35	13	32	prominent	21	8	plain	3	bidirectional	feather	chert	pebble
KGR 51	flake side	35	58	12	32	flat	57	15	plain	0	na	feather	porcellanite	angular clast
KGR 52	flake side	52	53	16	46	prominent	44	12	plain	3	irregular	feather	porcellanite	angular clast
KGR 54	flake side	38	45	17	29	prominent	23	12	plain	3	centripetal	feather	chert	indeterminate
KGR 55	flake side	28	57	13	27	prominent	57	9	cortical	1	unidirectional	feather	chalcedony	pebble
KGR 57	flake end	34	29	16	15	prominent	21	9	cortical	0	na	feather	chalcedony	pebble
KGR 58	flake side	36	37	13	21	prominent	19	12	cortical	2	irregular	feather	porcellanite	angular clast
KGR 59	flake end	39	27	9	9	prominent	22	6	semi-cortical	1	na	step	porcellanite	angular clast
KGR 61	flake side	24	41	7	7	prominent	25	6	abraded	3	irregular	feather	porcellanite	angular clast
KGR 62	flake side	25	26	9	8	prominent	13	5	semi-cortical	1	unidirectional	feather	agate	pebble
KGR 63	flake end	51	26	11	16	flat	25	9	cortical	3	unidirectional	hinge	porcellanite	angular clast
KGR 64	flake end	40	28	8	14	flat	27	11	plain	1	unidirectional	feather	porcellanite	angular clast
KGR 65	flake end	42	25	9	11	prominent	8	4	plain	0	na	feather	agate	pebble
KGR 67	flake side	19	30	8	5	flat	10	5	cortical	0	na	feather	chalcedony	pebble
KGR 71	flake end	45	28	16	20	prominent	15	7	plain	2	irregular	feather	porcellanite	angular clast
KGR 72	flake side	36	39	9	11	prominent	17	8	plain	2	unidirectional	feather	porcellanite	indeterminate
KGR 75	flake side	35	38	13	25	prominent	33	9	cortical	0	na	feather	chert	pebble
KGR 80	flake side	31	33	8	7	prominent	18	8	plain	4	unidirectional	feather	chert	indeterminate
KGR 83	flake end	34	24	8	7	prominent	19	8	cortical	3	unidirectional	feather	porcellanite	angular clast
KGR 84	flake side	30	31	9	8	prominent	16	10	cortical	1	unidirectional	feather	chert	pebble
KGR 86	flake end	37	34	8	10	prominent	16	7	plain	3	bidirectional	feather	porcellanite	indeterminate
KGR 87	flake end	29	25	10	6	prominent	21	10	abraded	1	unidirectional	feather	chert	pebble
KGR 89	flake end	41	33	7	12	prominent	24	6	plain	5	centripetal	feather	porcellanite	indeterminate
KGR 92	flake end	54	51	13	44	prominent	31	10	cortical	2	unidirectional	feather	porcellanite	angular clast

KGR 93	flake end	52	42	16	43	prominent	26	11	plain	2	unidirectional	feather	porcellanite	angular clast
KGR 95	flake side	42	54	18	53	flat	43	13	cortical	5	unidirectional	feather	porcellanite	angular clast
KGR 96	flake side	45	57	20	39	prominent	16	4	semi-cortical	1	unidirectional	feather	porcellanite	angular clast
KGR 98	flake side	24	31	16	16	prominent	29	9	plain	6	bidirectional	feather	porcellanite	angular clast
KGR 99	flake side	34	36	11	14	prominent	19	10	plain	3	irregular	feather	porcellanite	indeterminate
KGR 101	flake end	60	33	14	39	prominent	15	7	cortical	8	centripetal	step	porcellanite	angular clast
KGR 105	flake side	15	30	9	5	flat	18	4	cortical	4	unidirectional	feather	chert	angular clast
KGR 106	flake regular	27	27	10	10	prominent	23	10	plain	0	na	feather	chert	pebble
KGR 107	flake regular	47	47	15	27	prominent	22	10	cortical	4	unidirectional	feather	chert	angular clast
KGR 109	flake side	29	48	14	25	prominent	33	18	cortical	1	unidirectional	feather	porcellanite	angular clast
KGR 110	flake side	18	25	7	4	prominent	18	8	facetted	1	indeterminate	feather	porcellanite	indeterminate
KGR 116	flake end	35	29	10	8	flat	14	7	plain	4	centripetal	feather	porcellanite	indeterminate
KGR 117	flake end	22	21	8	4	flat	16	9	cortical	3	irregular	feather	porcellanite	angular clast
KGR 118	flake side	22	30	9	6	flat	25	11	plain	1	unidirectional	feather	porcellanite	indeterminate
KGR 120	flake end	25	23	6	3	prominent	17	7	cortical	2	unidirectional	feather	porcellanite	angular clast
KGR 125	flake end	30	27	8	6	prominent	28	8	cortical	2	bidirectional	feather	porcellanite	angular clast
KGR 126	flake end	47	32	13	15	broken	12	3	abraded	2	irregular	feather	porcellanite	angular clast
KGR 129	flake end	35	30	15	17	prominent	16	9	dihedral convex	3	irregular	feather	porcellanite	indeterminate
KGR 131	flake side	34	40	15	18	prominent	13	7	cortical	4	unidirectional	feather	porcellanite	angular clast
KGR 135	flake end	35	22	5	5	broken	6	2	abraded	2	unidirectional	feather	porcellanite	indeterminate
KGR 139	flake end	27	18	8	4	prominent	15	8	abraded	3	unidirectional	feather	chert	indeterminate
KGR 140	flake end	32	20	10	6	prominent	14	5	plain	1	unidirectional	feather	porcellanite	angular clast
KGR 142	flake oblique	30	25	7	6	prominent	10	5	facetted	1	unidirectional	feather	chert	indeterminate
KGR 144	flake side	25	29	7	7	prominent	19	8	plain	1	unidirectional	feather	porcellanite	angular clast
KGR 153	flake end	33	23	9	3	prominent	21	8	facetted	1	unidirectional	feather	quartzite	indeterminate
KGR 154	flake side	18	27	5	2	flat	11	4	plain	3	indeterminate	feather	porcellanite	indeterminate
KGR 164	flake end	32	25	9	8	prominent	15	5	plain	4	bidirectional	feather	quartz	indeterminate
KGR 165	flake end	28	16	7	3	flat	9	4	plain	2	unidirectional	feather	quartz	indeterminate
KGR 178	flake end	15	12	1	0	prominent	5	2	plain	1	unidirectional	feather	porcellanite	indeterminate
KGR 179	flake end	25	16	8	3	flat	10	3	abraded	3	centripetal	feather	quartz	indeterminate
KGR 182	flake end	28	21	9	5	prominent	6	3	plain	1	unidirectional	feather	quartz	pebble
KGR 184	flake end	34	17	10	5	prominent	10	5	plain	4	bidirectional	feather	quartz	angular clast
KGR 185	flake oblique	21	20	7	2	prominent	15	5	cortical	0	na	feather	quartz	pebble
KGR 188	flake side	8	13	1	0	prominent	4	1	plain	0	na	feather	porcellanite	indeterminate
KGR 198	flake end	23	14	5	0	flat	13	5	abraded	2	indeterminate	feather	chert	indeterminate
KGR 201	flake end	25	18	6	0	prominent	6	2	plain	4	irregular	feather	chert	indeterminate
KGR 218	flake end	29	30	13	14	prominent	23	10	cortical	0	na	feather	agate	pebble
KGR 222	flake end	58	45	15	44	prominent	35	15	cortical	0	na	feather	chalcedony	pebble
KGR 223	flake end	27	23	11	7	prominent	15	10	cortical	1	unidirectional	feather	chalcedony	pebble
KGR 224	flake end	33	24	11	6	prominent	18	10	cortical	0	na	feather	chalcedony	pebble
KGR 225	flake oblique	29	29	9	5	prominent	18	5	abraded	0	NA	feather	quartz	pebble

Table A 13. Kargara core measurements and other select attributes.

Code	Typological classification	Length (mm)	Width (mm)	Thickness (mm)	Weight(g)	No. of striking platform	Method of Flaking	Flaking Pattern	Type of Core	Raw material	Blank type
KGR 1	core	140	88	80	960	1	regular	unidirectional	single platform unifacial	quartzite	angular clast
KGR 2	core	45	38	19	38	2	prepared	centripetal, unidirectional	prepared	porcellanite	angular clast
KGR 4	core	63	47	32	99	1	discoid	discoid	discoid	quartzite	indeterminate
KGR 5	core	58	41	27	62	3	regular	multidirectional	multi-platform	porcellanite	angular clast
KGR 6	core	36	33	34	63	2	laminar	bidirectional	blade	porcellanite	angular clast
KGR 7	core	40	39	26	46	4	laminar	multidirectional	exhausted core	porcellanite	angular clast
KGR 8	core	35	34	25	41	2	laminar	unidirectional	blade	porcellanite	angular clast
KGR 10	core	35	27	23	25	2	laminar	unidirectional	blade	porcellanite	indeterminate
KGR 11	core	67	31	22	53	2	laminar	bidirectional	blade	porcellanite	angular clast
KGR 12	core	69	34	32	108	1	regular	unidirectional	single platform unifacial	chert	angular clast
KGR 14	core	25	19	13	5	2	laminar	bidirectional	microblade	chert	pebble
KGR 15	core	56	42	30	86	4	prepared	multidirectional	exhausted	porcellanite	angular clast
KGR 16	core	55	51	51	106	3	prepared	unidirectional, centripetal	prepared	porcellanite	angular clast
KGR 17	core	86	60	59	374	1	regular	unidirectional	single platform unifacial	quartzite	angular clast
KGR 18	core	56	51	48	175	2	regular	unidirectional	multi-platform	quartzite	angular clast
KGR 19	core	50	36	34	76	3	regular	multidirectional	multi-platform	quartzite	angular clast
KGR 20	core	35	22	22	33	2	laminar	bidirectional	blade	quartz	angular clast
KGR 25	core	47	36	14	34	2	laminar	bidirectional	blade	porcellanite	indeterminate
KGR 26	core	76	47	25	92	2	regular	unidirectional	multi-platform	quartz	pebble
KGR 30	core	30	32	16	22	3	laminar	bidirectional	core-on-flake	chert	indeterminate
KGR 32	core	53	33	22	43	1	regular	multidirectional	core-on-flake	porcellanite	indeterminate
KGR 33	core	48	33	27	37	2	regular	bidirectional	double platform	quartzite	angular clast
KGR 35	core	42	17	14	14	1	laminar	unidirectional	blade	porcellanite	angular clast
KGR 44	core	38	22	11	14	1	laminar	unidirectional	core-on-flake	porcellanite	angular clast
KGR 77	core	50	34	22	35	2	laminar	bidirectional	exhausted	porcellanite	angular clast
KGR 78	core	24	21	16	10	2	laminar	multidirectional	exhausted	porcellanite	indeterminate
KGR 100	core	41	30	18	25	1	laminar	unidirectional	blade	porcellanite	angular clast
KGR 102	core	29	18	10	6	1	laminar	unidirectional	microblade	porcellanite	angular clast
KGR 121	core	25	21	17	10	3	laminar	multidirectional	exhausted	porcellanite	indeterminate
KGR 127	core	64	26	13	2	1	laminar	unidirectional	core-on-flake	porcellanite	angular clast
KGR 221	core	38	22	22	16	1	regular	unidirectional	core-on-flake	chalcedony	pebble

Table A 14. Kargara blade and microblade measurements and other select attributes.

Code	Typological classification	Length (mm)	Width (mm)	Thickness (mm)	Weight(g)	Platform width (mm)	Platform thickness (mm)	Platform preparation	Dorsal ridges	Dorsal flake scars	Axial percussion	Termination	Shoulders	Bulb of percussion	Exterior core surface	Raw material	Blank type
KGR 85	microblade	27	14	3	5	6	3	plain	3	4	left	feather	2,4	prominent	3	chert	pebble
KGR 123	blade	46	19	4	5	12	4	Plain	2	3	parallel	feather	2	prominent	4	porcellanite	angular clast
KGR 148/	blade	51	17	5	8	3	2	abraded	1	1	right	feather	3	flat	7	porcellanite	angular clast
KGR 155	blade	36	9	5	4	na	na	na	0	1	left	feather	na	na	na	porcellanite	angular clast
KGR 159	blade	32	10	4	2	4	1	abraded	1	2	right	indeterminate	3	flat	3	chert	indeterminate
KGR 171	microblade	25	8	3	0	5	2	plain	1	2	parallel	feather	1	flat	3	quartz	indeterminate
KGR 180	microblade	29	14	4	1	5	2	plain	1	2	left	feather	2	flat	3	quartz	indeterminate

Table A 15. Newari flake measurements and other select attributes.

Code	Typological classification	Length(mm)	Width(mm)	Thickness(mm)	Weight(g)	Bulb of percussion	Platform width (mm)	Platform thickness (mm)	Platform preparation	No. of dorsalflake scars	Dorsal flake scarpattern	Flake termination	Raw material	Blank type
NRI 65	flake side	26	30	15	12	prominent	na	na	abraded	2	irregular	feather	chert	indeterminate
NRI 176	flake end	48	40	18	23	prominent	17	10	plain	4	irregular	feather	chert	indeterminate
NRI 181	flake side	23	37	9	9	prominent	19	10	plain	1	unidirectional	feather	chert	indeterminate
NRI 183	flake oblique	37	32	13	16	prominent	15	5	plain	3	crossed	feather	chert	indeterminate
NRI 184	flake end	51	27	10	13	flat	12	4	abraded	0	na	feather	chert	indeterminate
NRI 185	flake oblique	41	29	11	10	prominent	11	5	plain	8	irregular	feather	chert	indeterminate
NRI 186	flake end	51	26	11	14	flat	6	3	abraded	3	irregular	feather	chert	indeterminate
NRI 187	flake oblique	40	39	15	23	prominent	16	6	plain	3	irregular	feather	chert	indeterminate
NRI 190	flake end	37	35	12	17	prominent	20	10	plain	3	bidirectional	feather	chert	indeterminate
NRI 195	flake oblique	35	35	11	11	prominent	6	3	plain	1	unidirectional	feather	chert	indeterminate
NRI 196	flake end	36	30	12	13	prominent	24	10	plain	2	unidirectional	feather	chert	indeterminate
NRI 197	flake end	55	33	17	28	prominent	13	7	plain	3	irregular	feather	chert	indeterminate
NRI 198	flake side	25	41	12	11	prominent	14	7	plain	1	unidirectional	feather	chert	indeterminate
NRI 199	flake oblique	42	35	13	20	prominent	26	16	plain	0	na	feather	chert	indeterminate
NRI 203	flake side	28	30	11	12	prominent	26	10	cortical	1	unidirectional	feather	chert	indeterminate
NRI 204	flake end	30	20	16	13	prominent	12	10	cortical	1	unidirectional	feather	chalcedony	pebble
NRI 205	flake end	30	28	13	13	prominent	11	7	plain	1	unidirectional	feather	chert	pebble
NRI 206	flake side	33	37	12	16	flat	22	8	plain	2	unidirectional	feather	chert	pebble
NRI 209	flake oblique	34	34	14	17	prominent	14	5	plain	2	unidirectional	feather	chert	pebble
NRI 213	flake end	28	27	5	6	prominent	13	6	cortical	3	irregular	feather	chert	pebble
NRI 215	flake end	42	28	20	28	prominent	23	19	cortical	0	na	feather	chert	pebble
NRI 220	flake oblique	39	29	10	10	prominent	14	3	cortical	3	irregular	feather	chert	pebble
NRI 222	flake regular	22	22	8	4	prominent	na	na	na	0	na	feather	chert	pebble
NRI 224	flake end	42	31	10	13	broken	na	na	abraded	1	unidirectional	feather	chert	pebble
NRI 233	flake end	40	22	8	9	broken	na	na	abraded	3	unidirectional	feather	chert	pebble
NRI 241	flake side	25	40	12	9	prominent	13	14	plain	4	irregular	feather	quartz	indeterminate
NRI 242	flake side	17	36	5	4	prominent	15	3	plain	3	unidirectional	feather	chert	pebble
NRI 246	flake oblique	34	30	6	7	prominent	9	6	cortical	3	irregular	feather	chert	pebble

NRI 247	flake side	24	26	10	7	prominent	24	10	plain	0	na	feather	chert	pebble
NRI 248	flake end	35	23	8	8	prominent	12	5	plain	5	unidirectional	feather	chert	pebble
NRI 249	flake end	30	28	14	15	prominent	26	14	plain	2	unidirectional	step	chert	indeterminate
NRI 250	flake end	35	28	10	11	prominent	17	8	plain	1	unidirectional	feather	chert	pebble
NRI 254	flake side	24	33	10	7	prominent	21	5	plain	5	unidirectional	feather	quartz	indeterminate
NRI 255	flake oblique	39	21	10	9	prominent	12	5	plain	4	bidirectional	feather	chert	indeterminate
NRI 258	flake end	30	27	12	12	prominent	14	7	plain	3	unidirectional	step	chert	indeterminate
NRI 261	flake end	31	20	9	6	prominent	18	6	plain	2	unidirectional	feather	chert	indeterminate
NRI 262	flake side	27	31	8	7	flat	na	na	na	0	na	feather	quartz	pebble
NRI 263	flake oblique	33	28	8	6	prominent	21	7	semi-cortical	3	irregular	feather	chert	indeterminate
NRI 264	flake side	23	39	8	8	prominent	6	4	plain	4	unidirectional	feather	chert	indeterminate
NRI 266	flake oblique	32	27	11	9	prominent	16	10	plain	0	na	step	chert	indeterminate
NRI 268	flake end	30	20	9	4	prominent	12	6	plain	2	unidirectional	feather	chert	indeterminate
NRI 269	flake end	32	22	9	6	prominent	10	3	plain	1	unidirectional	step	chert	pebble
NRI 272	flake oblique	27	24	10	7	prominent	5	3	plain	4	unidirectional	step	chert	indeterminate
NRI 273	flake end	30	23	12	4	prominent	4	5	abraded	2	unidirectional	feather	chert	indeterminate
NRI 276	flake end	30	17	4	2	prominent	14	4	plain	3	unidirectional	feather	chert	indeterminate
NRI 278	flake oblique	24	24	8	4	prominent	10	8	cortical	1	unidirectional	feather	chert	pebble
NRI 279	flake end	37	18	8	7	prominent	7	5	plain	3	unidirectional	feather	chert	indeterminate
NRI 280	flake side	16	35	8	4	prominent	13	6	plain	3	unidirectional	feather	chert	indeterminate
NRI 281	flake end	28	24	6	3	prominent	19	5	cortical	1	unidirectional	feather	chert	indeterminate
NRI 282	flake end	36	12	14	4	prominent	7	3	plain	4	unidirectional	feather	chert	indeterminate
NRI 283	flake side	17	26	14	6	prominent	22	5	cortical	1	unidirectional	feather	chalcedony	pebble
NRI 284	flake oblique	24	25	10	6	prominent	19	10	facetted	2	unidirectional	feather	chert	pebble
NRI 290	flake oblique	26	25	6	4	prominent	14	5	cortical	6	centripetal	feather	chert	pebble
NRI 292	flake end	25	23	7	4	prominent	22	7	cortical	1	unidirectional	hinge	chert	pebble
NRI 293	flake end	27	24	5	2	prominent	7	4	plain	0	na	indeterminate	quartz	pebble
NRI 300	flake end	32	21	8	5	prominent	6	4	abraded	0	na	feather	quartz	pebble
NRI 305	flake end	26	18	7	3	prominent	17	7	cortical	0	na	feather	quartz	pebble
NRI 307	flake end	19	13	5	1	prominent	na	na	abraded	1	unidirectional	step	chert	pebble
NRI 309	flake regular	20	20	4	2	prominent	10	3	dihedral flat	0	na	feather	chert	pebble
NRI 311	flake side	15	25	6	1	prominent	17	5	plain	1	unidirectional	step/hinge	chert	pebble
NRI 313	flake end	23	12	5	1	flat	na	na	cortical	0	na	feather	chert	pebble
NRI 318	flake side	18	31	11	5	prominent	na	na	cortical	1	unidirectional	feather	chert	pebble
NRI 319	flake end	40	26	7	6	broken	na	na	abraded	2	unidirectional	feather	chert	pebble
NRI 321	flake end	40	29	11	12	prominent	24	10	cortical	2	unidirectional	feather	chert	pebble
NRI 322	flake side	20	34	9	6	prominent	33	11	cortical	1	unidirectional	hinge/feather	chert	pebble
NRI 324	flake end	24	19	11	5	flat	na	na	abraded	0	na	feather	chalcedony	pebble
NRI 327	flake end	37	20	8	7	flat	na	na	abraded	4	irregular	step	chert	pebble
NRI 328	flake end	33	19	6	3	prominent	7	2	plain	1	unidirectional	step	chert	pebble
NRI 329	flake end	31	22	4	3	prominent	8	4	plain	3	unidirectional	feather	chert	pebble
NRI 331	flake end	26	19	7	3	prominent	10	4	plain	4	unidirectional	step	chert	pebble
NRI 332	flake end	37	25	12	10	prominent	8	4	plain	4	irregular	feather	chert	pebble
NRI 333	flake end	30	18	9	4	prominent	12	6	plain	3	bidirectional	hinge/feather	chert	indeterminate
NRI 339	flake side	23	32	8	5	prominent	14	5	plain	2	bidirectional	feather	chert	pebble
NRI 340	flake end	26	18	10	4	prominent	na	na	abraded	3	centripetal	feather	chert	pebble
NRI 341	flake end	37	18	5	3	prominent	9	3	plain	1	unidirectional	hinge	chert	pebble
NRI 342	flake oblique	43	20	7	6	prominent	11	3	abraded	0	unidirectional	feather	agate	indeterminate

NRI 344	flake end	33	18	7	4	prominent	5	2	cortical	3	unidirectional	hinge	chert	pebble
NRI 346	flake oblique	27	16	5	2	prominent	7	3	plain	4	crossed/unidirectional		chert	pebble
NRI 347	flake end	25	14	7	3	prominent	7	5	abraded	3	unidirectional	feather	chert	pebble
NRI 348	flake end	26	10	10	3	prominent	10	4	plain	2	unidirectional	step?	chert	pebble
NRI 350	flake end	24	19	7	3	prominent	15	5	facetted	1	unidirectional	feather	chert	pebble
NRI 353	flake end	24	12	7	2	flat	7	3	abraded	0	na	feather	chert	pebble
NRI 360	flake end	28	18	6	3	prominent	10	5	plain	0	na	feather	chert	pebble
NRI 361	flake end	30	21	10	6	prominent	13	6	plain	2	unidirectional	feather	chert	pebble
NRI 365	flake side	18	28	8	4	prominent	13	5	cortical	0	na	feather	quartz	pebble
NRI 366	flake end	26	23	11	8	prominent	14	7	facetted	0	na	feather	chert	pebble
NRI 369	flake side	23	25	5	4	prominent	18	7	plain	2	unidirectional	feather	chert	indeterminate
NRI 374	flake end	29	18	6	4	flat	11	5	cortical	0	na	feather	chert	pebble
NRI 375	flake side	21	23	7	3	prominent	8	3	facetted	4	na	feather	chert	indeterminate
NRI 378	flake end	30	18	8	4	prominent	13	8	cortical	1	unidirectional	feather	chert	pebble
NRI 381	flake end	27	16	4	2	flat	8	3	abraded	0	na	feather	quartz	indeterminate
NRI 389	flake end	30	14	6	2	flat	4	2	plain	2	bidirectional	feather	chalcedony	pebble
NRI 396	flake end	30	25	9	5	prominent	10	5	facetted	6	unidirectional	feather	chert	pebble
NRI 400	flake side	33	36	9	8	flat	8	4	cortical	1	unidirectional	feather	chert	pebble
NRI 408	flake oblique	26	19	8	4	prominent	11	5	plain	5	bidirectional	feather	chert	pebble
NRI 411	flake end	15	13	2	0	prominent	8	2	abraded	2	unidirectional	feather	quartz	indeterminate
NRI 416	flake end	23	14	5	0	prominent	6	3	abraded	3	unidirectional	feather	chert	indeterminate
NRI 424	flake side	20	25	8	3	prominent	12	6	plain	1	irregular	feather	chert	pebble
NRI 425	flake side	16	21	6	0	prominent	15	5	cortical	1	unidirectional	feather	porcellanite	angular clast
NRI 426	flake end	26	14	6	1	prominent	7	2	plain	0	na	step	chert	pebble
NRI 432	flake end	19	13	4	0	prominent	12	4	facetted	3	irregular	feather	quartz	indeterminate
NRI 435	flake end	28	16	7	2	prominent	15	7	cortical	0	na	feather	chert	pebble
NRI 440	flake end	23	14	4	1	prominent	10	4	plain	2	unidirectional	feather	chert	pebble
NRI 441	flake side	20	36	12	7	prominent	7	6	cortical	2	irregular	feather	chalcedony	pebble
NRI 444	flake end	26	15	7	3	flat	12	4	plain	1	unidirectional	feather	chert	pebble
NRI 445	flake end	19	18	5	2	prominent	9	3	cortical	0	na	feather	chert	pebble
NRI 446	flake end	18	17	5	2	prominent	9	4	plain	3	unidirectional	feather	quartz	pebble
NRI 450	flake side	20	21	8	4	prominent	22	9	cortical	1	unidirectional	feather	chert	pebble
NRI 455	flake end	23	13	5	1	flat	6	3	plain	3	irregular	feather	chert	pebble
NRI 456	flake oblique	19	20	7	4	prominent	17	7	plain	3	unidirectional	feather	chert	pebble
NRI 460	flake end	21	17	4	1	flat	17	4	plain	1	unidirectional	feather	quartz	indeterminate
NRI 470	flake end	23	21	7	4	prominent	5	3	plain	0	na	feather	chert	pebble
NRI 482	flake end	17	13	5	1	flat	3	2	plain	5	unidirectional	feather	chert	indeterminate
NRI 485	flake end	19	16	3	0	flat	5	2	plain	2	bidirectional	feather	porcellanite	indeterminate
NRI 487	flake end	21	12	4	1	flat	11	3	facetted	2	unidirectional	feather	chert	pebble
NRI 488	flake end	18	9	6	1	prominent	8	5	plain	3	irregular	feather	chert	indeterminate
NRI 489	flake end	19	14	5	1	prominent	5	3	plain	3	unidirectional	step	chert	indeterminate
NRI 496	flake oblique	43	41	14	23	prominent	28	14	cortical	0	na	feather	chert	angular clast
NRI 498	flake end	39	25	10	10	prominent	23	10	facetted	2	unidirectional	feather	chert	angular clast
NRI 500	flake side	44	67	18	61	prominent	48	17	cortical	0	unidirectional	step	chert	angular clast
NRI 501	flake oblique	40	30	10	12	prominent	9	4	plain	1	unidirectional	feather	chert	angular clast
NRI 503	flake side	26	38	15	14	prominent	20	14	cortical	0	na	feather	chert	indeterminate
NRI 507	flake end	34	24	8	8	prominent	14	8	cortical	2	unidirectional	feather	chert	indeterminate
NRI 508	flake regular	37	37	7	7	prominent	17	5	cortical	2	unidirectional	feather	chert	indeterminate

NRI 511	flake side	23	33	7	5	prominent	14	7	cortical	4	unidirectional	hinge	chert	pebble
NRI 514	flake oblique	42	26	6	6	flat	16	5	cortical	2	unidirectional	feather	porcellanite	angular clast
NRI 517	flake side	21	27	11	7	prominent	24	11	cortical	0	na	feather	chert	pebble
NRI 522	flake end	41	21	9	8	prominent	18	9	plain	0	na	feather	chert	indeterminate
NRI 524	flake oblique	35	30	7	9	prominent	14	7	cortical	1	unidirectional	feather	chert	indeterminate
NRI 525	flake end	36	26	12	10	prominent	12	6	plain	3	irregular	feather	chert	indeterminate
NRI 526	flake side	25	32	12	9	prominent	32	12	cortical	1	unidirectional	feather	agate	indeterminate
NRI 535	flake oblique	56	28	15	32	flat	14	10	cortical	1	unidirectional	step	chert	indeterminate
NRI 536	flake end	42	40	16	36	prominent	33	14	abraded	2	unidirectional	feather	chert	indeterminate
NRI 540	flake end	35	26	12	13	prominent	17	7	plain	5	bidirectional	feather	chert	indeterminate
NRI 541	flake side	14	31	17	25	prominent	39	15	cortical	0	na	feather	chert	pebble
NRI 545	flake side	27	35	13	14	prominent	25	10	facetted	0	na	feather	agate	pebble
NRI 553	flake end	28	20	10	6	prominent	14	6	plain	3	bidirectional	feather	chalcedony	pebble
NRI 559	flake end	37	26	14	16	prominent	18	12	cortical	0	na	feather	chert	pebble
NRI 563	flake oblique	43	26	10	8	flat	25	4	plain	3	unidirectional	feather	chert	angular clast

Table A 16. Newari core measurements and other select attributes.

Code	Typological classification	Length (mm)	Width (mm)	Thickness (mm)	Weight (g)	No. of striking platform	Method ofFlaking	Flaking Pattern	Type of Core	Raw material	Blank type
NRI 1	core	47	37	35	86	3	laminar	bidirectional	microblade	chert	indeterminate
NRI 2	core	25	25	15	16	1	laminar	unidirectional	microblade	chert	pebble
NRI 3	core	38	21	18	16	2	laminar	bidirectional	microblade	chert	indeterminate
NRI 4	core	38	17	16	13	1	laminar	unidirectional	microblade	chert	pebble
NRI 5	core	29	22	17	13	1	laminar	unidirectional	microblade	chert	pebble
NRI 6	core	23	24	18	13	2	laminar	bidirectional	microblade	chert	indeterminate
NRI 7	core	39	34	34	77	1	laminar	unidirectional	microblade	quartz	pebble
NRI 8	core	38	40	26	54	2	laminar	bidirectional	microblade	chert	pebble
NRI 9	core	28	22	14	10	2	laminar	bidirectional	microblade	chert	pebble
NRI 10	core	39	31	24	35	2	laminar	bidirectional	exhausted	chert	pebble
NRI 11	core	23	22	23	18	2	laminar	bidirectional	microblade	chert	pebble
NRI 12	core	46	35	32	59	2	laminar	unidirectional	microblade	chert	pebble

NRI 13	core	39	31	20	25	2	laminar	unidirectional	microblade	chert	indeterminate
NRI 14	core	31	25	20	15	1	laminar	unidirectional	microblade	chert	pebble
NRI 15	core	35	17	13	11	1	laminar	unidirectional	exhausted	chert	indeterminate
NRI 16	core	25	35	27	21	3	prepared	multidirectional	prepared	chert	indeterminate
NRI 17	core	25	22	18	13	1	laminar	unidirectional	microblade	chert	pebble
NRI 18	core	48	31	21	43	2	laminar	unidirectional	microblade	chert	pebble
NRI 19	core	51	35	22	58	1	laminar	unidirectional	microblade	chert	pebble
NRI 20	core	35	20	20	14	1	laminar	unidirectional	microblade	chert	indeterminate
NRI 22	core	28	21	15	11	1	laminar	unidirectional	microblade	chert	pebble
NRI 23	core	43	35	18	43	1	laminar	unidirectional	microblade	chert	pebble
NRI 24	core	27	21	14	10	3	laminar	multidirectional	microblade	chert	pebble
NRI 25	core	26	18	8	4	1	laminar	unidirectional	core-on-flake	quartz	pebble
NRI 26	core	24	23	15	9	1	laminar	unidirectional	exhausted	chert	indeterminate
NRI 27	core	29	18	14	10	2	laminar	unidirectional	microblade	chert	pebble
NRI 28	core	40	25	15	18	2	laminar	unidirectional	microblade	chert	pebble
NRI 29	core	22	15	14	8	2	laminar	unidirectional	microblade	chert	pebble
NRI 30	core	29	24	19	17	2	laminar	unidirectional	microblade	chert	pebble
NRI 31	core	42	24	20	30	2	laminar	unidirectional	microblade	chert	pebble
NRI 33	core	27	13	13	5	3	laminar	unidirectional	microblade	chert	pebble
NRI 34	core	30	14	14	8	2	laminar	unidirectional	microblade	chert	pebble
NRI 35	core	32	15	9	8	2	laminar	unidirectional	microblade	quartz	indeterminate
NRI 36	core	28	23	21	22	1	laminar	unidirectional	microblade	chert	pebble
NRI 37	core	37	19	14	12	2	laminar	unidirectional	microblade	chert	pebble
NRI 38	core	33	23	15	14	2	laminar	unidirectional	microblade	chert	pebble
NRI 39	core	38	25	21	25	1	laminar	unidirectional	microblade	chert	pebble
NRI 40	core	29	22	20	17	1	laminar	unidirectional	microblade	chert	pebble
NRI 41	core	40	33	22	41	2	laminar	unidirectional	exhausted	chert	pebble
NRI 42	core	40	25	13	16	2	laminar	unidirectional	microblade	chert	pebble
NRI 43	core	31	22	13	14	1	laminar	unidirectional	exhausted	chert	pebble
NRI 44	core	46	41	26	56	3	laminar	unidirectional	exhausted	chert	pebble
NRI 45	core	24	26	17	17	3	laminar	unidirectional	exhausted	chert	pebble
NRI 46	core	29	24	17	16	2	laminar	unidirectional	microblade	chert	pebble
NRI 48	core	28	16	15	7	1	laminar	unidirectional	microblade	chert	pebble
NRI 49	core	34	18	16	8	1	laminar	unidirectional	exhausted	chert	indeterminate
NRI 50	core	25	16	15	8	2	laminar	unidirectional	exhausted	chert	indeterminate
NRI 51	core	9	10	8	1	1	laminar	unidirectional	microblade	quartz	indeterminate
NRI 52	core	25	20	15	10	1	laminar	unidirectional	microblade	quartz	pebble
NRI 53	core	28	28	19	19	2	laminar	unidirectional	microblade	chert	pebble
NRI 54	core	18	24	23	13	1	laminar	unidirectional	microblade	chert	pebble
NRI 56	core	32	22	8	8	1	laminar	unidirectional	core-on-flake	chert	indeterminate
NRI 57	core	20	14	13	4	1	laminar	unidirectional	microblade	chert	indeterminate
NRI 58	core	28	21	17	14	2	laminar	unidirectional	microblade	chert	pebble
NRI 59	core	25	13	7	3	1	laminar	unidirectional	core-on-flake	chert	indeterminate
NRI 60	core	54	38	38	84	4	laminar	unidirectional	microblade	chert	indeterminate
NRI 64	core	39	28	23	33	1	laminar	unidirectional	microblade	chert	pebble
NRI 68	core	34	16	10	5	1	laminar	unidirectional	microblade	chert	indeterminate
NRI 69	core	20	13	10	3	1	laminar	unidirectional	microblade	quartz	pebble
NRI 70	core	30	20	14	10	1	laminar	unidirectional	microblade	chert	pebble

NRI 71	core	25	24	19	11	2	laminar	unidirectional	microblade	chert	pebble
NRI 172	core	36	28	22	30	2	laminar	unidirectional	microblade	chert	pebble
NRI 178	core	39	37	18	37	2	laminar	unidirectional	microblade	chert	pebble
NRI 188	core	50	45	20	72	2	regular	multidirectional	amorphous	chert	pebble
NRI 189	core	38	25	23	26	2	regular	unidirectional	amorphous	chert	pebble
NRI 192	core	30	26	18	17	1	regular	unidirectional	single platform unifacial	quartz	pebble
NRI 194	core	39	28	28	34	1	regular	unidirectional	amorphous	chert	pebble
NRI 239	core	25	17	15	10	1	regular	multidirectional	amorphous	chert	pebble
NRI 275	core	25	18	15	10	2	laminar	unidirectional	blade	chert	pebble
NRI 277	core	24	16	7	4	2	laminar	unidirectional	core-on-flake	chert	pebble
NRI 299	core	16	27	16	8	1	laminar	unidirectional	blade	chert	indeterminate
NRI 314	core	32	24	12	8	1	laminar	unidirectional	core-on-flake	chert	pebble
NRI 376	core	25	20	12	5	1	centripetal	centripetal	exhausted	quartz	indeterminate
NRI 427	core	21	17	9	2	1	laminar	unidirectional	blade	chert	pebble
NRI 473	core	21	15	10	3	1	laminar	unidirectional	microblade	quartz	pebble
NRI 495	core	52	32	26	54	1	regular	unidirectional	single platform unifacial	chert	pebble
NRI 497	core	35	34	18	30	5	regular	multidirectional	amorphous	chert	pebble
NRI 499	core	48	28	19	29	2	1: laminar, 2: regular	unidirectional	amorphous	chert	pebble
NRI 502	core	56	31	14	24	2	laminar	unidirectional	blade	chert	pebble
NRI 512	core	34	30	22	22	1	laminar	unidirectional	blade	chert	pebble
NRI 513	core	41	32	15	20	2	regular	centripetal, unidirectional	multi-platform	chert	pebble
NRI 521	core	28	24	22	22	2	laminar	unidirectional	microblade	quartz	pebble
NRI 527	core	30	28	12	8	2	laminar	unidirectional	core-on-flake	chert	pebble
NRI 529	core	61	46	34	139	2	laminar	unidirectional, multidirectional	blade	chert	pebble
NRI 530	core	45	32	27	40	2	laminar	unidirectional	microblade	chert	pebble
NRI 532	core	58	44	23	60	3	laminar	unidirectional	blade	chert	pebble
NRI 534	core	87	51	51	336	1	regular	unidirectional	single platform unifacial	porcellanite	pebble
NRI 537	core	38	31	25	52	2	regular	bidirectional	amorphous	chert	pebble
NRI 543	core	41	23	21	22	1	laminar	unidirectional	blade	chert	pebble
NRI 549	core	28	27	21	22	1	laminar	unidirectional	blade	chert	pebble
NRI 550	core	84	65	45	330	3	regular	unidirectional, bidirectional	multi-platform	porcellanite	pebble
NRI 551	core	65	60	41	161	1	regular	unidirectional	single platform bifacial	porcellanite	pebble
NRI 552	core	41	22	16	18	2	laminar	unidirectional parallel	microblade	chert	pebble
NRI 554	core	34	17	15	11	2	laminar	unidirectional convergent; unidirectional	microblade	quartz	pebble
NRI 555	core	37	25	19	20	1	laminar	unidirectional convergent	microblade	chert	indeterminate
NRI 556	core	37	27	21	29	3	laminar	unidirectional parallel, unidirectional	microblade	chert	pebble
NRI 557	core	43	35	26	43	3	laminar	unidirectional parallel, unidirectional	exhausted	chert	pebble
NRI 558	core	40	20	10	13	2	laminar	unidirectional parallel, unidirectional	microblade	chert	pebble
NRI 561	core	29	20	13	8	2	laminar	unidirectional parallel	microblade	quartz	pebble
NRI 562	core	45	25	15	21	2	laminar	unidirectional parallel	microblade	chert	pebble
NRI 565	core	28	20	19	12	3	laminar	unidirectional parallel; unidirectional	microblade	chert	pebble

Table A 17. Newari blade and microblade measurements and other select attributes.

Code	Typological classification	Length (mm)	Width (mm)	Thickness (mm)	Weight (g)	Platform width (mm)	Platform thickness (mm)	Platform preparation	Dorsal ridges	Axial percussion	Termination	Shoulders	Bulb of percussion	Raw material	Blank type
NRI 85	blade	31	10	3	1	3	1	plain	1	parallel	feather	4	prominent	chert	indeterminate
NRI 91	microblade	20	10	4	1	2	1	abraded	3	right	feather	1	prominent	chert	indeterminate
NRI 111	blade	34	14	7	3	8	5	plain	1	left	feather	4	prominent	quartz	pebble
NRI 113	blade	39	14	3	2	6	2	plain	3	left	feather	2	prominent	chert	indeterminate
NRI 122	microblade	19	8	2	0	3	2	plain	2	parallel	feather	4	prominent	chert	indeterminate
NRI 130	microblade	23	6	2	0	2	1	abraded	2	left	feather	3	NA	chert	indeterminate
NRI 164	blade	30	8	2	0	2	1	plain	2	left	feather	3	prominent	chert	indeterminate
NRI 193	blade	54	20	9	7	4	2	plain	1	right	feather	2	prominent	chert	indeterminate
NRI 212	blade	37	17	4	3	12	3	plain	3	right	feather	2	flat	chert	angular clast
NRI 231	blade	43	21	7	9	8	5	plain	1	right	feather	2	prominent	chert	angular clast
NRI 270	blade	40	16	5	3	6	3	plain	1	parallel	feather	1	prominent	porcellanite	indeterminate
NRI 312	blade	31	13	6	1	8	6	abraded	2	right	feather	2	prominent	chert	indeterminate
NRI 330	blade	40	14	7	4	na	na	abraded	3	parallel	feather	3	prominent	chert	indeterminate
NRI 356	blade	44	22	8	8	10	7	plain	1	left	feather	3	prominent	chert	indeterminate
NRI 386	microblade	27	12	6	2	8	4	plain	1	left	feather	4	broken	porcellanite	indeterminate
NRI 412	microblade	29	14	5	1	7	3	abraded	0	right	feather	3	prominent	chert	indeterminate

Table A 18. Kone flake measurements and other select attributes.

Code	Typological classification	Length (mm)	Width (mm)	Thickness (mm)	Weight(g)	Bulb of percussion	Platform width (mm)	Platform thickness (mm)	Platform preparation	No. of dorsal flake scars	Dorsal flake scarpattern	Flake termination	Raw material	Blank type
KON 1	flake end	48	27	10	12	prominent	15	7	cortical	1	unidirectional	feather	porcellanite	angular clast
KON 5	flake regular	33	33	10	13	flat	30	10	cortical	0	na	feather	chert	angular clast
KON 6	flake regular	34	22	7	6	prominent	17	8	cortical	1	unidirectional	step	porcellanite	angular clast
KON 9	flake end	48	30	9	15	prominent	15	10	cortical	3	unidirectional	feather	porcellanite	angular clast
KON 12	flake end	23	19	5	2	prominent	11	5	cortical	2	indeterminate	feather	porcellanite	angular clast
KON 24	flake oblique	26	20	6	3	flat	8	2	plain	6	unidirectional	feather	porcellanite	indeterminate
KON 27	flake end	41	23	8	7	prominent	25	9	plain	2	unidirectional	feather	porcellanite	indeterminate
KON 37	flake end	40	31	8	12	prominent	12	6	plain	2	indeterminate	feather	porcellanite	indeterminate
KON 58	flake end	44	27	13	14	flat	9	3	plain	3	unidirectional	feather	chert	angular clast
KON 59	flake end	44	23	7	9	flat	15	7	indeterminate	2	unidirectional	feather	porcellanite	angular clast
KON 63	flake side	26	50	12	12	flat	36	13	plain	2	unidirectional	feather	porcellanite	indeterminate
KON 70	flake side	23	27	8	5	prominent	24	8	cortical	1	unidirectional	feather	chalcedony	subangular clast
KON 72	flake side	25	32	13	9	flat	32	13	cortical	0	na	feather	chalcedony	subangular clast
KON 87	flake end	37	30	9	11	flat	18	7	plain	2	unidirectional	feather	porcellanite	angular clast
KON 106	flake end	33	21	9	6	prominent	17	9	plain	2	indeterminate	feather	porcellanite	indeterminate
KON 112	flake side	48	55	14	43	prominent	46	15	facetted	1	unidirectional	feather	porcellanite	angular clast
KON 134	flake side	36	38	12	17	prominent	15	8	cortical	2	indeterminate	feather	porcellanite	indeterminate
KON 136	flake oblique	42	27	10	11	flat	12	3	plain	9	bidirectional opposed	feather	porcellanite	indeterminate

KON 139	flake side	22	34	10	10	prominent	22	7	plain	2	unidirectional	feather	porcellanite	angular clast
KON 163	flake end	84	56	8	60	prominent	48	9	cortical	5	unidirectional	feather	porcellanite	angular clast
KON 165	flake end	45	31	11	18	flat	20	7	cortical	1	unidirectional	feather	porcellanite	angular clast
KON 166	flake regular	43	69	20	73	flat	na	na	indeterminate	7	centripetal	feather	porcellanite	indeterminate
KON 168	flake regular	25	26	14	8	flat	22	15	cortical	2	bidirectional	feather	chalcedony	subangular clast
KON 171	flake end	57	33	11	19	prominent	25	5	abraded	4	unidirectional	feather	porcellanite	indeterminate
KON 172	flake end	79	43	19	58	flat	16	8	abraded	5	centripetal	feather	porcellanite	angular clast
KON 173	flake end	53	26	23	37	prominent	22	13	abraded	1	unidirectional	feather	chalcedony	subangular clast
KON 174	flake regular	25	25	7	4	flat	12	4	cortical	3	unidirectional	step	porcellanite	indeterminate
KON 180	flake side	20	25	7	4	prominent	13	5	plain	na	indeterminate	feather	porcellanite	indeterminate
KON 182	flake end	36	27	16	14	prominent	14	5	plain	2	indeterminate	feather	chalcedony	subangular clast
KON 183	flake side	29	30	13	11	prominent	9	6	plain	1	unidirectional	feather	chalcedony	subangular clast
KON 186	flake end	40	31	11	17	prominent	20	10	cortical	4	bidirectional	feather	chert	subangular clast
KON 187	flake end	32	28	7	8	prominent	14	8	cortical	2	unidirectional	feather	porcellanite	angular clast
KON 188	flake side	44	53	11	39	flat	52	16	plain	5	bidirectional	hinge	porcellanite	indeterminate
KON 191	flake end	25	16	5	2	flat	16	5	dihedral convex	3	unidirectional	feather	porcellanite	indeterminate
KON 192	flake side	23	27	10	9	flat	18	6	plain	0	na	feather	chert	subangular clast
KON 193	flake end	35	28	7	3	flat	10	7	plain	3	unidirectional	feather	porcellanite	indeterminate
KON 195	flake side	38	42	10	15	prominent	29	7	facetted	0	NA	feather	porcellanite	indeterminate
KON 197	flake end	37	14	10	5	prominent	15	10	cortical	1	unidirectional	feather	chert	angular clast
KON 201	flake end	43	33	15	25	prominent	34	16	cortical	3	unidirectional	feather	porcellanite	angular clast
KON 204	flake end	34	21	5	7	prominent	12	3	dihedral convex	5	bidirectional	feather	porcellanite	angular clast
KON 205	flake side	20	30	5	4	prominent	18	4	cortical	1	unidirectional	feather	porcellanite	angular clast
KON 208	flake end	30	28	10	10	prominent	25	9	cortical	1	unidirectional	feather	chert	subangular clast
KON 210	flake end	30	16	7	4	prominent	17	7	plain	4	bidirectional	feather	porcellanite	indeterminate
KON 211	flake end	28	21	6	5	flat	18	8	plain	1	unidirectional	feather	chalcedony	subangular clast
KON 212	flake end	55	39	15	42	prominent	25	13	plain	1	unidirectional	feather	chert	angular clast
KON 220	flake side	25	25	7	5	prominent	26	8	cortical	1	unidirectional	feather	chert	subangular clast
KON 227	flake end	35	26	18	14	prominent	19	7	cortical	1	unidirectional	feather	chert	subangular clast
KON 231	flake oblique	40	25	13	9	flat	19	7	cortical	3	bidirectional	feather	porcellanite	indeterminate
KON 244	flake oblique	28	18	10	5	prominent	15	6	plain	5	irregular	feather	porcellanite	indeterminate
KON 250	flake end	44	22	9	10	prominent	12	6	plain	6	centripetal	feather	porcellanite	angular clast
KON 252	flake end	64	40	17	48	prominent	18	9	plain	1	unidirectional	feather	porcellanite	angular clast
KON 258	flake end	33	21	10	8	prominent	20	8	plain	0	na	feather	porcellanite	indeterminate
KON 262	flake end	55	25	8	15	prominent	10	8	plain	5	bidirectional	feather	porcellanite	angular clast
KON 269	flake end	26	21	16	9	prominent	12	10	plain	2	irregular	feather	chert	subangular clast
KON 273	flake end	20	15	5	0	prominent	16	5	cortical	3	bidirectional	feather	chalcedony	indeterminate
KON 277	flake side	41	52	17	50	prominent	39	13	plain	6	centripetal	feather	porcellanite	angular clast
KON 287	flake end	37	31	11	11	prominent	24	10	plain	3	centripetal	feather	porcellanite	angular clast
KON 296	flake end	30	27	10	9	prominent	18	10	plain	3	unidirectional	feather	porcellanite	indeterminate
KON 305	flake end	36	18	8	4	prominent	17	7	dihedral convex	3	unidirectional	feather	porcellanite	indeterminate
KON 307	flake end	48	40	8	17	prominent	35	8	plain	7	centripetal	feather	porcellanite	indeterminate
KON 313	flake oblique	46	26	10	14	prominent	23	5	plain	2	unidirectional	feather	porcellanite	angular clast
KON 321	flake end	43	26	8	11	prominent	14	5	cortical	0	na	feather	chert	subangular clast
KON 322	flake end	27	25	7	8	prominent	19	4	plain	4	unidirectional	feather	porcellanite	angular clast

KON 324	flake oblique	31	22	7	6	prominent	11	6	cortical	2	unidirectional	feather	chert	angular clast
KON 335	flake end	30	20	10	7	prominent	14	6	abraded	0	NA	feather	chert	angular clast
KON 336	flake end	27	16	7	4	prominent	12	5	plain	2	bidirectional	feather	chalcedony	subangular clast
KON 342	flake side	21	27	10	6	prominent	27	6	cortical	2	bidirectional	indeterminate	chalcedony	subangular clast
KON 347	flake side	23	29	8	6	prominent	22	8	cortical	1	unidirectional	feather	chert	angular clast
KON 356	flake side	34	60	13	27	prominent	41	11	dihedral convex	3	unidirectional	feather	porcellanite	angular clast
KON 363	flake oblique	60	56	17	64	prominent	35	13	plain	7	irregular	step	porcellanite	indeterminate
KON 368	flake end	44	23	9	8	flat	14	5	abraded	5	unidirectional	feather	porcellanite	angular clast
KON 369	flake end	27	21	12	10	prominent	15	9	cortical	1	unidirectional	feather	chert	subangular clast
KON 375	flake end	16	9	4	0	prominent	3	2	plain	8	irregular	feather	quartz	indeterminate
KON 377	flake end	25	15	11	4	prominent	15	9	cortical	0	na	feather	chert	subangular clast
KON 378	flake end	24	13	3	1	flat	11	4	plain	7	unidirectional	feather	porcellanite	indeterminate
KON 388	flake side	14	21	6	2	prominent	16	4	plain	0	na	feather	chert	subangular clast
KON 389	flake side	16	25	4	2	prominent	24	5	plain	3	unidirectional	feather	porcellanite	angular clast
KON 395	flake oblique	57	33	8	17	prominent	28	8	abraded	6	irregular	feather	porcellanite	angular clast
KON 400	flake end	27	19	8	5	flat	18	9	dihedral convex	4	unidirectional	feather	chert	subangular clast
KON 431	flake side	52	80	20	99	prominent	70	17	plain	1	unidirectional	hinge	porcellanite	indeterminate
KON 432	flake end	77	49	12	49	prominent	22	10	cortical	4	unidirectional	feather	porcellanite	angular clast
KON 434	flake side	40	56	12	32	prominent	47	10	plain	5	indeterminate	indeterminate	porcellanite	indeterminate
KON 436	flake end	56	26	14	21	prominent	17	11	plain	3	unidirectional	feather	porcellanite	angular clast
KON 448	flake side	33	44	11	18	flat	25	7	plain	3	bidirectional	feather	porcellanite	indeterminate
KON 450	flake end	31	23	7	6	prominent	20	9	facetted	0	na	feather	chert	subangular clast
KON 458	flake end	30	22	8	6	prominent	15	8	cortical	3	indeterminate	feather	chert	subangular clast
KON 465	flake side	19	30	5	3	prominent	17	5	plain	1	indeterminate	feather	porcellanite	indeterminate
KON 476	flake side	28	32	8	9	prominent	25	8	cortical	1	unidirectional	feather	chert	subangular clast
KON 489	flake side	47	58	10	31	prominent	16	11	semi-cortical	4	unidirectional	feather	porcellanite	angular clast
KON 496	flake end	57	42	16	37	prominent	31	15	plain	3	unidirectional	feather	porcellanite	angular clast
KON 500	flake end	40	33	8	18	prominent	23	8	plain	1	indeterminate	feather	porcellanite	angular clast
KON 501	flake regular	30	30	14	14	prominent	25	14	semi-cortical	1	unidirectional	feather	chert	subangular clast
KON 504	flake side	39	40	9	17	prominent	30	8	plain	4	unidirectional	feather	porcellanite	indeterminate
KON 505	flake side	33	40	8	11	prominent	23	9	plain	2	unidirectional	feather	porcellanite	indeterminate
KON 507	flake side	30	40	13	15	prominent	12	8	cortical	0	na	feather	porcellanite	subangular clast

Table A 19. Kone core measurements and other select attributes.

Code	**Typological classification**	**Length (mm)**	**Width (mm)**	**Thickness (mm)**	**Weight (g)**	**No. of striking platform**	**Method ofFlaking**	**FlakingPattern**	**Type of Core**	**Raw material**	**Blank type**
KON 22	core	40	39	30	45	2	laminar	unidirectional	blade core	porcellanite	angular clast
KON 30	core	31	28	23	25	2	laminar	unidirectional	blade core	chalcedony	rounded clast
KON 46	core	31	23	17	13	1	laminar	unidirectional	blade core	porcellanite	indeterminate
KON 47	core	56	29	17	38	2	laminar	unidirectional	blade core	porcellanite	indeterminate
KON 73	core	44	40	27	64	1	laminar	unidirectional	blade core	porcellanite	angular clast
KON 79	core	35	26	20	21	1	laminar	unidirectional	blade core	porcellanite	indeterminate

KON 83	core	62	28	20	36	2	laminar	bidirectional	blade core	porcellanite	indeterminate
KON 111	core	49	30	18	35	2	1: laminar; 2: regular	bidirectional	blade core	porcellanite	indeterminate
KON 115	core	51	18	19	23	1	laminar	bidirectional	blade core	porcellanite	angular clast
KON 122	core	97	44	46	224	1	regular	unidirectional	single platform unifacial	porcellanite	angular clast
KON 123	core	29	25	25	22	1	laminar	unidirectional	microblade	porcellanite	indeterminate
KON 132	core	54	52	34	91	3	regular	multidirectional	multi-platform	porcellanite	angular clast
KON 133	core	51	27	26	47	1	regular	unidirectional	single platform	chalcedony	angular clast
KON 153	core	44	39	35	69	3	regular	multidirectional	multi-platform	porcellanite	indeterminate
KON 170	core	45	41	22	42	1	regular	unidirectional	single platform	chert	angular clast
KON 185	core	37	35	23	38	2	1: laminar; 2: regular	unidirectional	blade core	chert	angular clast
KON 194	core	37	32	25	29	3	regular	multidirectional	exhausted	porcellanite	indeterminate
KON 213	core	48	41	32	80	2	laminar	unidirectional	blade core	porcellanite	angular clast
KON 216	core	42	37	23	52	1	regular	unidirectional	single platform unifacial	chert	angular clast
KON 218	core	42	38	24	42	3	laminar	unidirectional	blade core	porcellanite	indeterminate
KON 240	core	44	19	14	21	2	laminar	bidirectional	core-on-flake	porcellanite	indeterminate
KON 251	core	44	31	22	30	2	laminar	bidirectional	blade core	porcellanite	indeterminate
KON 275	core	21	17	13	7	1	laminar	unidirectional	microblade	porcellanite	indeterminate
KON 311	core	51	49	20	66	2	regular	unidirectional	single platform bifacial	porcellanite	angular clast
KON 354	core	48	45	22	64	2	laminar	bidirectional	blade core	porcellanite	angular clast
KON 365	core	35	25	18	17	1	laminar	unidirectional	blade core	porcellanite	indeterminate
KON 415	core	35	22	11	12	2	laminar	unidirectional	blade core	porcellanite	angular clast
KON 449	core	24	20	14	9	1	laminar	unidirectional	microblade	chert	angular clast
KON 466	core	45	42	28	60	2	laminar	bidirectional	blade core	porcellanite	angular clast
KON 486	core	32	22	19	15	2	laminar	bidirectional	blade core	porcellanite	indeterminate
KON 487	core	55	44	28	69	2	laminar	unidirectional	blade core	porcellanite	angular clast

Table A 20. Kone blade and microblade measurements and other select attributes.

Code	Typological classification	Length (mm)	Width(mm)	Thickness (mm)	Weight(g)	Platform width (mm)	Platform thickness (mm)	Platform preparation	Dorsal ridges	Axial percussion	Termination	Shoulders	Bulb of percussion	Raw material	Blank type
KON 17	blade	37	15	6	3	14	5	abraded	3	parallel	feather	2	na	porcellanite	indeterminate
KON 33	microblade	27	12	5	2	10	5	plain	1	parallel	hinge	1	flat	porcellanite	angular clast
KON 45	blade	50	17	9	7	7	4	plain	1	right	feather	1	flat	porcellanite	indeterminate
KON 131	blade	42	19	9	6	14	6	indeterminate	1	parallel	feather	2	prominent	porcellanite	indeterminate
KON 295	microblade	25	14	4	1	13	5	facetted	1	right	feather	2	prominent	porcellanite	angular clast
KON 391	blade	60	16	10	10	8	4	plain	1	parallel	feather	2	prominent	porcellanite	indeterminate
KON 413	blade	30	12	3	1	9	4	cortical	2	parallel	feather	2	flat	porcellanite	angular clast

Table A 21. Field documentation form used during the survey in the LSV.

Date/Day/Time	
Site Name	
Village(district)	
Site size	
GPS Point	Lat, long., (Point No. and name)
Photograph No.	
Landscape	
Context	
Artefact type	
Artefact density	
Assemblage type	
Raw material	
Soil colour	
Sediment type	
Stratigraphy	
Landmark	

Table A 22. $\delta^{13}C$ and $\delta^{18}O$ values of calcrete at Pilikarar along with depth.

Samples ID	$\delta^{13}C_{VPDB}$	$\delta^{18}O_{VPDB}$	Depth (cm)
PLK_1_3A, B	-1.82	-2.63	10
PLK_1_5	-1.73	-2.90	30
PLK_1_6	-1.58	-2.82	50
PLK_1_7A,B	-1.62	-2.61	70
PLK_1_8A,B	-2.64	-2.93	90
PLK_1_9A,B	-1.53	-2.53	100
PLK_2_10	-2.11	-2.65	120
PLK_2_11A	-2.25	-2.94	140
PLK_2_12A,B	-5.39	-3.27	160
PLK_2_17A,B	-4.32	-2.78	180
PLK_2_23	-8.54	-3.97	200
PLK_3_30	-8.81	-4.14	220
PLK_3_34A,B	-7.95	-3.63	240
PLK_3_49	-0.05	-3.30	250
PLK_3_54B	0.02	-3.16	270
PLK_3_57	-0.29	-3.15	290
PLK_4_58	-1.06	-3.02	300
PLK_4_59A	-1.86	-3.78	310
PLK_4_60	0.38	-3.08	320
PLK_4_62A,B	0.47	-3.30	330
PLK_4_63A	0.64	-3.47	340
PLK_4_65	0.39	-3.56	350

Table A 23. $\delta^{13}C$ and $\delta^{18}O$ values of calcrete at Talayaghat along with depth

Samples ID	$\delta^{13}C_{VPDB}$	$\delta^{18}O_{VPDB}$	Depth (cm)
TLG_CS_1	-2.5	-2.6	10
TLG_CS_2A, B	-2.73	-2.8	20
TLG_CS_3A, B	-5.9	-3.6	30
TLG_CS_4A, B	-3.74	-3.2	40
TLG_CS_5A, B	-2.24	-2.9	50
TLG_CS_6	-2.1	-2.8	60
TLG_CS_7A,B	-3.17	-2.7	70
TLG_CS_8A,B	-2.48	-2.7	80
TLG_CS_9A, B	-5.92	-3.8	90
TLG_CS_10A, B	-5.88	-3.6	100
TLG_CS_11A,B	-6.90	-3.8	110
TLG_CS_12A, B	-6.70	-3.8	120
TLG_CS_13A,B	-2.6	-2.9	130
TLG_CS_15A, B	-6.65	-3.4	150
TLG_CS_16A,B	-3.53	-2.7	160
TLG_CS_18A,B	-3.50	-2.5	180
TLG_CS_19A,B	-4.08	-2.7	190
TLG_CS_20A,B	-7.44	-3.7	200
TLG_CS_21A,B	-3.60	-2.8	210
TLG_CS_22A,B	-5.05	-3.0	220
TLG_CS_23A,B	-3.5	-2.7	230
TLG_CS_24A,B	-3.9	-2.8	240
TLG_CS_25A,B	-4.33	-3.2	250
TLG_CS_26A,B	-6.1	-3.2	260
TLG_CS_27	-4.8	-2.8	270
TLG_CS_29	-0.3	-2.9	290
TLG_CS_30	-1.0	-3.3	300
TLGCS31A,B	-0.32	-3.3	310
TLGCS32A,B	-0.43	-4.5	320
TLGCS33A,B	-1.70	-3.5	330
TLGCS34A,B	-0.18	-4.1	340
TLGCS35A,B	-0.50	-3.6	350
TLGCS36A,B	0.1	-3.6	360
TLGCS37	-0.07	-4.05	370
TLGCS38	-0.58	-4.2	390
TLGCS42	-0.27	-4.04	430

TLGCS43	-0.92	-3.8	440
TLGCS44 A,B	-1.20	-3.9	450
TLGCS45	-0.86	-3.91	460
TLGCS46A,B	-1.67	-3.79	470
TLGCS47	-1.51	-4.74	480
TLGCS48	-0.60	-3.48	490
TLGCS49B	-3.02	-3.51	500
TLGCS51	-3.15	-3.46	520
TLGCS53	-2.60	-4.80	530
TLGCS54	-2.75	-4.34	540
TLGCS55	-7.40	-3.97	550
TLGCS56A,B,C	-6.79	-4.24	560
TLGCS57	-7.87	-4.86	570
TLGCS58A,B	-7.60	-4.50	580
TLGCS59	-9.40	-4.75	590
TLGCS60	-7.94	-4.74	600
TLGCS61A	-1.19	-4.60	610
TLGCS62	-0.90	-4.59	620
TLGCS63A,B	-1.60	-4.69	630

Table A 24. $\delta^{13}C$ and $\delta^{18}O$ values of calcrete at Devakachar along with depth

Samples ID	$\delta^{13}C_{VPDB}$	$\delta^{18}O_{VPDB}$	Depth (cm)
SRTS_1_ST_1CA	-1.48	-2.86	10
SRTS_1_ST_2C	-1.49	-2.83	20
SRTS_1_ST_3C	-7.13	-4.12	30
SRTS_1_ST_4CA	-2.05	-3.05	40
SRTS_1_ST_5CA	-1.57	-2.93	50
SRTS_1_ST_6C	-7.13	-4.19	60
SRTS_1_ST_7C	-0.92	-2.76	70
SRTS_1_ST_8CA	-1.42	-3.11	80
SRTS_1_ST_9C	-7.20	-4.19	90
SRTS_1_ST_10CA, B	-7.08	-4.09	100
SRTS_1_ST_11C	-5.06	-3.59	110
SRTS_1_ST_12C	-7.78	-4.72	120
SRTS_1_ST_13CA	-0.69	-3.51	130
SRTS_1_ST_15CA, B	0.28	-4.08	150
SRTS_1_ST_16CA,B,c	-1.97	-2.83	160
SRTS_1_ST_17CA,B,C	-1.43	-3.16	170
SRTS_1_ST_18CA,B	-0.94	-3.05	180
SRTS_1_ST_19CA,B	-1.98	-2.77	190
SRTS_1_ST_20CA, B	-1.76	-3.07	200
SRTS_1_ST_21CA, B	-1.51	-3.61	210
SRTS_1_ST_22C	-2.29	-3.20	220
SRTS_1_ST_23CA, B	-1.94	-2.74	230
SRTS_1_ST_24CA, B	-5.69	-3.90	240
SRTS_1_ST_25CA,B	-1.60	-3.01	250
SRTS_1_ST_26CA,B	-1.37	-2.81	260
SRTS_1_ST_27CA,B	-1.46	-3.04	270
SRTS_1_ST_28CA,B	-6.46	-4.02	280
SRTS_5_ST_30CA,B	-6.35	-3.94	300
SRTS_5_ST_31CA,B	-8.47	-4.41	310
SRTS ST16 139A, B	-5.01	-4.59	1390
SRTS ST16 140A, B	-1.26	-2.99	1400
SRTS ST16 141A,B	-3.08	-3.55	1410
SRTS ST16 142	-4.84	-3.55	1420
SRTS ST16 143	-1.46	-4.44	1430
SRTS ST16 144	-4.12	-3.46	1440

SRTS ST16 146A,B	-1.90	-3.84	1460
SRTS ST16 147	-1.73	-4.69	1470
SRTS ST17 152	-4.47	-5.24	1520
SRTS ST19 172	-1.32	-4.46	1720
SRTS ST19 173A, B	-3.59	-4.28	1730
SRTS ST19 174	-3.30	-3.99	1740
SRTS ST19 175	-3.53	-4.19	1750
SRTS ST19 176	-5.94	-5.57	1760
SRTS ST19 177A, B	-4.68	-5.06	1770
SRTS ST19 178	-5.73	-5.27	1780
SRTS ST19 179A,B	-1.02	-4.56	1790
SRTS ST19 180A,B	-2.33	-6.13	1800
SRTS ST19 181A,B	-1.63	-4.30	1810
SRTS ST19 182	-1.70	-4.17	1820
SRTS ST19 183A,B	-1.49	-4.31	1830
SRTS ST19 184	-4.22	-5.31	1840
SRTS ST19 185A,B	-3.08	-4.81	1850
SRTS ST19 186	-4.74	-4.36	1860
SRTS ST19 187	-4.91	-4.94	1870
SRTS ST19 188	-1.47	-4.13	1880
SRTS ST19 189.1	-1.54	-3.84	1890
SRTS ST19 190A,B	-0.77	-3.91	1900
SRTS ST19 191	-1.37	-4.17	1910
SRTS ST20 192A,B	-2.72	-4.36	1920
SRTS ST20 193A,B	-4.63	-4.59	1930
SRTS ST20 194	-1.35	-4.26	1940
SRTS ST20 195A,B	-1.32	-4.18	1950
SRTS ST20 196	-5.33	-5.62	1960
SRTS ST20 197	-1.02	-4.51	1970
SRTS ST20 198	-0.41	-4.33	1980
SRTS ST20 199	-5.34	-5.01	1990
SRTS ST20 200	0.18	-3.38	2000
SRTS ST20 201 A,B	-2.61	-4.74	2010
SRTS ST20 202A,B	-0.01	-4.07	2020
SRTS ST20 203	0.44	-3.70	2030
SRTS ST20 204A,B	0.46	-3.71	2040
SRTS ST20 205	-1.05	-4.56	2050
SRTS ST20 206	0.18	-4.72	2060
SRTS ST20 207	0.53	-4.41	2070

SRTS ST20 208A,B	-0.34	-4.43	2080
SRTS ST20 210	0.24	-4.94	2100
SRTS ST21 211	-0.45	-4.83	2110
SRTS ST21 212	-7.20	-6.07	2120
SRTS ST21 213A,B	-1.06	-4.50	2130
SRTS ST21 214	-0.65	-4.88	2140
SRTS ST21 216	-0.93	-4.12	2160
SRTS ST21 217	-2.84	-5.90	2170
SRTS ST21 219	-1.03	-5.06	2190
SRTS ST21 220	-6.75	-6.59	2200
SRTS ST21 221	-6.52	-6.29	2210
SRTS ST22 222	-5.81	-5.94	2220
SRTS ST22 223	-0.72	-5.56	2230
SRTS ST22 225	-0.11	-5.11	2250
SRTS ST22 226	-7.11	-6.19	2260
SRTS ST22 227	-1.28	-6.12	2270
SRTS ST22 228A,B	-4.44	-6.84	2280
SRTS ST22 229A,B	-4.76	-7.08	2290
SRTS ST22 230	-7.03	-5.99	2300
SRTS ST23 231	-7.50	-6.34	2310
SRTS ST23 232	-1.16	-5.91	2320
SRTS ST23 233A	-5.54	-5.41	2330
SRTS ST23 235A	-5.31	-4.65	2350

Figure A 1. 3D scans of different artefacts from Bagia, Doma, Kargara, Khempur, Kone, Newari, Parva Chinguri

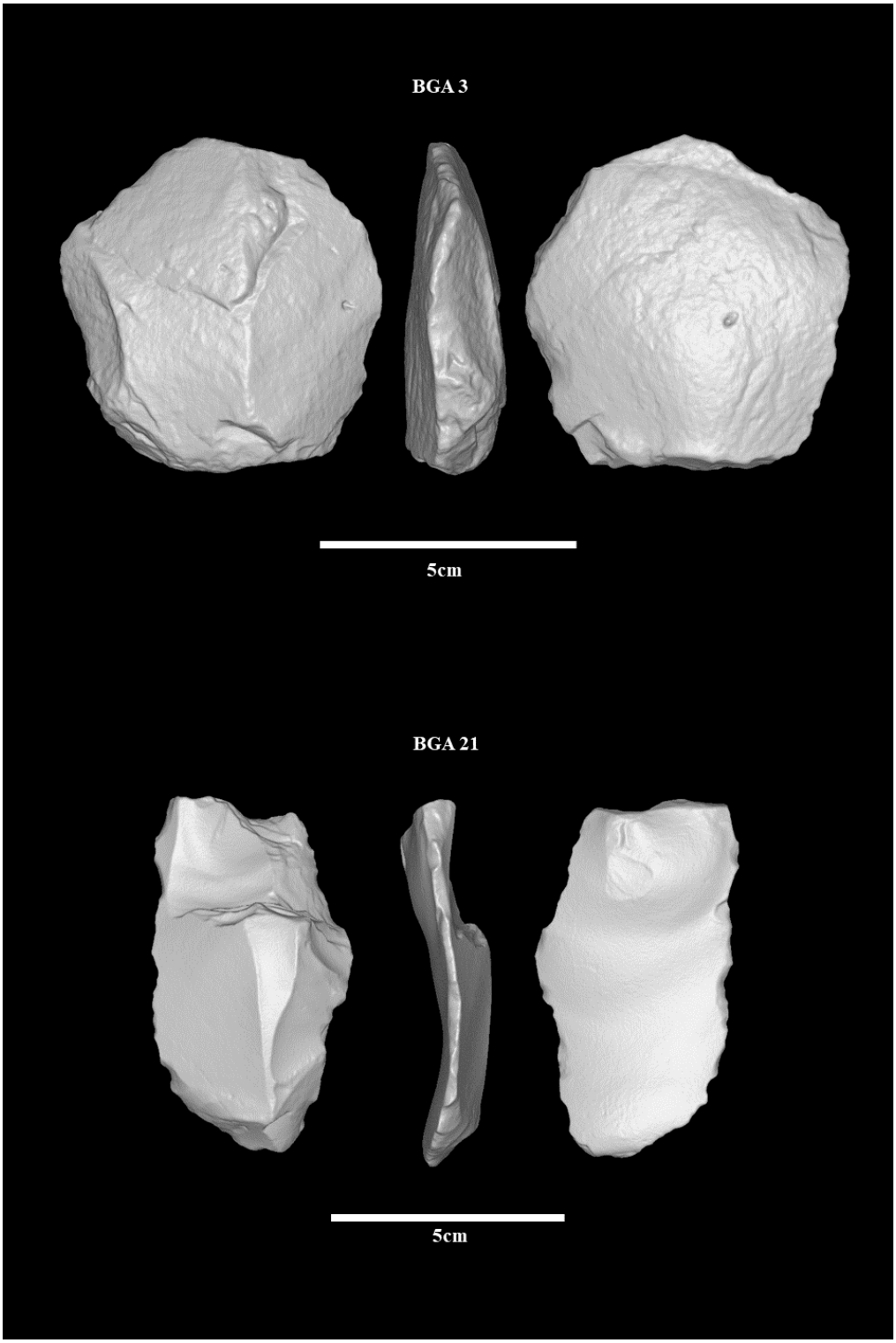

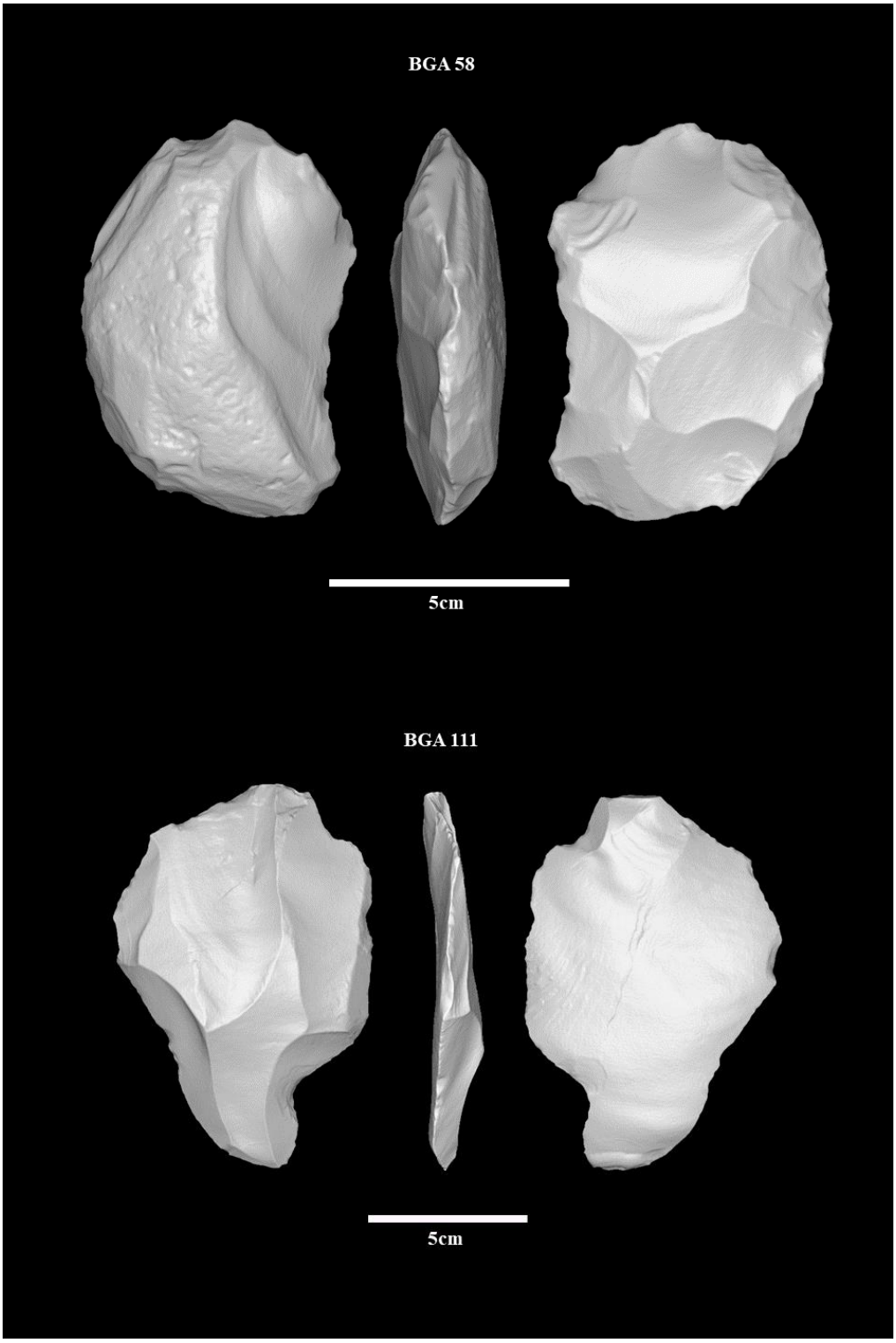
BGA 58
5cm
BGA 111
5cm

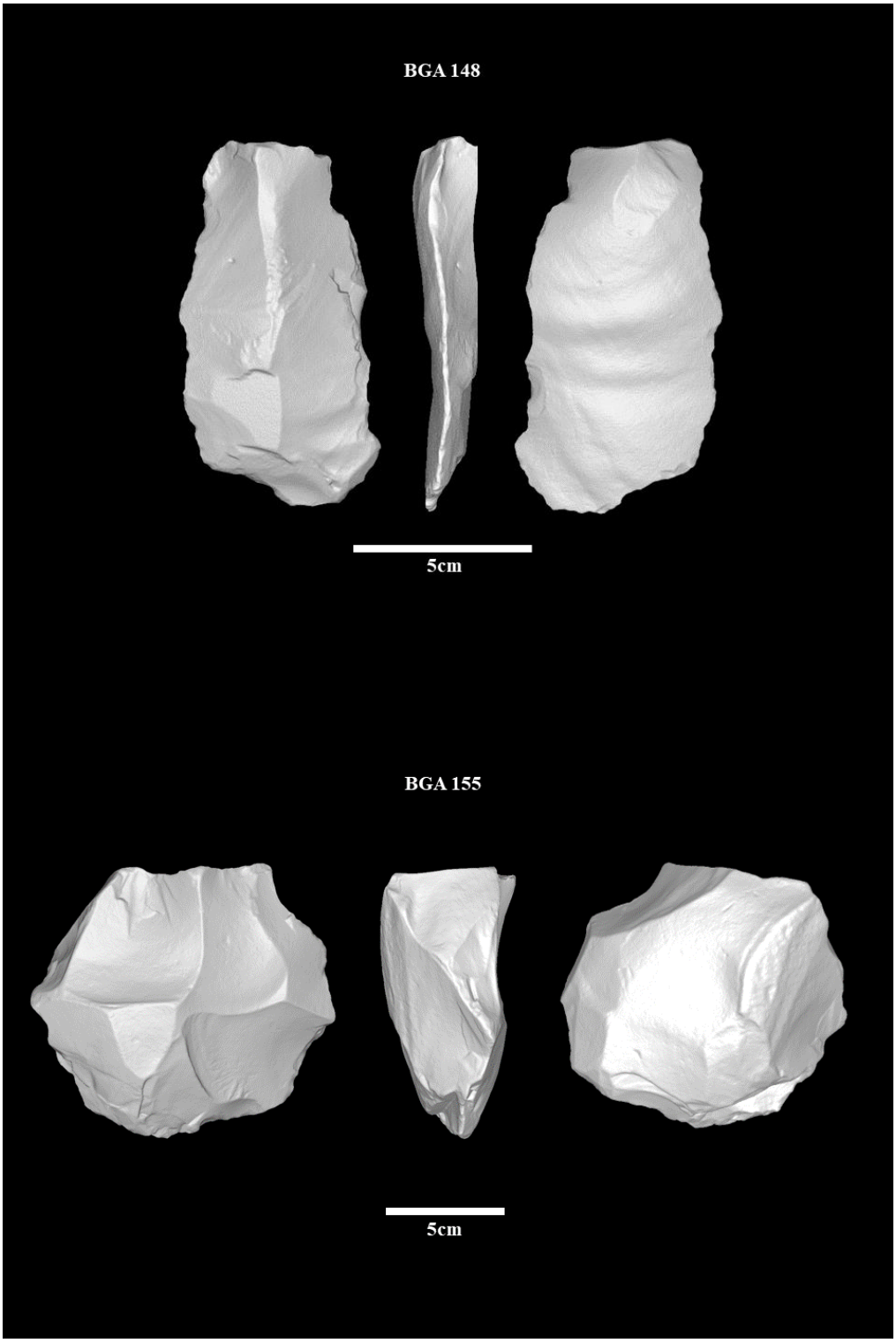
BGA 148
5cm
BGA 155
5cm

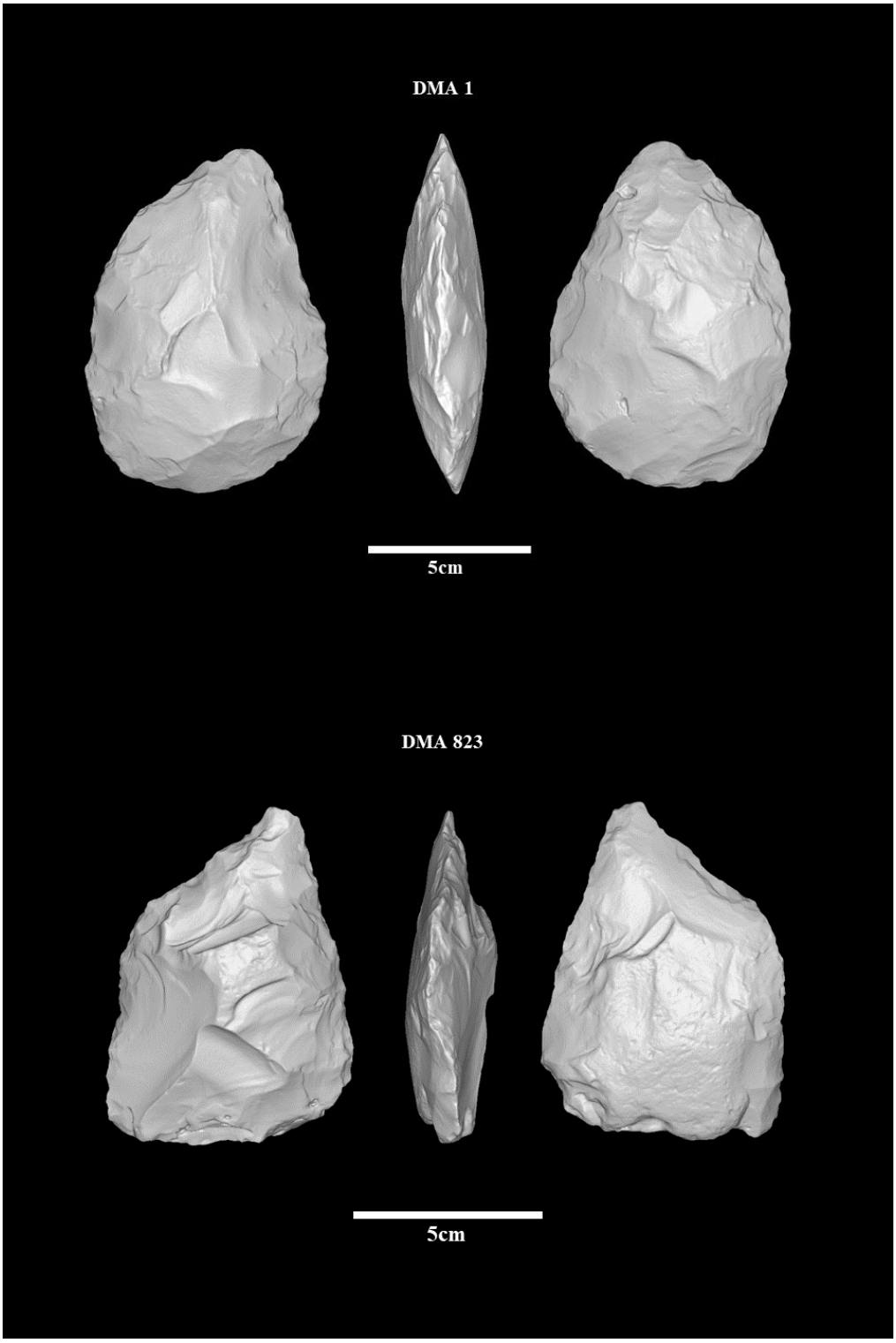
DMA 1
5cm
DMA 823
5cm

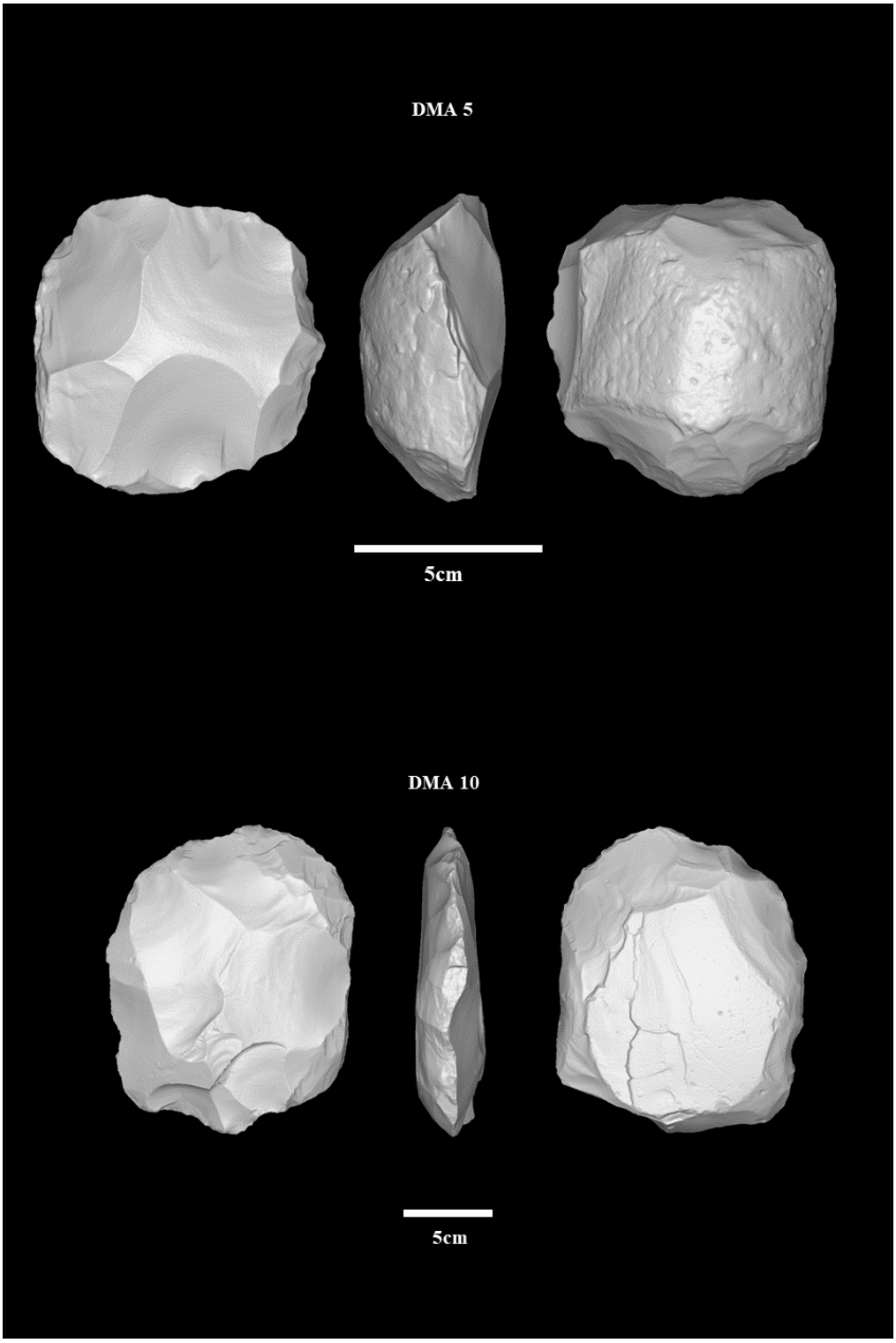
DMA 5
5cm
DMA 10
5cm

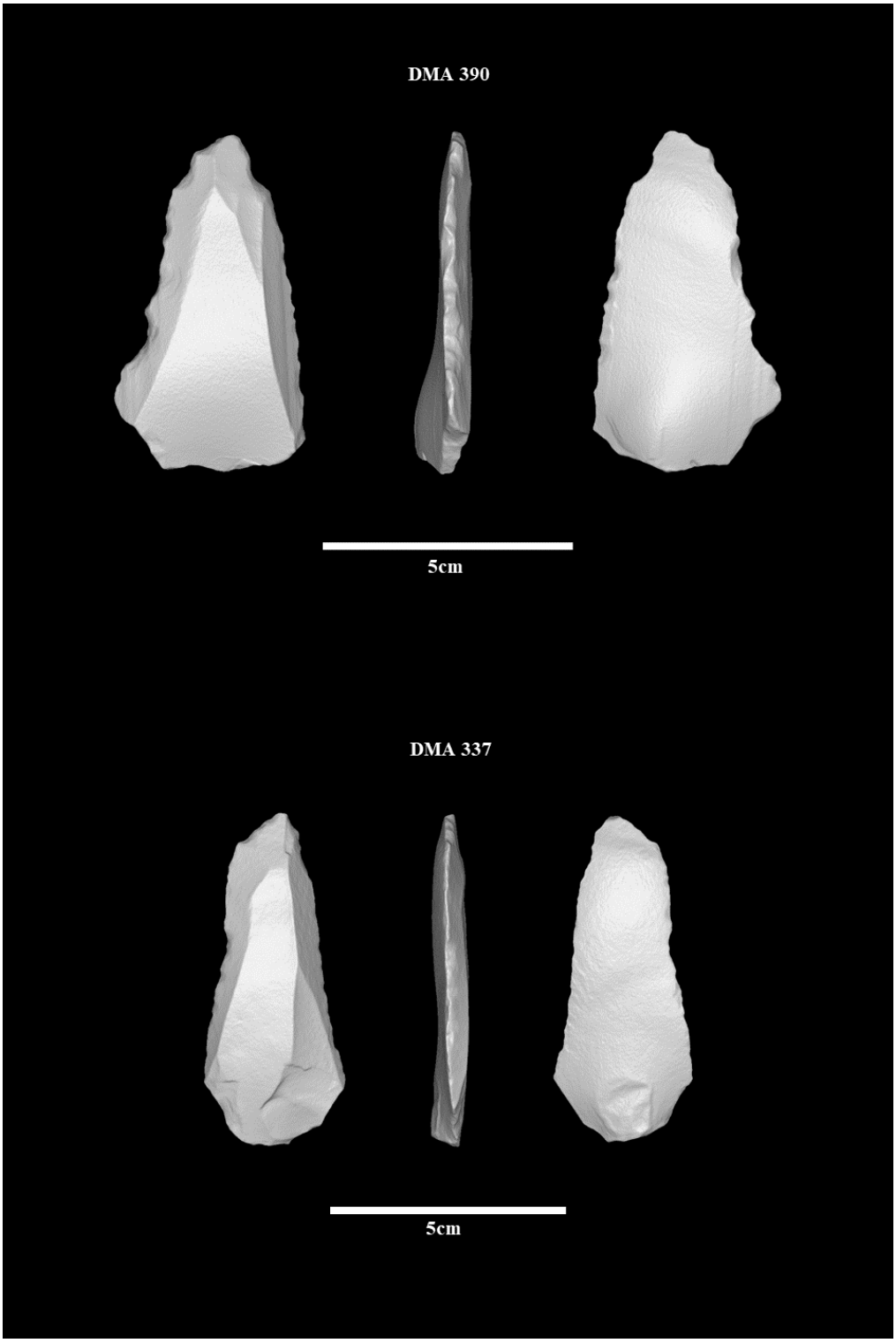
DMA 390
5cm
DMA 337
5cm

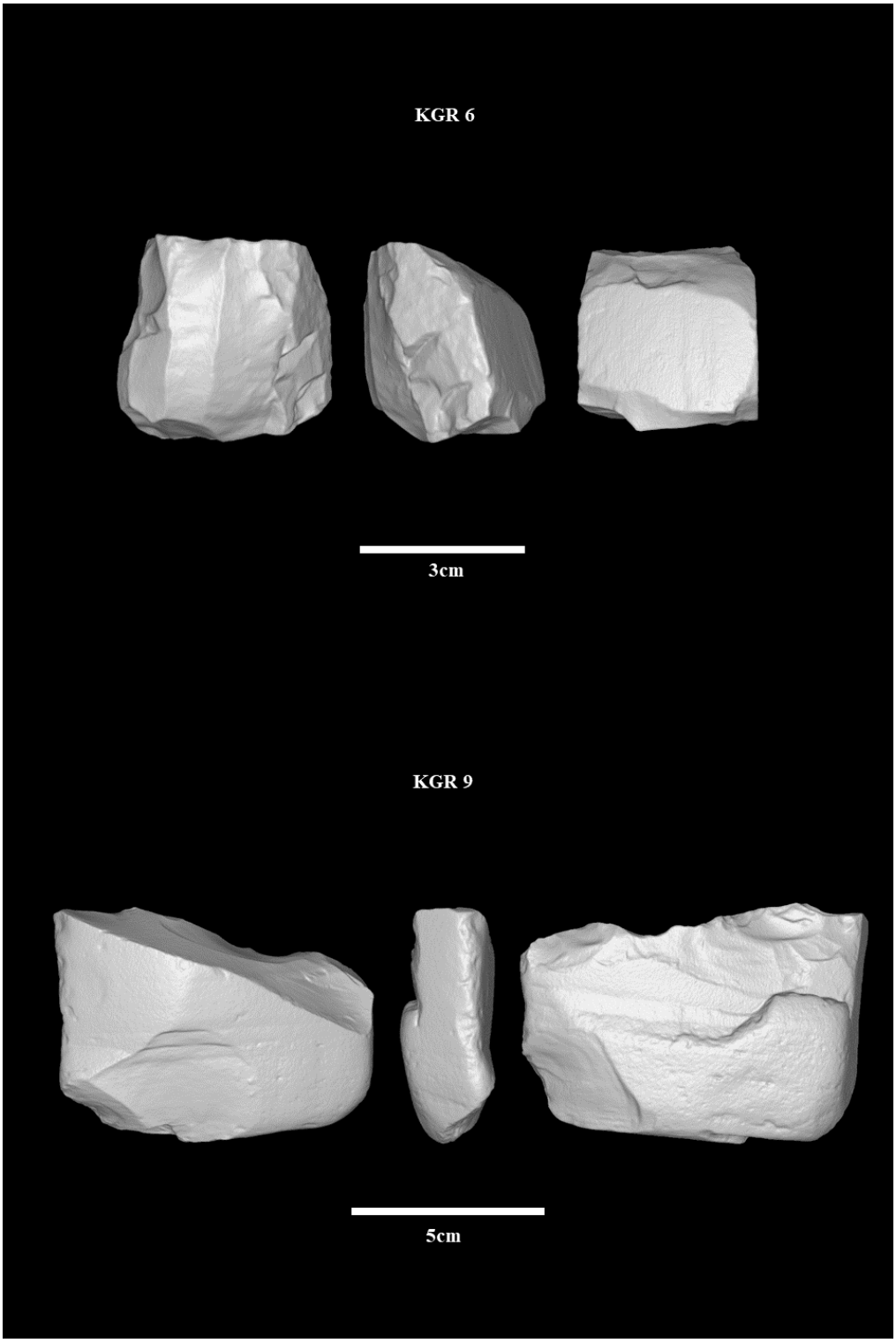
KGR 6
3cm
KGR 9
5cm

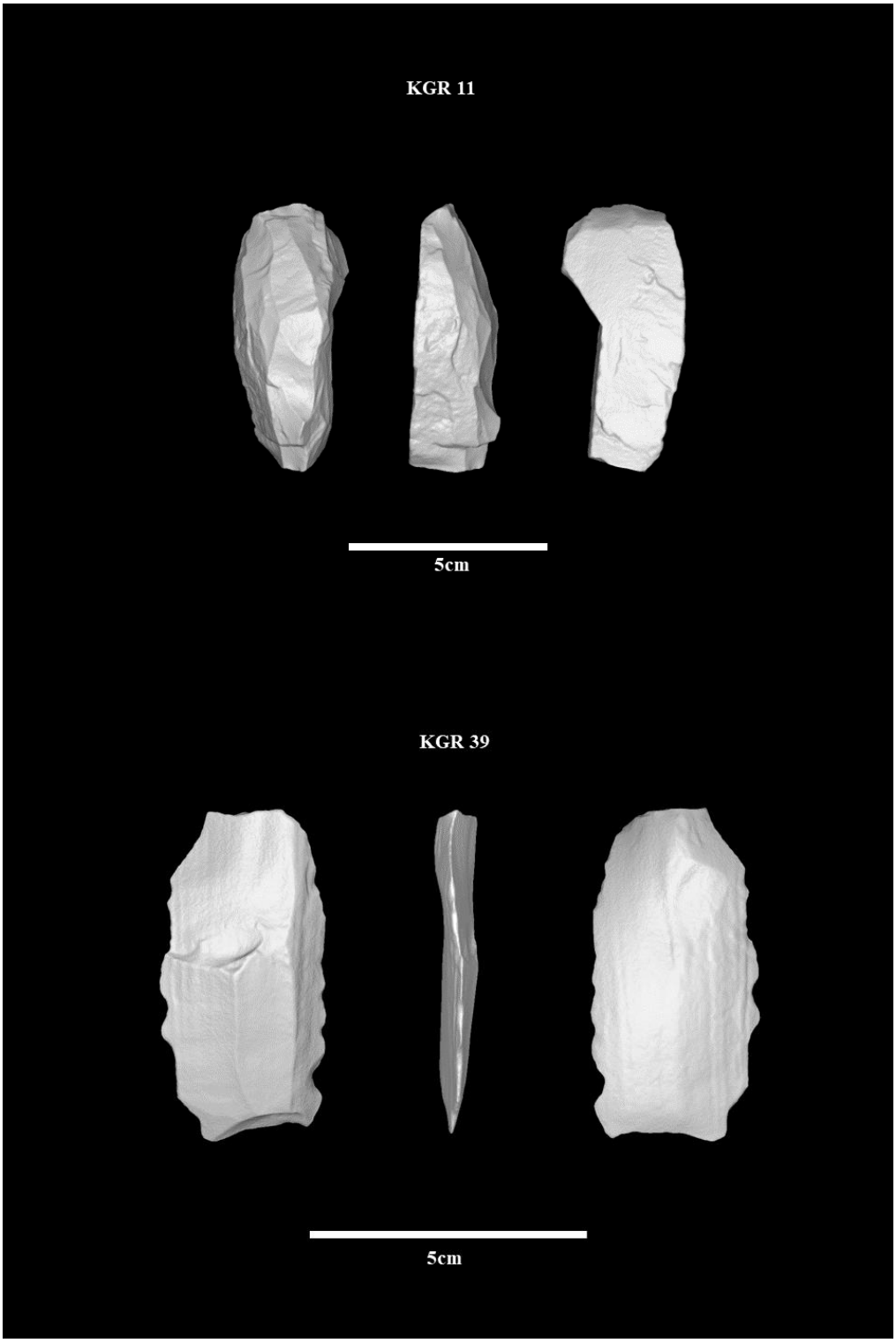
KGR 11
5cm
KGR 39
5cm


KGR 74
3cm
KGR 130
5cm

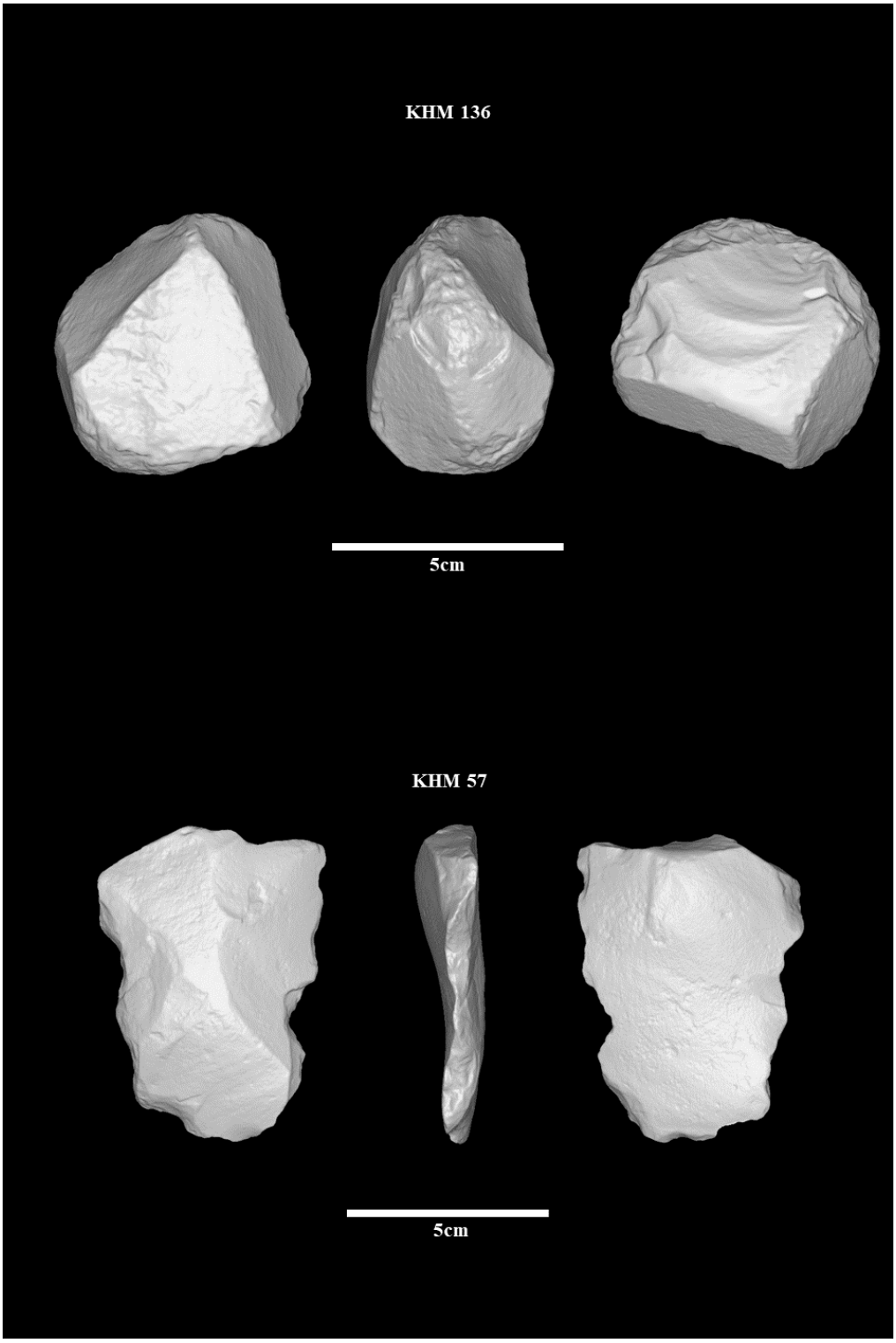
KHM 136
5cm
KHM 57
5cm

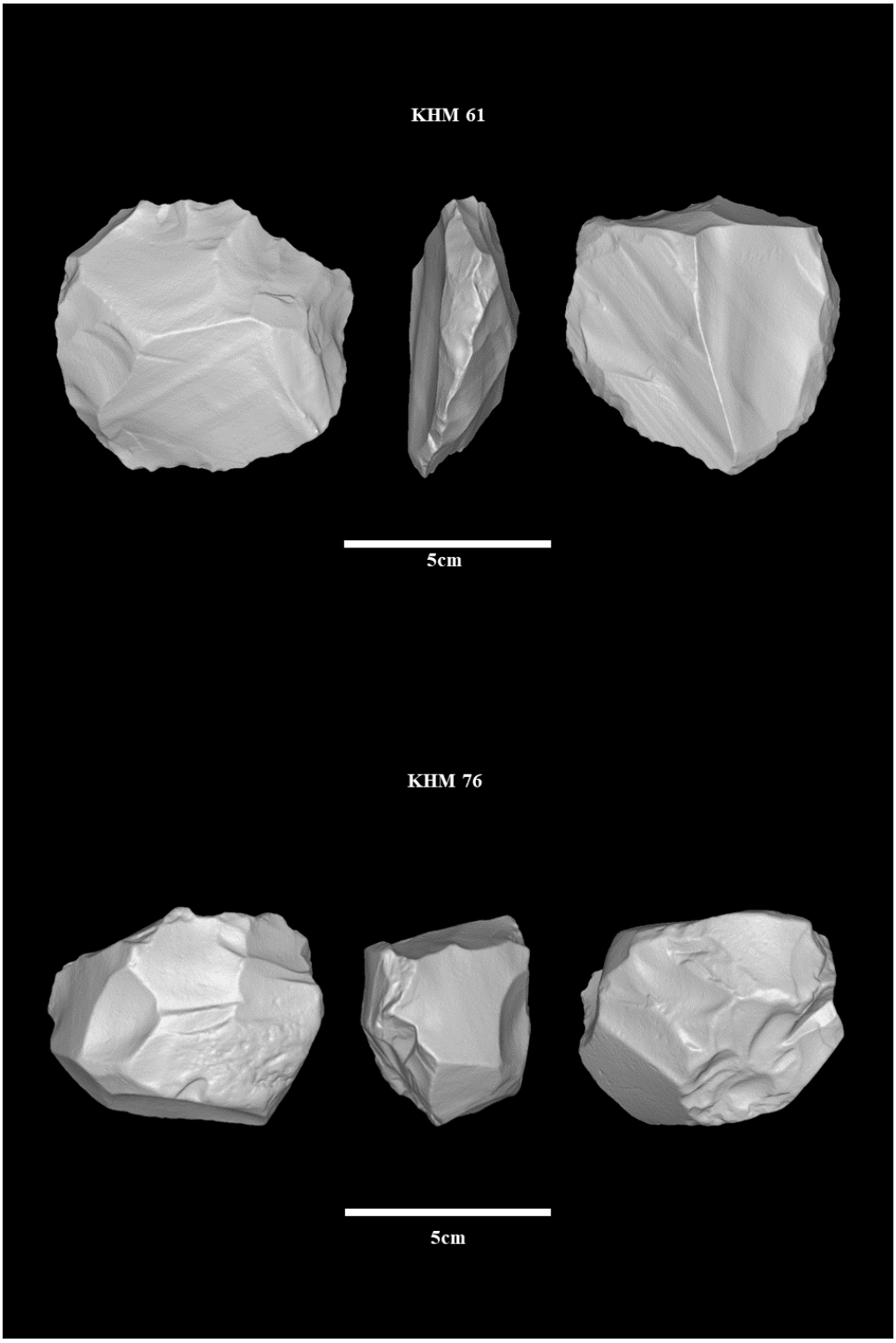
KHM 61
5cm
KHM 76
5cm

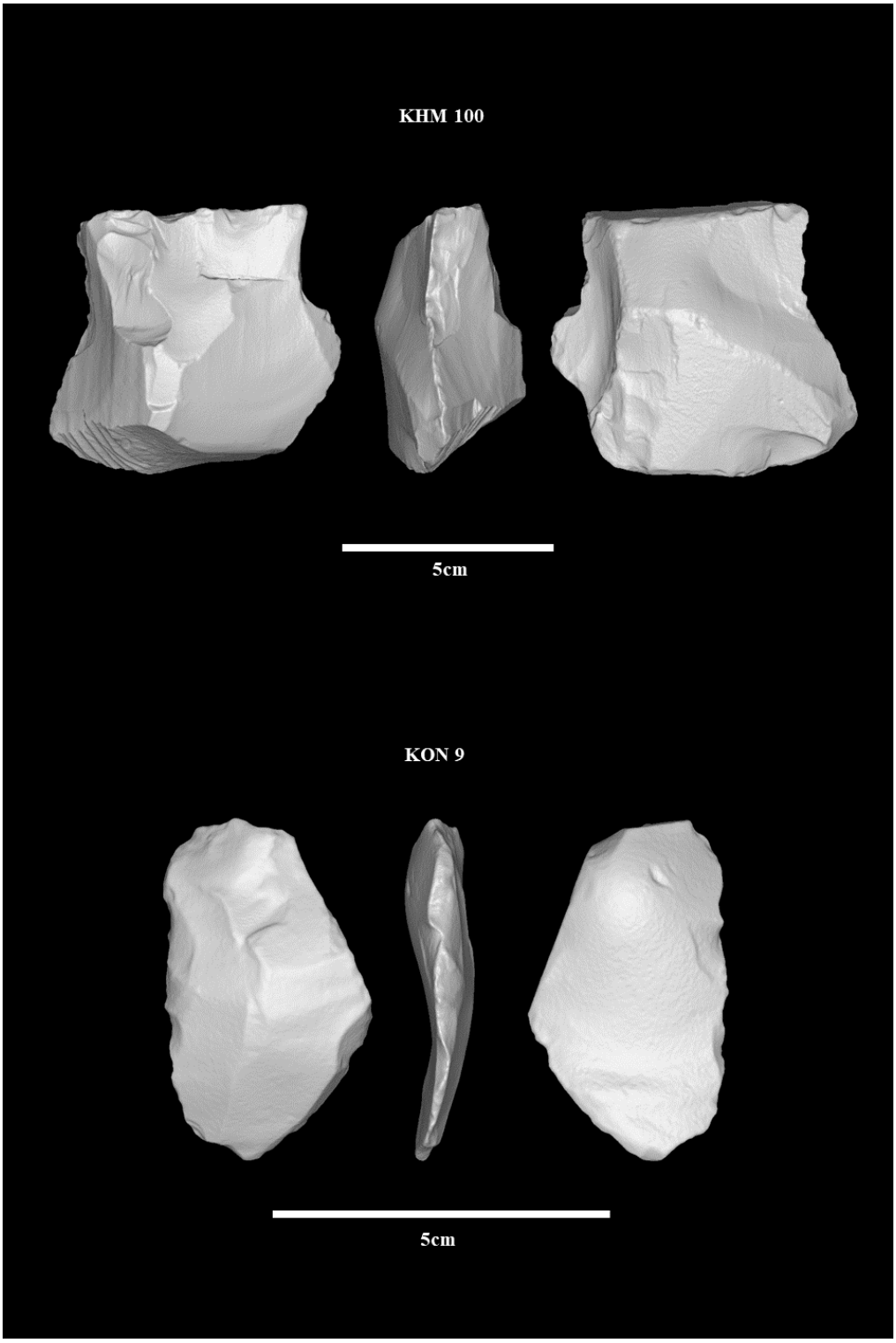
KHM 100
5cm
KON 9
5cm

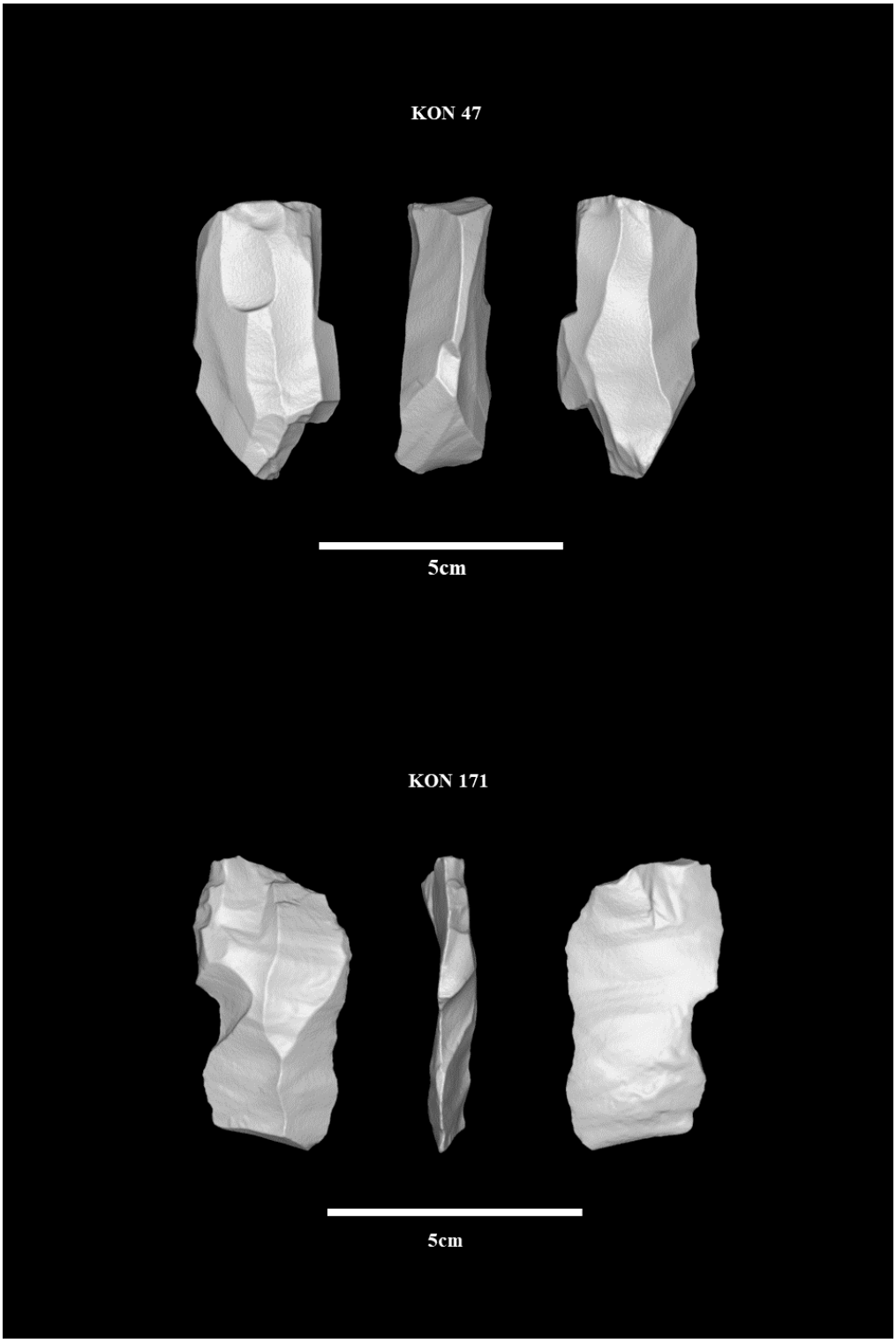
KON 47
5cm
KON 171
5cm

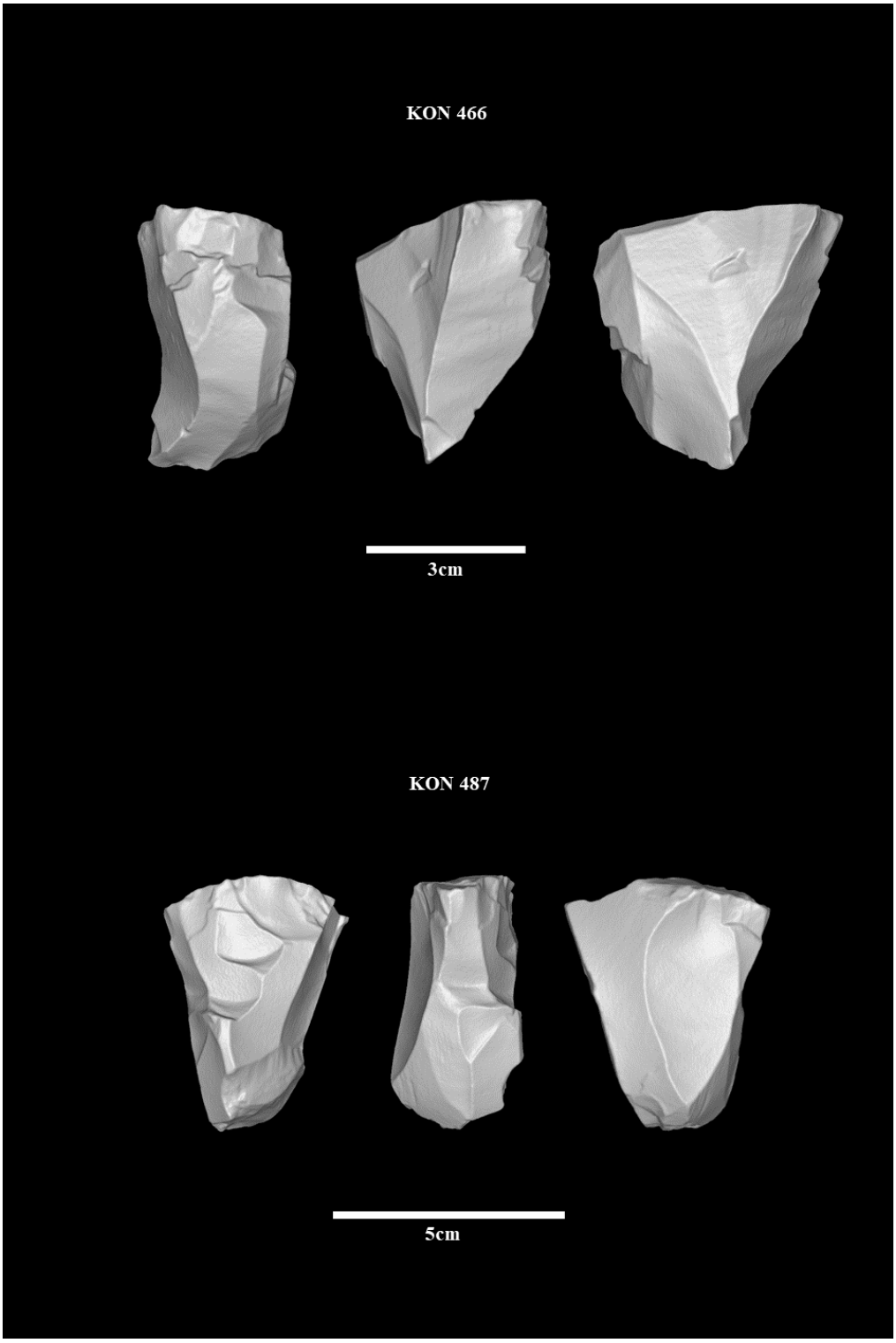
KON 466
3cm
KON 487
5cm

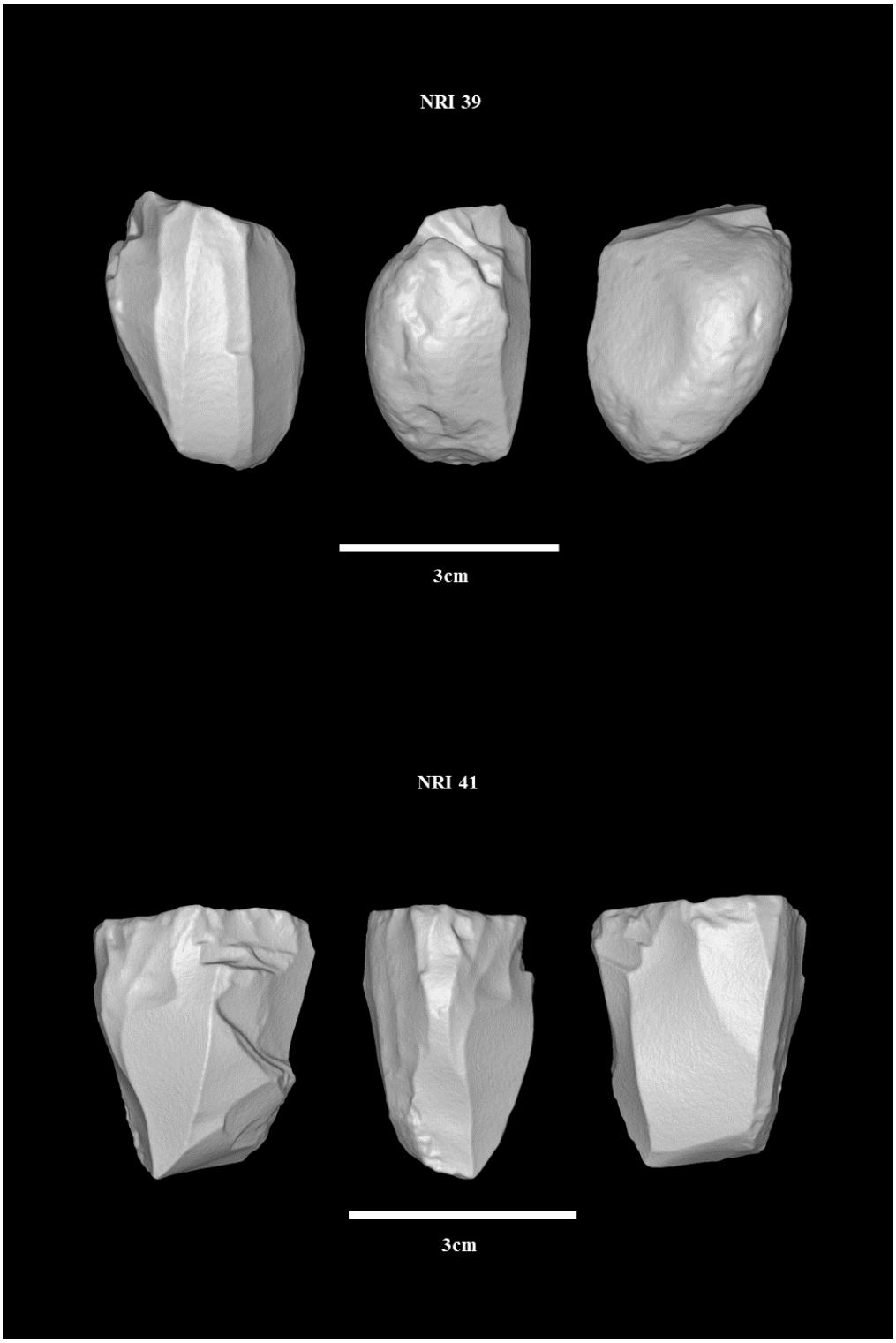
NRI 39
3cm
NRI 41
3cm

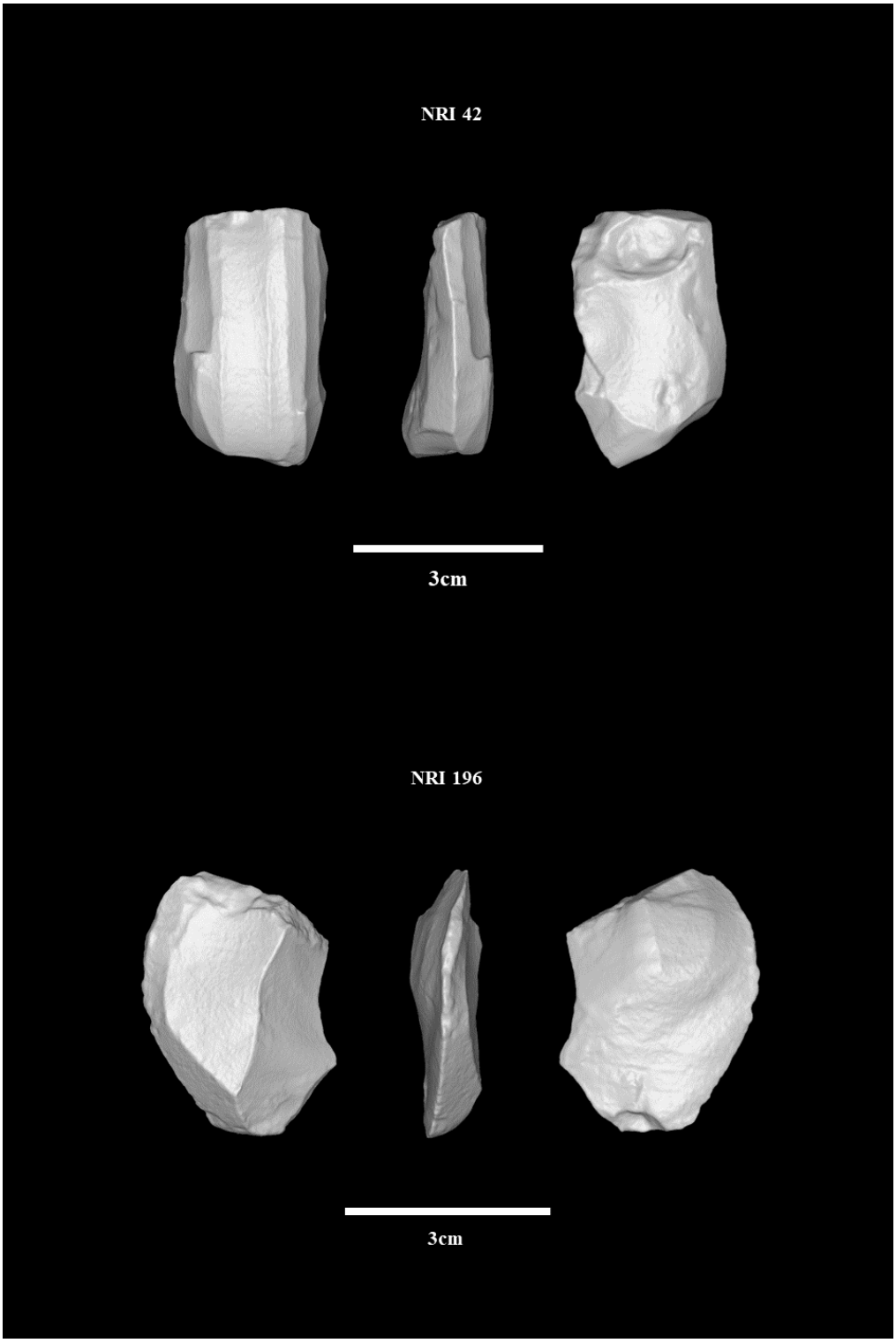
NRI 42
3cm
NRI 196
3cm

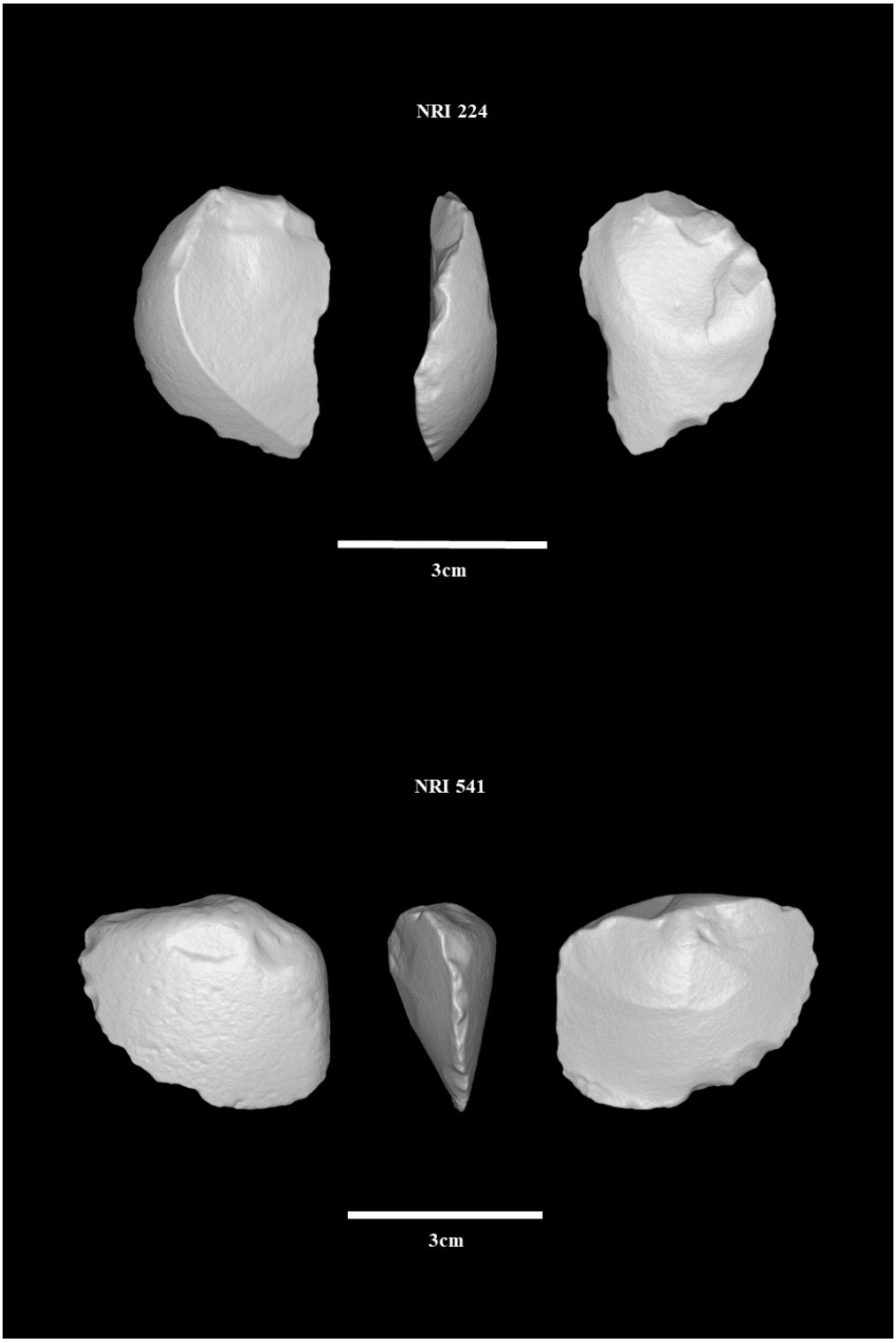
NRI 224
3cm
NRI 541
3cm

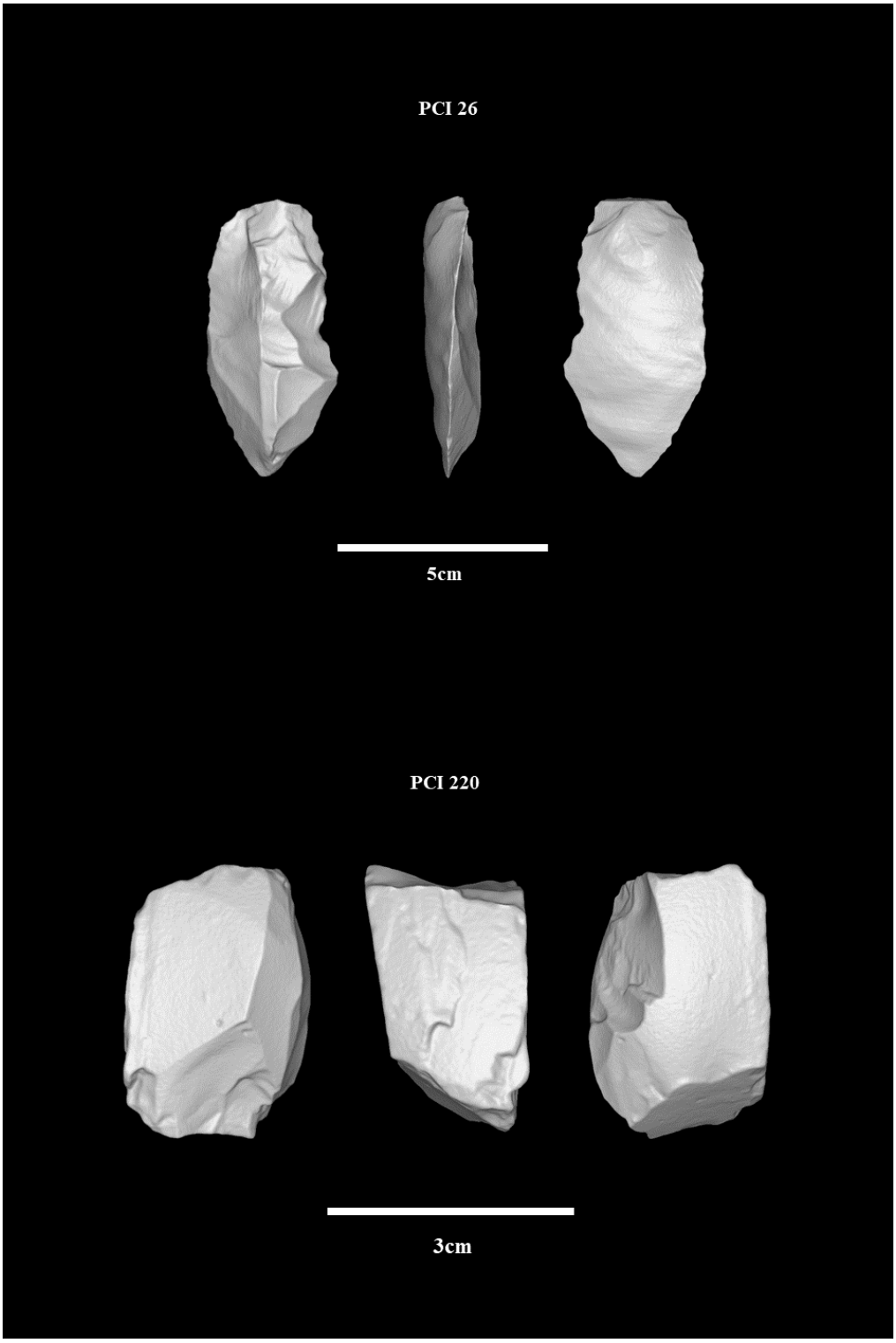
PCI 26
5cm
PCI 220
3cm

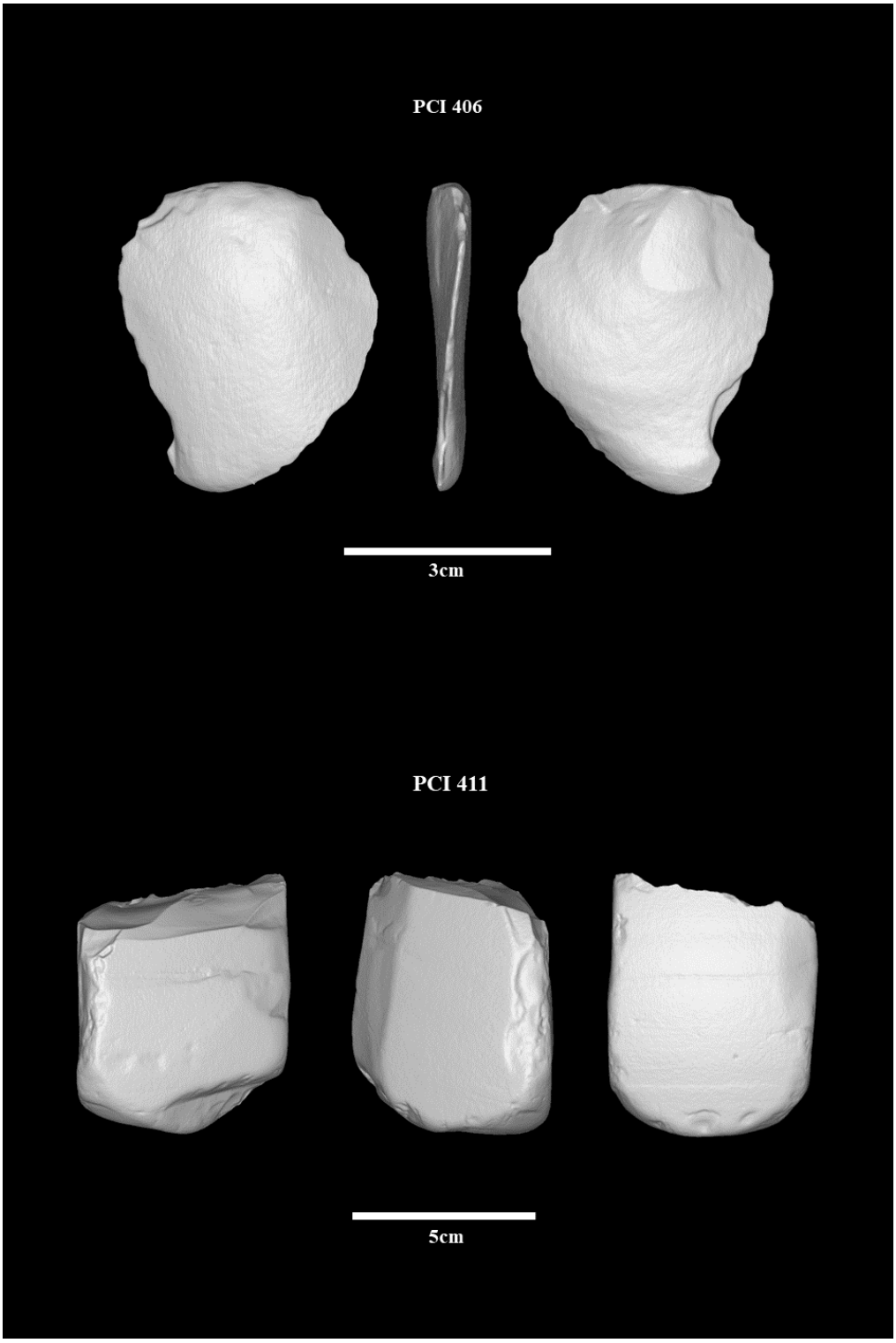
PCI 406
3cm
PCI 411
5cm

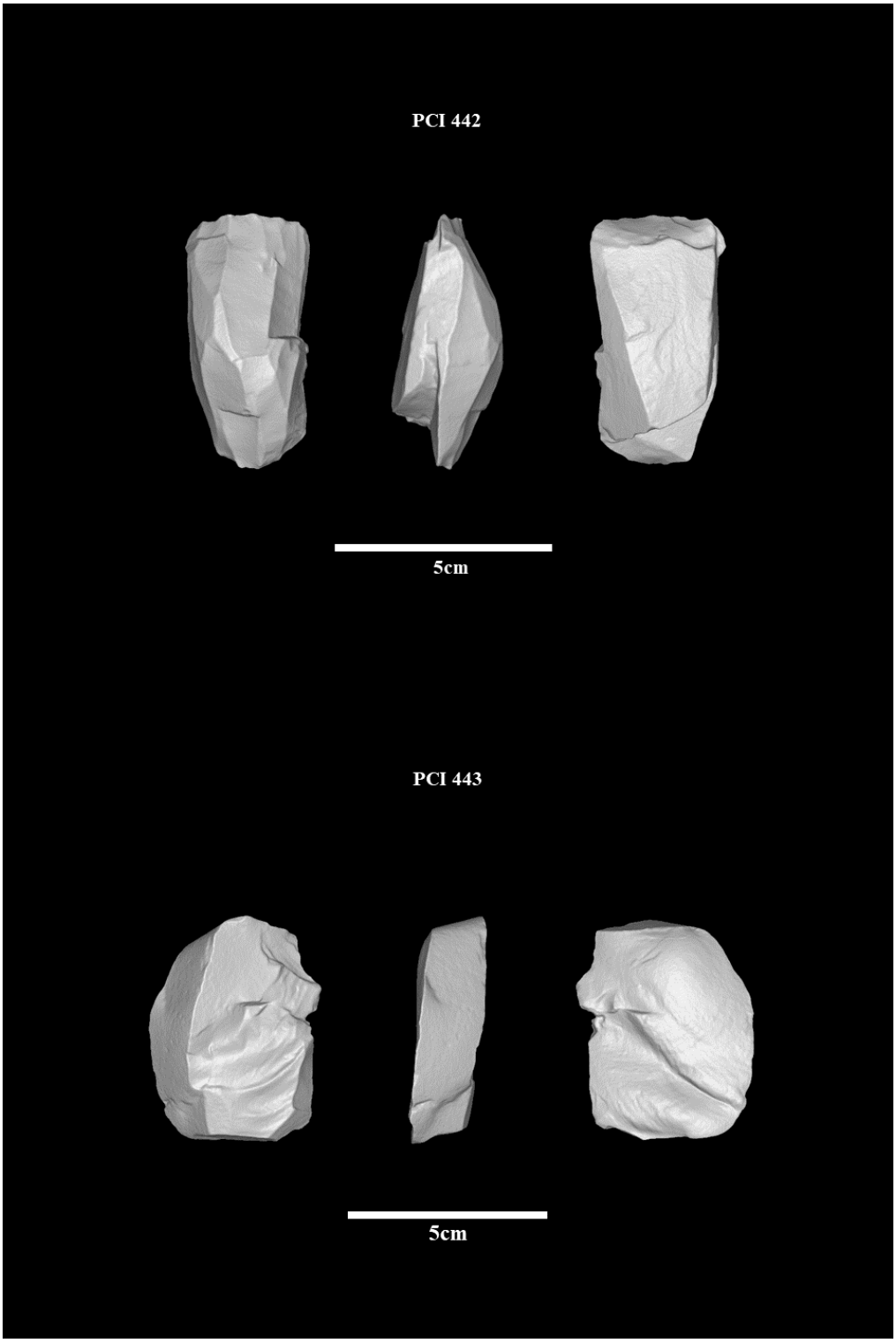
PCI 442
5cm
PCI 443
5cm